Mechanisms Underlying Memory Retrieval and the Effect of Amyloid Precursor Protein in a Transgenic Mouse Model

by

Nichola Whittingham

A thesis submitted in partial fulfilment for the requirements for the degree of Doctor of Philosophy at the University of Central Lancashire

April 2024

STUDENT DECLARATION FORM

Type of Award **Doctor of Philosophy**

School **School of Pharmacy and Biomedical Sciences**

1. Concurrent registration for two or more academic awards

I declare that while registered as a candidate for the research degree, I have not been a registered candidate or enrolled student for another award of the University or other academic or professional institution

2. Material submitted for another award

I declare that no material contained in the thesis has been used in any other submission for an academic award and is solely my own work

No proof-reading service was used in the compilation of this thesis.

Signature of Candidate 

Print name NICHOLA WHITTINGHAM

ABSTRACT

Introduction

Research into Alzheimer's disease (AD) would greatly benefit from a deeper understanding of the mechanisms underlying memory retrieval. Previous studies have found impairments in memory retrieval present in very young amyloid precursor transgenic (APPtg) mice, at a stage which would be considered preclinical in humans, however, the molecular and cellular mechanisms behind this impairment are unknown. Dysfunctional amyloid precursor protein (APP) processing is thought to be central to AD pathogenesis and mutations in the APP gene are one of the leading causes of familial Alzheimer's disease (FAD).

Objective

This thesis aims to contribute to a better understanding of the mechanisms underlying memory loss in a genetically modified preclinical mouse model resembling aspects of AD. These mechanisms will be elucidated via the quantitative analysis of certain mitochondrial protein levels, identification of biochemical and cellular pathways involved in memory retrieval via proteomics analysis, analysis of the activity of various enzymes in the mouse brain in the context of memory retrieval and the quantification of key mitochondrial metabolites in the mouse brain tissue samples.

Methods

Brain tissue from a mouse model overexpressing APP with two mutations linked to FAD (APPtg), was used in this project. Four groups consisting of APPtg and wild-type (WT) mice at basal levels (with no behavioural task) and during memory retrieval (sacrificed 20 seconds after 7-day probe trial, following Morris Water Maze behavioural task) were used in this study. Purified synaptosome samples were used for western blotting, enzymatic activity assays, and proteomic analysis.

Results

Western blotting against several synaptic and mitochondrial markers revealed increased expression of VDAC1 and the mitochondrial fission and fusion proteins Drp1 and Mfn1 in the APPtg mice at both the basal level and during memory retrieval. Several complexes of the electron transport chain also showed synapse specific expression increases in the APPtg mice at both the basal levels and during the attempted retrieval of a memory.

Using a combination of tools including gene-ontology (GO), protein-protein interaction (PPI) networks and functional dependency analysis, proteomic analysis revealed that the insertion of the

APP transgene causes upregulation of proteins implicated in mitochondrial dysfunction and disease pathology in both basal and memory retrieval groups . Based on the proteomics findings, failure to upregulate proteins involved in ATP production (Ndufa7, Ndufa6, Ndufb6, Ndufb4, Ndufb2) structural support (Nefl, Ina, Gfap), proteasome complex (Psma3, Psmb2, Psma7, Psmc1, Psmd4) response to oxidative stress (Prdx3, Prdx2, Gsr, Park7, Snca), and the negative regulation of apoptotic processes (Slc25a27, Nefl, Prdx3, Prdx2, Park7, Snca) are suggested to contribute to the memory deficits in this APPtg mouse model.

Whilst these methodologies have been previously used in Alzheimer's research, performing them in the context of memory retrieval (specifically, mice sacrificed at the point of attempted memory retrieval) is novel and provides new insights into the mechanisms underlying memory loss in preclinical APPtg mice.

Future work

Further work investigating the metabolic changes in WT mice during memory retrieval, when compared to basal levels, and how these changes differ in the preclinical model of FAD, can help to identify metabolites involved in healthy memory retrieval and how they differ in FAD. Alongside this, further assessment of the activity of enzymes involved in the various stages of aerobic respiration will provide insight into the disease process, offering opportunities for testing of enzymatic response to targeted therapies which, if delivered at a preclinical stage, could provide a means to prevent of delay memory loss in AD.

TABLE OF CONTENTS

ACKNOWLEDGEMENTS

First and foremost, I would like to thank my supervisor, Dr. Vassilios Beglopoulos, for the privilege of working on such an interesting project with important future implications, and for his continuing support, guidance, and advice throughout my academic endeavours.

Secondly, I would like to express my deepest appreciation to Dr. Emyr Bakker for his invaluable guidance and support regarding computational biology. The computational parts of this thesis would not have been possible without you.

I would also like to thank Dr. Jioji Tabudravu, Tamar Garcia-Sorribes, and Kathryn Dickens for their advice and guidance on the metabolomics aspect of this project and allowing me to access their laboratories to complete experiments. You have provided me with confidence in an area I knew very little about. Thank you.

My special thanks to my friends and colleagues, at UCLan and outside, for their support, patience, and understanding over the past three years. I couldn't ask for better friends.

Last, but certainly not least, I am deeply grateful to my parents and my partner Luke, for their unwavering love and support throughout this entire process. Your patience through tough times is what sustained me this far. None of this would be possible without you.

LIST OF TABLES

memory retrieval but were not upregulated in APPtg mice during memory retrieval. Inappropriately regulated= proteins that were upregulated during memory retrieval in APPtg mice but were not upregulated in WT mice.

Table 4.12. Differential protein regulations in APPtg mice during memory retrieval, when compared to WT mice during memory retrieval (group B).

Table 4.13. DAVID functional annotation clustering output for proteins upregulated in WT mice during memory retrieval, when compared to WT mice at the basal level (group A). Top 5 clusters are listed, in order of enrichment score.

Table 4.14. DAVID functional annotation clustering output for proteins downregulated in WT mice during memory retrieval, when compared to WT mice at the basal level (group A). The top 5 clusters are listed, in order of enrichment score.

Table 4.16. DAVID functional annotation clustering output for proteins downregulated in APPtg mice during memory retrieval, when compared to APPtg mice at the basal level (group C). The top 5 clusters are listed, in order of enrichment score.

Table 4.17. Table of the top 10 most connected proteins. Table lists the proteins with the greatest number of incoming and outgoing connections within differentially regulated proteins in APPtg mice during memory retrieval, when compared to APPtg mice at the basal level (group C) .

Table 4.18. Functional dependency matrix species dependency numbers in APPtg mice during memory retrieval, when compared to APPtg mice at the basal level (group C).

LIST OF FIGURES

type Basal average. T-testing was carried out between groups of synaptosome samples, and no significant differences were revealed.

Figure 3.6. A) Immunoblot analysis of PSD95 in P2 fractions from 8 different mice. WT-B= wild-type basal, WT-M= wild-type memory retrieval, APP-B= APPtg basal, APP-M=APPtg memory retrieval. Synaptophysin was used as a loading control. B) Densitometric analysis of blots shown in B. Protein abundance relative to normalised Wild-type Basal levels.

Figure 3.7. A) Immunoblot analysis of alpha synuclein levels in P2 fractions from 8 different mice. WT-B= wild-type basal, WT-M= wild-type memory retrieval, APP-B= APPtg basal, APP-M=APPtg memory retrieval. Synaptophysin was used as a loading control. B) Densitometric analysis of blot shown in A. Protein abundance normalised to synaptophysin levels, relative to WT basal average.

Figure 3.8. A) Immunoblot analysis of UQCRB levels in P2 fractions from 8 different mice. WT-B= wild-type basal, WT-M= wild-type memory retrieval, APP-B= APPtg basal, APP-M=APPtg memory retrieval. Synaptophysin was used as a loading control. B) Densitometric analysis of blots shown in A (P2 fraction). Normalised protein abundance relative to Wild-type Basal average.

Figure 3.9. Kinetic graph showing activity of malate dehydrogenase. Blank= assay buffer only. Blank + lysis)= assay buffer with additional lysis buffer. Assay carried out at 25°C, pH 7.4, with 5μg protein per sample. 16L & 24R= Wild-type memory retrieval group, total cell lysate.

Figure 3.10. Malate dehydrogenase 2 (MDH2) activity in synaptosome samples. A= MDH2 activity measured for each test sample. VG10,12,13,15= wild-type basal; VG2,4,5,8= wild-type memory retrieval; VG9,11,14,16= APPtg basal; VG1,3,6,7= APPtg memory retrieval. B= MDH2 activity measured via change in optical density per minute, measured at 450nm. Average activity calculated for each experimental group. Colour intensity at 450nm is directly proportional to MDH2 activity in each sample.

Figure 3.13. Kinetic graphs showing MDH2 activity, measured as change in optical density at 450nm per minute, over a 60-minute time frame. A= kinetic measurements of blank samples. B= kinetic measurements of sample backgrounds (no substrate). C= kinetic measurements of sample backgrounds (no substrate). D= kinetic measurements of biological samples. Assay carried out at 25°C, pH 7.4, with 5μg protein per sample.

Figure 3.14. A) Immunoblot analysis of MDH2 in synaptosome samples. Synaptophysin was used as a loading control. B) Average MDH2 expression plotted as a percentage of average wild-type basal MDH2 abundance.

Figure 3.15. Malate dehydrogenase 2 activity normalised against western blot quantification. A) normalised MDH2 activity by experimental group. No differences between groups were significant by t-test (a=0.05). B) Normalised MDH2 activity per sample. VG10,12,13,15= wild-type basal; VG2,4,5,8= wild-type memory retrieval; VG9,11,14,16= APPtg basal; VG1,3,6,7= APPtg memory retrieval.

Figure 3.16. Kinetic graph showing activity of 6-phosphofructokinase. Background= sample prepared without the addition of substrate. Background only= assay buffer. Assay carried out at 37°C, pH 7.4, with 5μg protein per sample.

Figure 3.17. 6-PFK activity in synaptosome samples. A=6-PFK activity measured by change in optical density per minute, measured at 450nm. Average activity calculated for each experimental group. Colour intensity at 450nm is directly proportional to PFK activity present in sample. B= 6-PFK activity measured by change in

optical density per minute. Activity measured for each individual sample. VG10,12,13,15= wild-type basal; VG2,4,5,8= wild-type memory retrieval; VG9,11,14,16= APPtg basal; VG1,3,6,7= APPtg memory retrieval.

Figure 3.18. Activity of 6-PFK. Kinetic graphs measuring change in absorbance at 450nm. A= Run 1- standard curve dilutions; positive controls; absolute blank; lysis buffer blank, B= Run 2- no-substrate sample backgrounds, C= Run 3- no-substrate sample backgrounds, D= Run 4- test samples, E= test samples. Assay carried out at 37°C, pH 7.4, with 5μg protein per sample.

Figure 3.19. A) NADH standard curve used to determine the amount of NADH in each test sample. B) The enzyme activity of 6-PFK was analysed within synaptosome samples of wild-type and APPtg mice during basal levels and during memory retrieval, here calculated as amount of NADH produced per minute, per 5μg protein. There were no significant differences identified between groups (α=0.05).

Figure 3.20. A) Immunoblot analysis of 6-PFK in synaptosome samples. Synaptophysin was used as a loading control. B) Average 6-PFK expression plotted as a percentage of average wild-type basal 6-PFK abundance.

Figure 3.21. Normalised 6-PFK activity in synaptosome samples in A) experimental groups, B) each test sample use, and C) activity expressed as the amount of NADH produced per minute, per 5μg protein. There were no significant differences identified between groups (α=0.05). VG10,12,13,15= wild-type basal; VG2,4,5,8= wild-type memory retrieval; VG9,11,14,16= APPtg basal; VG1,3,6,7= APPtg memory retrieval.

Figure 3.22. Average 6-PFK activity, normalised to western blotting results. Activity expressed as the amount of NADH produced per minute, per 5μg protein.

Figure 3.23. Kinetic graph showing activity of Hexokinase. Background WT-B= sample prepared without the addition of Hexokinase substrate. Background= only assay buffer. Assay carried out at 25°C, pH 7.4, with 5μg protein per sample.

Figure 3.24. Kinetic graph showing activity of pyruvate kinase. 16L & 24R= test wild-type memory retrieval sample (total cell lysate) . Background 16L & 24R= sample without the addition of substrate. Background= assay buffer only. Assay carried out at 25°C, pH 7.4, with 5μg protein per sample. 16L & 24R= Wild-type memory retrieval group, total cell lysate.

Figure 3.25. Kinetic graph showing activity of pyruvate dehydrogenase. Blank= assay buffer. Blank (lysis buffer)= blank with additional 3μl lysis buffer). Assay carried out at 25°C, pH 7.4, with 5μg protein per sample.

Figure 3.26. Kinetic graph showing activity of aconitase. Blank= assay buffer. Blank (lysis buffer)= blank with additional 3μl lysis buffer). Background, lysis + substrate= assay buffer blank with additional lysis buffer and substrate added. Assay carried out at 25°C, pH 7.4, with 5μg protein per sample. 16L & 24R= Wild-type memory retrieval group, total cell lysate.

Figure 3.27. Trailing different 96-well plates using NADH standards. Non developer= NADH standard alone, diluted with assay buffer. Developer= NADH standard with additional developer solution. B) non-developer and developer gained the same results exactly and therefore; results overlap on the graph. Assay carried out at 37°C, pH 7.4.

Figure 3.28. Kinetic graph showing activity of isocitrate dehydrogenase. Sample backgrounds= samples with no added substrate mix. Blank= assay buffer. Blank (lysis buffer)= blank with additional 3μl lysis buffer). Assay

carried out at 37°C, pH 7.4, with 5μg protein per sample. 16L & 24R= Wild-type memory retrieval group, total cell lysate.

Figure 3.29. Kinetic graph showing activity of fumarase. VG4= wild-type memory retrieval. 0.5x VG4= 0.5x volume. Background control= assay buffer only. Background control (lysis buffer)= assay buffer with additional lysis buffer. Background control (sample)= biological sample without the addition of substrate mix. Assay carried out at 25°C, pH 7.4, with 5μg protein per sample or 2.5μg protein (0.5 X Vg4).

Figure 3.30. Kinetic graph showing activity of complex 1. Blank= incubation buffer only. Blank+ lysis buffer= incubation buffer with additional lysis buffer. 5x 16L= 5x volume of 1x 16L sample. 10x 16L= 10x volume of 1x 16L sample. Assay carried out at 25°C, pH 7.4, with 5μg, 25μg or 50μg protein per sample. 16L & 24R= Wild-type memory retrieval group, total cell lysate.

Figure 3.31. Kinetic graph showing activity of complex II. Blank= assay buffer only. Blank+ lysis buffer= assay buffer with additional lysis buffer. Assay carried out at 25°C, pH 7.4, with 5μg protein per sample.

Figure 3.32. Kinetic graph showing activity of complex IV. 16L= Wild-type memory retrieval group, total cell lysate. Blank= incubation buffer only. Blank+ lysis buffer= incubation buffer with additional lysis buffer. Assay carried out at 25°C, pH 7.4, with 5μg, 20μg or 80μg protein per sample.

Figure 3.33 . Kinetic graph showing activity of complex V. WT-B (1/5)= 1/5th volume of standard 5μg WT-B (=1μg). Blank= assay buffer only. Blank+ lysis buffer=assay buffer with additional lysis buffer. Assay carried out at 25°C, pH 7.4, with 1μg or 5μg per sample.

Figure 3.34. Mass spectra of derivatised citric acid and pyruvic acid.

Figure 4.1. Raw LFQ (label-free quantitation) intensities for proteins targeted in western blot analysis. LFQ intensity shown for each of the experimental groups. Each group has 4 biological replicates.

Figure 4.2. LFQ (label-free quantitation) values for enzymes used for enzymatic activity assays. LFQ intensity shown for each experimental group. Each group has 4 biological replicates.

Figure 4.3. LFQ values for enzymes used for enzymatic activity assays. LFQ intensity shown for each experimental group. Each group has 4 biological replicates.

Figure 4.4. A) Differentially expressed proteins in WT mice at the point of memory retrieval, when compared to basal levels. Red plots denote statistical significance ($p<0.05$). A total of 1354 proteins were included in the plot, following FDR correction. B) Differentially expressed proteins in APPtg mice during memory retrieval, when compared to WT mice during memory retrieval. A total of 1480 proteins were included in the plot, after FDR correction. There are no statistically significant plots. C) Differentially expressed proteins in APPtg mice during memory retrieval, when compared to the basal levels. A total of 1497 proteins were included in the plot, following FDR correction. There are no statistically significant plots. D) Differentially expressed proteins in APPtg mice at Basal levels, when compared to WT controls. Red plots are statistically significant ($p<0.05$). A total of 1454 proteins were included in the plot, following FDR correction.

Figure 4.5 DAVID GO-term enrichment analysis. Table presents the top 5 biological processes enriched in upregulated proteins in WT mice during memory retrieval (when compared to WT basal levels; group A). Significant results denoted by *.

Figure 4.6. DAVID GO-term enrichment analysis. Table presents the top 5 biological processes enriched in upregulated proteins in APPtg mice during basal levels (when compared to WT mice during basal levels; group D). Significant results denoted by *.

Figure 4.23. DAVID GO term annotations for associated molecular functions enriched in APPtg mice at the basal level, when compared to WT mice at the basal level (group D). Significance denoted by *. Blue= downregulated proteins, Orange= upregulated proteins.

Figure 4.24. DAVID KEGG Pathway results for proteins differentially regulated in APPtg mice at the basal level, when compared to WT mice at the basal level (group D). Significance is denoted by *. Blue= downregulated proteins, Orange= upregulated proteins.

Figure 4.25. Functional dependency matrix for upregulated expressed proteins at the basal level in APPtg mic (when compared to WT mice at the basal level; group D). Y-axis labels are in reverse order to x-axis (starting from Lin7a and finishing with Cryab. Overlapping species labels can be deduced from X-axis labels.

Figure 4.26. DAVID GO enrichment analysis output for enriched biological processes within proteins that fail to become upregulated or become upregulated in APPtg mice during memory retrieval but are not upregulated in WT mice during memory retrieval. Significant results denoted by *. Blue= proteins upregulated when they shouldn't be, Orange= proteins that fail to become upregulated.

Figure 4.27. DAVID GO enrichment analysis output for enriched cellular components within proteins that fail to become upregulated or become upregulated in APPtg mice during memory retrieval but are not upregulated in WT mice during memory retrieval. Significant results denoted by *. Blue= proteins that fail to become upregulated, Orange= proteins upregulated when they shouldn't be.

Figure 4.28. DAVID GO enrichment analysis output for enriched biological processes within proteins that fail to become downregulated or become downregulated in APPtg mice during memory retrieval but are not downregulated in WT mice during memory retrieval. Significant results denoted by *. Blue= proteins downregulated when they shouldn't be, Orange= proteins that fail to become downregulated.

Figure 4.29. DAVID GO enrichment analysis output for enriched cellular components within proteins that fail to become downregulated or become downregulated in APPtg mice during memory retrieval but are not downregulated in WT mice during memory retrieval. Significant results denoted by *. Blue= proteins that fail to become downregulated, Orange= proteins that are downregulated when they shouldn't be.

Figure 4.30. DAVID GO enrichment analysis output for enriched molecular functions within proteins that fail to become downregulated or become downregulated in APPtg mice during memory retrieval but are not downregulated in WT mice during memory retrieval. Significant results denoted by *. Blue= proteins downregulated when they shouldn't be, Orange= proteins that fail to become downregulated.

Figure 4.31. Electron transport chain protein expression during memory retrieval in each experimental condition. Protein expression expressed as a percentage of WT basal expression levels, in terms of fold change. 1.2= 120%-fold change. Red= highest fold change, green= smallest fold change

Figure 4.32. Expression levels of key proteins involved in mitochondrial dynamics in each experimental condition. Protein expression expressed as a percentage of WT basal, in terms of fold change. 1.5= 150% fold change. Yellow- highest fold change, dark blue/black= smallest fold change.

Figure 4.33. DAVID GO term enrichment analysis results for enriched biological processes within proteins differentially regulated in WT mice during memory retrieval, when compared to WT mice at the basal level (group A). Significant results are denoted by *. Blue= downregulated proteins, Orange= upregulated proteins.

Figure 4.34. DAVID GO term enrichment analysis results for biological processes enriched within proteins differentially regulated in APPtg mice during memory retrieval, when compared to APPtg mice at the basal level. Significant results denoted by *. Blue= downregulated proteins, Orange= upregulated proteins.

Figure 4.35. DAVID GO term enrichment analysis results for enriched cellular components within WT mice during memory retrieval, when compared to WT mice at the basal level (group A). Significant results denoted by *. Blue= downregulated proteins, Orange= upregulated proteins.

Figure 4.36. DAVID GO term enrichment analysis results for enriched cellular components within APPtg mice during memory retrieval, when compared to APPtg mice at the basal level (group C). Significant results denoted by *. Blue= downregulated proteins, Orange= upregulated proteins.

Figure 4.37. DAVID GO term enrichment analysis results for molecular functions enriched within differentially regulated proteins in WT mice during memory retrieval, compared to WT mice at the basal level (group A). Significant results denoted by *. Blue= downregulated proteins, Orange= upregulated proteins.

Figure 4.38. DAVID GO term enrichment analysis results for molecular functions enriched within differentially regulated proteins in APPtg mice during memory retrieval, when compared to APPtg mice at the basal level (group C). Significant results are denoted with *.Blue= downregulated proteins, Orange= upregulated proteins.

Figure 4.39. DAVID enrichment analysis results. Top 10 enriched KEGG pathways in differentially regulated proteins in WT mice during memory retrieval, when compared to WT mice at the basal level (group A). Significant results denoted by *. Blue= downregulated proteins, Orange= upregulated.

Figure 4.40. DAVID enrichment analysis results. Table lists top 10 enriched KEGG pathways in differentially regulated proteins in APPtg mice during memory retrieval, when compared to APPtg mice at the basal level. Significant results donated by *. Blue= downregulated proteins, Orange= upregulated proteins.

Figure 4.41. STRING network map of proteins upregulated during memory retrieval in WT mice, when compared to basal levels (group A). All interactions are of the highest confidence interaction score (0.900+). Line thickness indicates strength of data support for each interaction. PPI Enrichment Value <1.0e-16.

Figure 4.42. STRING network maps of protein upregulated in APPtg mice during memory retrieval when compared to basal levels (group C). All interactions are of the highest confidence interaction score (0.900+). Line thickness indicates strength of data support for interaction. PPI Enrichment Value <1.0e-16.

Figure 4.43. Functional dependency matrix for upregulated proteins in APPtg mice during memory retrieval. Dependencies show the effect of the X node on the Y node. Figure includes all significantly upregulated and significantly downregulated proteins which pass the 20% regulation threshold.

GLOSSARY OF ABBREVIATIONS

2-DG- 2-deoxyglucose
AD- Alzheimer's disease
ADP- Adenosine diphosphate
AMP- Adenosine monophosphate
AMPA- Alpha-amino-3-hydroxy-5-methyl-4-isoxazolepropioinic acid
AMPARs- AMPA-type glutamate receptors
AMPK- AMP-activated protein kinase
AMPK- AMP-dependent protein kinase
ANOVA- Analysis of variance
APP- Amyloid precursor protein
Aß- Amyloid beta
AßPP- Amyloid beta precursor protein
ATP- Adenosine triphosphate
ATP5A- Mitochondrial ATP synthase subunit alpha
BCA- Bicinchoninic acid assay
BP- Biological process
c-NADP-MDH- Cytosolic $NADP^+$ dependent
CA- Cornu ammonis
Ca^{2+}- Calcium (minus 2 electrons)
cAco- Cytosolic
CaMKII- Calcium/calmodulin-dependent kinase II
cAMP- Cyclic adenosine monophosphate
CC- Cellular component
CcO- Cytochrome C oxidase
CI-AMPARs- Calcium-impermeable AMPAR
CNA- CellNetAnalyzer
COX4- Cytochrome C oxidase subunit 4
CP-AMPAR- Calcium-permeable AMPAR
CRE- CREB-responsive element
CREB- cAMP response element-binding protein
CSF- Cerebrospinal fluid
DAVID- Database for Annotation, Visualisation, and Integrated Discovery
DEPs- Differentially expressed proteins
DG- Dentate gyrus
DRP1- Dynamin-related protein 1
DTT- Dithiothreitol
ECL- Enhanced chemiluminescence
EOAD- Early-onset familial AD
ETC- Electron transport chain
FAD- Familial Alzheimer's disease
$FADH_2$- Flavin adenine dinucleotide
FAMEs- Fatty acid methyl esters
FDA- Food and Drug Administration
FDR- False discovery rate
FH- Fumarate hydratase

Fis1- Mitochondrial fission protein 1
GC-MS- Gas chromatography- mass spectrometry
GO- Gene ontology
GR- Glucocorticoid receptor
H.M- Henry Molaison
hAPP- Human APP
HK- Hexokinase
HP- Hippocampus proper
HRP- Horseradish peroxidase F
IMM- Inner mitochondrial membrane
KEGG- Kyoto encyclopedia of genes and genomes
KO- Knock-out
LC- Liquid chromatography
LFQ- Label-free quantification
LTM- Long-term memory
LTMs- Long-term memories
LTP- Long-term potentiation
m-NADP-MDH- Mitochondrial $NADP^+$ dependent
mAco- Mitochondrial aconitase
MADD- MAP-kinase activating death domain
MAL- L-malate
MAPKs- Mitogen-activated protein kinases
MCI- Mild cognitive impairment
MDH- Malate dehydrogenase
MDH1- Cytosolic malate dehydrogenase 1
MDH2- Mitochondrial malate dehydrogenase 2
MEK- Upstream activator of MAPK
MeOX- Methoxyamine hydrochloride
MF- Molecular function
Mff- Mitochondrial fission factor
Mfn1- Mitochondrial fusion protein 1
Mfn2- Mitochondrial fusion protein 2
mGluR- Metabotropic receptors
MS- Mass spectrometry
MSTFA- N-methyl-N-(trimethylsilyl)-trifluoroacetamide
mtDNA- Mitochondrial DNA
Mtfp1- Mitochondrial fission process 1
Mtfr1l- Mitochondiral fission regulator 1 like
MTT- Multiple trace theory
MW- Molecular weight
NAD- Nicotinamide adenine dinucleotide
NAD^+- Oxidised nicotinamide adenine dinucleotide
NADH- Nicotinamide adenine dinucleotide (+Hydrogen atom)
$NADP^+$- Nicotinamide adenine dinucleotide phosphate
NFT- Neurofibrillary tangle
NMDA- N-methyl-D-Aspartate
NMDAR- N-methyl-D-aspartate-type glutamate receptor

OAA- Oxaloacetate
OD- Optical density
OMM- Outer mitochondrial membrane
Opa1- Optic atrophy protein
OXPHOS- Oxidative phosphorylation
PDC- Pyruvate dehydrogenase complex
PDGF-ß- Platelet-derived growth factor beta
PDH- Pyruvate dehydrogenase
PEP- Posterior error probability
PET- Positron emission tomography
PFK- Phosphofructokinase
PFK-L- Phosphofructokinase (liver)
PFK-M- Phosphofructokinase (muscle)
PFK-P- Phosphofructokinase (platelet)
PFK1- Phosphofructokinase 1
PFK2- Phosphofructokinase 2
PK- Pyruvate kinase
PKA- Protein kinase A
PPI- Protein-protein interaction
PPPs- Protein phosphatases
PS- Presenilin
PS1- Presenilin 1
PS2- Presenilin 2
PSD- Postsynaptic density
PSD95- Postsynaptic density protein 95
PVDF- Polyvinylidene fluoride
ROS- Reactive oxygen species
SDH- Succinate dehydrogenase
SDHA- Succinate dehydrogenase complex flavoprotein subunit A
sEH- Hepatic soluble epoxide hydrolase
SEM- Standard error of the mean
STM- Short-term memory
STRING- Search Tool for the Retrieval of Interacting Genes
TCA- Tricarboxylic acid
UPLC-MS- Ultra-performance liquid chromatography-mass spectrometry
UQCRB- Ubiquinol-cytochrome C reductase binding protein
VDAC1- Voltage dependent anion channel 1
WT- Wild type

CHAPTER 1- INTRODUCTION

1.1 Memory

The primary function of the brain is to process and store information relating to the environment and control behavioural responses to this information. Over 3000 different cell types have been catalogued in the human brain, including excitatory neurons (the most abundant), inhibitory neurons, and glial cells, which together respond to the environment whilst maintaining functional connectivity and homeostasis (Conroy., 2023; Kennedy., 2013). Each excitatory neuron receives thousands of synaptic inputs and makes thousands of synaptic connections with other neurons. There are estimated to be over 85 billion neurons in the human brain, which allow us to carry out a multitude of complex cognitive functions essential for our survival including memory- the ability to retain information and recall it at a later time (Herculano-Houzel., 2009). Memories effectively shape our identities through guiding our thoughts and decisions, and influencing our emotional responses (Bisaz, et al., 2014).

The study of learning and memory has been at the forefront of three disciplines: philosophy, psychology, and more recently, biology (Squire., 2009). But what is memory? Psychologists define memory as 'the faculty of encoding, storing, and retrieving information,' divided into three main categories: sensory, short-term, and long-term (Squire, 2009). Each type of memory has its own qualities; sensory information is not consciously controlled, short-term memory has a finite storage capacity, and long-term memory has an unlimited storage capacity (Cowan., 2008). More recently, however, memory is beginning to be understood as a neuro-chemical process, which includes conditioning and stored experiences, occurring on a synaptic level in most organisms (Zlotnik & Vansintian., 2019).

In 1957, the modern era of memory research began, with studies by Milner, who documented the effects of a bilateral medial temporal lobe (including the hippocampus) resection on an epileptic patient, Henry Gustav Molaison, known as H.M, who exhibited significant forgetfulness following the surgery. The study's main findings led to the development of three principles which still guide research today: 1) memory is a distinct cerebral function and is separate from other cognitive abilities, 2) immediate memory does not require the medial temporal lobe, and 3) the structures that were damaged during H.M's surgery are not the ultimate repository of memory (Scoville & Milner., 1957). Milner's work was closely followed by the discovery of place cells (underlie spatial memory and navigation; 1971), the discovery of long-term potentiation (suggesting memories may be encoded in the strength of synaptic signals between neurons; 1973), the development of an

animal model of human memory impairment (1978), and evidence of multiple memory systems (1980). Efforts to achieve a working animal model of human memory impairment by Mishkin (1978) were initially successful and were followed by years of behavioural and anatomical studies, identifying the anatomical elements of the medial temporal lobe memory system, which supports declarative memory. Declarative memory is the first type of memory, focussed on facts, people, places, objects, and events. Non-declarative memory, the second type of memory, is focussed on perceptual and motor skills, and habit learning (Squire & Zola-Morgan., 1991). Eric Kandel (1981), in his Nobel prize winning studies, presented classical conditioning as a simple form of memory storage, observable on a molecular level within very simple organisms (classical conditioning was first defined by the psychologist, Pavlov, and defined on a molecular and cellular level by Kandel). His work extended the definition of memory to contain the storage of information within neural networks in different regions of the brain.

The hippocampus is a complex brain structure, located deep inside the temporal lobe. The hippocampus is formed from three distinct zones: the dentate gyrus (DG), hippocampus proper (HP), and the subiculum (Fogwe, Reddy & Mesfin., 2022). The HP is divided into the cornu ammonis (CA) 1 (CA1), CA2, CA3 and CA4 regions and is responsible for episodic memory (memory of events). These hippocampal sub-regions play an important role in the generation of episodic memory and would later be proven essential for learning, declarative memory, and spatial navigation, with long-term potentiation (the neural substrate of memory) first discovered in the region (Voss et al., 2017; Anand & Dhikav., 2012). The hippocampus is one of the earliest and most severely affected structures in neuropsychiatric disorders such as Alzheimer's disease (AD) ,(Rao et al., 2022), and damage to the hippocampal structures in humans leads to the impairment of memories formed from material learnt up to a month prior to the damage (Squire., 2009).

The key to understanding memory in its entirety is the question of how memories are formed, consolidated, and retrieved. In most organisms, long-term storage of memories occurs on a synaptic level, but in more complex organisms, like mankind, there is a second, more complex form of consolidation- systems consolidation (Zlotnik & Vansintjan., 2019). Systems consolidation relocates, processes, and stores memories more permanently (Frankland & Bontempi., 2005). There are many modern-day models of memory consolidation, which will be further discussed in the following sections. Although much is known about memory, the specific molecular and cellular mechanisms underlying encoding, consolidation, and retrieval are yet to be fully understood.

1.1.1 Memory Encoding

Whilst conducting research into the loss of memory, the primary and most devastating symptom of neurodegenerative disease, it is vital to first understand how a memory is formed, consolidated, and retrieved in a cognitively healthy individual so that we may begin to therapeutically target the aberrant pathologies in disease patients. The process of memory encoding begins with the processing of external stimuli from one or more sensory organs by the frontal lobe (predominantly the dorsolateral prefrontal cortex) and the parietal lobe of the cerebral cortex. The frontal lobe plays a vital role in establishing the sustained patterns of increased glutamatergic transmission that represent the information being received, and the functional organisation of the frontal lobe provides valuable information surrounding the nature of those representations (Postle & Pasternak., 2009). Information no longer accessible from the environment is then actively retained as short-term memory (STM) in a subset of neurons called an engram. STM allows recall for a period of several seconds to a minute without the need for rehearsal of the information, however, the estimated capacity of STM is generally thought to be only 7 ± 2 items, leaving information highly vulnerable to interference (Miller, 1956; Cowan, 2001). STM represents the initial, highly fragile phase of memory storage, which has limited capacity and duration. For the committal of information to long-term memory (LTM), repetition and synaptic-remodelling must be carried out, formally known as memory consolidation.

1.1.2 Memory Consolidation

It is widely accepted that memories must undergo a process of consolidation before committal to LTM. Immediately after learning, memories are temporary, susceptible to interference or trauma, and cannot be transformed into a more stable, LTM until consolidation has occurred. Consolidation is typically described as a process in which memories are reorganised with the passing of time, gradually lessening the dependence on the hippocampus for their storage and retrieval, until a more permanent memory is developed in alternate regions of the neocortex (Squire et al., 2015). Memory consolidation can be divided into two processes: synaptic consolidation (cellular mechanisms) and systems consolidation (reorganisation of neural circuits). A major mechanism by which experience-generated neural activity can modify brain function is synaptic plasticity- a series of synaptic transmission modifications. The long-term potentiation (LTP) of excitatory synaptic transmission, an experience-dependent and long-lasting strengthening of synaptic transmission, is one of the most important types of synaptic plasticity in memory consolidation (Goto., 2022). LTP can be divided into two main phases, early-LTP and late-LTP. One of the most well-characterised methods of LTP is early-LTP, which is dependent on N-methyl-D-aspartate-type glutamate receptor (NMDAR) in the CA1 region of the hippocampus. Ca^{2+} floods into the postsynaptic compartment during early-LTP

induction through NMDARs, activating calcium/calmodulin-dependent kinase II (CaMKII), which causes the phosphorylation of several proteins, including AMPA-type glutamate receptors (AMPARs) (Derkach et al., 1999). Phosphorylation of AMPAR subunits causes an increase in AMPAR channel conductance and the increase in CaMKII activity contributes to the insertion of AMPARs, leading to the potentiation of synapses (Hayashi et al., 2000). Concomitantly, new dendritic spines are formed, and the abundance of existing spines increases, leading to a modification of synaptic function (Engert and Bonhoeffer, 1999, Okamoto et al., 2004, Maletic-Savatic et al., 1999; Matsuzaki et al., 2004). The process of early-LTP occurs within hours and involves the stabilisation of changes in synaptic connectivity.

The onset of late-LTP is accompanied by the activation of adenylyl cyclase, triggered by the intracellular increase of $Ca^{2+,}$ resulting in an increased cAMP concentration. Protein kinase A (PKA) and mitogen-activated protein kinases (MAPKs) are activated in response to elevated intracellular cAMP. PKA translocates to the nucleus and phosphorylates the transcription factor cAMP response element-binding protein (CREB), ultimately triggering the transcription of genes containing CREB-responsive element (CRE), such as immediate early genes, kinases such as CaMKII and protein kinase Mzeta (Luis & Ryan., 2022). Proteins encoded by these genes act as upstream initiators of signalling pathways stemming from the membranes of dendritic spines to the postsynaptic density (PSD) and further in protein activation cascades (Zhu et al., 2016). Protein activation is most commonly enabled via phosphorylation, where phosphorylation cascades result in protein synthesis in the PSD, actin polymerisation, and alpha-amino-3-hydroxy-5-methyl-4-isoazolepropionic acid (AMPA) receptor trafficking on the spine membrane (Bosch et al., 2014). LTP can become more resistant to depotentiation stimuli 100 minutes after formation ,(Fujii et al., 1991), in a process called synaptic consolidation. Synaptic consolidation was originally thought to be explained by protein synthesis-dependent transport of postsynaptic density (PSD) scaffolding proteins to the synapses (Bosch et al., 2014, Frankland and Bontempi, 2005), however, memory storage does not end here. Consolidation can occur on a systems level, where memories that were initially dependent on the hippocampus are reorganised over time, until their dependence on the hippocampus is lessened and they are stored more permanently in the neocortex (Squire et al., 2015).

Today, there are many models of systems consolidation. For example, the standard model of consolidation proposes that the neocortex encodes and stores long-term memories (LTMs) via the strengthening of connections. It posits that the hippocampus supports the neocortex in doing so until the cortical connections are strong enough to become fully independent of the hippocampus and thus the hippocampus is no longer essential for the retrieval of remote, LTMs, only those which have yet to be consolidated (Alvarez & Squire., 1994). Multiple trace theory (MTT) was proposed in

1997 by Nadel and Moscovitch, which suggested the continued involvement of the hippocampus in the retrieval of all episodic memories (personal experiences that can be explicitly stated or conjured). It posits that upon each reactivation of a memory, a unique, contextually rich episodic memory trace (or code) is created within the hippocampus. It also suggests that memory traces created within the cortex are semantic and context-free, implying hippocampal involvement in the retrieval of all remote, episodic memories, independent of the age of the memory (Hintzman & Block., 1971; Hintzman., 1986, 1990; Versace et al., 2014; Briglia et al., 2018). Reactivation of hippocampal memory traces is thought to lead to the restoration of waking neural activity patterns, stabilizing existing hippocampal-cortical circuits. This process must occur several times for gradual remodelling of hippocampal-cortical circuits to occur, providing sites of permanent storage in the cortex (Frankland and Bontempi, 2005). Testing of these theories posed a significant challenge until the recent development of optogenetics, enabling researchers to modify specific cells to express light-sensitive ion channels, allowing the precise characterisation and manipulation of cellular functions (Emiliani, Entcheva & Hedrich., 2022). Even with the availability of optogenetic methodologies, there are still many avenues to be explored and understood before a more detailed and accurate model of consolidation can be formed.

1.1.3 Memory Retrieval

Memory retrieval is a highly regulated, complex process which aims to re-access previously stored information and its specific expression patterns in the brain. It is well documented that a wide range of molecular events underlie the different stages of memory formation and consolidation, however little is known about the molecular requirements of memory retrieval. This is perhaps surprising considering that retrieval is the first stage of memory to deteriorate in transgenic mouse models of AD, as demonstrated by Beglopoulos et al (2016) and Roy et al (2016). Research into memory retrieval falls into two main categories: research at the systems level or the molecular level.

Research at the systems level began with Semon (1921; 1923), who introduced the theory that reactivation of the memory-specific engram (population of neuronal cells which undergo persistent chemical and/or physical changes after exposure to specific experience), by cues available from the time of the experience, are required to induce memory retrieval. Studies in a pre-clinical mouse model of AD by Beglopoulos et al (2016) revealed that pre-pathological PDAPP mice (3-4 months old; express human APP with Indiana mutations (APPV717F); show absence of Aβ plaques via immunohistochemistry), who exhibited normal learning in a spatial memory task, displayed faster forgetting following performance to a pre-determined criterion than WT littermate mice. Memory

deficits were later rescued by immunotherapy with an anti-beta-amyloid antibody, suggesting that encoding and consolidation was largely normal, however, the ability to access and retrieve stored information was impacted (for a more detailed overview of this study, see section 1.4.1). Supporting evidence by Roy et al (2016) used transgenic mouse models of early AD to show that direct optogenetic activation of engram cells in the hippocampus resulted in the retrieval of memories in mice that were previously amnesic during long-term memory testing, even in the presence of retrieval cues. The authors directly induced long-term potentiation at perforant path synapses of DG engram cells, which restored LTM and dendritic spine density, restoring the memory. They proposed the restoration of dendritic spine density to be a mechanism of potential treatment of memory loss in the early stages of AD. Riedel et al (1999) reviewed the role of the hippocampus in retrieval via spatial memory tasking. They found that temporary inactivation of the hippocampus prior to memory testing impaired recall, suggesting the hippocampus to play an important role in retrieval.

Whilst research into the molecular mechanisms underlying retrieval is limited, progress into the initial events leading to retrieval has been made. Memory retrieval requires a coordinated chain of molecular events that occur on the synaptic level, supporting the temporary reactivation of neuronal networks previously established during consolidation (Szapiro et al., 2002; Rugg et al., 2015). Various neurobiological and behavioural theories about the mechanisms underlying memory retrieval have been developed over the past decades, focussing on specific molecular changes and brain regions. Studies by Szapiro et al (2000) found that blocking hippocampal AMPA/kainite receptors 10 minutes before memory-recall testing and the inactivation of AMPA/kainite receptors in a separate trial in rats, both impaired the retrieval of inhibitory avoidance responses, suggesting their involvement in retrieval mechanisms. The authors continued their studies by blocking metabotropic (mGluR) receptors using specific mGluR antagonists before memory retrieval testing, which was found to also prevent the retrieval of contextual fear memories. Additionally, the pre-test infusion of MEK (an upstream activator of MAPK) and a PKA inhibitor intrahippocampally effectively blocked memory retrieval. Memory retrieval was also associated with a rapid and selective increase in the levels of activated forms of p42 and p44 MAPKs in total hippocampal extracts of rats who performed very well during retrieval testing, highlighting the involvement of MAPK and PKA pathways in memory retrieval. The results of this study suggest that glutamate release, associated with testing, is critical for long-term memory retrieval and likely acts through mGluRs and AMPA/kainite receptors, which activate PKA and MAPK signalling cascades. The activity of such protein kinases implicated in memory retrieval, such as PKA, MAPKs and protein kinase C are modulated by dopaminergic D1, serotonergic-1A, beta-noradrenergic, and cholinergic muscarinic receptors in the hippocampus. Memory retrieval has historically been associated with changes in AMPAR, activated by glutamate,

the most prevalent neurotransmitter in the brain. The first studies on the role of AMPAR in memory retrieval studied AMPAR activation (Liang., 1991). Most AMPARs in the brain contain the GluA2 subunit, however, a small group of AMPARs which lack GluA2, termed calcium permeable AMPARs (CP-AMPAR), are associated with single-channel conductance. Calcium-impermeable AMPARs (CI-AMPARs) containing the GluA2 subunit play a role in basal synaptic transmission and have greater stability at the synapse. During memory retrieval and LTP associated processes, major synaptic changes occur at synapses strongly involved in memory retrieval, consisting of the rapid exchange of CI-AMPARs to CP-AMPARs. Blocking the synaptic removal of GluA2-containing CI-AMPARs during memory retrieval was shown to prevent the exchange of AMPAR composition, destabilising synaptic strength and resulting memory (Hong et al., 2013). Lopez at al (2015) theorised that protein synthesis to maintain pools of proteins was necessary for memory retrieval. They discussed the involvement of these proteins in activity-induced trafficking of AMPARs to the postsynaptic density and the subsequent need for these proteins to be replaced in order for retrieval to be completed. Using specific protein synthesis inhibitors (rapamycin or anisomycin), administered in the amygdala 10 minutes before memory testing, they demonstrated the impairment of memory expression. This proposed that memory retrieval requires ongoing protein synthesis and NMDAR activity-mediated AMPAR trafficking is required for the retrieval of fear memories.

Studies by Vianna et al (2000) highlighted the role of protein kinase isoenzymes in memory retrieval within inhibitory avoidance memory tasks in rats. Their results showed that inhibitors of the calcium-dependent isoforms, alpha and beta, blocked memory retrieval when infused into the CA1 region of the hippocampus 10 minutes before retrieval testing, highlighting their involvement in retrieval. Due to the rapid effect of protein synthesis inhibitors on memory retrieval, it is logical to assume that the proteins involved are locally translated at the synapse, with a rapid turnover rate. The period between the onset of conditioned stimulus and behavioural memory expression is a few seconds at most, indicating the continual synthesis of proteins necessary for memory retrieval by the specific synapses involved in the memory trace (Lopez et al., 2015). Once retrieval is initiated, sustenance of the protein pools required for effective retrieval requires ongoing protein synthesis. Introduction of a protein synthesis inhibitor would be manifested as an impairment in the previously learnt memory.

Research into memory retrieval has uncovered the involvement of glutamate receptors, cAMP-dependent protein kinase and mitogen-activated protein kinases, alongside the requirement of AMPA receptors. It has also shed light on the modulation by dopamine D1, beta noradrenergic, serotonin 1A and cholinergic neurons. Despite recent advancements, there are still many aspects of retrieval we do not yet understand, such as which processes are unquestionably involved, and which processes could be the most crucial. Elucidating the mechanisms that contribute to memory

retrieval failure in AD will allow for the potential development of cognitive therapies, drug development or optogenetic retrieval mechanisms to mitigate the devastating loss of precious memories.

1.2 Alzheimer's Disease

Alzheimer's disease (AD), an irreversible, complex, multifactorial disease characterised by extensive cortical atrophy, is the most common disorder involving the loss of memory (Emmady & Tadi., 2021). AD is the most common type of dementia, comprising 60-80% of cases worldwide, (Duong et al., 2017), and predominantly effecting the elderly population. As of 2022, there are over 55 million people living with dementia worldwide and this figure is projected to almost double every year, equating to 139 million people by 2050 (Alzheimer's Disease International., 2022). The total cost of care for dementia patients in the UK alone is over 33.7 billion, and with a new case presenting every 3.2 seconds, finding a cost-effective treatment is of the utmost importance to relieve some of the economic pressures (Alzheimer's Society., 2019). The risk of developing AD increases drastically with age: 34.6% of the population over the age of 85 currently have Alzheimer's dementia, (Alzheimer's Association., 2021), and this figure is projected to increase drastically over the next 25 years (Prince et al., 2014).

AD is defined pathologically by two main cellular hallmarks: the deposition of extracellular aggregates of amyloid-β protein (amyloid plaques) which interfere with neuronal communication,

and the presence of paired helical filaments of hyperphosphorylated tau protein within neurons (neurofibrillary tangles; NFTs), which block the transportation of nutrients and other molecules essential for neuronal survival (Emmady & Tadi., 2021; Furcila et al., 2019). Amyloid precursor protein (APP) is a type 1 integral membrane protein, and its expression is most concentrated in the synapses of neurons. Whilst the primary function of APP is unknown, it is thought to be implicated in the regulation of synapse formation and synaptic plasticity. Both APP and Aβ, its by-product, have been found to translocate inside mitochondria and play a role in mitochondrial dysfunction (Hoe, Lee & Pak, 2012). In 1991, the first mutation in the APP gene was discovered, closely followed by the discovery of mutaitons in presenilin 1 (PS1) and presenilin 2 (PS2). Together, these genes are responsible for the cleavage of APP into Aβ fragments of differing lengths, and mutations in these genes favour the production of longer fragments that accumulate abnormally in the brain, forming amyloid plaques (Chen et al., 2017). Plaques and NFTs are predominantly found in the entorhinal cortex, neocortex, and hippocampal formation, where their abundance and the proportion of

affected cortex progresses with the advancement of disease, although it is still currently unknown which protein is the primary trigger for neurodegeneration (Furcila et al., 2019).

AD can be separated into two main types, sporadic and familial. Familial AD (FAD) has an age of onset in the mid-40s and -50s and is caused by mutations in amyloid β precursor protein (AβPP), PS1 or PS2 encoding genes, representing the minority of AD cases (Quan et al,. 2020). Mutations within the APP gene account for 10-15% of early-onset familial AD (EOAD) cases and many of these mutations lie in or adjacent to the major component of amyloid plaques, the Aβ peptide sequence (Bekris et al., 2010). Sporadic AD accounts for more than 95% of cases and its onset is significantly influenced by a combination of environmental, lifestyle and genetic risk factors. The strongest genetic risk factor sporadic AD is apolipoprotein E ε4 allele, increasing the risk in homozygotes by as much as 15% (Raulin et al., 2022).

According to the National Institute on Aging (2011), AD may be divided into 3 basic stages: pre-clinical, mild cognitive impairment (MCI) and Alzheimer's dementia. During the pre-clinical stage, amyloid plaque build-up and other neuronal alterations have begun, but noticeable symptoms have yet to occur as the brain is able to compensate for the changes it is encountering, enabling normal functionality. Biomarkers for pre-clinical stages include abnormal beta-amyloid levels (detected using positron emission tomography (PET) scanning and cerebrospinal fluid (CSF) analysis), CSF and plasma tau protein changes, and decreased glucose metabolism as shown via PET scans (Alzheimers Association., 2023). Persons in the MCI stage have impairments in memory and cognitive abilities that are more advanced than what is typical for their age and educational status. These changes are not yet severe enough to interfere with normal daily functioning, but may be apparent to the sufferer, their close friends and family (Langa & Devine., 2014). MCI does not always progress to AD. The final stage, Alzheimer's dementia, presents symptoms including memory loss, visual and spatial problems, and behavioural changes, which are significant enough to impair a person's ability to function independently. In this late stage of disease, bodily functions become compromised, eventually leading to death most commonly by bronchitis, pneumonia, or acute myocardial infarction (Sakurai et al., 2023). Without any disease modifying treatments succeeding at clinical trial, AD presents one of the greatest global health challenges to date.

1.2.1 The Amyloid Hypothesis

Whilst several hypotheses for the pathogenesis of AD have been proposed over the past two decades, the amyloid hypothesis, proposed by Hardy and Allsop (1991), has been the prevailing concept underlying AD research among experts for the past 25 years (Kametani & Hasegawa., 2018).

The initial idea for the hypothesis came from researchers who had previously studied prion proteins, identifying similarities between amyloid plaques and causal entities in Creutzfeldt-Jakobs disease (Morris, Clark & Vissel., 2014). It posits that the deposition of toxic amyloid-beta (Aβ) aggregates in the brain initiates a cascade of neurodegenerative processes, leading to the loss of memory and cognitive ability seen in AD (Makin, 2018). The hypothesis states that in healthy aged subjects, Aβ undergoes excision from APP by β-secretase and γ-secretase, where it is subsequently released outside the cell for rapid degradation or removal. However, in AD patients, or aged subjects, Aβ fragments may begin to accumulate due to a decreased metabolic activity (Kametani & Hasegawa., 2018). This accumulation of Aβ oligomers is postulated to directly trigger formation of amyloid plaques and NFTs, synapse loss, neuronal death and neuroinflammation in regions concerned with learning and memory, notably the hippocampus. As the abundance of amyloid plaques increases, synaptic and neuronal loss progresses, eventually leading to disease (Morris, Clark & Vissel., 2014).

Although the amyloid hypothesis has dominated modern AD research, many clinical trials of anti-amyloidogenic agents have failed and a growing body of evidence is being amassed that disputes its core principles (Selkoe & Hardy., 2016). For example, various immunotherapy studies which targeted Aβ in mouse models of AD were effective in decreasing Aβ deposits in the brain but failed to improve symptoms of the disease and accumulation of tau (Ostrowitzki et al., 2012; Giacobini and Gold, 2013; Doody et al., 2014; Salloway et al., 2014). Additionally, studies by Kim et al (2007; 2013) using BRI2- Aβ mice demonstrated that, despite the presence of Aβ oligomers and fibrils and the development of amyloid plaques, no neuronal degeneration or impairment of cognitive function was observed, indicating that Aβ42 and its oligomers are not cytotoxic. Recent advances in imaging technologies have revealed the presence of amyloid deposits in non-demented individuals and very few deposits in AD patients (Morris et al., 2010; Edison et al., 2007; Li et al., 2008). In fact, the distribution of amyloid plaques in the brains of aged, non-demented patients can be just as widespread as that of AD patients, suggesting Aβ deposition to be a normal phenomenon of ageing (Davis et al., 1999; Fagan et al., 2009; Prince et al., 2009; Chetelat et al., 2013). Current data supports the notion that the aberrant expression and processing of APP may in some cases cause familial AD, and that excessive Aβ can be toxic. However, it does not support the conclusion that sporadic instances of AD are caused by aberrant Aβ expression thus alternative hypotheses of AD pathogenesis have gained steadily growing support (Morris, Clark & Vissel., 2014).

1.2.2 Alternative Hypotheses

Many alternative hypotheses for the pathogenesis of AD exist and are beyond the scope of this project and therefore, only those which are relevant to the project will be detailed.

An alternative hypothesis for AD, which focusses on the processing of Aβ rather than Aβ aggregates themselves, is the **presenilin hypothesis**, proposed by Shen and Kelleher (2007). According to the hypothesis, neurodegeneration and dementia are linked to the loss of Presenilin 1 (PS1) essential functions. The intermembranous protein PS1 is a component of γ secretase, which cleaves a plethora of type 1 transmembrane proteins including APP to generate Aβ peptides and notch (Kurkinen et al., 2023; Kelleher., 2017). Through a dominant-negative mechanism, pathogenic mutations in presenilin (PS) partly impair both γ secretase -dependent and -independent functions (Weggen & Beher., 2012; Veugelen et al., 2016). Elevated levels of Aβ, particularly Aβ42 (42 amino acid length), are produced by PS or APP mutations (perhaps in conjunction with sporadic AD), which can work to suppress PS function and mimic the effects of PS mutations. The partial loss of PS and γ secretase activity increases the synthesis of Aβ42, and Aβ42-mediated inhibition can create a vicious cycle, progressively worsening PS impairment (Shen & Kelleher., 2007). This decline in PS function leads to synaptic dysfunction, including alterations in molecular signalling events such as impairments of N-methyl-D-aspartate (NMDA) receptor-mediated function and deficits in synaptic plasticity. Ultimately, loss of essential PS function leads to progressive neurodegeneration (Saura et al., 2004). The hypothesis was motivated by earlier genetic discoveries that showed PS to be crucial for learning, memory, and neuronal survival during ageing in the adult mouse cerebral cortex (Saura et al., 2004;Watanabe et al., 2012). Subsequent studies showed PS1 mutations often result in loss of PS1 function and that more severe PS1 mutations eliminated γ secretase activity and Aβ production in the mouse brain, further supporting the hypothesis (Kelleher., 2017).

The **tau hypothesis** states that the aggregation of hyperphosphorylated tau protein impairs neuronal axons and reduces the affinity of tau to microtubules, thereby negatively influencing synaptic plasticity (Du, Wang & Geng., 2018). Abnormal interaction of hyperphosphorylated tau with filamentous actin induces the mis-stabilisation of actin, mitochondrial integrity deficits, and synaptic impairment (Kametani & Hasegawa., 2018). This propagation of tau pathology in the medial temporal lobe, specifically the entorhinal cortex, is strongly correlated with the severity of cognitive decline and the manifestation of clinical symptoms, to a greater extent than Aβ production. It has been reported that Aβ accumulation occurs after the appearance of tau lesions, providing support for the hypothesis (Braak & Del Tredici., 2014).

The **mitochondrial cascade hypothesis** provides an underlying framework for AD pathology and aims to extrapolate the amyloid cascade hypothesis to also cover sporadic forms of AD, instead of limiting itself to familial forms of the disease. According to the hypothesis, a person's genetically inherited mitochondrial starting line, along with their genetically and environmentally defined rate of mitochondrial decline, is the factor that defines the age at which neurological disease manifests itself (Swerdlow, Burns & Khan, 2013). It suggests mitochondrial dysfunction as an early event in sporadic forms of AD, enhancing pathologies that ultimately lead to neuronal death. Evidence has shown that soluble Aβ plaques can localize to mitochondrial membranes, altering their structures and causing a reduction in respiratory capacity and adenosine triphosphate (ATP) generation, alongside the generation of reactive oxygen species (ROS), leading to mitochondrial damage and neuronal incapacitation (Reddy & Beal, 2008).

The pathological alterations in AD are complicated and varied. Despite many criticisms, the amyloid hypothesis is still hugely influential today, although it has been built upon, modified, and challenged by researchers and alternative hypotheses over the years. AD is a complex and multifactorial disease, best explained by a combination of hypotheses.

1.2.3 Current treatments

There is currently no cure for Alzheimer's disease, however, several drugs have been approved for the temporary reduction in symptoms by modulating either acetylcholine or glutamate (Medscape., 2023). Cholinesterase inhibitors are commonly prescribed for mild to moderate AD and help control cognitive and behavioural symptoms. Cholinesterase inhibitors prevent the breakdown of acetylcholine, leading to increased neuronal transmission and a temporary stabilisation in symptoms (NIH., 2023). The most recently approved treatments are anti-amyloid drugs, including Lecanemab and Aducanumab, derived from mouse studies, which reduce the amyloid burden in patients. The medications function as monoclonal antibodies, removing Aβ fibrils (Lecanemab) and soluble oligomers (Aducanumab) which disrupts the pathogenic processes vital to the progression of AD. (Verger et al., 2023). NMDA antagonists are used to slow neurotoxicity in moderate to severe AD. NMDA antagonists block NMDA glutamate receptors, preventing the excessive activation of glutamine receptors, known to cause neuronal loss (Kuns, Rosani & Varghese., 2023). Whilst these treatments are effective at slowing cognitive decline in patients, research must continue in attempts to understand the molecular mechanisms underlying AD, with the hopes that new and effective cures will be identified along the way.

1.3 The role of mitochondria in Alzheimer's disease

Mitochondria are cellular organelles composed of two membranes, the outer mitochondrial membrane (OMM) and the inner mitochondrial membrane (IMM), surrounding the inner matrix. The outer membrane of mitochondria is porous and freely crossed by ions and small, uncharged molecules through porin membrane proteins such as the voltage-dependent anion channel (VDAC; Bayrhuber et al.,2008). Proteins and larger molecules are imported into the mitochondria via translocases (Kuhlbrandt., 2015). The IMM houses respiratory chain complexes which produce energy for the body via oxidative phosphorylation (OXPHOS), which generates an inner membrane potential used by ATP synthase (complex V) to synthesize ATP (figure 1.1). This process is entirely dependent on reducing equivalents produced via the tricarboxylic acid cycle (TCA) or β-oxidation in the mitochondrial matrix (Stock et al., 2000). The morphology and position of mitochondria within the cell are of crucial importance to cell function and are regulated by intricately balanced processes of fission and fusion, biogenesis, and autophagy, which work together to ensure a consistent and healthy mitochondrial population (Osellame et al., 2012). Mitochondrial dysfunction is implicated in metabolic and age-related disorders as well as neurodegenerative diseases (Johri & Beal., 2012).

Mitochondria communicate with the rest of the cell via four prominent mechanisms including the release of cytochrome C to induce cell death, the activation of AMP-activated protein kinase (AMPK) to control fission and fusion, production of ROS for transcription factor activation and the release of mitochondrial DNA (mtDNA) for the activation of immune response. A fifth mechanism, the release of TCA cycle metabolites, is known to control chromatin modifications, DNA methylation, post-translational modification of proteins and control cell cycle fate and mitochondrial function (Martinez-Reyes & Chandel., 2020).

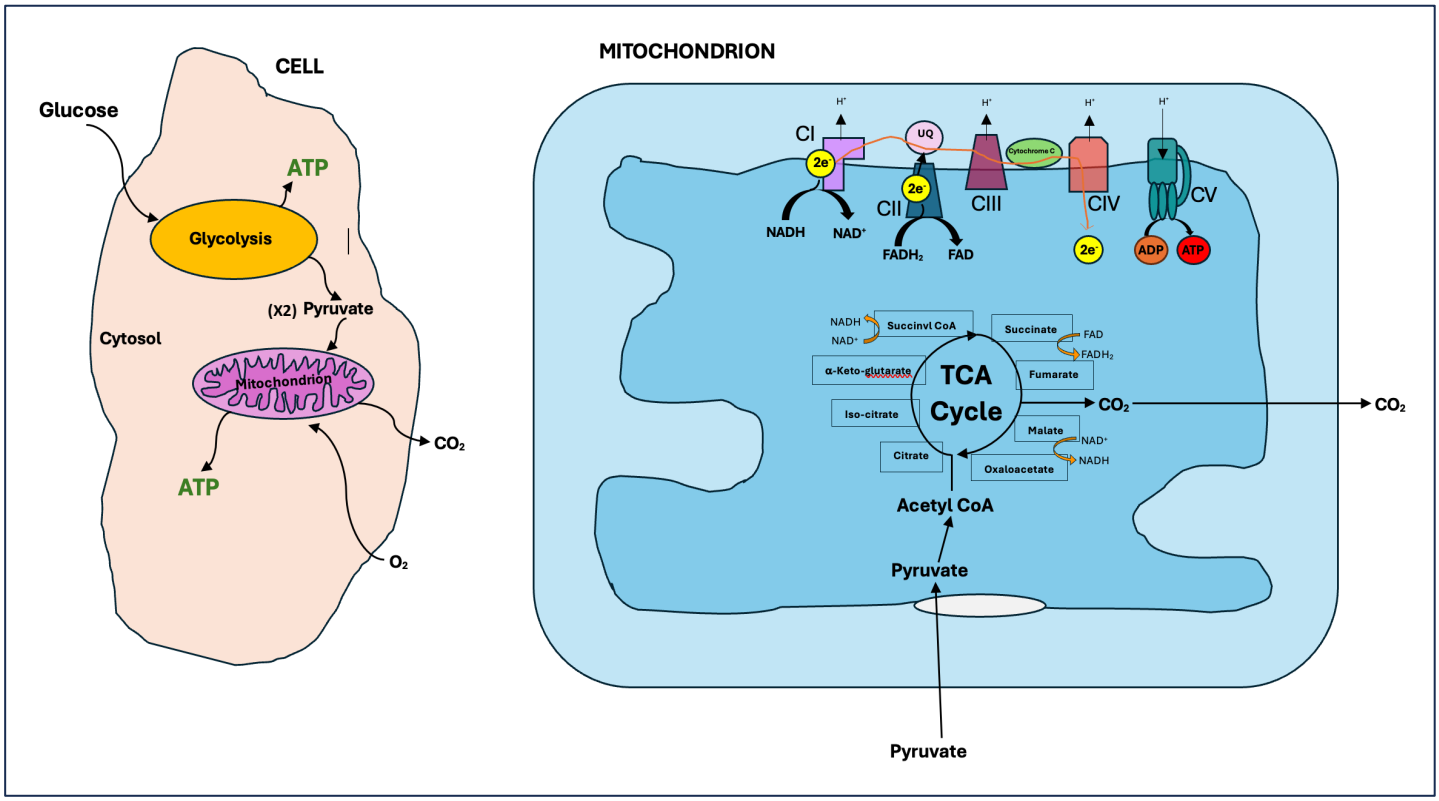

Figure 1.1. Simplified main stages and cellular locations of energy metabolism. At the top of the mitochondrion are the complexes of the electron transport chain, ending in ATP synthase (CV), where ADP and Pi are combined to create ATP. NAD plays a key role in its oxidised form (NAD+) and its reduced form NADH, in carrying and transferring protons and electrons to the intermembrane space and complex 1 respectively.

1.3.1 Glycolysis

Glycolysis is the cytosolic pathway in which a single molecule of glucose is catabolised into two molecules of pyruvate (figure 1.1), with the additional production of two molecules of ATP and nicotinamide adenine dinucleotide (NADH). Pyruvate from glycolysis is then metabolised in mitochondrial respiration to produce the ATP needed to sustain the brain and body (Zhang, Alshakhshir & Zhao., 2021). Glycolysis consists of two main phases: the investment stage (where ATP is consumed) and the payoff phase (where ATP is produced), (Chandel., 2021). First, glucose is converted into glucose-6-phospahte by hexokinase or glucokinase, using ATP and a phosphate group. Glucose-6-phosphate is then converted into fructose-6-phosphate by phosphoglucose isomerase. Next, phosphofructokinase (PFK) uses ATP to produce fructose-1,6-bisphosphate, which is then converted into dihydroxyacetone phosphate and glyceraldehyde 3-phosphate by fructose bisphosphate aldolase. Dihydroxyacetone phosphate is later converted into glyceraldehyde-3-phosphate by triosephosphate isomerase. Glyceraldehyde-3-phosphate becomes oxidised into 1,3-bisphospoglycerate, reducing NAD^+ into NADH and H^+ 1,3-bisphosphoglycerate will turn into 3-phosphoglycerate by phosphoglycerate kinase, alongside the production of the first molecule of ATP.

3-phosphoglycerate then converts into 2-phosphoglycerate, catalysed by phosphoglycerate mutase. Enolase then converts 2-phosphoglycerate into phosphoenolpyruvate, releasing one molecule of H_2O. Pyruvate kinase will finally remove a phosphate group from phosphoenolpyruvate, creating the second ATP of glycolysis (Chaudhry &Varacallo., 2023).

1.3.2 The Tricarboxylic Acid Cycle

In neurons (and other mitochondria-containing cells) pyruvate, the product of glycolysis in the cytoplasm, diffuses under aerobic conditions into mitochondria, where it enters the TCA cycle, a central metabolic pathway which oxidises nutrients to support cellular bioenergetics (Melkonian & Schury, 2021). The TCA cycle is composed of eight enzymes within the mitochondrial matrix, with the exception of succinate dehydrogenase, which is related to the electron transport chain (ETC) and thus is located on the IMM. In a series of enzymatic reactions, the reducing equivalents NADH and flavin adenine dinucleotide ($FADH_2$), required for the transfer of electrons to the mitochondrial ETC, are produced (Melkonian & Schury, 2021; figure 1.1). The initiating reaction for each turn of the TCA cycle is the condensation of oxaloacetate (OAA) with acetyl-CoA, generating citrate, catalysed by citrate synthase (Araujo et al., 2012). Citrate is then converted into isocitrate by aconitase 2. Next, isocitrate undergoes decarboxylation into alpha-ketoglutarate in an NAD^+ dependent manner, catalysed by isocitrate dehydrogenase, in an $NADP^+$ dependent manner, coupled with the release of CO_2 (Foyer, Noctor & Hodges., 2011). Alpha-ketoglutarate is decarboxylated by oxoglutarate dehydrogenase complex into succinyl-CoA, producing NADH and releasing CO_2. Succinyl-CoA is then converted to succinate by succinyl-CoA synthetase, coupled to the production of ATP in the only substrate-level phosphorylation step in the cycle. Succinate is further converted into fumarate by succinate dehydrogenase complex, which participates in both the TCA cycle and the ETC (Figueroa et al., 2001). Succinate dehydrogenase complex reduces flavin adenine dinucleotide, which donates two electrons to complex II of the ETC. Fumarate is converted into malate by fumarate hydratase, followed by the conversion of malate to OAA by malate dehydrogenase 2, regenerating the starting molecule to allow for subsequent turns of the cycle (Arnold & Finley., 2023). The completion of the cycle and production of ATP, NADH and flavin adenine dinucleotide feed into the ETC complex I and II, which pass their electrons through the ETC to produce ATP through OXPHOS (Martinez-Reyes & Chandel., 2020).

1.3.3 Oxidative Phosphorylation

The oxidative phosphorylation (OXPHOS) system in mitochondria is the final biochemical pathway producing ATP by the consumption of oxygen. Electrons from complexes I (NADH ubiquinone oxidoreductase, contains 42 subunits including Ndufa2 & Ndufa12) and II (Succinate ubiquinone oxidoreductase, contains three structural subunits: SDHA, SDHB, SDHD) are transferred to complex III (ubiquinol cytochrome C reductase, contains 11 subunits including UQCRB) by Coenzyme Q (glycerophosphate dehydrogenase) and the electron transferring flavoprotein. Electrons are then transferred from complex III to oxygen via cytochrome C and complex IV (cytochrome c oxidase (COX), contains 13 subunits including COX4) whilst an electrochemical proton gradient is simultaneously built across the IMM (figure 1.1). Generated proton motive force is used by complex V (ATP synthase) to produce ATP (Lanzillotta et al., 2019)

Enzymatic activity of the mitochondrial ETC has two additional effects; firstly, the generation of the inner membrane potential which is essential for mitochondrial import of nuclear encoded proteins and may reflect the health status of both the mitochondria and the cell. Secondly, the leakage of electrons from the ETC components is a contributor to the generation of reactive oxygen species (ROS), considered a by-product of bioenergetic pathways (Quinlan et al., 2013). In non-diseased states, ROS production is usually balanced by antioxidant systems, an equilibrium which becomes unbalanced during neurodegenerative disease, negatively effecting proteins involved in OXPHOS.

Dysfunction of single enzyme complexes of the respiratory pathways (glycolysis, TCA cycle, ETC) are frequently followed by loss of mitochondrial membrane potential, increased ROS production, and reduced ATP production. It is believed to critically contribute to the onset and progression of neurodegenerative pathology in AD (Bilsland et al., 2008). Deficiency of several key mitochondrial enzymes is well documented in AD, including enzymes involved in the TCA cycle such as ketoglutarate dehydrogenase, and pyruvate dehydrogenase, alongside enzymes involved in the ETC, such as cytochrome oxidase (Lanzillotta et al., 2019). Mitochondria are regulators of both the metabolism of energy and cell death pathways, highlighting their essential role in the survival or death of neurons (Moreira et al., 2010). Many adult-onset neurodegenerative diseases, including AD are characterised by the impairment of bioenergetics followed by disease related pathologies, suggesting mitochondrial dysfunction as a plausible hypothesis of AD (Yao & Brinton., 2011). Twelve enzymes were chosen to be studied, each from glycolysis, the TCA cycle or OXPHOS, in order to gain an overview of neuronal metabolic health. Of the enzymes chosen (chosen due to compatibility with sample type, cost, kit availability), two enzymatic activity assay kits were deemed functional/compatible with sample type after optimisation and therefore will be focussed on throughout this thesis; 6-phosphofructokinase, which catalyses the first committed step of

glycolysis, and mitochondrial malate dehydrogenase 2, a key enzyme of the TCA cycle. The enzymatic activity of these enzymes was measured, as detailed in the methods section.

1.3.4 Malate Dehydrogenase 2

Malate dehydrogenase (MDH) is a member of the nucleotide binding protein family, commonly termed nicotinamide adenine dinucleotide (NAD)-dependent dehydrogenases, or oxidoreductases (McCue & Finzel., 2022). There are two types of mammalian MDHs, cytosolic malate dehydrogenase 1 (MDH1), and mitochondrial malate dehydrogenase 2 (MDH2). MDH2 catalyses the oxidisation of L-malate (MAL) into oxaloacetate (OAA) in the citric acid cycle, simultaneously producing NAD^+ through the oxidation of NADH, and driving glycolysis (Priestly et al., 2022). There are three different MDH2 isoforms in mammals, based on their nucleotide specificity and cellular compartment: cytosolic $NADP^+$ dependent (c-NADP-MDH), mitochondrial $NADP^+$ dependent (m-NADP-MDH), and mitochondrial $NADP^+$ dependent (m-NAD-MDH) (Hung, Kuo, Chang & Lui., 2005). MDH2, the mitochondrial isoform, plays a critical role in preserving the NAD^+/NADH ratio between the mitochondria and the cytosol, through the reversible, NADH dependent catalysis of the oxidation of L-malate (MAL) to oxaloacetate (OAA) in the TCA cycle (Dasika, Vinnakota & Beard., 2015; McCue & Finzel, 2022). Catalysis of the unfavourable reactions by MDH2 necessitates the timely elimination of the product OAA in advance of the backwards reaction taking place (Mullinax et al., 1982). NAD^+ is reduced to NADH throughout the process, driving OXPHOS and crowning MDH2 an integral enzyme in energy homeostasis for the cell (Priestly et al., 2022).

The quaternary structure of m-NADP-MDH is a dimer of dimers, with stronger interactions at the dimer interface than the tetramer interface. Each monomer contains two independent binding sites-the active site and a separate, extra-nucleotide allosteric binding site, termed the exosite (Yang, Lanks & Tong., 2002). m-NADP-MDH has a complex regulatory system involving quaternary structure interconversion via ligand binding. The dissociation of the enzyme complex into dimers causes diminished enzyme activity, whilst the tetrameric organization is essential for full catalytic capacity. Activity is highly controlled by the energy status of the cell and is attributable to the sensitivity of the adenosine diphosphate (ADP)/ATP ratio as well as TCA cycle metabolites (Hsieh, Shih & Kuo., 2019). This specific ligand regulation is carried out by several molecules including NAD^+ and fumarate, which activate m-NADP-MDH under millimolar concentrations, triggering the conversion of malate to pyruvate, eventually leading to the production of ATP via the TCA cycle (Hsieh, Shih & Kuo, 2019). Kinetic studies have shown that NAD^+ and fumarate trigger such changes by binding allosterically to the enzyme, promoting reorganization of tetramers, thus activating the catalytic effects (Hung, Kuo,

Chang & Liu, 2005). Conversely, ATP can bind to the active site as a competitive inhibitor, but also allosterically binds to the exosite, causing the enzyme to dissociate into dimers, suppressing the enzymatic activity (Yang, Lanks & Tong., 2002). ATP suppresses the enzyme activity in this way when cells have sufficient ATP, as a negative feedback control for the metabolic pathway, preventing the generation of excess energy (Xu et al., 1999). When already bound to ATP, the additional binding of fumarate causes significantly more structural dissociation. However, binding of fumarate to the ATP-malate-bound enzyme causes rapid reassociation to the tetrameric form and increased enzymatic activity (Hsieh, Shih & Kuo, 2019).

In AD, disturbances in cellular metabolism, coupled with the accumulation of toxic beta-amyloid, may disrupt the normal allosteric regulation of MDH2, impairing the ability of the enzyme to appropriately respond to changing cellular demands. Decreased glucose and pyruvate availability may limit the supply of NADH, impeding the conversion of OAA into MAL and disrupting the flow of TCA cycle intermediates.

1.3.5 6-Phosphofructokinase

The Phosphofructokinases, phosphofructokinase 1 (PFK1), and phosphofructokinase 2 (PFK2), are tetrameric enzymes that together, in the presence of ATP, catalyse the first committed step of glycolysis- the phosphorylation of fructose-6-phosphate to fructose-2,6-diphosphate at position 1 (Brüser et al., 2012). The conversion of fructose-1,6-bisphosphate is catalysed by PFK1, while PFK2 catalyses the transfer of phosphate from adenosine triphosphate (ATP) to the second carbon of fructose-6-phopshate, generating fructose-2,6-bisphosphate (Raben., 2013). Fructose-2,6-bisphosphate is a stimulator of PFK1 through its capacity to heighten the affinity of PFK1 for fructose-6-phosphate, and diminish the reaction-inhibiting ability of ATP, thus regulating PFK1 activity (Litwack, 2018). PFK2 is a bifunctional enzyme with kinase and phosphatase activity. The kinase activity is inhibited by phosphorylation and the phosphatase activity is stimulated by phosphorylation (Patel & Harris, 2023). Thus, the same enzyme can covert fructose-6-phosphate to fructose-2,6-bisphsophate in the non-phosphorylated state and convert fructose-2,6-bisphosphate to fructose-6-phosphate in the phosphorylated state (Litwack, 2018)

There are three major mammalian isoforms of PFK1: PFK-M (muscle), PFK-L (liver) and PFK-P (platelet). All human tissues express each of the three isoforms in differing ratios, except for muscle tissues, which only express PFK-M (Fernandes et al., 2020). PFK2 has four known isoforms, identified in the liver, heart, brain and testis (Watanabe & Furuya, 1999). In eukaryotes, the N-terminal region

of the PFK1 enzyme is the mediator of its catalytic function, whilst the C-terminal region contains allosteric ligand binding sites, thought to have evolved from catalytic and regulatory sites from ancestral prokaryotic PFK (Brüser et al., 2012). Mammalian PFK is commonly accepted to have 4 active sites and 12 allosteric bindings sites; the structure of which suggest that one allosteric site may be specialised for small molecular regulators, such as citrate and phosphoenolpyruvate, and the other for AMP (adenosine monophosphate)/ADP (adenosine diphosphate), (Fernandes et al., 2020).

PFK activity is modulated allosterically by a variety of ligands, including the reaction products, its substrates, and more than 10 different metabolites, which fine-tune glycolytic activity to meet metabolic demands (Webb et al., 2015; Zancan et al., 2008). All three PFK1 isoforms show this ligand-dependent regulation, including sensitivity to inhibition by ATP and activation by the fructose-6-phosphate substrate (Webb et al., 2017). Mammalian PFK undergoes a complex regulatory process, switching assembly between monomers, dimers, and tetramers to tightly adjust cellular glycolytic activity in response to changing metabolic conditions (Webb et al., 2017). Enzyme formation and activity are directly correlated, as the PFK1 dimer exhibits minimal catalytic activity, whilst tetrameric forms exhibit full activity (Webb et al., 2017; Fernandes et al., 2020; Sola-Penna et al., 2010). Specific ligands favour the formation of the dimeric or tetrameric form of PFK1, with significant changes to the activity of the enzyme (Sola-Penna et al., 2010; Webb et al., 2015). Citrate, for example, favours the dissociation of tetramers, inhibiting the enzyme, whilst ADP and fructose-6-phosphate stabilize the tetrameric conformation, impeding the effects of citrate. Interestingly, ATP has a dual effect on PFK1, acting as an activator up to concentrations of 1mM, and an allosteric inhibitor at higher concentrations (Zancan et al., 2008). PFK1 is almost totally inactive under normal physiological concentrations of substrates and effectors, unless concentrations of fructose-2,6-bisphosphate rise, relieving the inhibition by ATP and allowing cells to maintain high glycolytic activity, even in the presence of ATP (Hue & Rider, 1987). Inhibition by ATP is part of a negative feedback loop that limits glycolytic flux when under aerobic conditions (Ros & Schulze, 2013).

In AD, conditions of oxidative stress may alter the availability of reducing factors, known to slow the dissociation of the active tetrameric form of PFK via allosteric binding sites (Fernandes., 2018). Limited availability of reducing factors would therefore lead to diminished PFK activity and a reduction in the glycolytic activity of the cell, contributing to glucose hypometabolism in AD.

1.3.6 Mitochondrial Dynamics in Alzheimer's Disease

Neurons, especially at the synapse, are dependent on mitochondria for fulfilment of their high energy requirements and the buffering of Ca^{2+} ion concentration, both of which are essential for effective neurotransmission and generation of axonal membrane potential. Healthy mitochondria regulate the homeostasis of $Ca^{2+,}$ a key regulator of neuronal plasticity and synaptic activity (Clavo-Rodrigues et al., 2020). Impaired regulation may lead to the influx of Ca^{2+} into the mitochondria, increasing ROS production, inhibiting ATP production, and triggering apoptosis- the foundations of neurodegeneration (Cali, Ottolini & Brini., 2012).

Mitochondria are highly dynamic organelles, constantly changing shape by two interchangeable processes known as fission and fusion, which regulate the morphology and structure of the mitochondrial network (a dynamic tubular network extended through the cytosol), (Cenini & Voos., 2019). Fission, mediated by proteins including the dynamin-related protein 1 (DRP1), is the fragmentation of large mitochondria into smaller ones and typically occurs when the cell needs to eliminate damaged mitochondria. As the metabolic needs of the cell change, mitochondria may increase their numbers or form interconnected networks via the fission process, maintaining the quality and bioenergetic functioning of mitochondria. Fusion is the process in which two mitochondria fuse together and exchange inner materials such as proteins and growth factors through the cytosol, effectively maintaining a healthy mitochondrial population. Fusion is mediated by a number of proteins including the GTPase dynamin-like proteins mitofusin 1 (Mfn1), mitofusin 2 (mfn2) and optic atrophy protein 1 (Opa1; Ranieri et al., 2013). Any modification to the structure of mitochondria can have drastic effects on the biogenesis of ATP, paving the way for neurodegenerative disease (Panchal & Tiwari, 2019).

Further to this, correct and efficient transport of mitochondria to the synaptic terminals is vital for their proper functioning (Cenini & Voos, 2019). Mitochondria can quickly switch between anterograde and retrograde movement and may be shifted between moving or stationary phases by changes in intracellular signalling or axonal growth. Thus, the mitochondrial membrane machinery must consist of motors, sensors, and anchoring proteins (Hollebeck & Saxton., 2005). The axonal transport of mitochondria via microtubules is also influenced by the metabolic demand and Ca^{2+} status at the synaptic level (Sheng & Cai., 2012).

1.4 Metabolic Responses and their Relevance to Alzheimer's Disease

As previously discussed, neurons are highly dependent on mitochondria for fulfilment of their high energy demands. They are also highly intolerant of insufficient energy supply, predisposing the brain

to disease if supplies are disrupted. Glucose, the obligatory brain fuel, fulfils many critical functions including the production of ATP, management of oxidative stress, and the synthesis of neurotransmitters, neuromodulators, and structural components (Mergenthaler et al., 2013). Decreased glucose availability has been shown to induce significant downregulation of glycosylation, an important mechanism of secondary protein processing within cells. Moreover, glycosylation may act as a metabolic sensor that can link the metabolism of glucose to normal neuronal functioning (Bukke et al., 2020). Independent of the amyloid cascade hypothesis, proteins involved in the metabolism of Aβ precursor protein have been identified as candidates of glycosylation. This presents the possibility that Aβ metabolism may be regulated by glycosylation, emphasizing the ideas that tightly controlled regulation of glucose metabolism is critical for brain physiology and glucose metabolic pathways may represent promising new areas for pharmacological intervention. Glucose metabolism is a multi-step process, including the transportation of glucose and its intracellular metabolism. Glucose hypometabolism is commonly understood as the impairment of glucose metabolism through OXPHOS, strongly implicating mitochondrial dysfunction as an early player in AD pathogenesis. In AD subjects, mitochondria are characterised by reduced OXPHOS, decreased ATP production, increased generation of ROS and perturbed antioxidant defence, although the mechanisms that cause bioenergetics deficits are yet to be fully understood (Lanzillotta et al., 2019).

It has long been recognised that brain glucose hypometabolism is a prominent irregularity occurring in the preclinical stages of AD, where abnormalities are found in almost every step of glucose metabolism. In fact, many neurodegenerative diseases also show a coexisting metabolic dysfunction, which is strongly correlated with the significant worsening of neurological symptoms and therefore, improving the neuronal energy state early in the disease progression may influence the level of cognitive and memory decline, presenting a promising new area for pharmacological intervention intervention (Constantini et al., 2008). By analysing the activity of each enzyme within energy metabolism pathways and identifying aberrant activity patterns, specific targeted agents can be developed (or existing drugs identified from drug databases) to increase or decrease the activity of the dysfunctional enzyme complexes thought to be causing the deficit then it may be possible to delay or reverse the glucose hypometabolism seen in AD and potentially, the memory loss that it causes.

Additionally, the use of mitochondrial therapy has been employed in a number of diseases to improve symptoms of mitochondrial dysfunction in a range of human diseases. For example, a mitochondrial targeted agent currently being trailed focusses on the mitochondrial pyruvate carrier which mediates the import of pyruvate into the mitochondrial matrix, linking glycolysis and OXPHOS.

Mitochondrial and metabolic dysfunction, linked to aberrant pyruvate uptake, is an important contributor to the pathogenesis of metabolic diseases. Pharmacological inhibition of the mitochondrial pyruvate carrier is being explored for treatment of AD and Parkinson's disease and has shown successful improvement of cerebral glucose metabolism and reduced AD patient brain damage in stage 2 clinical trials (Singh, Faccenda & Campanella., 2021). Targeting mitochondrial dysfunction and aberrant bioenergetics early on in disease pathogenesis presents a promising, new area for future treatments of neurodegenerative disease.

1.4.1 Memory-Associated Metabolic Responses and their Relevance to Alzheimer's Disease

Even with years of extensive research, a logical and chronological order of the events in AD and an effective treatment is still missing. The main concepts for this project were developed based on the previous work of the first supervisor. Beglopoulos et al (2016) conducted a series of behavioural, histochemical, and immunological methodologies in attempt to identify cryptic changes in spatial memory in a rodent model of FAD at a very young age, when memory encoding is normal. In humans, this is representative of a pre-diagnostic stage of disease. Firstly, very young (7-9 months) pre-pathological PDAPP mice, overexpressing mutant human APP, and WT littermate mice, were trained in a watermaze (Vorhees, Williams & Morris, 2006), using a spatial learning protocol specifically designed to dissect learning from forgetting.

For five days, the animals were subject to visual cue training, four times per day. The Atlantis platform placement varied across each trial. At the beginning of the trial, each animal was given a randomly assigned starting position in the pool and was allowed a maximum of 90 seconds to search for the platform, with a maximum of 30 seconds to remain on the platform at the end of the trial. This was carried out for 3-10 days until the daily-session training criterion with average escape latency <20 seconds was achieved. Probe tests consisted of a single 60 second trial followed by the release of the Atlantis platform to 1.5cm from the water surface with an additional 30 seconds to allow platform to be located. For the 7-day probe test, the Atlantis platform was not utilized, and mice were removed from the watermaze at the end of the 60 second period. Mice were trained to a predefined standard of quick and reliable escape from the water, no matter how many trials this required. Then, either retrieval was tested immediately (10 minutes), or consolidation was allowed to continue with retrieval tested after a long delay (7 days). A 'basal levels' group was used for each genotype, where mice were handled and learnt the memory task, but retrieval was not tested. Training to visible escape platform in the watermaze, as well as swim speed and average swim length, were normal for both genotypes. A small, but significant, difference was present in the

number of days to reach training criterion, which resulted in higher escape latencies by PDAPP mice in trials on days 1-2. However, overall, young PDAPP mice (representative of pre-symptomatic AD patients) with low levels of soluble Aβ can learn hippocampal-dependent tasks effectively (histochemical analysis confirmed Aβ plaque absence). Control mice showed good recall in memory retrieval testing at both the short- and long-term retention intervals. PDAPP mice, however, demonstrated strong recall at 10 minutes but displayed considerable memory loss, indicated by loss of search focus, at the 7-day interval (Analysis of variance (ANOVA) revealed highly significant interaction between group, quadrant occupancy and memory delay). Comparison of target quadrant occupancy scores between the 10-minute and 7-day tests showed no decline in performance of the WT mice.

In conjunction with behavioural protocols, the authors also performed analysis of glucose uptake in the brain, timed specifically to distinct phases of memory processing, through injection with [14C]-2-deoxyglucose (2-DG), measured across 32 brain areas. Autoradiographs from WT and PDAPP mice revealed a remarkable glucose hypometabolism in connection with memory retrieval in the PDAPP mice, which was absent in WT mice. Glucose uptake impairment in was largely seen in the neocortex, with a smaller but substantial alteration in the hippocampus. At the basal levels, glucose uptake in PDAPP mice was normal.

Lastly, immunotherapy using an antibody directed towards a section of the Aβ sequence was carried out to confirm the specificity of cognitive and physiological phenotypes to Aβ or other APP metabolites. Alone, the PDAPP mouse adopts transgene overexpression which may have non-specific effects on phenotypes related to insertion of the transgene. Administration of 10D5 antibody (specific to section of Aβ sequence) was initiated 4 weeks before watermaze training. Analysis of the 7-day probe trial swim patterns revealed a complete removal of memory retrieval deficit in PDAPP mice, as well as the memory-associated deficit in glucose uptake, which confirmed the specificity of the observed phenotypes to Aβ and other APP metabolites which contain the Aβ sequence and also proved 10D5 to be a successful therapy for the rescue of memory retrieval deficits in previously amnesic mice, as well as recovery of normal brain glucose metabolism.

Overall, the main findings of the study were accelerated behavioural forgetting in young PDAPP mice in absence of learning deficit and attenuation of memory-associated glucose uptake measured during the act of retrieval. Contribution to forgetting by young PDAPP mice may be due to failure to meet consolidation associated metabolic demands. Given the role of mitochondria in neuronal glucose metabolism and that mitochondrial transport is hindered by Aβ, the cellular mechanisms underlying the observed phenotypes might include impaired synaptic localization of mitochondria.

Additional recent studies have identified dysfunctional glucose metabolism in the brains of AD patients. When compared to aged-matched controls, AD brains showed a reduction in glucose utilisation, further evidenced in APP mouse models (Huang et al., 2020). Further, a reduction in the levels of glucose consumption at the hippocampal and posterior cingulate has been observed in patients at the early stages of AD (Chen et al., 2021). This decline in glucose metabolism can be correlated with synaptic density and function, suggesting a connection between cognitive impairment and brain glucose consumption. This previous work suggested important mechanistic insights but the exact biochemical mechanisms still are not known.

The aims of this project, detailed in section 1.6, are largely based on the hypothesis presented by the first supervisor that synaptic mitochondrial dynamics and activity are a strong candidate process for supporting the synaptic activity needed for the retrieval of memories, and dysfunction in these areas may cause the significant glucose hypometabolism seen in AD. Prior evidence, particularly the aforementioned anti- amyloid immunotherapy results (Beglopoulos et al., 2016), which reversed the behavioural phenotype of memory loss and has a very similar method of action to the most recently approved AD drugs, Lecanemab and Aducanumab, provides increased confidence to support the investigation of this hypothesis.

1.4.2 Justification of Mitochondrial Metabolite Methodology

The workflow for the analysis of mitochondrial metabolites was a source of consistent change. Different instruments became available over the course of a year, allowing for more sensitive and accurate analysis. This did, however, mean methods were developed for one instrument and then discontinued when a new instrument became available, with the focus then shifting to developing and optimising the new instrument for the changing experimental needs. The final instrument chosen to continue analysis was an ultra-performance liquid chromatography-mass spectrometry (UPLC-MS), a highly sensitive instrument that has the capability of analysing the metabolites required.

In the beginning, three standards were readily available for testing and method optimisation: tri-sodium citrate dihydrate, sodium pyruvate, and sodium succinate hexahydrate (as this was for optimisation purposes the conjugate anion forms of the organic acid metabolites citric acid, pyruvic acid and succinic acid were used, with the intention of spiking a biological sample to determine if samples were compatible with the instrument, contained detectable amounts of metabolites and the instrument displayed adequate sensitivity). 1mM stock solutions were created for each

metabolite (dissolved in dH2O) and subsequently diluted to 50µM in a 50:50 ratio of dH2O and solvent (methanol:acetonitrile). Calibration curve standards were made at 0.5,2.0,5.0,10,25,50µM. standards were injected into the gas chromatography- mass spectrometry instrument (GC-MS) using an autosampler (1ml/min He gas flow, 1.00µl injection volume; Trace 300 & ISQ LT Mass Spec (Thermo)). GC-MS analysis has many advantages, including its speed, stable retention times, and production of fragmentation patterns for which vast fragment databases exist, allowing quick identification of detected metabolites by comparison. However, GC-MS is more applicable to volatile and gaseous samples due to the inert gases used to transport vapourised samples to the stationary phase (Berg et al., 2013). Non-volatile samples must go through an additional derivatisation process before submission to the instrument. After submission of the standards to the instrument, a build-up of residue was found around the GC-MS injection site and thus analysis did not continue with this instrument. Instead, the organic acids citric acid, succinic acid, and pyruvic acid (primary metabolites) were ordered and used, and new stock solutions were created for each metabolite standard (50µM, 50:50 dH2O:solvent (methanol:acetonitrile)).

The coupling of liquid chromatography (LC) with mass spectrometry (MS) with the introduction of electrospray ionisation in the 1980s, created a new, highly sensitive method capable of detecting a broader range of complex mixtures including polar and non-polar compounds, as well as thermolabile molecules (Pitt, 2009). LC-MS technology-based methods have been widely used to analyse the alteration of glycolysis and TCA cycle metabolites, although these studies have primarily used serum or plasma samples. A newly available LC-MS (Finnigan Surveyor LCQ Advantage Max Mass Spectrometer System PDA Plus Detector, Autosampler Plus, LC Pump Plus, LCQ Advantage Max (Thermo)) became available for use and analysis continued with this instrument as the use of polarity switching is known to offer a more comprehensive metabolome coverage than the use of single polarity (Lei, Huhman & Sumner., 2011). Metabolites of the TCA cycle contain carboxyl and hydroxyl groups, which are less volatile and highly polar, requiring chemical derivatization. Standards were derivatized using methoxyamine hydrochloride (MeOX) solution in pyridine, N-methyl-N-(trimethylsiyl)-trifluoroacetamide (MSTFA) and mixture of fatty acid methyl esters (FAMEs), following method detailed by Fiehn (2016), further detailed in Appendix c, protocol 5, and standards injected into LC-MS. No presence of derivatising agent was detected in the standards, as detailed in results section 3.5.1, which confirmed the standards had not been derivatised and a new method would need to be developed. After trialling new methods of derivatisation to no avail, a UPLC-MS became available. After an extensive literature review and training period, analysis continued using this new instrument, following methods detailed by Smith, Plumb & Rainville, (2019), further detailed in the next section.

1.5 Proteomics

Proteomics is the large-scale experimental analysis of the functions, interactions, composition, and structures of complete sets of proteins present in an organism or biological sample (Aslam et al., 2017). A recently emerging field that has been playing a vital role in biomedical research over the past decade, proteomics involves the application of technologies for the identification and 0quantification of proteins in a cell, tissue, or organism, offering complimentary data to genomics and transcriptomics (Cui, Cheng & Zhang., 2022). With the increasing ability of high-throughput proteomics methodologies, and integration with other scientific disciplines, proteomics promises to revolutionise the detection of diagnostic markers, understanding of pathogenic mechanisms, alteration of expression patterns under specific situations and the interpretation of pathways in health and disease (Aslam et al., 2017). Most proteins accumulate at defined locations within the cell, with a large fraction of these taking up residence in multiple compartments. Many context-specific cellular processes are mediated by trafficking to and from organelles, and abnormal protein localisation has been implicated in numerous diseases (Paul et al., 2020). Determining typical patterns of protein expression and localisation in health and normal development, as well as studying how they are perturbed by disease is of fundamental importance for the advancement of biology. As the composition of the proteome is in a constant state of flux, proteomic analysis defines the state of the proteome during a certain condition or point in time within an organism (Chandramouli & Qian., 2009). Proteomics allows for the identification of quantitative changes across samples, providing important insights into the current understanding of how protein pathways are regulated across differing genotypes and the different roles of proteins in complex biological systems. A variety of proteomics techniques are used to analyse the expression of proteins at different levels, allowing for the assessment of quantitative and qualitative cellular responses related to each protein (Xiao et al., 2008). Quantitative proteomics is commonly carried out using label-free quantification (LFQ) of high mass resolution liquid chromatography-tandem mass spectrometry, and can provide insights into disease mechanisms, cellular functions, and biomarker discovery (Grønborg et al., 2006).

1.5.1 Testing for Multiple Comparisons

Scientific conclusions are often drawn from the statistical testing of a hypothesis, where a probability score of 0.05 or 0.01 is used as an acceptable cut-off. However, the probability of reporting false statistics greatly increases when multiple hypotheses are tested simultaneously, requiring proper adjustment for the multiple comparisons (Banerjee et al., 2009). The testing of

multiple hypotheses leaves us vulnerable to two types of error: type I- incorrectly rejecting the H0 (null hypothesis, proposes no statistical significance exists in a set of given observations), and type II- false negative results. Research that will eventually have important practical consequences, such as the changing of clinical practice or testing of new treatment strategies, requires vigorous control of type I errors and therefore the application of rigorous correction methods is essential. On the other hand, when research is intended to obtain primary candidates for further investigation, such as in 'omics' studies, committing too many type II errors should be avoided (Chen, Feng & Yi., 2017). Researchers can compensate for type I errors using false discovery rate (FDR) correction, a method that is frequently employed to account for multiple comparisons in proteomics experiments. However, they can only do so under a reasonable proportion by considering the total amount of H0 rejections. This method of FDR application successfully maintains the accuracy of protein identifications (Savitski et al., 2015).

Conversely, an increasing number of researchers hold the opinion that FDR correction is not always the best approach and should be reserved for particular experimental designs only. In non-targeted exploratory studies, such strict adjustment for multiple comparisons is less crucial, given that a clear statement declaring that a subsequent study should be conducted to confirm any observed associations is given. Adjusting for p-values in an exploratory study may effectively penalise an association from being identified in a large study rather than a smaller study and the cost of FDR application is to increase the frequency of incorrect statements that assert no relation between two factors, even when the relationship is not due to chance (Althouse., 2015). In exploratory biological studies, even the smallest of interactions may have important meaning and the null hypothesis should be carefully considered before readily rejecting. The hypothesis challenges the fundamental principles of empirical research, which asserts that nature follows consistent laws that may be understood through observations (Rothman., 1990). Not making adjustments (and instead using fold change thresholds) is preferable in exploratory studies only because it will lead to fewer errors of interpretation when the data under evaluation are real observations in nature and in this case, it may be best to let the readers use their own judgment about the weight of conclusions.

Either approach, correcting for multiple comparisons and the application of a fold change threshold, has many positives but also many limitations that make choosing the most appropriate method challenging. Using a combination criteria such as the t-test relative to a threshold provides information on whether the differential expression of a protein is biologically meaningful as well as statistically significant. It has become increasingly common to require differentially expressed genes to satisfy both p-value and fold change criteria, with many researchers believing that combination ranking improves upon FDR correction by also assessing the magnitude of differential expression for

biological meaning (McCarthy & Smyth., 2009). This method is especially useful in exploratory experiments with large amounts of differential expression, such as the current project and as such, was used for proteomics analysis. The percentage fold change value is often arbitrarily chosen based on the expected severity of the phenotype- the more severe the phenotype, the higher the fold change threshold. As the phenotype of the J20 mice is relatively mild, a lower threshold of 20%-fold change was used and combined with two-way t-testing to identify values that satisfied both percentage fold change threshold and p-value significance. In parallel, the same data was also be analysed using FDR correction, to satisfy both statistical and biological significance.

1.5.2 Network and Systems Biology

Network biology, often referred to as systems biology, facilitates the system-wide analysis of cellular components and processes to attempt to understand organisms or cells at various levels of functions or mechanisms (Altaf-Ul-Amin et al., 2014). Promising new tools are being offered by network and systems biology approaches for the study of intricate mechanisms involved in the development of diseases. Large sets of molecular interactions can be incorporated into representations using *in silico* models, enabling systematic testing and predictive simulations (Tian et al., 2013). In order to better understand the intricacy of network interactions and disease pathways, models of qualitative network representations are being created at various scales and levels of complexity for an increasing number of human diseases. For instance, understanding how proteins are expressed and localised at the cellular level may shed light on the functions, regulation, and heterogeneity of neurons that are affected in neurological diseases (Paul et al.,2020). Research by Bakker et al (2017) into glucocorticoid receptor (GR) signalling through the interactome utilised systems biology to create a model of the GR protein interaction network that encapsulated the functional relationships between the GR, its target genes, genes that target the GR and the interactions between genes that interact with the GR. The model was subsequently used as a predictive clinical tool and platform for future development by directing research and allowing further manipulation and addition of components into the model, providing a comprehensive overview of GR signalling. In this example, the model provided insight into the mechanisms of GR signalling and how resistance may appear, providing important understanding for future therapies. Utilising such a model in the context of pre-clinical AD may allow the deeper understanding of how target protein networks are altered from a healthy state. Once target protein mechanisms of action are understood, future manipulation of the model can be used to assess protein network changes that may be associated with positive clinical outcomes.

1.6 Aims and Objectives

The aim of this project is to study the mechanisms in the mouse brain underlying the action of retrieving a memory, as well as any impairments in these mechanisms related to Alzheimer's disease. Tissue from mice sacrificed in the context of a memory retrieval behavioural paradigm has been used, and genetically modified mice (together with wild-type controls) were used with regard to Alzheimer's disease. The aims and objectives of the project are:

1. To quantitatively analyse the levels of certain mitochondrial proteins in the laboratory
2. To identify the biochemical and cellular pathways involved in memory retrieval via computational analysis of proteomics results
3. To analyse the activity of various enzymes in the mouse brain in the context of memory retrieval
4. To quantify key mitochondrial metabolites in the same brain tissue samples

Given that Alzheimer's disease is largely a memory disorder and that there is currently no cure, the expected benefits of this project are a) a contribution to a better understanding of the underlying mechanisms (at the protein level) of memory loss in a genetically modified preclinical mouse model resembling some aspects of Alzheimer's disease, b) the identification of brain proteins that have the potential for possible drug targeting in the future towards contribution to the treatment of Alzheimer's disease, and c) the measurement of metabolites relating to energy metabolism in wild-type and APPtg mice at the point of attempted memory retrieval.

CHAPTER 2- METHODS

Statement of Ethical Application

Local university ethics approval was obtained from the Animal Welfare and Ethical Review Body for the use of animal tissues in this thesis. All behavioural experiments and tissue collection were conducted at the University of Edinburgh prior to this project in accordance with the scientific procedures Animals (Scientific Procedures) Act 1986 and relevant ethical procedures were followed.

Materials

The majority of reagents were purchased from Fisher Scientific (www.thermofisher.com) or Merck (www.merckgroup.com)

All metabolite standards purchased from Sigma-Aldrich (www.sigmaaldrich.com)

Western Blotting	Analysis of Mitochondrial Metabolites
Pierce RIPA Buffer (Thermo; 89900)	Pyruvic acid (Sigma; 107360)
Methanol	L-(+)-Lactic acid (Sigma; 46937)
dH2O	Citric acid (Sigma; 251275)
Glycine	Cis-Aconitic acid (Sigma; A3412)
Tri-Sodium citrate dihydrate (Fisher; 6132-04-3)	α-ketoglutaric acid (Sigma; 75890)
Sodium dodecyl sulphate	Succinic acid (Sigma; S-7501)
Transfer buffer (25mM Tris, 192mM Glycine, 20% Methanol)	Fumaric acid (Sigma; 47910)
Polyvinylidene Fluoride (PVDF) membrane	L-(-)-Malic acid (Sigma; 02288)
NuPAGE Dithiothreitol (Invitrogen; 2201429)	HPLC-Grade Water (VWR Chemicals; 7732-18-5)
NuPAGE Laemmli sample buffer (Bio-Rad; 1610747)	Formic acid (Acros Organics; 64-18-6)
Precision Plus Protein Dual Colour Standard (Bio-Rad; 1610394)	Acetonitrile
Phosphate buffer saline	Ammonium hydrogen carbonate
MOPS SDS Buffer (Thermo Fisher)	Dithiothreitol
Tween x20 (Bio-Rad)	Iodoacetamide
PSB Tween (PBS 1x, Tween 0.05%)	Speed Beads magnetic carboxylate modified particles (Sigma Aldrich; GE45152105050250)
Peroxide Solution (Bio-Rad)	Ethanol
Luminol Enhancer Solution (Bio-Rad)	Trypsin
Detection Reagent 1-Peroxide Solution (Thermo; 1859701) -OLD	Methoxyamine hydrochloride (Sigma; 89803-1G)
Detection Reagent 2- Luminol Enhancer Solution (Thermo; 1859698)	N-Methyl-N-(trimethylsiyl) trifluoroacetamide (Sigma; 69479-5ML) -GC derivatisation

Equipment

Western Blotting	Enzymatic Activity Assays	Analysis of Mitochondrial Metabolites
NuPAGE 4-12% Bis-Tris Mini Protein Gels (Thermo; 20110510-0945)	All assay ktis purchased from Abcam (www.abcam.com)	Kinetex 2.6µm C18 100Å LC Column 30x 2.1mm (H22-030955)
Invitrogen MiniGel Tank (Thermo Fisher)	Abcam 6-Phosphofructokinase enzymatic activity assay kit	Trace 300 & ISQ LT Mass Spec (Thermo)
Heating block	Abcam Malate Dehydrogenase 2 enzymatic activity assay kit	Finnigan Surveyor LCQ Advantage Max Mass Spectrometer System PDA Plus Detector, Autosampler Plus, LC Pump Plus, LCQ Advantage Max (Thermo)
Mini-PROTEAN Tetra System (Bio-Rad)	Clear, round bottomed 96 well plates (brand)	Acquity Ultra Performance UPLC- TQ Detector, Binary Solvent Manager, Sample Manager, Waters)- software: MassLynx 4.1
4x sponges	Tecan Spark Plate reader with heating function	
4x filter paper (Thermo Fisher)	Tecan GENios Pro platereader	
Transfer cassette	Tecan infinite f200 PRO platereader	
Chemi Doc XRS+ with ImageLab software	Thermo Scientific Multiskan FC platereader	

2.1. Mouse Lines

This study makes use of brain tissue from J20 and WT mice attained by the first supervisor prior to this project. J20 mice overexpress human APP (hAPP), bearing two mutations linked to FAD (APP KM670/671NL-Swedish, APP V717F-Indiana; genetic background: C57BL6 (75%) & DBA/2J (25%); strain name: B6.Cg-Zbtb20 $^{Tg(PDGFB-APPSwInd)20Lms}$/2Mmjax; Mucke et al.,2000). The platelet-derived growth factor beta (PDGF-β) was used for the transcription of hAPP, allowing expression exclusively

within the central nervous system, with highest levels of immunoreactivity within the hippocampus and neocortex (Balducci & Forloni., 2011 ;Alzforum., 2017).

Whilst the J20 mouse is indeed different to the PDAPP mouse (APP V717F-Indianna; genetic background C57B6 x DBA2 (Alzforum., 2013)) used in previous studies by the first supervisor, the transgene and phenotypes are both very similar, yet the J20 mouse is available commercially where the PDAPP mouse is not. J20 mice display increased Aβ in hippocampal neurons, deficits in basal synaptic transmission and significant neuronal loss in the CA1 region of the hippocampus between 3 and 6 months of age, clinically comparable to a preclinical stage of disease (Wright et al., 2013; Saganich et al., 2006). All animal husbandry was carried out by the first supervisor prior to the project start.

2.1.1 Behavioural Training

Morris watermaze behavioural protocol was carried out by the first supervisor at the University of Edinburgh prior to this project, as detailed by Beglopoulos et al (2016). Mice were sacrificed 20 seconds after the final probe test had been completed, and the brains were collected. The behavioural phenotype of long-term forgetting in APPtg mice previously observed in Beglopoulos et al (2016) was reproduced in the cohort of mice, from which brain tissue was used in this project.

2.1.2 Sample Preparation

All synaptosome preparation was carried out by Dr Anthony Ashton, University of Central Lancashire, prior to the project start. Two sample types were used throughout the project; P2 fractions and synaptosomes.

P2 Fractions Hippocampal and cortical homogenates were fractionated via two rounds of centrifugation and the second pellet, the mitochondrial pellet, containing membrane enriched organelles including both synaptic and non-synaptic mitochondria, was collected. The mitochondrial pellet will be referred to as the 'P2 fraction'.

Synaptosomes are created from the same neuronal homogenates, followed by three rounds of centrifugation (1 more than P2 fractions). A detailed guide on synaptosome preparation can be found in Appendix C, protocol 1. Synaptosomes are enriched in synapses, synaptic mitochondria, synaptic vesicles and often parts of the postsynaptic membrane and postsynaptic density. They are an indispensable *ex vivo* model of AD due to their preserved metabolic and enzymatic activities

(Ahmad & Liu., 2020). Additionally, analysing the synaptic proteome, including synaptic vesicles, postsynaptic densities, and synaptic membranes allows for deeper understanding of the processes orchestrating the activity of synaptic protein complexes, which support neuronal communication, information processing, learning and memory, under healthy and diseased states (Bai & Witzmann., 2007). All tissue samples were stored at -80°C.

P2 and synaptosome samples have been used throughout this project, dissolved in lysis buffer containing 50mM Tris HCl (pH 7.4), 150mM NaCl, 5mM EDTA, 0.5% NP-40, 0.5% Sodium deoxycholate, 1% SDS, protease inhibitors (Sigma, 1:200) and 1mM PMSF. All sample lysis steps were carried out by a previous student, prior to the start of this project.

Two additional samples '16L' and 24R' have been used throughout the thesis as 'practice samples'. Both 16L and 24R are from the same cohort of J20 mice used throughout the project, behaviourally trained in the same manner. Both mice belong to the WT group, sacrificed immediately after the retrieval of the spatial memory (WT memory retrieval group). 16L and 24R samples are total cell lysates, suspended in identical lysis buffer.

2.2 Western Blotting

Western blot analysis allows for the detection of specific native or denatured proteins within a protein mixture, via separation in order of molecular weight (MW). Proteins are separated by gel electrophoresis, transferred to a membrane, and subject to antibody-specific detection for a target protein (Ghosh, Gilda & Gomes., 2014). All samples were subjected to bicinchoninic acid (BCA) protein assay prior to the project start to verify the exact levels of protein. All samples were found to contain 5µg protein. Table 2.1 details the antibodies used for western blotting.

Table 2.1. Antibodies used for western blotting. All antibodies were purchased from Abcam.com and used at the recommended dilution.

Antibody	Justification for use	Species	Catalogue No.	Provider	Dilution
Anti-SDHA	Subunit of ETC complex II; located on the mitochondrial inner membrane (Renkema et al., 2015)	Rabbit	ab137040	Abcam	1:5,000

Anti-UQCRB	Plays essential roles in stability of ETC complex III; downregulated in early-onset AD, slowing the oxidation of NADH and $FADH_2$,effecting membrane proton gradient; affects ATP production by complex V (Adav, Park & Sze., 2019)	Rabbit	ab190360	Abcam	1:10,000
Anti-DRP1	Recruited to outer mitochondrial membrane and oligomerises to form active GTP-dependent mitochondrial fission sites; mediates fission events (Frank et al., 2001)	Rabbit	ab184247	Abcam	1:2,000
Anti-Mitofusin 1	Located on outer mitochondrial membrane, mediates mitochondrial fusion events (Ishihara, Eura & Mihara, 2004)	Rabbit	ab221661	Abcam	1:2,000
Anti-PSD95	Essential component involved in synaptic transmission and synaptic plasticity (Coley & Gao., 2019)	Rabbit	ab18258	Abcam	1:3,000
Anti-ATP5A	Subunit of ETC complex V; located in the inner mitochondrial membrane (Cha et al., 2015)	Mouse	ab14748	Abcam	1:50,000
Anti-VDAC1	Most abundant protein on the outer mitochondrial membrane; acts as a gatekeeper for the passage of metabolites crucial for metabolic functions; plays crucial role in apoptosis due to its interactions with apoptotic proteins (Camara et al., 2017)	Rabbit	ab15895	Abcam	1:15,000
Anti-COX4	Component of the ETC, located in the inner mitochondrial membrane; involved in the regulation of OXPHOS (Timon-Gomez et al., 2017)	Rabbit	ab16056	Abcam	1:10,000
Anti-cytochrome C	Electron transporter between complex III and complex IV, facilitating production of	Rabbit	ab133504	Abcam	1:5,000

	energy; located in large amounts in the inner mitochondrial membrane; (Eleftheriadis et al., 2016)				
Anti-alpha synuclein	Ubiquitously expressed in the brain, particularly the neocortex and hippocampus; strongly linked to several neurodegenerative diseases (Burré., 2015)	Rabbit	ab212184	Abcam	1:3,000
Anti-Synaptophysin	Major integral membrane protein of synaptic vesicles, commonly used as synaptic marker (Thiel.,1993)	Rabbit	ab32127	Abcam	1:300,000
Anti-Ndufa2	Part of the ETC complex I which transfers electrons from NADH to ubiquinone, establishing proton gradient for ATP generation during OXPHOS (Triepels et al., 2000)	Rabbit	ab198196	Abcam	1:1,000
Anti-DAP13/Ndufa12	Subunit of ETC complex I (Triepels et al., 2000)	Rabbit	ab192617	Abcam	1:2,000

2.2.1 Electrophoresis

Proteins separated following SDS-PAGE methodology (Invitrogen Mini Gel Tank). Samples (5µg protein per sample) were made up to a total volume of 40µl using RIPA buffer, NuPAGE sample buffer (7.5µl; NuPAGE Laemmli Sample Buffer, Bio-Rad) and dithiothreitol (DTT; 3µl), then heated for 10 minutes at 70°C. Samples loaded into wells of the gel (10 well NuPage 4-12% Bis-Tris), using Precision Plus Protein Dual Colour Standard (Bio-Rad). Gel subjected to electrophoresis in 1X MOPS SDS at 200V for 35minutes.

2.2.2 Transfer of Proteins to Polyvinylidene Fluoride membrane

After electrophoresis, the gel was removed and the PVDF membrane was activated in methanol for 10seconds, washed in dH2O, and soaked in transfer buffer. Transfer cassette was assembled under transfer buffer (25mM Tris, 192mM Glycine, 20% Methanol) as follows; 2x sponges; filter paper; gel; PVDF membrane; filter paper; 2x sponges. Assembly was then locked into transfer cassette and the

cassette was placed into the transfer chamber (Bio-Rad Mini-PROTEAN Tetra System), pre-filled with chilled transfer buffer. Transfer ran at 250mA for 2 hours at 4°C.

2.2.3 Immunodetection

For the detection of proteins of interest, a series of stages were followed. PVDF membrane was washed in PBS-tween (3x 5 minutes) before blocking in 5% milk for 1 hour. Milk proteins bind non-specifically to all proteins present on the membrane. Primary antibodies were diluted in 5% milk for 1 hour (Table 2.1). This results in high binding specificity and reduction of background as primary antibody competes with blocking buffer proteins to bind the target protein. Primary probed membranes then washed in PBS-tween (3x 5 minutes) before incubation with secondary antibody for 1 hour (1:10,000). Secondary antibody conjugated with horseradish peroxidase (HRP), which allows for subsequent detection using enhanced chemiluminescence (ECL) protocol. Interpretation of western blot (WB) results requires the use of a loading control and thus, synaptophysin, a primary antibody specific to the presynaptic terminal protein synaptophysin, was used for normalisation of synaptic abundance across samples.

2.2.4 Enhanced Chemiluminescence Detection

Enhanced chemiluminescence reagents (Thermo Scientific) were prepared 1:1 according to manufacturers instructions and used to incubate the membrane for 4 minutes, before the mixture was discarded and membrane placed on imaging tray. Membrane covered with cling film and imaging carried out using Bio-Rad ChemiDoc XRS+ in manual signal accumulation mode.

2.2.5 Densitometry Analysis of Western Blot Data Using ImageLab

Densitometry was employed through the use of ImageLab (https://www.bio-rad.com/en-uk/product/image-lab-software?ID=KRE6P5E8Z). Densitometry allows for a semi-qualitative analysis of blot data through the measurement of lane optical density. Readings were obtained for each band for the protein of interest, background signal subtracted and values normalised to the loading control protein (synaptophysin) signal (See Appendix C- protocol 2 for more detailed description). Normalised band readings were expressed as a percentage of the control (Wild-Type Basal) and bar charts were created using the average values and standard error of the mean (SEM), combining

results from independent experiments. Two tailed, type two t-tests were carried out between each experimental group (a=0.05) to determine any significant differences.

2.3 Optimisation of Enzymatic Activity Assays

The biological samples used throughout the project have been subject to multiple freeze-thaw processes, which has the potential to impact the retention of enzymatic activity (Bortolin et al., 2017). Studies by Acin-Perez et al (2020) revealed that tissue samples that had been through freeze-thaw processes were able to maintain an intact ETC and were still actively respiring. Enzymatic activity is essential for all stage of cellular respiration, from glycolysis and the TCA cycle to the ETC and OXPHOS, providing confidence that the samples used throughout the project will have retained sufficient enzymatic activity.

The optimisation of enzymatic activity assays is a complex, multi-step process which requires many trials and adjustments. A total of 12 enzymatic activity kits were purchased from Abcam (https://www.abcam.com/; Table 2.2 details all assay kits purchased) and tested firstly using wild-type control samples with no behavioural training, at a range of concentrations (0.25, 0.5, 0.75, 1-x amount required for 5µg protein). The first optimisation was carried out following the manufacturer's instructions exactly, including shaking steps, temperature, incubation steps, the use of positive controls, blanks, and standards, if included in the guidance. Blanks were carried out in sets of 4 initially, including 2 absolute blanks (just assay buffer OR incubation buffer) and 2 blanks with lysis buffer (absolute blank buffer + 3µl lysis buffer, as is present in the sample preparation). Any mention of 'lysis buffer' in assay optimisation or data accumulation assays is referring to the specific lysis buffer the homogenates have been prepared in. Sample backgrounds were included where assay instructions required the addition of 'activity mix' or 'reaction mix', which consist of biological sample, made up exactly as directed for comparative samples, without the substrate added. No-substrate mixes are labelled as 'background mix' in manufacturer's instructions and ensures any comparative samples can be normalised via the subtraction of the sample background. Assays were run in a kinetic mode, where the progress of the reaction is continuously measured, and the rate of reaction measured as the change in optical density per minute, per milligram (ΔmOD/min/mg). After the first optimisation run, results were analysed. If the assay worked well, no major adjustments were made, and the next trial would introduce a small number of samples from each of the experimental groups. If the assay showed enzymatic activity in the samples only but at a smaller level than expected, a number of factors could be introduced, removed, or adjusted. For example, if the assay was initially carried out at room temperature, it could be carried out again at

37°C, longer periods of reading or shaking steps could be implemented between reads if there were non prior. Each time an assay was carried out and gained sub-optimal results, another factor would be studied and adjusted until they assay was deemed non-functional or functional. Each assay was carried out using three different available plate readers and the results compared to ensure the plate reader chosen for the final comparative assays (Tecan Spark) was working correctly. Details of all 12 assays and their trial conditions are detailed in Table 3.2. Details of optimization workflow is detailed in Appendix C, protocol 3. After initial optimisation, 2 assays were deemed functional based on overall performance and progressed to the final comparative experiments: malate dehydrogenase 2 and 6-phosphofructokinase. Assays not selected for final experiments were eliminated for reasons including: blanks appearing to show mild enzymatic activity and insufficient activity shown in biological samples over time.

Table 2.2. Enzymatic activity assay kits purchased from Abcam.com.

Assay Kit	**Catalogue No.**	**Provider**	**Justification**
Hexokinase	*ab136957*	*Abcam*	*Controls the rate-limiting first step of glycolysis and is therefore a fundamental enzyme in glycolysis (Roberts & Miyamoto., 2014)*
6-Phosphofructokinase	*ab155898*	*Abcam*	*Catalyses the first committed step of glycolysis (Brüser et al., 2012)*
Pyruvate Kinase	*ab83432*	*Abcam*	*Key enzyme of glycolysis acting on phosphoenolpyruvate to form pyruvate (Zhang, Deng & Liu., 2019)*
Pyruvate Dehydrogenase	*ab109902*	*Abcam*	*Catalyses the oxidative decarboxylation of pyruvate, linking the glycolytic pathway to the oxidative pathway of the TCA cycle (Patel et al., 2014)*
Aconitase	*ab83459*	*Abcam*	*Thought to control cellular ATP production via regulation of TCA cycle intermediate flow (Lushchak., 2014)*
Fumarase	*ab196992*	*Abcam*	*Catalyses the hydration and dehydration of fumarate into malate in the TCA cycle (Yogev et al., 2010)*

Isocitrate Dehydrogenase	*ab102528*	*Abcam*	*Catalyses the oxidative carboxylation of isocitrate in the TCA cycle, producing α-ketoglutarate whilst converting NAD^+ to NADH (Al-Khalla., 2017)*
Malate Dehydrogenase 2	*ab119693*	*Abcam*	*Catalyses oxidisation of L-malate into oxaloacetate in the TCA cycle, producing NAD+ through oxidation of NADH and driving glycolysis (Priestly et al., 2022)*
NADH-Coenzyme Q Oxidoreductase	*ab109721*	*Abcam*	*Largest enzyme complex of the ETC (Ohnishi, Shinzawa-Ito & Yoshikawa., 2008)*
Succinate Dehydrogenase	*ab109908*	*Abcam*	*Catalyses oxidation of succinate to fumarate in the TCA cycle and feeds electrons from succinate to ubiquinone in the ETC (Rustin, Munnich & Rötig., 2002)*
Cytochrome C Oxidase	*ab109911*	*Abcam*	*Complex IV of the ETC which links the conversion of molecular oxygen to water (Watson & McStay., 2020)*
ATP synthase	*ab109714*	*Abcam*	*Synthesises ATP from ADP and inorganic phosphate (Jonckheere, Smeitink & Rodenburg., 2012)*

2.3.1 Malate Dehydrogenase Assay

Malate Dehydrogenase 2 (MDH2) activity was assessed using a Malate Dehydrogenase 2 Activity Assay Kit (Abcam, ab119693), following the manufacturer's instructions. MDH2 activity is determined by following the production of NADH in the reaction it catalyses: malate + NAD $\rightarrow$ oxaloacetic acid + NADH. The 1:1 reduction of a reporter dye to a yellow product is coupled to the generation of NADH; its concentration can be determined by measuring the increase in absorbance at 450nm. The assay kit immunocaptures only native MDH2 in each well, removing all other enzymes, including cytosolic MDH1.

5μg of protein was added to the 96 well antibody capture plate and buffer containing a reagent dye was added. MDH2 activity was measured using a kinetic mode for 60mins at 20sec intervals using a microplate reader (Tecan Spark) that measured the absorbance at 450nm. Two time points were

selected within the linear growth phase of absorbance and MDH2 activity was calculated from these, as per manufacturer's instructions. Final units of enzyme activity were expressed as the change in absorbance per minute, per amount of sample (ΔmOD/min/μg).

2.3.2 6-Phosphofructokinase Assay

Phosphofructokinase (PFK) activity was assessed using a 6-Phosphofructokinase Activity Assay Kit (Abcam, ab155898), following the manufacturer's instructions. In this assay, PFK converts fructose-6-phosphate and ATP to fructose-diphosphate and ADP. ADP is converted to AMP and NADH in the presence of substrate and enzyme mix, which reduces a colourless probe to a coloured product with absorbance at 450nm.

Standard curves were generated from NADH prepared from 0 to 3nmol/well. PFK reaction mixes were assembled in a 96 well plate by mixing 5μg of protein with Assay Buffer, PFK Developer, ATP, and PFK Substrate, as provided within the kit. The PFK activity was measured using a kinetic mode for 60mins at 20sec intervals using a microplate reader (Tecan Spark) that measured the absorbance at 450nm. Two time points were selected within the linear growth phase of absorbance and PFK activity was calculated from these, as detailed by the manufacturer. Final units of PFK activity were expressed in two ways; firstly- the change in absorbance per minute, per amount of sample (ΔmOD/min/μg); secondly- nmol/min/mL, where 1 Unit PFK activity = amount of PFK that will generate 1.0 μmol of NADH per minute at pH 7.4 at 37°C.

2.3.3 Normalisation of Assay Data using Western Blot Data

Western blotting was employed to control for enzyme amount within each experimental sample. Enzymatic activity assay results (change in OD/min) were normalised against protein expression levels after normalisation against loading control (change in optical density value divided by protein expression value for each individual sample. Group averages were calculated using values normalised using this method, final units were ΔmOD/min/μg). Normalisation via western blotting results include two blots, one blot of eight samples carried out as part of this project (VG10,12,4,8,9,11,3,7) and another blot consisting of the remaining eights samples (VG1,2,5,6,13,14,15,16) carried out by another student (the two sets of blots were shared by this project and the other student's project due to sample limitations).

Similarly, all enzymatic assays were indeed carried out in duplicate, using the full set of 32 test samples (8 replicates of each genotype and behavioural group combination). One replicate of the 32 samples was used as part of this project, whereas, due to limited sample volume, the other replicates were used by another student. The results and statistical analyses of the normalised, combined set of samples are described in Appendix A-3.

2.4 Standards

A total of 8 metabolite standards from Smith, Plumb & Rainville (2019) were chosen for analysis, based on availability, analytical grade quality and relevance (table 2.4). Each metabolite has a 100% quality grade, with the exceptions of Pyruvic acid and *Cis*-Aconitic acid (98%). Two glycolytic products and six TCA cycle intermediates were chosen for analysis, in parallel with antibodies chosen for western blotting and enzymatic assays, to offer a more holistic, although admittedly limited, overview of the main processes of aerobic respiration. Both glycolysis and the TCA cycle are under constant regulation based on the energy requirement of the cell and thus during highly energetically demanding processes such as memory retrieval, these processes are likely to be upregulated.

A Waters UPLC-MS system and a Kinetex 2.6µm C18 100Å LC Column (30x 2.1mm) column were used for standard analysis. The temperature of the column was set at 40°C with a sample temperature of 6°C. the mobile phases used were water (980ml HPLC- grade water (VWR Chemicals; solvent A) and acetonitrile (20ml solvent B), both modified with 0.01% formic acid (Acros Organics) with an initial flow rate of 0.2ml/min. The volume of standard injected was 4µl and all standards were at 1nM. Optimum cone voltage was determined by trialling each standard at 60, 70, & 80v and mass ranges were set to ± 5 known molecular weight (MW) of metabolites. Once optimal cone voltage was determined and mass ranges tightened, standard curves were generated for each metabolite standard with concentrations of 1M, 1mM, 1µM and 1nM. 4µl standards loaded up into autosampler and left overnight, defined by parameters outlined in table 2.3.

Table 2.3. UPLC-MS parameters used for the detection of metabolite standards.

Parameters	
Run time	14 minutes
Flow rate	0.2ml/min
Column temperature	40°C

Sample temperature	6°C
Weak solvent	H2O- 600µl
Strong solvent	ACN- 200µl
M/Z range	50-500
Cone voltage	30-80
Source temperature	150°C
Desolvation temperature	350°C
Desolvation flow	600µl/min

In between each metabolite standard, a blank sample containing only mobile phase was inserted to ensure no autosampler carryover residue remained from previous standard which would contaminate results and result in unwanted analyte peak.

Table 2.4. Metabolite standards ordered for UPLC-MS analysis. All standards were ordered from Sigma-Aldrich.

Standard	**Supplier**	**Catalogue No.**	**Amount used**	**Justification**	**Enzyme Responsible for Metabolite Production**
Pyruvic acid	Sigma-Aldrich	107360	0.088g/ml	Product of glycolysis	Pyruvate Kinase
L-(+)-Lactic acid	Sigma-Aldrich	46937	0.09g/ml	Product of glycolysis-anaerobic respiration	Lactate Dehydrogenase
Citric acid	Sigma-Aldrich	251275	0.192g/ml	TCA cycle intermediate	Citrate Synthase
***Cis*-Aconitic acid**	Sigma-Aldrich	A3412	0.17411g/ml	TCA cycle intermediate	Aconitase
α-ketoglutaric acid	Sigma-Aldrich	75890	0.146g/ml	TCA cycle intermediate	Isocitrate dehydrogenase
Succinic acid	Sigma-Aldrich	S7501	0.118g/ml	TCA cycle intermediate	Malate Dehydrogenase

Fumaric acid	Sigma-Aldrich	47910	0.116g/ml	TCA cycle intermediate	Succinate Dehydrogenase
L-(-)-Malic acid	Sigma-Aldrich	02288	0.134g/ml	TCA cycle intermediate	Fumarate Hydratase

2.5 Proteomics Mass-Spectrometry Workflow

Quantification of protein expression via mass spectrometry was carried out on synaptosome samples from all experimental groups. Synaptosomes were chosen over P2 fractions for proteomics to align with the underlying hypothesis that synaptic mitochondrial dynamics and activity are strong candidate processes for supporting the synaptic activity required for the retrieval of memories, and dysfunction in these areas, which can be revealed by proteomic analysis, may cause significant glucose hypometabolism, seen in AD. Furthermore, synaptosomes also allow for the investigation of synapses, where memories are thought to be stored long-term, on a proteomic level.

The generation of initial (processed into Excel file) data was arranged prior to this project by the first supervisor and carried out at the Fingerprints proteomics facility, University of Dundee, using MaxQuant software. 16 samples (4 from each group) have been analysed. Label-free quantification (LFQ) was carried out using Q Exactive quadrupole/orbitrap tandem mass-spectrometer at the University of Dundee.

2.5.1 Correction for Multiple Comparisons

This project utilises exploratory proteomics in an unbiased, untargeted manner. There are two main approaches used within this thesis: FDR corrected proteomics and non-FDR corrected proteomics, which instead utilises a regulatory fold change threshold of ±20% and unpaired two-sample t-test. However, in the 20% regulation threshold proteomics, FDR is still utilised: all results from DAVID analyses have FDR correction applied automatically and significance values presented in the output charts. FDR analysis offers the removal of false positives but also removes some true positives, whilst non-FDR correction retains all true positives but also retains many false positives. Using both

methods on the same data, a more holistic view of the data can be gained, favouring both statistical and biological significance.

-both methods have limitations, none better than the other, most inclusive way is for both to be used, keeping in mind the limitations of both methods

2.5.2 Differentially Expressed Synaptic Proteins

Data was then analysed through the application of a series of data filters. Firstly, each individual protein was required to have n=3 data points present across the 4 experimental groups. Proteins with less than n=3 data were removed from analysis. Proteins with one missing value substituted average LFQ intensity of the 3 available data in place of the missing data. Any missing protein IDs or gene names were rectified using UniProt (https://www.uniprot.org/). Percentage fold change was calculated, and proteins ranked from highest to lowest change. The second filter was a threshold of ≥+20% or ≤-20% fold change. Proteins with a fold change between -20% and 20% were deemed 'unchanged'. Fold changes were combined with p-value <0.05 (two-tailed, type 2 t-test)Significantly upregulated ($\geq_{+}$20%, p <0.05) and significantly downregulated (≤-20%, p<0.05) protein lists compared to ensure exclusivity. Final protein lists were utilised for gene-ontology (GO), functional annotation, protein-protein interaction network analysis and further proteomic analyses, each with their own significance threshold.

2.5.3 DAVID Functional Analysis

Database for Annotation, Visualisation, and Integrated Discovery (DAVID, version 6.8) online tools (DAVID: Functional Annotation Result Summary (ncifcrf.gov)) were used to annotate differentially expressed proteins (DEPs) with associated GO terms (Molecular function, cellular component & biological process), highlighting functional similarities. Benjamini-Hochberg false discovery rate (FDR) correction used to assess statistical significance. Enriched GO terms with FDR-corrected P<0.05 are considered statistically significant. DAVID was also used for the annotation of functional classification, Kyoto Encyclopedia of Genes and Genomes (KEGG) pathways, and the application of functional annotation clustering. Functional annotation clustering classifies highly related genes into functionally related groups and ranks these clusters in order of enrichment score. Enrichment scores used by DAVID are overall enrichment scores for the group based on the EASE scores (Modified Fisher's Exact P-Value, adopted to measure gene-enrichment scores) of each group member; the

higher, the more enriched. The whole protein set for wild-type basal mice (n=1573) was chosen as the background list for all DAVID analyses and uploaded to DAVID database for subjection to Fisher's exact test, which includes correction by Benjamini-Hochberg method. For each individual DAVID analyses were performed using an EASE score of 0.1 (default score, Fisher Exact p-value= 0 represents perfect enrichment).

2.5.4 STRING Protein Network Mapping

Differentially expressed protein lists inputted into Search Tool for the Retrieval of Interacting Genes (STRING) database and predicted protein association networks generated. Within STRING network maps, nodes represent proteins and edges represent predicted functional associations. Edges can be drawn in up to 7 different ways based upon user preference. Edge variations represent different types of evidence for each predicted interaction, including experimental evidence, text mining evidence, database evidence and expression evidence. Edge thickness can be edited to display the degree of confidence of each interaction. Confidence scores of 0.9 or above (highest confidence) were used for interaction mapping.

2.5.4.1 Functional Dependency Analysis

STRING (version 11; STRING: functional protein association networks (string-db.org) database was searched for predicted functional and physical interactions between proteins in the *mus musculus* genome. Interaction lists downloaded and filtered for highest confidence interactions (greater than or equal to 0.9). Interaction records were then further processed into a node transcript and reaction transcript readable by CellNetAnalyzer (CNA). The node transcript includes the gene identifiers, and the reaction transcript includes interaction types (activation or inhibition) and the identifiers of the two interacting genes.

2.5.4.2 MATLAB and CellNetAnalyzer

CellNetAnalyzer is a MATLAB toolbox offering a graphical user interface alongside a plethora of computational methods and algorithms for the comprehensive structural analysis of signalling, metabolic and regulatory networks (Klamt et al., 2007). One particularly useful asset of *CellNetAnalyzer* (CNA) is its methods for functional network analysis, i.e., functional state characterisation, functional dependency detection, identification of intervention strategies and for

providing qualitative predictions on the effects of perturbations (Klamt & Von Kamp., 2011). CellNetAnalyzer Version 2022.1 was used to provide structural and functional analysis of cellular networks.

2.5.4.3 Import and Analysis in CellNetAnalyzer

Interaction list was imported into CNA and dependency matrix generated. Dependency matrices calculate the overall effect of every node (gene/protein) within the model upon every other node by tracing paths based on the edges (interactions) connecting nodes. Six types of effect are defined, based on the interaction type between nodes: no effect, ambivalent factor, strong inhibitor, strong activator, weak inhibitor, and weak activator. Using a similar example to Tian et al. (2013), these effects are defined below in relation to nodes *A* and *B*:

1) If there is neither a positive nor negative path from node *A* to node *B*, then *A* has no effect on *B*
2) *A* is an ambivalent factor of *B* if there exists both positive and negative paths from node *A* to node *B*
3) If only negative paths exist from node *A* to node *B* and there are no negative feedback loops present in these paths, then *A* is a strong inhibitor of *B*
4) If only positive paths exist from node *A* to node *B* and there are no negative feedback loops in these positive paths, then *A* is a strong activator of *B*
5) If only negative paths exist from nodes *A* to *B* and negative feedback loops are present in these negative paths, then *A* is a weak inhibitor of *B*
6) If only positive paths exist between nodes *A* and *B*, and there are negative feedback loops present in these paths, then *A* is a weak activator of *B*

Comparison of WT and knock-out (KO) model (KO meaning a gene/protein of interest was turned 'off' in the analysis, simulating a KO effect) dependency matrices will allow for further understanding of how the system behaves following deviation from its usual state. An in-silico KO model involves removing nodes of interest from the network and analysing any significant alterations thus mimicking in-vivo mutation effects.

2.5.5 Functional Connectivity Analysis

A combined list proteins differentially regulated during memory retrieval in APPtg mice (when compared to WT) was compared against the previously attained list of predicted functional and physical protein-protein interactions, downloaded from STRING (version 11). Interactions data was mined to highlight protein interactions present in the differentially regulated proteins during memory retrieval. Data was filtered to identify which proteins have the greatest number of incoming connections (connections from other proteins to the protein of interest), thus were the most greatly affected, and those with the greatest number of outgoing connections (connections stemming from protein of interest to surrounding proteins), thus had the greatest effect on other proteins.

2.5.6 Heatmap Generation

For heatmaps specific to mitochondrial proteins, extraction of known mitochondrial proteins from proteomics data was required. The 'Mouse.Mitocarta3.0.xls' was downloaded from Broad Institute (https://www.broadinstitute.org/mitocarta/mitocarta30-inventory-mammalian-mitochondrial-proteins-and-pathways). The mouse Mitocarta is an inventory of 1140 genes encoding proteins with strong support of mitochondrial localisation, providing evidence of mitochondrial protein localisation and protein distribution across 14 different tissue types. Protein lists were compared to the Mouse Mitocarta to extract any mitochondrial-specific proteins. Extracted proteins were then separated into functions, including those involved in each complex of the ETC. Only proteins with data from each of the four experimental groups were taken forward for heatmap generation. Data was imported into R Studio and heatmaps generated using 'ggplot2' package. For non-mitochondrial specific heatmaps, 'ggplot2' was also used.

CHAPTER 3- RESULTS

3.1 Western blotting

All western blot results were carried out once per antibody. Blots were quantified in terms of band signal intensity and subjected to t-tests between groups for determination of significant differences in protein abundance. Both sample fractions, P2 and synaptosomes, were used for western blotting. The main focus of the analysis was on the results of the synaptosome samples, which contain synaptic mitochondria only. Long-term memories are thought to be stored in the brain in the form of synapses, meaning any synapse-specific trends in the levels of target proteins may be directly

relevant to the mechanisms underlying memory retrieval. Conversely, the P2 samples contain both synaptic and non-synaptic mitochondria, which will act as a form of non-synaptic control. Any trends seen in both P2 and synaptosome samples will reflect non-synaptic trends in protein expression.

All western blots were normalised against synaptophysin, a presynaptic vesicle membrane protein expressed extensively throughout the brain (Tarsa & Goda., 2002; Kwon & Chapman., 2011). Synaptophysin is localised to synaptic vesicles, present within synaptosomes and P2 fractions, and thus was used as a synaptic marker for western blot normalisation.

3.1.1 Cytochrome C Oxidase Subunit 4 (COX4)

Cytochrome C oxidase subunit 4 is a subunit of the fourth complex of the ETC, located in the IMM. It catalyses the final step of the mitochondrial ETC and is regarded as one of the major sites of OXPHOS (Li et al., 2006). Western blotting analysis of COX4 expression was carried out using P2 and synaptosome samples.

Figure 3.1 depicts the western blot results and analysis for both sample types. COX4 expression in the synaptosome samples showed very little difference between groups. WT mice on average showed greater expression, with slightly lower expression during memory retrieval than at basal levels. Expression in WT mice during memory retrieval was very closely matched to the expression levels in transgenic mice at the basal level. None of the differences between groups were statistically significant.

COX4 expression in P2 samples was greater in the transgenic mice than the WT mice. WT COX4 expression was higher at the basal level than during memory retrieval, although this was not reflected in the transgenic mice. APPtg mice showed very similar expression levels at both the basal level and during memory retrieval, with the slightly greater expression during memory retrieval.

A small, synapse specific increase in COX4 expression can be seen in the WT mice during memory retrieval.

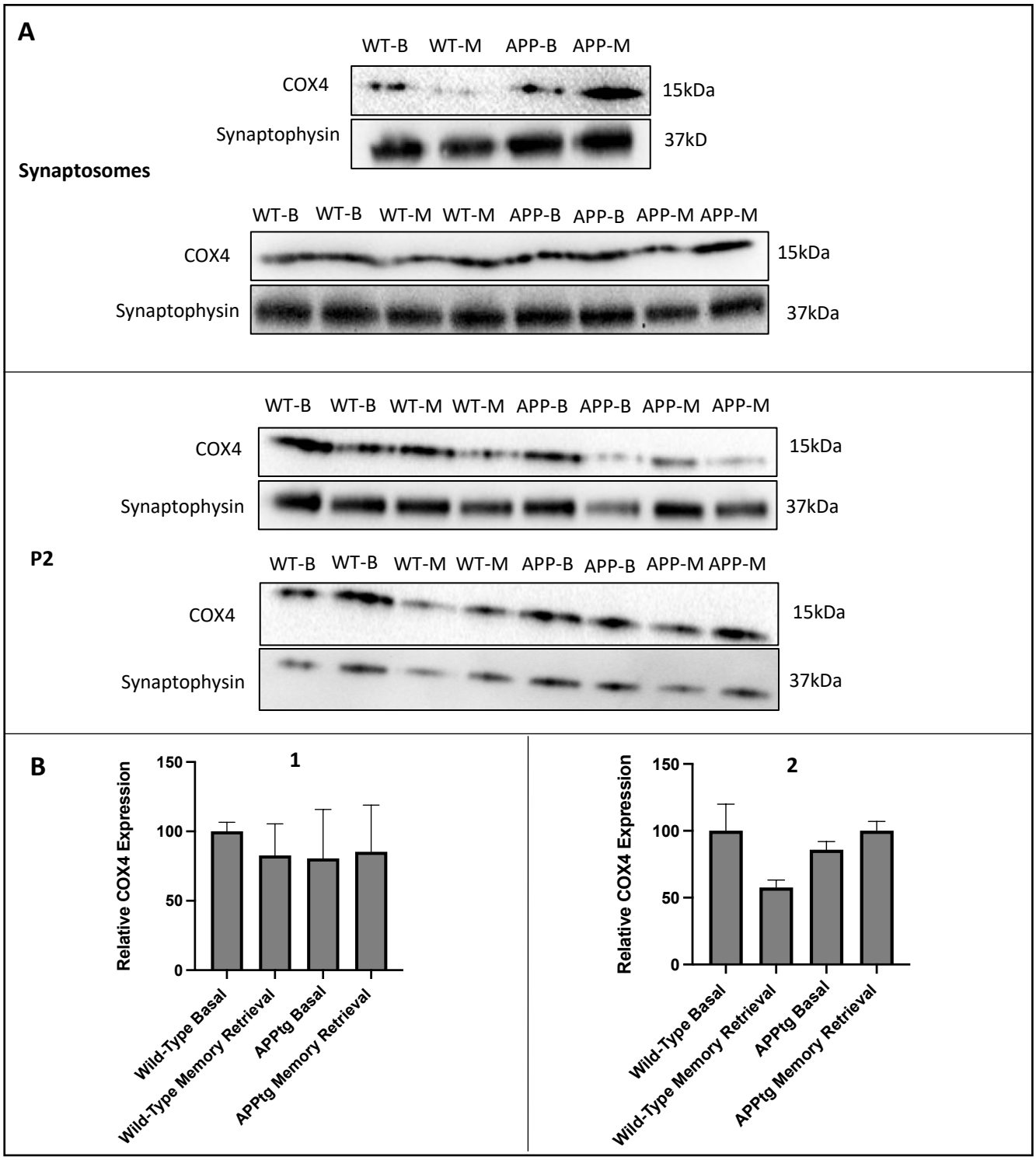

*Figure 3.11. A) Immunoblot analysis of COX4 expression in P2 fraction and synaptosome samples from 16 and 12 mice respectively. WT-B= wild-type basal, WT-M= wild-type memory retrieval, APP-B= APPtg basal, APP-M=APPtg memory retrieval. Synaptophysin was used as a loading control. B**) Densitometric analysis of blots shown in A (1-synaptosomes, 2-P2).** Normalised protein abundance relative to Wild-type Basal average. T-testing was carried out between groups for P2 and synaptosome samples and no significant differences were found.*

3.1.2 Cytochrome C

Cytochrome C is an electron carrier protein, located in the IMM, where it participates in the ETC by accepting electrons from cytochrome reductase and transferring them to the terminal cytochrome oxidase complex. The activity of cytochrome c is necessary for effective energy production (Garrido et al., 2006).

Western blotting for the expression of cytochrome c was carried out using P2 samples, and synaptosome samples. Figure 3.2 presents the western blotting results from both samples types. In the synaptosome samples, expression of cytochrome c was also higher, on average, in the WT mice, with the highest expression at the basal level. Expression levels in the transgenic mice at the basal level closely matched that of the WT mice during memory retrieval. Expression in transgenic mice during memory retrieval was consistent with expression during basal levels. None of the differences between groups were statistically significant. In the P2 samples, cytochrome c expression is higher in the WT mice than in the transgenic mice, with the highest levels expressed during memory retrieval. In the transgenic mice, expression was consistent across the basal and memory retrieval groups. None of the differences between groups could be tested for statistical significance due to sample number limitation. A small synapse specific decrease in cytochrome C expression can be seen in the transgenic mice during memory retrieval. Conversely, in the WT mice, a synapse specific decrease in expression can be seen during memory retrieval.

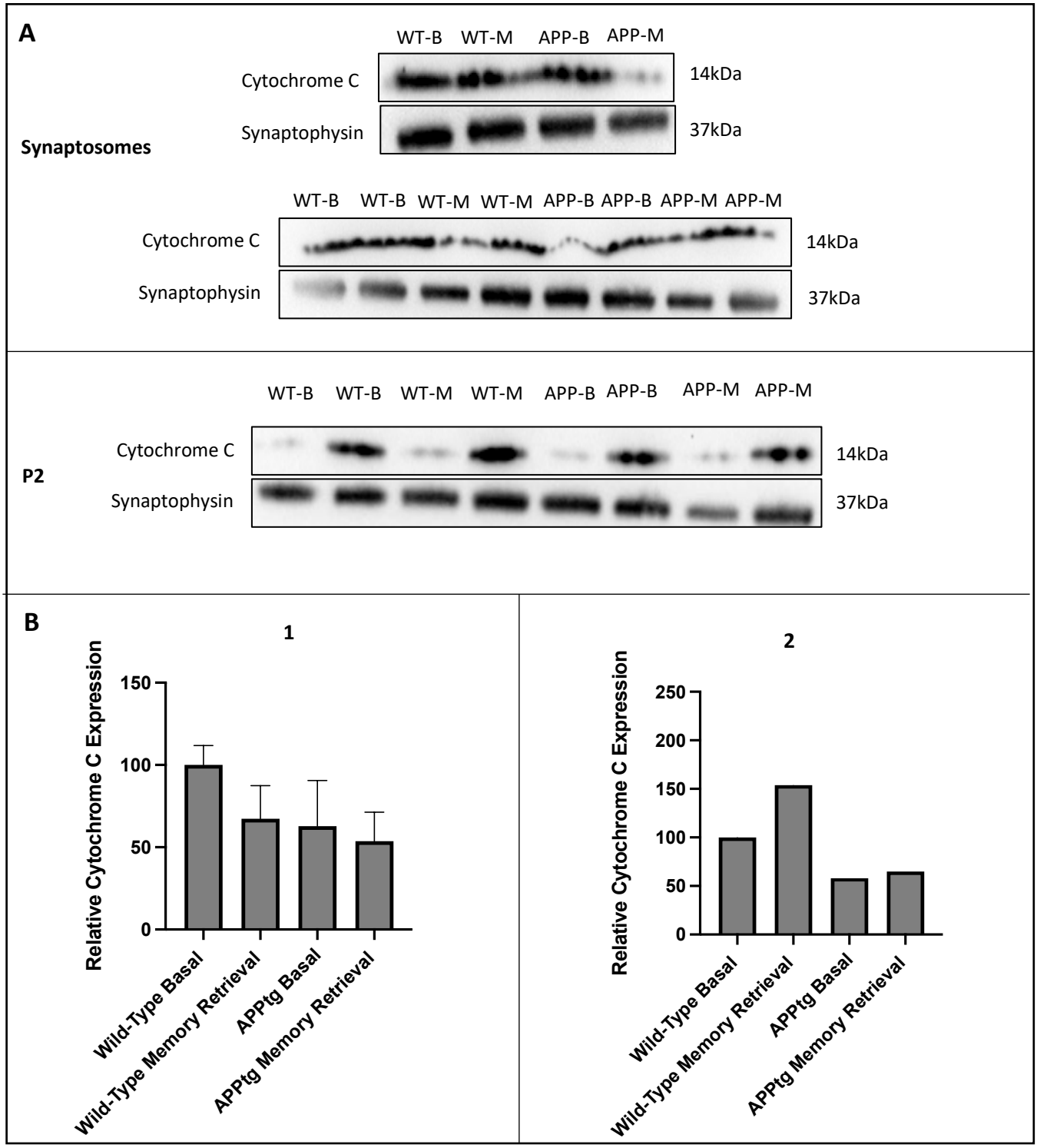

Figure 3.12. A) Immunoblot analysis of cytochrome c levels in P2 fraction and synaptosome samples from 8 and 12 different mice respectively. WT-B= wild-type basal, WT-M= wild-type memory retrieval, APP-B= APPtg basal, APP-M=APPtg memory retrieval. Synaptophysin was used as a loading control. B) Densitometric analysis of blots shown in ***A (1- synaptosomes, 2-P2).*** *Normalised protein abundance relative to Wild-type Basal average. T-testing was carried out between groups of synaptosome samples, and no significant differences were revealed.*

3.1.3 Mitochondrial ATP Synthase Subunit Alpha (ATP5A)

ATP5A is a catalytic subunit of the mitochondrial complex ATP synthase, responsible for the hydrolysis of ATP. It couples the hydrolysis of ATP with the transport of ions across the IMM, and thus is regarded as a direct regulator of mitochondrial polarity and an essential component for the maintenance of metabolic homeostasis (Goldberg et al., 2018).

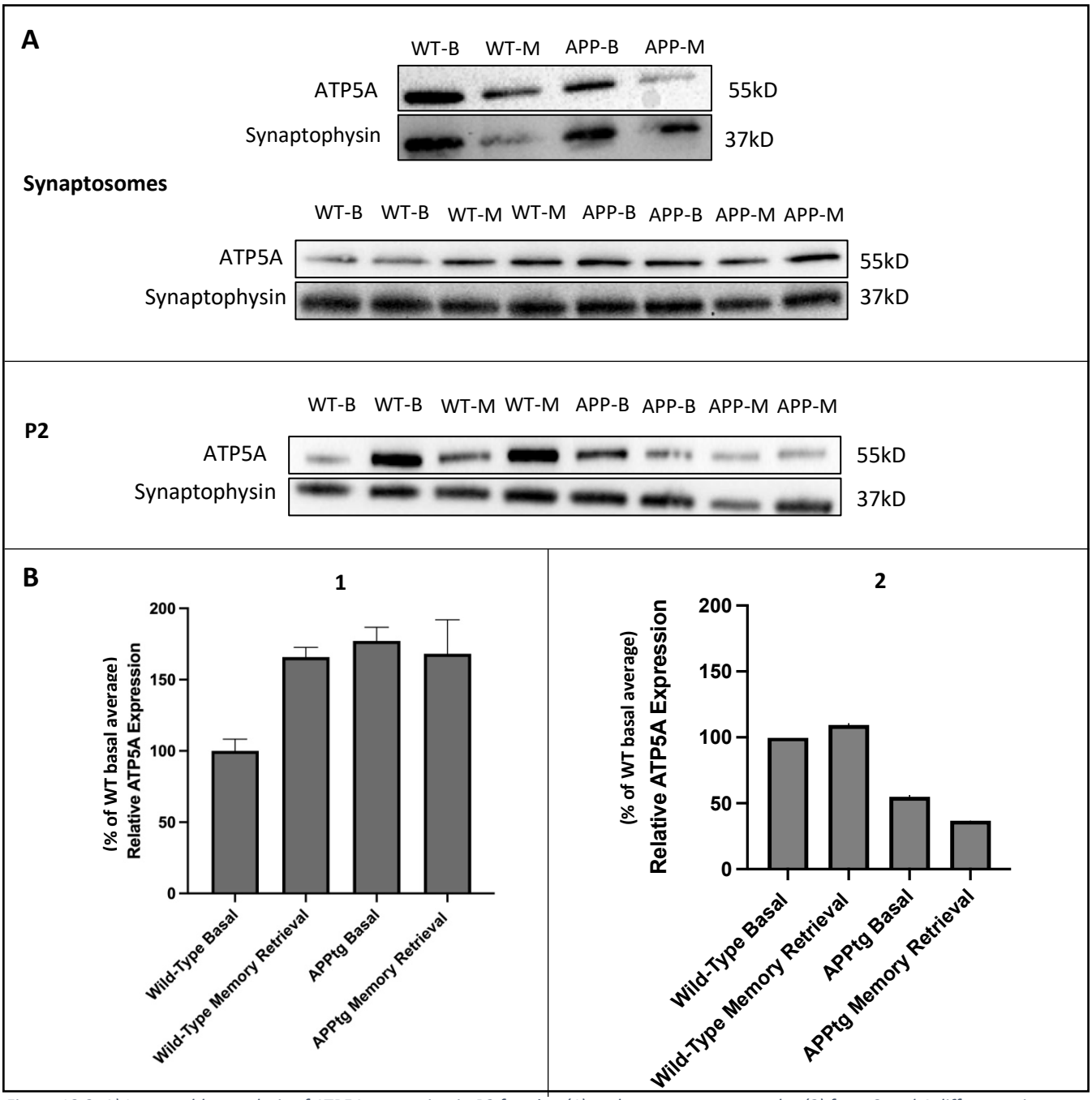

*Figure 13.3. A) Immunoblot analysis of ATP5A expression in P2 fraction (1) and synaptosome samples (2) from 8 and 4 different mice respectively. WT-B= wild-type basal, WT-M= wild-type memory retrieval, APP-B= APPtg basal, APP-M=APPtg memory retrieval. Synaptophysin was used as a loading control. B**)** Densitometric analysis of blots shown in **A (1-synaptosomes, 2-P2).** Normalised protein abundance relative to Wild-type Basal average. T-testing was carried out between groups of synaptosome samples, and no significant differences were revealed.*

Figure 3.3 depicts the western blotting results using the P2 samples. In the synaptosome samples, the expression of ATP5A is higher in the transgenic mice than the WT mice, although there is little difference between the basal and memory retrieval groups. In the WT mice on the other hand, there is a large increase in ATP5A expression during memory retrieval when compared to basal levels. None of the differences between groups were statistically significant. In the P2 samples, expression of ATP5A is higher in the WT mice than the transgenic mice, however, there is little difference between WT basal and memory retrieval groups. In the transgenic mice, expression is much lower, however, the greatest expression is in the basal group. Due to the expression difference between genotypes in the different sample fractions, it can be noted that increased expression of ATP5A in transgenic mice is synapse specific.

3.1.4 Succinate Dehydrogenase Complex Flavoprotein Subunit A (SDHA)

SDHA is one of four nuclear encoded subunits of succinate dehydrogenase (SDH), a component of the tricarboxylic acid cycle (TCA) which catalyses the oxidation of succinate into fumarate (Rustin, Munnich & Rotig., 2002). Dysfunction of SDH caused by mutations in SDHA could impair mitochondrial activity and physiology, making neurons more susceptible to degeneration and the onset of AD (Farshbaf & Kiani-Esfahani,. 2018). Western blotting was carried out using P2 samples and synaptosome samples.

Figure 3.4. reflect the respective SDHA expression. In the synaptosome samples at the basal level, the expression of SDHA was consistent between the WT and transgenic mice. During memory retrieval, expression was higher in the transgenic mice compared to the WT mice. None of the differences between groups were statistically significant. In the P2 samples, expression was higher in the WT mice than the transgenic mice. Expression was only slightly higher at the basal level than during memory retrieval for the WT mice. In the transgenic mice, expression was very slightly higher during memory retrieval than during the basal levels. None of the differences between groups could be tested for statistical significance due to sample number limitations.

There is a small synapse specific decrease in SDHA expression in WT mice during memory retrieval and a synapse specific increase in SDHA expression in APPtg mice at the basal level.

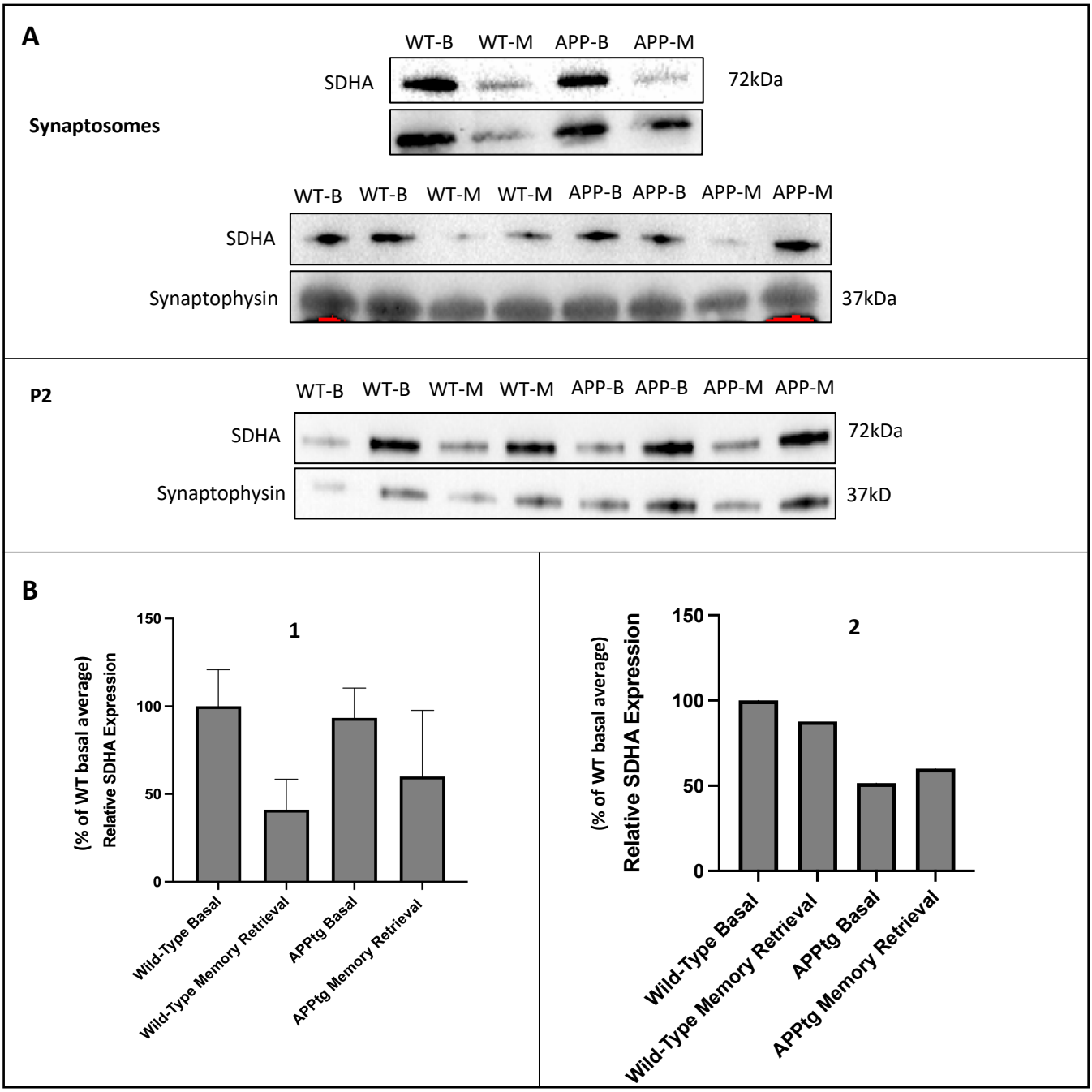

*Figure 3.14. A) Immunoblot analysis of SDHA levels in P2 fraction and synaptosome samples from 8 and 12 different mice respectively. WT-B= wild-type basal, WT-M= wild-type memory retrieval, APP-B= APPtg basal, APP-M=APPtg memory retrieval. Synaptophysin was used as a loading control. B) Densitometric analysis of blots shown in **A (1-synaptosomes, 2-P2).** Normalised protein abundance relative to Wild-type Basal average. T-testing was carried out between groups of synaptosome samples, and no significant differences were revealed.*

3.1.5 Dynamin-Related Protein 1 (DRP1)

Drp1, a member of the dynamin family of large GTPases, influences cell survival by mediating mitochondrial fission. Drp1 oligomerises on the OMM in a ring-like structure which constricts to divide mitochondria (Gao et al., 2021). Fission is an intricately balanced process which regulates

cellular and organ dynamics, including the regulation of mitochondrial apoptosis. Any perturbation to the physiological balance between fission and fusion induces the fragmentation of synaptic mitochondria from its usual tubular-like morphology into pieces, leading to synaptic dysfunction, neuronal damage, and abnormal mitochondrial redistribution (Hu, Huang & Li., 2017; Bera et al., 2022).

Figure 3.5 shows the expression levels of DRP1 in P2 samples and synaptosomes. In the synaptosome samples, WT mice at the basal level demonstrated higher levels of DRP1 expression than the memory retrieval group. Expression in the transgenic mice showed very little difference between basal and memory groups. None of the differences between groups were statistically significant. In the P2 samples, expression is higher in the WT mice than the transgenic mice, with the greatest DRP1 expression in WT mice at the basal level. In the transgenic mice, expression was slightly higher in the memory group than the basal group, however, none of these differences could be tested for statistical significance due to sample limitation. Due to the same behavioural group trend being witnessed in both sample types, the increased expression cannot be interpreted as synapse specific, however, the increased expression in the transgenic mice, compared to the WT mice is only seen in the synaptosome samples and so this small increase can be seen as synapse specific.

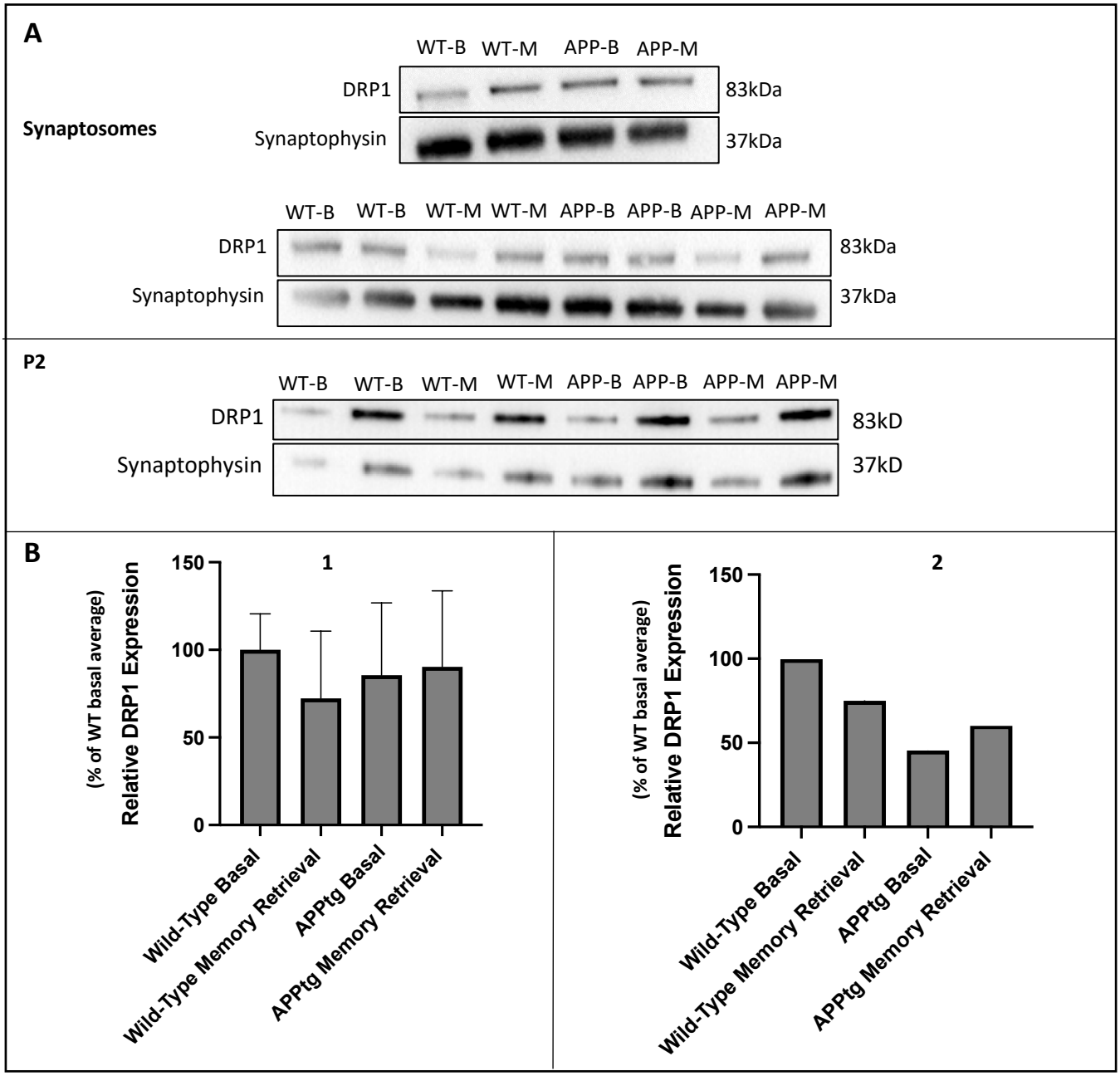

Figure 3.15. A) Immunoblot analysis of DRP1 in P2 fraction and synaptosome samples from 8 and 12 different mice respectively. WT-B= wild-type basal, WT-M= wild-type memory retrieval, APP-B= APPtg basal, APP-M=APPtg memory retrieval. Synaptophysin was used as a loading control. B) Densitometric analysis of blots shown in ***A (1-synaptosomes, 2-P2).*** *Normalised protein abundance relative to Wild-type Basal average. T-testing was carried out between groups of synaptosome samples, and no significant differences were revealed.*

3.1.6 Mitofusin 1 (MFN1)

Members of the mitofusin family promote the fusion of mitochondrial outer membranes. MFN1 is critical in the remodelling of mitochondrial membranes, required for effective fusion events to

facilitate the exchanging of materials between mitochondrial populations (Escobar-Henriques & Joaquim,. 2019). The ability of mitochondria to undergo fusion events influences the overall fitness of the cell and any possible reduction in levels of the mitofusins could suggest a significant level of dysfunction (Wang et al., 2009). Reduced MFN1 is an abnormality commonly seen in AD and thus, western blotting was used to assess the levels of the protein in WT and APPtg mice.

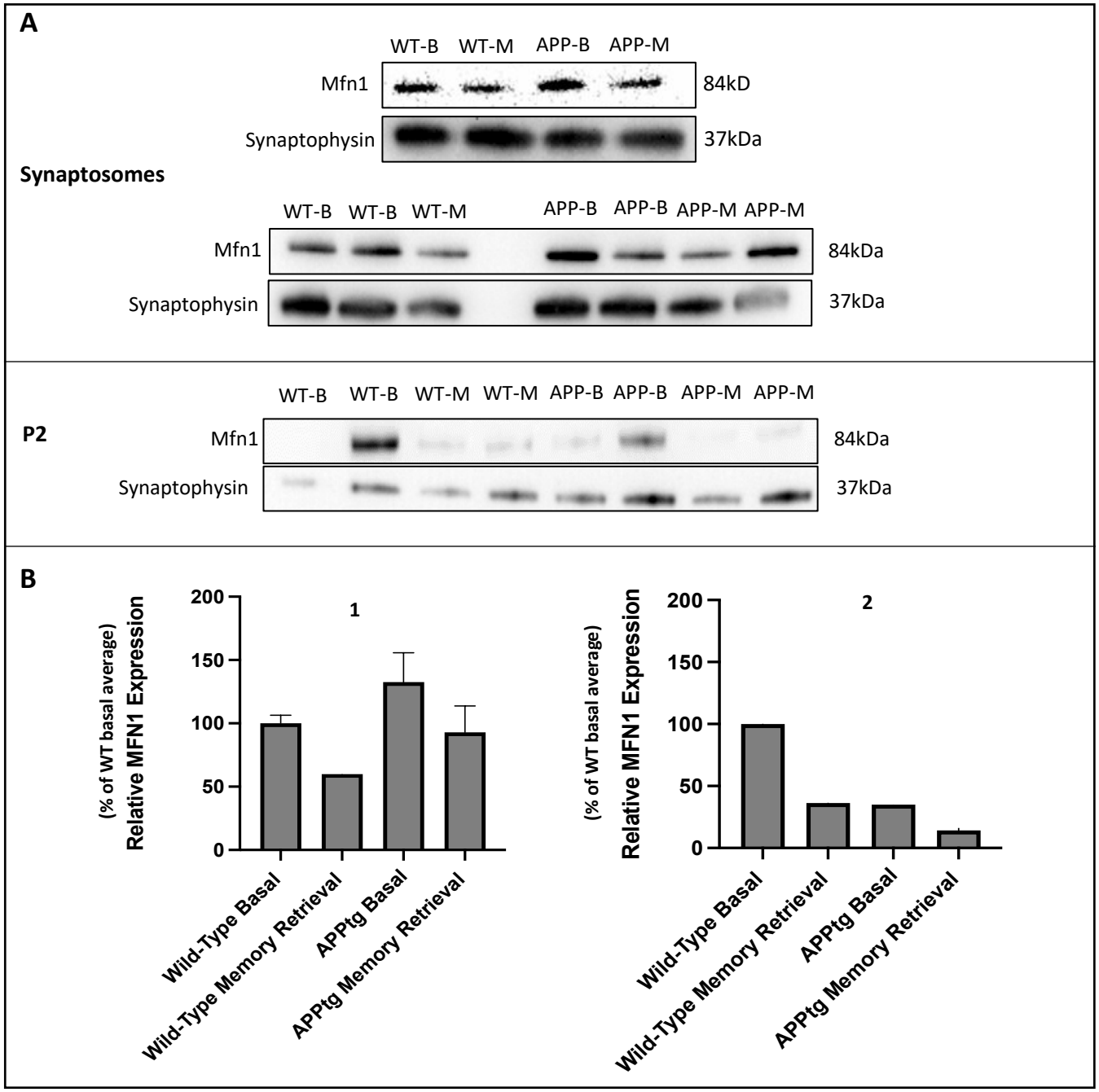

Figure 3.16. ***A)*** *Immunoblot analysis of MFN1 levels in P2 fraction and synaptosome samples from 8 and 11 different mice respectively. WT-B= wild-type basal, WT-M= wild-type memory retrieval, APP-B= APPtg basal, APP-M=APPtg memory retrieval. Synaptophysin was used as a loading control.* ***B)*** *Densitometric analysis of blots shown in* ***A (1-synaptosomes, 2-P2).*** *Protein abundance relative to Wild-type Basal average. T-testing was carried out between groups of synaptosome samples (n=3), and no significant differences were revealed. Figure B1 lacks error bar for 'Wild-type Memory Retrieval' group due to only two replicates included.*

One sample belonging to the WT memory retrieval group failed to properly transfer to the PVDF membrane. When carrying out statistical analyses on these samples, the average value for all remaining samples in the WT memory retrieval group was substituted in its place.

Figure 3.6 reveals the MFN1 expression levels in both sample types. In the synaptosome samples, both genotypes have greater MFN1 expression at the basal level, however, the transgenic mice display a higher expression than the WT mice. In WT mice, MFN1 expression is visually higher during basal levels than during memory retrieval, however the difference was not significant. Although in APPtg mice, MFN1 expression was also higher during basal levels than memory retrieval, the difference was not significant. When looking at the results from the P2 samples, a different pattern emerges. The expression of MFN1 in P2 samples is more than 50% greater in the WT mice than the transgenic mice, at both basal levels and during memory retrieval. Wild-type mice also presented with much lower MFN1 levels during memory retrieval, when compared to the basal level (75% lower). Due to sample limitation, statistical analyses could not be carried out to determine significance of these trends. In the P2 control samples, transgenic mice display a much lower expression of MFN1 than WT mice. When looking at synaptosome samples, the transgenic mice express higher levels of MFN1 than the WT mice, a trend which is synapse specific.

3.1.7 Voltage Dependent Anion Channel 1 (VDAC1)

VDAC1 is the most abundant protein on the OMM and is a key player in the regulation of mitochondrial function, acting as a gatekeeper for the passage of ions, metabolites, and nucleotides. VDAC1 interacts with several apoptotic and anti-apoptotic proteins and therefore plays a central role in apoptosis. The regulation of VDAC1 is essential not only for metabolic functions, but also cell survival (Camara et al., 2017).

Western blotting for VDAC1 was carried out using both P2 and synaptosome samples. Figure 3.7 represents the western blot results for both sample types. In the synaptosome samples, expression of VDAC1 was relatively consistent across genotype-phenotype combinations. The lowest levels of VDAC1 expression were seen in the transgenic mice during memory retrieval. None of the differences between groups were significant (t-test, a=0.05).

By contrast, in the P2 samples, visual expression of VDAC1 was greater in the WT mice than the transgenic mice, both at the basal level and during memory retrieval. In control mice, the expression of VDAC1 was greater during memory retrieval than at the basal level, however, this was not

reflected in the transgenic mice, who displayed higher expression during basal levels. Results from these samples could not be tested for statistical significance due to limited sample number.

A synapse specific increase in VDAC1 expression can be seen in APPtg basal and APPtg memory groups, however, a 50% decrease in VDAV1 expression was highlighted in WT mice during memory retrieval.

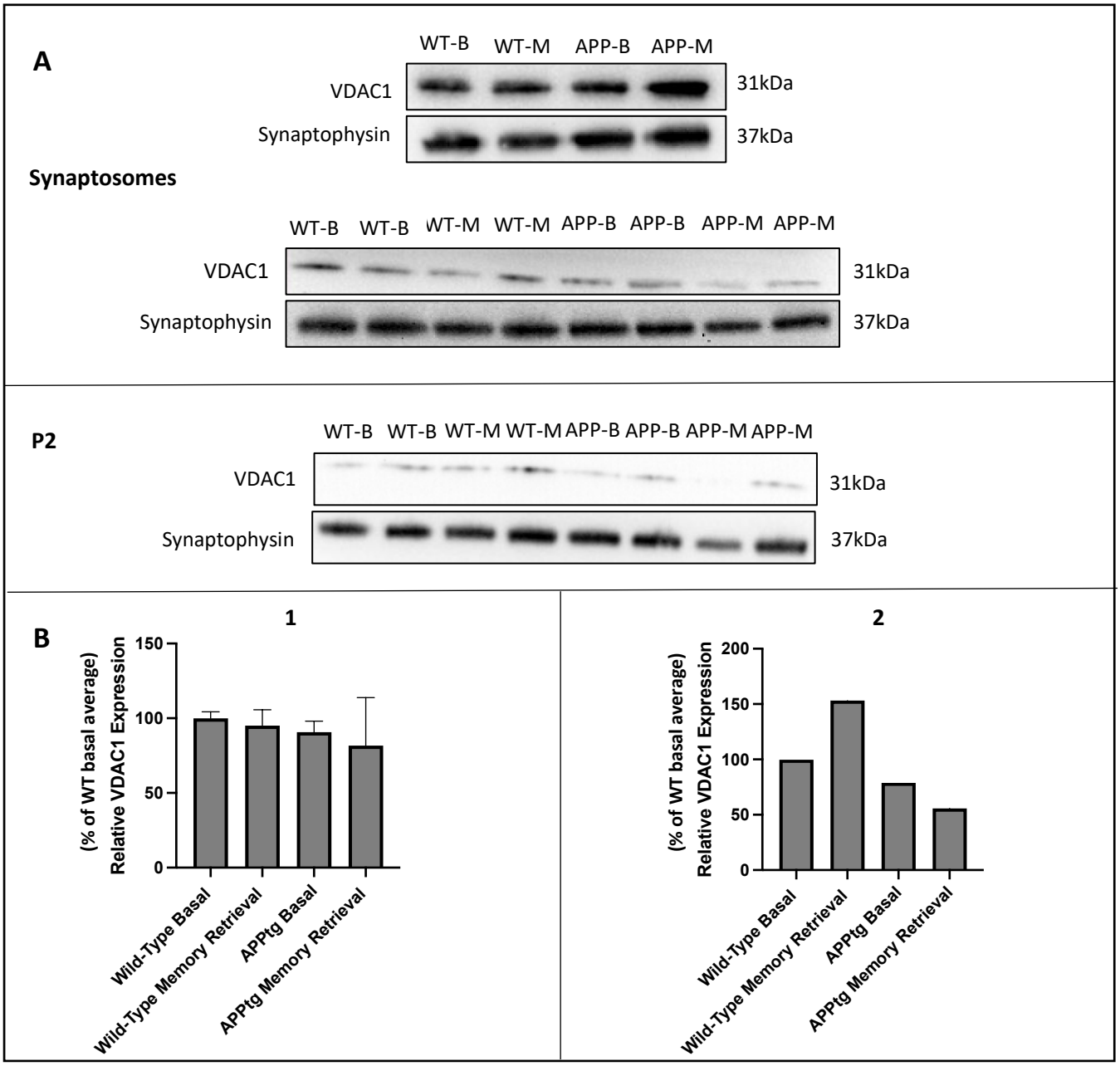

Figure 3.17. A) Immunoblot analysis of VDAC1 levels in P2 fraction (1) and synaptosome samples (2) from 8 and 12 different mice respectively. WT-B= wild-type basal, WT-M= wild-type memory retrieval, APP-B= APPtg basal, APP-M=APPtg memory retrieval. Synaptophysin was used as a loading control. ***B)*** *Densitometric analysis of blots shown in* ***A (1-synaptosomes; 2-P2).*** *Protein abundance normalised to synaptophysin, relative to Wild-type Basal average. T-testing was carried out between groups of synaptosome samples, and no significant differences were revealed.*

Thus far, western blotting has been carried out on both sample fractions, the P2 and synaptosomes, however, due to limited sample, the following western blots could not be carried out using full sets of either sample fractions and therefore, no statistical tests were applied the result. To determine the significance of any results, further western blots would need to be carried out, using a higher n number for each experimental group (n=3).

3.1.8 Postsynaptic Density Protein 95 (PSD95)

PSD95 is an important synaptic scaffolding protein, localised to the postsynaptic density of excitatory synapses, where it participates in the regulation of signalling molecules, channels, and receptors. Recent studies have shown PSD95 to be a vital player in the molecular mechanisms underlying synaptic maturation and plasticity (Jeong et al., 2019). Synaptic loss has been reported to better correlate with cognitive decline in AD, rendering PSD95 an interesting target for biomarker development, especially at the preclinical level. Expression of PSD95 was assessed in P2 samples from each experimental group.

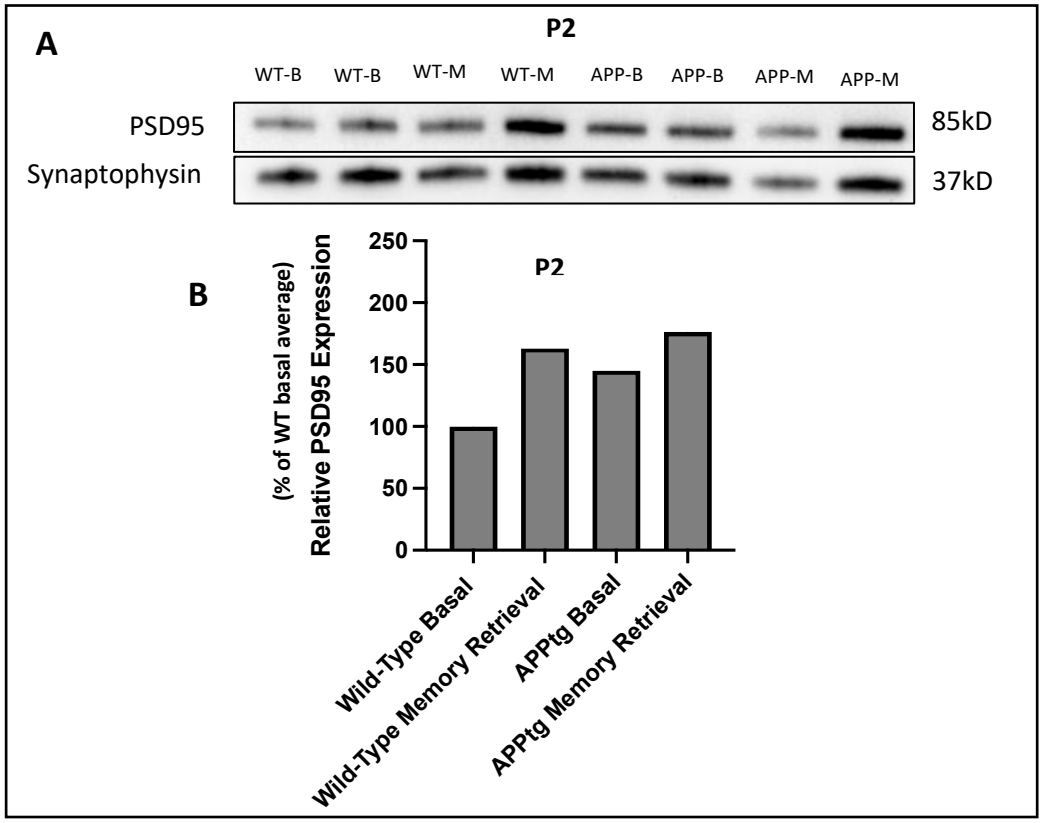

*Figure 3.18. **A)** Immunoblot analysis of PSD95 in P2 fractions from 8 different mice. WT-B= wild-type basal, WT-M= wild-type memory retrieval, APP-B= APPtg basal, APP-M=APPtg memory retrieval. Synaptophysin was used as a loading control. **B)** Densitometric analysis of blots shown in **B.** Protein abundance relative to normalised Wild-type Basal levels.*

Figure 3.8 depicts the wester blotting results against the PSD95 protein, normalised with synaptophysin, a presynaptic terminal marker.

Whilst sample limitation prevented statistical analyses from being carried out between groups, some visual trends can be seen from the western blot signal. There appears to be higher levels of PSD95 in the APPtg mice, when compared to the WT mice, both at the basal level and during memory retrieval. These results are only visual trends and cannot be assessed for significance without further experimentation.

3.1.9 Alpha Synuclein

Alpha synuclein is an abundant neuronal protein, ubiquitously expressed in the brain, particularly presynaptic terminals in the neocortex and hippocampus. Whilst the main function of alpha synuclein remains largely unclear, it has a strong genetic link to Parkinson's disease and other neurodegenerative diseases. Known to aggregate and propagate through the neuraxis, alpha synuclein has been identified as the non-amyloid component of amyloid plaques (Burré., 2015). Due to sample limitation, western blotting for alpha synuclein was only carried out using P2 samples, using 2 samples from each genotype-phenotype combination.

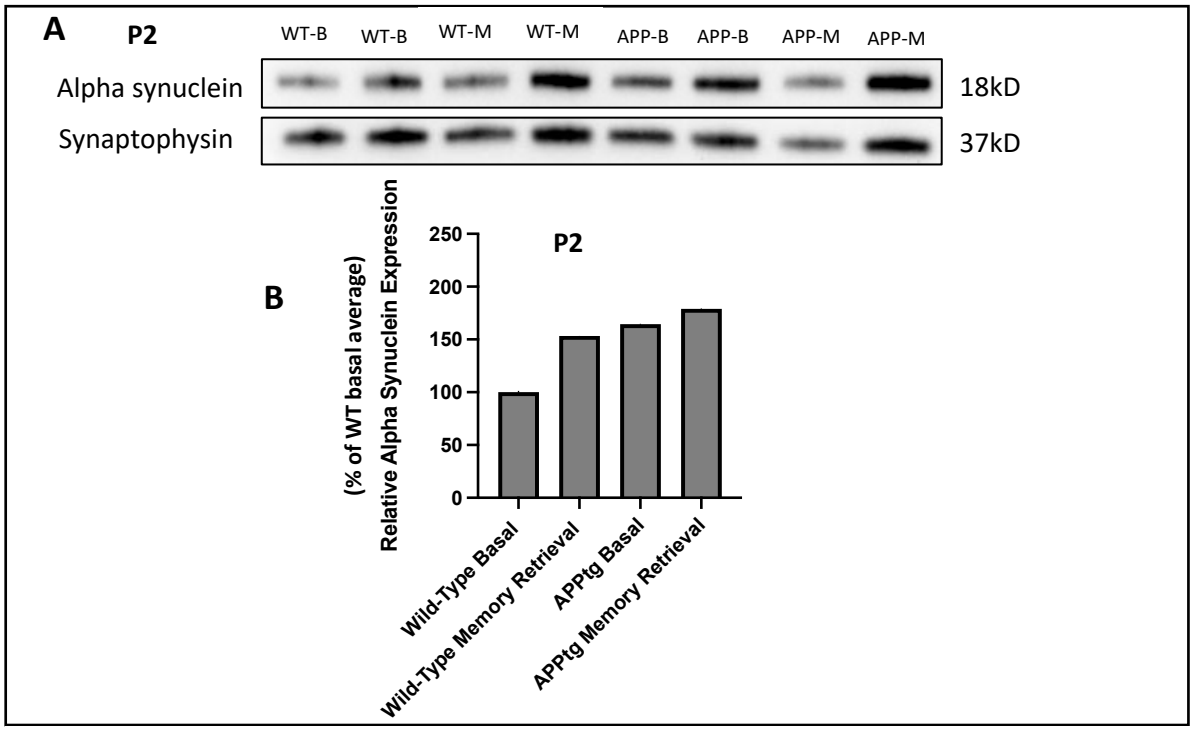

Figure 3.19. A) Immunoblot analysis of alpha synuclein levels in P2 fractions from 8 different mice. WT-B= wild-type basal, WT-M= wild-type memory retrieval, APP-B= APPtg basal, APP-M=APPtg memory retrieval. Synaptophysin was used as a loading control. ***B)*** *Densitometric analysis of blot shown in* ***A.*** *Protein abundance normalised to synaptophysin levels, relative to WT basal average.*

Figure 3.9 depicts the expression of alpha synuclein in each genotype-phenotype combination. Visually, there is a higher expression of alpha synuclein in APPtg mice compared to WT mice, at both basal levels and during memory retrieval. The increase in expression between basal levels and memory retrieval (1.5-fold increase) is not replicated in the APPtg mice, whose expression is very similar at both levels. Although these results appear interesting, they cannot be analysed statistically for significance without further experimentation with a higher sample number.

3.1.10 Ubiquinol-Cytochrome C Reductase Binding Protein (UQCRB)

Ubiquinol-cytochrome C oxidoreductase (UQCRB), commonly referred to as complex III or cytochrome bc1 complex, is an integral component of the ETC, localised to the IMM. UQCRB contributes to the generation of electrochemical potential by catalysing electron transfer from ubiquinol to cytochrome C, coupled to the translocation of protons across the membrane (Xia et al., 2013).

Western blotting was carried out to analyse the levels of UQCRB expression in P2 samples. Western blotting was also attempted for UQCRB expression in synaptosome samples; however, reliable results could not be obtained with this antibody.

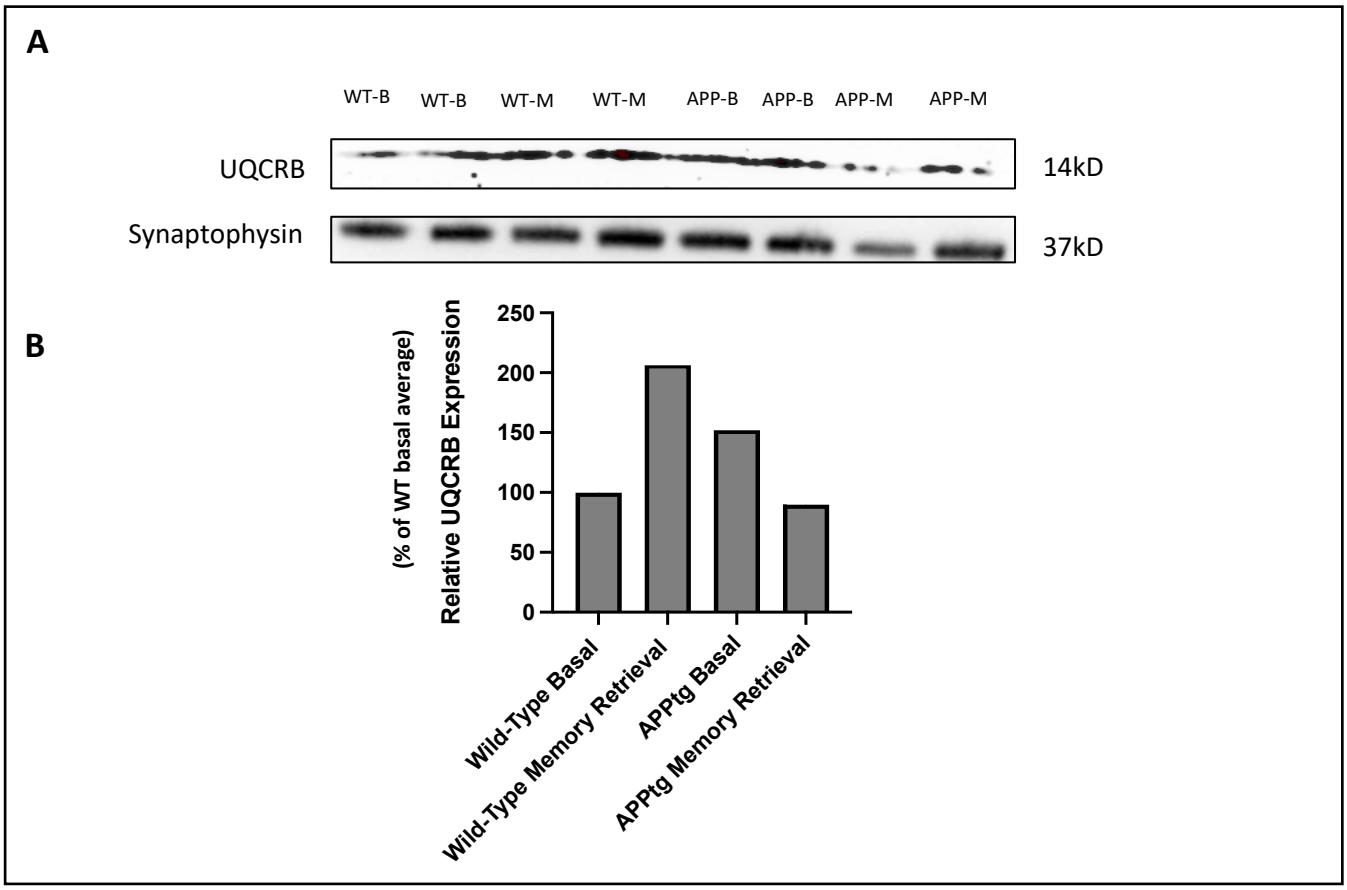

*Figure 3.20. A) Immunoblot analysis of UQCRB levels in P2 fractions from 8 different mice. WT-B= wild-type basal, WT-M= wild-type memory retrieval, APP-B= APPtg basal, APP-M=APPtg memory retrieval. Synaptophysin was used as a loading control. B**)** Densitometric analysis of blots shown in **A (P2 fraction).** Normalised protein abundance relative to Wild-type Basal average.*

Figure 3.10 represents the relative UQCRB expression levels across the four groups. Expression was the highest in WT mice during memory retrieval. In the transgenic mice, expression at the basal level was higher than WT mice at the basal level. Expression in transgenic mice during memory retrieval was the lowest of the four groups. None of these differences could be tested for statistical significance due to limited sample number.

3.2 Enzymatic Activity Assays

Measuring enzymatic activity is a tried-and-tested means of determining the amount of enzyme present under defined conditions, in this case, during basal levels or during memory retrieval in WT and APPtg mice. The activity of the enzyme can be compared between experimental conditions, and with a complete study of the parameters that affect enzyme activity, it should be possible to extrapolate to the activity expected to occur *in vivo.* The enzymatic activity of two key enzymes were

tested using enzymatic activity assay kits purchased from Abcam.com, and their activity was compared against each genotype and behavioural group interaction. Full set of tables detailing kit reagents, assay reding parameters, recorded OD readings, calculations of the changes in OD, and standard curve straight line equation are listed in Appendix A, tables 1,2,3,6,7,8,9 & 12.

3.2.1 Optimisation of Malate Dehydrogenase 2

MDH2, a key enzyme in the TCA cycle which catalyses the interconversion between malate and oxaloacetate, utilising NAD^+/NADH as a cofactor, was optimised for factors including: sample concentration, effect of lysis buffer, incubation period, and temperature (for more detail, see section 1.3.4). The MDH2 activity kit works by following the production of NADH, coupled to the reduction of a reporter dye to yield a coloured product with strong absorbance at 450nm.

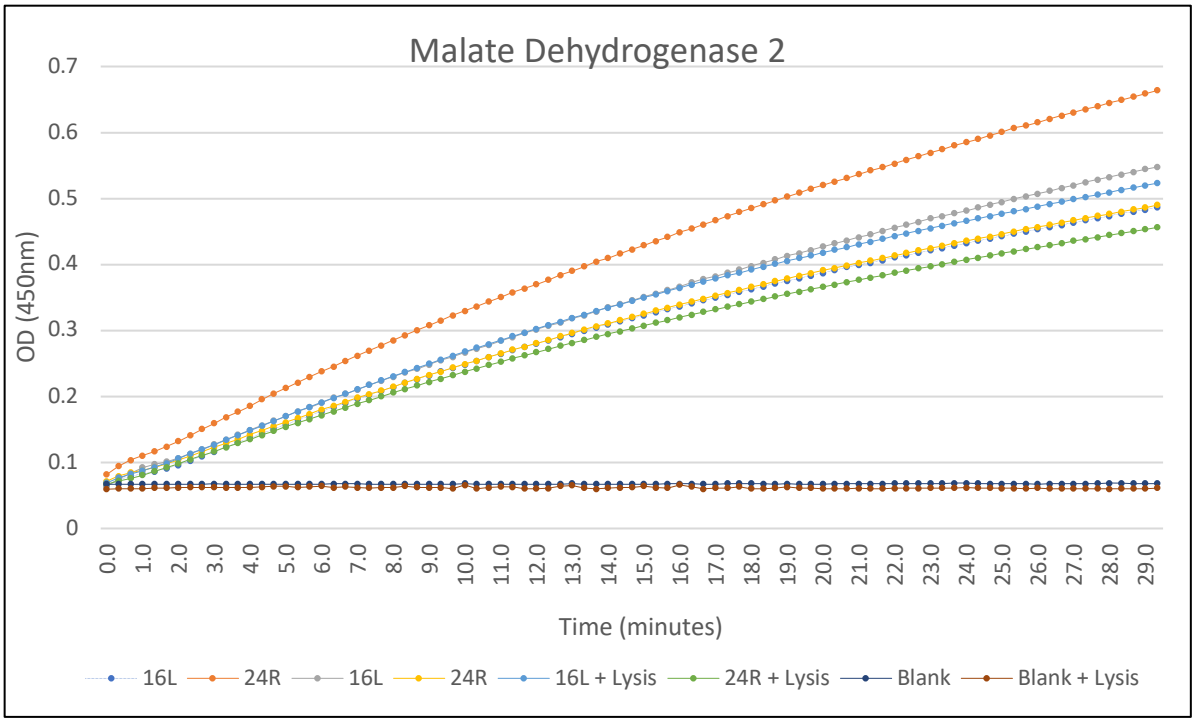

Figure 3.21. Kinetic graph showing activity of malate dehydrogenase. Blank= assay buffer only. Blank + lysis)= assay buffer with additional lysis buffer. Assay carried out at 25℃, pH 7.4, with 5μg protein per sample. 16L & 24R= Wild-type memory retrieval group, total cell lysate.

This kit contained no positive controls or standards. The MDH2 enzyme is captured within the wells of the microplate, ensuring confidence in kit specificity.

Figure 3.11 reflects the success of the second optimisation trial of MDH2. Both blanks produced no change in activity over the 30-minute period, and all biological samples used produced strong, positive linearity over the course of the reaction, reflective of MDH2 activity. After this optimisation

trial, samples from each of the genotype-phenotype interactions were introduced to the assay, at differing concentrations. Sample backgrounds without the addition of activity solution were also included to allow for normalisation in the comparative assays.

3.2.2 Malate Dehydrogenase 2 Results

Malate dehydrogenase 2 is located in the mitochondrial matrix, where it participates in the TCA cycle, catalysing the oxidation of malate (as detailed in the introduction, section 1.3.1.4).

In this assay, MDH2 activity is expressed as the change in absorbance per minute, per amount of sample loaded into each well (Figure 3.12). Figure 3.12A shows the MDH2 activity within each individual sample tested, whilst figure 3.12B shows the average enzymatic activity for each of the four experimental groups. In the wild-type mice, MDH2 activity was greater in the basal group (0.0116OD/min), compared to the memory retrieval group (0.01OD/min). In the APPtg mice, the MDH2 activity was consistent across phenotypes; basal MDH2 activity was 0.0108OD/min and during memory retrieval, MDH2 activity was 0.0108OD/min. Overall, there were no statistically significant differences in MDH2 activity between groups (α=0.05).

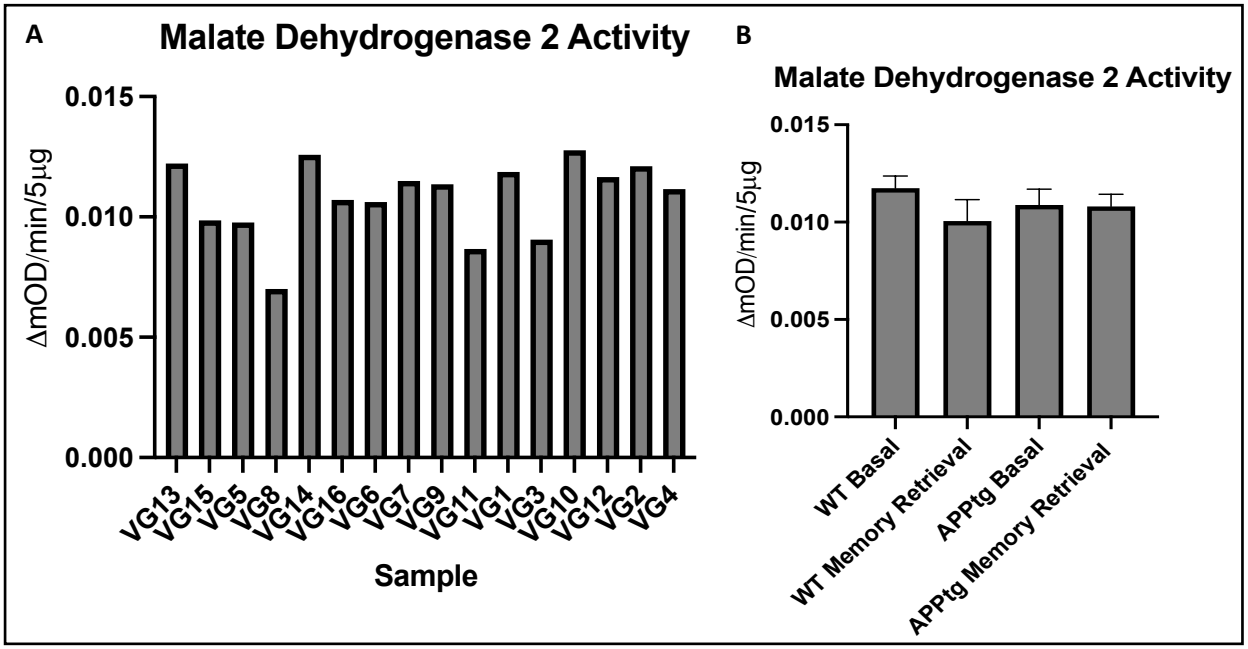

*Figure 3.22. Malate dehydrogenase 2 (MDH2) activity in synaptosome samples. **A=** MDH2 activity measured for each test sample. VG10,12,13,15= wild-type basal; VG2,4,5,8= wild-type memory retrieval; VG9,11,14,16= APPtg basal; VG1,3,6,7= APPtg memory retrieval. **B=** MDH2 activity measured via change in optical density per minute, measured at 450nm. Average activity calculated for each experimental group. Colour intensity at 450nm is directly proportional to MDH2 activity in each sample.*

Within a kinetic assay method, the rate at which substrates are converted into products is continually measured, and readings are affected by changes in the concentrations of both the substrate and the product. Measurement methods are based on tracking changes in product formation or substrate utilisation over a predetermined time frame. For the purpose of analysis, the linear range of the rection curve is vital and frequently observed during the earliest stages of the reaction. During this time, the reaction is not yet hindered by diminishing substrate or potential product inhibitory effects.

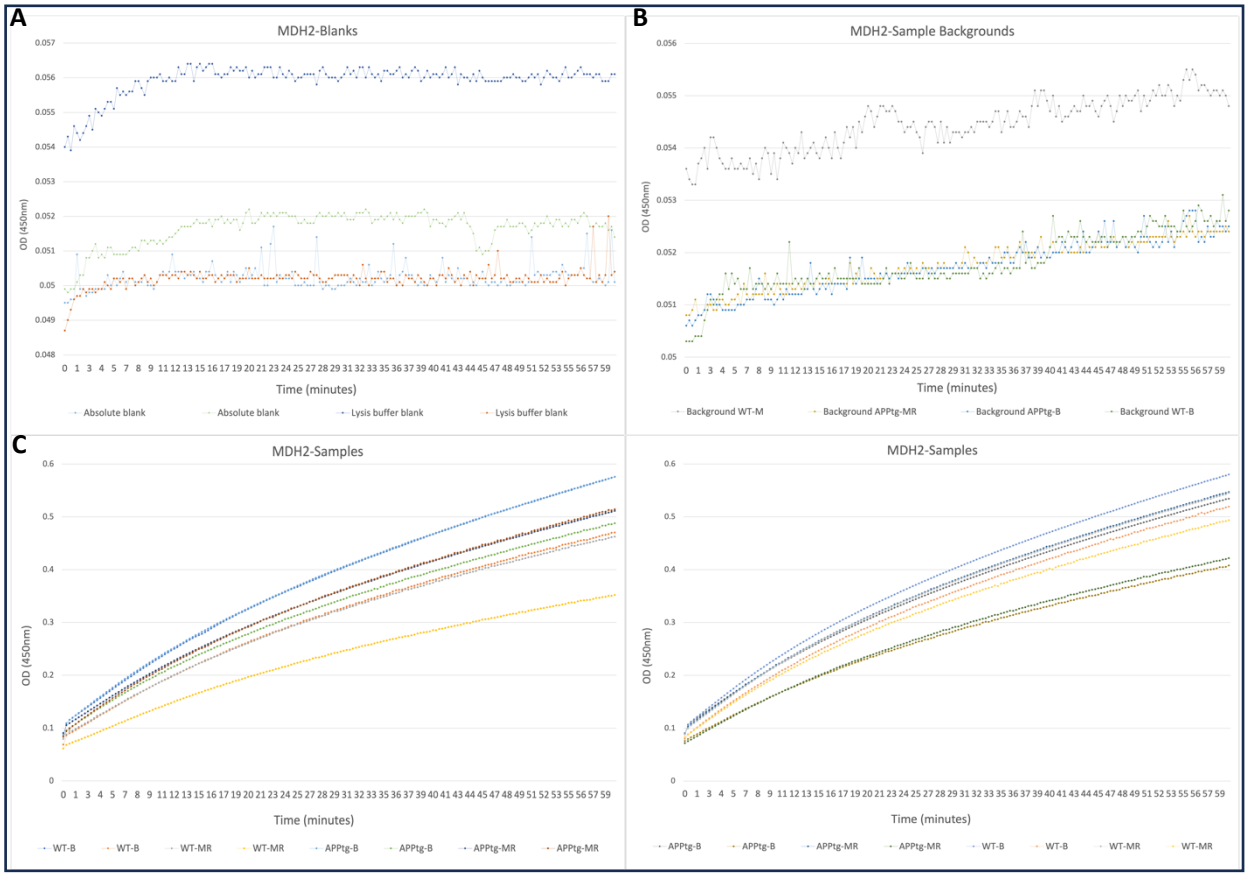

Figure 3.13. Kinetic graphs showing MDH2 activity, measured as change in optical density at 450nm per minute, over a 60-minute time frame. A= kinetic measurements of blank samples. B= kinetic measurements of sample backgrounds (no substrate). C= kinetic measurements of sample backgrounds (no substrate). D= kinetic measurements of biological samples. Assay carried out at 25 ℃, pH 7.4, sample conc= 5 μg/50 μl. Assay linear for 59 minutes.

The kinetic graphs shown in figure 3.13 depicts the reaction occurring within the 60-minute period. Figure 3.13A reveals there was no activity in either the absolute blanks (assay buffer only) or the lysis buffer blanks (assay buffer with additional lysis buffer). Figure B depicts the reaction course of the sample backgrounds (sample with no substrate added). The sample backgrounds (1 from each experimental group) show minimal change in OD over the course of the reaction period, confirming minimal activity occurring with endogenous substrate. Whilst the VG5 (WT basal) background

sample reads at a higher OD than the other sample backgrounds, the rate of reaction is no different. Graphs C & D show the reaction of the test samples themselves (4 mice from each experimental group). The rate of reaction here is much greater than that of the sample backgrounds, with the greatest reaction occurring before the 620 second time point.

3.2.3 Western Blotting- MDH2

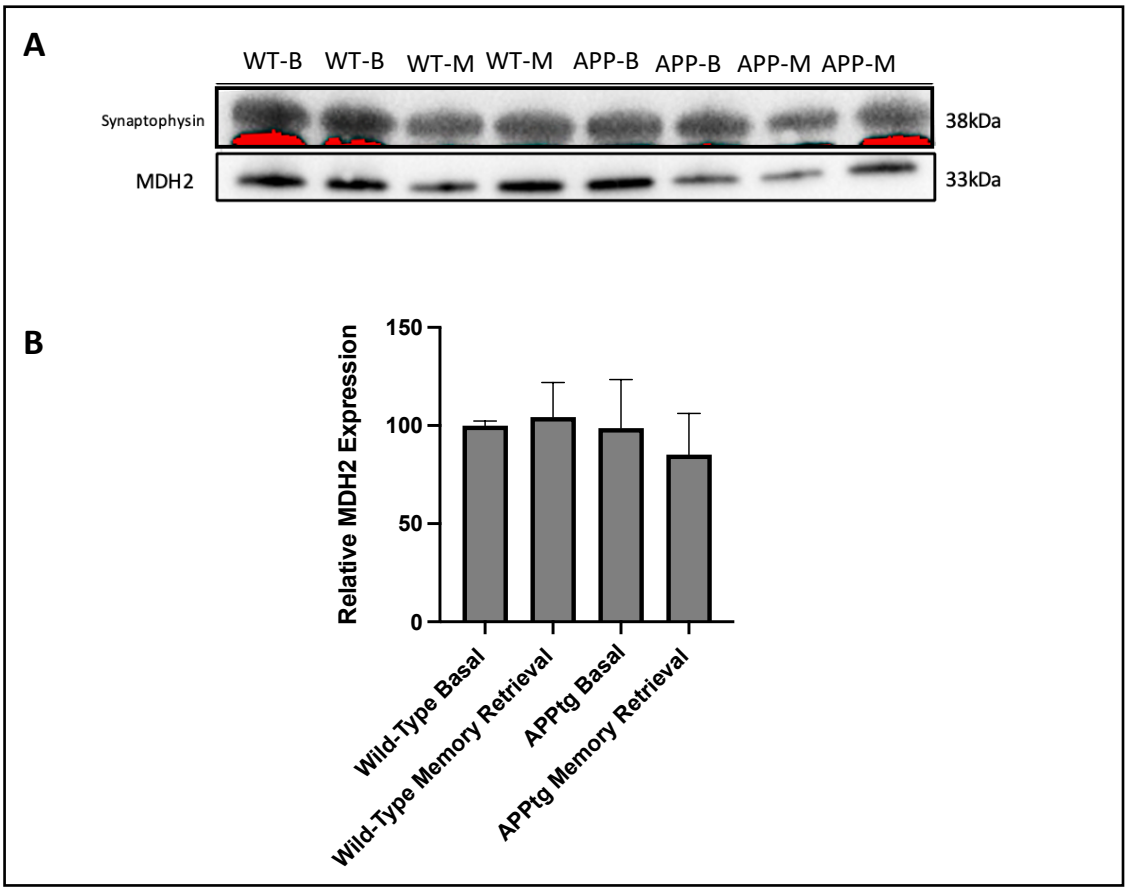

*Figure 3.14. **A)** Immunoblot analysis of MDH2 in synaptosome samples. Synaptophysin was used as a loading control. **B)** Average MDH2 expression plotted as a percentage of average wild-type basal MDH2 abundance.*

Figure 3.14 reveals that In WT mice, MDH2 expression is very similar at the basal level and during memory retrieval, however, in the transgenic mice, a different pattern emerges; the expression of MDH2 is greater in APPtg mice during basal levels than during memory retrieval. Overall, the expression of MHD2 is not affected by either genotype-phenotype interaction. None of the differences between groups could be tested for statistical significance due to limited sample number. Western blots using the second set of 8 synaptosome samples was carried out by another member of the research group, allowing for statistical comparisons to be made between all 16

samples. Results can be found in Appendix B, figure 4. Combined results reveal no significant differences in MDH2 expression between any of the genotype and behavioural group interactions.

3.2.4 Malate Dehydrogenase 2 Results Normalised to Western Blot Results

All MDH2 activity data was normalised against the abundance of MDH2, determined via western blotting. Figure 3.15A represents the average MDH2 activity in each experimental group, whilst 3.15B represents the enzymatic activity within each sample tested.

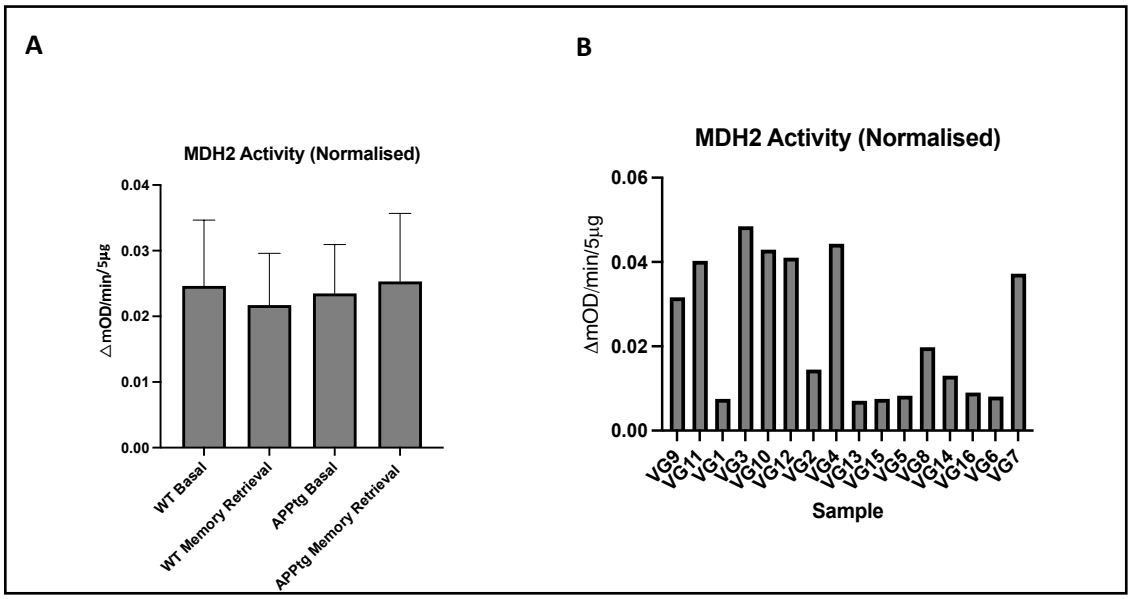

Figure 3.15. Malate dehydrogenase 2 activity normalised against western blot quantification. A) normalised MDH2 activity by experimental group. No differences between groups were significant by t-test (a=0.05). B) Normalised MDH2 activity per sample. VG10,12,13,15= wild-type basal; VG2,4,5,8= wild-type memory retrieval; VG9,11,14,16= APPtg basal; VG1,3,6,7= APPtg memory retrieval.

After normalisation of results against western blot quantification, there remained no significant interaction between genotype and behavioural training for MDH2 activity. Two-way ANOVA revealed no significant differences in the MDH2 activity for either of the genotype and behavioural group interactions ($F(1,12)=0.06949$; $p=0.7966$). Assay was carried out in duplicate using 32 samples (16 samples carried out by another student in the group). Combined normalised assay results (Appendix B, figure 1) revealed no significant interaction between genotype and behavioural group for MDH2 activity. Two-way ANOVA was carried out on duplicate assay data, results shown in Appendix A, table 16. No significant interactions exist between genotype and behavioural group.

3.2.5 Optimisation of 6-Phosphofructokinase

For the initial optimisation of 6-PFK, a key regulatory enzyme of glycolysis (further detailed in section 1.3.1.5, including how the kit works), 4 background samples (assay buffer only), biological samples (1x wild-type memory retrieval, 1x APPtg memory retrieval), 2 positive controls (1 & 5µl) and 2 standards (1nmol & 0.5nmol) were trialled (Figure 3.16). Both memory retrieval samples showed a steep slope of results, indicating high levels of enzymatic activity. Both sample backgrounds produced a much smaller level of activity, reflective of endogenous substrate reactivity. All assay background (assay buffer only) samples showed no activity. Overall, this assay appeared to be working optimally with minimal optimisation and thus was continued to the comparative experiments.

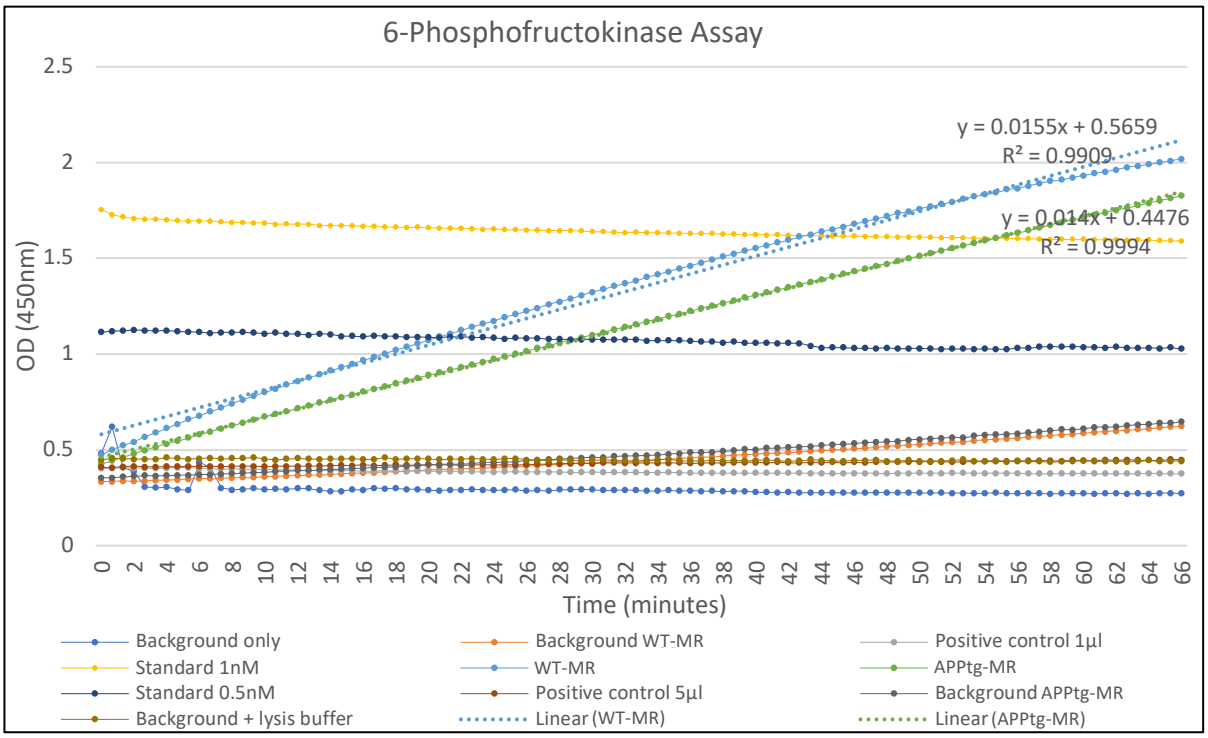

Figure 3.16. Kinetic graph showing activity of 6-phosphofructokinase. Background= sample prepared without the addition of substrate. Background only= assay buffer. Assay carried out at 37℃, pH 7.4, sample conc= 5µg/50µL. Assay linear for 66 minutes.

3.2.6 6-Phosphofructokinase Results

6-phosphofructokinase is a key regulatory enzyme in glycolysis, which catalyses the phosphorylation of fructose-6-phosphate to fructose-1,6-biphosphate (detailed in introduction section 1.3.5).

The activity of PFK in this assay is expressed, through the production of NADH, which correlates with a change in absorbance, per minute, at 450nm (Figure 3.17B). The use of PFK-specific substrate and

the inclusion of a positive control provides full confidence that the assay kit is exclusively measuring the activity of 6-PFK.

PFK activity was found to be the most consistent across both genotypes at the basal level, with a change of 0.126OD/min for the wild-type mice and 0.121OD/min for APPtg mice. For both genotypes, mice had consistently lower PFK activity when tasked with memory retrieval, with wild-type mice showing a change of 0.096OD/min and APPtg mice with a change of 0.107OD/min. None of the differences between groups were statistically significant (α=0.05).

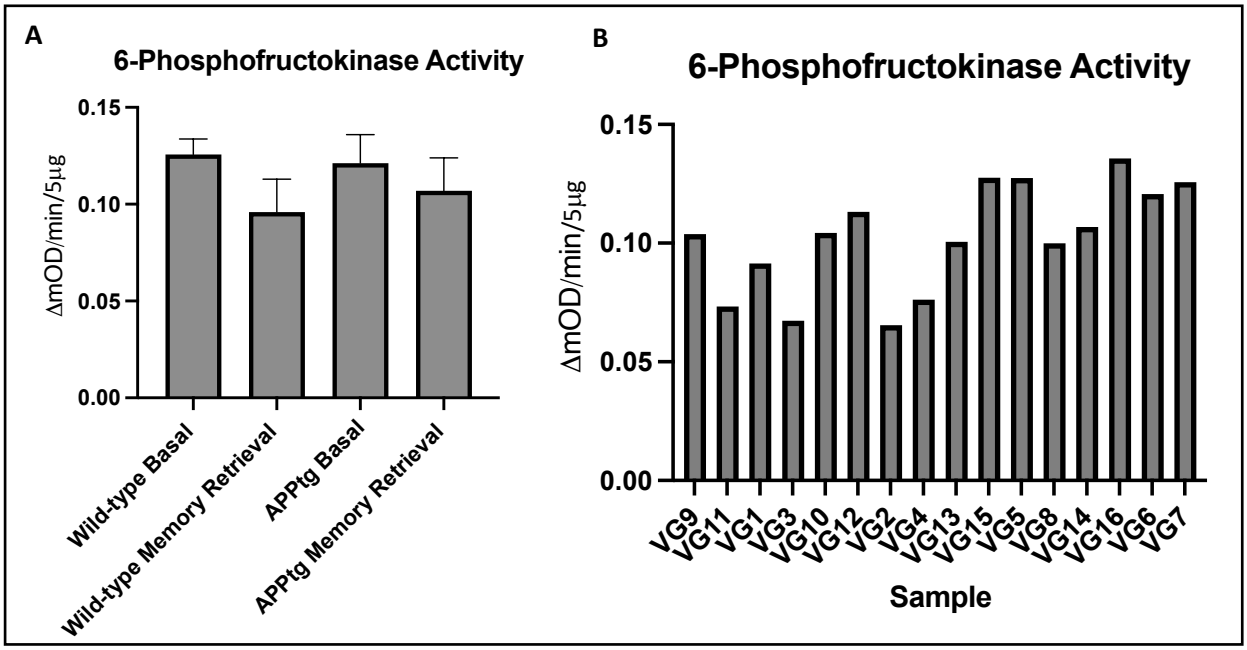

*Figure 3.17. 6-PFK activity in synaptosome samples. **A**=6-PFK activity measured by change in optical density per minute, measured at 450nm. Average activity calculated for each experimental group. Colour intensity at 450nm is directly proportional to PFK activity present in sample. **B**= 6-PFK activity measured by change in optical density per minute. Activity measured for each individual sample. VG10,12,13,15= wild-type basal; VG2,4,5,8= wild-type memory retrieval; VG9,11,14,16= APPtg basal; VG1,3,6,7= APPtg memory retrieval.*

The kinetic graphs in figure 3.18 show the reaction over a 60-minute period. 3.18A shows the kinetic graph for the assay blanks (assay buffer only), positive controls and assay standards at a range of concentrations. The two positive controls (at 10µl & 20µl) contain a known quantity of purified enzyme to allow confidence that the assay is indeed working and is able to detect the enzyme. All of the blanks gave no change in readings over time, reflective of no enzymatic activity. The assay standards all demonstrated no change in OD over time and appeared evenly spaced across the graph, proportional to their concentration. The standards, blanks, and positive control patterns of reaction confirm the assay kit is performing well/as expected.

Figure 3.18B & C show the kinetic reaction of the sample backgrounds. In this assay, the 'sample background' consists of test sample with assay buffer, ATP, developer, and enzyme mix, only without the addition of substrate, thus the only reaction that should occur within a sample background would be due to endogenous substrate. There is a clear difference between the reaction rates of some of the sample backgrounds, likely due to the different genotype-phenotype interactions. Overall, the sample backgrounds displayed a slower rate of reaction over a longer time period (peaking at 1261-2002 seconds) than the test samples themselves and the total change in OD, proportional to product formation, was much lower than the test samples. The rate of reaction can be seen decreasing after the initial reaction period, instead of plateauing. The kinetic graph for the test samples (samples with added substrate), figures 3.18D & E, show a much steeper rate of reaction than figures 3.18B & C. After the initial phase of the reaction (400-800 seconds), the graph begins to plateau as all of the enzyme active sites become saturated with substrate and the reaction rate does not increase any further. Accumulation of product can also have an inhibitory effect upon the enzyme, leading to a plateau in the rate of reaction.

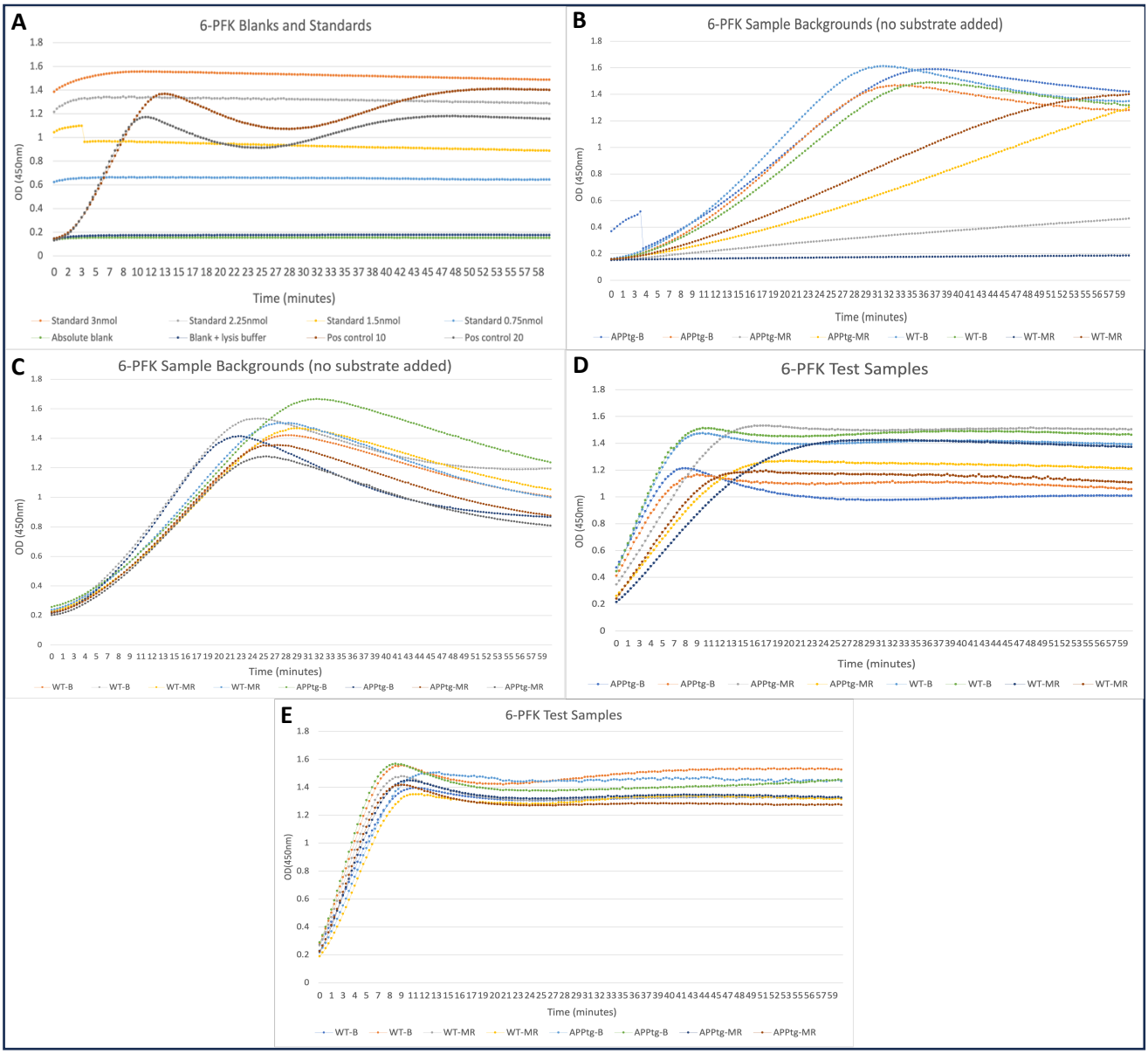

Figure 3.18. Activity of 6-PFK. Kinetic graphs measuring change in absorbance at 450nm. A= Run 1- standard curve dilutions; positive controls; absolute blank; lysis buffer blank, B= Run 2- no-substrate sample backgrounds, C= Run 3- no-substrate sample backgrounds, D= Run 4- test samples, E= test samples. Assay carried out at 37℃, pH 7.4,sample conc= 5μg/50μL. Assay linear for: B- 59 minutes, C- 32 minutes, D- 25 minutes, E- 9 minutes.

PFK activity was also expressed through a second means, measured as the amount of PFK that would generate 1.0μmol of NADH per minute, per 5μg protein sample (5μg/50μL) at pH 7.4 at 37° (Figure 3.19B), calculated using the NADH standard curve (Figure 3.19A). Here, PFK activity was at its highest in both genotypes at the basal level, with PFK activity at 0.385nmol/min/μg in the wild-type mice and 0.348nmol/min/μg in the APPtg mice. When tasked with memory retrieval, PFK activity fell to 0.247nmol/min/μg in the wild-type mice and 0.285nmol/min/μg in the APPtg mice and thus, APPtg mice had the highest rate of enzymatic activity when tasked with memory retrieval. Overall, none of the differences in PFK activity between groups were statistically significant (α=0.05).

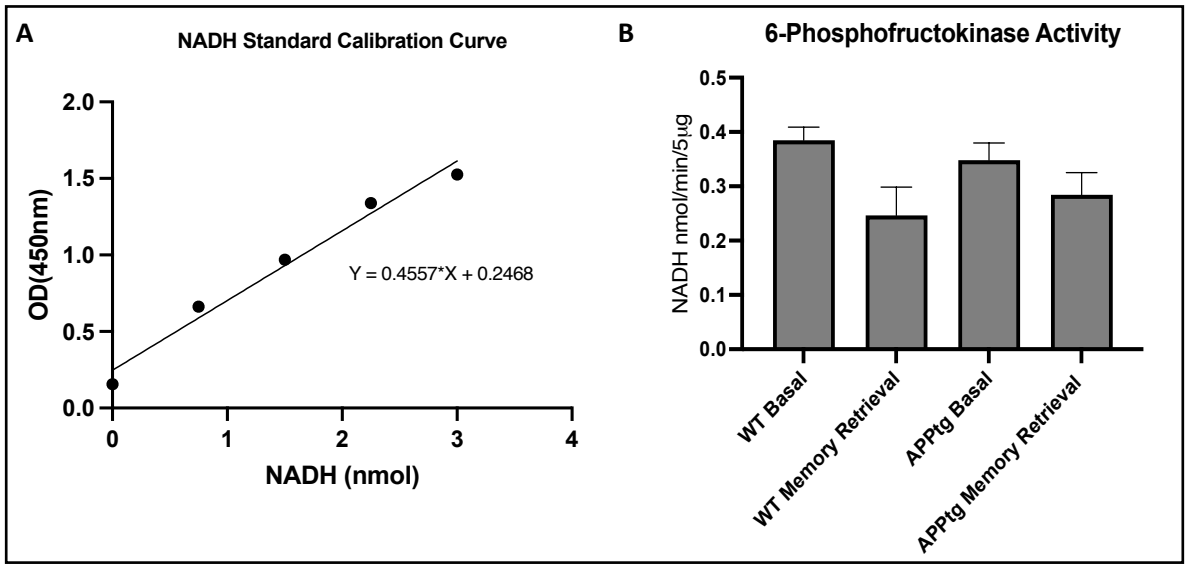

Figure 3.19. A) NADH standard curve used to determine the amount of NADH in each test sample. B) The enzyme activity of 6-PFK was analysed within synaptosome samples of wild-type and APPtg mice during basal levels and during memory retrieval, here calculated as amount of NADH produced per minute, per 5μg protein. There were no significant differences identified between groups (α=0.05).

3.2.7 Western blotting- 6-PFK

Figure 3.20 reveals the expression levels of 6-PFK in synaptosome samples. In WT mice, the expression of 6-PFK is higher during the basal levels than during memory retrieval, however, this pattern is not reflected in the transgenic mice, whose 6-PFK expression is consistent between both behavioural groups. None of the differences between groups could be tested for statistical significance due to limited sample number. The full set of 16 synaptosome samples have been analysed in Appendix B, figure 4, where these samples have been combined with another 8 samples, analysed by another student. Results were combined to allow for statistical comparison of all 16 samples. Combined blot results revealed a significant difference between the expression of 6-PFK in

WT mice during memory retrieval, when compared to WT mice during the basal level (p=0.017925, α=0.05). There were no significant differences in expression between the other experimental groups.

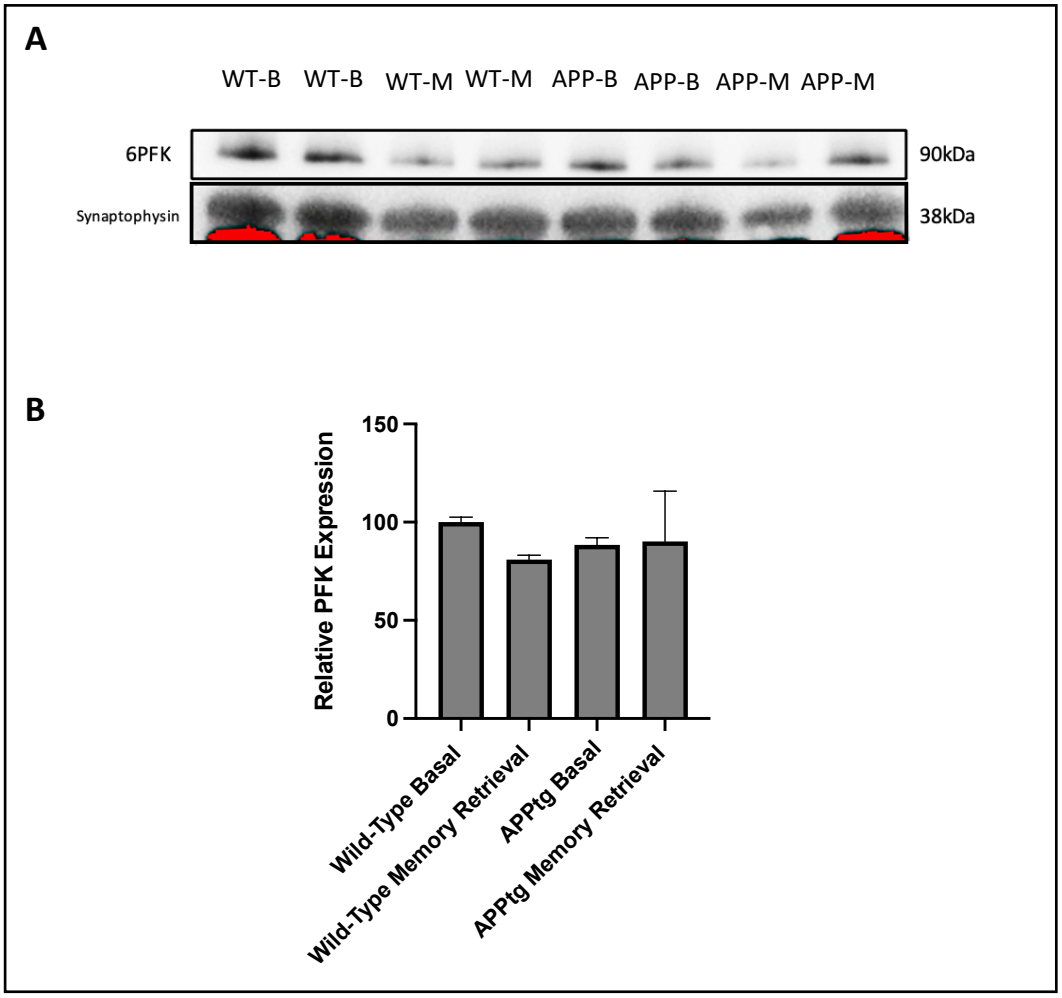

Figure 3.20. ***A)*** *Immunoblot analysis of 6-PFK in synaptosome samples. Synaptophysin was used as a loading control.* ***B)*** *Average 6-PFK expression plotted as a percentage of average wild-type basal 6-PFK abundance.*

3.2.8 6-Phosphofructokinase Results Normalised to Western Blot Results

After normalisation against western blotting quantification, there remained no significant genotype and behavioural group interaction for 6-PFK activity (Figure 3.21A & B). Two-way ANOVA revealed no significant interactions between genotype and behavioural group when comparing PFK activity (measured by change in OD/min) ($F(1,12)=0.05205$;$p=0.8234$). Two-way ANOVA revealed there was no statistically significant difference in the PFK activity (measured via NADH nmol/min/5μg; Figure 3.22) between any of the genotype and behavioural group interactions ($F(1,12)=0.01313$;$p=0.9107$). Assay was carried out in duplicate using 32 samples (16 samples carried out by another student in the group). Results shown in Appendix B, figure 2. Combined results normalised to western blotting

data revealed no significant difference in the activity of 6-PFK between any of the genotype and behavioural groups. Two-way ANOVA was carried out on duplicate assay results, detailed in Appendix A, table 21. ANOVA revealed no significant interaction between genotype and behavioural group.

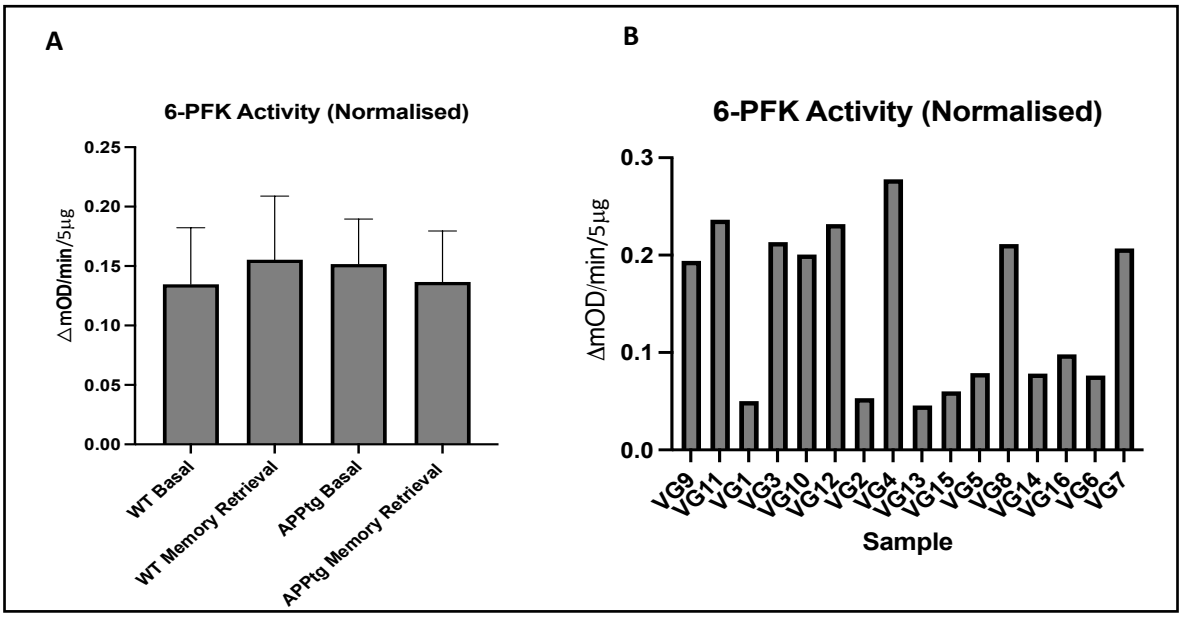

Figure 3.21. Normalised 6-PFK activity in synaptosome samples in A) experimental groups, B) each test sample use, and C) activity expressed as the amount of NADH produced per minute, per 5μg protein. There were no significant differences identified between groups (α=0.05). VG10,12,13,15= wild-type basal; VG2,4,5,8= wild-type memory retrieval; VG9,11,14,16= APPtg basal; VG1,3,6,7= APPtg memory retrieval.

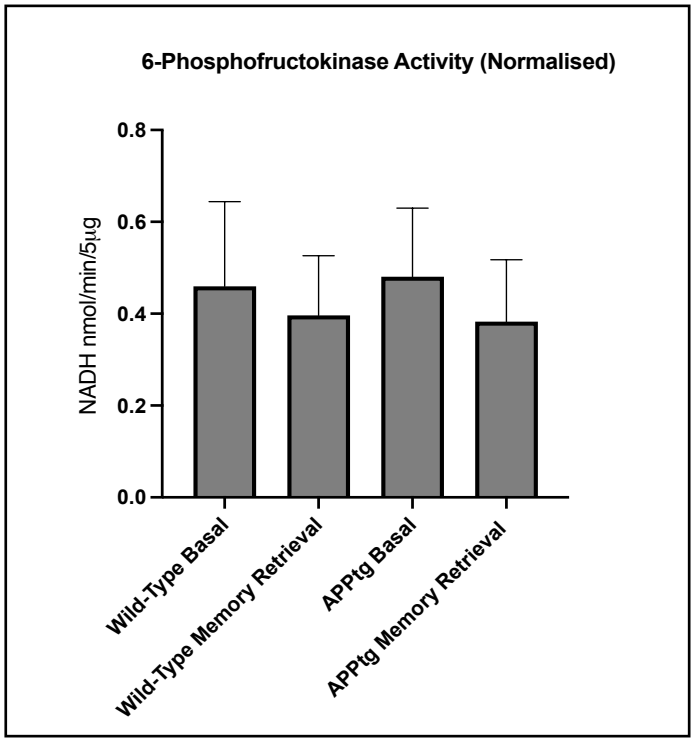

Figure 3.22. Average 6-PFK activity, normalised to western blotting results. Activity expressed as the amount of NADH produced per minute, per 5μg protein.

Appendix B, figure 3 reveals the activity of 6-PFK, expressed as the amount of PFK that would generate 1.0μmol of NADH per minute, per 5μg protein sample at pH 7.4 at 37°. This data utilised 32 samples (16 samples carried out in duplicate (8 samples from each group), 16 of the samples used by another student in the group) and was normalised against western blot data. Combined results revealed no significant difference in the 6-PFK activity between any of the groups. Two-way ANOVA was carried out on combined blot results, detailed in Appendix A, table 21. ANOVA revealed no significant interaction between genotype and behavioural group.

3.3 Assay Optimisation

A total of 12 enzymatic activity assay kits were purchased from Abcam.com (detailed in methods section), targeted to different stages of cellular respiration. All 12 assay kits were optimised, starting by following the manufacturer's instructions exactly, using 'control' samples- homogenates from wild-type littermate mice with no behavioural training (5μg protein per sample, 5μg/50μL). Synaptosome samples were previously prepared and are suspended in lysis buffer. Any tissue not prepared in lysis buffer was used for electron microscopy in previous studies and therefore, the only sample available for enzymatic analysis was the lysates. From the beginning of the study, it was known that the presence of detergent within the samples may be problematic, as certain enzymatic activity kits are not compatible with detergent and require the enzyme intact, however this is not the case will all assay kits. The purpose of this section is to describe those which did not work due to the presence of lysis buffer or limited sample volume.

One graph from one respective optimisation is included for each assay in this thesis, however, each assay was optimised >4 times, using 3 different plate readers, different temperatures, addition of shaking steps, and sample concentrations to achieve optimal results. Specificity of each assay kit was achieved through either: the addition of target enzyme-specific substrate to prepared samples (hexokinase, 6-phosphofructokinase, pyruvate kinase, aconitase, fumarase, isocitrate dehydrogenase), or the coating of microplate wells with capture antibodies specific to the target enzyme (pyruvate dehydrogenase, malate dehydrogenase 2, NADH coenzyme Q oxidoreductase, succinate dehydrogenase, cytochrome C oxidase, ATP synthase).

Table 3.1 highlights the main observations made for each individual assay, including the reasons they did or did not work. The next sections will detail the results from each assay in turn, and the different steps taken for optimisation.

Table 3.1. Enzymatic activity kits purchased from Abcam. Table details the specific justification of why assays were deemed to have worked or not worked.

Assay Kit	Function of enzyme	Result	Detail
Hexokinase	*First enzyme of glycolysis*	**Did not work**	-all samples showed very little activity -sample backgrounds showed no activity -positive controls showed negative rate of reaction
6-Phosphofructokinase	*Key regulator of glycolysis, early glycolysis enzyme*	**Worked**	-blanks, standards, positive controls, and sample backgrounds all displaying correct trends -test samples showed strong enzymatic activity
Pyruvate Kinase	*Enzyme involved in the last step of glycolysis*	**Did not work**	-negative slope of results when should be positive linearity -background samples showed no activity
Pyruvate Dehydrogenase	*Enzyme linking glycolysis and the TCA cycle*	**Did not work**	-blanks showed positive linearity -no activity in samples after normalisation against blanks
Aconitase	*Early TCA cycle enzyme*	**Did not work**	-denatured background samples showed greater activity than test samples -change in OD minute, may be plate reader drift
Isocitrate Dehydrogenase	*TCA cycle enzyme*	**Did not work**	-no activity present within samples or sample backgrounds -positive controls not producing desired rate of reaction
Fumarase	*TCA cycle enzyme*	**Did not work**	-no activity detected in test samples -activity present within background samples
Malate Dehydrogenase 2	*TCA cycle enzyme*	**Worked**	-blanks did not change over course of reaction -samples showed good enzymatic activity
NADH-Coenzyme Q Oxidoreductase	*Complex I mitochondrial electron transport chain*	**Did not work**	-no activity detected
Succinate Dehydrogenase	*Complex II mitochondrial electron transport chain/ also TCA cycle enzyme*	**Did not work**	-no activity detected
Cytochrome C Oxidase	*Complex IV mitochondrial electron transport chain*	**Did not work**	-blanks read at higher OD than any other sample -no activity detected
ATP Synthase	*Complex V mitochondrial electron transport chain*	**Did not work**	-no activity detected

3.3.1 Hexokinase

Hexokinase (HK) is an important glycolytic enzyme which catalyses the phosphorylation of glucose, the rate-limiting first step of glycolysis (Roberts & Miyamoto., 2014). The hexokinase assay works by following the conversion of glucose into glucose-6-phosphate by hexokinase after the addition of enzyme and substrate mix. Glucose-6-phosphate is then oxidised by glucose-6-phosphate dehydrogenase to form NADH, coupled to the reduction of a colourless probe to a coloured product with a strong absorbance at 450nm.

Hexokinase was optimised initially according to manufacturers instructions. The positive control in this assay kit was HK-II (one of the four HK isoforms), derived from bacillus subtilis. For this first optimisation, two standards (1nmol & 2.5nmol, the lower end of standard concentrations) were used alongside positive controls at 25µl and 50µl (mid- and highest-range). Figure 3.23 shows the course of the kinetic reaction, over a 60-minute period. Whilst the 16L practice sample showed hexokinase activity and a quick rate of reaction in the initial reaction phase, the wild-type basal (VG12) sample showed no hexokinase activity. Similarly, the background 16L and VG12 samples showed no enzymatic activity over the 60-minute period; whilst sample backgrounds have no substrate added, the endogenous substrate within the samples is expected to produce a small level of activity. Positive controls provided with the hexokinase kit are used as a benchmark sample to ensure all components of the kit are working correctly. The positive control is a purified enzyme and as such, should quickly reduce the colourless probe into a coloured product with strong absorbance at 450nm. In figure 3.23, the positive controls do not appear to have worked, instead reducing in activity in the initial reaction phase, until plateauing after 1760 seconds. Due to the absence of activity within the wild-type basal sample and respective sample background, coupled with the lack of positive control activity, this assay was deemed non-functional.

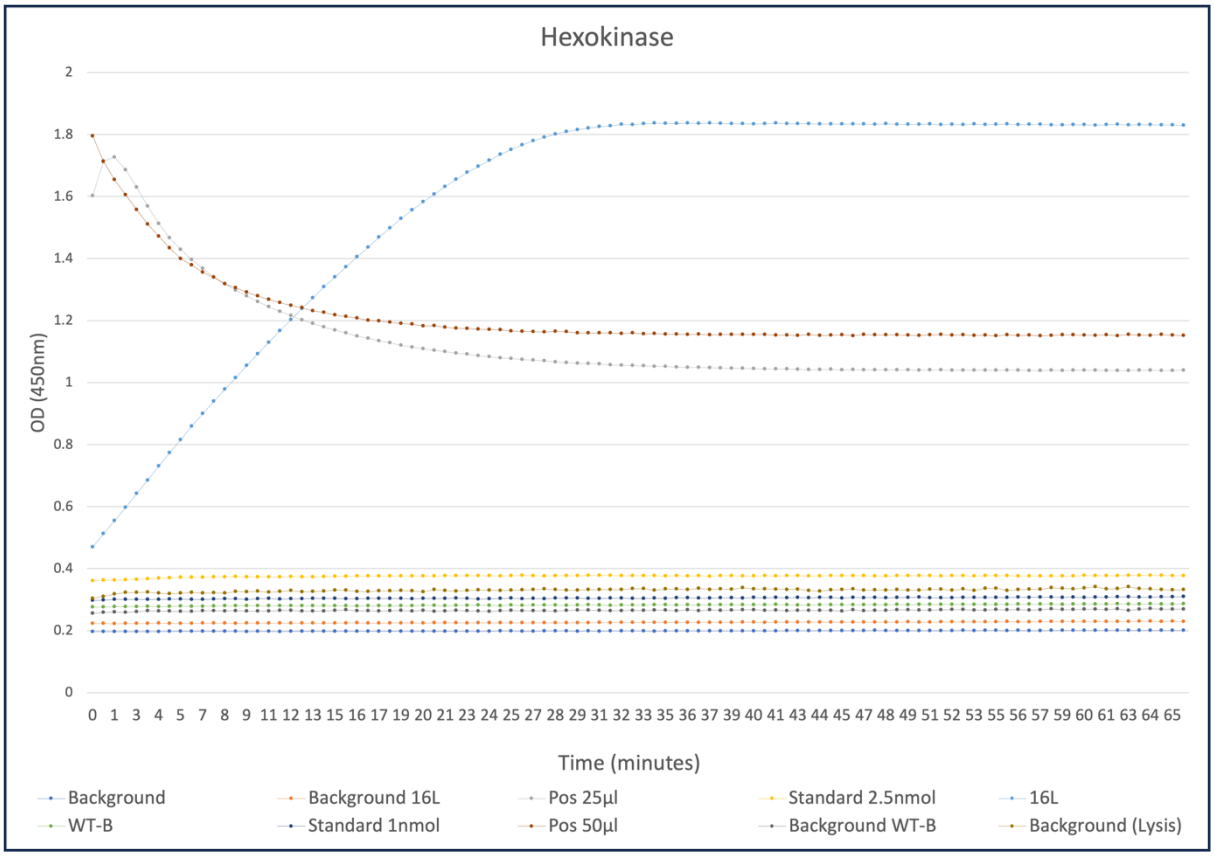

Figure 3.23. Kinetic graph showing activity of Hexokinase. Background WT-B= sample prepared without the addition of Hexokinase substrate. Background= only assay buffer. Assay carried out at 25 ℃, pH 7.4, sample conc=5µg/50µL. Assay linear for 35 minutes.

3.3.2 Pyruvate Kinase

Pyruvate kinase (PK) is one of the key enzymes of glycolysis, acting on phosphoenolpyruvate to form pyruvate. There are four PK subtypes, L,R,M1 & M2. PKM2 is mainly expressed in brain and liver tissues, where it regulates glycolysis and can be used as a switch for energy metabolism and material synthesis, routing glucose metabolism to pyruvate into the TCA cycle (Zhang, Deng & Liu., 2019). The pyruvate kinase assay works by following the generation of pyruvate and ATP, from PEP and ADP, catalysed by pyruvate kinase after the addition of enzyme and substrate mix. Pyruvate is oxidised by pyruvate oxidase to produce a coloured product with absorbance at 570nm, or fluorescence Ex/m 535/587nm. The fluorescence assay is approximately 10x more sensitive than the colorimetric assay.

As the fluorometric assay is 10x more sensitive, it was trialled for optimisation (figure 3.24). Whilst some components of the assay worked well, such as the blanks and standards, the samples tested produced negative slope of results and the sample backgrounds did not exhibit any enzymatic

activity this assay follows the production of pyruvate coupled to the reporter molecule, a positive slope of results would be expected. This assay was discontinued.

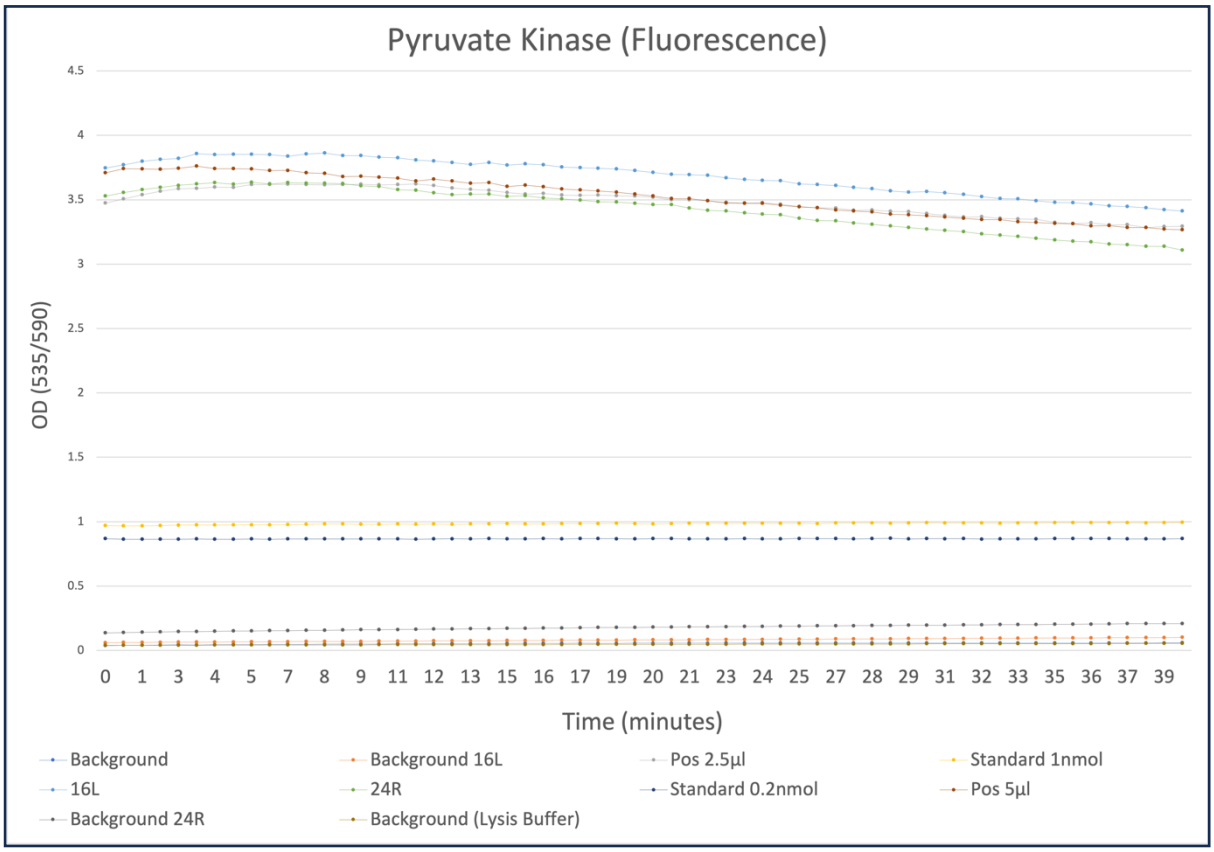

Figure 3.24. Kinetic graph showing activity of pyruvate kinase. 16L & 24R= test wild-type memory retrieval sample (total cell lysate) . Background 16L & 24R= sample without the addition of substrate. Background= assay buffer only. Assay carried out at 25℃, pH 7.4, sample conc=5µg/50µL.

3.3.3 Pyruvate Dehydrogenase

The pyruvate dehydrogenase complex (PDC) catalyses the oxidative decarboxylation of pyruvate, alongside the formation of acetyl-coA, CO_2 and NADH. The PDC links the glycolytic pathway to the oxidative pathway of the TCA cycle, occupying a key position in the oxidation of glucose. PDC acts as a gatekeeper in the maintenance of glucose homeostasis via the metabolism of pyruvate (Patel et al., 2014). The pyruvate dehydrogenase kit contains pre-coated wells with anti-PDH monoclonal antibody, which immunocaptures the PDH complex for determination of activity. PDH activity is measured by following the reduction of NAD^+ to NADH, coupled to the reduction of a reporter dye, with strong absorbance at 450nm.

Optimisation of the PDH assay began by testing one sample from each of the experimental conditions (genotype-phenotype interactions) and 4 blanks. This assay does not include a positive control or standard.

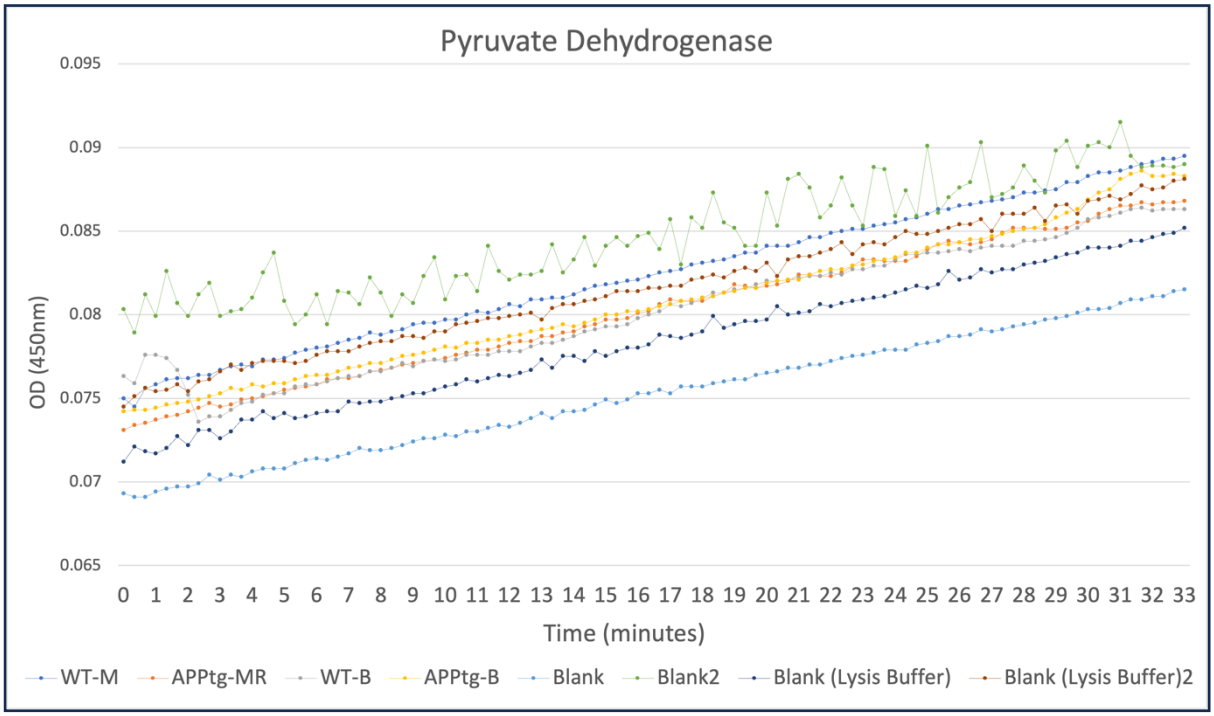

Figure 3.25. Kinetic graph showing activity of pyruvate dehydrogenase. Blank= assay buffer. Blank (lysis buffer)= blank with additional 3µl lysis buffer). Assay carried out at 25 ℃, pH 7.4, sample conc=5µg/50µL. Assay linear for 33 minutes.

Figure 3.25 reflects the enzymatic activity over a 30-minute period, as described in the manufacturers instructions. Although visually, figure 3.25 shows a steady increase in optical density over the reaction period, all samples and blanks increase at the same rate, with a final change in OD of 0.01. Such a small change is likely due to plate reader drift and cannot be interpreted as enzymatic activity. This pattern of activity was reflected over all 4 optimisation trials for PDH, and thus the assay was deemed non-functional. The pyruvate dehydrogenase assay is highly sensitive to detergent and should be repeated utilising fresh tissue homogenates from newly trained mice.

3.3.4 Aconitase

Aconitase is an enzyme involved in the regulation of cellular metabolism that catalyses the isomerisation of citrate into isocitrate via cis-aconitate intermediate. There are two isoenzymes of aconitase, mitochondrial aconitase (mAco) and cytosolic (cAco). mAco is thought to control cellular ATP production via the regulation of intermediate flow in the TCA cycle (Lushchak et al., 2014). The

aconitase assay kit follows the catalysis of the equilibrium between aconitate, cis-aconitate and iso-citrate. Activity can be measured by the increase in absorbance at 240nm, associated with the formation of isocitrate after the addition of enzyme and substrate mix into the reaction wells.

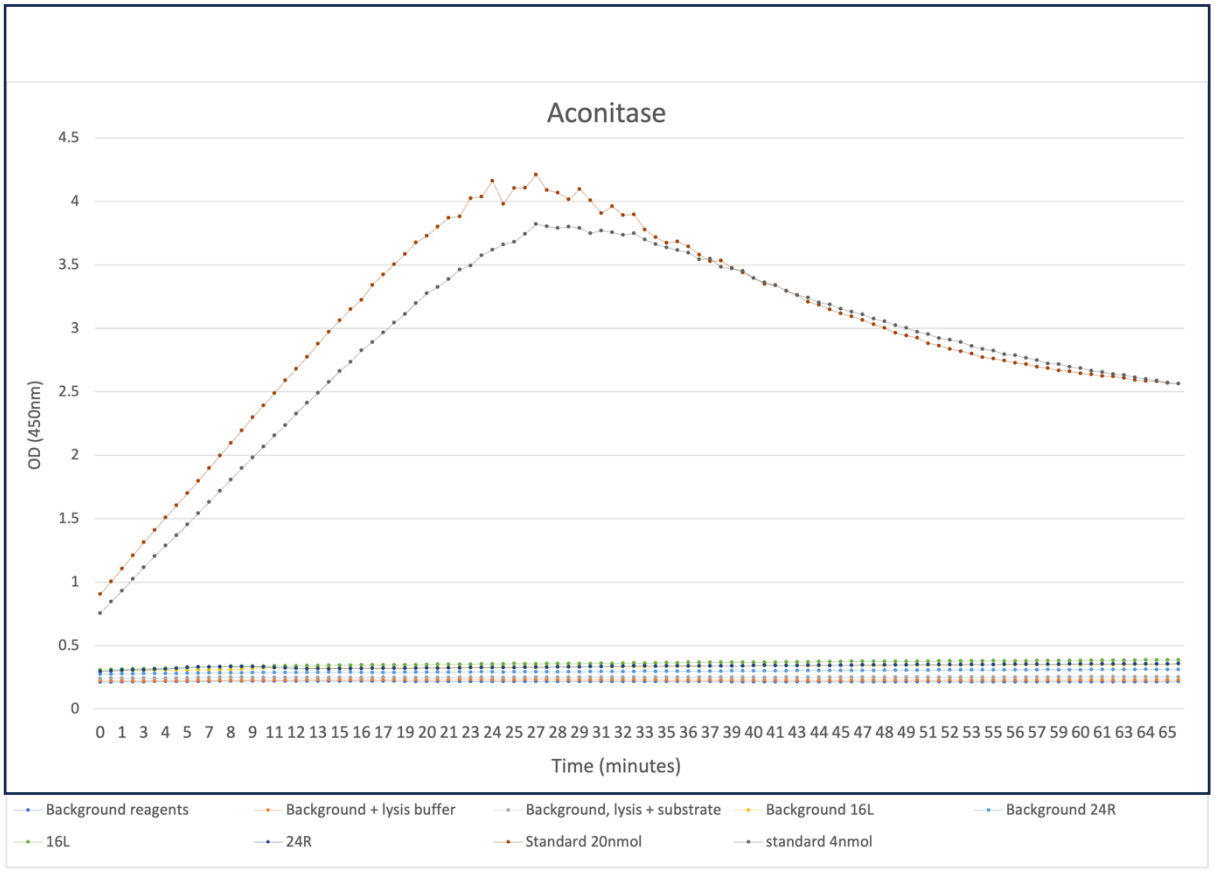

Figure 3.26. Kinetic graph showing activity of aconitase. Blank= assay buffer. Blank (lysis buffer)= blank with additional 3µl lysis buffer). Background, lysis + substrate= assay buffer blank with additional lysis buffer and substrate added. Assay carried out at 25 ℃, pH 7.4, sample conc=5µg/50µL. 16L & 24R= Wild-type memory retrieval group, total cell lysate. Assay linear for 28 minutes (standards only).

The optimisation of the aconitase assay (figure 3.26) started by first using the 16L and 24R control samples (WT memory retrieval total cell lysates) and one sample background, consisting of the control sample with no added substrate. The standards were trialled at the upper (20nmol) and lower (4nmol) limits of the suggested range and three assay blanks, consisting of assay buffer only, assay buffer with additional lysis buffer and one with assay buffer, lysis buffer and substrate mix added. The two standards produced strong positive linearity of results and a fast rate of reaction; however, the samples showed no enzymatic activity across any of the optimisation trials and thus this assay was discontinued.

3.3.5 Isocitrate Dehydrogenase

Isocitrate dehydrogenase is an enzyme that has a well-established role in the TCA cycle. The IDH3 isoform catalyses the oxidative decarboxylation of isocitrate, producing α-ketoglutarate and CO_2 while converting NAD^+ to NADH (Al-Khalla., 2017). The assay kit works by utilizing isocitrate as a specific substrate which leads to a colour change with strong absorbance at 450nm. The isocitrate dehydrogenase assay is carried out at 37°C, over a 30 minute to 2-hour period.

Before optimising the assay, three different types of 96-well plate were trialled to compare effects on assay results. The three plates available were clear, flat bottomed 96-well plates (figure 3.27 A), rounded bottom 96-well plates (figure 3.27 C) and opaque yellow 96-well plates (figure 3.27 B). The isocitrate dehydrogenase assay requires the generation of an NADH standard curve, complete with the addition of 'reaction mix' containing a developer solution. Standards were tested with the addition of developer and without to determine the effects, as manufacturer's instructions did not specify. Figure 3.27 presents the data gained from each of the different plates and developer combinations.

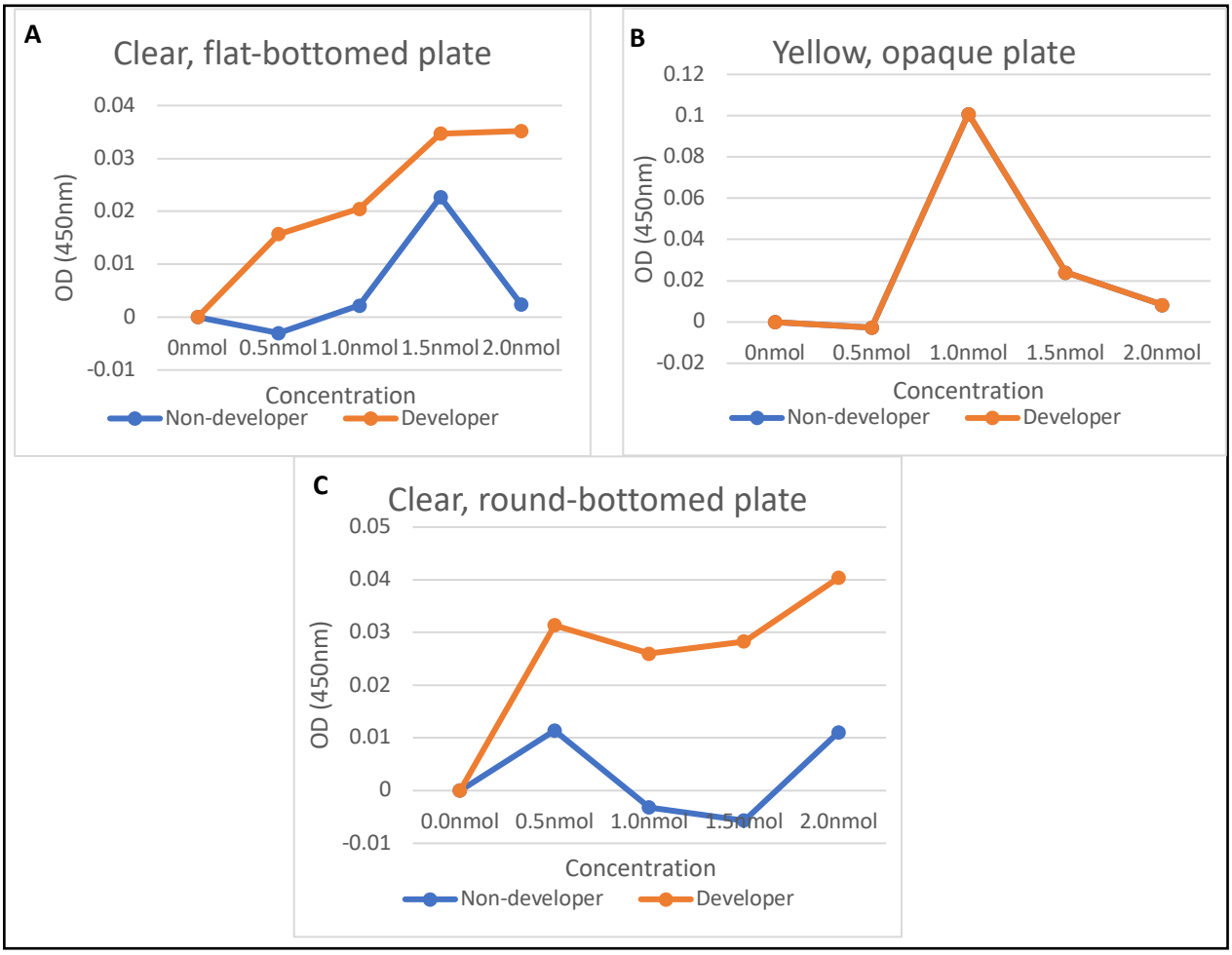

Figure 3.27. Trailing different 96-well plates using NADH standards. Non developer= NADH standard alone, diluted with assay buffer. Developer= NADH standard with additional developer solution. B) non-developer and developer gained the same results exactly and; therefore, results overlap on the graph. Assay carried out at 37℃, pH 7.4.

It was determined from the results shown in figure 3.27A that the clear flat-bottomed 96 well plate with the addition of developer produced the best linearity of results and thus this combination was continued for the assay optimisation. Following manufacturers recommendations, a 2µl and 5µl positive control was used, alongside two control samples with no behavioural training, 1 standard, and a combination of background controls. As samples require the addition of 'reaction mix' for this assay, background controls had reaction mix added.

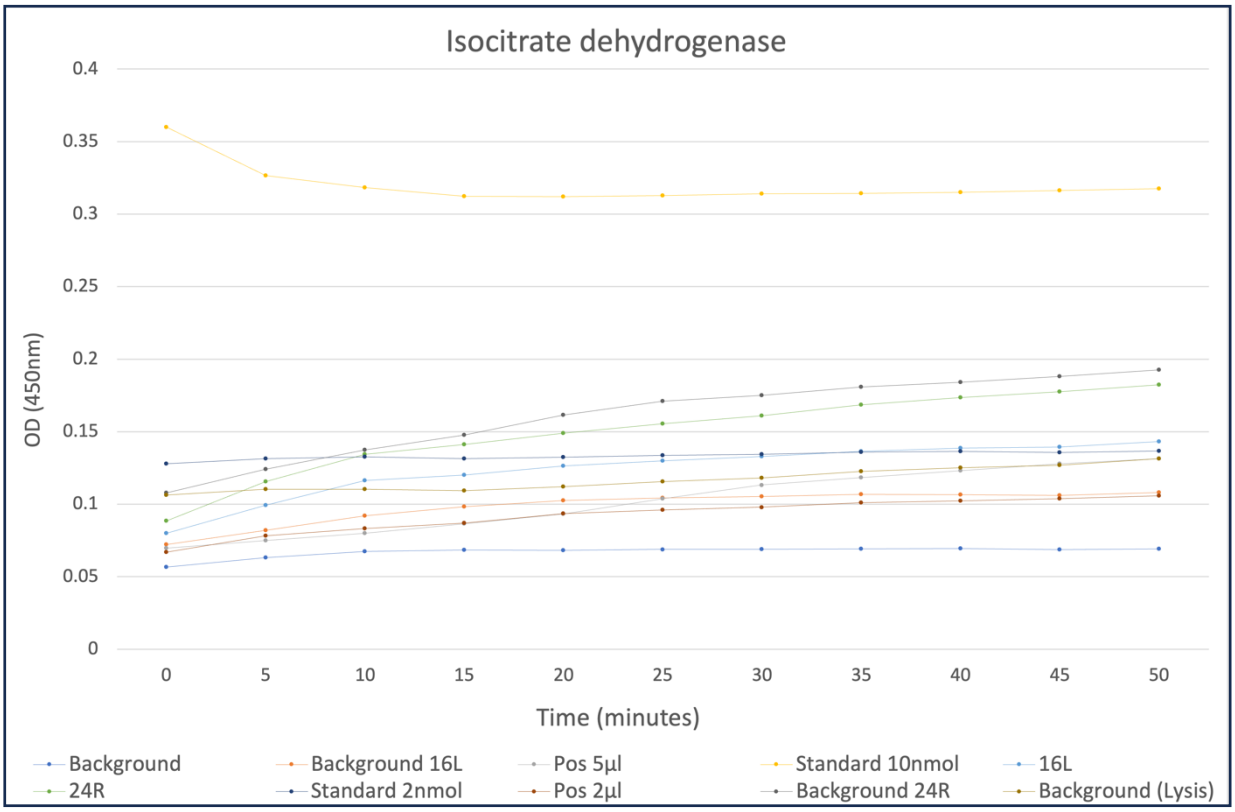

Figure 3.28. Kinetic graph showing activity of isocitrate dehydrogenase. Sample backgrounds= samples with no added substrate mix. Blank= assay buffer. Blank (lysis buffer)= blank with additional 3µl lysis buffer). Assay carried out at 37℃, pH 7.4, sample conc=5µg/50µL. 16L & 24R= Wild-type memory retrieval group, total cell lysate.

The results shown in figure 3.28 reflect the non-functionality of this assay kit. After four separate optimisation runs, there was no detectable isocitrate dehydrogenase activity within any of the biological samples tested, no matter which 96-well plate was used. All sample backgrounds possessed the same levels of activity as the test samples, with an increase of only 0.025OD over the course of the reaction. This assay was deemed non-functional and not continued to the comparative tests.

3.3.6 Fumarase

Fumarase (fumarate hydratase (FH)) is an enzyme found in the cytoplasm and in the mitochondria which catalyses the reversible hydration and dehydration of fumarate into malate. FH is involved in the generation of ATP for the cell via the TCA cycle (Yogev et al., 2010). The FH assay works by following the production of malate, which reacts with the enzyme mix to form an intermediate which reduced the developer to form a coloured product with strong absorbance at 450nm.

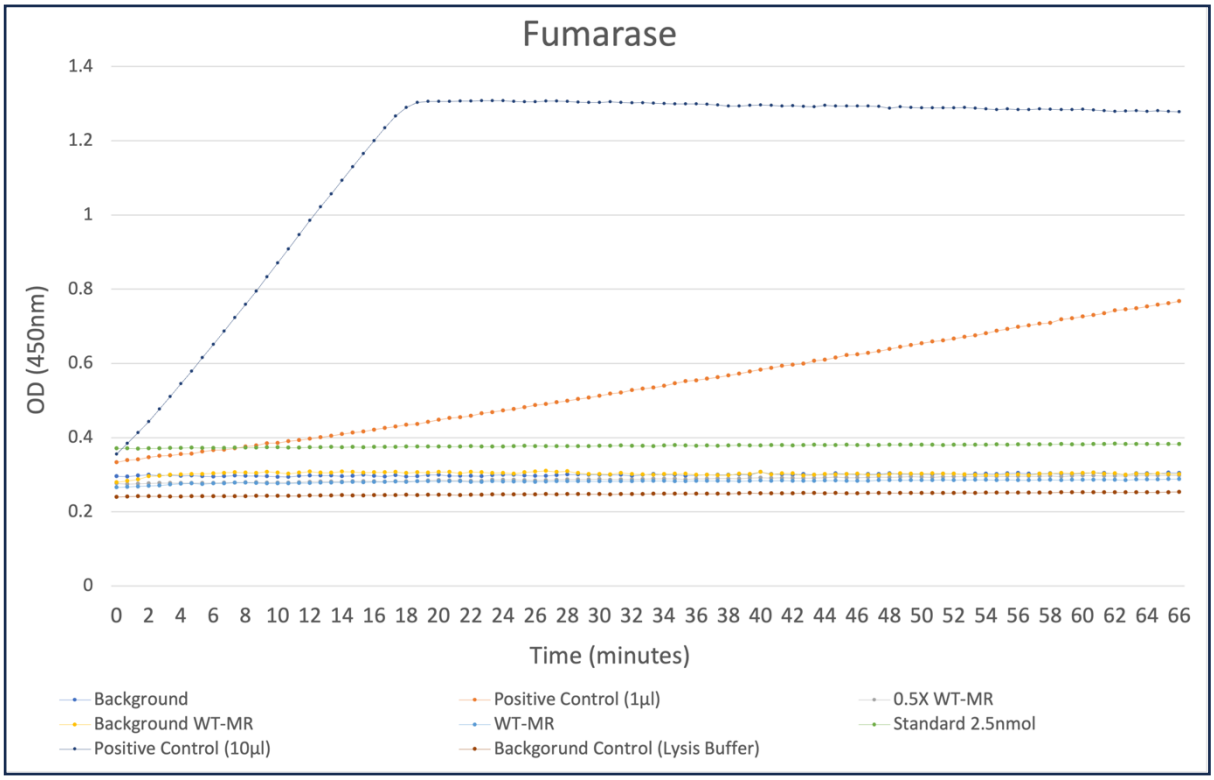

Figure 3.29. Kinetic graph showing activity of fumarase. VG4= wild-type memory retrieval. 0.5x VG4= 0.5x volume. Background control= assay buffer only. Background control (lysis buffer)= assay buffer with additional lysis buffer. Background control (sample)= biological sample without the addition of substrate mix. Assay carried out at 25℃, pH 7.4, with sample conc=5µg/50µL or sample conc=2.5µg/50µL. (0.5 X Vg4). Assay linear for 66 minutes (positive control-1µl).

Fumarase assay was optimised for factors including optimal sample concentration, optimal positive control volume, standard concentration, and background control reagents. Figure 3.29 depicts the reaction progress over a 60-minute period. Both positive controls can be seen to exhibit fast rates of reaction and sharp increases in OD, however, the samples and sample backgrounds do not exhibit the same pattern. Whilst there appears to be no enzymatic activity present within the samples, the results from the blanks and positive controls show that the assay kit is functional, although not compatible with the current sample preparation method. This assay would need to be repeated with fresh tissue homogenates, prepared according to the manufacturer's guidance.

3.3.7 NADH-Coenzyme Q Oxidoreductase

NADH-Coenzyme Q Oxidoreductase (complex 1) is the largest of the energy converting enzyme complexes of the mitochondrial respiratory chain (Ohnishi, Shinzawa-Ito & Yoshikawa., 2008). Complex 1 uses two electrons to convert ubiquinone to ubiquinol by oxidising NADH produced by the TCA cycle in the mitochondrial matrix (Sharma, Lu & Bai., 2009). The complex 1 activity kit works by following the oxidation of NADH to NAD^+, coupled to the reduction of a reporter dye with strong absorbance at 450nm. Capture antibodies for complex 1 are pre-coated in the wells, which capture target from samples. After target is captured, the activity of the enzyme can be accurately measured.

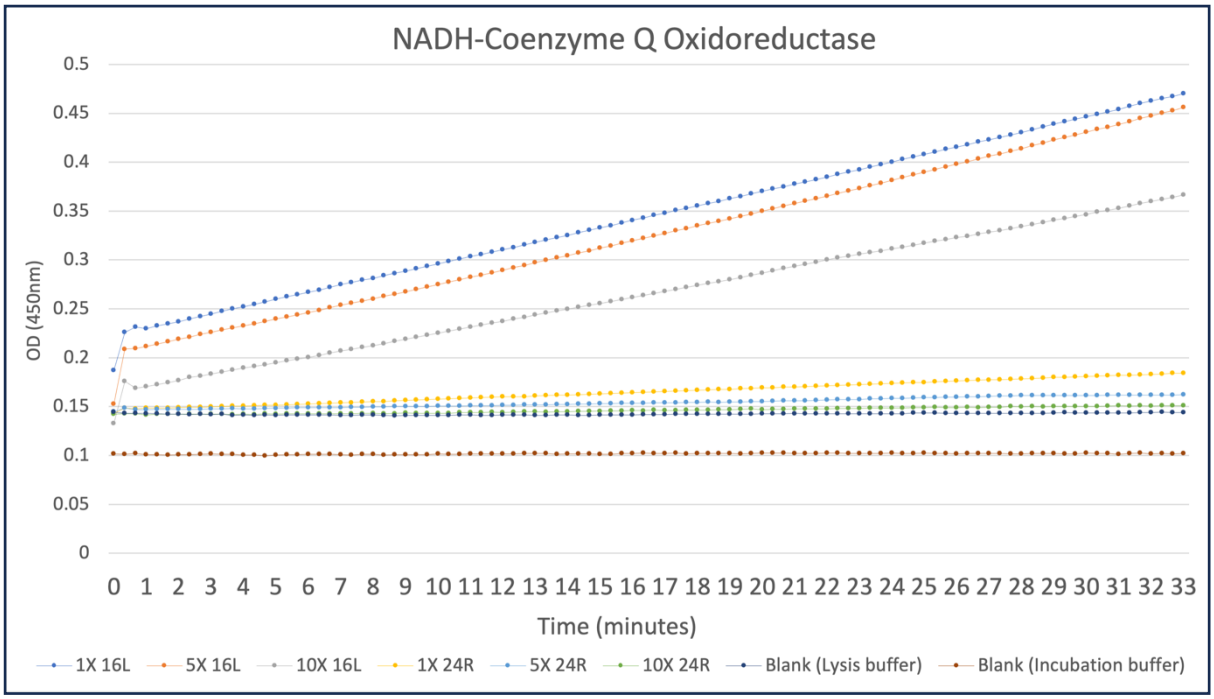

Figure 3.30. Kinetic graph showing activity of complex 1. Blank= incubation buffer only. Blank+ lysis buffer= incubation buffer with additional lysis buffer. 5x 16L= 5x volume of 1x 16L sample. 10x 16L= 10x volume of 1x 16L sample. Assay carried out at 25℃, pH 7.4, with 5μg, 25μg or 50μg protein per 50μL sample. 16L & 24R= Wild-type memory retrieval group, total cell lysate. Assay linear for 33 minutes.

This optimisation aimed to determine the optimal sample volume for greatest complex 1 activity, whilst also assessing how the addition of lysis buffer affected the incubation buffer blank. As all samples are prepared in lysis buffer, it is important to note any differences that may result from its presence. Results from the assay show that across all volumes of 16L and 24R, there are strong levels of complex 1 activity. Samples with the highest volumes, and therefore the highest amount of lysis buffer, produced the lowest changes in optical density and the lowest rates of activity. As the lysis buffer can be seen to negatively impact the complex 1 activity, only samples at 1x volume use for

western blotting (1-3µl) were continued. Although from figure 3.30 it would seem the assay had worked, it was later determined to be non-functional. The samples used for this trial were non-behaviourally trained control mice only and when repeated with experimental samples from each genotype-phenotype combination, there was no detectable complex 1 activity over the course of the reaction.

3.3.8 Succinate Dehydrogenase

The succinate dehydrogenase complex catalyses the oxidation of succinate to fumarate in the TCA cycle and feeds electrons from succinate to ubiquinone in the respiratory chain (Rustin, Munnich & Rötig., 2002). The succinate dehydrogenase activity kit works by following the production of ubiquinol coupled to the reduction of a reporter dye with a reduction in absorbance at 600nm. The microplate wells are coated with an anti-complex II monoclonal antibody which purifies enzyme, ready for reaction monitoring.

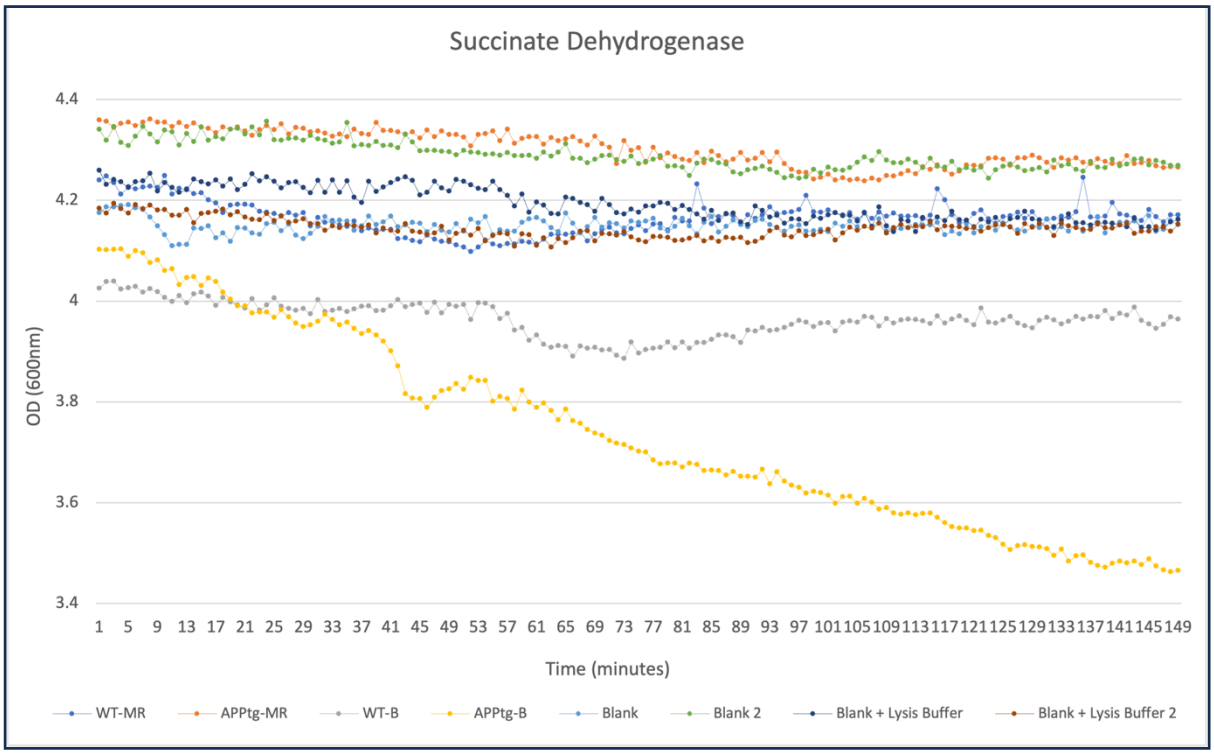

Figure 3.31. Kinetic graph showing activity of complex II. Blank= assay buffer only. Blank+ lysis buffer= assay buffer with additional lysis buffer. Assay carried out at 25℃, pH 7.4, sample conc=5µg/50µL. Assay linear for 149 minutes.

Figure 3.31 shows that up to 880 seconds, all samples produced a decrease in absorbance over time, reflective of complex II activity. Both blanks produced no activity over the course of the reaction. However, after further optimisation attempts for this assay, the same trends could not be replicated

with larger groups of test samples (from each experimental condition), instead gaining positive linearity of results and therefore, this assay was deemed non-functional.

3.3.9 Cytochrome C Oxidase

Cytochrome C oxidase (CcO) is the terminal OXPHOS complex in mitochondria. CcO links the conversion of molecular oxygen to water, the reduction of electron carriers during metabolism, and the translocation of protons into the intermembrane space (Watson & McStay., 2020).

The CcO assay kit works by following the oxidation of reduced cytochrome C by the change in absorbance at 550nm. The wells of the microplate are coated with monoclonal antibody, specific to the enzyme.

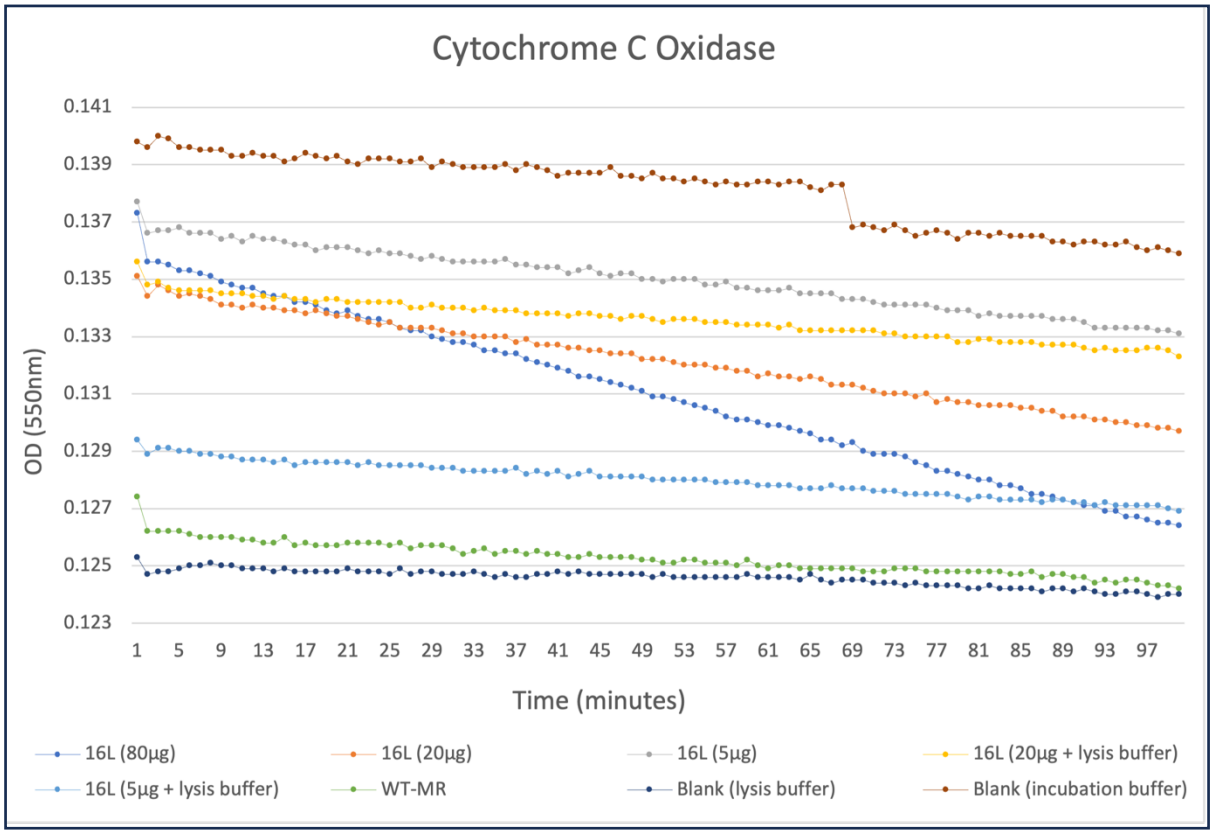

Figure 3.32. Kinetic graph showing activity of complex IV. 16L= wild-type memory retrieval group, total cell lysate. Blank= incubation buffer only. Blank+ lysis buffer= incubation buffer with additional lysis buffer. Assay carried out at 25℃, pH 7.4, with 5µg, 20µg or 80µg protein per 50µL. Assay linear for 97 minutes.

Figure 3.32 depicts the third optimisation trial for complex IV, which tested different 16L sample concentrations ranging from 5-80µg. The results from this assay confirmed that the assay kit was non-functional. Over the 2-hour reaction period, the largest change in OD (16L 80µg) was 0.009,

reflecting minimal enzymatic activity and likely due to plate reader drift. This assay may be notably sensitive to specific methods of sample preparation, favouring fresh homogenates.

3.3.10 ATP Synthase

The last assay to be optimised was ATP synthase, the fifth OXPHOS complex, which synthesises ATP from ADP and inorganic phosphate in the mitochondrial matrix, using energy derived from the proton gradient (Jonckheere, Smeitink & Rodenburg., 2012). The ATP synthase assay kit works by following the production of ADP which is coupled to the oxidation of NADH to NAD^+, detected as a decrease in absorbance at 340nm. ATP synthase is immunocaptured within the microplate wells and its activity can then be precisely measured.

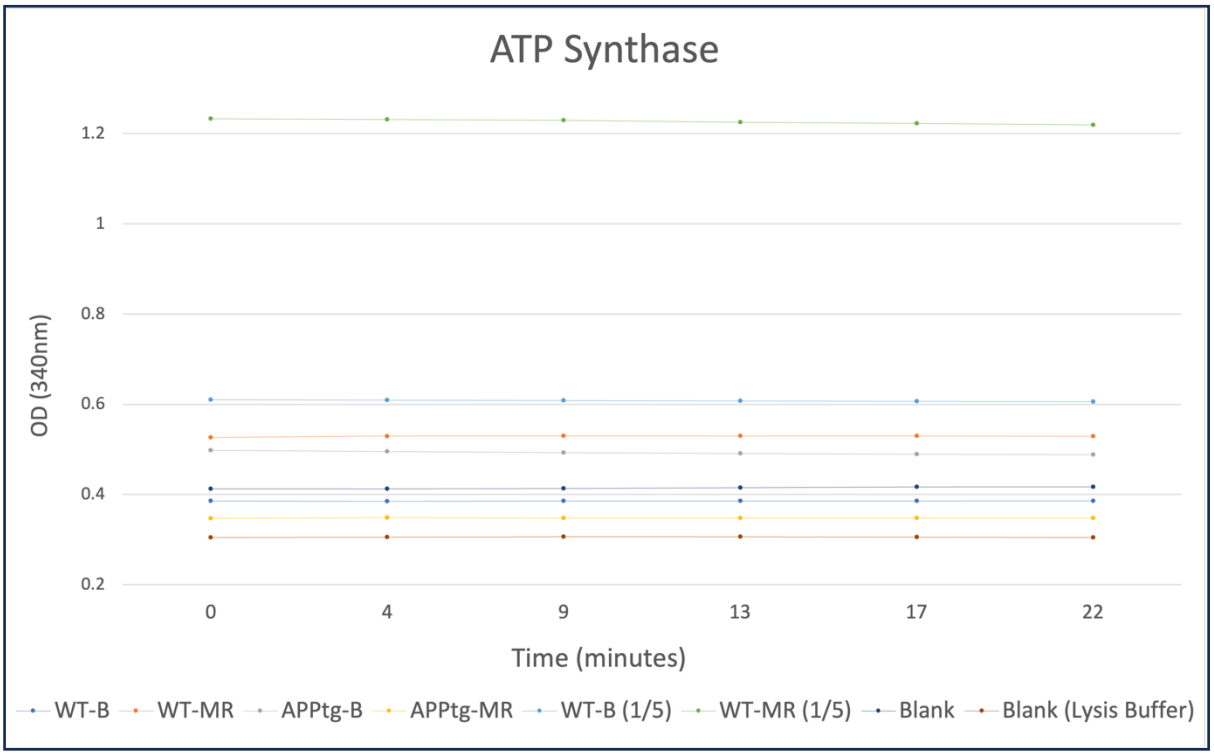

Figure 3.33 . Kinetic graph showing activity of complex V. WT-B (1/5)= 1/5th volume of standard 5μg WT-B (=1μg). Blank= assay buffer only. Blank+ lysis buffer=assay buffer with additional lysis buffer. Assay carried out at 25 ℃, pH 7.4, with 1μg or 5μg per 50μL.

Figure 3.33 depicts the second attempt at optimising the ATP synthase assay, trialling samples from each experimental condition, at different concentrations. Similar to the first attempt, no activity was present over the 20-minute reaction period. The ATP synthase assay was designed for use with purified mitochondria, noting that homogenised tissue may also be used but specific activity may be

lower. Due to unavailability of fresh tissue homogenates and resulting lack of detected ATP synthase activity, this assay was disregarded for the comparative experiments.

Table 3.1 provides a brief summary of all 12 enzymatic activity assay kits purchased from Abcam and the final outcome for each kit, whereas table 3.2, below, details the different variables tested during optimisation for each assay.

Table 3.2. Summary of enzymatic activity assay kits purchased from Abcam, the outcome of each assay and some of the variables tested in the initial optimisation period.

Assay Kit	Subcellular location	Justification	Variables tested
Hexokinase (measures total hexokinase- HKI, HKII, HKIII, HKIV)	· HK1- all mammalian tissues · HK2- OMM and cytoplasmic compartments, muscle, heart · HK3- lung, kidney, liver · HK4- certain neuroendocrine cells	Glycolysis	· Plate reader · Sample concentration · Amount of positive control · Standard concentration · Addition of lysis buffer
6-Phosphofructokinase	Cytoplasm	Glycolysis	· Plate reader · Temperature (37°C) · Sample concentration · Positive control amount · Standard concentration · Addition of lysis buffer
Pyruvate Kinase	Cytoplasm	Glycolysis	· Plate reader · Sample concentration · Addition of lysis buffer · Amount of positive control · Standard concentration · Colourimetric/fluorometric
Pyruvate Dehydrogenase	Mitochondrial matrix	Links glycolysis and TCA cycle	· Plate reader · Sample concentration · Addition of lysis buffer
Aconitase	m-type- Mitochondrion	TCA cycle	· Plate reader · Sample concentration · Addition of lysis buffer · Single measurement/kinetic measurements
Fumarase	Mitochondrion & cytosol	TCA cycle	· Plate reader · Amount of positive control · Standard concentration · Sample concentration · Addition of lysis buffer
Isocitrate Dehydrogenase	IDH2- IMM	TCA cycle enzyme	· Plate reader · Temperature (37°C) · Amount of positive control · Standard concentration · Addition of lysis buffer · Different types of 96 well plates (round or flat, clear, or translucent)
Malate Dehydrogenase 2	MDH2- mitochondrial matrix	TCA cycle	· Plate reader · Sample concentration · Addition of lysis buffer

NADH-Coenzyme Q Oxidoreductase	IMM	ETC complex I	· Plate reader · Sample concentration · Addition of lysis buffer
Succinate Dehydrogenase	IMM, matrix side	ETC complex II	· Plate reader · Addition of lysis buffer ·
Cytochrome C Oxidase	IMM	ETC complex IV	· Plate reader · Sample concentration · Lysis buffer volume · Length of assay · Inter-reading interval
ATP synthase	IMM	ETC complex V	· Plate reader · Sample concentration · Addition of lysis buffer · Inter-reading interval and overall reaction time

3.4 Analysis of Mitochondrial Metabolites

Ideally, the quantification of metabolites would require unprocessed brain tissue to allow for sample preparation methods, compatible with the instrument of analysis. However, within this project, it has not been possible to utilise fresh tissue, as all remaining tissue from both hemispheres of each mouse has been used for other purposes, such as western blotting. The premise of these experiments was to attempt the analysis in the hopes that sample preparation may not have a substantial impact on the compatibility of the methods used for metabolite detection, even with the knowledge that it may not be feasible due to limited sample volume and sample preparation methods. Due to these factors, no conclusive comparative result were obtained, however, the presentation of these results may go some way to developing a future method of analysing samples prepared in such fashion.

Significant progress was made in the optimisation of each instrument to the different metabolite standards chosen and the development of a UPLC-MS method for future continuation of the project. As analysis of mitochondrial metabolites in brain tissue homogenates of mice with preclinical FAD

has not been carried out previously, this method is novel and can be continued to determine changes in metabolite levels between cognitively normal WT mice and APPtg mice.

3.4.1 Standards

Chromatograms from GC-MS analysis of citric acid showed a good base peak at the correct molecular weight (MW; see figure 3.34, however, for succinic acid, a peak was detected at an incorrect MW. In both chromatograms, no presence of derivatising agent was detected, confirming the derivatisation method was inappropriate for the standards used.

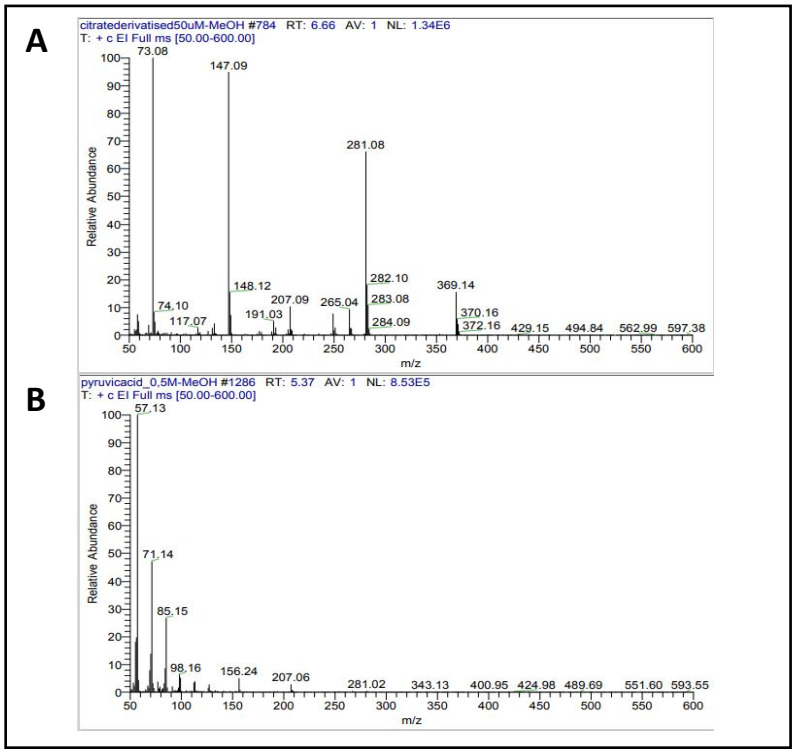

Figure 3.34. Mass spectra of derivatised citric acid and pyruvic acid.

Standards were run through UPLC-MS at three different cone voltages (60v,70v,80v) to determine optimum voltage and retention times for each metabolite. Table 3.3 details the results from the optimisation of each metabolite standard, including the retention time and observed peak parameters. These parameters can be used in the future for further analysis.

Table 3.3. Table of optimum parameters for each metabolite standard.

Metabolite	Optimum cone voltage	Observed Peak m/z	Retention time (mins)

Pyruvic acid	70v	88.2	6.36
L-(+)-Lactic acid	60v	91	11.48
Citric acid	70v	193	8.34
***Cis*-Aconitic acid**	60v	175.2	4.76
α-ketoglutaric acid	80v	147.1	4.01
Succinic acid	80v	119.2	6.91
Fumaric acid	80v	117.5	5.74
L-(-)-Malic acid	80v	135.1	12.87

Standard curves were generated for each metabolite standard, at 1M, 1mM, 1µM and 1nM, however, due to software constraints, the resulting curves could not be exported for presentation.

Although brief, the results presented from the analysis of mitochondrial metabolites within lysed brain tissue homogenates is novel and allows for the further development of an experimental method compatible with this type of biological sample and sample preparation method.

CHAPTER 4- PROTEOMICS RESULTS

The general approach for untargeted, exploratory proteomics analysis is to apply unbiased statistical filters to the whole proteomic dataset and corroborate the results and pathways discovered in one database with many other databases to remove database selection bias. Higher confidence results can be gained using multiple independent parameters, so long as the same pathway is identified by each one. All outputs of proteomics results are placed in the appendix, including interesting results that did not meet statistical significance but might still be important to note. In this case, the reader can come to their own conclusions, although it may be more important to focus on the general patterns as a whole, rather than focussing on each individual result.

As the proteomic analysis has been carried out using two separate methods (FDR correction & application of t-tests relative to threshold), the result will be split into two sections; firstly, FDR corrected results, and secondly, the 20% regulation threshold results.

4.1 Key Markers

The raw LFQ intensity values gained from sample mass-spectrometry were used to plot bar graphs of the levels of key synaptic and mitochondrial proteins. The values were used before the application of FDR correction or the 20% regulation threshold. The average LFQ intensity value for each experimental group is presented. For enzyme complexes with multiple detected subunits, e.g. 12 different subunits of ETC complex I, the average of all of the subunits was used as the overall value, calculated for each experimental condition.

Figure 4.1 represents the average LFQ intensities for proteins targeted in western blot analysis in each experimental group. SDHA showed the same expression pattern in both genotypes, with highest levels in the basal group. WT mice had the greatest difference between behavioural groups, whereas in transgenic mice, the difference was minimal. The expression patterns of alpha synuclein were also the same in each genotype (greater expression in the memory groups) however, the difference between behavioural groups was much bigger in the WT mice, where the expression in WT memory was much larger than WT basal. Expression of ATP5A was very similar in APPtg mice at the basal level, when compared to during memory retrieval, however, in the WT mice, expression was much greater at the basal level than during memory retrieval. VDAC1 expression also was very similar between the two behavioural groups in the transgenic mice, whereas WT mice showed greater expression during memory retrieval. The expression pattern of COX4 was the same across both genotypes. Expression of 6-PFK revealed an interesting pattern; WT mice showed greater overall expression across both behavioural groups (higher expression at the basal level), however the expression pattern between behavioural groups was reversed in the transgenic mice (greater expression during memory retrieval). The expression pattern of MDH2 was consistent across genotypes (higher expression during memory retrieval), however, overall expression was higher in the transgenic mice.

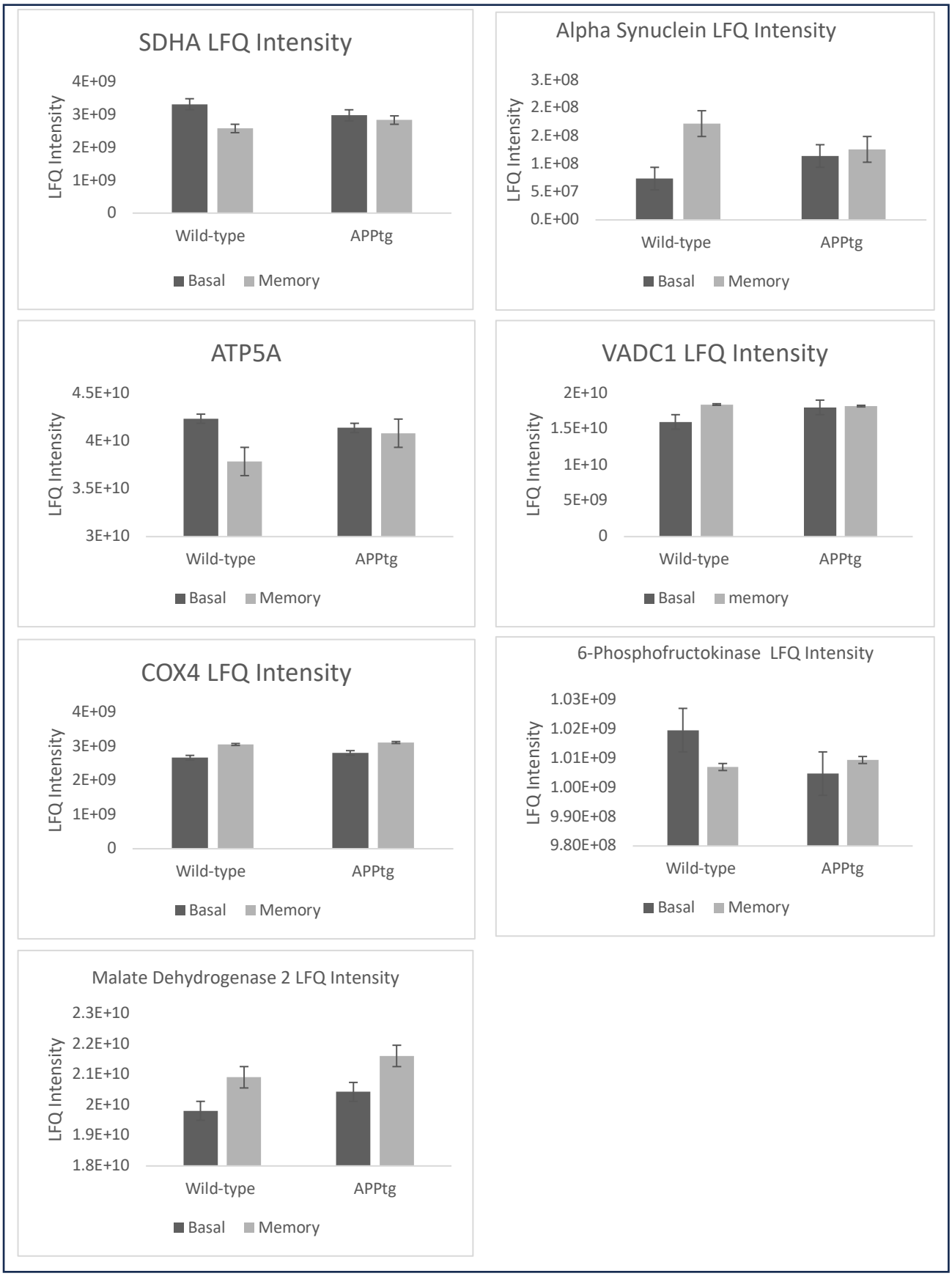

Figure 4.1. Raw LFQ (label-free quantitation) intensities for proteins targeted in western blot analysis. LFQ intensity shown for each of the experimental groups. Each group has 4 biological replicates.

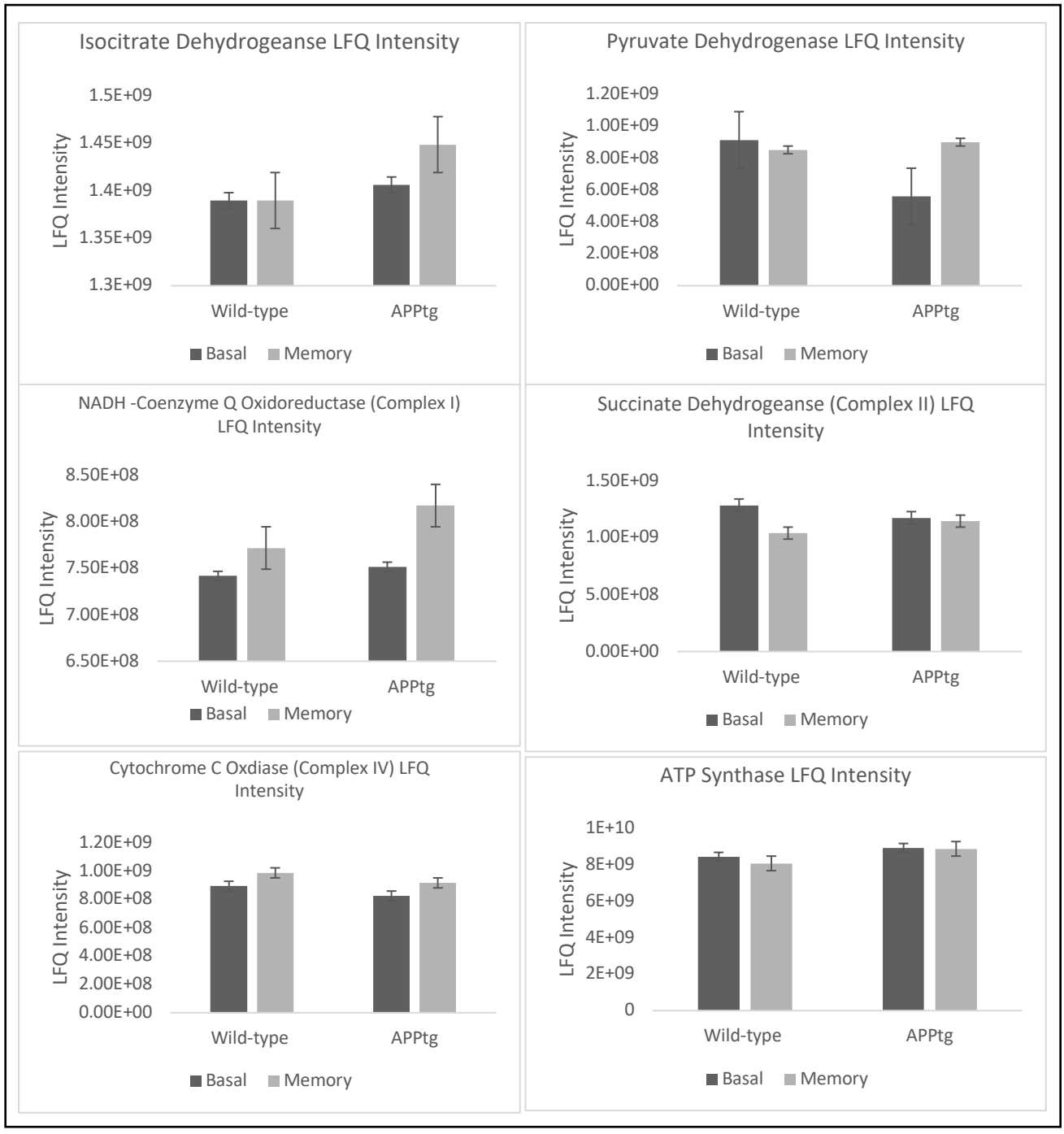

Figure 4.2. LFQ (label-free quantitation) values for enzymes used for enzymatic activity assays. LFQ intensity shown for each experimental group. Each group has 4 biological replicates.

Figure 4.2 displays the average LFQ intensities of enzymes also used for enzymatic activity assay, per experimental group. The expression of isocitrate dehydrogenase was consistent in WT mice across behavioural groups, however, in the transgenic mice, the expression showed an entirely different pattern; overall expression was much higher than in the WT mice and expression during memory retrieval was greater than during basal levels. Expression of pyruvate dehydrogenase was greater in

the WT mice overall, with little difference between the two behavioural groups. In the transgenic mice, expression was much higher in the memory group than during basal levels. Expression of complex I showed the same patterns across the two genotypes, with higher expression in the memory retrieval groups. The greatest expression was in transgenic mice during memory retrieval. Expression of complex II was consistent across behavioural groups in the transgenic mice, however, in the WT mice, expression was highest at the basal level. Complex IV expression pattern was the same across genotypes, however, the WT mice had an overall higher expression than the transgenic mice. Expression of ATP synthase was much lower in the WT mice than the transgenic mice, whose expression was consistent across behavioural groups. Figure 4.3 depicts the average LFQ intensity across experimental groups for the remaining 4 enzymes. Hexokinase expression patterns were the same across genotypes, with higher expression during basal levels. The expression of pyruvate kinase is consistent across behavioural groups in transgenic mice, however in WT mice, there is a higher expression at the basal level, when compared to during memory retrieval. The expression pattern of fumarase was the same across genotypes, however, the expression in WT mice at the basal level was considerably higher than any other genotype and behavioural group combination. The last enzyme analysed was aconitase, whose expression levels were consistent across all genotype and behavioural groups.

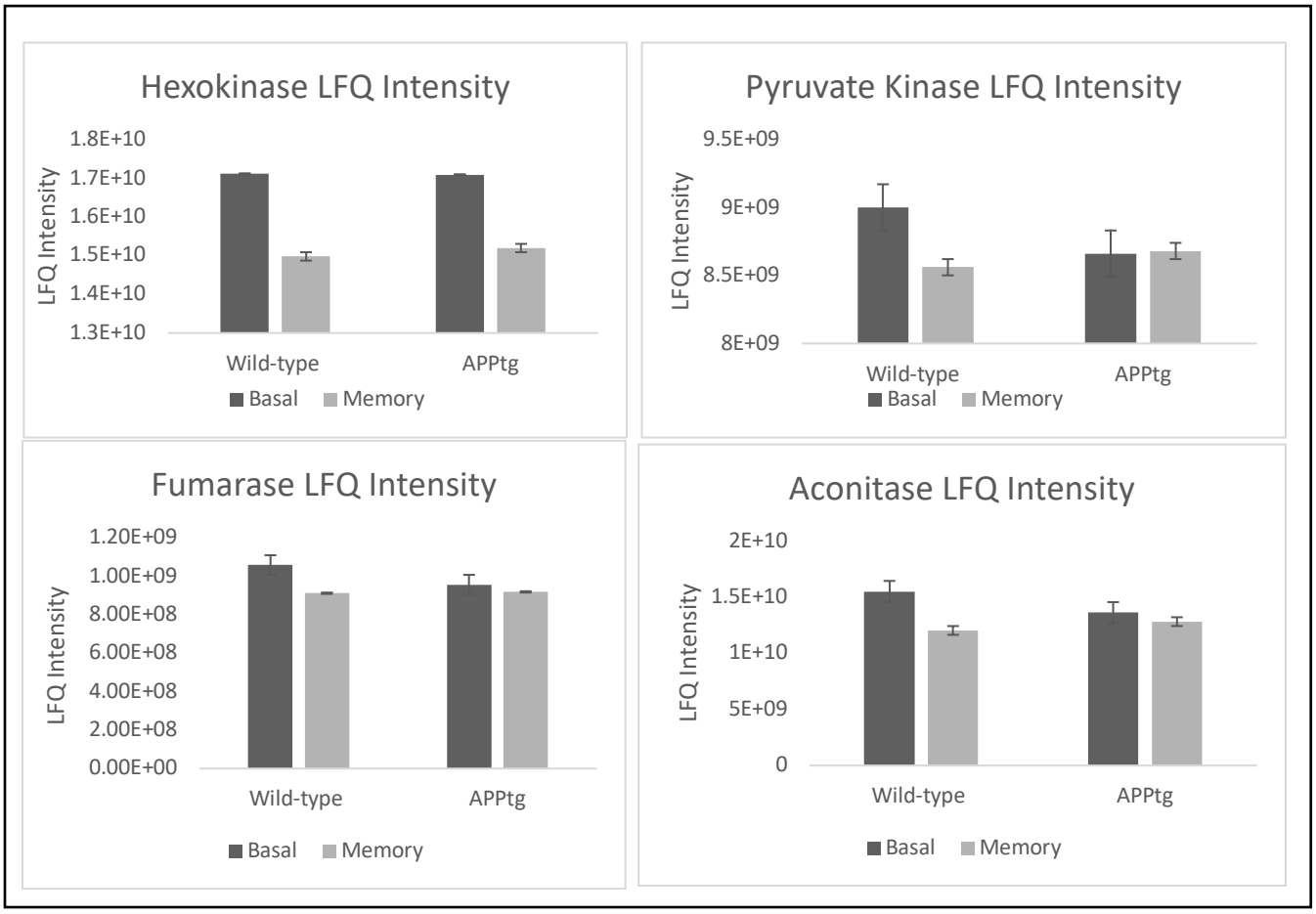

Figure 4.3. LFQ values for enzymes used for enzymatic activity assays. LFQ intensity shown for each experimental group. Each group has 4 biological replicates.

4.2 FDR Corrected results

After the application of FDR correction to the whole set of stage 1 proteins from each experimental group (following method detailed by Lee & Lee., 2018), proteins that returned a statistically significant result were further separated into up- and down-regulated groups, based on percentage fold change (table 4.1). Whilst the number of total stage 1 proteins were very similar between groups, the number of significant adjusted p-values were strikingly different between groups. WT mice (group A) had 40 significant protein regulations, 30 of which were upregulated and 10 of which were downregulated. In the APPtg mice on the other hand, none of the protein regulations were significant after FDR application (group C). When comparing APPtg mice at the point of memory retrieval against their WT counterparts (group B), none of the protein regulations were significant after FDR correction. However, when comparing APPtg mice at basal levels with WT mice (group D), 83 statistically significant protein regulations were identified, 47 of which were upregulations and 36 of which were downregulations.

Table 4.1. Table showing the numbers of differentially regulated proteins in each experimental group. Total proteins equals the number of proteins remaining after stage 1 analysis (e.g. removal of proteins with more than one missing value) but before the application of FDR. Total significant proteins equals the number of stage 1 proteins that returned a statistically significant result after FDR correction.

Group	Total Significant Proteins	Significantly Upregulated	Significantly Downregulated	Total Proteins
A- WT Basal v. WT Memory	40	30	10	1454
B- WT Memory v. APPtg Memory	0	0	0	1481
C- APPtg Basal v. APPtg Memory	0	0	0	1497
D- WT Basal v. APPtg Basal	83	47	36	1354

To quickly visualise proteins with large fold changes and statistical significance against the whole dataset analysed, volcano plots were created using GraphPad Prism (https://www.graphpad.com/). Figure 4.4 represents the magnitude of fold change, and whether statistical significance was reached for each protein within each experimental group.

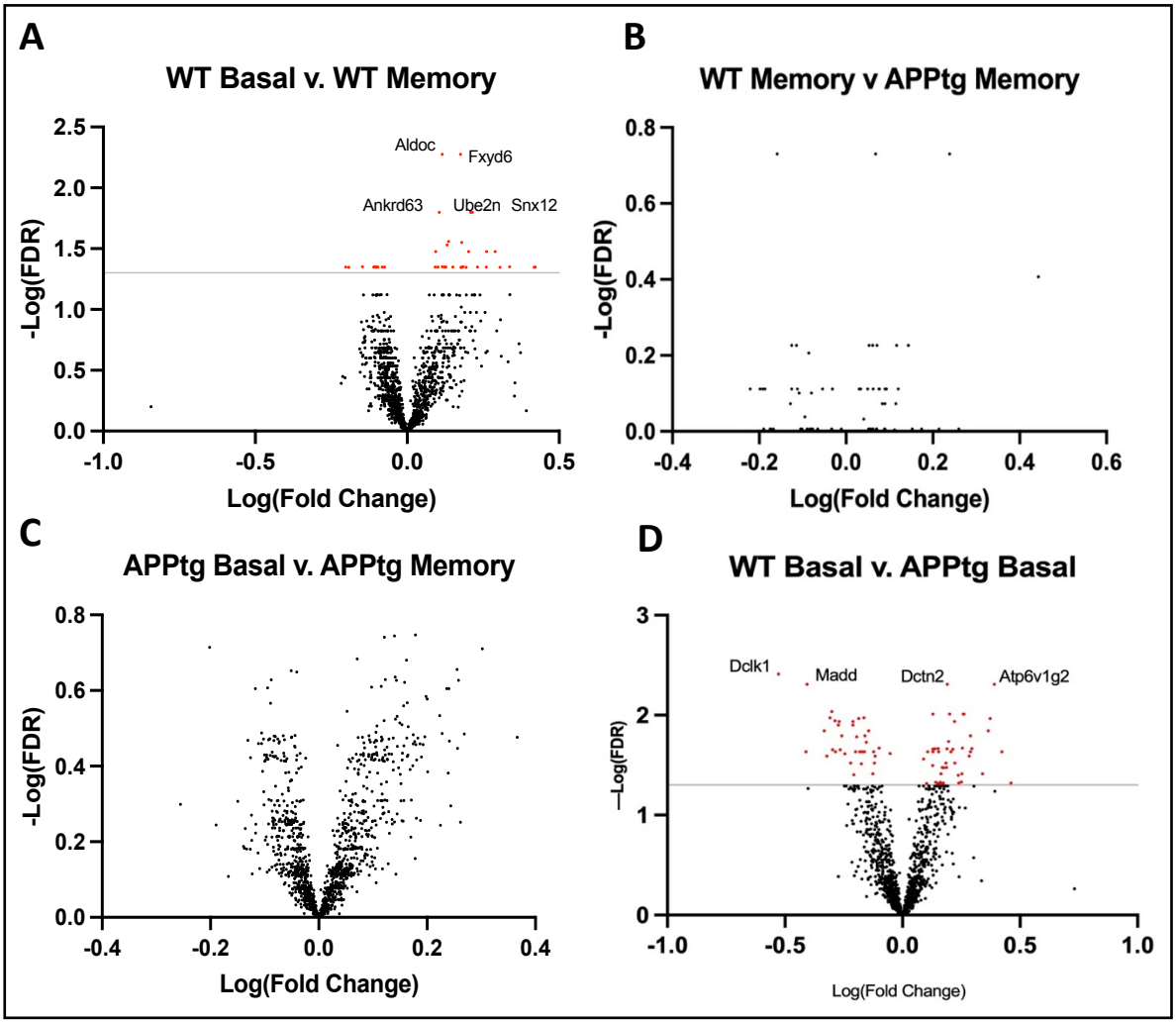

Figure 4.4. A) Differentially expressed proteins in WT mice at the point of memory retrieval, when compared to basal levels. Red plots denote statistical significance ($p<0.05$). A total of 1354 proteins were included in the plot, following FDR correction. B) Differentially expressed proteins in APPtg mice during memory retrieval, when compared to WT mice during memory retrieval. A total of 1480 proteins were included in the plot, after FDR correction. There are no statistically significant plots. C) Differentially expressed proteins in APPtg mice during memory retrieval, when compared to the basal levels. A total of 1497 proteins were included in the plot, following FDR correction. There are no statistically significant plots. D) Differentially expressed proteins in APPtg mice at Basal levels, when compared to WT controls. Red plots are statistically significant ($p<0.05$). A total of 1454 proteins were included in the plot, following FDR correction.

Two of the four groups, WT Memory v. APPtg Memory (Group B) and APPtg Basal v. APPtg Memory (group C), had no statistically significant protein regulations within the dataset after the application of FDR correction (Figure 4.4). The two experimental conditions with significant protein regulations remaining after FDR correction, WT basal v. APPtg basal (group D) and WT basal v. WT memory retrieval (group A), had a number of proteins that were up- or down-regulated to a much greater extent than other proteins. In the APPtg mice at basal levels (when compared to WT mice at basal levels), 83 protein regulations were identified as significant, with 47 significant upregulations and 36 significant downregulations (4.1; figure 4.4D). Highlighted in the volcano plots are the top 5 results

with the greatest fold changes. For this group, the greatest fold changes in the significantly upregulated proteins were Dctn2 and Atp6vlg2. Dctn2 is a subunit of dynactin, a macromolecular complex which binds microtubules and cytoplasmic dynein. It has multiple known functions including endoplasmic reticulum (ER)-Golgi transport, axogenesis , and the centripetal movement of endosomes and lysosomes, which it carries out via activation of dynein for transport along microtubules. It is thought that the protein may play a key role in synapse formation during development of the brain (GeneCards., 2017). The second greatest significant upregulation, Atp6vlg2 is a subunit of mitochondrial ATP synthase, and may play a direct role in translocation of protons across the membrane, via the F0 proton channel domain (UniProt., 2023). The greatest significant downregulations in APPtg mice during memory retrieval were Dclk1 and Madd. Dclk1, a member of the doublecortin and protein kinase superfamily, contains two N-terminal doublecortin domains, facilitating binding of microtubules and regulation of microtubule polymerisation. Another of its domains, which lies between the doublecortin and protein kinase domains, is involved in the mediation of protein-protein interactions. The encoded protein functions within a number of cellular processes including neuronal migration, neuronal apoptosis, neurogenesis and retrograde transport. Upregulation of Dclk1 by brain-derived neurotropic factor is associated with general cognitive ability and memory function (NIH., 2023). Madd protein is a signalling molecule which interacts with one of two receptors on cells that have been targeted for apoptosis. The MAP-kinase activating death domain (Madd) interacts with the death domain of TNF-alpha receptor 1, activating MAPK, propagating the apoptotic signal. Madd has several functions including roles in vesicle trafficking at the neuromuscular junction, upregulating post-docking step of synaptic exocytosis in central synapses, formation of synaptic vesicles, and the motor-dependent transport of vesicles to presynaptic nerve terminals (NIH., 2023).

The second condition with significant differential protein expression, WT basal v. WT memory (table 4.1; figure 4.4A) also has the top 5 significant differential protein regulations highlighted in the volcano plots. For this group, the greatest fold changes were in the significantly upregulated proteins; Fxyd6, Ube2n, Aldoc, and Ankrd63. Fxyd6 is a phosphohippolin, which is thought to affect the activity oof Na, K-ATPase (GeneCards., 2023). Aldoc is a member of the class I fructose-biphosphate aldolase gene family, expressed specifically in the hippocampus and Purkinje cells and is a member of the enzyme family aldolase (NIH., 2023). Aldoc is an enzyme of the glycolytic pathway which catalyses the reversible aldol cleavage of fructose-1,6-bisphosphate to dihydroxyacetone and fructose-1-phosphate to glyceraldehyde-3-phosphate or glyceraldehyde (GeneCards., 2023). Fxyd6 is a protein which has yet to be fully characterised but is thought to participate in the regulation of sodium ion transmembrane transporter activity and is active in the glutamatergic synapse,

postsynaptic membrane, and presynaptic membrane (PubChem., 2023). Ankrd63 gene encodes a protein which, in eukaryotic cells, serves as an adaptor protein that links membrane proteins to the cytoskeleton, forming protein complexes of integral membrane proteins, cytoskeletal components and signalling molecules. The ankyrin proteins stabilise and organise protein networks though their ability to mediate protein-protein interactions, stablishing the infrastructure of specialised membrane domains (Cunha & Mohler., 2009).

4.2.1 DAVID Annotations

Due to two of the four experimental groups having no significant differentially expressed proteins, only the two groups with significant expressions were analysed by DAVID and therefore, the results are slightly limited in number. The top 5 results from the analyses are listed, in order of highest significance or largest enrichment value. The full list of outputs can be found in appendix D, section 1, where the reader can come to their own conclusions on the data; data that does not meet statistical significance thresholds (p=0.05) may still be biologically meaningful in exploratory proteomics studies.

4.2.2 Gene Ontology

The first stage of analysis was to gain an understanding of the biological meaning and functions behind the large protein lists identified as differentially regulated between genotype and phenotype combinations. The **D**atabase for **A**nnotation, **V**isualisation and **I**ntegrated **D**iscovery (DAVID) was employed to provide a comprehensive list of enriched biological themes within the protein lists, particularly focussing on Gene Ontology (GO) terms.

4.2.3 Biological Process

GO provides a framework for describing the functions of gene products (proteins) of target organisms. A GO annotation is an association between a specific protein and a GO term, together making a statement important to the function of the protein. The two biological conditions with significant protein regulations after FDR correction were submitted to DAVID GO tool for annotation with associated biological processes. Figure 4.5 shows the top 5 biological processes (BPs) enriched in the upregulated protein lists for their respective experimental condition.

In the WT mice, four significant BPs were found to be associated with upregulated proteins during memory retrieval (when compared to basal levels), including melanosome transport, vesicle-mediated transport, cellular oxidant detoxification and establishment of protein localisation to membrane. There were no upregulations in the APPtg mice during memory retrieval (group C).

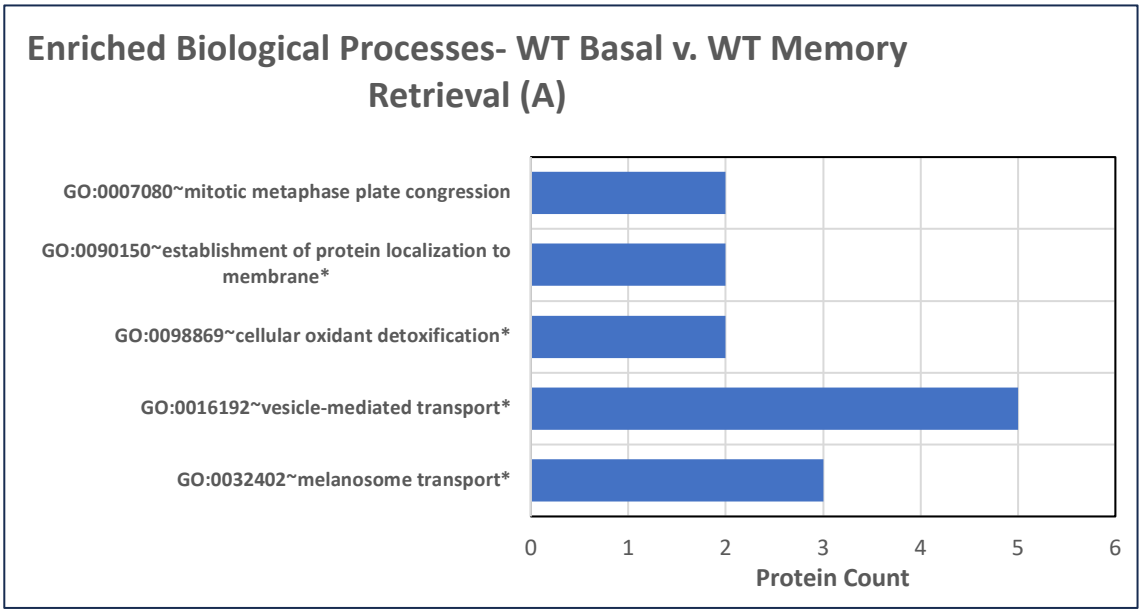

*Figure 4.5 DAVID GO-term enrichment analysis. Table presents the top 5 biological processes enriched in upregulated proteins in WT mice during memory retrieval (when compared to WT basal levels; group A). Significant results denoted by *.*

Figure 4.6 reveals three BPs were found to be significantly associated with proteins upregulated in transgenic mice at the basal level (when compared to WT mice at the basal level; group D), including mitochondrial electron transport, cytochrome c to oxygen, fatty acid metabolic process and gene expression. Negative regulation of neuron death was also identified and although it did not reach the significance threshold, its meaning may still be biologically important.

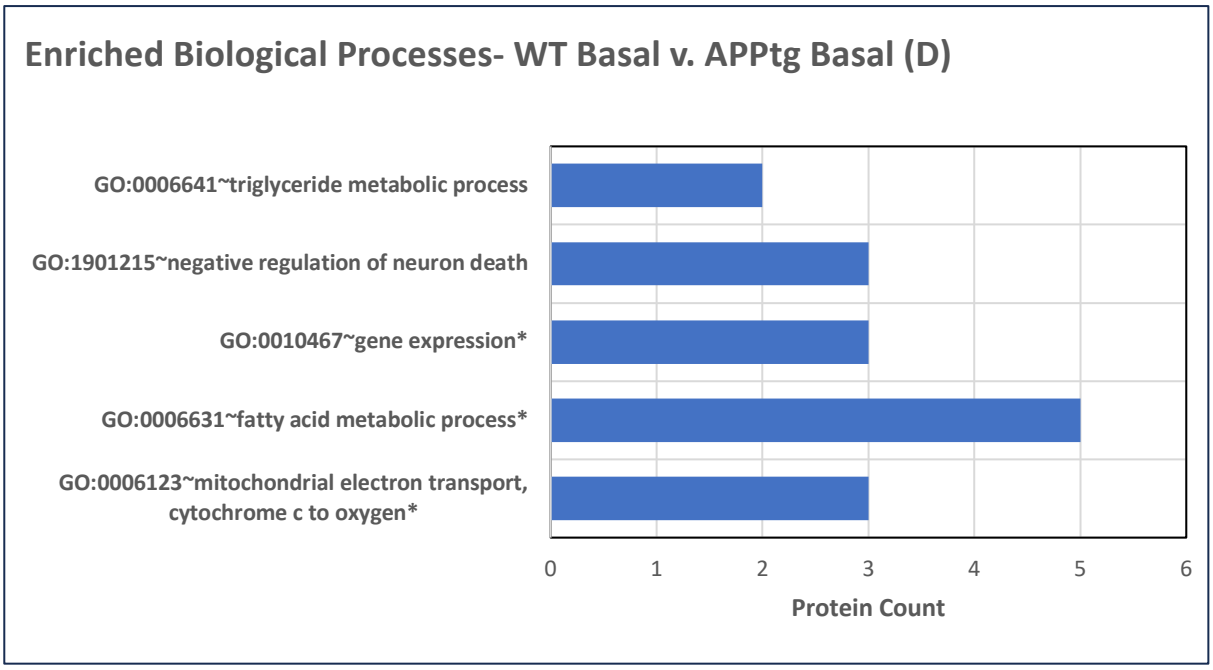

*Figure 4.6. DAVID GO-term enrichment analysis. Table presents the top 5 biological processes enriched in upregulated proteins in APPtg mice during basal levels (when compared to WT mice during basal levels; group D). Significant results denoted by *.*

In WT mice during memory retrieval (when compared to basal; group A) there were two BPs identified by DAVID in the significantly downregulated proteins (figure 4.7), although they did not reach the significance threshold; apoptotic process and liver development. There were no results for APPtg mice during memory retrieval (group C).

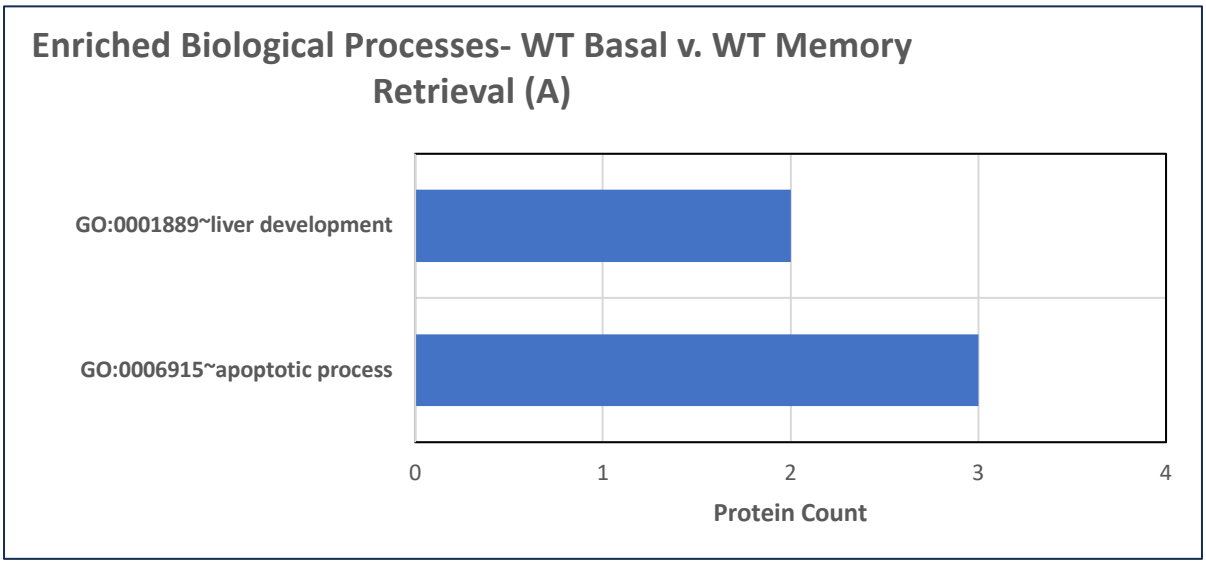

*Figure 4.7. DAVID GO-term enrichment analysis results for proteins downregulated in WT mice during memory retrieval (when compared to WT mice during basal levels; group A). Significant results denoted by *.*

In the transgenic mice during basal levels (when compared to WT basal; group D), one result was statistically significant- barbed-end actin filament capping, as listed in figure 4.8.

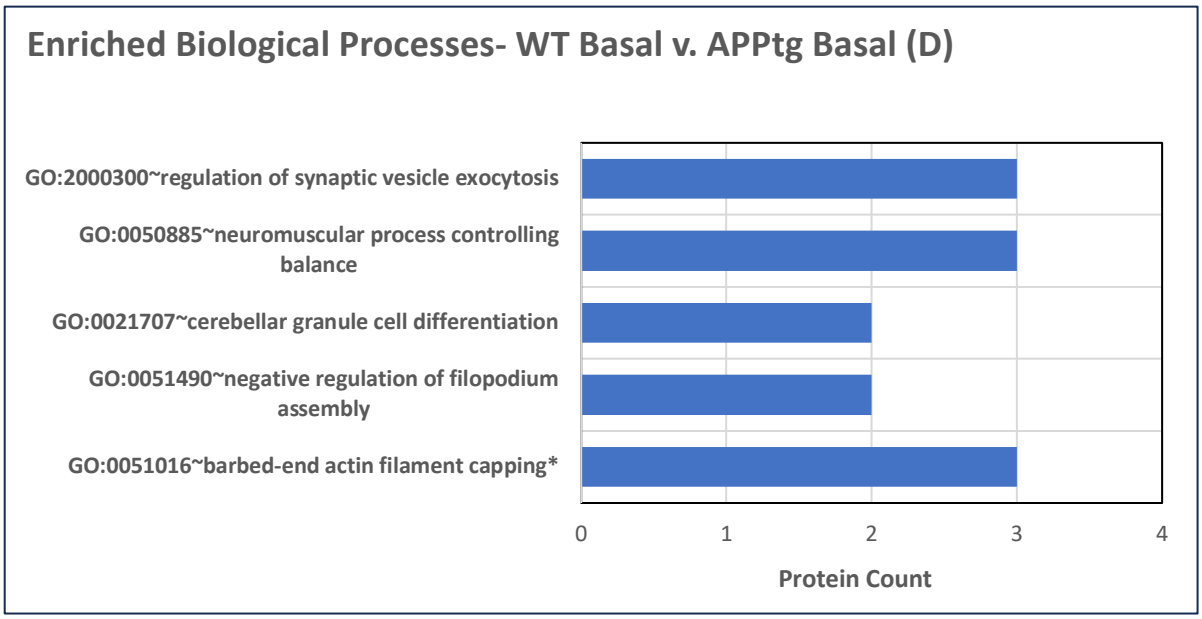

*Figure 4.8. DAVID GO-term enrichment analysis. Table presents the top 5 biological processes enriched in downregulated proteins in APPtg mice during basal levels (when compared to WT mice during basal levels; group D). Significant results denoted by *.*

4.2.4 Cellular component

The next GO term to be annotated to inputted proteins was the cellular component (CC). CC provides information about the subcellular structures and macromolecular complexes where inputted proteins are located, helping localise specific protein functions of interest.

Figure 4.9 reflects the cellular components where each protein's function is localised within the two experimental conditions. In WT mice during memory retrieval (compared to basal levels; group A), two CCs were identified as significantly enriched; the postsynaptic endocytic zone cytoplasmic component and clathrin coat of trans-golgi network vesicle. There were no results for APPtg mice during memory retrieval (group C).

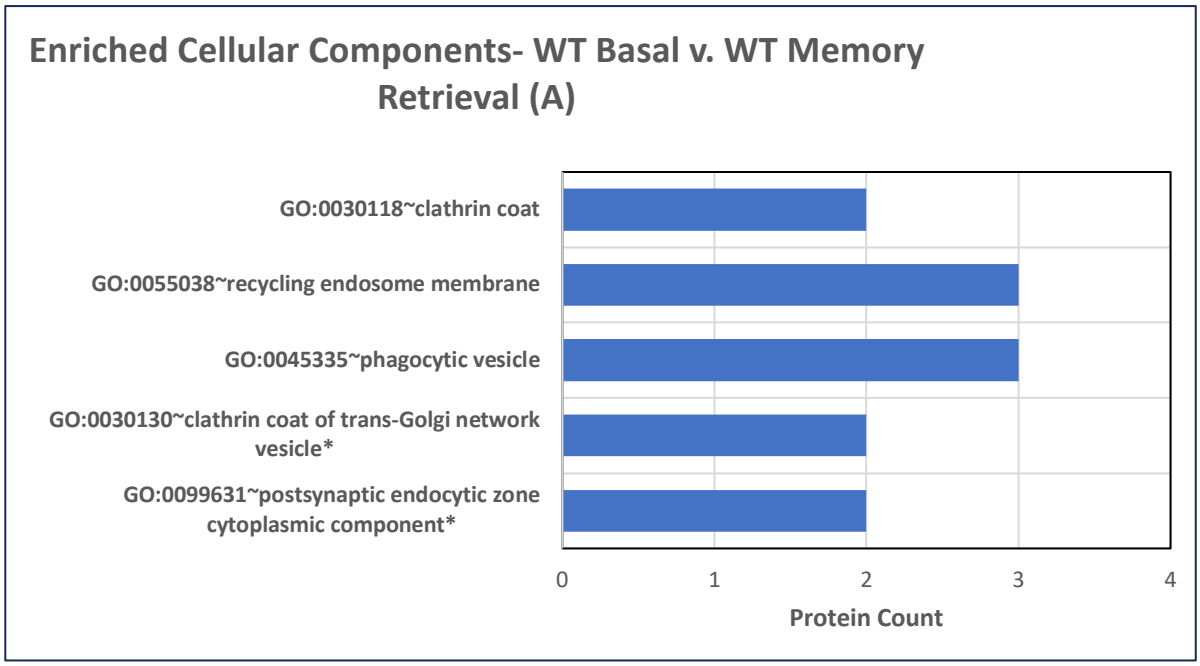

*Figure 4.9. DAVID GO-term results. Table represents the cellular components enriched in upregulated proteins in WT mice during memory retrieval (when compared to WT mice at basal levels; group A). The top 5 results are shown, in order of significance. Significant results denoted by *.*

In the transgenic mice at the basal level (compared to WT basal; group D), three CCs were statistically significant including the IMM (most enriched), mitochondrial respiratory chain complex IV and the postsynaptic endocytic zone cytoplasmic component, listed in figure 4.10.

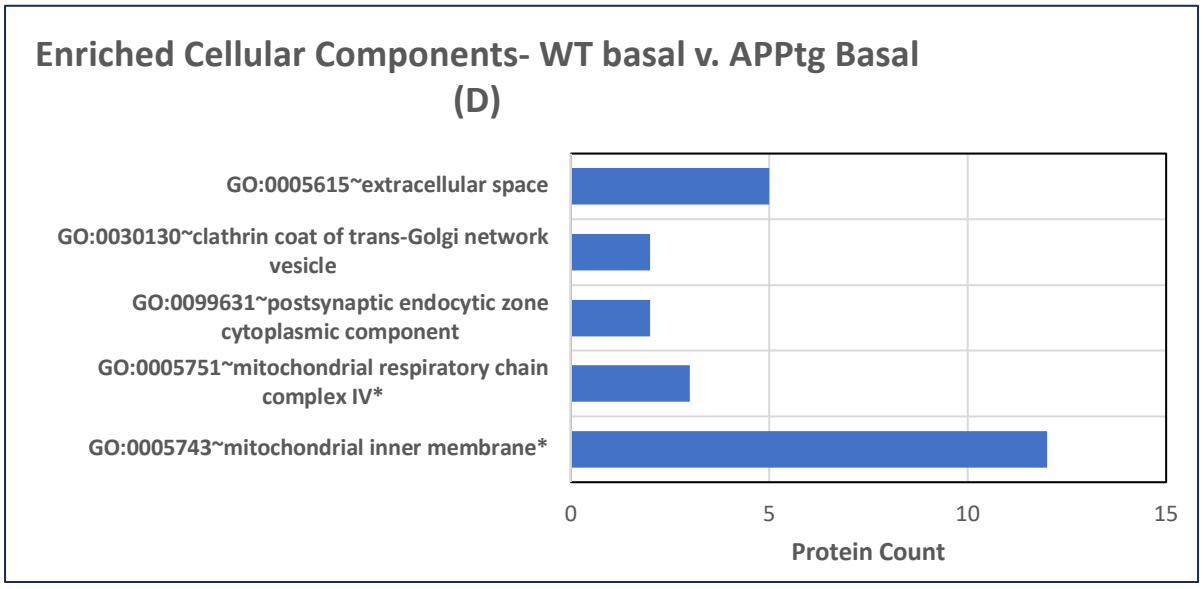

*Figure 4.10. DAVID GO-term enrichment analysis. Table presents the top 5 cellular components enriched in upregulated proteins in APPtg mice during basal levels (when compared to WT mice during basal levels; group D). Significant results denoted by *.*

Only one CC was identified in proteins downregulated within WT mice during memory retrieval (group A), the synapse, suggesting most proteins identified as significant downregulated in WT mice during memory retrieval have functions in the synapse, however this was not statistically significant. There were no results for APPtg mice during memory retrieval (group C).

In the transgenic mice, the two significant CC results were the glutamatergic synapse and the Schaffer collateral- CA1 synapse, listed in figure 4.11.

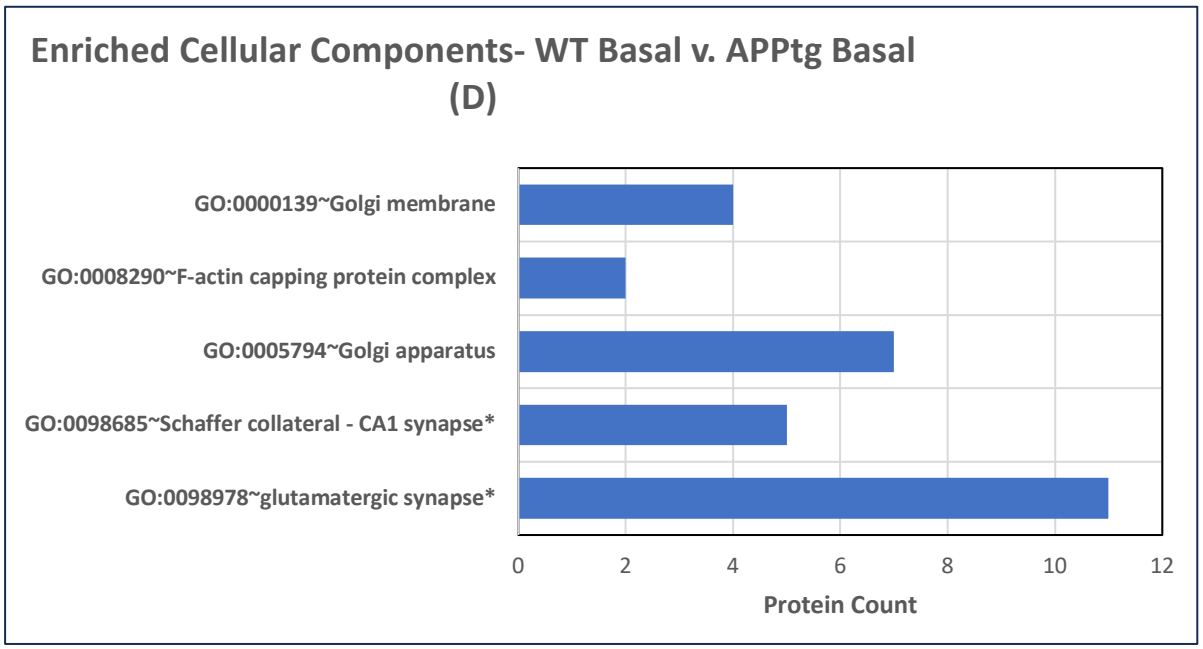

*Figure 4.11. DAVID GO-term enrichment analysis. Table presents the top 5 cellular components enriched in downregulated proteins in APPtg mice during basal levels (when compared to WT mice during basal levels). Significant results denoted by *.*

4.2.5 Molecular Function

The molecular function (MF) GO terms describe actions that can be carried out on a molecular level via the direct physical interactions with other molecular entities (Thomas., 2017).

Figure 4.12 represents the MF annotations enriched in the inputted significantly upregulated gene lists. None of the results for either condition were statistically significant. There were also no MFs significantly enriched in the proteins significantly downregulated in either condition. There were no results for APPtg mice during memory retrieval (group C).

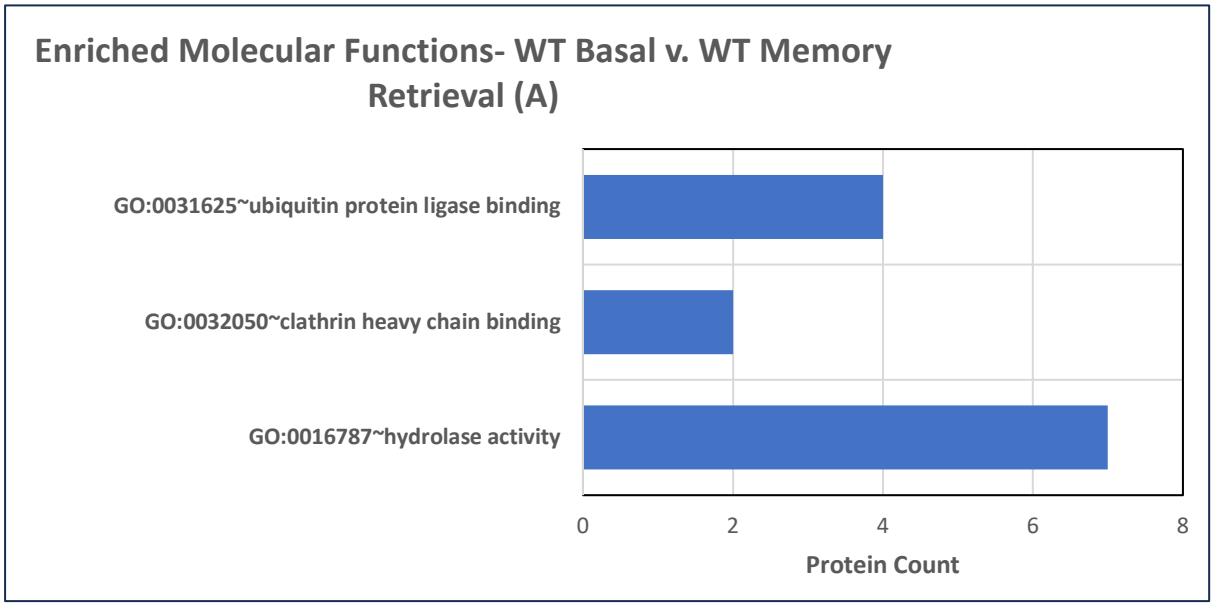

*Figure 4.12. DAVID GO-term enrichment analysis results. Table presents the top enriched molecular processes in proteins upregulated in WT mice during memory retrieval (when compared to basal levels; group A). Significant results denoted by *.*

Only one, non-significant result was returned for transgenic mice at the basal level (group D), which was calmodulin binding.

4.2.6 KEGG Pathways

KEGG pathway annotations identify the enriched networks that each inputted protein is functionally associated with via molecular interactions. Corresponding KEGG pathways maps can be visualised for each specific term and utilise KEGG Orthology groups which allow experimental results from specific organisms to be generalised to other organisms using genomic information (GenoneNet., 2011).

Figure 4.13 represents the KEGG pathways proteins significantly upregulated in each condition are associated with. In the WT mice during memory retrieval (when compared to basal levels), three pathways were identified as significantly enriched- endocytosis, synaptic vesicle cycle and vasopressin-regulated water reabsorption.

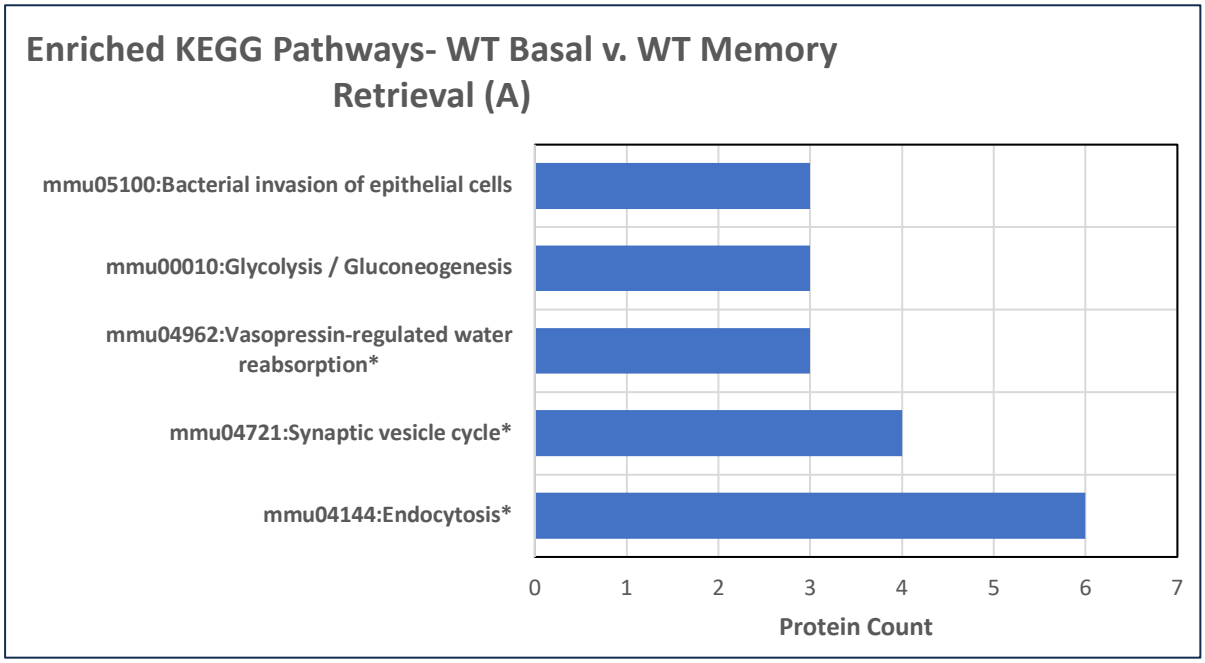

*Figure 4.13. Table of DAVID enriched KEGG pathways identified in upregulated proteins in WT mice during memory retrieval (when compared to basal levels; group A). Significant results denoted by *.*

In transgenic mice at the basal level (compared to WT mice at the basal level; group D), all 55 results were statistically significant and included OXPHOS, AD and pathways of neurodegeneration- multiple diseases (figure 4.14).

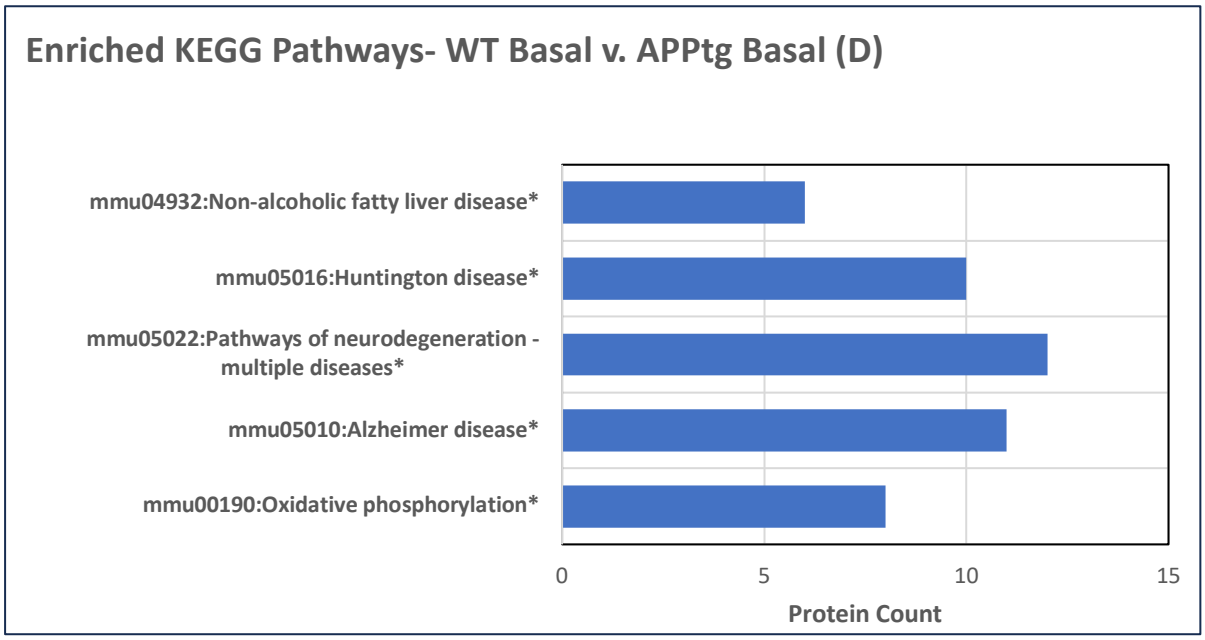

*Figure 4.14. Table of DAVID enriched KEGG pathways identified in upregulated proteins in APPtg mice at the basal level (when compared to WT counterparts; group D). Significant results denoted by *.*

In the significantly downregulated proteins, there were no enriched KEGG pathways in WT mice during memory retrieval (group A), and only one significantly enriched KEGG pathway, sulfur metabolism, in the transgenic mice at the basal level (when compared to WT mice at the basal level; group D).

4.2.7 Functional Annotation Clustering

DAVID functional annotation clustering tool groups proteins with similar functions/annotations together to make the biological interpretation of large protein lists clearer and more focussed. The top 5 clusters are listed in the output tables, in order of enrichment score (the higher, the more enriched). The enrichment score is the geometric mean (in -log scale) of members' p-values in a corresponding annotation cluster, is used to rank their biological significance. Thus, top ranked annotation groups most likely have consistent lower p-values . More detail about enrichment scores can be found on the DAVID website (https://david.ncifcrf.gov/helps/functional_annotation.html). Full clustering output tables can be found in Appendix D, section 1.

7 clusters were identified in the WT group and 10 clusters were identified in the APPtg mice at basal levels (when compared to WT mice at basal levels; group D). Table 4.2 lists the top most enriched clusters within inputted significantly upregulated protein lists. During memory retrieval in WT mice (when compared to basal levels; group A), the top functional clusters were synaptic vesicle cycle, protein transport, GTPase activity, ion transport and lipid metabolism. There were no results for APPtg mice during memory retrieval (group C).

*Table 4.2. DAVID functional annotation clustering results for upregulated proteins in WT mice during memory retrieval (when compared to WT basal; group A). The top 5 clusters are shown, in order of enrichment score. Significant results denoted by *.*

A- WT Basal v. WT Memory Retrieval
Upregulated
Synaptic vesicle cycle (2.67)
Protein transport (1.33)
GTPase activity (1.21)
Ion transport (0.93)
Lipid metabolism (0.88)

In transgenic mice at the basal level (compared to WT; group D), the top enriched clusters were metabolic pathways, GTPase activity, synaptic vesicle cycle, identical protein binding and lipid binding (table 4.3).

*Table 4.3. DAVID functional annotation clustering results for upregulated proteins in APPtg mice at the basal level when compared to WT mice at the basal level (group D). The top 5 clusters are shown, in order of enrichment score. Significant results denoted by *.*

D- Wild-type Basal v. APPtg Basal
Upregulated
Metabolic pathways (3.63)
GTPase activity (1.81)
Synaptic vesicle cycle (1.73)
Identical protein binding (1.28)
Lipid binding (1.15)

4 clusters were identified in the WT mice and a total of 11 clusters were identified in the APPtg mice at basal levels (when compared to WT mice at basal levels; group D). In the proteins significantly downregulated during memory retrieval in WT mice (group A), four clusters were generated, including synapse, mitochondrion, membrane, and phosphoprotein (table 4.4). There were no results for APPtg mice during memory retrieval (group C).

*Table 4.4. DAVID functional annotation clustering results. Annotation clusters present in genes downregulated in WT mice during memory retrieval (when compared to basal levels; group A). Significant results denoted by *.*

A- WT Basal v. WT Memory Retrieval
Downregulated
Synapse (2.05)
Mitochondrion (1.64)
Membrane (0.62)
Phosphoprotein (0.62)

In the transgenic mice during basal levels (group D), the top enriched clusters were calmodulin binding, intracellular transport, cytoskeleton, membrane, and Golgi apparatus (table 4.5).

*Table 4.5. DAVID functional annotation clustering results for upregulated proteins in APPtg mice at the basal level when compared to WT mice at the basal level (group D)l. The top 5 clusters are shown, in order of enrichment score. Significant results denoted by *.*

D- Wild-type Basal v. APPtg Basal
Upregulated
Calmodulin binding (2.91)
Intracellular transport (2.51)
Cytoskeleton (2.31)
Membrane (1.70)
Golgi apparatus (1.70)

4.2.8 STRING Protein Network Mapping

The STRING database was used to generate visual protein connectivity maps for significantly differentially regulated proteins within biological conditions. The STRING database aims to integrate all known and predicted protein associations, including physical interactions and functional associations. STRING collects and scores evidence from multiple sources including automated text mining of scientific literature (Szklarczyl et al., 2021). STRING network maps can be used to identify major differences in protein connectivity between genotypes or experimental conditions.

Figure 4.15 captures the protein interactions present within proteins significantly downregulated in WT mice during memory retrieval (when compared to basal levels; group A). The associated protein-protein interaction (PPI) enrichment p-value for this network was 0.00234, meaning the inputted proteins have more interactions among themselves than what would be expected for a set of proteins of the same size and degree distribution. The score indicated that these proteins are at least partially biologically connected as a group. The two main groups connected in this figure have functions in mitochondrial dynamics (Opa1, Immt and Aco2), and synapse maintenance and cell death (Dmxl2, Madd and Srcin1).

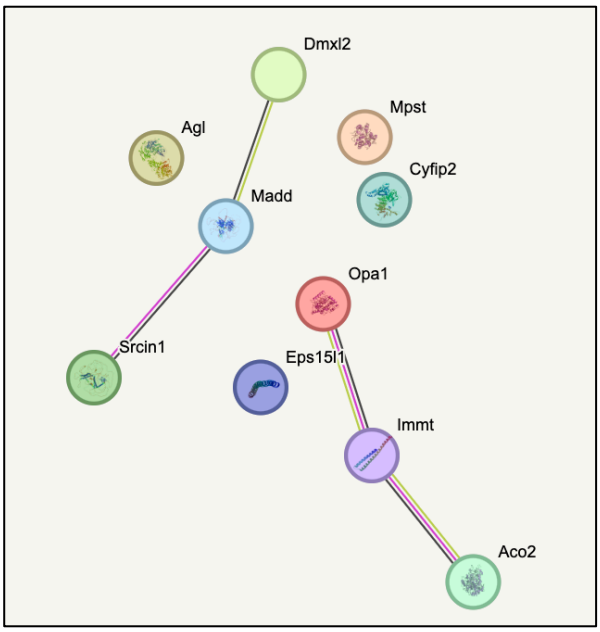

Figure 4.15. STRING protein connection network for proteins significantly downregulated in wild-type mice during memory retrieval (when compared to basal levels; group A).

Figure 4.16 represents the PPI network map for proteins significantly upregulated in WT mice during memory retrieval, when compared to WT mice at the basal level (group A). There are two main groups of connected proteins, a smaller group involved in intracellular membrane trafficking (Rab11b, Rab11a & Dctn2), and a larger group, involved in phosphoprotein activity (Rap1a, Aldoc, Prdx6, Akr1a1, Tpi1 & Ywhaz). The associated PPI enrichment p-value for this network was 0.0172.

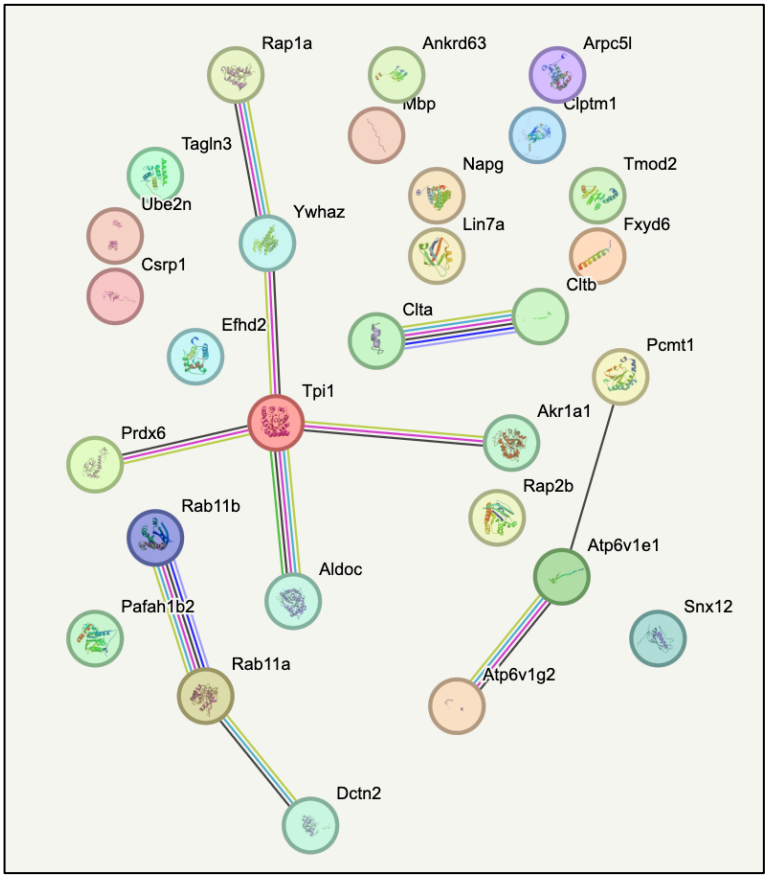

Figure 4.16. STRING PPI map for proteins significantly upregulated in wild-type mice during memory retrieval (when compared to basal levels; group A).

Figure 4.17 represents the PPI network map for proteins significantly upregulated in transgenic mice at the basal level, when compared to their WT counterparts (group D). In this PPI network map, there is one highly connected functional group, consisting of proteins involved in energy biosynthesis pathways. The top group consists of proteins located in the ETC, which produce energy via OXPHOS. The purple node in the centre, alpha synuclein, connects this group to the smaller group below, which functions in fatty acid catabolism. The associated PPI enrichment p-value for this network was 6.91e-07.

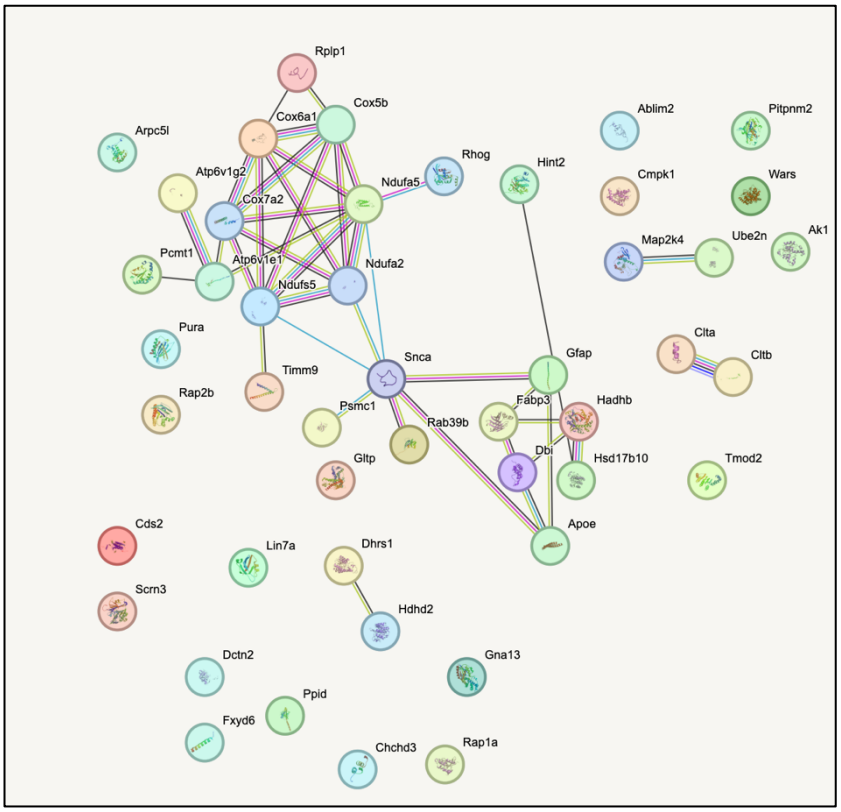

Figure 4.17. STRING protein network map for proteins upregulated in APPtg mice during basal levels, when compared to WT mice at the basal level (group D).

Figure 4.18 shows the PPIs existing between proteins significantly downregulated in APPtg mice at the basal level, when compared to WT mice at the basal level (group D). This protein group is involved in biological functions such as actin cytoskeleton regulation and cell surface proteins involved in cell-cell interactions and regulation of signal transmission. The associated PPI enrichment p-value for this network was 0.000207.

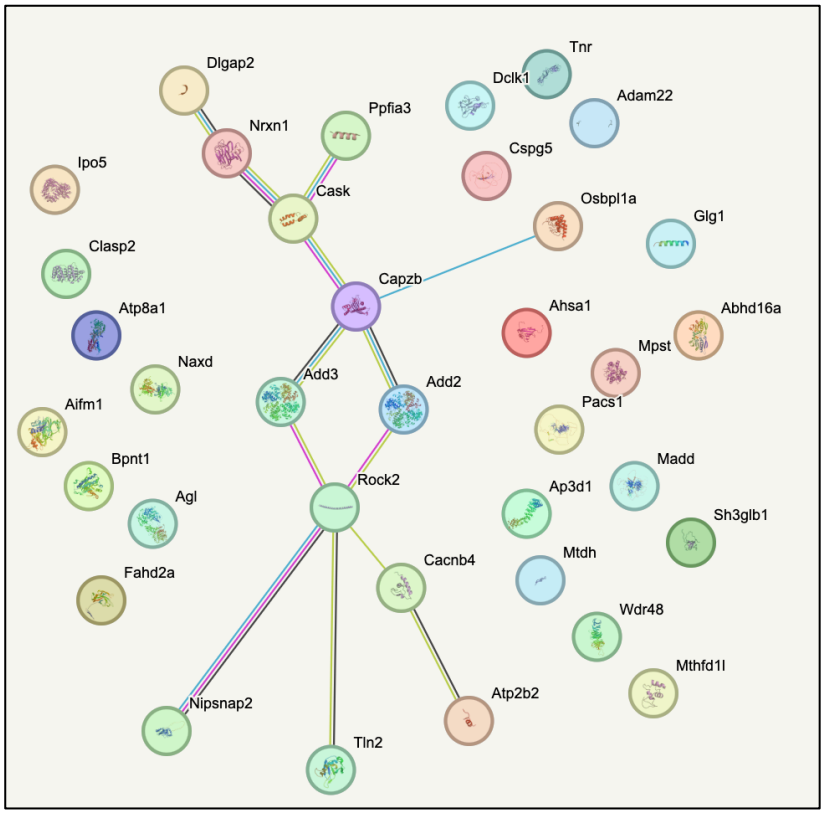

Figure 4.18. STRING PPI network map for proteins significantly downregulated in APPtg mice at the basal level, when compared to WT mice at the basal level (group D).

4.2.9 Functional Dependency Analysis

As detailed in the methods section, CNA carries out in-depth analysis of the effects of every model component on every other model component in the inputted data. This is completed via the generation of dependency matrices- fully encompassing analyses accounting for all possible signalling and feedback loops present within the model and determines the effect of every node on every other node. Nodes can have any of the following effects: Dark green = strong activator; Light green= weak activator; Yellow= ambivalent factor; Light red= weak inhibitor; Dark red= strong inhibitor; Black= no effect.

MATLAB was used to generate the dependency matrix, using the CellNetAnalyser graphical user interface application. Only the highest confidence interactions (0.900 or above) were contained within the matrix, as determined on the STRING database. A confidence score does not indicate the strength or specificity of any interaction, instead, it indicates how much evidence, experimental or otherwise (as described in section 2.5.4) there is to indicate the interaction to be true, which may explain the absence of APP, PS1 and PS2 from the matrix.

When generating a knock-out dependency matrix, the yellow, ambivalent factors would be targeted first. When targeting an ambivalent factor, changes in the biological system are most likely. This is because ambivalent factors exert both activator and inhibitory influences on the target nodes (usually these factors will exert the different types of effects at different times or under different conditions) and thus changing this node is likely to effect targets in two ways, whereas a dark red, strong inhibitory, node would only be changing this one type of inhibitory influence.

What we would be looking for in a knock-out dependency matrix is any colour changes in the matrix, indicating that nodes change the type of effects they exert on their target nodes. A desired effect in terms of therapeutics would be that the knocking-out of an ambivalent node would in turn activate nodes corresponding to genes involved in functions positive to either bioenergetics, mitochondrial or neuronal function or memory retrieval as a whole. Conversely, if we see that genes which negatively effect mitochondrial function or memory retrieval as a whole are turned red/inhibited by the removal of an ambivalent factors, then we can identify this factor as an optimal point of therapeutic intervention.

Figure 4.19 displays the functional dependency matrix generated using MATLAB from the proteins significantly upregulated in APPtg mice at the basal level, when compared to WT mice at the basal level. Functional dependency matrices represent the effects of every node (protein) in the matrix on every other node within the model.

The matrix consists of 47 species and 2209 reactions, 5 of which were strong inhibitors and 50 of which were strong activators. The rest of the interactions have no effect. There are no negative feedbacks present in the matrix and no ambivalent factors.

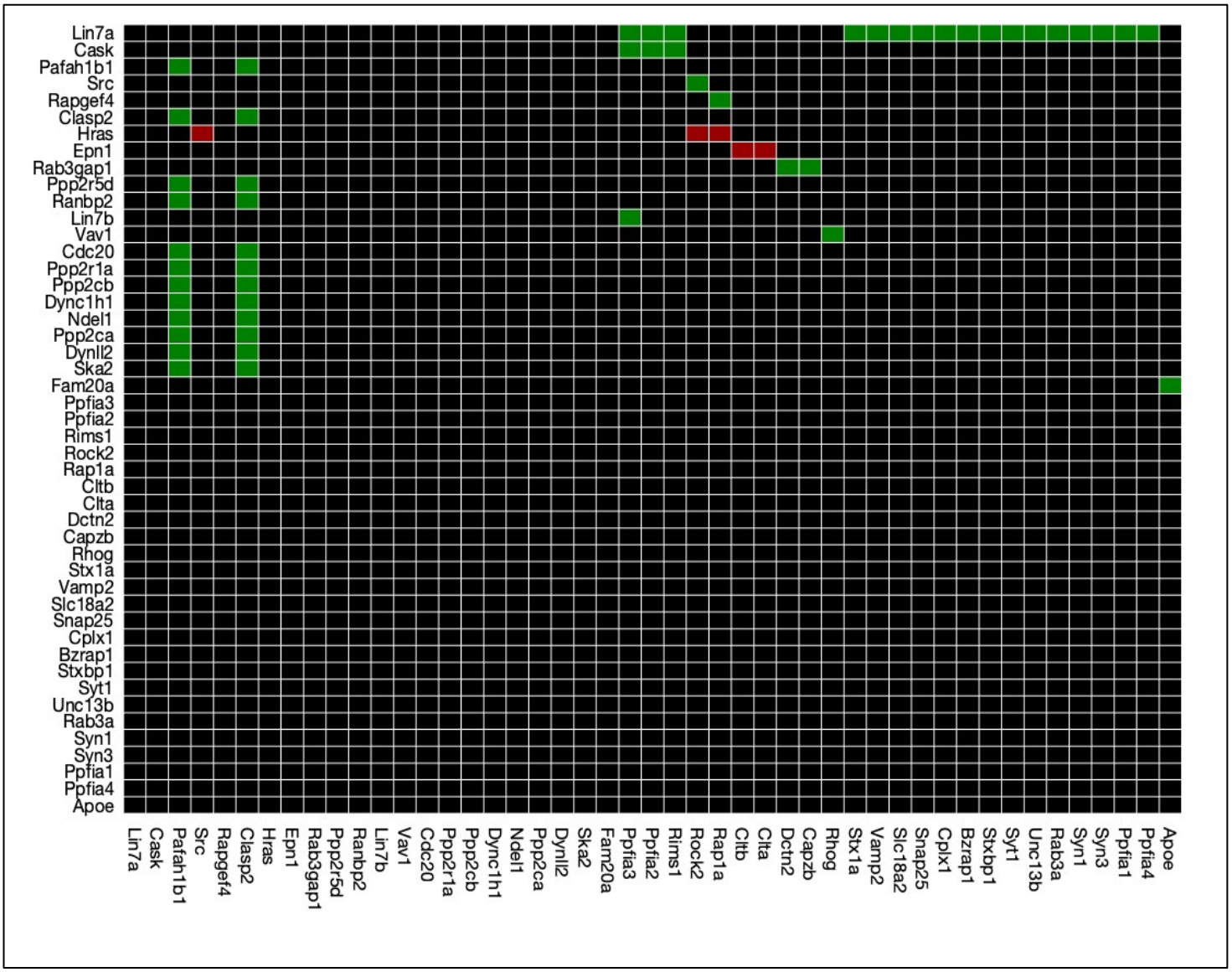

Figure 4.19. Functional dependency matrix for protein-protein interactions in proteins upregulated in APPtg mice at the basal level, when compared to WT mice at the basal level (group D). Black= no relationship. Dark green= strong activation of X-axis node by Y-axis node. Dark red= strong inhibition of X-axis node by Y-axis node.

One benefit to computational biology is the ability to conduct numerous different analyses to determine how models may change following the loss of certain network elements (proteins). Knock-out matrices were generated, focussing on removing proteins with the highest connectivity (highest number of proteins strongly activated or strongly inhabited by KO protein). The results are presented in table 4.6. KO models have a total number of 2116 dependencies due to removal of the target node and all of its dependencies. Due to the presence of no ambivalent factors (yellow nodes) or feedback loops (pink or pale green nodes), removal of proteins did not have any effect on the matrix. Feedback loops within biological networks are usually crucial for the maintenance of network integrity and offer the highest resistance to perturbations (Tian et al., 2013).

Table 4.6. Dependency matrix was manipulated to simulate a knock-out model of specific proteins. Protein KO effects on the rest of the model detailed, including the number of activations that changed.

Scenario	Number of Each Dependency						
	No Effect	Ambivalent	Weak Inhibitor	Weak Activator	Strong Inhibitor	Strong Activator	Total
Full model	2154	0	0	0	5	50	2209
Fam20a KO	2065	0	0	0	5	46	2116
Lin7a KO	2078	0	0	0	5	33	2116
Hras KO	2064	0	0	0	2	50	2116
Epn1 KO	2063	0	0	0	3	50	2116

4.3 20% Threshold Results

Similar to the reporting of the FDR corrected results, the 20% threshold results will contain the top 5 or top 10 results from their respective DAVID analyses, listed in order of most significant p-value or the greatest enrichment score. The whole outputted results from DAVID are too vast to be included in the results section of this thesis and thus all of the output tables are listed in Appendix D, section 2, including the full results tables from analyses shown below (beyond the top 5 or 10 results). When FDR correction is not used in proteomics studies, further experimental testing should be carried out to confirm the validity of any observed associations.

4.3.1 General overview

After initial processing, stage 1 protein lists (each protein had data for at least ¾ mice in each of the experimental groups and no missing protein IDs or gene names) were divided into upregulated, downregulated, significantly upregulated, significantly downregulated, and unchanged proteins. Figure 4.20 depicts the numbers of protein regulations that fit into each category. The values used here just include the application of the 20% regulation threshold- they have not yet had the t-test applied for significance testing.

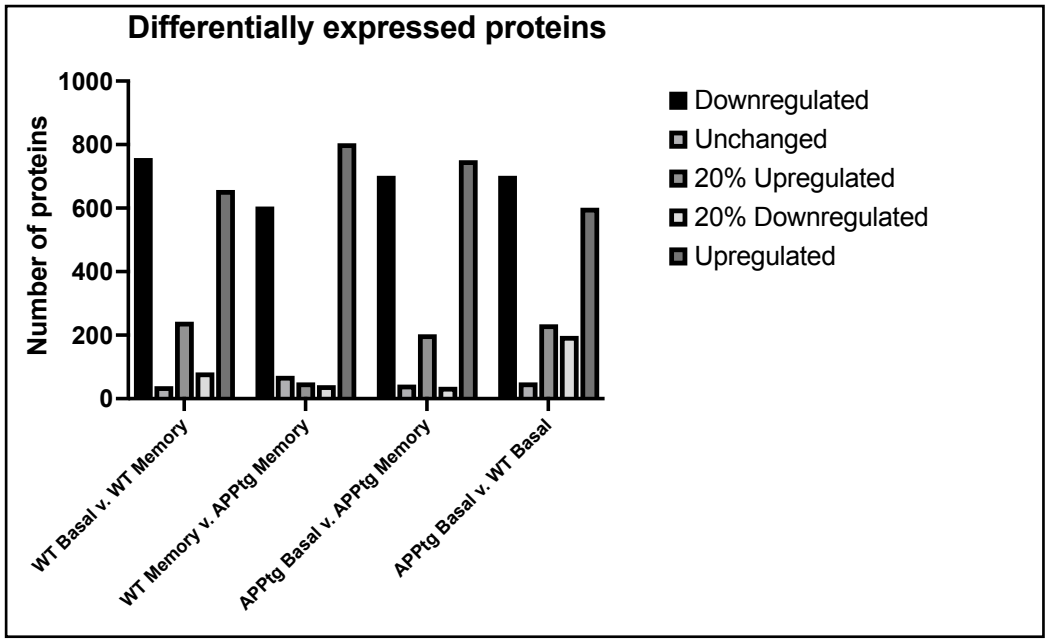

Figure 4.20. Differentially expressed proteins after application of 20% regulation threshold. Upregulated= all proteins with a positive fold change, 20% upregulated= all proteins with positive fold change of 20% or above.

Table 4.7 reflects the different levels of protein regulations within each of the four experimental groups. Unchanged proteins have a fold change score of 0. 20% upregulated and 20% downregulated categories consist of proteins with a statistically significant positive or negative fold change respectively, followed by application of the 20% regulation threshold. Upregulated or downregulated categories consist of proteins with a positive or negative fold change before the application of statistical testing or regulation threshold.

Table 4.7. Numbers of differentially regulated significant and non-significant proteins. Only the 20% stats are significant.

Group	Upregulated	Downregulated	20% Upregulated	20% Downregulated	Unchanged	Total Proteins
A-WT Basal v. WT Memory	657	758	139	49	39	1454
B- WT Memory v. APP Memory	804	605	4	5	72	1481
C- APPtg Basal v. APPtg Memory	751	702	107	15	44	1497

D- APPtg Basal v. WT Basal	601	702	154	139	51	1354

4.3.2 Differentially Regulated Proteins At The Basal Level

This section will detail the proteomic results from group D 'Wild-type basal v. APPtg basal', which details the proteins differentially expressed in the transgenic mice at the basal level, when compared to expression in WT mice at the basal level.

4.3.2.1 DAVID Annotations

The following sections will list the top 10 results from each type of analysis carried out using DAVID tools. The GO term and KEGG pathway results will be listed in order of most significant p-value and the functional annotation clustering results will be listed in order of enrichment score.

4.3.2.2 Biological Process

Within the significantly upregulated proteins in transgenic mice at the basal level (when compared to WT mice; group D), there were 18 biological processes significantly enriched (figure 4.21). Within the top 10 most enriched results were endocytosis, synaptic transmission-glutamatergic, chemical synaptic transmission, and positive regulation of long-term synaptic depression. Other significant results not listed within figure 4.21 were glutamate secretion, positive regulation of aspartic-type endopeptidase activity involved in amyloid precursor protein catabolic process, and negative regulation of long-term synaptic potentiation. Within the downregulated proteins, only two biological processes were significantly enriched: mitochondrial electron transport-cytochrome c to oxygen and activation of phospholipase D activity.

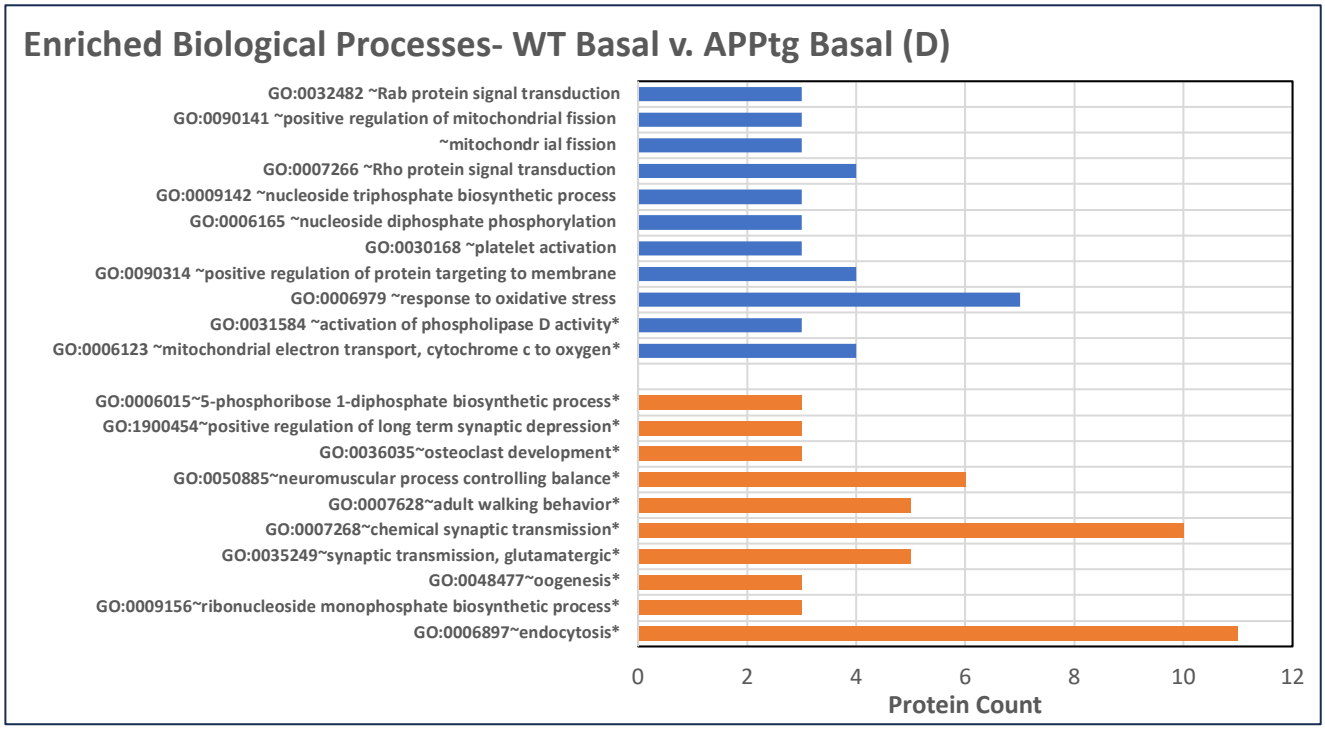

*Figure 4.21. DAVID GO biological process results for proteins upregulated and downregulated in APPtg mice at the basal level, when compared to wild-type mice at the basal level (group D). Significant results denoted by *. Blue= downregulated proteins, Orange= upregulated proteins.*

4.3.2.3 Cellular Component

Figure 4.22 represents the DAVID-identified enriched cellular component annotations within APPtg mice at the basal level, when compared to WT mice at the basal level (group D). Within the upregulated proteins, 14 significantly enriched cellular components were identified, including presynaptic active zone, postsynaptic density, glutamatergic synapse, dendritic spine, neuronal cell body and synapse. Within the downregulated proteins, 5 cellular components were significantly enriched including mitochondrial respiratory chain, IMM, mitochondrial respiratory complex IV and actin filament bundle.

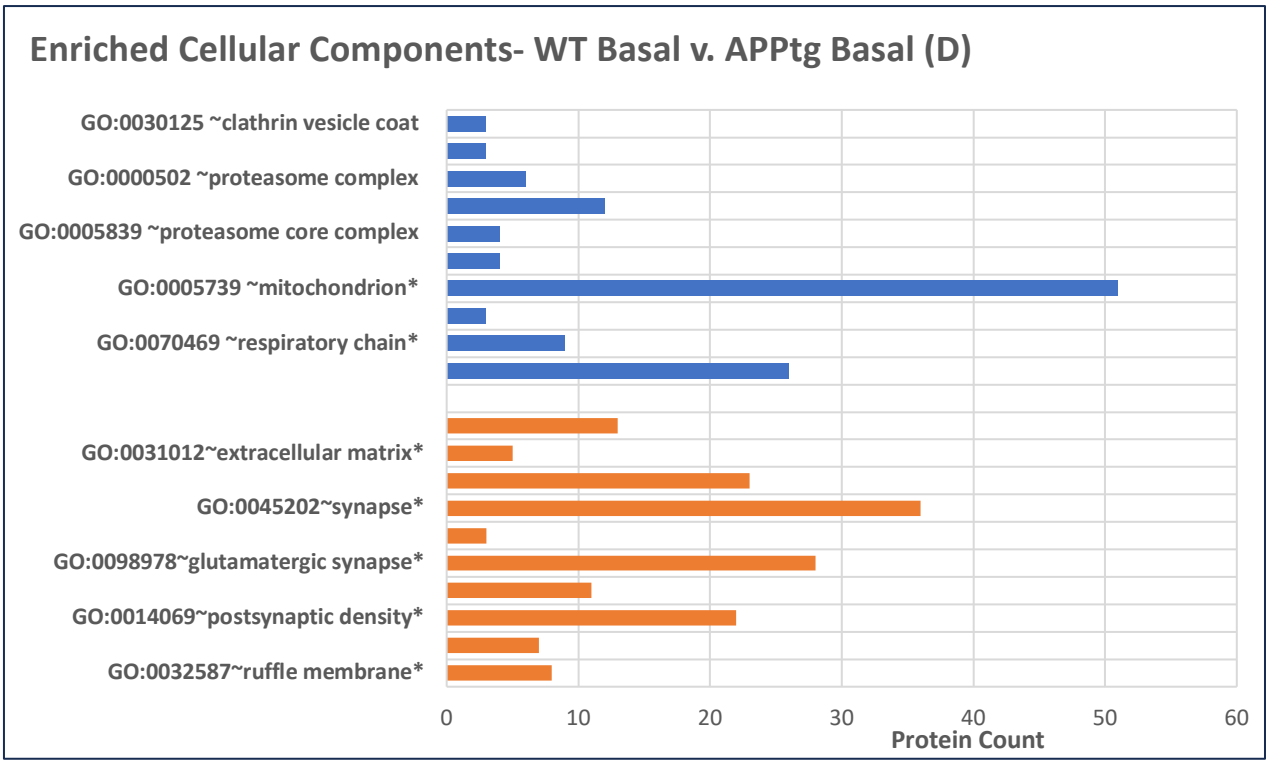

*Figure 4.22. DAVID GO analysis- enriched cellular component annotations within differentially expressed proteins in APPtg mice at the basal level, when compared to WT mice at the basal level (group D). Significance denoted by *. Blue= downregulated proteins, Orange= upregulated proteins.*

4.3.2.4 Molecular Function

Enriched molecular function annotations within proteins differentially regulated in transgenic mice at the basal level (when compared to their WT counterparts; group D) are listed in figure 4.23. 7 molecular functions were found to be significantly enriched, including actin filament binding, calcium channel activity, ATP binding and receptor binding. Within the downregulated proteins, two molecular functions were significantly enriched- oxidoreductase activity and nucleobase-containing compound kinase activity.

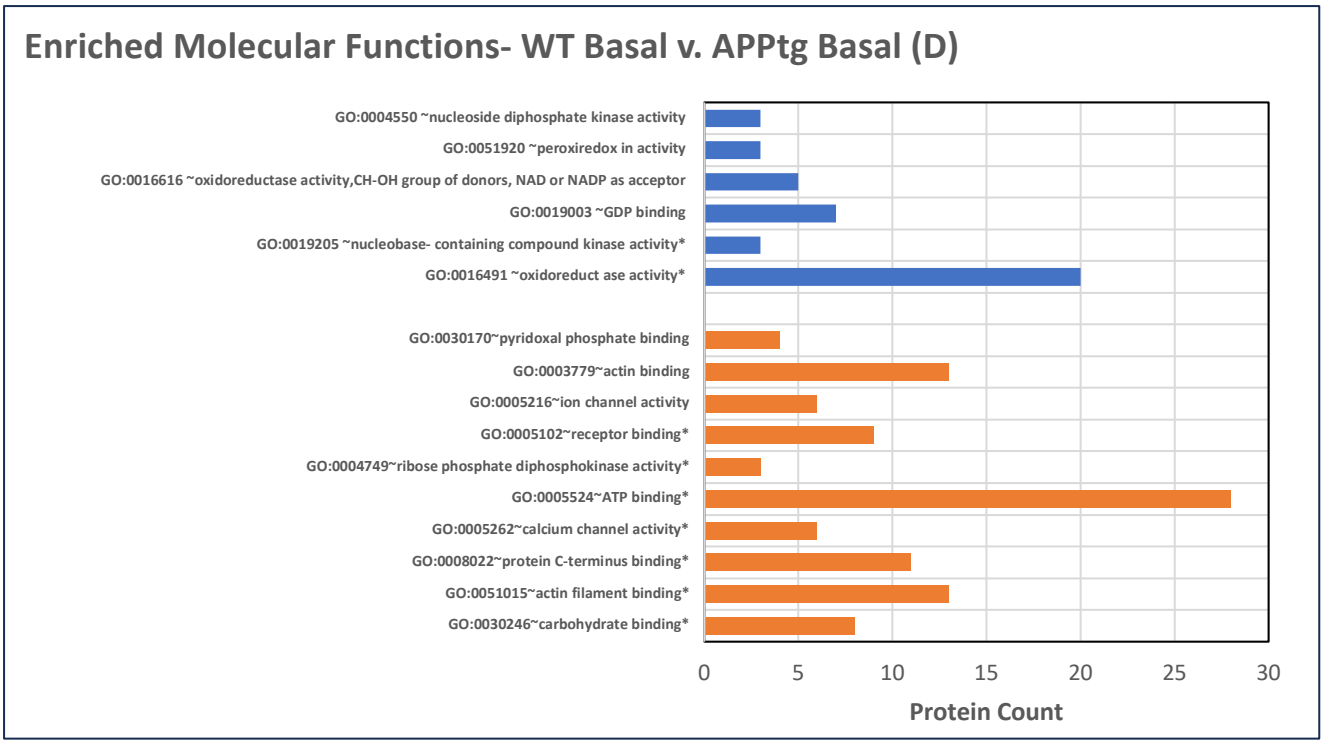

*Figure 4.23. DAVID GO term annotations for associated molecular functions enriched in APPtg mice at the basal level, when compared to WT mice at the basal level (group D). Significance denoted by *. Blue= downregulated proteins, Orange= upregulated proteins.*

4.3.2.5 KEGG Pathways

Figure 4.24 represents the KEGG Pathway annotations enriched in APPtg mice at the basal level (when compared to WT mice at the basal level; group D). Within the input list of upregulated proteins, 12 annotations were identified as significantly upregulated, including Alzheimer's disease, OXPHOS, prion disease and metabolic pathways. Within the proteins downregulated , only one result was returned which was the significantly enriched endocytosis pathway.

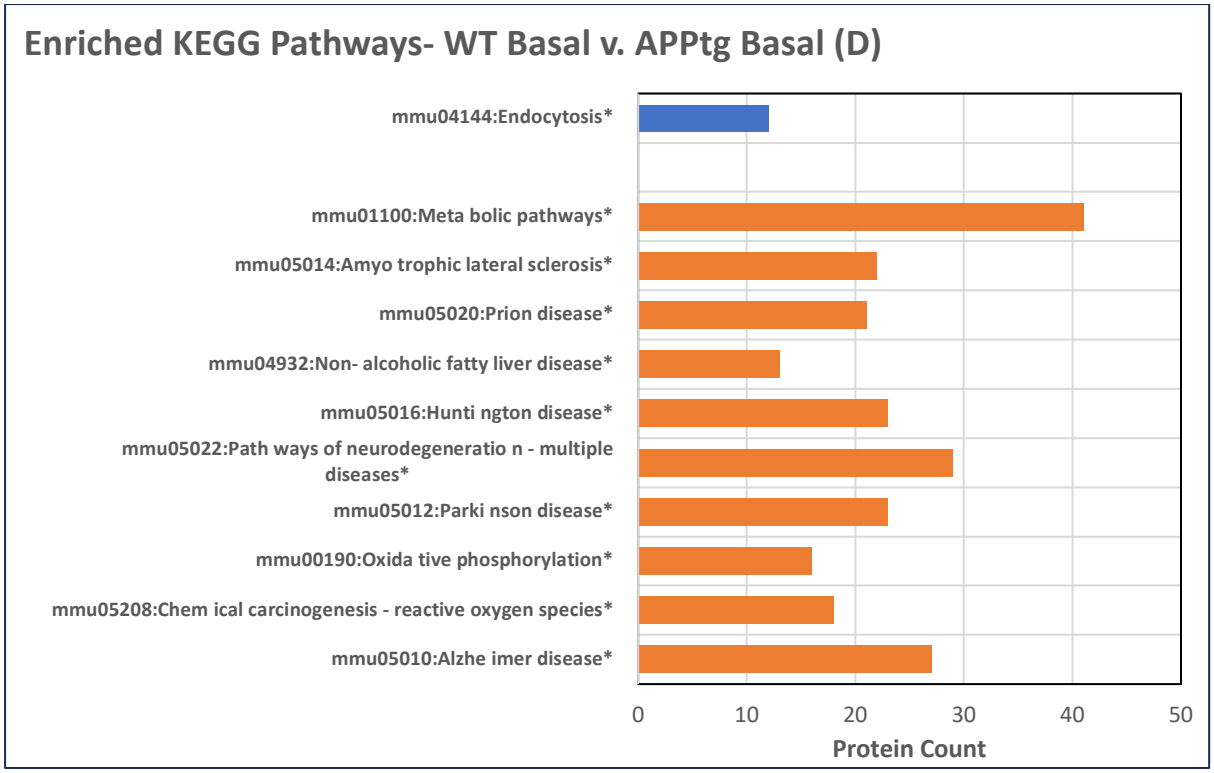

*Figure 4.24. DAVID KEGG Pathway results for proteins differentially regulated in APPtg mice at the basal level, when compared to WT mice at the basal level (group D). Significance is denoted by *. Blue= downregulated proteins, Orange= upregulated proteins.*

4.3.2.6 Functional Annotation Clustering

Results from DAVID functional annotation clustering analysis for proteins significantly differentially regulated in APPtg mice at the basal level (when compared to WT mice at the basal level; group D). The top 10 results are listed in table 4.8, in order of enrichment score (the larger, the more enriched). Enrichment score is listed next to each clustering output in brackets.

Table 4.8. DAVID functional annotation clustering analysis results for proteins significantly differentially regulated in APPtg mice at the basal level, when compared to WT mice at the basal level (group D). Enrichment score is listed next to each cluster in brackets.

D- Wild-type Basal v. APPtg Basal	
Upregulated	**Downregulated**
PDZ Domain (1.72)	Pathways of neurodegeneration (2.32)
Endocytosis (1.68)	Mitochondrial inner membrane (1.68)

Ribonucleoside monophosphate biosynthetic process (1.16)	Mitochondrial respiratory chain complex IV (1.36)
Synapse (1.16)	Cx9C motif 1 (biogenesis of respiratory enzyme complexes) (1.33)
Synaptic vesicle docking (1.14)	GTPase activity (1.06)
Actin binding (1.13)	Actin binding, cofilin/tropomyosin type (0.99)
Regulation of dendritic spine morphogenesis (1.07)	Nucleobase-containing compound metabolic process (0.94)
Golgi apparatus (1.04)	Proteasome core complex (0.87)
Epidermal growth factor-like domain (0.92)	Mitochondrial respiratory chain complex III (0.85)
Calcium channel activity (0.85)	Mitochondrion (0.80)

Within proteins upregulated in transgenic mice at the basal level, clusters including endocytosis, synapse, regulation of dendritic spine morphogenesis and calcium channel activity were identified as enriched. Within downregulated proteins, annotation clusters including pathways of neurodegeneration, IMM, respiratory chain complex IV, and respiratory chain complex III were identified as enriched. DAVID identified a total of 41 functional clusters in the upregulated proteins and a total of 43 clusters in the downregulated proteins.

4.3.2.7 STRING Protein Network Mapping

The list of protein interactions downloaded from STRING for the generation of functional dependency matrices was filtered to identify proteins with the greatest number of outgoing connections, which therefore have the greatest effect on other proteins, and the proteins with the greatest number of incoming connections, which therefore are the greatest affected by others. The top 10 most connected proteins are listed in table 4.9, with the number of each type of connection stated. This analysis encompasses all of the upregulated and downregulated proteins within APPtg mice at the basal level, to identify the most enriched in the experimental category, regardless of directionality.

The vast majority of highly connected proteins identified by the analysis were members of the Ppp2 family, a family of catalytic subunits of protein phosphatases (ppp's), the major serine/threonine

phosphatases, implicated in the negative regulation of cell growth and division. Post-mortem studies of AD patients have linked Ppp2 to AD. Within the disease, Ppp2 shows reduced activity, owing to increased inhibition, reduced levels, and alterations to subcellular localisation and specificity (Braithwaite et al., 2012). Further, Ppp2c has been shown to be downregulated in AD, leading to induction of tau hyperphosphorylation. In health, Ppp's serve a neuroprotective role and regulate the autophagic degradation of proteins (Sinsky, Pichlerova & Hanes., 2021). In vivo studies from Sontag (2004) have shown the selective Pp1/pp2A inhibitor, okadaic acid, induces the hyperphosphorylation of tau, deposition of Aß, changes in synaptic plasticity, memory impairment and neurodegeneration.

Table 4.9. Numbers of incoming and outgoing protein interactions within APPtg mice at the basal level, when compared to WT mice at the basal level (group D).

D- Wild-type basal V. APPtg basal				
	Most outgoing connections	**No.**	**Most incoming connections**	**No.**
1	Ppp2r1a	100	Ppp2r1a	112
2	Ppp2ca	100	Ppp2ca	111
3	Ppp2cb	100	Ppp2cb	111
4	Ppp2r1b	100	Ppp2r1b	108
5	Ppp2r5a	100	Ppp2r5a	108
6	Ppp2r5b	100	Ppp2r5b	108
7	Ppp2r5c	100	Ppp2r5c	108
8	Ppp2r5d	95	Ppp2r5d	108
9	Ppp2r5e	95	Ppp2r5e	108
10	BC048507	95	BC048507	97

4.3.2.8 Functional Dependency Analysis

Functional dependency matrix was created for all proteins upregulated in APPtg mice at the basal level (when compared to WT mice at the basal level; group D). A total of 213 species with 45,369 reactions were included in the basal model (Figure 4.25). The majority of

dependencies in the matrix have no effect, however, a considerable number (5944) of dependencies are strong activators, and a portion of results are strong inhibitors (99). Similar to the memory retrieval matrix, there are no negative feedback loops present within the model, however, in contrast to the previous model, there are also no ambivalent dependencies within the basal model.

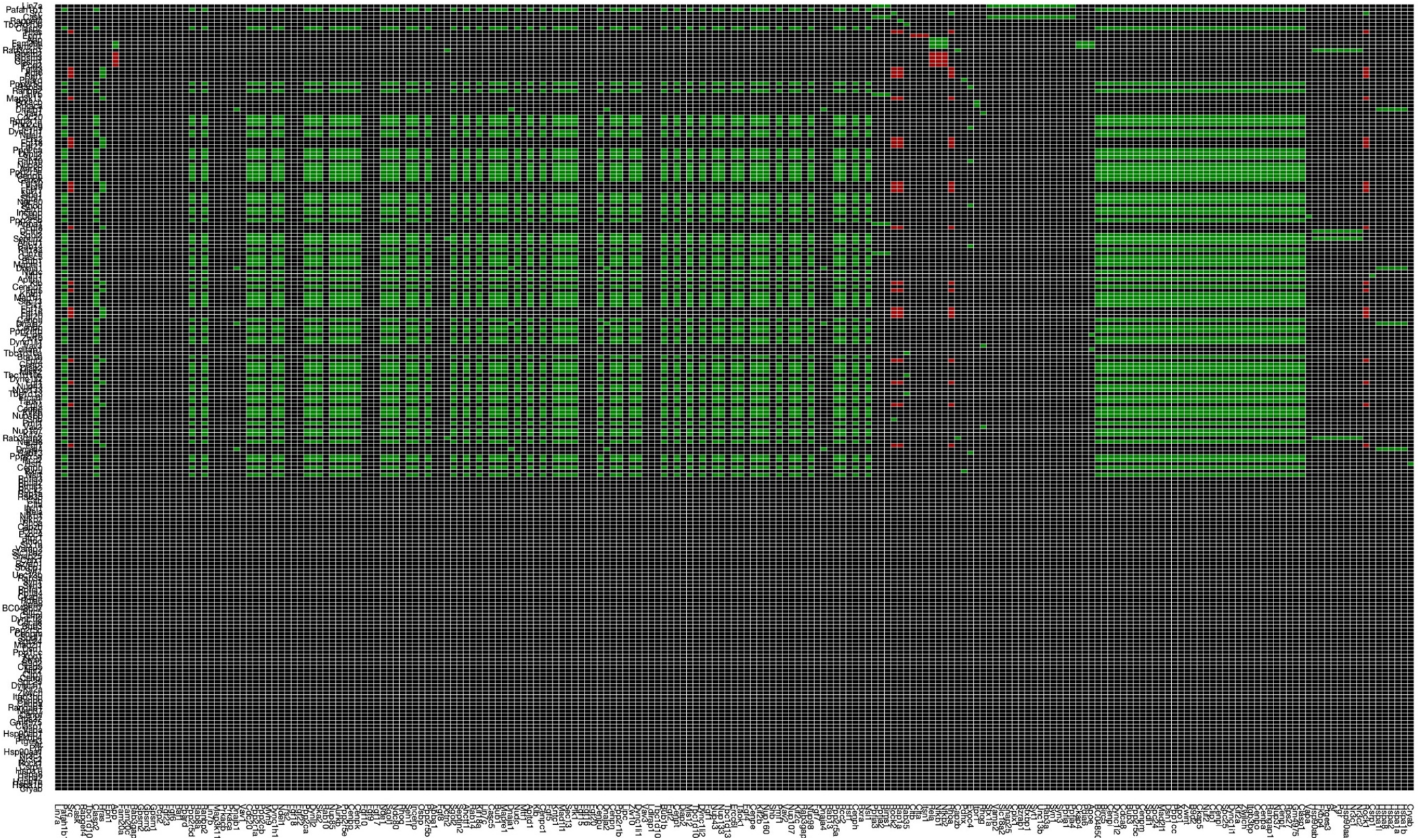

Figure 4.25. Functional dependency matrix for upregulated expressed proteins at the basal level in APPtg mic (when compared to WT mice at the basal level; group D). Y-axis labels are in reverse order to x-axis (starting from Lin7a and finishing with Cryab. Overlapping species labels can be deduced from X-axis labels.

KO models were generated, removing specific proteins from the matrix. Proteins that strongly activated a large amount of other nodes in the model or proteins that strongly inhibited a large amount of other proteins in the model were targeted for removal. Table 4.10 lists the effect of node removal on the model. Due the lack of feedback loops (positive or negative) and ambivalent factors in the model, none of the protein KO models had any effect on the rest of the model dependencies. All KO scenarios have only 44,944 reactions as opposed to 45,369 due to removal of target node and all of its dependencies.

Table 4.10. Functional dependency matrix Knock-out results.

Scenario	Number of Each Dependency						
	No Effect	Ambivalent	Weak Inhibitor	Weak Activator	Strong Inhibitor	Strong Activator	Total
Full model	39326	0	0	0	99	5944	45,369
Cdc20 KO	39054	0	0	0	99	5791	44,944
Ppp2cb KO	39054	0	0	0	99	5791	44,944
Src KO	39016	0	0	0	78	5850	44,944
Clasp2 KO	39056	0	0	0	99	5789	44,944

A functional dependency matrix could not be generated for proteins upregulated in APPtg mice during memory retrieval (when compared to WT mice during memory retrieval; group B) due to the lack of significant protein expression in APPtg mice during memory retrieval after the application of FDR correction.

4.3.3 Differentially Regulated Proteins During Memory Retrieval

The following sections contain the results for proteins differentially regulated during memory retrieval in each genotype when compared to their own respective basal levels, and a direct

comparison of transgenic mice during memory retrieval and WT mice during memory retrieval (group B).

Protein lists were compared between genotypes to identify those which were properly regulated (upregulated in APPtg as well as WT mice), failed to be properly regulated, (upregulated in WT mice but not in APPtg mice), and inappropriately regulated (upregulated in APPtg mice but not in WT mice). Table 4.11 details the differential protein upregulations in APPtg mice during memory retrieval, when compared to WT mice during memory retrieval. 58 proteins were found to be mutually upregulated, 98 failed to become upregulated during memory retrieval and 61 proteins were inappropriately regulated.

Upregulated:

Table 4.11. Proteins differentially regulated during memory retrieval in APPtg mice, when compared to WT mice during memory retrieval (group B). Mutually upregulated proteins= upregulated in both WT memory retrieval and APPtg memory retrieval. Failed to become upregulated= proteins upregulated in WT mice during memory retrieval but were not upregulated in APPtg mice during memory retrieval. Inappropriately regulated= proteins that were upregulated during memory retrieval in APPtg mice but were not upregulated in WT mice.

Mutually Upregulated During Memory Retrieval	**Failed to become upregulated during memory retrieval**	**Inappropriately regulated during memory retrieval e.g., upregulated in APPtg but not in WT**
Mbp	Fam162a	Cox6c
Atp6v1g2	Snca	Rps18;Gm10260
Ndufa2	Cox7a2	Arf5
Tmod2	Gap43	Psmd7
Hint2	Slc9a3r1	Usmg5
Atp5i;Atp5k	Ndufa7	Atp6v1g1
Arpc5l	Nme1	Sod1
Lin7a	Park7	Psma2
Ndufb1	Fabp5	Dnaja2
Cltb	Scrn3	Uqcr10
Pcmt1	Psma3	Comtd1
Atp5o	Clptm1	Marcks
Cycs	Gfap	Impact
Atp6v1e1	Ndufa6	Arpc3
Ak1	Dctn2	Psmd6
Ndufa5	Rab8a	Crip2
Sgta	Cox5a	Mras
Ube2n	Asrgl1	Cbr3

Cox6a1	Ndufb6	Ndufb10
Snx12	Pafah1b2	Cisd1
Ndufs4	Fxyd6	Wipf3
Cox6b1	Nudt3	Acaa1a;Acaa1b
Dynll2	Ndufb4	Mtpn
Clta	Tppp	Psma1
Tpi1	Nefl	Atl2
Efhd2	Fam213a	Ndufb3
Ndufa4	Lrrc57	Stip1
Ndufv2	Ndufb2	Lgalsl
Uqcrb	Wars	Psmc6
Hrsp12	Ina	Vps29
Mapt	Apool	Ndufa8
Prdx5	Cfl2	Sdhb
Fis1	Slc27a1	Atp5l
Atp5h	Purb	Dpysl5
Prdx6	Lpgat1	Hprt1
Rpl18	Pura	Rab35
Uqcrq	Pebp1	Sod2
Gng7	Prdx2	Snap25
Atp6v1d	Nipsnap3b	Gars
Nsfl1c	Rap1a	Nefm
Akr1a1	Gmfb	Pgam5
Txnl1	Rab1b	Ndufb7
Ppia	Napg	Clu
Cbr1	Tmed9	D10Jhu81e
Tagln3	Psmd4	Ckb
Psma6	Psmb2	Timm44
Ndufs5	Tollip	Mapk8ip3
Scp2	Ndrg1	Pgrmc1
Fkbp1a	Pam	Mcu
Prdx1	Dusp3	Slc4a3
Psat1	Ube2v1;Gm20431;Ube2v2	Fam49b
Napb	Arpc5	Ak4
Ywhaz	Myadm	Psma5
Cfl1	Aldoc	Grb2

Dynll1	Rab11b;Rab11a	Ndufb9
Mtx2	Cds2	Syt12
Eef1a2	Pcbp2	Chchd3
Capzb	Dstn	Tom1l2
	Slc6a9	Homer1
	Prdx3	Stx12
	Slc25a27	Ndrg2
	Ankrd63	
	Abcb8	
	Ddt;Gm20441	
	Arhgdia	
	Pcbp1	
	Csrp1	
	Ddost	
	Reep5	
	Tmx4	
	Rap2b	
	Hsd17b12	
	Psma7;Psma8	
	Gsr	
	Rhog	
	Cnrip1	
	Ywhae	
	Ppa1	
	Vsnl1	
	Gna11	
	Ahsa1	
	Map2k4	
	Aspa	
	Psmc1	
	Necap1	
	Aldoa	
	Tecr	
	Rab6b	
	Adgrl3;Lphn3	
	Slc44a2	

	Ywhaq	
	Dgke	
	Pdia6	
	Prune	
	Cyb5b	
	Flot1	
	Kxd1	
	Sparcl1	

DAVID functional analysis tools were used to provide information on the enriched BP, CC, and MF present within the lists of inappropriately regulated proteins (table 4.11).

In APPtg mice during memory retrieval, a number of proteins fail to become upregulated when they are upregulated in their WT counterparts. DAVID provided information on the enriched biological process annotations identified within the list. Cellular response to oxidative stress was the only significantly enriched biological process, out of a total of 9 processes. Figure 4.26 reveals that within the list of proteins identified as upregulated in APPtg mice during memory retrieval when they were not upregulated in their WT counterparts, none of the biological process annotations were significantly enriched. A total of 10 biological processes were enriched non-significantly, including mitochondrial ATP synthesis coupled proton transport, aerobic respiration, mitochondrial respiratory chain complex I and superoxide anion generation.

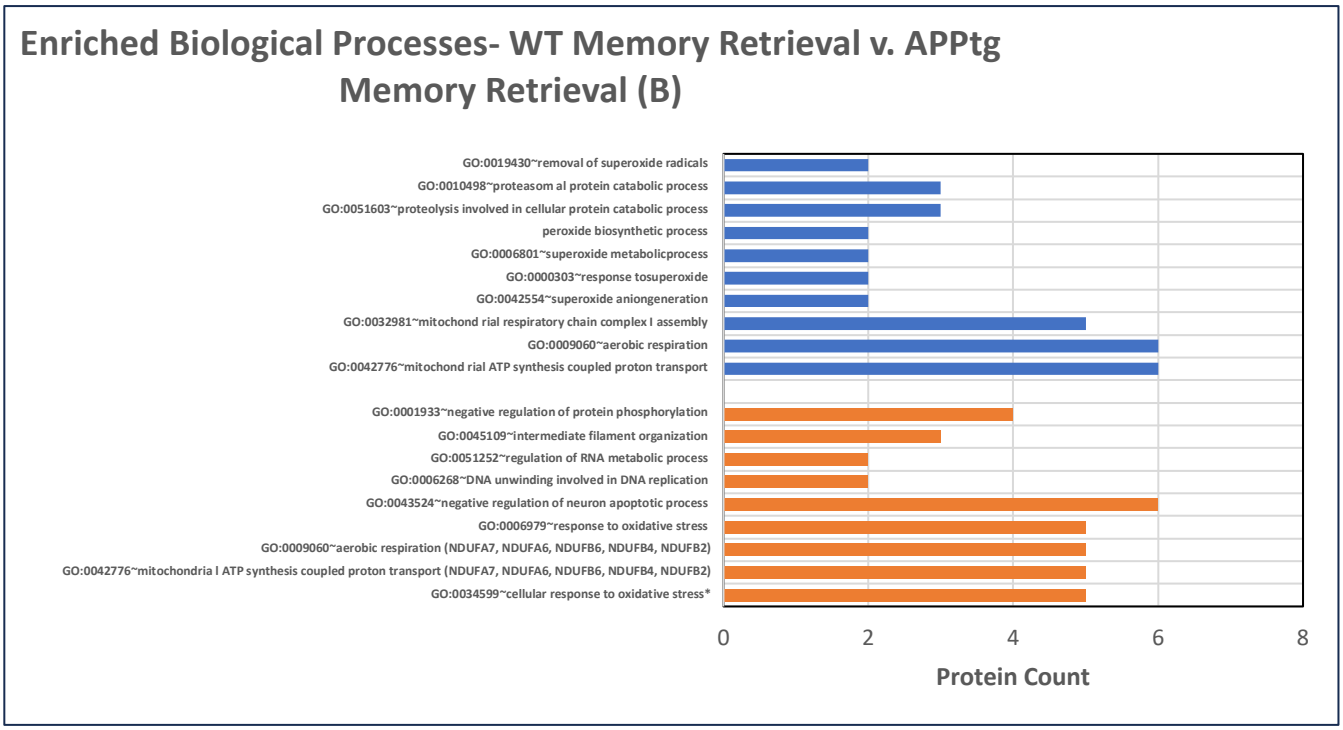

*Figure 4.26. DAVID GO enrichment analysis output for enriched biological processes within proteins that fail to become upregulated or become upregulated in APPtg mice during memory retrieval but are not upregulated in WT mice during memory retrieval. Significant results denoted by *. Blue= proteins upregulated when they shouldn't be, Orange= proteins that fail to become upregulated.*

Figure 4.27 summarises the top 10 cellular components identified as enriched within the protein lists. Within the proteins that fail to become upregulated, 7 cellular components were identified as enriched, with 6 of these significantly enriched, including, myelin sheath, endoplasmic reticulum-Golgi intermediate compartment, and intermediate filament. In the proteins upregulated when they should not have been, 8 cellular components were identified as enriched, with 7 significantly enriched, including proteasome complex, mitochondrial inner membrane, and respiratory chain.

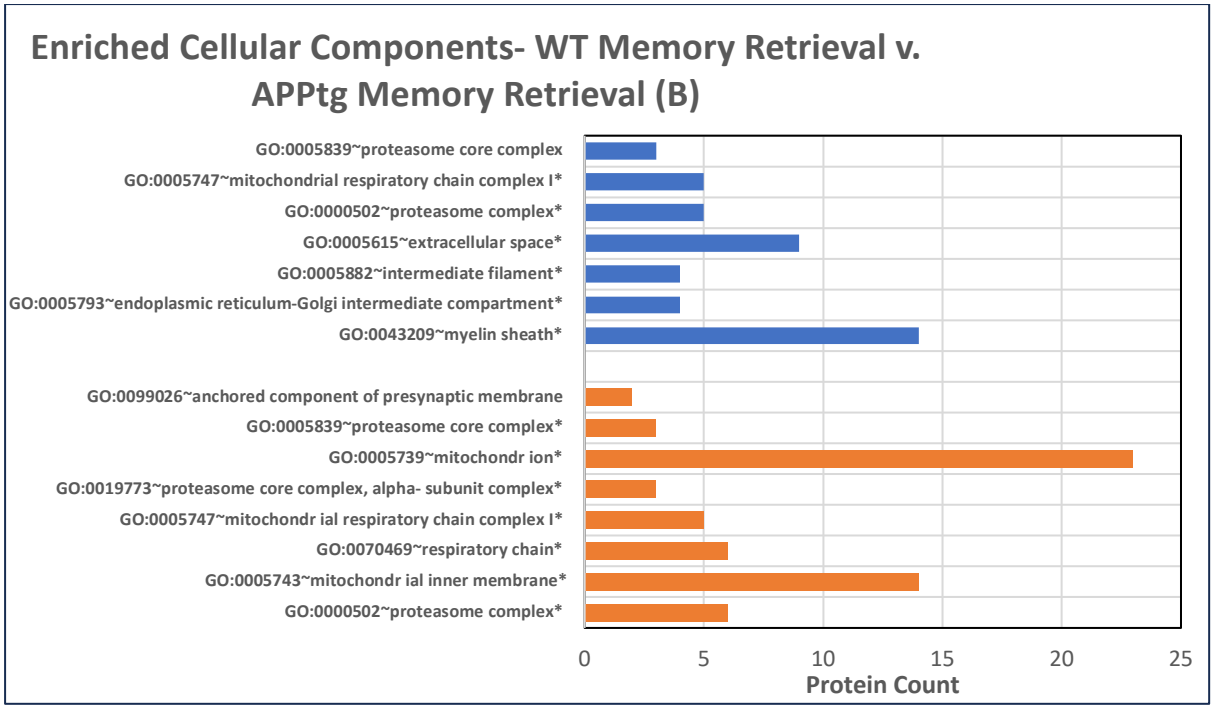

*Figure 4.27. DAVID GO enrichment analysis output for enriched cellular components within proteins that fail to become upregulated or become upregulated in APPtg mice during memory retrieval but are not upregulated in WT mice during memory retrieval. Significant results denoted by *. Blue= proteins that fail to become upregulated, Orange= proteins upregulated when they shouldn't be.*

Figure 4.28 highlights the enriched molecular function annotations identified within the protein lists. Within proteins that failed to become upregulated during memory retrieval, 10 categories were enriched, with 5 significantly enriched, including single-stranded DNA binding, RNA polymerase II transcription factor activity- sequence specific DNA binding, and RNA polymerase II regulatory region sequence-specific DNA binding. Only two molecular function annotations were enriched within the proteins inappropriately upregulated which were superoxide dismutase activity and chaperone binding- both of which were significantly enriched.

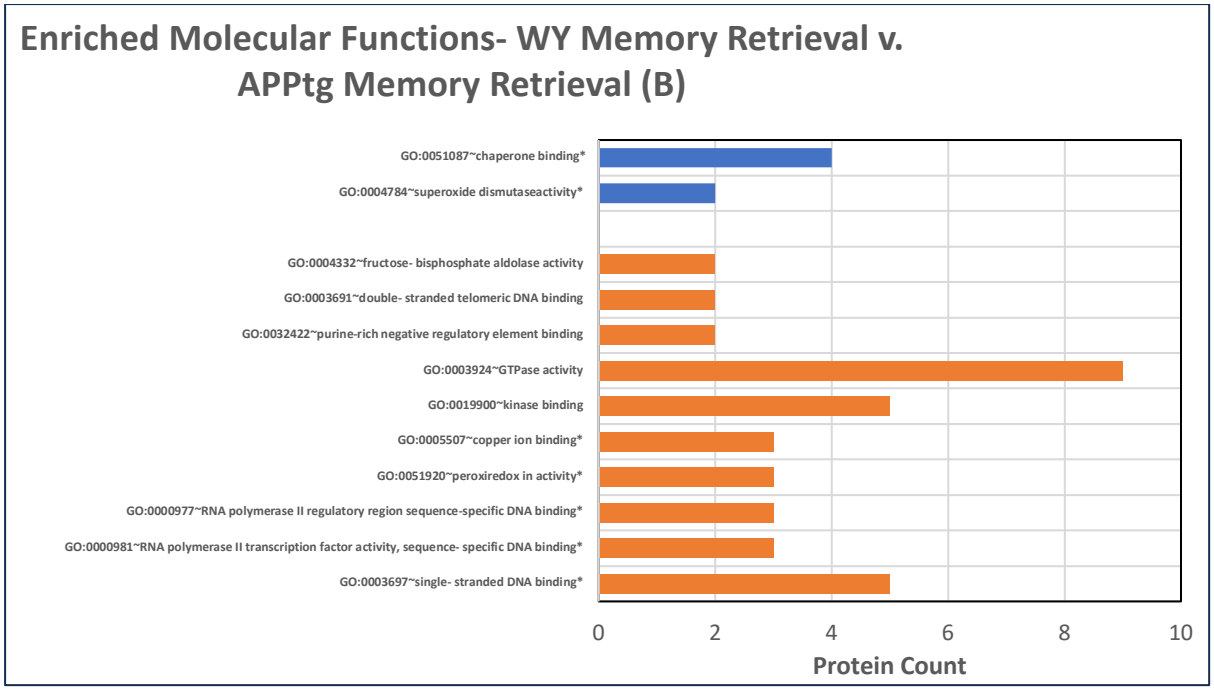

Figure 4.28. DAVID GO enrichment analysis output for enriched molecular functions within proteins that fail to become upregulated or become upregulated in APPtg mice during memory retrieval but are not upregulated in WT mice during memory retrieval. Significant results denoted by. Blue= proteins upregulated when they shouldn't*

Downregulated:

Table 4.12 details the differential protein upregulations in APPtg mice during memory retrieval, when compared to WT mice during memory retrieval. 15 proteins were found to be mutually downregulated, 109 failed to become downregulated during memory retrieval and 42 proteins were inappropriately downregulated in the APPtg mice.

Table 4.12. Differential protein regulations in APPtg mice during memory retrieval, when compared to WT mice during memory retrieval (group B).

Mutually Downregulated During Memory Retrieval	Failed to become downregulated during memory retrieval	Inappropriately regulated during memory retrieval e.g. downregulated in APPtg mice but not in WT
Ap3d1	Mpst	Scyl2
Akap5	Agl	Tpp2
Pip5k1c	Stam	Pdk1
Snap91	Bcs1l	Hexb
6430548M08Rik;Kiaa0513	Wdr7	Psmd1
Ppfia2	Madd	Vps26a

Pacs1	Dnajc5	Blmh
Dmxl2	Lrpprc	Ap3b2
Mink1	Adcy5	Ap3s1
Aak1	Unc13a	Nrxn2
Dclk1	Pcx;Pc	Gsk3a
Dlg2	Myo6	Rimbp2
Dnajc6	Plcb1	Slc2a13
Nbea	Kif21a	Sacm1l
Ap2b1	Pygm	Mtor
	Dip2b	Tnik
	Rock2	Adgrb2;Bai2
	Rims1	Adss
	Aldh6a1	Mpi
	Ogdhl	Cdc42bpb
	Grm3	Psmd3
	Ppp1r9a	Ank1
	Synj1	Adrbk1
	Rasgrf2	Pdp1
	Ppfia3	Atp8a1
	Gls	Apmap
	Oat	Mllt4
	Aco2	Stk32c
	Sdha	Cltc
	Opa1	Ppp5c
	Acadsb	Gabbr1
	Abat	Atp2b4
	Elfn2	Pafah1b1
	Wnk2	Usp14
	Dbn1	Grm2
	Immt	Map4
	Hspa9	Ptk2b
	Cyfip2	Slc25a22
	Dld	Sgip1
	Atp6v0a1	Epb4.1l1;Epb41l1
	Dctn1	Afg3l2
	Eps15l1	Pfkp

	Pcdh1	
	Synpr	
	Ogdh	
	Samm50	
	Syngap1	
	Brsk2	
	Smap1	
	Oxr1	
	Mthfd1l	
	Cadps	
	Atp6ap1	
	Rph3a	
	Por	
	Glud1	
	Camk2g	
	Shank3	
	Nrxn3	
	Adam22	
	Pcdhgc5	
	Myo18a	
	Bsn	
	Dlgap1	
	Epha4	
	Ctnnd2	
	Clasp2	
	Ppp1r9b	
	Sv2b	
	Ndufs1	
	Nckap1	
	Tln2	
	Atp2b1	
	Ogt	
	Wdr1	
	Srcin1	
	Stxbp5l	
	Actn1	

	Dnm3	
	Lancl2	
	Pkp4	
	Slc12a5	
	Sptbn1	
	Prkcb	
	Cap1	
	Syt1	
	Anxa7	
	Ntrk2	
	Shank2	
	Syn1	
	Abi2	
	Sptan1	
	Dlgap2	
	Camkv	
	Gpi	
	Gda	
	Atp2b2	
	Hk1	
	Map6	
	Npepps	
	Ctnnb1	
	Lonp1	
	Prkar2b	
	Nrcam	
	Smpd3	
	Atp2b3	
	Sptbn2	
	Amph	
	Nrxn1	

Within the lists of inputted proteins downregulated during memory retrieval, 51 biological processes were enriched, with 33 significantly enriched, including learning, synaptic vesicle exocytosis, and regulation of dendritic spine morphogenesis, highlighted in figure 4.28. Other biological processes identified were chemical synaptic transmission, long-term synaptic potentiation, cellular calcium ion

homeostasis, regulation of NMDA receptor activity, and postsynaptic neurotransmitter receptor internalization. Within the proteins inappropriately downregulated, 19 BP were identified, 10 of which were significant, including protein phosphorylation, phosphorylation, and chemical synaptic transmission.

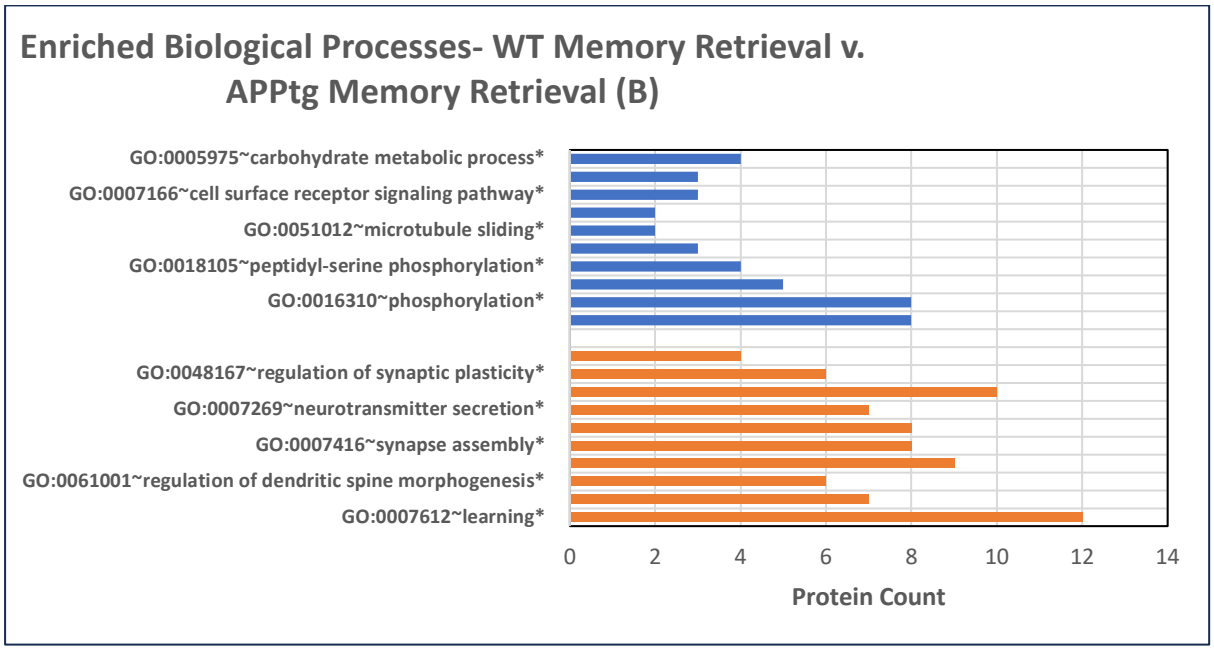

*Figure 4.28. DAVID GO enrichment analysis output for enriched biological processes within proteins that fail to become downregulated or become downregulated in APPtg mice during memory retrieval but are not downregulated in WT mice during memory retrieval. Significant results denoted by *. Blue= proteins downregulated when they shouldn't be, Orange= proteins that fail to become downregulated.*

Within the inputted protein lists, 42 cellular component annotations were identified as enriched, with 30 significantly enriched including glutamatergic synapse, cortical actin cytoskeleton, and cell projection. Within the proteins downregulated during memory retrieval when they shouldn't have been downregulated, 6 cellular components were identified, with only membrane coat and membrane significantly enriched (figure 4.29).

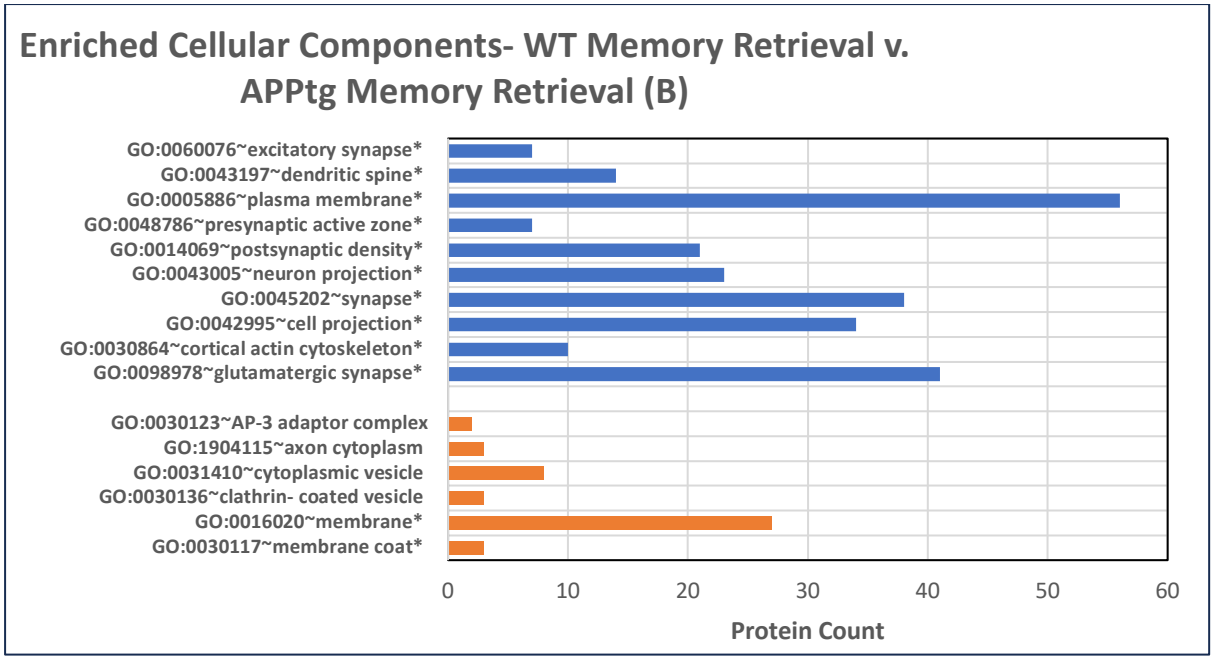

*Figure 4.29. DAVID GO enrichment analysis output for enriched cellular components within proteins that fail to become downregulated or become downregulated in APPtg mice during memory retrieval but are not downregulated in WT mice during memory retrieval. Significant results denoted by *. Blue= proteins that fail to become downregulated, Orange= proteins that are downregulated when they shouldn't be.*

Figure 4.30 highlights the top enriched molecular function annotations within the inputted protein lists. Within the proteins that failed to become downregulated during memory retrieval, 16 functions were identified as enriched, with 13 of these significantly enriched, including calmodulin binding, actin filament binding, and calcium-transporting ATPase activity involved in regulation of presynaptic cytosolic calcium ion concentration. Within the list of proteins downregulated during memory retrieval when they shouldn't be downregulated were 13 enriched molecular functions, with 8 significantly enriched, including protein kinase activity, ATP binding, and kinase activity.

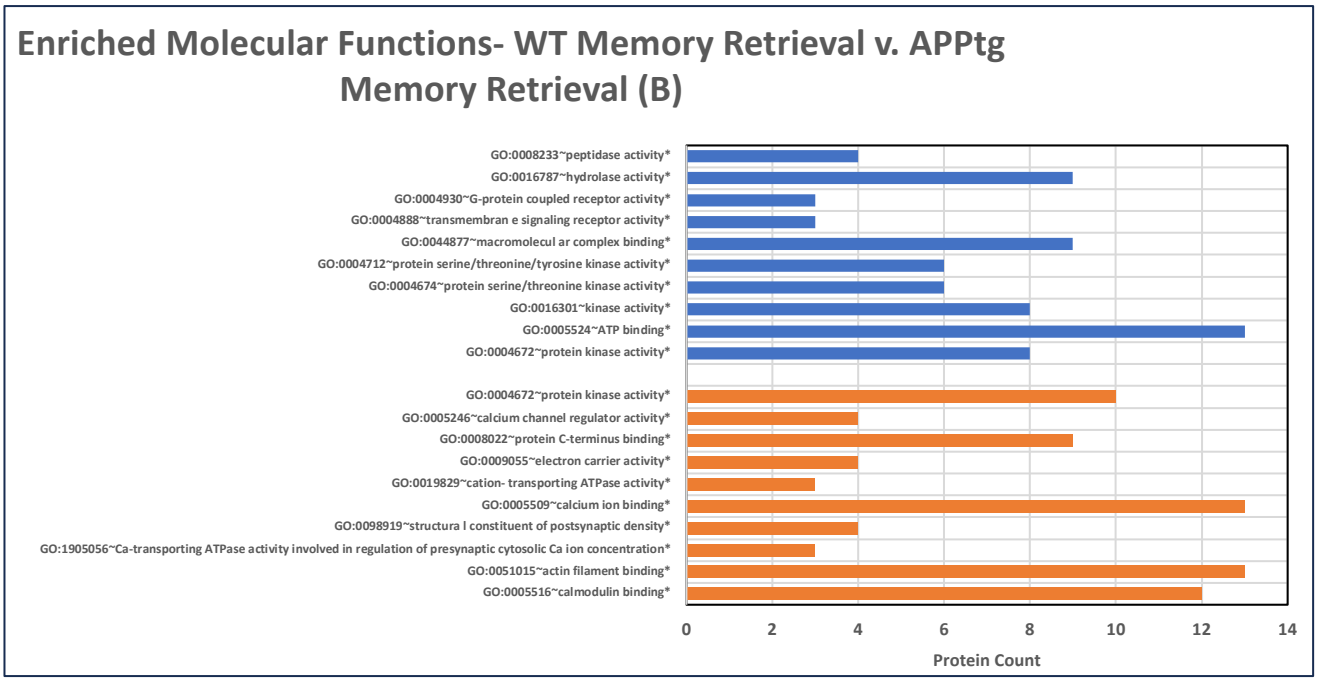

*Figure 4.30. DAVID GO enrichment analysis output for enriched molecular functions within proteins that fail to become downregulated or become downregulated in APPtg mice during memory retrieval but are not downregulated in WT mice during memory retrieval. Significant results denoted by *. Blue= proteins downregulated when they shouldn't be, Orange= proteins that fail to become downregulated.*

Using mus musculus Mitocarta 3.0 from Broad Institute, proteins involved in the ETC (figure 4.31) and mitochondrial dynamics (figure 4.32) were extracted from each experimental condition. Heatmaps were generated to represent the expression of these proteins when compared to WT basal expression levels. Only proteins with 4 data points for each of the four experimental conditions were continued to heatmap generation. All proteins were expressed as a percentage of WT basal expression levels.

Figure 4.31 reveals a number of differential regulations within protein subunits of the ETC. During memory retrieval in WT mice and APPtg mice, complex I and complex IV proteins are upregulated when compared to basal levels. In APPtg mice during memory retrieval, complex II proteins are upregulated at a greater amount than in WT mice during memory retrieval. Complex I and V proteins are regulated consistently across both behavioural groups in WT mice and APPtg mice.

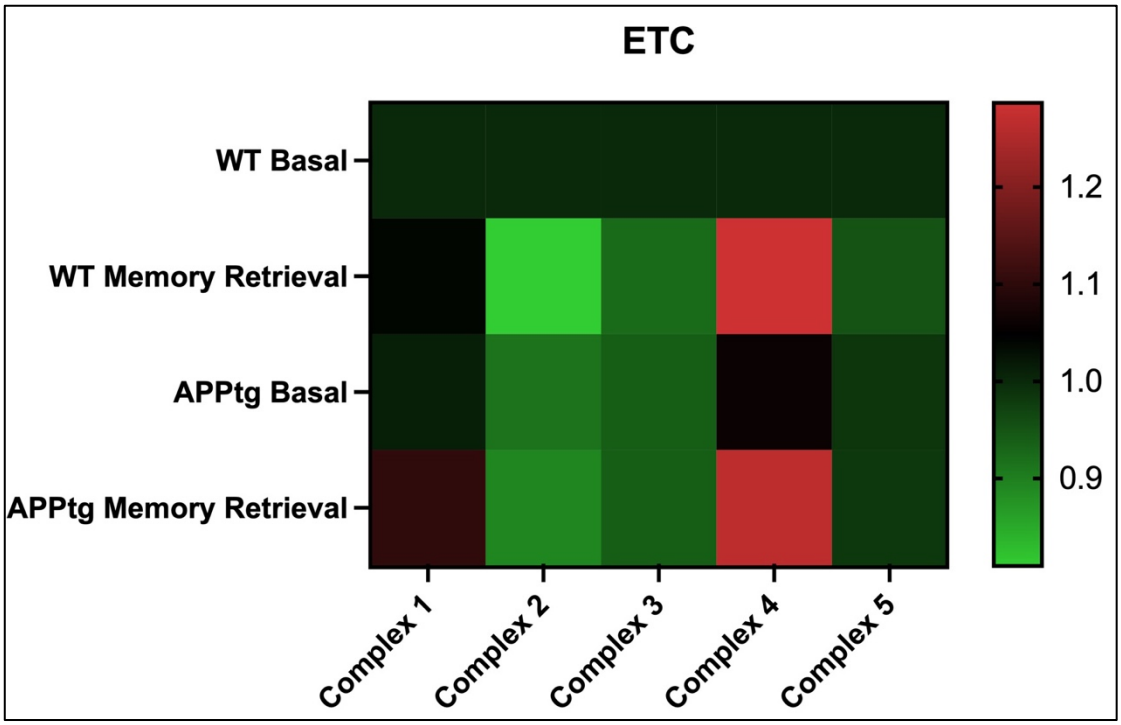

Figure 4.31. Electron transport chain protein expression during memory retrieval in each experimental condition. Protein expression expressed as a percentage of WT basal expression levels, in terms of fold change. 1.2= 120%-fold change. Red= highest fold change, green= smallest fold change.

Figure 4.32 reveals the different regulation levels of proteins involved in mitochondrial dynamics, in relation to WT basal levels. During memory retrieval in both genotypes Cycs, which associates with the IMM and accepts electrons from cytochrome b and transfers them to cytochrome oxidase (GeneCards., 2023), and Park7, co-chaperone protein which modulates the autophagic removal of misfolded protein cargoes generated via oxidative stress (NCBI.,2023), are the most highly upregulated, with a fold change of 150% from WT basal levels. The Ahcyl1, Aifm1 Slc25a46, and Mfn2 proteins were the most unchanged between the behavioural groups, displaying consistent regulation levels during basal levels and during memory retrieval. Samm50 was downregulated in WT mice during memory retrieval but failed to become downregulated to the same level in the APPtg mice. When compared to WT mice at the basal level, VDAC1 was upregulated in WT mice during memory retrieval and in APPtg mice both during basal levels and during memory retrieval.

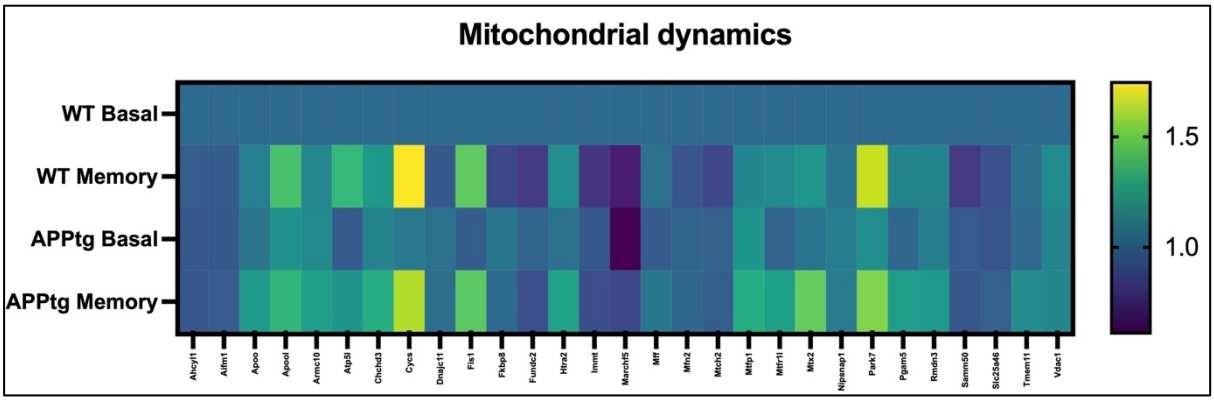

Figure 4.32. Expression levels of key proteins involved in mitochondrial dynamics in each experimental condition. Protein expression expressed as a percentage of WT basal, in terms of fold change. 1.5= 150% fold change. Yellow- highest fold change, dark blue/black= smallest fold change.

4.3.3.1 DAVID Annotations- Gene Ontology

The results from DAVID GO term enrichment analyses are listed in the below sections for the three memory retrieval-specific experimental groups. The top 10 results for each annotation term and presented, and the results are listed in order of significance value.

4.3.3.2 Biological Process

Within proteins identified as upregulated in WT mice during memory retrieval, when compared to WT mice at the basal level (group A), 18 biological processes were found to be significantly enriched, including mitochondrial ATP synthesis coupled proton transport, aerobic respiration, mitochondrial respiratory chain complex I assembly and mitochondrial electron transport- cytochrome c to oxygen (figure 4.33). Within proteins downregulated in WT mice during memory retrieval, 5 biological processed were identified as significantly enriched, including synaptic vesicle docking, neurotransmitter secretion, and postsynaptic actin cytoskeleton organisation.

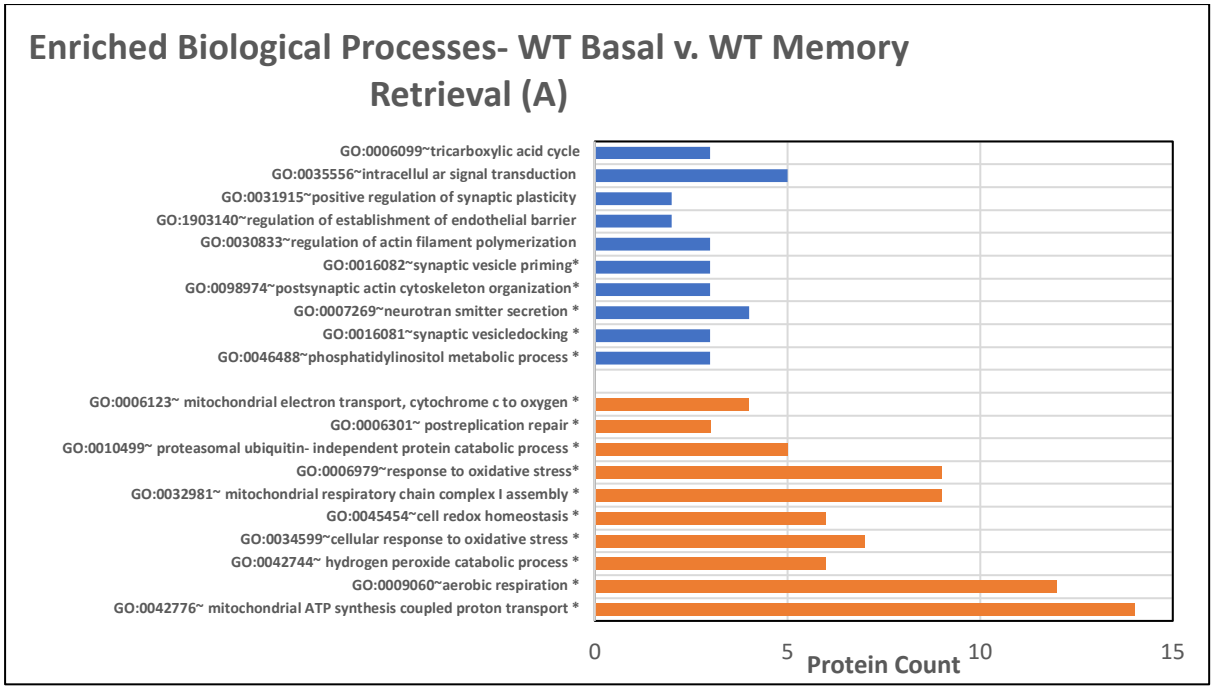

*Figure 4.33. DAVID GO term enrichment analysis results for enriched biological processes within proteins differentially regulated in WT mice during memory retrieval, when compared to WT mice at the basal level (group A). Significant results are denoted by *. Blue= downregulated proteins, Orange= upregulated proteins.*

Within proteins identified as downregulated in APPtg mice during memory retrieval, when compared to APPtg mice at the basal level (group C), 15 biological processes were found to be significantly enriched, including mitochondrial ATP synthesis coupled proton transport, aerobic respiration, mitochondrial respiratory chain complex I assembly, response to reactive oxygen species and respiratory electron transport chain (figure 4.34). The list of enriched biological processes in APPtg mice during memory retrieval is strikingly similar to that of the WT mice during memory retrieval; the majority of proteins upregulated in these conditions are involved in the same biological processes. When analysing proteins downregulated in APPtg mice during memory retrieval (compared to APPtg mice at the basal level; group C), 11 biological processes were found to be significantly enriched including intracellular transport, synaptic vesicle recycling, and anterograde axonal transport.

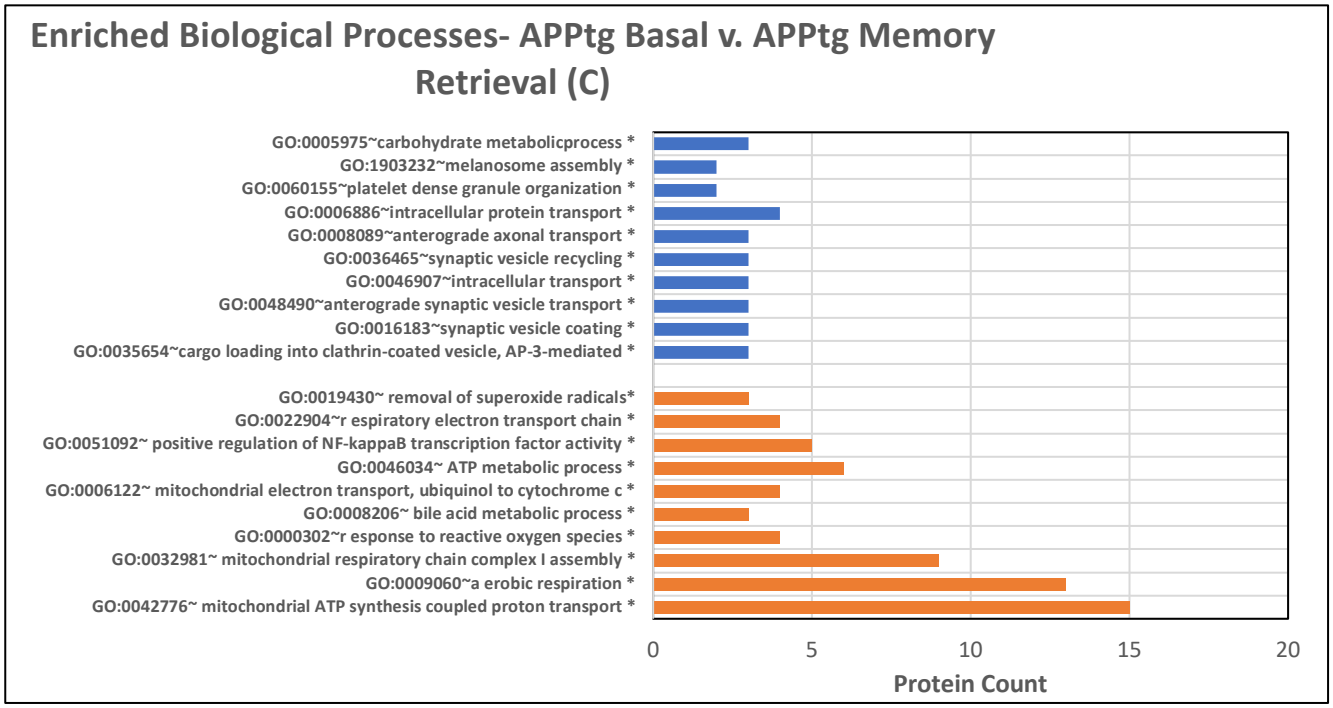

*Figure 4.34. DAVID GO term enrichment analysis results for biological processes enriched within proteins differentially regulated in APPtg mice during memory retrieval, when compared to APPtg mice at the basal level. Significant results denoted by *. Blue= downregulated proteins, Orange= upregulated proteins.*

When comparing proteins upregulated in APPtg mice during memory retrieval with WT mice during memory retrieval (group B), no biological processes were found to be enriched. When comparing downregulated proteins between the two genotypes, only two biological processes were found to be enriched which were cellular response to hypoxia (significantly enriched) and the negative regulation of cell proliferation.

4.3.3.3 Cellular Component

Figure 4.35 presents the enriched cellular component annotations identified by DAVID within submitted lists of differentially expressed proteins in WT mice during memory retrieval, when compared to WT mice at the basal level (group A). Within the upregulated protein list, 10 cellular components were significantly enriched including respiratory chain, mitochondrial respiratory chain complex I, mitochondrial membrane, IMM, mitochondrial respiratory chain complex IV and myelin sheath. Within the downregulated protein lists, 5 cellular components were found to be significantly enriched, including mitochondrial matrix, glutamatergic synapse, and postsynaptic actin cytoskeleton.

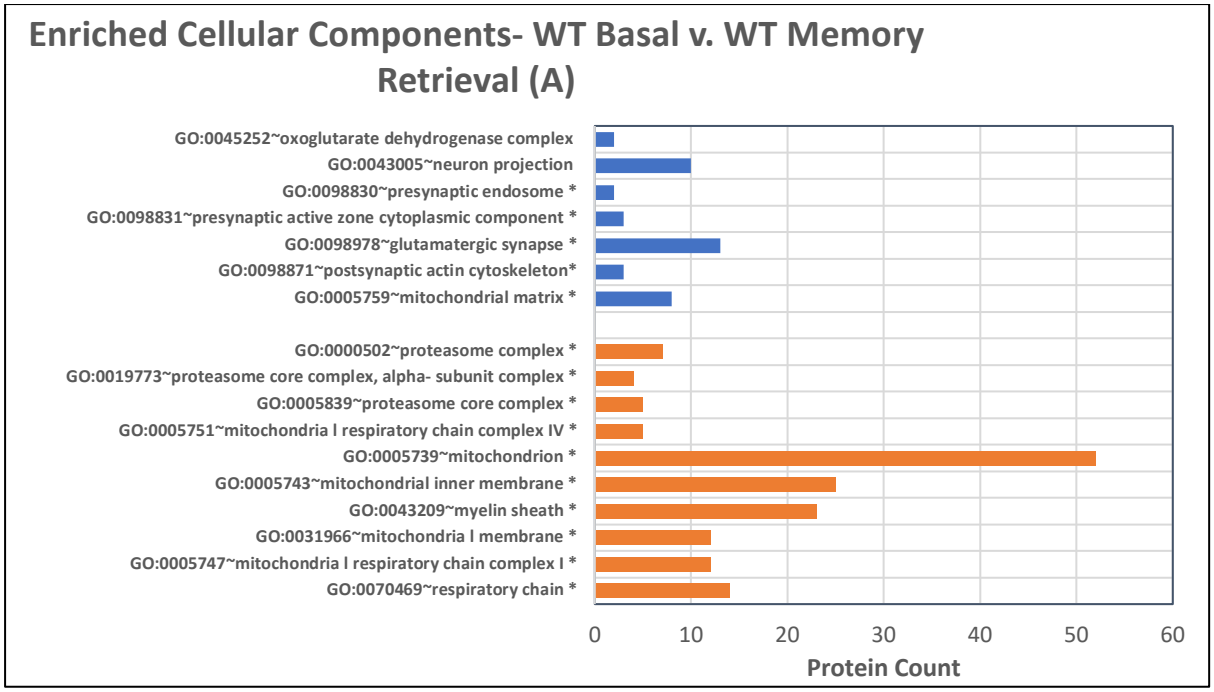

*Figure 4.35. DAVID GO term enrichment analysis results for enriched cellular components within WT mice during memory retrieval, when compared to WT mice at the basal level (group A). Significant results denoted by *. Blue= downregulated proteins, Orange= upregulated proteins.*

Enriched cellular components in the proteins identified as upregulated in APPtg mice during memory retrieval returned very similar results to those enriched in WT mice during memory retrieval, when compared to WT mice at the basal levels (group A). 16 cellular components were significantly enriched in APPtg mice during memory retrieval including respiratory chain, mitochondrial respiratory chain complex I, IMM, mitochondrial respiratory chain complex IV and neurofibrillary tangle (figure 4.36). 7 significantly enriched cellular components were identified as significantly enriched with downregulated proteins in APPtg mice during memory retrieval, including axon cytoplasm, endosome membrane and AP-3 adaptor complex.

When analysing proteins differentially regulated in APPtg mice during memory retrieval, when compared to basal levels (group C), DAVID returned no significantly enriched cellular components within upregulated proteins. Within the inputted downregulated protein lists, DAVID returned 5 enriched cellular components, three of which were significantly enriched. Enriched cellular components were perinuclear region of cytoplasm, myelin sheath, and perikaryon.

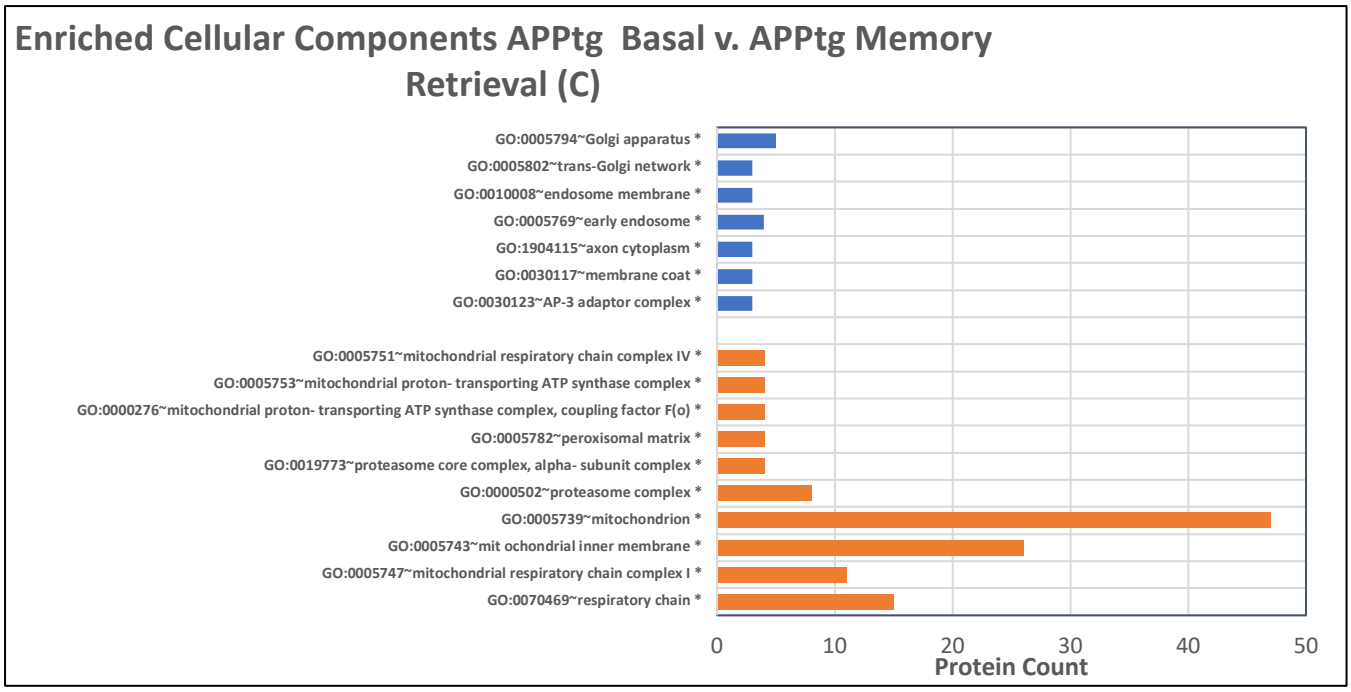

*Figure 4.36. DAVID GO term enrichment analysis results for enriched cellular components within APPtg mice during memory retrieval, when compared to APPtg mice at the basal level (group C). Significant results denoted by *. Blue= downregulated proteins, Orange= upregulated proteins.*

4.3.3.4 Molecular Function

Lists of differentially regulated proteins were submitted to DAVID GO tools and enriched molecular functions were annotated (figure 4.37). Within the proteins upregulated in WT mice during memory retrieval, 9 molecular functions were identified as significantly enriched including, antioxidant activity, macromolecular complex binding, NADH dehydrogenase activity and peroxidase activity. In the downregulated proteins, only one molecular function was significantly enriched- pyridoxal phosphate binding.

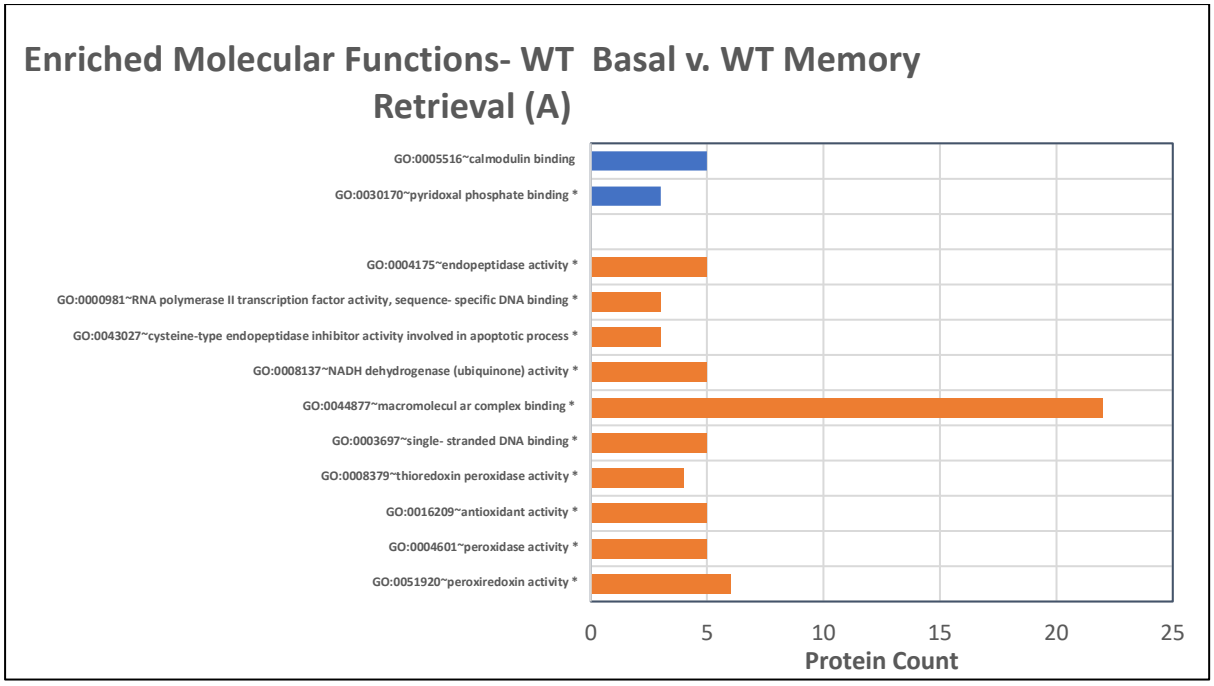

*Figure 4.37. DAVID GO term enrichment analysis results for molecular functions enriched within differentially regulated proteins in WT mice during memory retrieval, compared to WT mice at the basal level (group A). Significant results denoted by *. Blue= downregulated proteins, Orange= upregulated proteins.*

DAVID tools were used to annotate differentially regulated proteins in APPtg mice during memory retrieval (when compared to APPtg mice at the basal level; group C) with significantly enriched molecular functions (figure 4.38). The molecular functions enriched in the transgenic mice were strikingly similar to those of the WT mice, especially in the upregulated proteins, where significantly enriched molecular functions included NADH dehydrogenase activity, antioxidant activity, peroxidase activity and acetyl-CoA C-acetyltransferase activity. Within the downregulated proteins, only one molecular function, aminopeptidase activity, was significantly enriched.

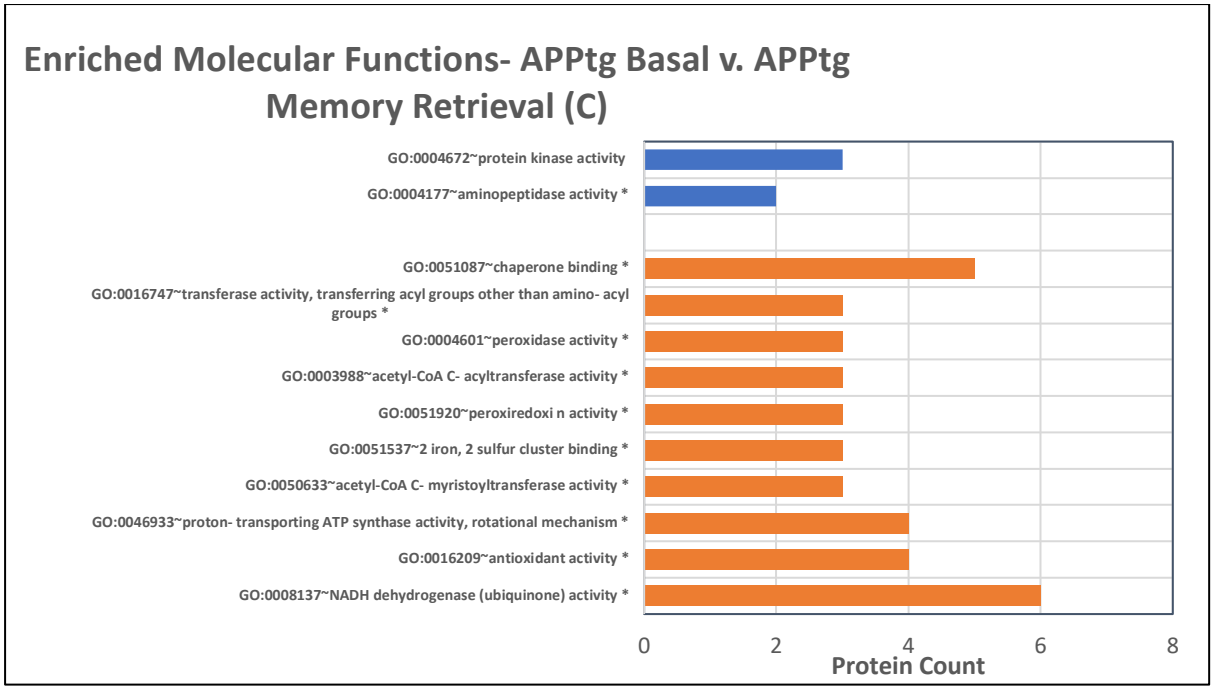

*Figure 4.38. DAVID GO term enrichment analysis results for molecular functions enriched within differentially regulated proteins in APPtg mice during memory retrieval, when compared to APPtg mice at the basal level (group C). Significant results are denoted with *.Blue= downregulated proteins, Orange= upregulated proteins.*

Analysis of proteins upregulated in APPtg mice during memory retrieval when directly compared to WT mice during memory retrieval (group B) returned one, non-statistically significant molecular function enriched within the input list- identical protein binding. No molecular function annotations were found to be enriched in the downregulated protein list for this condition.

4.3.3.5 KEGG Pathways

After submission to DAVID tools for the annotation of enriched KEGG pathways, 14 pathways were identified as significantly enriched within the proteins upregulated in WT mice during memory retrieval, when compared to basal levels (group A ;figure 4.39). Significantly enriched pathways included OXPHOS, AD, prion disease, metabolic pathways (not listed in the top 10 results but still statistically significant) and chemical carcinogens- reactive oxygen species. Within proteins downregulated in WT mice during memory retrieval, four pathways were identified as significantly enriched out of 7 pathways annotated to the list. Significantly enriched pathways in the downregulated proteins included the TCA cycle, metabolic pathways, inositol phosphate metabolism and carbon metabolism.

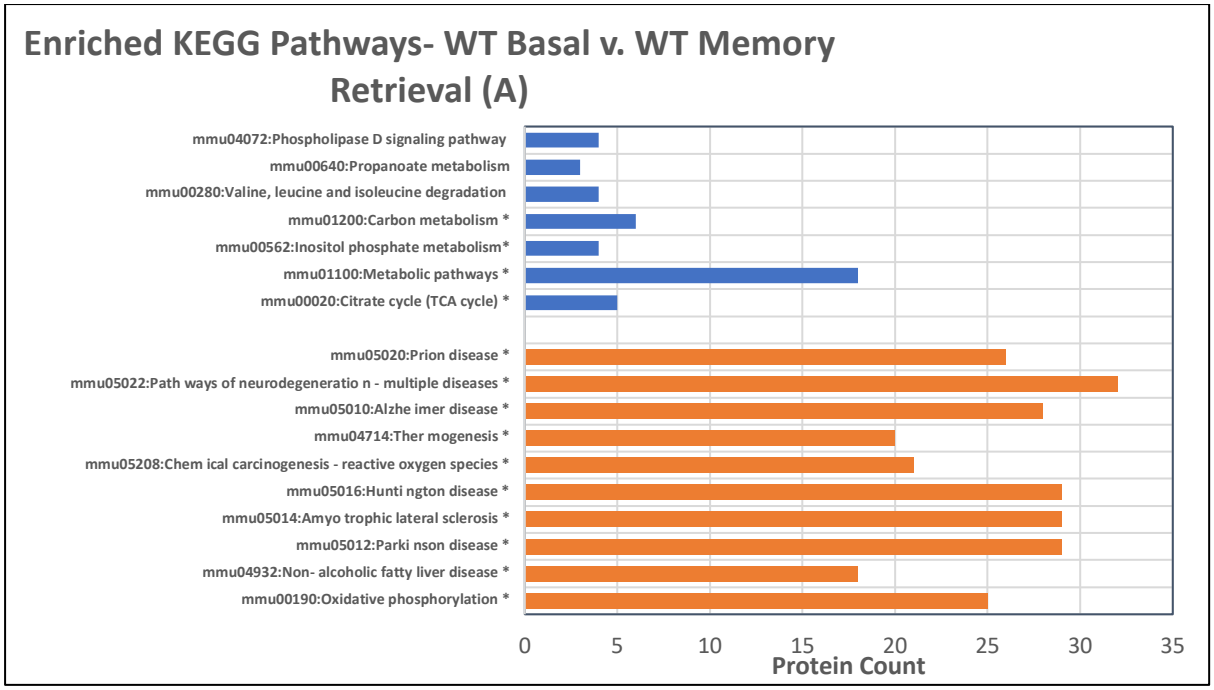

*Figure 4.39. DAVID enrichment analysis results. Top 10 enriched KEGG pathways in differentially regulated proteins in WT mice during memory retrieval, when compared to WT mice at the basal level (group A). Significant results denoted by *. Blue= downregulated proteins, Orange= upregulated.*

Figure 4.40 presents the top 10 enriched KEGG pathways annotated to differentially regulated proteins in APPtg mice during memory retrieval, when compared to APPtg mice during basal levels (group C). Within the upregulated proteins, 15 KEGG pathways were significantly enriched and the top 10 most enriched of these can be found in figure 4.40. Significantly enriched pathways in upregulated proteins include OXPHOS, prion disease, AD, pathways of neurodegeneration and chemical carcinogenesis-reactive oxygen species. The enriched KEGG pathways during memory retrieval in APPtg mice were very similar to that of the WT mice during memory retrieval. Only one significantly enriched KEGG pathway, lysosome, was identified in the downregulated proteins.

No KEGG 175pathways were 175annotated to any of the differentially regulated proteins in APPtg mice during memory retrieval (when directly compared to WT mice during memory retrieval; group B).

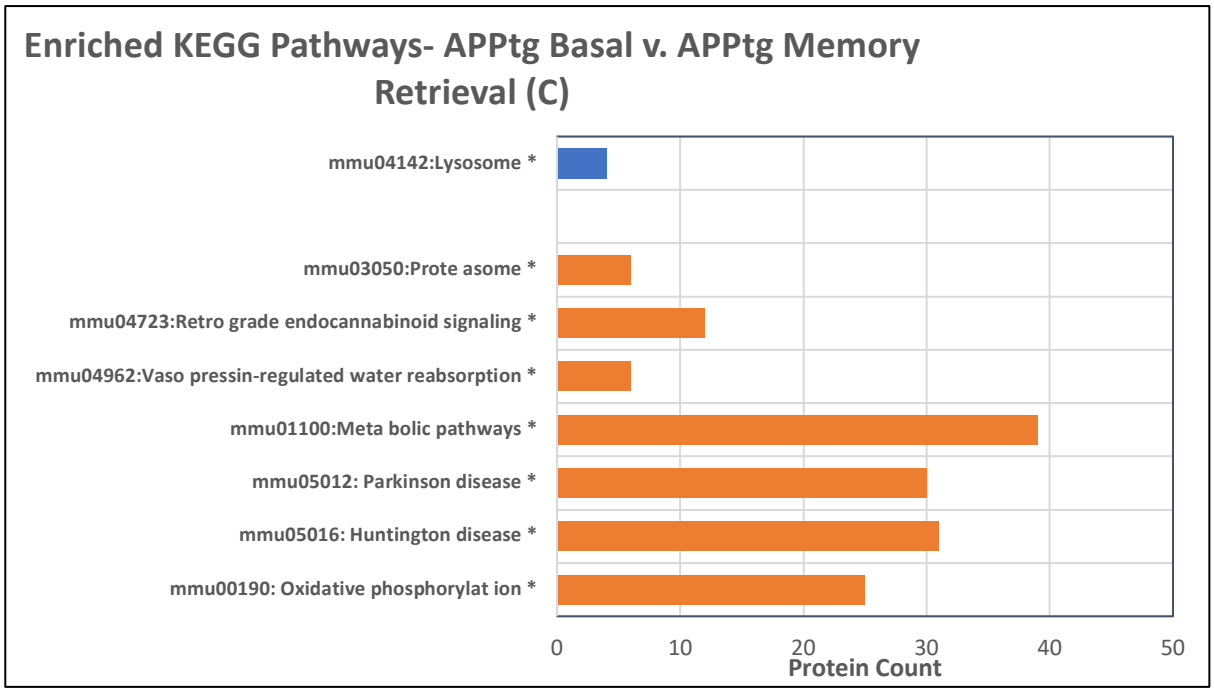

*Figure 4.40. DAVID enrichment analysis results. Table lists top 10 enriched KEGG pathways in differentially regulated proteins in APPtg mice during memory retrieval, when compared to APPtg mice at the basal level. Significant results donated by *. Blue= downregulated proteins, Orange= upregulated proteins.*

4.3.3.6 Functional Annotation Clustering

DAVID functional annotation tools were used to group protein lists into groups of functionally related proteins. The top 5 functional annotation clusters for proteins differentially regulated during memory retrieval are listed below, in order of enrichment score (the higher, the more enriched). Redundant terms were condensed into one overall cluster name, reflective of the functions of each protein within the cluster. The full clustering output tables can be found in Appendix D, section 2.

The top 5 enriched functional annotation clusters within proteins upregulated during memory retrieval in WT mice, when compared to WT mice at the basal level (group A; table 4.13) were as follows; the most enriched cluster was pathways of neurodegeneration, followed by proteasomal ubiquitin-independent protein catabolic process and mitochondrial motif carriers. Fourth came antioxidant activity, followed by ATP biosynthetic processes.

A- Wild-Type Basal v. Wild-Type Memory Retrieval – Upregulated

Table 4.13. DAVID functional annotation clustering output for proteins upregulated in WT mice during memory retrieval, when compared to WT mice at the basal level (group A). Top 5 clusters are listed, in order of enrichment score.

Annotation Cluster	Representative Annotation Terms	Enrichment Score
1	Pathways of neurodegeneration-multiple diseases	7.68
2	Proteasomal ubiquitin-independent protein catabolic process	5.16
3	Mitochondrial motif carriers	3.65
4	Antioxidant activity	2.18
5	ATP biosynthetic processes	1.79

A- Wild-Type Basal v. Wild-Type Memory Retrieval – Downregulated

Table 4.14 lists the top 5 functional annotation clusters, out of 19 in total, identified in proteins downregulated in WT mice during memory retrieval, when compared to WT mice at the basal level (group A). Clusters listed in order of enrichment score. The top 5 clusters were mitochondrion, mesenchymal migration, receptor binding, positive regulation of microtubule nucleation and neurotransmitter secretion.

Table 4.14. DAVID functional annotation clustering output for proteins downregulated in WT mice during memory retrieval, when compared to WT mice at the basal level (group A). The top 5 clusters are listed, in order of enrichment score.

Annotation Cluster	Representative Annotation Terms	Enrichment Score
1	Mitochondrion	1.74
2	Mesenchymal migration	1.69
3	Receptor binding	1.43
4	Positive regulation of microtubule nucleation	1.24
5	Neurotransmitter secretion	1.23

C- APPtg Basal v. APPtg Memory Retrieval- Upregulated

Table 4.15 lists the top 5 functional annotation clusters, out of a total of 23, connected with upregulated proteins in APPtg mice during memory retrieval, when compared to APPtg mice at the basal level (group C). The top 5 most enriched clusters were pathways of neurodegeneration, mitochondrial motif carriers, mitochondrial electron transport, neurofilament cytoskeleton organisation and response to oxidative stress.

Table 4.15. DAVID functional annotation clustering output for proteins upregulated in APPtg mice during memory retrieval, when compared to APPtg mice at the basal level (group C). The top 5 clusters are listed, in order of enrichment score.

Annotation Cluster	**Representative Annotation Terms**	**Enrichment Score**
1	Pathways of neurodegeneration- multiple diseases	6.87
2	Mitochondrial motif carriers	2.60
3	Mitochondrial electron transport	1.56
4	Neurofilament cytoskeleton organization	1.42
5	Response to oxidative stress	1.35

C- APPtg Basal v. APPtg Memory Retrieval- Downregulated

Table 4.16 lists the 3 functional annotation clusters annotated to proteins downregulated in APPtg mice during memory retrieval, when compared to APPtg mice at the basal level. The top 5 most enriched clusters were protein transport, synaptic vesicle transport, cytoplasmic vesicle, protein kinase activity and myristoylation.

Table 4.16. DAVID functional annotation clustering output for proteins downregulated in APPtg mice during memory retrieval, when compared to APPtg mice at the basal level (group C). The top 5 clusters are listed, in order of enrichment score.

Annotation Cluster	Representative Annotation Terms	Enrichment Score
1	Synaptic vesicle transport	2.04
2	Protein phosphorylation	0.82
3	Hydrolase activity	0.60

B- Wild-Type Memory Retrieval v. APPtg Memory Retrieval

When analysing proteins differentially regulated in APPtg mice during memory retrieval, when compared to WT mice during memory receival (group B), the number of enriched clusters was drastically reduced. Only one cluster was enriched in upregulated proteins which was protein binding, with an enrichment score of 0.47. In downregulated proteins, only one cluster, perinuclear region of cytoplasm was enriched, with an enrichment score of 0.84.

4.3.3.7 STRING Protein Network Mapping

PPI network maps were created by inputting lists of differentially expressed (upregulated or downregulated) proteins within different experimental conditions to STRING. Interaction confidence score was set to medium confidence (0.400).

Figure 4.41 depicts the PPI networks within proteins upregulated in WT memory retrieval, when compared to WT mice at the basal level (group A). Two distinct protein clusters can be seen within the network; the largest cluster is comprised of subunits of the ETC, and the second, smaller cluster is comprised of protein subunits of the proteasome.

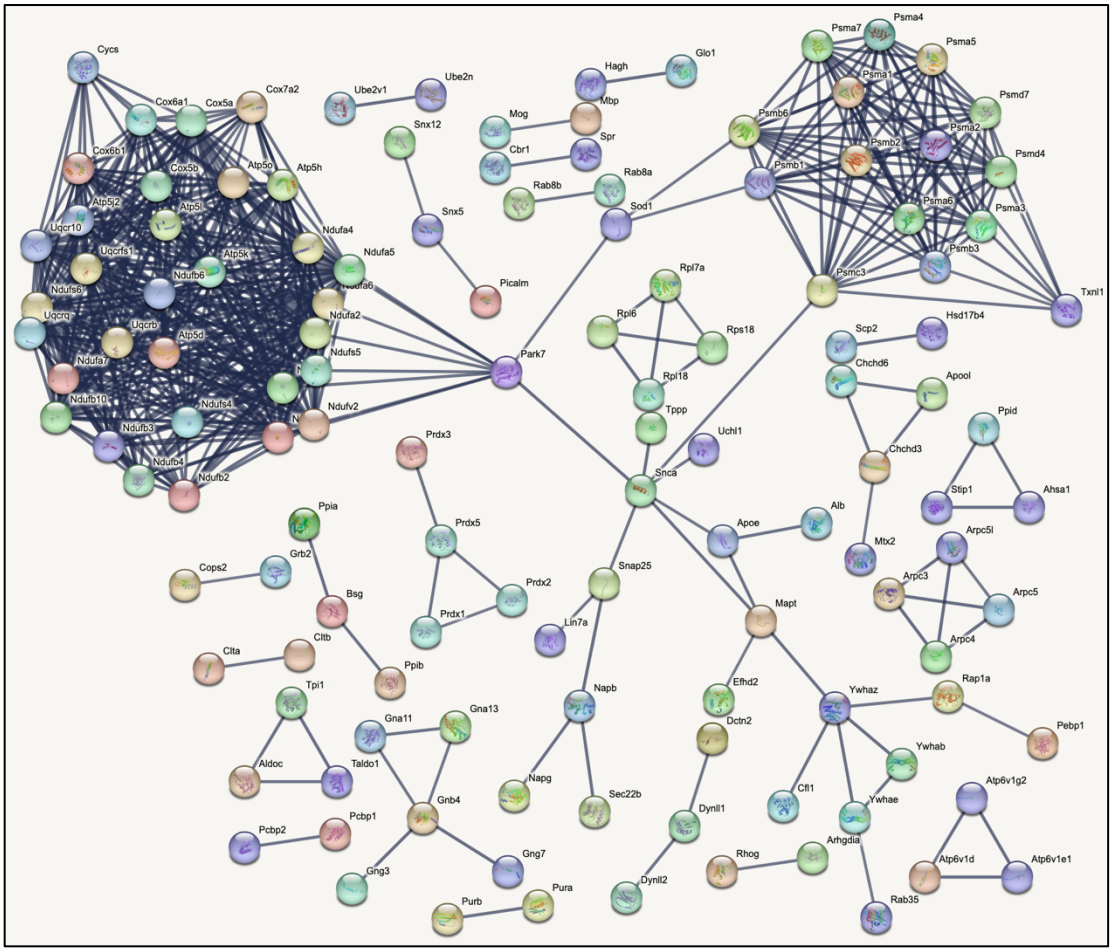

Figure 4.41. STRING network map of proteins upregulated during memory retrieval in WT mice, when compared to basal levels (group A). All interactions are of the highest confidence interaction score (0.900+). Line thickness indicates strength of data support for each interaction. PPI Enrichment Value <1.0e-16.

When we look at the PPI network maps for APPtg mice during memory retrieval (figure 4.42, when compared to basal levels (group C), the number of distinct clusters is altered. Although there is a greater number of highly connected proteins within the network, there is only one main densely populated cluster, comprised of protein subunits of the electron transport chain, similar to WT mice. However, the second protein interaction cluster seen in WT mice, consisting of proteasome proteins, is significantly reduced in the transgenic mice.

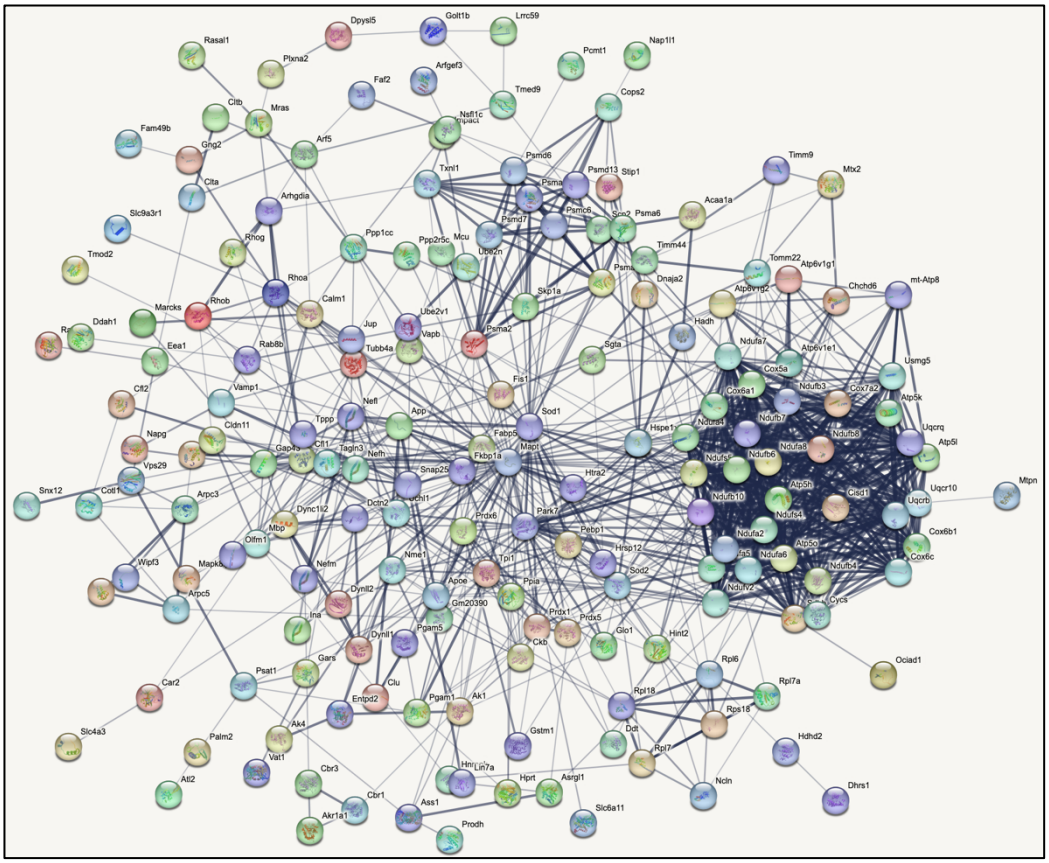

Figure 4.42. STRING network maps of protein upregulated in APPtg mice during memory retrieval when compared to basal levels (group C). All interactions are of the highest confidence interaction score (0.900+). Line thickness indicates strength of data support for interaction. PPI Enrichment Value <1.0e-16.

4.3.3.8 Most Connected Proteins Analysis

STRING interactions data was filtered to detect the most highly connected proteins within those identified to be differentially regulated in APPtg mice during memory retrieval, when compared to APPtg mice during basal levels (group C). The top 10 proteins with the greatest number of outgoing connections (has the greatest effect on others) and the top 10 proteins with the greatest number of incoming connections (greatest affected by others) were highlighted by this type of analysis. This type of analysis utilises the upregulated and downregulated proteins in APPtg mice during memory retrieval, when compared to WT mice during memory retrieval (group B), to highlight the most connected proteins in the experimental condition, irrespective of the directionality.

Table 4.17 shows the most highly connected proteins in APPtg mice during memory retrieval, when compared to APPtg mice at the basal level (group C). The top three proteins with the greatest number of outgoing connections. Rab3gap1, was the protein with the greatest number of outgoing

connections. Rab3gap1 interacts with Rab3gap2 to form the Rab3gap complex, which activates Rab18, involved in vesicle trafficking, autophagy, and endoplasmic reticulum organisation, when in its GTP-bound active state. The Rab3gap complex is also thought to activate the Rab3 GTPase, which plays key roles in the release of neurotransmitters (Medline Plus., 2018). The second and third most connected proteins are subunits of the cytoplasmic dynein complex, which is thought to be involved in the intracellular retrograde motility of vesicles and organelles along microtubules (Medline Plus 2018; UniProt., 2023). Due to the nature of protein trafficking, Dync1h1 was in the top 3 proteins with the most outgoing connections and also the most incoming connections. Hsp90aa1 was the top protein with the most incoming connections, closely followed by Rhoa. Hsp90aa1 functions as molecular chaperone aiding in the maturation, structural maintenance, regulation and proper folding or specific target proteins. It is also known to play a role in mitochondrial import, delivering preproteins to the intracellular import receptor TOMM70 (GeneCards., 2023). Rhoa functions as an intracellular molecular switch, critical for many functions including migration, cell survival, adhesion, and vesicle trafficking (Zhou & Zheng., 2013). Identifying 'hub' proteins, that is, proteins with the highest connectivity, can underpin important predictions into the functions of target proteins. It is widely accepted that 'hub' proteins play more important biological roles than proteins with low connectivity, and networks are much more sensitive to their removal. This kind of information can be reasonably used in future functional predictions of unannotated proteins, as the functions of hub proteins are likely to be correlated with the functions of unannotated proteins (Hou., 2017).

Table 4.17. Table of the top 10 most connected proteins. Table lists the proteins with the greatest number of incoming and outgoing connections within differentially regulated proteins in APPtg mice during memory retrieval, when compared to APPtg mice at the basal level (group C) .

C- APPtg basal V. APPtg memory retrieval				
	Most outgoing connections	**No.**	**Most incoming connections**	**No.**
1	Rab3gap1	24	Hsp90aa1	19
2	Dync1h1	14	Rhoa	15
3	Dynll2	14	Dync1h1	7
4	Dync1li1	14	Dynll2	7
5	Dync1li2	14	Dync1li1	7
6	BC048507	7	Dync1li2	7
7	Dync1i2	7	BC048507	7
8	Dync1i1	7	Dync1i2	7

9	Gpsm2	4	Dync1i1	7
10	Gpsm3	4	App	7

4.3.3.9 Functional Dependency Analysis

Functional dependency matrix was generated for proteins upregulated during memory retrieval in APPtg mice, when compared to proteins upregulated at the basal level (group C).

Figure 4.43 reveals that most dependencies in the matrix have no effect, however, a number of strong activators (122) exist, alongside a number of strong inhibitors (31). Out of 52 species and a total of 2704 reactions, only 3 dependencies in the model were ambivalent factors. Table 4.18 summarises the direction dependencies changed after removal of specific proteins in generated KO models. Ambivalent factors were targeted in KO models, as these are the most likely to change with manipulation.

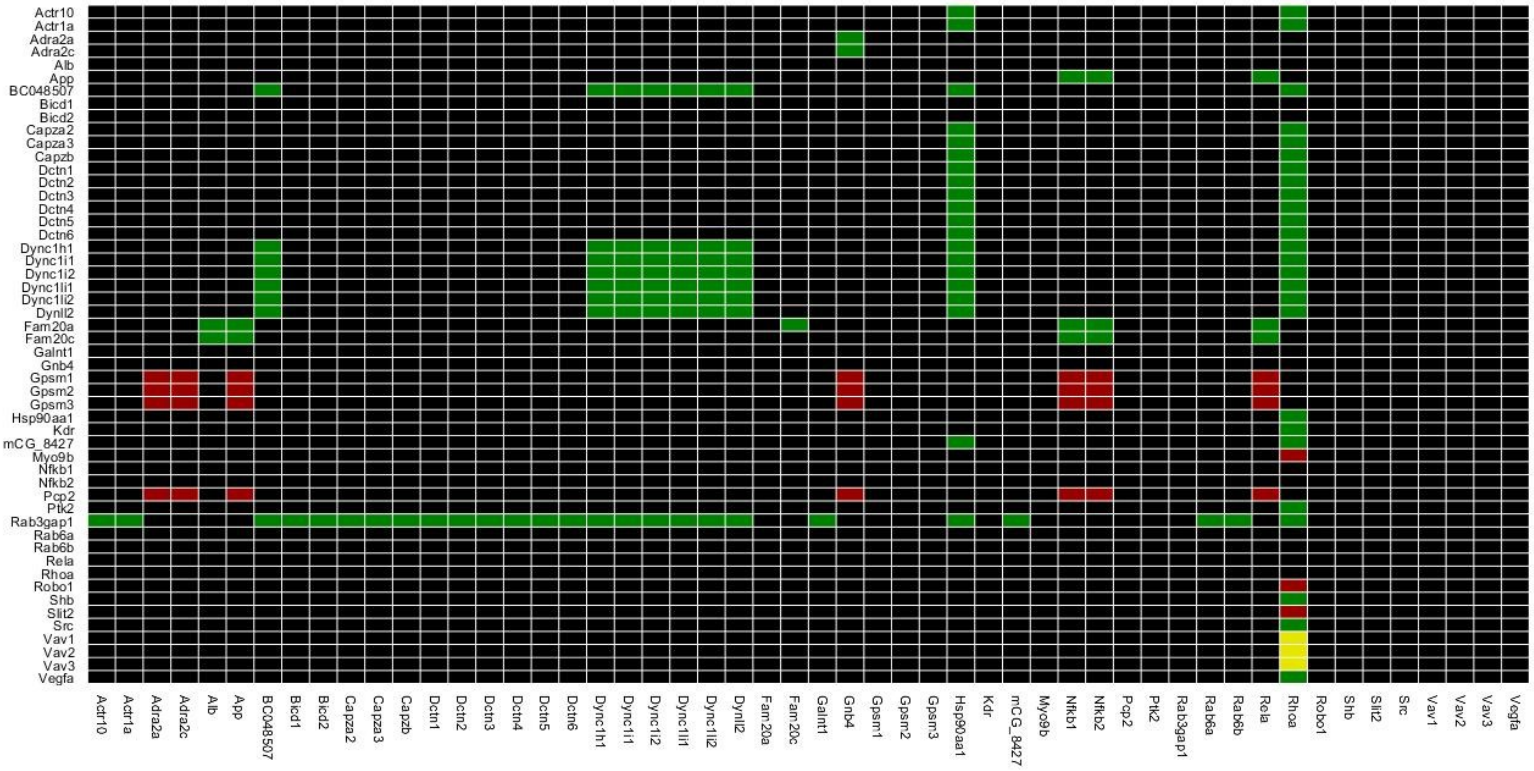

Figure 4.43. Functional dependency matrix for upregulated proteins in APPtg mice during memory retrieval. Dependencies show the effect of the X node on the Y node. Figure includes all significantly upregulated and significantly downregulated proteins which pass the 20% regulation threshold.

Table 4.18 reveals the number of each dependency within the network, following different *in silico* knockout simulations, generated to analyse the potential effects of the loss of network elements. Target nodes were selected based on likelihood of network changes and thus the Rhoa, Vav1, Vav2, and Vav3 nodes were chosen. KO matrices consist of 2601 total reactions, after removal of the KO node and all of its dependencies.

Table 4.18. Functional dependency matrix species dependency numbers in APPtg mice during memory retrieval, when compared to APPtg mice at the basal level (group C).

Scenario	Number of Each Dependency						
	No Effect	Ambivalent	Weak Inhibitor	Weak Activator	Strong Inhibitor	Strong Activator	Total
Full model	2548	3	0	0	31	122	2704
Rhoa KO	2477	0	0	0	28	96	2601
Vav1 KO	2448	2	0	0	31	122	2601
Vav2 KO	2448	2	0	0	31	122	2601
Vav3 KO	2448	2	0	0	31	122	2601

CHAPTER 5- DISCUSSION

5.1. Mitochondrial Dynamics

It has long been established that mitochondrial dysfunction is an early event in the onset and progression of AD (Misrani et al., 2021; Bhatia et al., 2022; Friedman & Nunnari., 2014). The overall morphology and function of mitochondria is dynamically controlled by the balance between fission and fusion events (Wang et al., 2009). Two proteins with central roles in mitochondrial dynamics were measured via western blotting in this project: DRP1, mediator of fission, and mfn1, mediator of

fusion. Mfn1 was found to be expressed at a greater level during basal levels compared to memory retrieval in P2 samples from both genotypes, however, expression in WT basal mice was twice as high as in the APPtg basal mice. A synapse-specific increase in Mfn1 expression was detected in the preclinical APPtg model, across both behavioural groups. Whilst the literature surrounding protein expression in AD typically uses post-mortem brain tissue from known AD cases, and thus is not directly comparable to a preclinical stage, some interesting insights can still be made. Wang et al (2009) found a 27.8% reduction in Mfn1 expression in human post-mortem AD brains compared to age-matched controls. It could be that at a very early, preclinical stage, overexpression of Mfn1 is a compensatory mechanism for mitochondrial dysfunction, attempting to mix molecules and mtNDA throughout the mitochondrial compartment, optimising function and preventing the mitophagy of damaged mitochondria (Suarez-Rivero et al., 2017). In the current study, DRP1 expression was found to follow the same patterns across P2 and synaptosome samples, however, a synapse-specific increase in DRP1 was found in the APPtg mice. Several groups have found increased levels of Drp1 in post-mortem brain tissue from known AD cases, which induced mitochondrial fragmentation and defective mitochondrial function (Oliver & Reddy.,2019). Studies by Misrani et al (2021) also observed increased levels of Drp1 in APP/PS1 mice, as early as 4-5 months, supporting the notion that mitochondrial dysfunction is a key player in the development of neurovegetative disease and begins at a preclinical level, as seen here as an increased expression of Mfn1 and Drp1 in APPtg mice. Upregulation of Drp1 in APPtg mice during memory retrieval, and subsequent increased mitochondrial fission may be a strong contributing factor to memory loss in AD.

Whilst western blotting results cannot be compared with proteomics LFQ intensity of Drp1 and Mfn1 due to missing data points in their entries, several other proteins involved in mitochondrial fission (Mitochondrial fission factor (Mff), mitochondrial fission process 1 (Mtfp1), mitochondrial fission regulator 1 like (Mtfr1l), mitochondrial fission protein 1 (Fis1)) and fusion (mitofusin 2 (Mfn2) were identified within the data (raw LFQ intensity graphs for these proteins can be found in Appendix B, figure 5). Whilst the expression of Mtfp1, Mtfr1l, and Fis1 did not change between genotypes or behavioural conditions, expression of Mfn2 and Mff were found to be increased in APPtg mice during memory retrieval (when compared to WT mice during memory retrieval).

An increase in the expression in mitochondrial fission and fusion related proteins, especially when synapse specific, leads to limitations in mitochondrial motility, decreased energy production , promotion of oxidative stress, and impairment of Ca^{2+} buffering in the mouse model of AD, leading to neuronal death (Knott & Bossy-Wetzel., 2008).

The development and progression of AD are also associated with mitochondrial dysfunction stemming from the cytotoxic effects of AB. One such effect is the interaction of increased levels of VDAC1 protein in the brains of AD patients interacting with AB and phosphorylated tau, leading to the blockage of mitochondrial pores, and increasing mitochondrial dysfunction (Manczak & Reddy., 2012). Western blot analysis revealed VDAC1 expression exhibited a synapse specific increase in transgenic mice, coupled with a reduction in expression in WT mice during memory retrieval. Since VADC1 overexpression is associated with the apoptotic response, its overexpression and interaction with AB in synaptic mitochondria at the preclinical level may be a central mechanism for neurodegeneration (Shoshan-Barmatz., 2018).

5.2 Electron Transport Chain

It is widely accepted that metabolic dysregulation is one of the hallmarks of AD and that metabolic alterations can be associated with AD-related comorbidities, cognitive decline, and brain pathology (Dodart et al., 1999; Mosconi, Pupi & De Leon., 2008; Beglopoulos et al., 2016; Yan et al., 2020;Kumar, Kim & Bishayee., 2022;Batra et al., 2022). Western blotting for proteins involved in mitochondrial energy metabolism pathways revealed several synapse specific regulation changes. SDHA and ATP5A, ETC complex II and V respectively, showed synapse specific expression increases in APPtg mice, compared to WT mice. Oxidative stress is known to regulate the expression of SHDA, which contributes to its overexpression in AD (Shi & Gibson., 2011). Conversely, studies by Misrani et al (2021) found reduced ATP5A expression in the brains of 4–5-month-old APP/PS1 mice. The synapse specific increase in SDHA and ATP5A expression, shown here at the preclinical level, may be an attempt to regulate mitochondrial membrane potential for the high levels of ATP synthesis needed to sustain memory retrieval in the mouse model of AD. Other protein subunits of the ETC showed differential expression in synaptosome samples. Cytochrome C demonstrated a small, synapse specific increase in expression in APPtg mice during memory retrieval but exhibited a small decrease in WT mice during memory retrieval. Studies by Kumar, Giani & Mason (2016) linked the peroxidase activity of cytochrome c to alpha synuclein radical formation and oligomerisation, contributing to increased neuronal death. Excessive peroxidase activity in APPtg mice during memory retrieval could be a result of oxidative damage caused by the presence of amyloid ß, which subsequently leads to alpha synuclein radical formation and oligomerisation, initiating neuronal apoptotic processes.

Western blotting for UQCRB was only carried out using P2 samples and thus any difference in expression is not synapse specific, however, an interesting expression pattern reversal was detected

in the transgenic mice (higher during basal levels than memory retrieval), when compared to WT mice (higher during memory retrieval). COX4 results showed no change in expression between genotypes, only a small, synapse specific decrease in WT mice during memory retrieval. Current literature on UQCRB and COX4 expression are contradictory, with many studies detailing a reduction in the enzymatic activity of the two enzyme complexes, most dramatically COX (Wang et al., 2020). Dysfunction of COX increases ROS production, reduced energy stores, and disturbs energy metabolism, contributing to neurodegeneration (Mutisya et al., 1994). In the WT mice, COX4 expression is increased during memory retrieval, as a means to upregulate OXPHOS and support neuronal energy requirements. Downregulation and dysfunction of COX4 in APPtg mice during memory retrieval (when compared to WT mice during memory retrieval) may be a contributing factor to the glucose hypometabolism seen in APPtg mice.

Western blotting of synaptic proteins PSD95 and alpha synuclein were only carried out in P2 samples, however, both proteins were expressed more highly in the mouse model of AD than their WT counterparts. Elevated alpha synuclein in AD has also been found by Twohig & Nielsen (2019) and Winkel et al (2021), however, these studies utilised CSF, rather than tissue homogenates used throughout this thesis. Literature surrounding PSD95 expression in AD is inconsistent and contradictory. Studies by Shao et al (2011) found PSD95 was increased in hippocampal Hirano bodies in AD brains, however, Savioz, Leuba & Vallet (2014) found decreased expression in the temporal cortex of AD brains coupled with an increase in PSD95 in the frontal cortex. Here, western blotting provides support for the increased expression of PSD95 in preclinical AD models, which likely contributes to disease pathogenesis through its rapid aggregation and propagation.

Whilst western blotting in the context of memory retrieval, especially in the context of AD, is novel, it is important to note that existing literature has studied the expression of proteins in AD brains whilst at the basal level and therefore literature can be used for guidance but not direct comparisons. To gain a more thorough overview of metabolomic pathways implicated in memory retrieval and how they are perturbed in AD, enzymatic activity analysis should be combined with the analysis of mitochondrial metabolites (both substrates and products of each enzyme in question) to provide a more in-depth view of enzyme function. Metabolomic studies should be carried out, as detailed in section 5.5.1.

5.3 Metabolic Signatures of Preclinical Alzheimer's Disease

No differences were identified in the expression or activity of 6-PFK or MDH2 enzymes between WT and APPtg mice, regardless of behavioural group. Several studies have looked at the roles of key glycolytic enzymes in AD and their potential contributions to AD pathogenesis, however, these results were mainly obtained from post-mortem brain specimens of known AD cases and are inconsistent. Studies by Bowen et al (1979) found a 10% decrease in PFK activity in autopsy studies of AD patients, which was contradicted by later studies by Bigl et al (1999), who found increased levels of PFK activity in AD brain tissue. Another study, more closely representative of the current experimental model, studied primary neurodegenerative dementia in young patients at very early stages of disease, found no change in the activity of PFK between demented and control patients (Sims et al., 1987). Studies on the enzymatic activity of the TCA cycle enzyme, MDH2, in preclinical AD patients is lacking, thus a direct comparison of results to literature cannot be made, however, studies by Shi & Gibson (2011) revealed an elevation in MDH2 activity in postmortem tissue samples from the brains of AD patients. It could be that similar to 6-PFK, the activity of MDH2 is unaffected in very early disease stages, before any alteration to activity has occurred. The study by Shi & Gibson (2011) progressed by analysing the effect of oxidative stress on enzymatic activity of MDH2 through induction of MDH gene expression. It was found that H_2O_2, an inducer of oxidative stress, did indeed increase the activity of MDH2 and mRNA expression in mouse hippocampal cell lines. Proteomics data looking at biological processes significantly enriched within APPtg mice during memory retrieval supports the notion that excessive production of ROS is occurring, however, the levels of MDH2 expression were not elevated in the current study.

It is important to remember that the method of sample preparation, including detergents and lysis buffer, and available sample volumes were not reflective of optimal conditions, as advised by the manufacturer, and thus these factors may have led to the activity patterns detected; the reduced sample volume could have impacted the ability to detect any metabolic differences between biological samples. The sample preparation method and presence of lysis buffer, combined with limited sample volume availability, significantly impacted the number of assay kits that were deemed functional or compatible. As only 2 assay kits out of an initial 12 were completed using experimental samples, the intended holistic overview of metabolic health during memory retrieval in the preclinical model of AD was not achieved. The sample preparation method also significantly impacted the ability to progress with analysing mitochondrial metabolites via UPLC-MS. Together, these methodologies would have enabled a thorough evaluation of metabolic regulation (including identifying any metabolic alterations) and mitochondrial health in the model of AD, allowing for the identification of key contributors to memory loss and potential areas for therapeutic intervention.

5.4 Proteomics Results

Determination of LFQ intensity values for mitochondrial proteins also targeted by western blotting provided information on the levels of specific proteins involved in energy metabolism and mitochondrial dynamics. Expression of protein subunits of the ETC (SDHA, COX4) were expressed more greatly during basal levels than during memory retrieval. Enzymes of the ETC are unaffected by feedback inhibition, but the rate of electron transport through the pathway is affected by the levels of ADP and ATP. If previous pathways of energy metabolism, such as the TCA cycle, were under negative feedback control, the flux of ADP and ATP would be reduced, and the ETC would be subsequently downregulated until the cell increases its energetic requirements. Expression of further enzyme complexes of the ETC (NADH-Coenzyme Q Oxidoreductase (complex I), ATP synthase (complex V), succinate dehydrogenase (complex II)) was also identified to be differentially expressed between genotypes. Complex I and complex V were expressed at higher levels in the transgenic mice than the WT mice, reflecting defective pathways of energy metabolism in the preclinical model, which requires subsequent upregulation of key complexes in attempt to compensate for the reduced energy availability. Complex V and complex II showed increased expression during basal levels than during memory retrieval in WT mice, however, their expression in APPtg mice was consistent across behavioural groups, suggesting a dysregulation of glucose metabolism in APPtg mice, which requires a subsequent upregulation in attempt to compensate for the increased energetic requirement.

Increased expression of complexes of the ETC in the AD model does not seem to support the impaired glucose metabolism seen at the preclinical level. However, the extensively reported increase in mitochondrial fission may be the root cause of this observation. Studies by Zhang et al (2016) found increased mitochondrial fission to represent an essential compensatory adaption to bioenergetic stress. Increased mitochondrial fission provides protection against mitophagy, effectively preserving residual mitochondrial function. An increase in the levels of mitochondrial fission by this mechanism would thereby increase the levels of ETC complex machinery, without increasing the production of ATP, if the complexes themselves are dysfunctional.

VDAC1 expression is crucial for the passage of ions and metabolites essential for energy metabolism (Shoshan-Barmatz et al.,2017). LFQ intensity of VDAC1 was higher in WT mice at the basal level, when compared to during memory retrieval. As VDAC1 controls metabolic flux into the mitochondrial matrix or out to the cytosol, maintaining the control of metabolic cross-talk between mitochondria and the rest of the cell, increased expression during memory retrieval is essential to sustain the high levels of metabolic demand (Shoshan-Barmatz, Shteinfer-Kuzmine & Verma., 2020).

In APPtg mice, however, VDAC1 was overexpressed in both behavioural conditions. Increased expression in the AD model may be reflective of increased stress conditions, known to cause VDAC1 overexpression and oligomerisation, forming large channels in the mitochondrial membrane which facilitates the release of pro-apoptotic proteins into the cytosol (Verma et al., 2022). In this way, VDAC1 effectively switches from the promotion of metabolic processes to the promotion of apoptosis (Shoshan-Barmatz et al., 2010).

Proteomic analysis also highlighted a number of proteins which failed to become upregulated or were upregulated in APPtg mice during memory retrieval when they were not upregulated in WT mice during memory retrieval (table 4.28). Failure to upregulate proteins involved in the cellular response to oxidative stress in APPtg mice during memory retrieval could signify that these proteins are already upregulated in the APPtg mice at the basal level, as a result of transgene insertion and therefore, do not present as upregulated in this analysis. Failure to upregulate proteins involved in the cellular response to oxidative stress would lead to increased oxidative damage of neuronal lipids, proteins, and DNA, significantly impairing cellular signalling pathways and contributing to increased apoptosis. Mitochondria, major sites of ROS production, would be especially susceptible to oxidative damage, which can lead to mitochondrial dysfunction and energy deficits, further exacerbating oxidative damage. Additionally, oxidative damage can lead to protein misfolding and increased propensity to aggregate, causing disruption to signalling and metabolic pathways but also altering the functions of key synaptic proteins, impairing synaptic function and neuronal communication. Interestingly, all proteins which fail to become upregulated during memory retrieval and are involved in aerobic respiration are subunits of ETC complex I (NADH ubiquinone oxidoreductase; Ndufa7, Ndufa6, Ndufb6, Ndufb4, Ndufb2). Impairment of complex I would lead to significantly impaired OXPHOS, increased ROS production, mitochondrial dysfunction, and impaired cellular functions, which would render the cell unable to meet the energetic requirement of memory retrieval, presenting as memory loss and subsequent neurodegeneration.

Combined, these effects may be a key contributor in AD pathogenesis and impaired metabolism, contributing to memory loss in the transgenic mice. Furthermore, proteins involved in the negative regulation of neuronal apoptosis would increase the susceptibility of neurons, especially those in a state of oxidative stress, to undergo apoptosis, leading to widespread neuronal loss and impaired neuronal plasticity. Proteins involved in aerobic respiration and mitochondrial ATP synthesis coupled protein transport were upregulated in APPtg mice during memory retrieval but not in WT mice during memory retrieval, likely as a compensatory mechanism to attempt to increase energy production to overcome the heightened oxidative stress sustain the energetic demand of memory retrieval.

Two key enzymes, 6-PFK and MDH2 were differentially expressed between the two genotypes. Expression of 6-PFK in WT mice was much greater at the basal level than during memory retrieval. This may be partially explained by the allosteric inhibition of 6-PFK by ATP, at concentrations higher than 1mM (detailed in section 1.3.5). If levels of ATP already surpassed this level by the time the mice were sacrificed following memory retrieval, ATP inhibition may have already occurred, reducing the overall expression of the enzyme. In the APPtg mice, expression of 6-PFK is greater during memory retrieval than at the basal levels, implying an upregulation of metabolic pathways to meet the rising metabolic demand of memory retrieval mechanisms. As PFK catalyses the rate-limiting step of glycolysis, an upregulation of this enzyme would increase the overall glycolytic flux throughout the cell (McKenna et al., 2012). The expression of MDH2 was greater during memory retrieval in both WT and APPtg mice, although the overall expression in both behavioural groups was higher in APPtg mice. Increased expression during memory retrieval supports the increased metabolic demands of retrieval. These results may suggest different dysregulations in protein expression in the APPtg mice, or during memory retrieval, however, they are based off LFQ intensity measurements alone and so should be taken in combination with other analyses and experimental methodologies.

Part of the proteomic analysis of this thesis utilised two different methods, namely the application of FDR correction for the testing of multiple hypotheses and the application of a regulation threshold with subsequent t-testing. The results seen here follow the current debate over the use of correcting procedures for multiple testing in proteomics studies and the differing opinions in the field. FDR can be seen to penalise biological associations for being identified in a larger study, over a smaller study and challenges the idea that nature may be understood through observations (Althouse., 2015; Rothman., 1990). Failing to apply FDR correction, however, can significantly increase the number of false positive associations, leading to false interpretations of the data. The results from the two analyses are both different and interesting. After the application of FDR correction, two of the four experimental conditions had no significant differential protein regulation remaining. The application of FDR to this project, which is exploratory by nature, could be seen as too harsh, eliminating all differential regulations in half of the study conditions. Consequently, none of the differential protein regulations in APPtg mice during memory retrieval, when compared to APPtg mice at the basal level, could be analysed for biological functions or affected pathways specific to the AD transgene. The aims of this project are to provide insight into the molecular and cellular mechanisms underlying memory retrieval and how they are perturbed in a model of preclinical FAD. Without significant protein regulations within APPtg mice during memory retrieval, the ability to draw conclusions and comparisons between the two genotypes is significantly impacted. Whilst the application of FDR in

targeted proteomics experiments is useful, it should be carefully considered before being applied to exploratory experiments, where even the smallest, non-statistically significant regulatory change could be highly biologically significant.

5.4.1 FDR Corrected Results

The first, and arguably the most striking, result from the FDR corrected proteomics was the significant failure of APPtg mice to differentially regulate protein expression. After the application of FDR correction, there were no significantly differentiated proteins in the mouse model of AD during memory retrieval, when compared to basal levels. Such a significant regulatory failure would have massive consequences for the cell, preventing the proper expression of proteins involved in responses to changing environmental conditions. Not only would this lead to a failure to upregulate the pathways required to support memory retrieval, but it would also cause a failure to properly regulate pathways involved in cell survival, including apoptosis and autophagy. Further research into the mechanisms behind this regulatory failure may have important clinical benefits in the treatment of AD.

Using DAVID bioinformatic tools, the data revealed that upregulated proteins within WT mice during memory retrieval were significantly enriched in vesicle-mediated transport, cellular oxidant detoxification and establishment of protein localisation to membrane biological processes and hydrolase activity, clathrin heavy chain binding and ubiquitin protein ligase binding molecular functions. Proteins were also found to be significantly enriched in the endocytosis, synaptic vesicle cycle and vasopressin-regulated water reabsorption pathways. Other, non-statistically significant results included the enrichment of glycolytic pathways, supporting the increased ATP demands of memory retrieval processes. The WT memory retrieval group provides a model of the molecular and cellular mechanisms underlying memory retrieval in healthy states. One mechanism significantly enriched was cellular oxidant detoxification, relating to any processes involved in the removal of toxicity superoxide radicals. The two major sites of superoxide radical production are known to be the election transport chain complexes I and III. Healthy WT mice use upregulation of this pathway to offset the high amounts of ROS generated during upregulation of ETC complexes during memory retrieval (Phaniendra, Jestadi & Periyasamy., 2015). Enrichment of vesicle-mediated transport is indicative of increased neurotransmitter transportation across the synapses during memory retrieval, supporting the excitation of neurons in complex circuits that were previously activated during learning (Tayler et al., 2013). Enrichment of hydrolase activity in the WT mouse could be representative of central defence mechanisms for the prevention of AB aggregate formation, known

to degrade synapses and impair memory formation. Studies by Wu et al (2023) found hepatic soluble epoxide hydrolase (sEH) to be a key modulator of AB metabolism. sEH regulates plasms levels of 14,15-epoxyeicosatrienoic acid, which crosses the blood-brain barrier and modulates AB metabolism, preventing excessive AB metabolism. Ubiquitin protein ligase binding is a key process involved in ubiquitination, where proteins marked for degradation are targeted to the proteasome (Suresh et al., 2016). Ubiquitination regulates protein stability, function, and localisation and is known to be critical for synaptic plasticity and long-term memory (Jarome & Helmstetter., 2013). Proteins downregulated in the WT model of memory retrieval were found to be enriched in apoptotic processes, which are generally characterised by energy-dependent biochemical mechanisms. The energy expenditure of memory retrieval may be so great that apoptotic pathways are downregulated in nondemented mice to ensure maximum energy utilisation in retrieval.

Comparing the pathways enriched within WT mice during memory retrieval with those of the APPtg mice can illuminate key differences that may be causative of AD induced memory loss. Proteins upregulated within APPtg mice at the basal level, when compared to WT mice at the basal level, were found to be significantly enriched in mitochondrial electron transport-cytochrome C to oxygen and fatty acid metabolic process. Non-significant but highly enriched other terms included the negative regulation of neuron death. Significantly enriched pathways of oxidative phosphorylation, Alzheimer disease, pathways of neurodegeneration, Huntington disease and non-alcoholic fatty liver disease pathways were also identified. Contrary to literature which suggests glucose metabolism in PDAPP mice is normal at the basal level, (Beglopoulos et al., 2016), APPtg mice present with significant enrichment of pathways involved in neurodegeneration and energy metabolism at the basal level. This could be due to the age difference between the mice, as the mice used by the authors were 3-4 months old, whereas the mice used for the studies in this thesis were 7-9months old and may have developed further pathologies. Additionally, whilst there is an identifiable difference between the studies in regard to glucose metabolism, we cannot be sure that the enrichment of pathways identified in this study will translate to the glucose hypometabolism clinically. The oxidation of energy-rich fatty acids presents with three main problems for the cell: it demands more oxygen consumption than glucose utilisation, enhancing the risk for neurons to become hypoxic; it generates superoxides which can cause severe oxidative stress; and the rate of ATP generation from fatty acid oxidation is slower than using glucose as the main fuel. During periods of rapid neuronal firing, fatty acid metabolism cannot guarantee the required rate of ATP generation and thus it is not utilised as the main source of energy metabolism (Schonfel & Reiser., 2013). Upregulation of this process, together with the upregulation of mitochondrial electron

transport processes, suggests APPtg mice are under metabolic stress, likely due to dysfunctional OXPHOS complex components, even at the basal level.

Proteins downregulated within APPtg mice at the basal level, when compared to WT mice at the basal level were significantly enriched in barbed-end filament capping, glutamatergic synapse, and Schaffer collateral-CA1 synapse. Owing to their pivotal role in excitatory neurotransmission, the disruption of normal signalling via glutamate receptors, due to synaptic protein downregulations, observed here in APPtg mice at the basal level, is implicated in a range of neuropathological diseases, including AD (Wang & Reddy., 2017). The majority of excitatory transmission in mammals is mediated by glutamate and its receptors, which also play a fundamental role in synaptic plasticity, the underlying molecular mechanisms of learning and memory (Riedel, Platt & Micheau., 2003). Any downregulation of proteins within glutamatergic synapses could have drastic impacts on memory.

5.4.2 Differential Regulation Threshold Results

5.4.2.1 Differentially Regulated Proteins at the Basal Level

Studying the difference in protein expression between WT and APPtg mice at the basal level revealed several interesting differences related to the insertion of the AD transgene. Proteins downregulated in the transgenic mice at basal levels were significantly enriched in mitochondrial electron transport-cytochrome c to oxygen, and non-significantly enriched in response to oxidative stress and mitochondrial fission. Additional significant enrichments in the mitochondrial inner membrane, respiratory chain, particularly complex IV, and actin filament bundle components. Downregulation of proteins involved in mitochondrial fission leads to an imbalance of fission and fusion events, and subsequent mitochondrial dysfunction, as previously discussed. Aberrant mitochondrial morphology can lead to increased ROS production, which deteriorates mitochondrial health further and can lead to the progression of disease (Jezek, Cooper & Strich., 2018; Pizzino et al., 2017). Aberrant mitochondrial morphology is further supported by the significant enrichment of actin filament bundle components in downregulated proteins. Actin filament bundles play essential roles in the structural support of the plasma membrane, cell division, and cell motility and thus are essential for the maintenance of mitochondrial function (Jones & Naylor., 2022). Furthermore, downregulation of protein complexes of the ETC shows evidence of energetic deficit in the transgenic mice at the basal level, which may be caused by the increase in ROS, exacerbated by dysfunctional mitochondrial dynamics. The is further supported by the upregulation of proteins

significantly enriched in neurons antioxidant defence system in response to oxidative stress. It seems likely that the insertion of the APP transgene causes an imbalance of mitochondrial dynamic events, further supported by the western blot data, which in turn, subjects the cell to oxidative stress and damages the protein complexes of the ETC via cristae remodelling. Damage to the ETC leaves the cell unable to produce ATP at the rate required to sustain memory retrieval and possible apoptosis occurs, which may explain the symptoms of memory loss in AD.

Enriched pathways within proteins upregulated in APPtg mice at the basal level, when compared to WT mice at the basal level were pathways of neurodegeneration, which further confirms the onset of disease has already begun at an age which is defined as preclinical.

The use of STRING PPI database allowed for the identification of the most highly connected proteins within those upregulated in APPtg mice at the basal level. Protein phosphatases dominated the results, showing the greatest number of incoming and outgoing interactions. Post-mortem studies have previously linked Ppp2 to AD. Within the disease, Ppp2 expression and activity is reduced, leading to the induction of tau hyperphosphorylation, deposition of Aß, memory impairment, and a reduction in autophagic degradation of faulty or damaged proteins (Braithwaite., 2012; Sontag., 2004; Sinsky Pichlerova & Hanes., 2021). Within the APPtg mice at the basal level, Ppp's are upregulated, providing mechanisms of neuroprotection against AD pathologies.

5.4.2.2 Differentially Regulated Proteins During Memory Retrieval

Proteins that failed to become upregulated in APPtg mice during memory retrieval (when compared to WT mice during memory retrieval) were enriched in cellular response to oxidative stress, mitochondrial ATP synthesis coupled proton transport, aerobic respiration, and negative regulation of neural apoptotic processes. They are enriched in the myelin sheath, endoplasmic reticulum-golgi intermediate compartment, intermediate filament, extracellular space, proteasome complex, and respiratory chain. The intermediate filaments, together with actin filaments and microtubules, form the cytoskeleton, a complex and highly dynamic network that provide major mechanical support for the cell. Intermediate filaments thus influence mitochondrial morphology, subcellar localisation, and function through direct and indirect interactions. A failure to upregulate these proteins in APPtg mice could lead to disease through the negative regulation of mitochondrial morphology (Schwarz & Leube., 2016). The degradation of intracellular proteins is carried out by the proteasome in a process requiring large amounts of metabolic energy. The ubiquitin-proteasome system controls almost all basic cellular processes such as metabolism, cell death, signal transduction and protein quality

control (Tanaka., 2009). Failure to upregulate the proteasome complex would lead to the accumulation of damaged and structurally aberrant proteins within the neuron, contributing to neurodegeneration in the APPtg mouse. This result was supported by the STRING PPI network maps, which illuminated a strong reduction in the proteasome protein cluster in the APPtg mice, when compared to WT mice. These results show that preclinical APPtg mice present with key pathways of neurodegeneration during memory retrieval. AD causes mitochondrial dysfunction and high levels of oxidative stress, leading to the production of ROS, which in turn, reduces the mitochondrial energetic-transducing capacity, which, combined with the accumulation of dysfunctional proteins, eventually leads to neuronal apoptosis. Owing to these conditions, proteins enriched in the aforementioned pathways fail to become upregulated during memory retrieval, which culminates in symptoms of memory loss.

Conversely, when studying proteins that were inappropriately upregulated in the APPtg mice during memory retrieval (where they were not upregulated in WT mice during memory retrieval) were enriched in the IMM and proteasome and were enriched in processes including mitochondrial respiratory chain complex I assembly and response to superoxides. Superoxides play vital roles in cell signalling and survival by activating membrane-bound receptors and altering mitochondrial membrane permeability to promote apoptosis (Varela & Farhana., 2023). The peroxisome plays important roles metabolism, detoxification of ROS and signalling, however, the process leads to the generation of superoxides, which require upregulation of response to superoxide pathways to negate the effects on the cell. Peroxisomes also participate in the oxidation of fatty-acids, providing an additional major energy source for the cell (Cooper., 2000). It may be that during memory retrieval in APPtg mice, the failure of OXPHOS pathways leads to the upregulation of the peroxisome, in order to generate ATP via the oxidation of fatty acids. Previous enrichments in APPtg mice at the basal level also found an enrichment of fatty acid oxidation pathways, further supporting the notion that the insertion of the APPtg causes failure of traditional aerobic respiration, causing a reliance on the increased oxidation of fatty acids to support the energy requirements of the cell, particularly during memory retrieval.

Proteins that fail to become downregulated during memory retrieval in APPtg mice (when compared to WT mice during memory retrieval) were significantly enriched in learning, synaptic vesicle exocytosis, regulation of dendritic spine morphogenesis, synapse organisation, neurotransmitter assembly and the regulation of synaptic plasticity. They are significantly enriched within the glutamatergic synapse, cortical actin cytoskeleton, plasma membrane and dendritic spine. Processes included in learning, such as synaptic plasticity, neurotransmission, synapse organisation, and dendritic spine morphogenesis in glutamatergic neurons may be downregulated in the WT mice so

conserve energy expenditure during memory retrieval- itself, a very highly energy demanding process. These processes may be downregulated to ensure that energy is predominantly dedicated to retrieval and not directed to the formation of memory circuits during this time of increased demand to ensure that the requirements of receival can be fulfilled by the cell. A failure in the downregulation of these pathways would increase the metabolic requirement of the cell, which cannot be sustained in APPtg mice who already suffer a downregulation of OXPHOS pathways, leading to symptoms of memory loss.

Conversely, proteins that are downregulated in APPtg mice during memory retrieval when they aren't downregulated in WT mice during memory retrieval are significantly enriched in protein phosphorylation, synaptic transmission, cell surface receptor signalling pathway, carbohydrate metabolic process and microtubule sliding. They are significantly enriched within membranes and are significantly enriched in protein kinase activity, ATP binding, transmembrane signalling receptor activity and hydrolase activity. Aberrant protein phosphorylation recognised as a critical step in AD pathogenesis and progression. Changes in protein phosphorylation patterns are thought to promote the transition from presymptomatic to symptomatic states as a response to AB accumulation (Perluigi et al., 2016). Microtubule sliding is the movement of microtubules relative to other microtubules or to non-microtubule structures such as the actin cytoskeleton and is a significant contributor to the establishment, organisation, and preservation of axonal microtubule arrays (Guha & Patil., 2021). Downregulation of microtubule sliding would negatively impact the growth and upkeep of axons, leading to dysfunctions and reduced neuronal branching, contributing to neurodegeneration.

Heatmaps of average LFQ intensity for complexes of the ETC chain revealed a number of key differential expressions within the different experimental groups. Proteins associated with complexes I, IV and V were upregulated more highly in APPtg mice during memory retrieval than in WT mice during memory retrieval. However, complex II proteins were downregulated in WT and APPtg mice during memory retrieval. The upregulation of complex I, IV and V in APPtg mice during memory retrieval is likely due to the dysfunction of energy metabolism pathways and subsequent upregulation in attempt to compensate for the reduced capacity to meet energetic demand during retrieval. The downregulation of complex II, whilst unexpected, is matched in the WT mice during memory retrieval and so may be a natural phenomenon of memory retrieval. Complex II plays a dual role in respiration via the catalysis of succinate oxidation in the TCA cycle and transference of electrons from succinate to ubiquinone in the ETC (Bandara, Drake & Brown., 2021). It is possible that at the time of sacrifice, the ETC was upregulated with preference over the TCA cycle, which may have already generated sufficient levels of intermediates to sustain the ETC. In this instance, given

the dual role of complex II, its expression would be both upregulated (for its ETC participation) and downregulated (for its TCA cycle participation), producing an overall downregulation pattern.

Proteins upregulated in WT mice during memory retrieval (when compared to WT mice at the basal level) are significantly enriched in processes involved in aerobic respiration and cellular response to oxidative stress within the respiratory chain (complex I and V specifically- matches heatmaps) and the proteasome complex. They are also significantly enriched in functions including peroxidase activity, NADH dehydrogenase activity, antioxidant activity and chaperone binding. These functions are essential to sustain and maintain the energetic requirements of memory retrieval and are apparently lacking in APPtg mice, as previously discussed. Interestingly, upregulated proteins during memory retrieval were found to be significantly enriched in OXPHOS, non-alcoholic fatty liver disease, chemical carcinogens, AD, pathways of neurodegeneration, and prion disease pathways. This could, however, be due to increased activation of the unfolded protein response during memory retrieval, which is functionally associated with the neurodegeneration and prion protein pathways. The unfolded protein response ensures the protection from misfolded proteins that may inhibit memory retrieval and result in memory loss. Proteins downregulated in WT mice during memory retrieval (when compared to WT mice at the basal level) are significantly enriched in phosphatidylinositol metabolic process, synaptic vesicle docking, neurotransmitter secretion, postsynaptic actin cytoskeleton organisation within the mitochondrial matrix, glutamatergic synapse, postsynaptic actin cytoskeleton, presynaptic endosome, and presynaptic active zone. They are significantly enriched in the TCA cycle and metabolic pathways, which are upregulated to meet the increased energetic demands of retrieval. The processes highlighted by DAIVD in WT mice during memory retrieval including phosphatidylinositol metabolic process, synaptic vesicle docking, neurotransmitter secretion and postsynaptic actin cytoskeleton organisation are all functions of healthy neurotransmission, synaptic organisation, and regulation.

Proteins upregulated in APPtg mice during memory retrieval (when compared to APPtg mice at the basal level) were significantly enriched in processes involved in aerobic respiration and response to oxidative stress. This is the same as their WT counterparts, which, in combination with the pathways enriched within downregulated proteins and proteins that fail to become upregulated in APPtg mice, suggests the proteins properly upregulated in APPtg mice during memory retrievals are functional and not the cause of neurodegenerative symptoms. Proteins downregulated in APPtg mice during memory retrieval (when compared to APPtg mice at the basal level) were significantly enriched in cargo loading into clathrin coated vesicle and anterograde synaptic transport in the AP-3 adaptor complex, membrane coat, axon cytoplasm and early endosome.

5.5 Study Limitations

5.5.1 Limitations of Wet Laboratory Research

One limitation of the current study is the use of the mouse model to study AD, a uniquely human disease (Toledano et al., 2012). Whilst experimental models in the mouse are critical to gain a better understanding of disease pathogenesis, they do not encapsulate the whole disease. Most mouse models, including the J20 mouse, overexpress human APP genes linked to FAD, leading to the formation of amyloid plaques in brain regions which typically have a high amyloid burden in AD, namely the cortex and hippocampus (Yokoyama et al., 2022). AD, however, is defined by the presence of plaques and neurofibrillary tangles of hyperphosphorylated tau and thus, it is often overlooked that mouse models, such as the J20, only present with specific pathological features of AD and they do not themselves suffer the disease (Tai et al., 2021). A crucial limitation to mouse models of AD is the lack of widespread neurodegeneration and regional brain atrophy which occurs in human presentation. These major differences greatly impact the translational accuracy from animals to humans (Elder, Gama Sosa & De Gasperi., 2010). An ideal mouse model would contain both amyloid plaques and tau tangles, as well as display widespread neurodegeneration at a similar age as human development. Despite the translational limitations, the J20 mouse model is more ethical than human alternatives, and more practical than cultured cell lines, which cannot attempt to encapsulate complex human physiology and especially behaviour. The J20 model remains an extremely useful mechanism of studying the biochemical mechanisms underlying memory retrieval and AD.

A second major limitation of the current study is the sample preparation and availability. All samples used throughout the project were created prior to the project. Both the P2 and synaptosome samples had to be lysed with detergents. The use of lysis buffer and detergents has proved difficult, and in some instances, incompatible, with some of the methodologies used throughout the project, namely the enzymatic activity assays and the analysis of mitochondrial metabolites. Certain enzymatic activity assays provided instructions on how to best prepare samples for optimal use with assay reagents, often tissue homogenisation in assay buffer with no additional reagents, and metabolomics protocols often require fresh tissue homogenates, prepared to a specified concentration, without the use of detergents that can damage expensive equipment.

Death may also impact the viability of neuronal mitochondria. Moments after death, the brain is subject to asphyxia, depriving the tissues of oxygen, which is required as the final electron acceptor

in the ETC. Consequently, the generation of ATP stops, causing the destruction of cellular membrane and the beginning of organelle degradation (Barksdale et al., 2010). As a result of this, any deficits seen in mitochondrial dynamics or energy metabolism may be, in part, due to the effect of death on mitochondria, and findings in mitochondrial physiology are difficult to translate into patient care and clinical trials. On the other hand, studies by Nukala et al (2006) found that mitochondria that are cryopreserved soon after death exhibit preserved bioenergetics and are structurally intact.

Another limitation of the study, particularly the western blotting, is the lack of technical replicates performed. Whilst biological replicates from each experiential group were included (n=4), helping to evaluate the variability between samples and allowing for statistical analysis to be performed, the lack of technical replicates do not allow for the assessment of experimental variability and the reduction of experimental error. To further reduce the large variation between western blots, all biological replicates from the same experimental groups should be carried out on the same gel, in adjacent lanes, to avoid between-gel variation. Between-gel variation was much larger than between-lane variation, which may have contributed to the size of the standard error bars. To improve the reliability, accuracy and reproducibility of western blotting results, all western blotting should be repeated with technical replicates the further validate findings.

Furthermore, the study suffers from a lack of biological replicates spanning different age groups. The current study focusses exclusively on 'preclinical mice' at a very young age (7-9 months) but does not attempt to track changes in behaviour with age. Using mice spanning different age ranges (J20 mice behaviourally trained in identical conditions) would allow for the tracking of alterations in protein expression as disease pathology progresses. Moreover, it would allow the identification of specific pathways or biological processes which become significantly dysregulated in the transgenic mice with the progression of AD (when compared to WT aged-matched controls). It may also identify any specific pathways or biological processes which become significantly dysregulated in the WT mice, due to natural ageing. The ability to pinpoint an age at which dysfunction becomes widespread and significant would allow for the identification of an optimal age for therapeutic intervention, where treatment would have the best chance of alleviating or even beginning to prevent memory loss in AD.

Additionally, the amount of sample available for use in the project was limited and impacted the number of experiments, experimental repeats, and result quality. Enzymatic activity assay protocols suggested up to 100µg protein per well in each assay, instead of the 5µg used in these experiments. The limited sample volume may have significantly impacted the ability of the assay kit to measure any enzymatic activity present with the samples. Despite this, a number of western blots, enzymatic

activity assays and proteomic studies were successfully carried out, allowing for the elucidation of memory retrieval and disease mechanisms.

Other limitations that impacted this project were equipment constraints effecting progression of the metabolomics work, as optimisation was required for each new instrument available and full, supervised training was required before use.

5.5.2 Limitations of Computational Research

A persistent limitation of complex biological models, such as the functional dependency matrix, is the qualitative nature of results that are ultimately drawn, limiting the amount of information that could otherwise be gained from the study. Due to the STRING database listing all of the known PPIs combined with predicted functional and physical PPI data, these models are mechanistically imprecise and can only be used predictively, although they remain a good starting point for *in silico* knockout models to allow predictions for *in vivo* behaviours, following network perturbations. In the present study, functional dependency matrices did not include any positive- or negative-feedback loops, significantly impacting the model's predictive capacity for knockout alterations (feedback loops are the most likely nodes to induce changes across the model when removed). Especially when using the FDR corrected proteomics data, the dependency matrix models are very small (48 species, 188 reactions for the smallest model generated) and thus they cannot fully simulate AD or memory retrieval-associated pathways. These models therefore represent a starting point for future work.

When attempting to elucidate biological mechanisms underlying memory retrieval in health and disease, even the smallest of differential expressions may have significant biological impact but may be falsely removed by corrections for multiple comparisons. Such correction, in the present study, significantly limited the extent of analyses carried out on proteins within the FDR corrected group, however, disregarding the need to correct for multiple comparisons incurs high levels of false positive results.

5.6 Future Directions

5.6.1 Future Directions for Wet Laboratory Research

Studying the metabolic changes in WT mice during memory retrieval when compared to basal levels, and how these changes differ in the preclinical model of FAD can help identify metabolites involved

in healthy memory retrieval but also how these usual metabolic changes are perturbed in FAD. Using fresh tissue homogenates from behaviourally trained WT and APPtg mice, prepared without the use of lysates and strong detergents would allow for analysis of the metabolome during memory retrieval in healthy and diseased states.

Western blotting should be employed to offer some validation of proteomic findings. Proteins identified with the greatest differential expression, along with those proteins with the largest number of incoming and outgoing connections should be targeted for western blot analysis to confirm the elevated expression in specific behavioural groups and presence of hub proteins. If the mouse model and behavioural training could be replicated in new mice and fresh tissue homogenates created, further western blotting could be carried out using the antibodies used throughout this thesis, using n=4 for each genotype and behavioural condition, allowing for two-way ANOVA to be carried out on each blot, assessing the change in protein levels according to both variables. Fresh homogenate tissue could then be employed for enzymatic activity assays, targeting the remaining 10 assay kits that were not compatible with available sample volume and preparation. Assessing the activity of enzymes involved in the various stages of aerobic respiration, insight into the disease process can be gained and further assessed, testing the enzymatic response of targeted therapies.

Further investigation of the proteins identified in table 4.28 as failing to become upregulated in APPtg mice during memory retrieval would provide a comprehensive insight into the underlying mechanisms, functional implications, and consequences of complex I dysregulation in APPtg mice. An oxygen consumption assay and Seahorse Extracellular Flux Analysis could be carried out to measure oxygen consumption and ATP production, assessing the impact of complex I dysregulation on energy metabolism. An additional investigation into the levels of oxidative stress and ROS production could be carried out by measuring the levels of ROS and oxidative stress markers using fluorescent probes and oxidative stress assays. This would help to evaluate the impact of complex I dysregulation on oxidative stress, mitochondrial ROS production and cellular redox homeostasis. If cohorts of mice from different age groups could be trained and used in these experiments, it may be possible to determine the age at which dysregulation of complex I ensues, helping to pinpoint the ideal window for therapeutic intervention.

Further validation of key proteomics findings should be carried out via western blotting to analyse expression levels within the experimental group. Findings such as the significant enrichment of mitochondrial electron transport: cytochrome c to oxygen, oxidative phosphorylation, and pathways of neurodegeneration in APPtg mice at the basal level (when compared to WT basal mice) should be

validated for all proteins identified by DAVID as belonging to the annotation category and significantly upregulated within the group. Identifying which proteins within each pathway are highly upregulated may lead to further understanding of which aberrant protein expressions contribute to the pathogenesis of AD, even at the preclinical level.

Since glucose hypometabolism has been described in AD, even at the preclinical level, (Belgopoulos et al,.2016), it would be sensible to investigate sodium-independent glucose transporters (GLUT proteins) to determine the levels of glucose transport into neurons and related expression of glucose transporters in neurons and whether disease mechanisms may begin with dysfunctional transport of glucose into neurons.

5.6.1.1 Metabolomics

Due to time constraints, metabolite precipitation was not carried out on the samples, and they were not submitted to the instrument. Due to the sample preparation containing SDS detergent and no reliable method of completely removing it or testing for its presence after attempted removal, the decision was made to cease the experiment. Detergent contamination of a mass spectrometer is very costly (ruined columns/tubing) and would be extremely time consuming to completely ensure its removal.

To continue with the analysis of mitochondrial metabolites, a method for the precipitation of metabolites from complex biological samples would need to be developed to ensure the complete removal of detergents and extraction of metabolites of interest. Once metabolites have been extracted from the homogenates and detergent removed, samples will be fed into the instrument using the auto sampling tool. After each sample, a blank solution of mobile phase will be passed through the instrument to prevent contamination. The levels of endogenous metabolites within each sample can be determined via the peak area ratio between the analyte and the specific standard at a known concentration. Concentration of endogenous metabolites can then be determined by dividing the figure by the volume of the analyte. Any high background noise on the resulting spectra can be subtracted using Waters software. If metabolite levels do not reach the lower detection limit, samples can be spiked using a cocktail of standards (each standard made to 1nM, mixed thoroughly and 4µl extracted for use), whereby the peak area of the analyte is compared against the peak area of the standard cocktail. Once the data has been accumulated, multiple processing steps may be performed to ensure the data is easily interpretable and comparable across runs. Examples of processing include: outlier screening, for the elimination of

anomalous peaks; filtering, which removes noise and any possible contamination from the data; and peak matching and retention time alignment, which enable metabolomic data to be compared across samples and can be carried out using Waters' MassLynx or MarkerLynx software (Zhou et al., 2012). After data pre-processing, statistical analyses including t-tests, fold-change analyses, and ANOVA may be carried out to assess the significance of each peak and any significantly altered metabolites within the experimental groups.

5.6.2 Future Directions for Proteomics Research

For the purpose of this project, proteomics analysis focussed on four experimental groups and only directly compared either different behavioural groups within the same genotype or the same behavioural group across both genotypes. A fifth comparative group, group E- wild-type memory retrieval v. APPtg basal, was not considered within the scope of this project. It would be interesting to carry out analysis on this group in the same manner as the four groups analysed in this thesis to identify genotype-specific differences in memory function. It may become apparent that pathways involved in memory retrieval or disease processes are already significantly upregulated in the APPtg mice at the basal level, giving the illusion that these pathways are not upregulated when compared to the APPtg memory retrieval group, which could have potentially impacted the interpretation of results.

Initial MS data not only provided LFQ measures of peptides within biological samples but also contains information on the protein oxidation state, providing information on posttranslational modifications which may be relevant to physiological processes, signalling mechanisms, and disease pathology. In depth analysis of oxidation data should be performed, identifying oxidised proteins, determining the extent and location of oxidative modifications within each of the experimental conditions and placing oxidatively modified proteins in specific molecular pathways to provide insight into disease pathways.

The majority of functional dependency matrices generated within this project were very small in size and therefore, model expansion and re-evaluation should be considered. This can be carried out by mining STRING for any updated protein interaction information and including all predicted interactions in the model, regardless of confidence level (not just highest confidence interactions).

5.7 Conclusions and Summary of Key Findings

Upon review of the key findings presented in this thesis, it seems likely that the insertion of the APP transgene causes a cascade of multiple pathways of neurodegeneration, and a significant failure to properly regulate protein expression at a very early age, comparable to preclinical AD. I propose that the overexpression of Aß blocks or partially blocks VDAC1 channels, causing a compensatory upregulation of VDAC1 channels, contributing to increased levels of neuronal apoptosis. Upregulations of key proteins involved in mitochondrial fission and fusion (Mfn1, Drp1, Mfn2 and Mff) causes an imbalance of mitochondrial dynamics, which in turn, subjects neurons to increased levels of oxidative stress. Oxidative stress causes aberrant morphological changes in protein complexes of the ETC, via mechanisms of mitochondrial cristae remodelling. Failures to upregulate intermediate filaments, actin filaments and microtubules, reduces the mechanical support of the mitochondrial cytoskeleton, causing further mitochondrial dysfunction and distortion of the IMM. Failure to upregulate the proteasome protein complex to clear subsequent structurally abnormal proteins leads to the accumulation of damaged and dysfunctional proteins within the cell, further blocking protein channels within the mitochondria and increasing mitochondrial dysfunction. Additionally, the dysfunction of OXPHOS pathways in APPtg mice consequently leads to the upregulation of the peroxisome, which attempts to meet the energetic requirements of the cell via the oxidation of fatty acids, generating superoxide by-products which amplifies oxidative stress mechanisms. Failure to downregulate biological processes such as learning, synaptic plasticity and synapse organisation in glutamatergic synapses causes excessive energy expenditure, reducing levels of ATP available for memory retrieval. In combination, these molecular and cellular mechanisms exacerbate mitochondrial dysfunction, leading to a failure to meet the energetic demands of memory retrieval and accumulation of ROS, triggering neurodegeneration, and culminating in the progressive memory loss seen in early-stage AD.

To summarise, western blot analysis revealed altered mitochondrial dynamics in APPtg mice, comprising the increased expression of mitochondrial fission and fusion factors. Some subunits of the ETC were also upregulated in APPtg mice (during basal levels and during memory retrieval; SDHA, ATP5A, cytochrome C, Complex II and complex V), alongside VDAC1 and the synaptic proteins alpha synuclein and PSD95. Enzymatic activity assay revealed no significant differences in the activity of MHD2 or 6-PFK between WT and APPtg mice, within either of the behavioural groups. Western blot analysis revealed no significant differences in the expression of MDH2 or 6-PFK between WT and APPtg mice, within either of the behavioural groups. Proteomics results revealed that after the application of FDR correction, there was a complete failure to differentially regulate protein expression in APPtg mice during memory retrieval (when compared to basal levels). Proteomics results also revealed several biological processes and pathways significantly enriched in WT mice

during memory retrieval, including vesicle-mediated transport, cellular oxidant detoxification, ubiquitin protein ligase binding and endocytosis. In comparison, APPtg mice significantly upregulated very different biological processes and pathways during memory retrieval, including oxidative phosphorylation, Alzheimer disease and pathways of neurodegeneration. Several proteins failed to become upregulated in APPtg mice at the point of memory retrieval (when compared to WT mice at the point of memory retrieval), which were significantly enriched in processes such as cellular response to oxidative stress, mitochondrial ATP synthesis coupled proton transport, aerobic respiration, and negative regulation of neural apoptotic processes. Additionally, several proteins were found to be upregulated in APPtg mice during memory retrieval, which were not upregulated in WT mice during memory retrieval. These proteins were involved in mitochondrial respiratory chain complex I assembly and response to superoxides. The aims of this project have been met by quantitatively analysing the levels of certain mitochondrial proteins via western blotting, identifying biochemical and cellular pathways significantly enriched during memory retrieval (in WT and APPtg mice) and by measuring the activity of key enzymes in the mouse brain, in the context of memory retrieval. By comparing the molecular and cellular mechanism significantly enriched within WT and APPtg mice during memory retrieval, we can begin to build a picture of the processes underlying memory retrieval in health and identify the key areas of deviation in the mouse model of AD. Understanding the interrelationships between the different AD mechanisms may begin to illuminate common areas for future therapeutic intervention, with the hopes that targeting aberrant pathways at a preclinical stage can provide a means to prevent or delay the memory loss symptoms seen in AD.

REFERENCES

Abu-Hamad, S., Sivan, S., Shoshan-Barmatz, V. (2006) The expression level of the voltage-dependent anion channel controls life and death of the cell. *PNAS,* 103 (15) 5787-5792.

Acin-Perez, R., Benador, IY., Petcherski, A., Veliova, M., Benavides, GA., Lagarrigue, S., Caudal, A., Vergnes, L., Murphy, AN., Karamanlidis, G., Tian, R., Reue, K., Wanagat, J., Sacks, H., Amati, F., Darley-Usmar, VM., Liesa, M., Divakaruni, AS., Stiles, L., Shirihai, OS. (2020) A novel approach to measure mitochondrial respiration in frozen biological samples*. EMBO J,* 1;39(13).

Adav, S.S., Park, J.E., Sze, S.K. (2019) Quantitative profiling brain proteomes revealed mitochondrial dysfunction in Alzheimer's disease. *Mol Brain* 12, 8.

Ahmad, F., & Liu, P. (2020). Synaptosome as a tool in Alzheimer's disease research. *Brain research*, 1746, 147009.

Al-Khallaf H. (2017). Isocitrate dehydrogenases in physiology and cancer: biochemical and molecular insight. *Cell & bioscience*, 7, 37.

Altaf-Ul-Amin, M., Afendi, F. M., Kiboi, S. K., & Kanaya, S. (2014). Systems biology in the context of big data and networks. *BioMed research international*, 428570.

Althouse, AD. (2016) Adjust for Multiple Comparisons? It's Not That Simple. *Ann Thorac Surg*, 101(5):1644-5.

Alvarez P, Squire LR. (1994) Memory consolidation and the medial temporal lobe: a simple network model. *Proc Natl Acad Sci,* 91:7041–7045.

Alzforum (2013) Reseach Models: PDAPP (line109). https://www.alzforum.org/research-models/pdappline109.

Alzforum (2017) Research Models: J20 (PDGF-APPSw,Ind). https://www.alzforum.org/research-models/j20-pdgf-appswind.

Alzheimer's Disease International. (2022) Dementia statistics. https://www.alzint.org/about/dementia-facts-figures/dementia-statistics/.

Alzheimer's Society. (2019) What are the costs of dementia care in the UK? Available at: https://www.alzheimers.org.uk/about-us/policy-and-influencing/dementia-scale-impact-numbers.

Anand, K. S., & Dhikav, V. (2012). Hippocampus in health and disease: An overview. *Annals of Indian Academy of Neurology*, *15*(4), 239–246.

Anjum, A., Jaggi, S., Varghese, E., Lall, S., Bhowmik, A., & Rai, A. (2016). Identification of Differentially Expressed Genes in RNA-seq Data of Arabidopsis thaliana: A Compound Distribution Approach. *Journal of computational biology : a journal of computational molecular cell biology*, 23(4), 239–247.

Araújo, W.L., Nunes-Nesi, A., Nikoloski, Z., Sweetlove, L.J., Fernie, A.R. (2012), Metabolic control and regulation of the tricarboxylic acid cycle in photosynthetic and heterotrophic plant tissues*. Plant, Cell & Environment*, 35: 1-21.

Arnold, P. K., & Finley, L. W. S. (2023). Regulation and function of the mammalian tricarboxylic acid cycle. *The Journal of biological chemistry*, 299(2), 102838.

Aslam, B., Basit, M., Nisar, M.A., Khurshid, M., Rasool, M.H. (2017) Proteomics: Technologies and Their Applications, *Journal of Chromatographic Science*, 55(2), 182–196.

Bai, F., Witzmann, F.A. (2007) Synaptosome proteomics. *Subcell Biochem* 43,77-98.

Balducci, C., Forloni, G. (2011) APP Transgenic Mice: Their Use and Limitations. *Neuromol Med* 13, 117-137.

Bandara, A.B., Drake, J.C. & Brown, D.A. (2021) Complex II subunit SDHD is critical for cell growth and metabolism, which can be partially restored with a synthetic ubiquinone analog. *BMC Mol and Cell Biol,* 22, 35.

Banerjee, A., Chitnis, U. B., Jadhav, S. L., Bhawalkar, J. S., & Chaudhury, S. (2009). Hypothesis testing, type I and type II errors. *Industrial psychiatry journal*, 18(2), 127–131.

Barksdale, KA., Perez-Costas, E., Gandy JC., Melendez-Ferro, M., Roberts, RC., Bijur, GN. (2010) Mitochondrial viability in mouse and human postmortem brain. *FASEB J,* 24(9):3590-9.

Bayrhuber, M., Meins, T., Habeck, M., Becker, S., Giller, K., Villinger, S., Vonrhein, C., Griesinger, C., Zweckstetter, M., Zeth, K. (2008). Structure of the human voltage-dependent anion channel. *Proceedings of the National Academy of Sciences,* 105(40), 15370-15375.

Bera, A., Lavanya, G., Reshmi, R., Dev, K., & Kumar, R. (2022). Mechanistic and therapeutic role of Drp1 in the pathogenesis of Alzheimer's disease. *European Journal of Neuroscience*, 56(9), 5516–5531.

Bhatia, S., Rawal, R., Sharma, P., Singh, T., Singh, M., & Singh, V. (2022). Mitochondrial Dysfunction in Alzheimer's Disease: Opportunities for Drug Development. *Current neuropharmacology,* 20(4), 675–692.

Bigl M., Bruckner M. K., Arendt T., Bigl V., Eschrich K. (1999). Activities of key glycolytic enzymes in the brains of patients with Alzheimer's disease. *J. Neural Transm,* 106 499–511.

Bisaz, R., Travaglia, A., & Alberini, C. M. (2014). The neurobiological bases of memory formation: from physiological conditions to psychopathology. *Psychopathology*, 47(6), 347–356.

Bliss, T.V., Lomo, T. (1973). Long-lasting potentiation of synaptic transmission in the dentate area of the anaesthetized rabbit following stimulation of the perforant path. *J Physiol*. ;232(2):331-56.
Bortolin, RC., Gasparotto, J., Vargas, AR., da Silva Morrone, M., Kunzler, A., Henkin, BS., Chaves, PR., Roncato, S., Gelain, DP., Moreira, JCF. (2017) Effects of Freeze-Thaw and Storage on Enzymatic Activities, Protein Oxidative Damage, and Immunocontent of the Blood, Liver, and Brain of Rats. *Biopreserv Biobank*, 15(3):182-190.

Bosch, M., Castro, J., Saneyoshi, T., Matsuno, H., Sur, M., & Hayashi, Y. (2014). Structural and molecular remodeling of dendritic spine substructures during long-term potentiation. *Neuron,* 82(2), 444-459.

Bowen D. M., White P., Spillane J. A., Goodhardt M. J., Curzon G., Iwangoff P., Meier-Ruge, W., Davison, AN. (1979). Accelerated ageing or selective neuronal loss as an important cause of dementia? *Lancet,* 1 11–14.

Braak, H., Del Tredici, K. (2014). Are cases with tau pathology occurring in the absence of Abeta deposits part of the AD-related pathological process? *Acta Neuropathol,* 128, 767–772.

Braithwaite, S.P., Stock ,J.B., Lombroso, P.J., Nairn, A.C. (2012) Protein phosphatases and Alzheimer's disease. *Prog Mol Biol Transl Sci,* 106:343-79.

Briglia, J., Servajean, P., Michalland, A.-H., Brunel, L., & Brouillet, D. (2018). Modeling an enactivist multiple-trace memory. ATHENA: A fractal model of human memory. *Journal of Mathematical Psychology,* 82, 97–110.

Brüser,A., Kirchberger,J., Kloos, M., Sträter,N., Schöneberg T. (2012) Functional Linkage of Adenine Nucleotide Binding Sites in Mammalian Muscle 6-Phosphofructokinase. *Enzymology*, 287 (21), pp17546-17553.

Burré, Jacqueline. (2015) The Synaptic Function of α-Synuclein. *IOS Press,* 699 – 713.

Camara, A., Zhou, Y., Wen, P., Tajkhorshid, E., Kwok, W. (2017) Mitochondrial VDAC1: A Key Gatekeeper as Potential Therapeutic Target. *Frontiers in Physiology, 8.*

Carew, T.J., Walters, E.T., Kandel, E.R (1981) Classical conditioning in a simple withdrawal reflex in Aplysia californica. *Journal of Neuroscience,* 1(12). 1426-1437.

Cha, M. Y., Cho, H. J., Kim, C., Jung, Y. O., Kang, M. J., Murray, M. E., Hong, H. S., Choi, Y. J., Choi, H., Kim, D. K., Choi, H., Kim, J., Dickson, D. W., Song, H. K., Cho, J. W., Yi, E. C., Kim, J., Jin, S. M., & Mook-Jung, I. (2015). Mitochondrial ATP synthase activity is impaired by suppressed O-GlcNAcylation in Alzheimer's disease. *Human molecular genetics,* 24(22), 6492–6504.

Chandel N. S. (2021). Glycolysis. *Cold Spring Harbor perspectives in biology,* 13(5), a040535.

Chandramouli K, Qian PY (2009) Proteomics: challenges, techniques and possibilities to overcome biological sample complexity. *Hum Genomics Proteomics*, 239204.

Chandrasekaran, K., Giordanao, T., Brady, D.R., Stoll, J., Martin, L.J., Rapoport, S.I. (1994) Impairment in mitochondrial cytochrome oxidase gene expression in Alzheimer disease. *Brain Res Mol Brain Res,* 24(1-4) 336-340.

Chaudhry R, Varacallo M. (2023) Biochemistry, Glycolysis. *In: StatPearls [Internet]. Treasure Island (FL): StatPearls Publishing*; 2-. https://www.ncbi.nlm.nih.gov/books/NBK482303/

Chen, H., & Chan, D. C. (2010). Physiological functions of mitochondrial fusion. *Annals of the New York Academy of Sciences,* 1201, 21–25.

Chen, P., Shen, Z., Wang, Q., Zhang, B., Zhuang, Z., Lin, J., Shen, Y., Chen, Y., Dai, Z. and Wu, R. (2021). Reduced cerebral glucose uptake in an Alzheimer's rat model with glucose-weighted chemical exchange saturation transfer imaging. *Frontiers in Aging Neuroscience,* 13.

Chen, S. Y., Feng, Z., & Yi, X. (2017). A general introduction to adjustment for multiple comparisons. *Journal of thoracic disease,* 9(6), 1725–1729.

Chételat G., La Joie R., Villain N., Perrotin A., De La Sayette V., Eustache F., Vandenberghe, R. (2013). Amyloid imaging in cognitively normal individuals, at-risk populations and preclinical Alzheimer's disease. *Neuroimage Clin*, 2, 356–365.

Coley, A.A., Gao, W.J. (2019) PSD95: A synaptic protein implicated in schizophrenia or autism? *Prog Neuropsychopharmacol Biol Psychiatry*, 82:187-194.

Conroy, G. (2023) This is the largest map of the human brain ever made. *Nature*, 622, 679-680. d

Cooper GM.(2000) The Cell: A Molecular Approach. 2nd edition. Sunderland (MA): Sinauer Associates. Peroxisomes. Available from: https://www.ncbi.nlm.nih.gov/books/NBK9930/

Cowan N. (2008). What are the differences between long-term, short-term, and working memory?. *Progress in brain research,* 169, 323–338.

Cowan, N. (2001). The magical number 4 in short-term memory: A reconsideration of mental storage capacity. *Behavioral and Brain Sciences*, 24(1), pp. 87-114.

Cui, M., Cheng, C. & Zhang, L. (2022) High-throughput proteomics: a methodological mini-review. *Lab Invest* 102, 1170–1181

Cunha, SR., Mohler, PJ. (2009) Ankyrin protein networks in membrane formation and stabilization. *J Cell Mol Med*, 13(11-12):4364-76.

Dasika, SK., Vinnakota, KC., Beard, DA. (2015) Determination of the catalytic mechanism for mitochondrial malate dehydrogenase. *Biophys J*, 108(2):408-19.

Davis D. G., Schmitt F. A., Wekstein D. R., Markesbery W. R. (1999). Alzheimer neuropathologic alterations in aged cognitively normal subjects. *J. Neuropathol. Exp. Neurol,* 58, 376–388.

Derkach, V., Barria, A., Soderling, T.R. (1999) $Ca^{2+/}$calmodulin-kinase II enhances channel conductance of α-amino-3-hydroxy-5-methyl-4-isoxazolepropionate type glutamate receptors. *PNAS.* 96 (6) 3269-3274.

Dodart, J. C., Mathis, C., Bales, K. R., Paul, S. M. & Ungerer, A. (1999) Early regional cerebral glucose hypometabolism in transgenic mice overexpressing the V717F beta-amyloid precursor protein. *Neurosci. Lett*. 277, 49–52.

Doody R. S., Thomas R. G., Farlow M., Iwatsubo T., Vellas B., Joffe S., Kieburtz, K., Raman, R., Sun, X., Aisen, P.S., Siemers, E., Liu-Seifert, H., Mohs, R. (2014). Phase 3 trials of solanezumab for mild-to-moderate Alzheimer's disease. *N. Engl. J. Med.* 370, 311–321.

Drummond, E., & Wisniewski, T. (2017). Alzheimer's disease: experimental models and reality. *Acta neuropathologica*, 133(2), 155–175.

Du, X., Wang, X. & Geng, M. (2018) Alzheimer's disease hypothesis and related therapies. *Transl Neurodegener* 7, 2.

Edison P., Archer H. A., Hinz R., Hammers A., Pavese N., Tai Y. F., Hotton,G., Cutler, D., Fox, N., Kennedy, M., Rossor, M., Brooks, D.J (2007). Amyloid, hypometabolism, and cognition in Alzheimer disease: An [11C]PIB and [18F]FDG PET study. *Neurology* 68, 501–508.

Elder, G. A., Gama Sosa, M. A., & De Gasperi, R. (2010). Transgenic mouse models of Alzheimer's disease. *The Mount Sinai journal of medicine, New York*, 77(1), 69–81.

Eleftheriadis, T., Pissas, G., Liakopoulos, V., & Stefanidis, I. (2016). Cytochrome c as a Potentially Clinical Useful Marker of Mitochondrial and Cellular Damage. *Frontiers in Immunology*, 7, 279.

Emiliani, V., Entcheva, E., Hedrich, R., Hegemann, P., Konrad, K.R., Luscher, C., Mahn, M., Pan, Z.H., Sims, R.R., Vierock, J., Yizhar, O. (2022) Optogenetics for light control of biological systems. *Nat Rev Methods Primers,* 2, 55.

Emmady, P.D., Tadi, P., (2021) Dementia. *In: StatPearls [Internet]. Treasure Island* (FL): StatPearls Publishing; . https://www.ncbi.nlm.nih.gov/books/NBK557444/

Engert, F., Bonhoeffer, T. (1999) Dendritic spine changes associated with hippocampal long-term synaptic plasticity. *Nature* 399, 66–70.

Escobar-Henriques, M., Joaquim, M. (2019) Mitofusins: Disease Gatekeepers and Hubs in Mitochondrial Quality Control by E3 Ligases. *Font. Physiol,* 10.

Fagan A. M., Mintun M. A., Shah A. R., Aldea P., Roe C. M., Mach R. H., Marcus, D., Morris, J. C., Holtzman, D. (2009). Cerebrospinal fluid tau and ptau (181) increase with cortical amyloid deposition in cognitively normal individuals: implications for future clinical trials of Alzheimer's disease. EMBO *Mol. Med*, 1, 371–380.

Farshbaf, M.J., Kiana-Esfahani, A. (2018) Succinate dehydrogenase: Prospect for neurodegenerative diseases. *Mitochondrion,* 42(1).

Fernandes, P.M (2018) Phosphofructokinase isoforms as metabolic targets for treating neurological diseases. Era. Available at: https://era.ed.ac.uk/handle/1842/31270.

Fernandes, PM., Kinkead, J., McNae, I., Michels, P., Walkinshaw, M.(2020) Biochemical and transcript level differences between the three human phosphofructokinases show optimisation of each isoform for specific metabolic niches. *Biochem J 21*; 477 (22): 4425–4441.

Figueroa P., Leon G., Elorza A., Holuigue L., Jordana X. (2001) Three different genes encode the iron-sulfur subunit of succinate dehydrogenase in Arabidopsis thaliana. *Plant Molecular Biology* 46, 241–250.

Fogwe, L.A., Reddy, V., Mesfin, F.B. (2022) Neuroanatomy, Hippocampus. *In: StatPearls [Internet]. Treasure Island* (FL): StatPearls Publishing; https://www.ncbi.nlm.nih.gov/books/NBK482171/

Foyer C.H., Noctor G. & Hodges M. (2011) Respiration and nitrogen assimilation: targeting mitochondria-associated metabolism as a means to enhance nitrogen use efficiency. *Journal of Experimental Botany* 62, 1467–1482.

Frank, S., Gaume, B., Bergmann-Leitner, E., Leitner, W., Robert, E., Catez, F., Smith, C., Youle, R. (2001) The Role of Dynamin-Related Protein 1, a Mediator of Mitochondrial Fission, in Apoptosis. *Developmental Cell*, 1(4). 515-525.

Frankland, P. W., & Bontempi, B. (2005). The organization of recent and remote memories. *Nature reviews. Neuroscience*, *6*(2), 119–130.

Friedman, J. R., & Nunnari, J. (2014). Mitochondrial form and function. *Nature,* 505(7483), 335–343.

Fujii, S., Saito, K., Miyakawa, H., Ito, K. I., & Kato, H. (1991). Reversal of long-term potentiation (depotentiation) induced by tetanus stimulation of the input to CA1 neurons of guinea pig hippocampal slices. *Brain research*, 555(1), 112-122.

Furcila, D., Domínguez-Álvaro, M., DeFelipe, J., Alonso-Nanclares, L. (2018) Subregional Density of Neurons, Neurofibrillary Tangles and Amyloid Plaques in the Hippocampus of Patients With Alzheimer's Disease. *Frontiers in Neuroanatomy*, 13.

Gao, F., Reynolds, M., Passalacqua, K., Sexton, J.Z., Abuaita, B., O'Riordan, M.X.D. (2021) The Mitochondrial Fission Regulator DRP1 Controls Post-Transcription Regulation of TNF- α. *Front. Cell. Infect. Microbiol*, 10.

Garrido, C., Galluzzi, L., Brunet, M., Puig, P.E., Didelot, C., Kroemer, G. (2006). Mechanisms of cytochrome *c* release from mitochondria. *Cell Death Differ* 13, 1423–1433.

GeneCards (2017) DCTN2 Gene-Dynactin Subunit 2. https://www.genecards.org/cgi-bin/carddisp.pl?gene=DCTN2#summaries

GeneCards (2023) ALDOC Gene-Aldolase, Fructose-Bisphosphate C. https://www.genecards.org/cgi-bin/carddisp.pl?gene=ALDOC#summaries.

GeneCards (2023) CYCS Gene. https://www.genecards.org/cgi-bin/carddisp.pl?gene=CYCS

GeneCards (2023) FXYD6 Gene.https://www.genecards.org/cgi-bin/carddisp.pl?gene=FXYD6#summaries

GeneCards (2023) HSP90AA1 Gene. https://www.genecards.org/cgi-bin/carddisp.pl?gene=HSP90AA1#summaries

GenomeNet (2011) KEGG Pathway Maps. Available at: https://www.genome.jp/kegg/kegg3a.html.

Ghosh, R., Gilda, J. E., & Gomes, A. V. (2014). The necessity of and strategies for improving confidence in the accuracy of western blots. *Expert review of proteomics,* 11(5), 549–560.

Giacobini E., Gold G. (2013). Alzheimer disease therapy-moving from amyloid-[beta] to tau. *Nat. Rev. Neurol.* 9, 677–686.

Goldberg, J., Currais, A., Prior, M., Fischer, W., Chiruta, C., Ratliff, E., Daugherty, D., Dargusch, R., Finley, K., Esparza-Moltó, P. B., Cuezva, J. M., Maher, P., Petrascheck, M., & Schubert, D. (2018). The mitochondrial ATP synthase is a shared drug target for aging and dementia. *Aging cell,* 17(2), e12715.

Goto, A. (2022) Synaptic plasticity during systems memory consolidation. *Neuroscience Research,* 183. 1-6.

Grønborg, M., Kristiansen, T. Z., Iwahori, A., Chang, R., Reddy, R., Sato, N., Molina, H., Jensen, O.N., Hruban, R.H., Goggins, M.G., Maitra, A., Pandey, A. (2006). Biomarker Discovery from Pancreatic Cancer Secretome Using a Differential Proteomic Approach* S. *Molecular & Cellular Proteomics,* 5(1), 157-171.

Guha, S., Patil, A., Muralidharan, H., & Baas, P. W. (2021). Mini-review: Microtubule sliding in neurons. *Neuroscience letters,* 753, 135867.

Hardy, J., Allsop, D. (1991) Amyloid deposition as the central event in the aetiology of Alzheimer's disease. *Trends Pharmacol. Sci*, 12, 383–388.

Hayashi, Y., Shi, S.H., Esteban, J.A., Piccini, A., Poncer, J.C., Malinow, R. (2000) Driving AMPA receptors into synapses by LTP and CaMKII: requirement for GluR1 and PDZ domain interaction. *Science*, 287, 2262-2267.

Herculano-Houzel S. (2009) The human brain in numbers: a linearly scaled-up primate brain. *Front Hum Neurosci*, 9;3:31.

Hintzman, D. L., & Block, R. A. (1971). Repetition and memory: Evidence for a multiple-trace hypothesis. *Journal of Experimental Psychology,* 88(3), 297–306.

Hong, I., Kim, J., Kim, J., Lee, S., Ko, H.G., Nader, K., K, B.K., Tsien, R.W., Choi, S. (2013) AMPA receptor exchange underlies transient memory destabillisation on retrieval. *PNAS,* 110 (20) 3218-8223.

Hou, J. (2017) Chapter 7- Protein Function Prediction from Functional Connectivity. *New Approaches of Protein Function Prediction from Functional Connectivity*, 97-105.

Hsieh, JY., Shih, WT., Kuo, YH., Lui, GW., Hung, HC. (2019) Functional Roles of Metabolic Intermediates in Regulating the Human Mitochondrial NAD(P)+-Dependent Malic Enzyme. *Sci Rep 9,* 9081.

Hu C, Huang Y, Li, L. (2017) Drp1-Dependent Mitochondrial Fission Plays Critical Roles in Physiological and Pathological Progresses in Mammals. *Int J Mol Sci*, ;18(1):144.

Huang, J., van Zijl, P.C., Han, X., Dong, C.M., Cheng, G.W., Tse, K.H., Knutsson, L., Chen, L., Lai, J.H., Wu, E.X. and Xu, J., (2020). Altered d-glucose in brain parenchyma and cerebrospinal fluid of early Alzheimer's disease detected by dynamic glucose-enhanced MRI. *Science advances,* 6(20)

Hue, L., Rider, M. (1987) Role of fructose 2,6-bisphosphate in the control of glycolysis in mammalian tissues. *Biochem J,* 245, pp 313-324.

Hung, H., Kuo, M.,Chang, G.,Liu, G. (2005) Characterization of the functional role of allosteric site residue Asp102 in the regulatory mechanism of human mitochondrial NAD(P)+-dependent malate dehydrogenase (malic enzyme). *Biochem J*, 392 (1): 39–45.

Ishihara, N., Eura,Y., Mihara, K. (2004) Mitofusin 1 and 2 play distinct roles in mitochondrial fusion reactions via GTPase activity. *J Cell Sci*, 117 (26): 6535–6546.

Jarome, T. J., & Helmstetter, F. J. (2013). The ubiquitin-proteasome system as a critical regulator of synaptic plasticity and long-term memory formation. *Neurobiology of learning and memory*, 105, 107–116.

Jeong, J., Pandey, S., Li, Y., Roche, K. (2019) PSD-95 binding dynamically regulates NLGN1 trafficking and function. *PNAS*, 116 (24). 12035-12044.

Ježek, J., Cooper, K. F., & Strich, R. (2018). Reactive Oxygen Species and Mitochondrial Dynamics: The Yin and Yang of Mitochondrial Dysfunction and Cancer Progression. *Antioxidants* (Basel, Switzerland), 7(1), 13.

Johri, A., & Beal, M. F. (2012). Mitochondrial dysfunction in neurodegenerative diseases. *The Journal of pharmacology and experimental therapeutics,* 342(3), 619–630.

Jonckheere, A. I., Smeitink, J. A., & Rodenburg, R. J. (2012). Mitochondrial ATP synthase: architecture, function and pathology. *Journal of inherited metabolic disease,* 35(2), 211–225.

Jones, M. D., & Naylor, K. (2022). Simple to Complex: The Role of Actin and Microtubules in Mitochondrial Dynamics in Amoeba, Yeast, and Mammalian Cells. *International journal of molecular sciences,* 23(16), 9402.

Kametani, F., Hasegawa, M., (2018) Reconsideration of Amyloid Hypothesis and Tau Hypothesis in Alzheimer's Disease. *Front Neurosci,* 12:25.

Karimi Abadchi, J., Nazari-Ahangarkolaee, M., Gattas, S., Bermudez-Contreras, E., Luczak, A., McNaughton, B. L., & Mohajerani, M. H. (2020). Spatiotemporal patterns of neocortical activity around hippocampal sharp-wave ripples. *eLife*, *9*, e51972.

Kelleher, R J. (2017) Presenilin-1 mutations and Alzheimer's disease. *Proceedings of the National Academy of Sciences,* 114(4) pp629-631.

Kennedy, M. B. (2013) Synaptic Signaling in Learning and Memory. *Cold Spring Harb Perspect Biol*, 30;8(2):a016824.

Kim J., Chakrabarty P., Hanna A., March A., Dickson D. W., Borchelt D. R., Golde, T., Janus, C. (2013). Normal cognition in transgenic BRI2-Abeta mice. *Mol. Neurodegener,* 8, 15.

Kim J., Onstead L., Randle S., Price R., Smithson L., Zwizinski C., Dickson, D.W., Golde, T., Klamt S, von Kamp A. (2011) An application programming interface for CellNetAnalyzer. *Biosystems,* ;105(2):162-8.

Klamt, S., Saez-Rodriguez, J. & Gilles, E.D. (2007). Structural and functional analysis of cellular networks with CellNetAnalyzer. *BMC Syst Biol* 1, 2.

Knott, A. B., & Bossy-Wetzel, E. (2008). Impairing the mitochondrial fission and fusion balance: a new mechanism of neurodegeneration. *Annals of the New York Academy of Sciences,* 1147, 283–292.

Kühlbrandt, W. (2015) Structure and function of mitochondrial membrane protein complexes. *BMC Biol* 13, 89.

Kumar, A., Ganini, D. & Mason, R.P. (2016) Role of cytochrome c in α-synuclein radical formation: implications of α-synuclein in neuronal death in Maneb- and paraquat-induced model of Parkinson's disease. *Mol* Neurodegeneration 11, 70.

Kumar, V., Kim, S. H., & Bishayee, K. (2022). Dysfunctional Glucose Metabolism in Alzheimer's Disease Onset and Potential Pharmacological Interventions. *International journal of molecular sciences,* 23(17), 9540.

Kuns B, Rosani A, Varghese D. (2023) Memantine. In: StatPearls [Internet]. Treasure Island (FL): StatPearls Publishing;. https://www.ncbi.nlm.nih.gov/books/NBK500025/

Kurkinen, M., Fułek, M., Fułek, K., Beszłej, JA., Kurpas, D., Leszek, J. (2023). The Amyloid Cascade Hypothesis in Alzheimer's Disease: Should we Change our Thinking? *Biomolecules*, *13*(3), 453

Langa, K. M., & Levine, D. A. (2014). The diagnosis and management of mild cognitive impairment: a clinical review. *JAMA,* 312(23), 2551–2561.

Lee S, Lee DK. (2018) What is the proper way to apply the multiple comparison test? *Korean J Anesthesiol,* ;71(5):353-360.

Lei, Z., Huhman, D. V., & Sumner, L. W. (2011). Mass spectrometry strategies in metabolomics. *The Journal of biological chemistry,* 286(29), 25435–25442.

Li Y., Rinne J. O., Mosconi L., Pirraglia E., Rusinek H., Desanti S., Kemppainen, N., Nagren, K., Kim, B.C., Tsui, W., de Leon, M.J. (2008). Regional analysis of FDG and PIB-PET images in normal aging, mild cognitive impairment, and Alzheimer's disease. Eur. J. *Nuclear Med. Mol*, 2169–2181.

Li, Y., Park, J. S., Deng, J. H., & Bai, Y. (2006). Cytochrome c oxidase subunit IV is essential for assembly and respiratory function of the enzyme complex. *Journal of bioenergetics and biomembranes*, *38*(5-6), 283–291.

Liang, K. C. (1991). Pretest intra-amygdala injection of lidocaine or glutamate antagonists impairs retention performance in an inhibitory avoidance task. *In Society for Neuroscience Abstracts*, 17(486) 237-249

Litwack, G. (2018) Glycolysis and Gluconeogenesis, *Human Biochemistry,* 183–198.

Lopez J, Gamache K, Schneider R, Nader K. (2015) Memory retrieval requires ongoing protein synthesis and NMDA receptor activity-mediated AMPA receptor trafficking. *J Neurosci,* 35(6):2465-75.

Luis, C., Ryan, T.J (2022) Understanding the physical basis of memory: Molecular mechanisms of the engram. *JBC Reviews*, 298 (5).

Luo, D., Li, J., Liu, H., Wang, J., Xia, Y., Qiu, W., Wang, N., Wang, X., Wang, X., Ma, C., Ge, W. (2023) Integrative Transcriptomic Analyses of Hippocampal–Entorhinal System Subfields Identify Key Regulators in Alzheimer's Disease. *Adv. Sci* , 10, 2300876

Lushchak, O. V., Piroddi, M., Galli, F., & Lushchak, V. I. (2014). Aconitase post-translational modification as a key in linkage between Krebs cycle, iron homeostasis, redox signaling, and metabolism of reactive oxygen species. *Redox report : communications in free radical research*, 19(1), 8–15.

Makin, S. (2018) The amyloid hypothesis on trial*. Nature* 559, S4-S7.

Maletic-Savatic, M., Malinow, R., & Svoboda, K. (1999). Rapid dendritic morphogenesis in CA1 hippocampal dendrites induced by synaptic activity. *Science,* 283(5409), 1923-1927.

Manczak, M., & Reddy, P. H. (2012). Abnormal interaction of VDAC1 with amyloid beta and phosphorylated tau causes mitochondrial dysfunction in Alzheimer's disease. *Human molecular genetics,* 21(23), 5131–5146.

Marinesco, S., & Carew, T. J. (2002). Serotonin release evoked by tail nerve stimulation in the CNS of aplysia: characterization and relationship to heterosynaptic plasticity. *The Journal of neuroscience : the official journal of the Society for Neuroscience*, *22*(6), 2299–2312.

Martínez-Reyes, I., Chandel, N.S. (2020) Mitochondrial TCA cycle metabolites control physiology and disease. *Nat Commun,* 11, 102

Matsuzaki, M., Honkura, N., Ellis-Davies, G. C., & Kasai, H. (2004). Structural basis of long-term potentiation in single dendritic spines. *Nature*, 429(6993), 761-766.

McCarthy, D. J., & Smyth, G. K. (2009). Testing significance relative to a fold-change threshold is a TREAT. *Bioinformatics (Oxford, England*), 25(6), 765–771.

McCue WM, Finzel BC (2021) Structural Characterization of the Human Cytosolic Malate Dehydrogenase I. *ACS Omega ;*7(1):207-214.

McGowan, E. (2007). Abeta40 inhibits amyloid deposition *in vivo. J. Neurosci,* 27, 627–633

McKenna, M., Dienek, G.A., Sonnewald, U., Waagepetersen, H.S., Schousboe, A. (2012) Chapter 11- ENergy Metaoblism of the Brain. *Basic Neuroschemistry (Eighth Edition),* 200-231.

Medline Plus (2018) DYNC1H1 gene. https://medlineplus.gov/genetics/gene/dync1h1/

Medline Plus (2018) RAB3GAP1 gene. https://medlineplus.gov/genetics/gene/rab3gap1/

Medscape (2023) Alzheimer Disease Treatment & Management.https://emedicine.medscape.com/article/1134817-treatment.

Miller, G. (1956). The magical number seven, plus or minus two: Some limits on our capacity for processing information. *Psychological Review,* 63(2), pp. 81-97.

Mishkin, M. (1978) Memory in monkeys severely impaired by combined but not by separate removal of amygdala and hippocampus. *Nature* 273, 297–298.

Misrani, A., Tabassum, S., Huo, Q., Tabassum, S., Jiang, J., Liu, S., Feng, X., Long, C., Yang, L. (2021) Mitochondrial Deficits With Neural and Social Damage in Early-Stage Alzheimer's Disease Model Mice. *Front. Aging Neurosci,* 13.

Mosconi, L., Pupi, A. and De Leon, M.J. (2008), Brain Glucose Hypometabolism and Oxidative Stress in Preclinical Alzheimer's Disease. *Annals of the New York Academy of Sciences*, 1147: 180-195.

Mucke L, Masliah E, Yu GQ, Mallory M, Rockenstein EM, Tatsuno G, Hu K, Kholodenko D, Johnson-Wood K, McConlogue L. (2000) High-level neuronal expression of abeta 1-42 in wild-type human amyloid protein precursor transgenic mice: synaptotoxicity without plaque formation. *J Neurosci,* 1;20(11):4050-8.

Müller, T., & Winter, D. (2017). Systematic Evaluation of Protein Reduction and Alkylation Reveals Massive Unspecific Side Effects by Iodine-containing Reagents. Molecular & cellular proteomics : *MCP,* 16(7), 1173–1187.

Mullinax, TR., Mock, JN., McEvily, AJ., Harrison, JH. (1982) Regulation of Mitochondrial Malate Dehydrogenase. Evidence for an allosteric Citrate-binding site. *The Journal Of Biological Chemistry,* 257(22). Pp13233-132393.

Mutisya, E.M., Bowling, A.C. and Beal, M.F. (1994), Cortical Cytochrome Oxidase Activity Is Reduced in Alzheimer's Disease. *Journal of Neurochemistry,* 63: 2179-2184.

NIH (2023) Aldoc aldolase C, fructose-bisphosphate [Mus musculus (house mouse)].https://www.ncbi.nlm.nih.gov/gene?Db=gene&Cmd=DetailsSearch&Term=11676

NIH (2023) Dclk1 doublecortin-like kinase 1 [Mus musculus (house mouse)]. https://www.ncbi.nlm.nih.gov/gene?Db=gene&Cmd=DetailsSearch&Term=13175

NIH (2023) How Is Alzheimer's Disease Treated? Available at: https://www.nia.nih.gov/health/how-alzheimers-disease-treated.

NIH (2023) Madd MAP-kinase activating death domain [Mus musculus (house mouse)]. https://www.ncbi.nlm.nih.gov/gene?Db=gene&Cmd=DetailsSearch&Term=228355

NIH (2023) PARK7 Parkinsonism associated deglycase [Homo sapiens (human)]. https://www.ncbi.nlm.nih.gov/gene/11315#

Nukala, VN., Singh, IN., Davis, LM., Sullivan, PG. (2006) Cryopreservation of brain mitochondria: A novel methodology for functional studies. *Journal of Neuroscience Methods,* 152 (1-2), 48-54.

Ohnishi, T., Ohnishi, S. T., Shinzawa-Ito, K., & Yoshikawa, S. (2008). Functional role of coenzyme Q in the energy coupling of NADH-CoQ oxidoreductase (Complex I): stabilization of the semiquinone state with the application of inside-positive membrane potential to proteoliposomes. *BioFactors* (Oxford, England), 32(1-4), 13–22.

Okamoto, K. I., Nagai, T., Miyawaki, A., & Hayashi, Y. (2004). Rapid and persistent modulation of actin dynamics regulates postsynaptic reorganization underlying bidirectional plasticity. *Nature neuroscience,* 7(10), 1104-1112.

Oliver, D., & Reddy, P. H. (2019). Dynamics of Dynamin-Related Protein 1 in Alzheimer's Disease and Other Neurodegenerative Diseases. *Cells,* 8(9), 961.

Ono, R., Sakurai, T., Sugimoto, T., Uchida, K., Nakagawa, T., Noguchi, T., Komatsu, A., Arai, H., & Saito, T. (2023). Mortality Risks and Causes of Death by Dementia Types in a Japanese Cohort with Dementia: NCGG-STORIES. *Journal of Alzheimer's disease : JAD,* 92(2), 487–498.

Osellame, L. D., Blacker, T. S., & Duchen, M. R. (2012). Cellular and molecular mechanisms of mitochondrial function. Best practice & research. *Clinical endocrinology & metabolism,* 26(6), 711–723.

Osto, C., Benador, I. Y., Ngo, J., Liesa, M., Stiles, L., Acin-Perez, R., & Shirihai, O. (2020). Measuring mitochondrial respiration in previously frozen biological samples. *Current Protocols in Cell Biology,* 89, e116.

Ostrowitzki S., Deptula D., Thurfjell L., Barkhof F., Bohrmann B., Brooks D. J., Klunk, W.E., Ashford, E., Yoo, K., Xu, Z.X., Loetscher, H., Santarelli, L. (2012). Mechanism of amyloid removal in patients with Alzheimer disease treated with gantenerumab. *Arch. Neurol.* 69, 198–207.

Patel, M. S., Nemeria, N. S., Furey, W., & Jordan, F. (2014). The pyruvate dehydrogenase complexes: structure-based function and regulation. *The Journal of biological chemistry,* 289(24), 16615–16623.

Patel, MS., Harris RA. (2023) Metabolic Regulation. *Encyclopedia of Cell Biology,* 1 (2). Pp 353-365.

Paul, I., White, C., Turcinovic, I. and Emili, A. (2020), Imaging the future: the emerging era of single-cell spatial proteomics. *FEBS J,* 288: 6990-7001.

Perluigi, M., Barone, E., Di Domenico, F., Butterfield, D.A. (2016) Abberrant protein phosphorylation in ALzheimer disease brains disturbs pro-survival and cell death pathways. *Biochemica et Biophysica Acta (BBA)-Molecular Basis of Disease,* 1862 (10). 1871-1882.

Phaniendra, A., Jestadi, D. B., & Periyasamy, L. (2015). Free radicals: properties, sources, targets, and their implication in various diseases. *Indian journal of clinical biochemistry : IJCB,* 30(1), 11–26

Pizzino, G., Irrera, N., Cucinotta, M., Pallio, G., Mannino, F., Arcoraci, V., Squadrito, F., Altavilla, D., & Bitto, A. (2017). Oxidative Stress: Harms and Benefits for Human Health. *Oxidative medicine and cellular longevity,* 2017, 8416763.

Postle, B.R., Pasternak, T. (2009). Short Term and Working Memory. *Encyclopedia of Neuroscience,* 783-789.

Price J. L., Mckeel D. W., Jr., Buckles V. D., Roe C. M., Xiong C., Grundman M., Hansen, L.A., Peterson, R.C., Parisi, J.E., Dickson, D.W., Smith, C.D., Davis, D.G., Schmitt, F.A., Markesbery, W.R., Kayw, J., Kurlan, R., Hu;ette, C., Kurland, B.F., Higdon, R., Kukull, W., Morris, J.C. (2009). Neuropathology of nondemented aging: presumptive evidence for preclinical Alzheimer disease. *Neurobiol. Aging* 30, 1026–1036.

Priestley, JRC., Pace, LM., Sen, K., Aggarwal, A.., Alves, CAPF., Campbell, IM., Cuddapah, SR., Engelhardt, NM., Eskandar, M., Jolín García, PC., Gropman, A., Helbig, I., Hong, X., Gowda, VK., Lusk, L., Trapane, P., Srinivasan,

VM., Suwannarat, P., Ganetzky, RD. (2022) Malate dehydrogenase 2 deficiency is an emerging cause of pediatric epileptic encephalopathy with a recognizable biochemical signature. *Mol Genet Metab Rep,* 33:100931.

PubChem (2023) Fxyd6- FXYD domain-containing ion transport regulator 6 (house mouse).https://pubchem.ncbi.nlm.nih.gov/gene/59095.

Raben, D. (2013) Phosphofructokinase-2/Fructose Bisphosphatase-2, *Encyclopedia of Biological Chemistry,* pp. 456–458.

Ramirez, A., & Arbuckle, M. R. (2016). Synaptic Plasticity: The Role of Learning and Unlearning in Addiction and Beyond. *Biological psychiatry,* 80(9), e73–e75.

Ranieri, M., Brajkovic, S., Riboldi, G., Rinchi, D., Rizzo, F., Bresolin, N., Corti, S., Comi, GP. (2013) Mitochondrial fusion proteins and human diseases. *Neurol Res Int,* 293893.

Rao, Y. L., Ganaraja, B., Murlimanju, B. V., Joy, T., Krishnamurthy, A., & Agrawal, A. (2022). Hippocampus and its involvement in Alzheimer's disease: a review. *3 Biotech*, *12*(2), 55.

Raulin, AC., Doss, S.V., Trottier, Z.A.., Ikezu, T.C., Bu, G., Liu, CC. (2022) ApoE in Alzheimer's disease: pathophysiology and therapeutic strategies. *Mol Neurodegeneration,* 17, 72.

Renkema, G., Wortmann, S., Smeets, R., Venselaar, H., Antoine, M., Visser, G., Ben-Omran, T., Van der Heuvel, L.P., Timmers, H.J.L.M., Smeitink., Rodenburg, R.J.T. (2015) SDHA mutations causing a multisystem mitochondrial disease: novel mutations and genetic overlap with hereditary tumors. *Eur J Hum Genet,* 23, 202–209.

Riedel G, Platt B, Micheau J. (2003) Glutamate receptor function in learning and memory. *Behav Brain Res,* ;140(1–2):1–47.

Riedel, G., Micheau, J., Lam, A. G. M., Roloff, E. V. L., Martin, S. J., Bridge, H., de Hoz, L., Poeschel, B., McCulloch, J., & Morris, R. G. (1999). Reversible neural inactivation reveals hippocampal participation in several memory processes. *Nature neuroscience,* 2(10), 898-905.

Roberts DJ, Miyamoto S. (2015) Hexokinase II integrates energy metabolism and cellular protection: Akting on mitochondria and TORCing to autophagy. *Cell Death Differ,* 22(2):248-57.

Ros, S., Schulze, A. (2013) Balancing glycolytic flux: the role of 6-phosphofructo-2-kinase/fructose 2,6-bisphosphatases in cancer metabolism. *Cancer Metab* 1, 8.

Rothman, KJ. (1990) No adjustments are needed for multiple comparisons. *Epidemiology*, Jan;1(1):43-6.

Roy, D. S., Arons, A., Mitchell, T. I., Pignatelli, M., Ryan, T. J., & Tonegawa, S. (2016). Memory retrieval by activating engram cells in mouse models of early Alzheimer's disease. *Nature,* 531(7595), 508–512.

Rustin, P., Munnich, A. & Rötig, A. (2002) Succinate dehydrogenase and human diseases: new insights into a well-known enzyme. *Eur J Hum Genet* 10, 289–291.

Saganich MJ, Schroeder BE, Galvan V, Bredesen DE, Koo EH, Heinemann SF. (2006) Deficits in synaptic transmission and learning in amyloid precursor protein (APP) transgenic mice require C-terminal cleavage of APP. *J Neurosci,* 26(52):13428-36

Salloway S., Sperling R., Fox N. C., Blennow K., Klunk W., Raskind M., Sabbagh, M., Honig, L.S., Porteinsson, A.P., Ferris, S., Reichert, M., Ketter, N., Nejadnik, B., Guenzler, V., Miloslavsky, M., Wang, D., Lu, Y., Lull, J., Tudor, L.C., Liu, E., Grundman, M., Yuen, E., Black, R., Brashear, H.R. (2014). Two phase 3 trials of bapineuzumab in mild-to-moderate Alzheimer's disease. *N. Engl. J. Med,* 370, 322–333.

Saura, C. A., Choi, S. Y., Beglopoulos, V., Malkani, S., Zhang, D., Shankaranarayana Rao, B. S., Chattarji, S., Kelleher, R. J., 3rd, Kandel, E. R., Duff, K., Kirkwood, A., & Shen, J. (2004). Loss of presenilin function causes impairments of memory and synaptic plasticity followed by age-dependent neurodegeneration. *Neuron*, 42(1), 23–36.

Savioz, A., Leuba, G., Vallet, P.G (2014) A framework to understand the variations of PSD-95 expresison in brain aging and in Alzheimer's disease. *Ageing Research Reviews,* 18. 86-94.

Savitski, M. M., Wilhelm, M., Hahne, H., Kuster, B., & Bantscheff, M. (2015). A Scalable Approach for Protein False Discovery Rate Estimation in Large Proteomic Data Sets. Molecular & cellular proteomics : *MCP,* 14(9), 2394–2404.

Schönfeld, P., & Reiser, G. (2013). Why does brain metabolism not favor burning of fatty acids to provide energy? Reflections on disadvantages of the use of free fatty acids as fuel for brain. *Journal of cerebral blood flow and metabolism : official journal of the International Society of Cerebral Blood Flow and Metabolism,* 33(10), 1493–1499.

Schwarz, N., & Leube, R. E. (2016). Intermediate Filaments as Organizers of Cellular Space: How They Affect Mitochondrial Structure and Function. *Cells,* 5(3), 30.

Scoville, WB., Milner ,B. (1957) Loss of recent memory after bilateral hippocampal lesions. J *Neurol Neurosurg Psychiatry* 20:11–21.

Selkoe, DJ., Hardy, J. (2016). The amyloid hypothesis of Alzheimer's disease at 25 years. *EMBO Mol Med.* 8: pp595-608.

Semon, R.W. (1921). The Mneme. London: G. Allen and Unwin Limited.

Semon, R.W. (1923). Mnemic psychology. London: Allen, Unwin.

Sexton, Z., Abuaita, B.H., O'Riordan, M.X.D (2021) The Mitochondrial Fission Regulator DRP1 Controls Post-Transcriptional Regulation of TNF-α. *Front.Cell.Infect.Microbiol,* 10.

Shao, C. Y., Mirra, S. S., Sait, H. B., Sacktor, T. C., & Sigurdsson, E. M. (2011). Postsynaptic degeneration as revealed by PSD-95 reduction occurs after advanced Aβ and tau pathology in transgenic mouse models of Alzheimer's disease. *Acta neuropathologica,* 122(3), 285–292.

Sharma, L. K., Lu, J., & Bai, Y. (2009). Mitochondrial respiratory complex I: structure, function and implication in human diseases. *Current medicinal chemistry*, 16(10), 1266–1277.

Shekhar, S., Pernier, J., Carlier, M.F. (2016) Regulators of actin filaments barbed ends at a glance. *J Cell Sci,* 129 (6). 1085-1091.

Shen, J.; Kelleher, R.J. 3rd. (2007) The presenilin hypothesis of Alzheimer's disease: Evidence for a loss-of-function pathogenic mechanism. *Proc. Natl. Acad. Sci,* 104, 403–409.

Sheng M, Sabatini BL, Südhof TC. (2012) Synapses and Alzheimer's disease. *Cold Spring Harb Perspect Biol,* 4(5):a005777.

Shi, Q., & Gibson, G. E. (2011). Up-regulation of the mitochondrial malate dehydrogenase by oxidative stress is mediated by miR-743a. *Journal of neurochemistry,* 118(3), 440–448.

Shim, K. H., Kang, M. J., Youn, Y. C., An, S. S. A., & Kim, S. (2022). Alpha-synuclein: a pathological factor with Aβ and tau and biomarker in Alzheimer's disease. *Alzheimer's research & therapy*, 14(1), 201

Shoshan-Barmatz V, Maldonado EN, Krelin Y. (2017) VDAC1 at the crossroads of cell metabolism, apoptosis and cell stress. *Cell Stress,* 11-36.

Shoshan-Barmatz, V., De Pinto, V., Zweckstetter, M., Raviv, Z., Keinan, N., Arbel, N. (2010) VDAC, a multi-functional mitochondrial protein regulating cell life and death. *Molecular Aspects of Medicine,* 31(3). 227-285.

Shoshan-Barmatz, V., Nahon-Crystal, E., Shteinfer-Kuzmine, A., & Gupta, R. (2018). VDAC1, mitochondrial dysfunction, and Alzheimer's disease. *Pharmacological research,* 131, 87–101.

Shoshan-Barmatz, V., Shteinfer-Kuzmine, A., & Verma, A. (2020). VDAC1 at the Intersection of Cell Metabolism, Apoptosis, and Diseases. *Biomolecules,* 10(11), 1485.

Sims N. R., Bowen D. M., Smith C. C., Flack R. H., Davison A. N., Snowden J. S., Neary, D. (1980). Glucose metabolism and acetylcholine synthesis in relation to neuronal activity in Alzheimer's disease. *Lancet 1* 333–336.

Singh, A., Faccenda, D., Campanella, M. (2021) Pharmacological advances in mitochondrial therapy. *eBioMedicine*, 65,103244.

Sinsky J, Pichlerova K, Hanes J. (2021) Tau Protein Interaction Partners and Their Roles in Alzheimer's Disease and Other Tauopathies. *Int J Mol Sci, (*17):9207.

Sola-Penna, M., Da Silva, D., Coelho, W.S., Marinho-Carvalho, M.M. and Zancan, P. (2010) Regulation of mammalian muscle type 6-phosphofructo-1-kinase and its implication for the control of the metabolism. *IUBMB Life*, 62: 791-796.

Squire LR, Genzel L, Wixted JT, Morris RG. (2015) Memory consolidation. *Cold Spring Harb Perspect Biol,* 7(8):a021766.

Squire, L. (2009). Memory and Brain Systems: 1969-2009. *Journal of Neuroscience*, 29 (41) 12711-12716

Squire, L.R., Zola-Morgan, S. (1991) The Medial Temporal Lobe Memory System.*Science,* 253,1380-1386.

Suarez-Rivero, J.M., Villanueva-Paz, M., De la Cruz-Ojeda, P., De le Mata, M., Cotan, D., Oropesa-Avila, M., De Lavera, I., Alvarez-Cordoba, M., Luzon-Hidalgo, R., Sanchez-Alcazar, J. (2017) Mitochondrial Dynamics in Mitochondrial Diseases. *Diseases,* 5(1).

Suresh, B., Lee, J., Kim, K. S., & Ramakrishna, S. (2016). The Importance of Ubiquitination and Deubiquitination in Cellular Reprogramming. *Stem cells international,* 2016, 6705927.

Szapiro, G., Galante, J. M., Barros, D. M., Levi de Stein, M., Vianna, M. R., Izquierdo, L. A., Izquierdo, I., & Medina, J. H. (2002). Molecular mechanisms of memory retrieval. *Neurochemical research,* 27(11), 1491–1498.

Szapiro, G., Izquierdo, L. A., Alonso, M., Barros, D., Paratcha, G., Ardenghi, P., Pereira P., Medina, J. H., and Izquierdo, I. (2000) Participation of hippocampal metabotropic receptors, protein kinase A and mitogen-activated protein kinases in memory retrieval. *Neuroscience* 99:1–5

Szklarczyk, D., Gable, A.L., Nastou, K.C., Lyon, D., Kirsch, R., Pyysalo, S., Doncheva, N.T., Legeay, M., Fang, T., Bork, P., Jensen, L.J., von Mering, C. (2021) The STRING database in 2021: customizable protein–protein networks, and functional characterization of user-uploaded gene/measurement sets*, Nucleic Acids Research,* 49(1),605-612

Tai, L. M., Maldonado Weng, J., LaDu, M. J., & Brady, S. T. (2021). Relevance of transgenic mouse models for Alzheimer's disease. *Progress in molecular biology and translational science,* 177, 1–48.

Tanaka K. (2009). The proteasome: overview of structure and functions. Proceedings of the Japan Academy. Series B, *Physical and biological sciences,* 85(1), 12–36.

Tarsa, L., & Goda, Y. (2002). Synaptophysin regulates activity-dependent synapse formation in cultured hippocampal neurons. *Proceedings of the National Academy of Sciences of the United States of America*, *99*(2), 1012–1016.

Tayler, K.K., Tanaka, K., Reijmers, L., Wiltgen, B.J. (2013) Reactivation of Neural Ensembles during the Retrieval of Recent and Remote Memories. *Current Biology,* 23(2). 99-106.

Thiel, G. (1993), Synapsin I, Synapsin II, and Synaptophysin: Marker Proteins of Synaptic Vesicles. *Brain Pathology,* 3: 87-95.

Thomas P. D. (2017). The Gene Ontology and the Meaning of Biological Function. *Methods in molecular biology* (Clifton, N.J.), 1446, 15–24.

Tian, K., Rajendran, R., Doddananjaiah, M., Krstic-Demonacos, M., Schwartz, J.M. (2013) Dynamics of DNA Damage Induced Pathways to Cancer. *Plos One,* 8(9).

Timón-Gómez, A., Nývltová, E., Abriata, L. A., Vila, A. J., Hosler, J., & Barrientos, A. (2018). Mitochondrial cytochrome c oxidase biogenesis: Recent developments. *Seminars in cell & developmental biology,* 76, 163–178.

Toledano, A., Alvarez, M.I., Lopez-Rodrigues, A.B., Toledano-Riza, A., Fernandez-Verdecia, C.I. (2012) Does Alzheimer's disease exist in all primates? Alzheimer pathology in non-human primates and its pathophysiological implications. *Neurologia (English Edition)* 27 (6) 354-369.

Tonegawa, S., Pignatelli, M., Roy, D., Ryan, T. (2015) Memory engram storage and retrieval. *Current Opinion in Neurobiology,* 35, 101-109.

Triepels, R., Smeitink, J., Loeffen, J., Smeets, R.,Trijbels, F., van den Heuvel, L. (2000) Characterization of the human complex I NDUFB7 and 17.2-kDa cDNAs and mutational analysis of 19 genes of the HP fraction in complex I-deficient-patients. *Hum Genet,* 106(4):385-91.

Twohig, D., Nielsen, H.M. (2019) α-synuclein in the pathophysiology of Alzheimer's disease. *Mol Neurodegeneration* 14, 23.

UniProt (2023) P00848.ATP6_MOUSE. https://www.uniprot.org/uniprotkb/P00848/entry

UniProt (2023) Q96FJ2 DYL2 HUMAN. https://www.uniprot.org/uniprotkb/Q96FJ2/entry

Varela CD, Farhana A. (2023) Biochemistry, Superoxides. In: StatPearls [Internet]. Treasure Island (FL): StatPearls Publishing; . https://www.ncbi.nlm.nih.gov/books/NBK555982/

Verger, A., Yakushev, I., Albert, N. L., van Berckel, B., Brendel, M., Cecchin, D., Fernandez, P. A., Fraioli, F., Guedj, E., Morbelli, S., Tolboom, N., Traub-Weidinger, T., Van Weehaeghe, D., & Barthel, H. (2023). FDA approval of lecanemab: the real start of widespread amyloid PET use? - the EANM Neuroimaging Committee perspective*. European journal of nuclear medicine and molecular imaging,* 50(6), 1553–1555.

Verma, A., Shteinfer-Kuzmine, A., Kamenetsky, N., Pittala, S., Paul, A., Nahon Crystal, E., Ouro, A., Chalifa-Caspi, V., Pandey, S. K., Monsonego, A., Vardi, N., Knafo, S., & Shoshan-Barmatz, V. (2022). Targeting the overexpressed mitochondrial protein VDAC1 in a mouse model of Alzheimer's disease protects against mitochondrial dysfunction and mitigates brain pathology. *Translational neurodegeneration,* 11(1), 58.

Veugelen, S., Saito, T., Saido, T C., Chavez-Gutierrez, L., Strooper, B. (2016) Familial Alzheimer's Disease Mutations in Presenilin Generate Amyloidogenic Aβ Peptide Seeds. *Neuron,* 90. Pp410-416.

Vianna, M. R., Barros, D. M., Silva, T., Choi, H., Madche, C., Rodrigues, C., Medina, J. H., and Izquierdo, I. (2000) Pharmacological demonstration of the differential involvement of protein kinase C isoforms in short- and long-term memory formation and retrieval of one-trial avoidance in rats. *Psychopharmacology* 150:77–84

Vorhees, C., Williams, M. (2006) Morris water maze: procedures for assessing spatial and related forms of learning and memory. *Nat Protoc* 1, 848–858.

Voss, J. L., Bridge, D. J., Cohen, N. J., & Walker, J. A. (2017). A Closer Look at the Hippocampus and Memory. *Trends in cognitive sciences*, *21*(8), 577–588.

Wang, R., & Reddy, P. H. (2017). Role of Glutamate and NMDA Receptors in Alzheimer's Disease. Journal of Alzheimer's disease : *JAD*, 57(4) 1041-1048.

Wang, W., Zhao, F., Ma, X., Perry, G., Zhu, X. (2020) Mitochondria dysfunction in the pathogenesis of Alzheimer's disease: recent advances. *Mol Neurodegeneration* 15, 30.

Wang, X., Su, B., Lee, H. G., Li, X., Perry, G., Smith, M. A., & Zhu, X. (2009). Impaired balance of mitochondrial fission and fusion in Alzheimer's disease. *The Journal of neuroscience : the official journal of the Society for Neuroscience*, 29(28), 9090–9103.

Wang, X., Su, B., Zheng, L., Perry, G., Smith, M. A., & Zhu, X. (2009). The role of abnormal mitochondrial dynamics in the pathogenesis of Alzheimer's disease. *Journal of neurochemistry*, *109 Suppl 1*(Suppl 1), 153–159.

Watanabe, F., and Furuya, E. (1999), Tissue-specific alternative splicing of rat brain fructose 6-phosphate 2-kinase/fructose 2,6-bisphosphatase, *FEBS Letters,* 458.

Watanabe, H., Xia, D., Kanekiyo, T., Kelleher, R.J., Shen, J. (2012) Familial frontotemporal dementia-associated presenilin-1 c.548G>T mutation causes decreased mRNA expression and reduced presenilin function in knock-in mice. *J Neurosci* 32, 5085–5096.

Watson, S. A., & McStay, G. P. (2020). Functions of Cytochrome c oxidase Assembly Factors. *International journal of molecular sciences,* 21(19), 7254.

Webb, BA., Dosey, AM., Wittmann, T., Kollman, J.,Barber; D. (2017) The glycolytic enzyme phosphofructokinase-1 assembles into filaments. *J Cell Biol* 7; 216 (8): 2305–2313.

Webb, BA., Forouhar, F., Szu, FE., Seetharaman, J., Tong, L., Barber, DL. (2015) Structures of human phosphofructokinase-1 and atomic basis of cancer-associated mutations. *Nature*, 523(7558):111-4.

Weggen, S., Beher, D. (2012) Molecular consequences of amyloid precursor protein and presenilin mutations causing autosomal-dominant Alzheimer's disease. *Alz Res Therapy* 4, 9.

Winkel, I., Ermann, N., Żelwetro, A. Sambor, B., Mroczko, B., Kornhuber, J., Paradowski, B., Lewczuk, P. (2021) Cerebrospinal fluid α synuclein concentrations in patients with positive AD biomarkers and extrapyramidal symptoms. *J Neural Transm* 128, 817–825.

World Health Organisation (2023) Dementia. https://www.who.int/news-room/fact-sheets/detail/dementia
Wright AL, Zinn R, Hohensinn B, Konen LM, Beynon SB, Tan RP, Clark IA, Abdipranoto A, Vissel B. (2013) Neuroinflammation and neuronal loss precede Aβ plaque deposition in the hAPP-J20 mouse model of Alzheimer's disease. *PLoS One,* 8(4):e59586.

Wu, Y., Dong, J.H., Dai, Y.F., Zhu, M.Z., Wang, M.Y., Zhang, Y., Pan, Y.D., Yuan, X.R.., Gui, Z.X., Wang, C.X., Li, Y.Q., Zhu, X.H. (2023) Hepatic soluble epoxide hydrolase activity regulates cerebral AB metabolism and the pathogenesis of Alzheimer's disease in mice. *Neuron.*

Xia, D., Esser, L., Tang, W. K., Zhou, F., Zhou, Y., Yu, L., & Yu, C. A. (2013). Structural analysis of cytochrome bc1 complexes: implications to the mechanism of function. *Biochimica et biophysica acta*, 1827(11-12), 1278–1294.

Xiao, G. G., Recker, R. R., & Deng, H. W. (2008). Recent advances in proteomics and cancer biomarker discovery. Clinical medicine. *Oncology,* 2, CMO-S539.

Yalcin, A., Telang, S., Clem, B., Chesney, J. (2009) Regulation of glucose metabolism by 6-phosphofructo-2-kinase/fructose-2,6-bisphopshatases in cancer, *Experimental and Molecular Pathology,* 86 (3), pp174-170.

Yan, X., Hu, Y., Wang, B., Wang, S., & Zhang, X. (2020). Metabolic Dysregulation Contributes to the Progression of Alzheimer's Disease. *Frontiers in neuroscience,* 14, 530219.

Yang, Z., Lanks, CW., Tong, L. (2002) Molecular Mechanism for the Regulation of Human Mitochondrial NAD(P)+-Dependent Malic Enzyme by ATP and Fumarate. *Structure*, 10(7):951-960.

Yogev, O., Yogev, O., Singer, E., Shaulian, E., Goldberg, M., Fox, T. D., & Pines, O. (2010). Fumarase: a mitochondrial metabolic enzyme and a cytosolic/nuclear component of the DNA damage response. *PLoS biology*, 8(3), e1000328.

Yokoyama, M., Kobayashi, H., Tatsumi, L., & Tomita, T. (2022). Mouse Models of Alzheimer's Disease. *Frontiers in molecular neuroscience,* 15, 912995.

Yu, C.A., Yu, L., Xia, D. (2013) Ubiquinol-Cytochrome x Oxidoreductase (Complex III). *Encyclopedia of Biophysics.* 2679-2684.

Zancan, P., Marinho-Carvalho, M.M., Faber-Barata, J., Dellias, J.M.M. and Sola-Penna, M. (2008) ATP and fructose-2,6-bisphosphate regulate skeletal muscle 6-phosphofructo-1-kinase by altering its quaternary structure. *IUBMB Life,* 60: 526-533.

Zhang, X., Alshakhshir, A., Zhao, L. (2021) Glycolytic Metabolism, Brain Resilience, and Alzheimer's Disease*. Front. Neurosci,* 15 .

Zhang, Z., Deng, X., Liu, Y. (2019) PKM2, function and expression and regulation. *Cell Biosci* 9, 52

Zhou, B., Xiao, J. F., Tuli, L., & Ressom, H. W. (2012). LC-MS-based metabolomics. *Molecular bioSystems,* 8(2), 470–481.

Zhou, X., & Zheng, Y. (2013). Cell type-specific signaling function of RhoA GTPase: lessons from mouse gene targeting. *The Journal of biological chemistry,* 288(51), 36179–36188.

Zhu J, Shang Y, Zhang M. (2016) Mechanistic basis of MAGUK-organized complexes in synaptic development and signalling. *Nat Rev Neurosci* 17: 209–223, .

Zlotnik, G., & Vansintjan, A. (2019). Memory: An Extended Definition. *Frontiers in psychology*, *10*, 2523.

APPENDIX A- TABLES

Malate Dehydrogenase 2

Table 1. MDH2 assay protocol set-up parameters.

Parameter	**Value**
Temperature	20
Mode	Kinetic
Kinetic duration	60m
Interval time	20s
Measurement wavelength	450nm
Number of flashes	10
Settle time	50ms
Double-orbital shaking duration	5s
Double-orbital shaking amplitude	1
Double-orbital shaking frequency	270

Table 2. MDH2 assay kit components.

Components
100X Coupler
100X NAD^+
100X Reagent Dye
100X Sodium Malate
10X Blocking Buffer
20X Buffer
Base Buffer
Extraction Buffer (ab260490)
MDH2 Microplate x96 tests

Table 3. Raw OD values for MDH2 assay. Results from start and end time points are T1 and T2 respectively. Values all pre-normalisations. Absolute blank= assay buffer only. Lysis buffer blank= assay buffer + 3μl lysis buffer (3μl is average, the equivalent volume within each test sample).

Sample	Group	T1-20seconds	T2-620seconds	Change in OD	Change in OD/min
VG13	WT Basal	0.1088	0.2321	0.1233	0.01233
VG15	WT Basal	0.0861	0.1858	0.0997	0.00997
VG5	WT Mem	0.0876	0.1857	0.0981	0.00981
VG8	WT Mem	0.068	0.1385	0.0705	0.00705
VG14	APPtg Basal	0.1086	0.2349	0.1263	0.01263
VG16	APPtg Basal	0.0954	0.2029	0.1075	0.01075
VG6	APPtg Mem	0.1053	0.212	0.1067	0.01067
VG7	APPtg Mem	0.0939	0.2093	0.1154	0.01154
VG9	APPtg Basal	0.1067	0.2207	0.114	0.0114
VG11	APPtg Basal	0.0792	0.1664	0.0872	0.00872
VG1	APPtg Mem	0.1028	0.222	0.1192	0.01192
VG3	APPtg Mem	0.0752	0.1662	0.091	0.0091
VG10	WT Basal	0.1062	0.235	0.1288	0.01288
VG12	WT Basal	0.0881	0.2058	0.1177	0.01177
VG2	WT Mem	0.0994	0.2208	0.1214	0.01214
VG4	WT Mem	0.0878	0.1998	0.112	0.0112
Blank	Absolute	0.0495	0.0503	0.0008	8E-05
Blank	Absolute	0.0498	0.0513	0.0015	0.00015
Blank	+Lysis buffer	0.0543	0.0561	0.0018	0.00018
Blank	+Lysis buffer	0.049	0.0503	0.0013	0.00013

Bck VG5	**WT Mem**	0.0534	0.0538	0.0004	4E-05
Bck VG6	**APPtg Mem**	0.0508	0.0513	0.0005	0.00005
Bck VG11	**APPtg Basal**	0.0507	0.0512	0.0005	0.00005
Bck VG10	**WT Basal**	0.0503	0.0514	0.0011	0.00011

Table 4. Two-way T-test results for MDH2 data after normalisation against western blot data. T-tests performed on change in optical density values, with average blank and respective sample background subtracted prior to testing.

Comparison	Mean	SD	t-value	df	p-value
WT Basal v. WT Mem	0.02 ; 0.02	0.02 ; 0.02	0.23	6	0.83
WT Mem v. APPtg Mem	0.02 ; 0.03	0.02 ; 0.02	-0.28	6	0.79
APPtg Basal v. APPtg Mem	0.02 ; 0.03	0.01 ; 0.02	-0.14	6	0.89
WT Basal v. APPtg Basal	0.02 ; 0.02	0.02 ; 0.01	0.09	6	0.93

Table 5. Two-way ANOVA results for MDH2 activity. Data has been normalised against western blotting quantification.

Source of Variation	% of total variation	P value	P value summary	Significant?	
Interaction	0.5746	0.7966	ns	No	
Row Factor	0.03027	0.9528	ns	No	
Column Factor	0.1545	0.8935	ns	No	
ANOVA table	**SS**	**DF**	**MS**	**F (DFn, DFd)**	**P value**
Interaction	2.26E-05	1	2.26E-05	F (1, 12) = 0.06949	P=0.7966
Row Factor	1.19E-06	1	1.19E-06	F (1, 12) = 0.003660	P=0.9528

Column Factor	6.09E-06	1	6.09E-06	F (1, 12) = 0.01869	P=0.8935
Residual	0.003908	12	0.000326		
Difference between column means		**Difference between row means**		**Interaction CI**	
Mean of Wild-Type	0.02317	**Mean of Basal**	0.02406	**Mean diff, A1 - B1**	0.001145
Mean of APPtg	0.02441	**Mean of Memory Retrieval**	0.02352	**Mean diff, A2 - B2**	-0.003612
Difference between means	-0.001233	**Difference between means**	0.000546	**(A1 -B1) - (A2 - B2)**	0.004757
SE of difference	0.009023	**SE of difference**	0.009023	**95% CI of difference**	-0.03456 to 0.04408
95% CI of difference	-0.02089 to 0.01843	**95% CI of difference**	-0.01911 to 0.02021	**(B1 - A1) - (B2 - A2)**	-0.004757
Normality of Residuals					
Test name	**Statistics**	**P value**	**Passed normality test (alpha=0.05)?**	**P value summary**	
D'Agostino-Pearson omnibus (K2)	9.223	0.0099	No	**	
Anderson-Darling (A2*)	0.908	0.0156	No	**	
Shapiro-Wilk (W)	0.8506	0.0139	No	**	
Kolmogorov-Smirnov (distance)	0.1787	0.1	No	**	

6- Phosphofructokinase

Table 6. PFK assay protocol set-up parameters

Parameter	**Value**
Temperature	37
Mode	Kinetic
Kinetic duration	60m
Interval time	20s
Measurement wavelength	450nm
Number of flashes	10
Settle time	50ms
Double-orbital shaking duration	60s
Double-orbital shaking amplitude	1
Double-orbital shaking frequency	270

Table 7. PFK assay kit components

Components
ATP
NADH Standard
PFK Assay Buffer
PFK Developer
PFK Enzyme Mix
PFK Positive Control
PFK Substrate

Table 8. Raw OD values for 6-PFK assay. Results from start and end time points are T1 and T2 respectively. Values all pre-normalisations. Absolute blank= assay buffer only. Lysis buffer blank= assay buffer + 3μl lysis buffer (3μl is average, the equivalent volume within each test sample).

Sample	Group	T1-0secs	T2-320secs	Change in OD	Change in OD/min
3nmol	Standard	1.3858	1.5257	0.1399	0.026247655
2.25 nmol	Standard	1.2152	1.3397	0.1245	0.023358349
1.5nmol	Standard	1.0434	0.9687	-0.0747	-0.014015009
0.75 nmol	Standard	0.6226	0.6628	0.0402	0.007542214
blank	Absolute blank	0.1406	0.1552	0.0146	0.002739212
blank	Blank+ lysis buffer	0.1478	0.1718	0.024	0.004502814
Pos control 10	Pos	0.1456	0.5667	0.4211	0.079005629
Pos control 20	Pos	0.1317	0.596	0.4643	0.087110694
Bckg VG9	APPtg Basal	0.3683	0.2896	-0.0787	-0.014765478
Bckg VG11	APPtg Basal	0.1541	0.2494	0.0953	0.017879925
Bckg VG1	APPtg Mem	0.1521	0.1779	0.0258	0.004840525
Bckg VG3	APPtg Mem	0.1597	0.204	0.0443	0.008311445
Bckg VG10	WT Basal	0.1617	0.2735	0.1118	0.02097561
Bckg VG12	WT Basal	0.1566	0.2415	0.0849	0.015928705
Bckg VG2	WT Mem	0.1509	0.1577	0.0068	0.001275797
Bckg VG4	WT Mem	0.1584	0.2134	0.055	0.010318949
Bckg VG13	WT Basal	0.212	0.351	0.139	0.026078799
Bckg VG15	WT Basal	0.2289	0.399	0.1701	0.031913696
Bckg VG5	WT Mem	0.2249	0.3569	0.132	0.024765478
Bckg VG8	WT Mem	0.2364	0.3762	0.1398	0.026228893
Bckg VG14	APPtg Basal	0.2567	0.3907	0.134	0.025140713
Bckg VG16	APPtg Basal	0.2156	0.3696	0.154	0.028893058
Bckg VG6	APPtg Mem	0.22	0.3464	0.1264	0.023714822

Bckg VG7	APPtg Mem	0.2007	0.3263	0.1256	0.023564728
VG9	APPtg Basal	0.4717	1.1023	0.6306	0.118311445
VG11	APPtg Basal	0.4095	0.9972	0.5877	0.110262664
VG1	APPtg Mem	0.3447	0.8787	0.534	0.100187617
VG3	APPtg Mem	0.2599	0.6851	0.4252	0.079774859
VG10	WT Basal	0.4451	1.2184	0.7733	0.145084428
VG12	WT Basal	0.4442	1.2538	0.8096	0.151894934
VG2	WT Mem	0.2137	0.5802	0.3665	0.068761726
VG4	WT Mem	0.2394	0.7343	0.4949	0.092851782
VG13	WT Basal	0.27	1.0043	0.7343	0.137767355
VG15	WT Basal	0.2837	1.2478	0.9641	0.180881801
VG5	WT Mem	0.2666	1.1724	0.9058	0.169943715
VG8	WT Mem	0.1882	0.8965	0.7083	0.132889306
VG14	APPtg Basal	0.216	0.9632	0.7472	0.140187617
VG16	APPtg Basal	0.288	1.3067	1.0187	0.191125704
VG6	APPtg Mem	0.2269	1.0723	0.8454	0.158611632
VG7	APPtg Mem	0.2234	1.1159	0.8925	0.167448405

Table 8. Raw T2-T1 change in optical density values with corresponding sample background subtracted from each test sample (column 2). Change in OD values with background removed, minus the average absolute blank value (column 3). Column 3 values used for further analysis. All values are pre-normalisation with western blot data.

Sample	**Group**	**Change in OD-background**	**(Change OD-background)-blank**
VG9	**APPtg Basal**	0.133076923	0.128574109
VG11	**APPtg Basal**	0.092382739	0.087879925
VG1	**APPtg Mem**	0.095347092	0.090844278
VG3	**APPtg Mem**	0.071463415	0.0669606
VG10	**WT Basal**	0.124108818	0.119606004
VG12	**WT Basal**	0.135966229	0.131463415
VG2	**WT Mem**	0.067485929	0.062983114
VG4	**WT Mem**	0.082532833	0.078030019
VG13	**WT Basal**	0.111688555	0.107185741

VG15	**WT Basal**	0.148968105	0.144465291
VG5	**WT Mem**	0.145178236	0.140675422
VG8	**WT Mem**	0.106660413	0.102157598
VG14	**APPtg Basal**	0.115046904	0.11054409
VG16	**APPtg Basal**	0.162232645	0.157729831
VG6	**APPtg Memory**	0.134896811	0.130393996
VG7	**APPtg Memory**	0.143883677	0.139380863

Table 9. Two-way T-test results for PFK assay data post-normalisation against western blot data. T-tests performed on change in optical density values with average absolute blank and respective sample backgrounds subtracted before testing.

Comparison	**Mean**	**SD**	**t-value**	**df**	**p-value**
WT Basal v. WT Mem	0.14 ; 0.14	0.09 ; 0.07	0.11	6	0.91
WT Mem v. APPtg Mem	0.14 ; 0.13	0.07 ; 0.07	0.16	6	0.88
APPtg Basal v. APPtg Mem	0.15 ; 0.13	0.07 ; 0.07	0.47	6	0.65
WT Basal v. APPtg Basal	0.14 ; 0.15	0.09 ; 0.07	-0.16	6	0.88

Table 10. Two-way ANOVA results- PFK normalised assay data. This data is change in OD .

Source of Variation	**% of total variation**	**P value**	**P value summary**	**Significant?**	
Interaction	0.4262	0.8234	ns	No	
Row Factor	1.298	0.6975	ns	No	
Column Factor	0.002317	0.9869	ns	No	
ANOVA table	**SS**	**DF**	**MS**	**F (DFn, DFd)**	**P value**
Interaction	0.000294	1	0.000294	F (1, 12) = 0.05205	P=0.8234

Row Factor	0.000894	1	0.000894	F (1, 12) = 0.1585	P=0.6975
Column Factor	1.6E-06	1	1.6E-06	F (1, 12) = 0.0002830	P=0.9869
Residual	0.06766	12	0.005639		
Difference between column means		**Difference between row means**		**Interaction CI**	
Mean of Wild-Type	0.1386	**Mean of Basal**	0.1464	**Mean diff, A1 - B1**	-0.009197
Mean of APPtg	0.1392	**Mean of Memory Retrieval**	0.1314	**Mean diff, A2 - B2**	0.007934
Difference between means	-0.000632	**Difference between means**	0.01495	**(A1 -B1) - (A2 - B2)**	-0.01713
SE of difference	0.03755	**SE of difference**	0.03755	**95% CI of difference**	-0.1807 to 0.1465
95% CI of difference	-0.08244 to 0.08117	**95% CI of difference**	-0.06686 to 0.09675	**(B1 - A1) - (B2 - A2)**	0.01713
				95% CI of difference	-0.1465 to 0.1807
Normality of Residuals					
Test name	**Statistics**	**P value**	**Passed normality test (alpha=0.05)?**	**P value summary**	
D'Agostino-Pearson omnibus (K2)	8.917	0.0116	No	**	
Anderson-Darling (A2*)	0.7943	0.0308	No	**	
Shapiro-Wilk (W)	0.8803	0.0392	No	**	
Kolmogorov-Smirnov (distance)	0.2136	0.0493	No	**	

Table 12. Values derived from equation of NADH standard curve. Y value= OD at end point of reaction (320seconds). M value= gradient. C value= y-intercept. X value= nmol NADH in sample.

Sample	Y Value	M Value	C Value	X Value
VG9	1.1023	0.4557	0.2468	1.87733158
VG11	0.9972	0.4557	0.2468	1.64669739
VG1	0.8787	0.4557	0.2468	1.38665789
VG3	0.6851	0.4557	0.2468	0.96181698
VG10	1.2184	0.4557	0.2468	2.13210445
VG12	1.2538	0.4557	0.2468	2.20978714
VG2	0.5802	0.4557	0.2468	0.73162168
VG4	0.7343	0.4557	0.2468	1.06978275
VG13	1.0043	0.4557	0.2468	1.66227781
VG15	1.2478	0.4557	0.2468	2.19662058
VG5	1.1724	0.4557	0.2468	2.03116085
VG8	0.8965	0.4557	0.2468	1.42571867
VG14	0.9632	0.4557	0.2468	1.5720869
VG16	1.3067	0.4557	0.2468	2.32587228
VG6	1.0723	0.4557	0.2468	1.81149879
VG7	1.1159	0.4557	0.2468	1.90717577

Formula:

PFK Activity= (B/Change T)

Change T= T2-T1

B= Amount NADH in sample, calculated from standard curve

Table 13. PFK activity calculation raw values. NADH values were derived using equation of standard curve. PFK activity per sample calculated using PFK activity formula. Change T= T2=T1.

Sample	Change T	B- NADH from Standard curve	PFK activity per sample
VG9	5.33	1.877331578	0.352219808
VG11	5.33	1.646697389	0.308948853
VG1	5.33	1.386657889	0.260160955
VG3	5.33	0.961816985	0.180453468
VG10	5.33	2.132104455	0.400019598
VG12	5.33	2.209787141	0.41459421
VG2	5.33	0.731621681	0.137264856
VG4	5.33	1.069782752	0.20070971
VG13	5.33	1.662277814	0.31187201
VG15	5.33	2.196620584	0.412123937
VG5	5.33	2.031160851	0.381080835
VG8	5.33	1.425718675	0.267489432
VG14	5.33	1.572086899	0.294950638
VG16	5.33	2.325872284	0.436373787
VG6	5.33	1.811498793	0.339868441
VG7	5.33	1.907175774	0.357819094

Table 14. Two-way T-test results for PFK activity (nmol NADH/min/5µg) data post-normalisation.

Comparison	Mean	SD	t-value	df	p-value
WT Basal v. WT Mem	0.46 ; 0.4	0.37 ; 0.23	0.28	6	0.79
WT Mem v. APPtg Mem	0.4 ; 0.38	0.23 ; 0.27	0.07	6	0.94
APPtg Basal v. APPtg Mem	0.48 ; 0.38	0.3 ; 0.27	0.49	6	0.64
WT Basal v. APPtg Basal	0.46 ; 0.48	0.37 ; 0.3	-0.09	6	0.93

Table 15. Two-way ANOVA results-PFK normalised assay data. This data is measuring PFK activity by calculating the production of NADH in nmol/min/5µg.

Source of Variation	% of total variation	P value	P value summary	Significant?	
Interaction	0.1068	0.9107	ns	No	
Row Factor	2.313	0.6036	ns	No	
Column Factor	0.004724	0.9812	ns	No	
ANOVA table	**SS**	**DF**	**MS**	**F (DFn, DFd)**	**P value**
Interaction	0.0012	1	0.0012	F (1, 12) = 0.01313	P=0.9107
Row Factor	0.026	1	0.026	F (1, 12) = 0.2844	P=0.6036
Column Factor	5.31E-05	1	5.31E-05	F (1, 12) = 0.0005810	P=0.9812
Residual	1.097	12	0.0914		

Difference between column means					
Mean of Wild-Type	0.4279				
Mean of APPtg	0.4316				
Difference between means	-0.003643				
SE of difference	0.1512				
95% CI of difference	-0.3330 to 0.3257				
Difference between row means	0.4701				
Mean of Basal	0.3895				
Mean of Memory Retrieval	0.08062				
Difference between means	0.1512				
SE of difference	-0.2487 to 0.4100				
95% CI of difference	0.4701				
Interaction CI	-0.02096				
Mean diff, A1 - B1	0.01368				
Mean diff, A2 - B2	-0.03464				
(A1 -B1) - (A2 - B2)	-0.6933 to 0.6241				
95% CI of difference	0.03464				

(B1 - A1) - (B2 - A2)	-0.6241 to 0.6933				
95% CI of difference	-0.02096				
Normality of Residuals					
Test name	**Statistics**	**P value**	**Passed normality test (alpha=0.05)?**	**P value summary**	
D'Agostino-Pearson omnibus (K2)	14.98	0.0006	No	**	
Anderson-Darling (A2*)	1.33	0.0013	No	**	
Shapiro-Wilk (W)	0.8206	0.0052	No	**	
Kolmogorov-Smirnov (distance)	0.2351	0.0183	No	**	

Combined enzymatic acitivty results (full 32 sample results)

Combined Assay Results:

MDH2

Table 16. Combined MDH2 assay data. Average values for each replicate sample.

Sample	Group	Average Change in OD/min	Western Blot Protein Abundance	Normalised Average Value
VG13	**WT Basal**	0.0115	1.72523444	0.00666576
VG15	**WT Basal**	0.011115	1.31162417	0.00847423
VG5	**WT Mem**	0.01023	1.17996454	0.00866975
VG8	**WT Mem**	0.008645	0.35472836	0.02437076
VG14	**APPtg Basal**	0.011285	0.96454362	0.01169983
VG16	**APPtg Basal**	1.18748369	0.01028225	0.00964645
VG6	**APPtg Mem**	0.01123	1.31257738	0.00855569
VG7	**APPtg Mem**	0.01135	0.30874585	0.03676163
VG9	**APPtg Basal**	0.01092	0.35905421	0.03041323
VG11	**APPtg Basal**	0.00981	0.21517712	0.04559035
VG1	**APPtg Mem**	0.00879	1.15251082	0.00762683
VG3	**APPtg Mem**	0.008125	0.18675967	0.04350511

VG10	**WT Basal**	0.012085	0.29753485	0.04061709
VG12	**WT Basal**	0.011555	0.28427509	0.04064725
VG2	**WT Mem**	0.009445	0.8349512	0.01131204
VG4	**WT Mem**	0.00996	0.25188861	0.03954129

Table 17. T-test results MDH2 combined assay results

Comparison	**Mean**	**SD**	**t-value**	**df**	**p-value**
WT Basal v. WT Mem	0.02 ; 0.02	0.02 ; 0.01	0.26	6	0.80
WT Mem v. APPtg Mem	0.02 ; 0.02	0.01 ; 0.02	-0.27	6	0.80
APPtg Basal v. APPtg Mem	0.02 ; 0.02	0.02 ; 0.02	0.02	6	0.99
WT Basal v. APPtg Basal	0.02 ; 0.02	0.02 ; 0.02	-0.02	6	0.99

Table 18. Two-way ANOVA results for MDH2 activity. Data has been normalised against western blot quantification. Combined data using full set of 32 samples.

Source of Variation	**% of total variation**	**P value**	**P value summary**	**Significant?**	
Interaction	0.2314	0.8699	ns	No	
Row Factor	0.3088	0.8499	ns	No	
Column Factor	0.3129	0.849	ns	No	
ANOVA table	**SS**	**DF**	**MS**	**F (DFn, DFd)**	**P value**
Interaction	8.42E-06	1	8.42E-06	F (1, 12) = 0.02801	P=0.8699
Row Factor	1.12E-05	1	1.12E-05	F (1, 12) = 0.03737	P=0.8499
Column Factor	1.14E-05	1	1.14E-05	F (1, 12) = 0.03787	P=0.8490
Residual	0.00361	12	0.000301		
Difference between column means					
Mean of Wild-Type	0.02254				
Mean of APPtg	0.02422				
Difference between means	-0.001688				
SE of difference	0.008672				
95% CI of difference	-0.02058 to 0.01721				
Difference between row means					
Mean of Basal	0.02422				

Mean of Memory Retrieval	0.02254				
Difference between means	0.001676				
SE of difference	0.008672				
95% CI of difference	-0.01722 to 0.02057				
Interaction CI					
Mean diff, A1 - B1	-0.000236				
Mean diff, A2 - B2	-0.003139				
(A1 -B1) - (A2 - B2)	0.002902				
95% CI of difference	-0.03489 to 0.04069				
(B1 - A1) - (B2 - A2)	-0.002902				
95% CI of difference	-0.04069 to 0.03489				
Normality of Residuals					
Test name	**Statistics**	**P value**	**Passed normality test (alpha=0.05)?**	**P value summary**	
D'Agostino-Pearson omnibus (K2)	12.31	0.0021	No	**	
Anderson-Darling (A2*)	1.127	0.0042	No	**	
Shapiro-Wilk (W)	0.8264	0.0062	No	**	

Kolmogorov-Smirnov (distance)	0.2333	0.02	No	**	

PFK

Table 19. T-test results PFK combined data

Comparison	Mean	SD	t-value	df	p-value
WT Basal v. WT Mem	0.13 ; 0.16	0.09 ; 0.11	-0.42	6	0.69
WT Mem v. APPtg Mem	0.16 ; 0.13	0.11 ; 0.08	0.42	6	0.69
APPtg Basal v. APPtg Mem	0.15 ; 0.013	0.08 ; 0.08	0.31	6	0.77
WT Basal v. APPtg Basal	0.13 ; 0.15	0.09 ; 0.08	-0.32	6	0.76

Table 20. Two-way ANOVA results on PFK activity. Combined data using full set of 32 test samples. Data has been normalised against western blot quantification. Data measures change in OD/min.

Source of Variation	**% of total variation**	**P value**	**P value summary**	**Significant?**	
Interaction	2.221	0.6107	ns	No	
Row Factor	0.1402	0.8977	ns	No	
Column Factor	0.08301	0.9212	ns	No	
ANOVA table	**SS**	**DF**	**MS**	**F (DFn, DFd)**	**P value**
Interaction	0.002225	1	0.002225	F (1, 12) = 0.2733	P=0.6107
Row Factor	0.00014	1	0.00014	F (1, 12) = 0.01725	P=0.8977
Column Factor	8.31E-05	1	8.31E-05	F (1, 12) = 0.01021	P=0.9212
Residual	0.09769	12	0.008141		
Difference between column means					
Mean of Wild-Type	0.1436				
Mean of APPtg	0.139				
Difference between means	0.004559				
SE of difference	0.04511				
95% CI of difference	-0.09374 to 0.1029				
Difference between row means					

Mean of Basal	0.1383				
Mean of Memory Retrieval	0.1443				
Difference between means	-0.005925				
SE of difference	0.04511				
95% CI of difference	-0.1042 to 0.09237				
Interaction CI					
Mean diff, A1 - B1	-0.01902				
Mean diff, A2 - B2	0.02814				
(A1 -B1) - (A2 - B2)	-0.04716				
95% CI of difference	-0.2438 to 0.1494				
(B1 - A1) - (B2 - A2)	0.04716				
95% CI of difference	-0.1494 to 0.2438				
Normality of Residuals					
Test name	**Statistics**	**P value**	**Passed normality test (alpha=0.05)?**	**P value summary**	
D'Agostino-Pearson omnibus (K2)	13.02	0.0015	No	**	
Anderson-Darling (A2*)	1.248	0.002	No	**	
Shapiro-Wilk (W)	0.8329	0.0077	No	**	

Kolmogorov-Smirnov (distance)	0.2644	0.0039	No	**	

Table 21. Values derived from equation of NADH standard curve. Y value= OD at end point of reaction (320seconds). M value= gradient. C value= y-intercept. X value= nmol NADH in sample. Data from full set of 32 samples, after normalisation against western blotting abundance.

Sample	Y Value	M Value	C Value	X Value
VG9	1.00025	0.4557	0.2468	1.65339039
VG11	0.98715	0.4557	0.2468	1.62464341
VG1	0.7109	0.4557	0.2468	1.01843318
VG3	0.645	0.4557	0.2468	0.8738205
VG10	1.06465	0.4557	0.2468	1.79471143
VG12	1.08255	0.4557	0.2468	1.83399166
VG2	0.5231	0.4557	0.2468	0.60631995
VG4	0.8145	0.4557	0.2468	1.24577573
VG13	1.03705	0.4557	0.2468	1.73414527
VG15	1.2443	0.4557	0.2468	2.18894009
VG5	1.1709	0.4557	0.2468	2.02786921
VG8	1.06355	0.4557	0.2468	1.79229756
VG14	0.99235	0.4557	0.2468	1.63605442
VG16	1.25155	0.4557	0.2468	2.20484968
VG6	1.12235	0.4557	0.2468	1.92132982
VG7	1.12955	0.4557	0.2468	1.93712969

Table 22. PFK activity calculation raw values. NADH values were derived using equation of standard curve. PFK activity per sample calculated using PFK activity formula. Change T= T2=T1. Data from full set of 32 samples, after normalisation against western blotting abundance.

Sample	Change T	B- NADH from Standard curve	Normalised PFK activity per sample
VG9	5.33	1.653390388	0.579468244
VG11	5.33	1.624643406	0.618581387
VG1	5.33	1.01843318	0.129262691
VG3	5.33	0.873820496	0.436495442
VG10	5.33	1.794711433	0.56502409
VG12	5.33	1.833991661	0.607202275
VG2	5.33	0.606319947	0.096077837
VG4	5.33	1.24577573	0.511412707
VG13	5.33	1.734145271	0.141803433
VG15	5.33	2.188940092	0.249359899
VG5	5.33	2.027869212	0.28758243
VG8	5.33	1.792297564	0.695624549
VG14	5.33	1.636054422	0.242204079
VG16	5.33	2.204849682	0.257452305
VG6	5.33	1.921329822	0.21142795
VG7	5.33	1.937129691	0.539722568

Table 23. Two-way ANOVA results of PFK activity. Combined results using full set of 32 test samples. Data has been normalised against western blot quantification. Data measuring PFK activity as amount of NADH produced in nmol/min/5µg.

Source of Variation	% of total variation	P value	P value summary	Significant?	
Interaction	0.5061	0.7861	ns	No	
Row Factor	20.42	0.1033	ns	No	
Column Factor	0.2432	0.8507	ns	No	

ANOVA table	**SS**	**DF**	**MS**	**F (DFn, DFd)**	**P value**
Interaction	0.000575	1	0.000575	F (1, 12) = 0.07705	P=0.7861
Row Factor	0.02321	1	0.02321	F (1, 12) = 3.109	P=0.1033
Column Factor	0.000276	1	0.000276	F (1, 12) = 0.03702	P=0.8507
Residual	0.08958	12	0.007465		
Difference between column means					
Mean of Wild-Type	0.3101				
Mean of APPtg	0.3018				
Difference between means	0.008311				
SE of difference	0.0432				
95% CI of difference	-0.08581 to 0.1024				
Difference between row means					
Mean of Basal	0.3441				
Mean of Memory Retrieval	0.2679				
Difference between means	0.07617				
SE of difference	0.0432				
95% CI of difference	-0.01796 to 0.1703				

Interaction CI					
Mean diff, A1 - B1	0.0203				
Mean diff, A2 - B2	-0.00368				
(A1 -B1) - (A2 - B2)	0.02398				
95% CI of difference	-0.1643 to 0.2122				
(B1 - A1) - (B2 - A2)	-0.02398				
95% CI of difference	-0.2122 to 0.1643				
Normality of Residuals					
Test name	**Statistics**	**P value**	**Passed normality test (alpha=0.05)?**	**P value summary**	
D'Agostino-Pearson omnibus (K2)	0.42	0.8106	No	**	
Anderson-Darling (A2*)	0.531	0.1474	No	**	
Shapiro-Wilk (W)	0.9323	0.2652	No	**	
Kolmogorov-Smirnov (distance)	0.1771	0.1	No	**	

APPENDIX B- FIGURES

The following figures present the results of MDH2 and 6-PFK assays using full set of samples, in combination with another student.

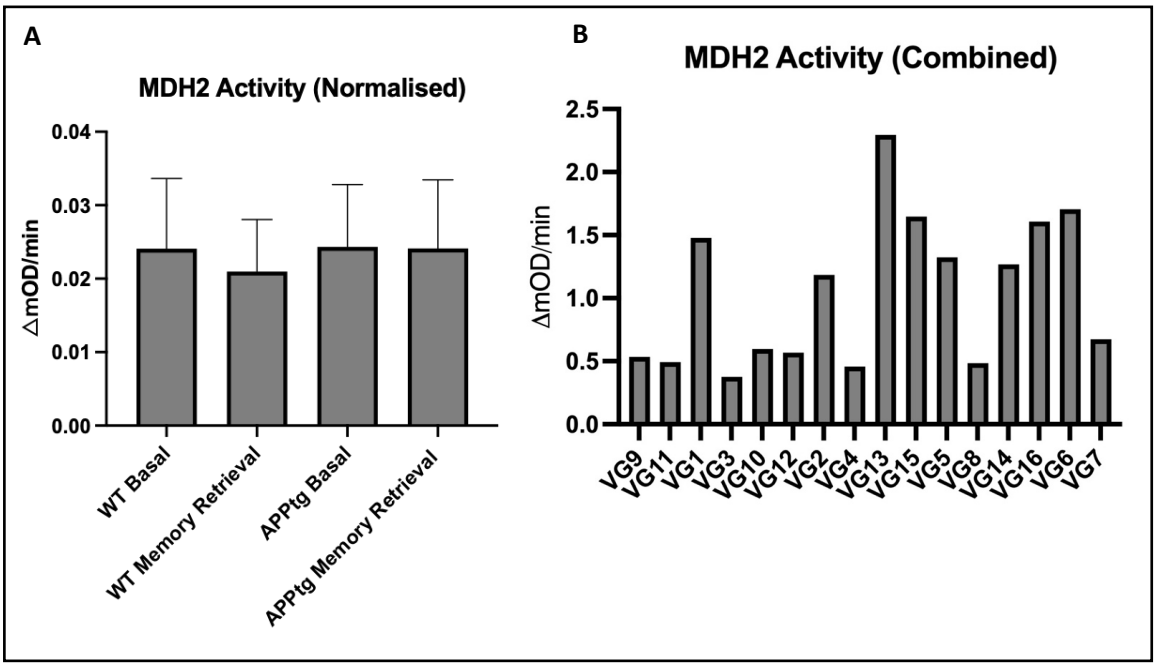

Figure 23. MDH2 assay data, normalised to western blot data. Assay utilising 32 samples (16 samples, carried out in duplicate), 16 from another student in the group to allow for full statistical comparison. Figure A shows the MDH2 activity expressed as change in OD per minute, per group average (n=8). Figure B shows the MDH2 activity per sample, expressed as change in OD per minute, per sample average.

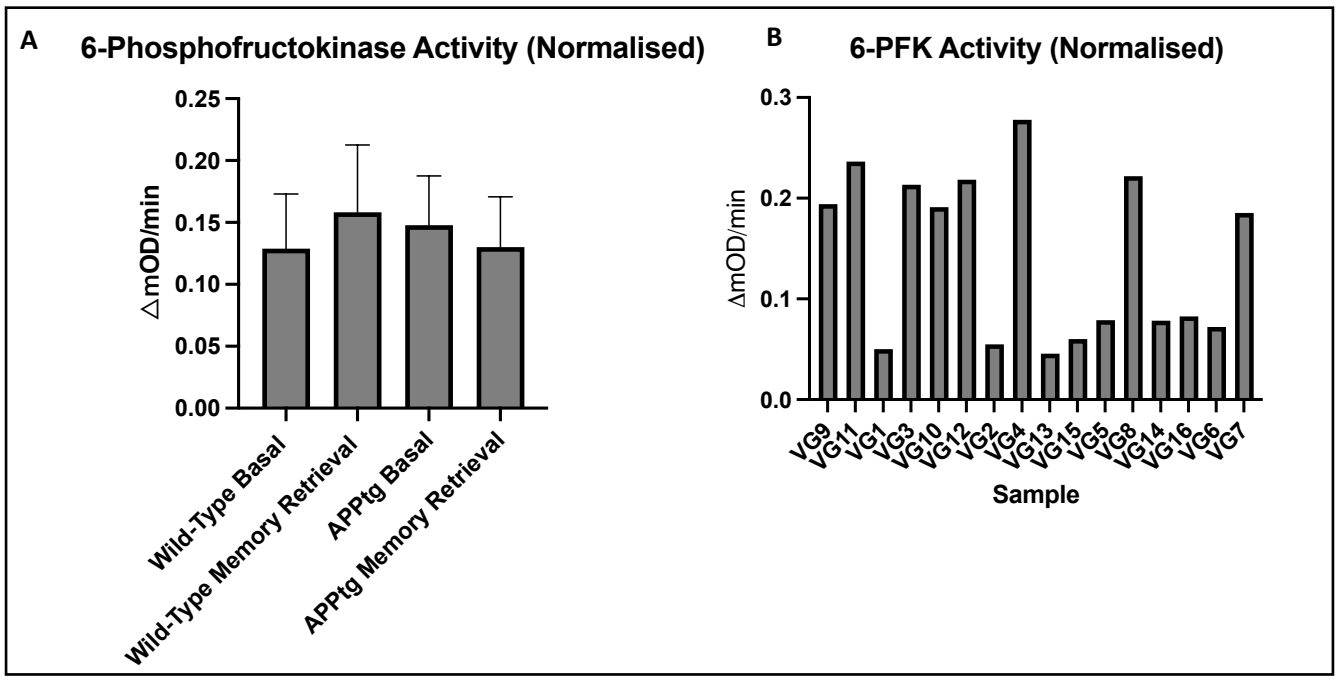

Figure 24.6-PFK assay data, normalised to western blot data. Assay utilising 32 samples (16 samples, carried out in duplicate), 16 from another student in the group to allow for duplicate statistical comparison. Figure A shows the 6-PFK activity, expressed as a change in OD per minute, per group average (n=8). Figure B shows the 6-PFK activity per sample, expressed as the change in OD per minute, per sample average.

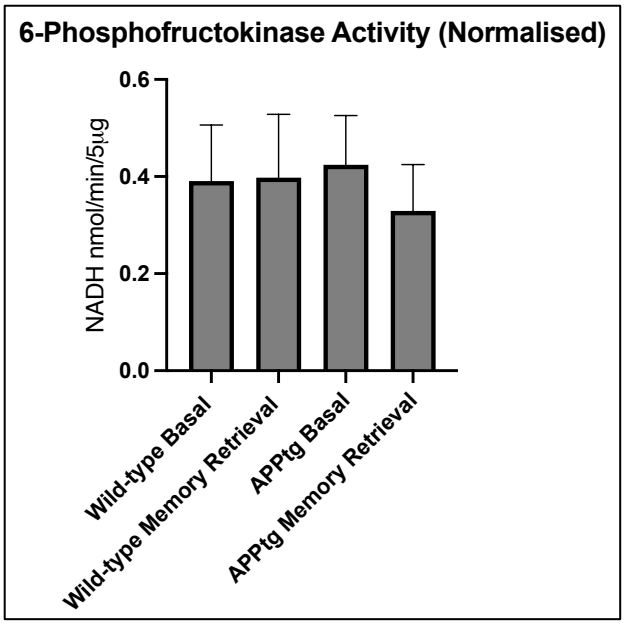

Figure 25. 6-PFK assay data, normalised to western blot data. Assay utilised 32 samples (16 samples, carried out in duplicate), 16 carried out by another student in the group to allow for duplicate statistical comparison. Activity is expressed as the amount of NADH produced per minute, per 5μg protein.

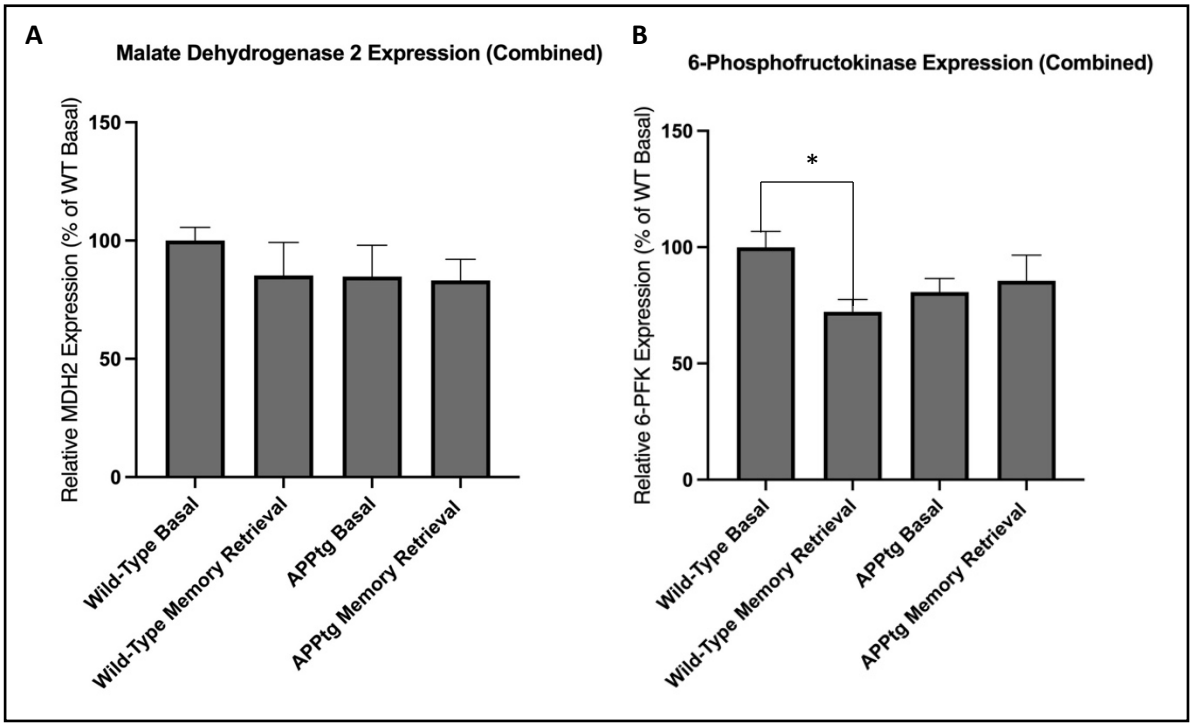

Figure 26. Western blot assay data. Blots were carried out in duplicate using full set of 16 samples (8 from another student in the group). Figure A shows the average MDH2 expression per group, expressed as a percentage of WT basal average. Figure B shows the average 6-PFK expression per group, expressed as a percentage of WT basal average. 6-PFK activity in WT basal mice was significantly higher than in WT mice during memory retrieval (p=0.017925, α=0.05).

PROTEOMICS FIGURES

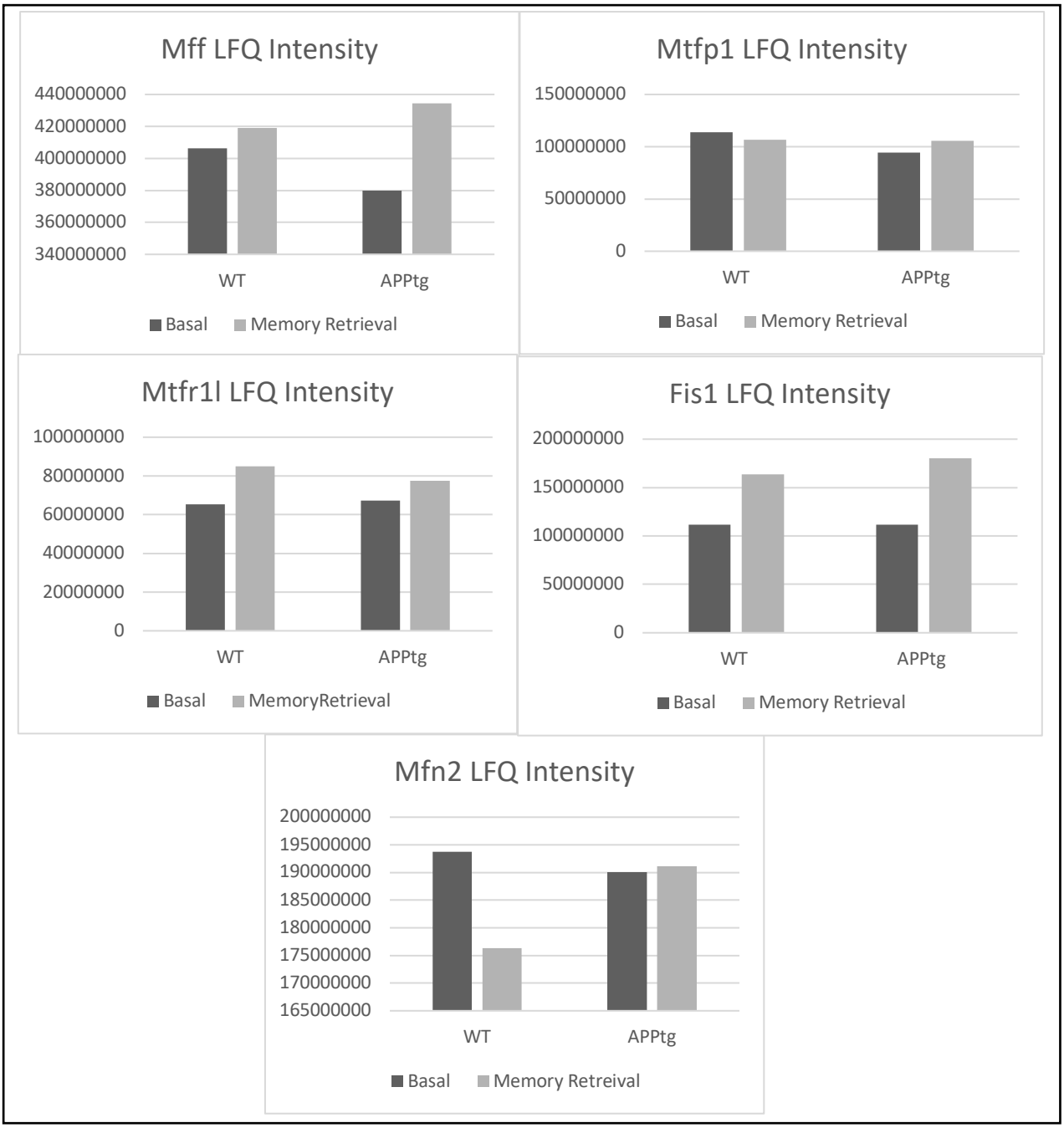

Figure 27. LFQ Intensity figures for proteins involved in mitochondrial fission and fusion. Raw LFQ intensities before the application of FDR correction or 20% regulation threshold.

APPENDIX C- PROTOCOLS

1. Synaptosome preparation method

Synaptosome preparation was carried out by Dr Anthony Ashton, UCLan

1) Whole cerebellum (n=16) homogenized (900RPM) in 40ml of 0.32M sucrose (10nM Hepes pH 7.4) containing 1:100 protease inhibitors, 1:500 EDTA and 1:1000 PMSF. Homogenisation technique used 12 strokes of motor-driven Teflon pestle at 900ROM, lasting approximately 2 minutes.
2) Supernatant retrieved and spun down in a Beckman Avanti 17 rotor (4400RPM) to retrieve second supernatant (S2), whilst removing nuclear pellet (P1). S2 was centrifuged again at 14500RPM for 20 minutes. Second pellet (P2) retrieved.
3) P2 solubilised and resuspended in 8ml of 0.32M sucrose containing 1:100 protease inhibitors, 1:500 EDTA and 1:1000 PMSF. This was placed on top of a sucrose gradient of 1.2M and 0.8M layers (also containing protease inhibitors cocktail) using 27ml tubes. P2 samples spun down through gradient for 90minutes at 51000RPM. Purified synaptosomes collected at the interface between 0.8M and 1.2M
4) Purified synaptosomes diluted slowly 3.125-fold with 10mM Hepes (pH 7.4) to prevent osmotic shock. Purified synaptosomes resuspended in 0.32M sucrose and centrifuged down in the Beckman Avanti 17 at 14500RPM for 20 minutes to retrieve purified synaptosome pellet.

2. Western Blot ImageLab Quantification

1. Open WB image file with Image Lab
2. Choose Volume Tools from Analysis Tool Box
3. Choose rectangles
4. Draw a rectangle around the first lane, ensuring minimum background
5. Copy the rectangle and paste around all other sample lanes
6. Cope all of the rectangles around sample lanes
7. Paste them into clean background area, close to sample lanes and aligned with each band

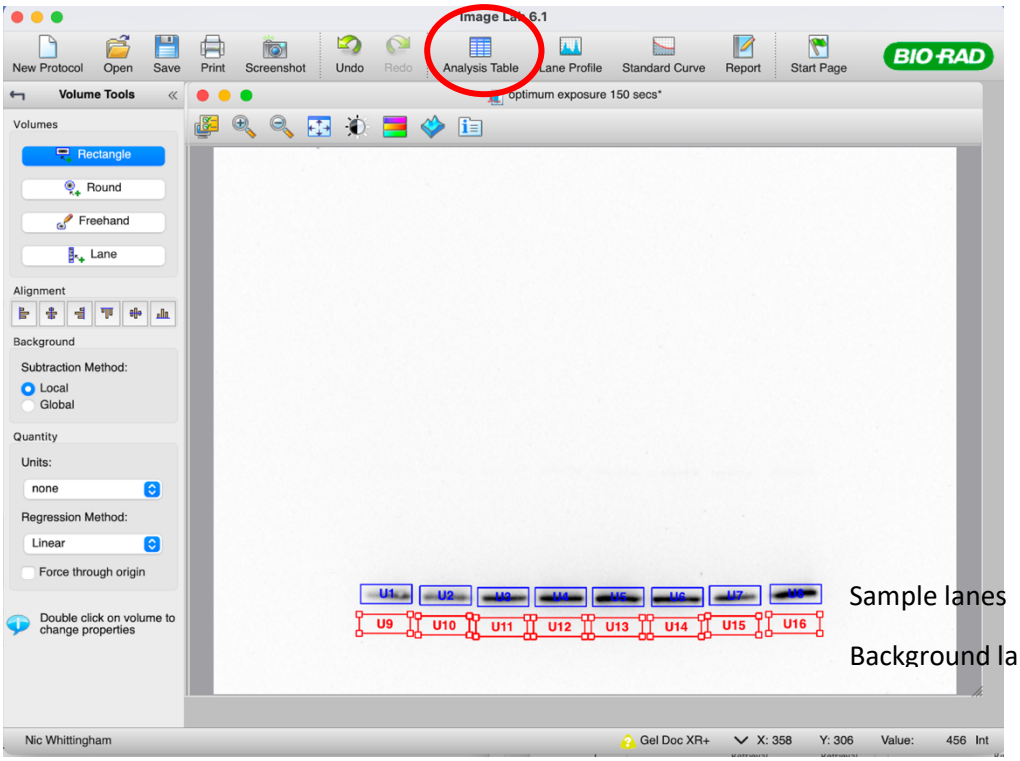

8. Once all samples and respective background rectangles are in place, choose Analysis Table

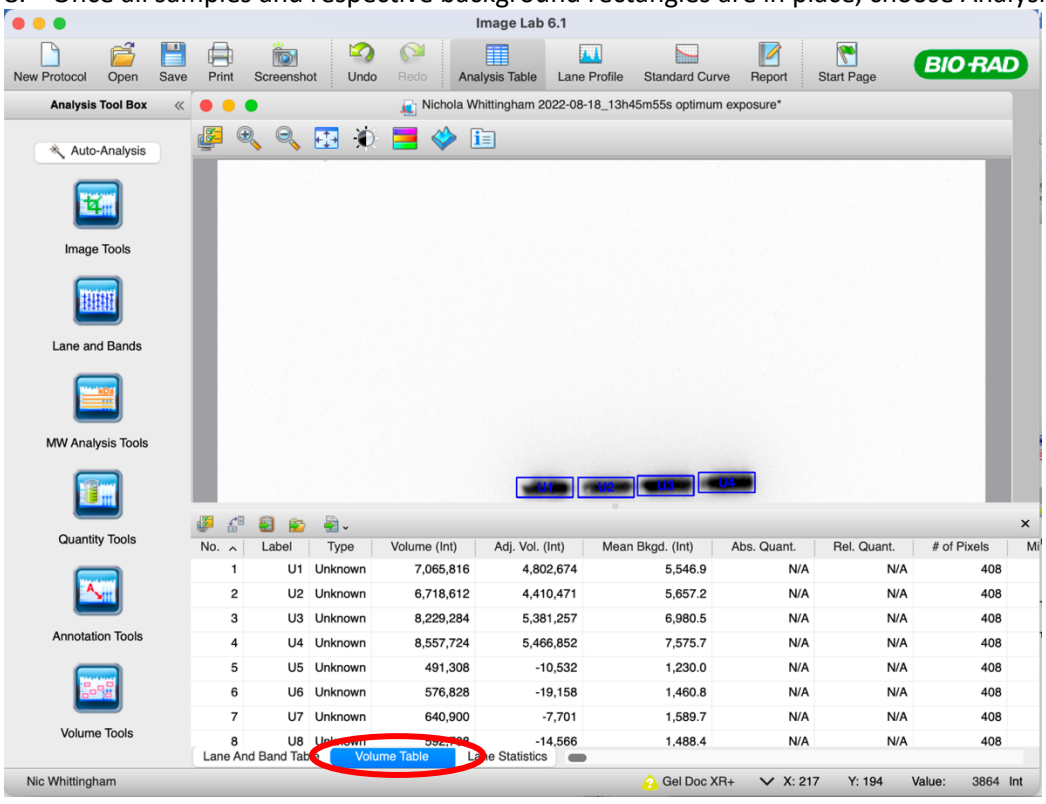

9. Export the table for Excel
10. Calculate average of background values
11. Subtract background from the volume of each sample band
12. Repeat 1-11 again for Loading Control Image
13. Divide the quantification of the test antibody by the loading control

14. Do T-test to verify any differences

3. Enzymatic activity assay optimization workflow

1) Carry out assay precisely following manufacturers protocol utilising 'practice' (WT) samples at concentrations ranging from 5-0.0125µg/µl; blanks (assay buffer or incubation solution), blanks with an additional 3µl of lysis buffer (3µl is the same amount present within test samples). Blanks test kits are working correctly and producing no activity. Lysis buffer blank included to determine if the addition of lysis buffer has any effect on enzymatic activity or whether the lysis buffer reads at a higher optical density than the absolute blanks
2) Select sample concentration with best linearity of results
3) If kit utilises standards and positive controls, trial concentrations of standard and volume of positive controls until results closest match that of test samples
4) Trial experimental sample at concentration determined in step 2
5) If assay produces expected linearity of samples, positive controls and standards, and blanks show no linearity, inspect results over kinetic cycle and determine if kinetic cycle should be extended, reduced, or shaking steps implemented
6) Trial assay at room temperature AND at 37°C. Compare activity levels
7) Once optimal kinetic cycle timing and all samples and kit components have been optimised, progress to final assay

4. Metabolomics workflow

1) Prepare standards (tri-sodium citrate dihydrate, sodium pyruvate, sodium succinate) into working solutions of 1M (1M of metabolite, not whole salt; dissolve in H20 then 50:50 methanol:acetonitrile)
2) Submit to GC-MS
3) Locate acidic forms of standards (salts left to much residue around injection site)
4) Acidic standards need to be derivatised (introduction of additional pyruvic acid standard)
5) Calculate amount of derivatising agent to maintain correct molar ratio
6) Dilute 1/10
7) Submit to GC-MS- detect metabolites at correct M/Z
8) Submit non-derivatised standards to LC-MS- enhanced resolution and no need for derivatisation, saving cost and time
9) Switch to UP-LC-MS
10) Make up mobile phase (0.0001% formic acid, 20ml acetonitrile, 980ml LC-MS grade water)
11) Dissolve standards in mobile phase to final concentration of 1M
12) Serial dilutions of standard: 1M, 1mM, 1 µM, 1nM
13) Prime solvents and wash syringes
14) Run each standard (1mM) in MRM mode at a range of cone voltages: 30, 40, 50, 60, 70, 80. Run 1 blank (mobile phase) in between each new metabolite to ensure no residue carried over from previous metabolite
15) Select: cone voltage that produced the strongest signal for each metabolite; retention time for each metabolite (± 2 minutes)

16) Run standards again in MRM mode using selected cone voltage, retention time frame and expected m/z
17) Standard curve generation

5. GC-MS Derivatisation Protocol: Fiehn O. (2016). Metabolomics by Gas Chromatography-Mass Spectrometry: Combined Targeted and Untargeted Profiling. *Current protocols in molecular biology*, *114*, 30.4.1–30.4.32. https://doi.org/10.1002/0471142727.mb3004s114

1. Prepare 20mg/mL Methoxyamine hydrochloride [MeOX] solution in pyridine
2. Vortex MeOX solution and sonicate at 60°Cfor 15 min to dissolve
3. Ensure that all samples are completely dry before derivatization. If samples taken from freezer, ensure they have reached room temperature before opening, otherwise water will condense inside the tubes and render MSTFA unsuitable
4. Add 10µl MeOX solution to each dried standard
5. Shake at max speed at 30°C for 1.5hours
6. To 1ml MSTFA add 10µ of FAME marker. Vortex for 10 seconds
7. Add 91µl of MSTFA + FAME mixture to each sample and standard. Cap immediately
8. Shake at max speed for 0.5 hours at 37°C
9. Transfer contents to glass vials with micro-inserts inserted and cap immediately
10. Submit to GC-MS data acquisition

APPENDIX D- PROTEOMICS DATA

SECTION 1- FDR CORRECTED PROTEOMICS RESULTS

1. **Gene Ontology-Biological Process**

Wild-Type Basal v. Wild-Type Memory Retrieval- Upregulated

Table 24. DAVID Gene Ontology output of enriched biological processes within proteins upregulated in WT mice during memory retrieval, when compared to WT mice at the basal level.

Term	Count	%	PValue	Genes	Fold Enrichment	FDR
GO:0032402~melanosome transport	3	9.677419	0.005512	DCTN2, RAB11A, RAB11B	24.61607	1
GO:0016192~vesicle-mediated transport	5	16.12903	0.034409	CLTB, CLTA, NAPG, RAB11A, RAB11B	3.816445	1
GO:0098869~cellular oxidant detoxification	2	6.451613	0.043449	HBB-BS, PRDX6	43.7619	1
GO:0090150~establishment of protein localization to membrane	2	6.451613	0.043449	RAB11A, RAB11B	43.7619	1
GO:0007080~mitotic metaphase plate congression	2	6.451613	0.071398	DCTN2, RAB11A	26.25714	1
GO:0032486~Rap protein signal transduction	2	6.451613	0.071398	RAP1A, RAP2B	26.25714	1

Wild-Type Basal v. APPtg Basal-Upregulated

Table 25. DAVID Gene Ontology output of enriched biological processes within proteins upregulated in APPtg mice at the basal level, when compared to WT mice at the basal level.

Term	Count	%	PValue	Genes	Fold Enrichment	FDR
GO:0006123~mitochondrial electron transport, cytochrome c to oxygen	3	6.122449	0.014313	COX7A2, COX5B, COX6A1	15.31667	1
GO:0006631~fatty acid metabolic process	5	10.20408	0.024099	HADHB, FABP3, DBI, HSD17B10, SNCA	4.345154	1
GO:0010467~gene expression	3	6.122449	0.048274	HADHB, APOE, GFAP	8.168889	1
GO:1901215~negative regulation of neuron death	3	6.122449	0.067242	PSMC1, APOE, SNCA	6.807407	1
GO:0006641~triglyceride metabolic process	2	4.081633	0.092445	DBI, APOE	20.42222	1

Wild-Type Basal v. Wild-Type Memory Retrieval- Downregulated

Table 26. DAVID Gene Ontology output of enriched biological processes within proteins downregulated in WT mice during memory retrieval, when compared to WT mice at the basal level.

Term	Count	%	PValue	Genes	Fold Enrichment	FDR

GO:0006915~apoptotic process	3	30	0.05416	CYFIP2, OPA1, MADD	6.971875	1
GO:0001889~liver development	2	20	0.062834	MPST, ACO2	27.8875	1

Wild-Type Basal v. APPtg Basal- Downregulated

Table 27. DAVID Gene Ontology output of enriched biological processes within proteins downregulated in APPtg mice at the basal level, when compared to WT mice at the basal level.

Term	Count	%	PValue	Genes	Fold Enrichment	FDR
GO:0051016~barbed-end actin filament capping	3	9.090909	0.007704	CAPZB, ADD3, ADD2	20.88636	1
GO:0051490~negative regulation of filopodium assembly	2	6.060606	0.051354	CAPZB, NRXN1	37.13131	1
GO:0021707~cerebellar granule cell differentiation	2	6.060606	0.051354	NRXN1, ATP2B2	37.13131	1
GO:0050885~neuromuscular process controlling balance	3	9.090909	0.068705	NRXN1, TNR, ATP2B2	6.683636	1
GO:2000300~regulation of synaptic vesicle exocytosis	3	9.090909	0.073639	CACNB4, CSPG5, CASK	6.426573	1
GO:0007158~neuron cell-cell adhesion	2	6.060606	0.084161	NRXN1, TNR	22.27879	1
GO:0048490~anterograde synaptic vesicle transport	2	6.060606	0.084161	MADD, AP3D1	22.27879	1
GO:0072659~protein localization to plasma membrane	4	12.12121	0.090651	PACS1, ROCK2, CASK, CLASP2	3.593353	1

2. Gene Ontology- Cellular Component

Wild-Type Basal v. Wild Type Memory Retrieval- Upregulated

Table 28. DAVID Gene Ontology output of enriched cellular components within proteins upregulated in WT mice during memory retrieval, when compared to WT mice at the basal level.

Term	Count	%	PValue	Genes	Fold Enrichment	FDR
GO:0099631~postsynaptic endocytic zone cytoplasmic component	2	6.451613	0.029636	CLTB, CLTA	64.68966	1
GO:0030130~clathrin coat of trans-Golgi network vesicle	2	6.451613	0.044134	CLTB, CLTA	43.12644	1
GO:0045335~phagocytic vesicle	3	9.677419	0.052168	RAP1A, RAB11A, RAB11B	7.762759	1
GO:0055038~recycling endosome membrane	3	9.677419	0.059934	RAP2B, RAB11A, RAB11B	7.187739	1
GO:0030118~clathrin coat	2	6.451613	0.072507	CLTB, CLTA	25.87586	1
GO:0030132~clathrin coat of coated pit	2	6.451613	0.086387	CLTB, CLTA	21.56322	1
GO:0098835~presynaptic endocytic zone membrane	2	6.451613	0.086387	CLTB, CLTA	21.56322	1
GO:0030125~clathrin vesicle coat	2	6.451613	0.086387	CLTB, CLTA	21.56322	1

Wild-Type Basal v. APPtg Basal- Upregulated

Table 29. DAVID Gene Ontology output of enriched cellular components within proteins upregulated in APPtg mice at the basal level, when compared to WT mice at the basal level.

Term	Count	%	PValue	Genes	Fold Enrichment	FDR
GO:0005743~mitochondrial inner membrane	12	24.4898	0.002701	HADHB, CHCHD3, NDUFA5, TIMM9, NDUFS5, NDUFA2, COX7A2, DHRS1, COX5B, COX6A1, HSD17B10, SNCA	2.692823	0.418627
GO:0005751~mitochondrial respiratory chain complex IV	3	6.122449	0.02476	COX7A2, COX5B, COX6A1	11.6281	1
GO:0099631~postsynaptic endocytic zone cytoplasmic component	2	4.081633	0.045329	CLTB, CLTA	42.63636	1
GO:0030130~clathrin coat of trans-Golgi network vesicle	2	4.081633	0.067234	CLTB, CLTA	28.42424	1
GO:0005615~extracellular space	5	10.20408	0.08975	PCMT1, FABP3, DBI, APOE, SNCA	2.842424	1

Wild-Type Basal v. Wild-Type Memory Retrieval- Downregulated

Table 30. DAVID Gene Ontology output of enriched cellular components within proteins downregulated in WT mice during memory retrieval, when compared to WT mice at the basal level.

Term	Count	%	PValue	Genes	Fold Enrichment	FDR
GO:0045202~synapse	5	50	0.05977	CYFIP2, MPST, MADD, DMXL2, SRCIN1	2.797794	1

Wild-Type Basal v. APPtg Basal- Downregulated

Table 31. DAVID Gene Ontology output of enriched cellular components within proteins downregulated in APPtg mice at the basal level, when compared to WT mice at the basal level.

Term	Count	%	PValue	Genes	Fold Enrichment	FDR
GO:0098978~glutamatergic synapse	11	33.33333	0.007257	CACNB4, ROCK2, NRXN1, AP3D1, ADAM22, CSPG5, TNR, ATP2B2, DLGAP2, PPFIA3, ADD2	2.451996	1
GO:0098685~Schaffer collateral - CA1 synapse	5	15.15152	0.021506	CAPZB, ROCK2, NRXN1, TNR, CASK	4.441288	1
GO:0005794~Golgi apparatus	7	21.21212	0.079047	SH3GLB1, ATP8A1, PACS1, AP3D1, CSPG5, GLG1, CLASP2	2.206317	1
GO:0008290~F-actin capping protein complex	2	6.060606	0.080019	CAPZB, ADD2	23.45	1
GO:0000139~Golgi membrane	4	12.12121	0.086395	SH3GLB1, AP3D1, CSPG5, GLG1	3.664063	1

3. Gene Ontology- Molecular Function

Wild-Type Basal v. Wild Type Memory Retrieval- Upregulated

Table 32. DAVID Gene Ontology output of enriched molecular functions within proteins upregulated in WT mice during memory retrieval, when compared to WT mice at the basal level.

Term	Count	%	PValue	Genes	Fold Enrichment	FDR
GO:0016787~hydrolase activity	7	22.58065	0.064171	RAP1A, RAP2B, ATP6V1E1, PRDX6, PAFAH1B2, RAB11A, RAB11B	2.295741	1
GO:0032050~clathrin heavy chain binding	2	6.451613	0.071359	CLTB, CLTA	26.23704	1
GO:0031625~ubiquitin protein ligase binding	4	12.90323	0.094407	TPI1, UBE2N, YWHAZ, PRDX6	3.498272	1

Wild-Type Basal v. APPtg Basal- Upregulated

Table 33. DAVID Gene Ontology output of enriched molecular functions within proteins upregulated in APPtg mice at the basal level, when compared to WT mice at the basal level.

Term	Count	%	PValue	Genes	Fold Enrichment	FDR
GO:0008289~lipid binding	5	10.20408	0.071434	GLTP, FABP3, PITPNM2, DBI, APOE	3.074653	1

Wild-Type Basal v. Wild-Type Memory Retrieval- Downregulated

No results.

Wild-Type Basal v. APPtg Basal- Downregulated

Table 34. DAVID Gene Ontology output of enriched molecular functions within proteins downregulated in APPtg mice at the basal level, when compared to WT mice at the basal level.

Term	Count	%	PValue	Genes	Fold Enrichment	FDR
GO:0005516~calmodulin binding	4	12.12121	0.066671	CASK, ATP2B2, ADD3, ADD2	4.071264	1

4. <u>KEGG Pathways</u>

Wild-Type Basal v. Wild Type Memory Retrieval- Upregulated

Table 35. DAVID annotation tools output of enriched KEGG pathways within proteins upregulated in WT mice during memory retrieval, when compared to WT mice at the basal level.

Term	Count	%	PValue	Genes	Fold Enrichment	FDR
mmu04144:Endocytosis	6	19.35484	0.009425	ARPC5L, CLTB, SNX12, CLTA, RAB11A, RAB11B	4.05614	0.584341
mmu04721:Synaptic vesicle cycle	4	12.90323	0.025578	ATP6V1G2, CLTB, CLTA, ATP6V1E1	5.708642	0.792921

mmu04962:Vasopressin-regulated water reabsorption	3	9.677419	0.042969	DCTN2, RAB11A, RAB11B	8.376812	0.812017
mmu00010:Glycolysis / Gluconeogenesis	3	9.677419	0.065485	TPI1, AKR1A1, ALDOC	6.643678	0.812017
mmu05100:Bacterial invasion of epithelial cells	3	9.677419	0.065485	ARPC5L, CLTB, CLTA	6.643678	0.812017
mmu04961:Endocrine and other factor-regulated calcium reabsorption	3	9.677419	0.082291	CLTB, CLTA, RAB11A	5.838384	0.850339

Wild-Type Basal v. APPtg Basal- Upregulated

Table 36. DAVID annotation tools output of enriched KEGG pathways within proteins upregulated in APPtg mice at the basal level, when compared to WT mice at the basal level.

Term	Count	%	PValue	Genes	Fold Enrichment	FDR
mmu00190:Oxidative phosphorylation	8	16.32653	0.003679	ATP6V1G2, NDUFA5, NDUFS5, NDUFA2, COX7A2, ATP6V1E1, COX5B, COX6A1	3.658228	0.185349
mmu05010:Alzheimer disease	11	22.44898	0.004119	NDUFA5, NDUFS5, PSMC1, NDUFA2, COX7A2, APOE, COX5B, COX6A1, HSD17B10,	2.631623	0.185349

				PPID, SNCA		
mmu05022:Pathways of neurodegeneration - multiple diseases	12	24.4898	0.009561	DCTN2, NDUFA5, NDUFS5, PSMC1, NDUFA2, RAB39B, COX7A2, COX5B, COX6A1, HSD17B10, PPID, SNCA	2.200508	0.278543
mmu05016:Huntington disease	10	20.40816	0.012576	DCTN2, NDUFA5, NDUFS5, PSMC1, NDUFA2, CLTB, CLTA, COX7A2, COX5B, COX6A1	2.424497	0.278543
mmu04932:Non-alcoholic fatty liver disease	6	12.2449	0.015475	NDUFA5, NDUFS5, NDUFA2, COX7A2, COX5B, COX6A1	3.802632	0.278543
mmu05208:Chemical carcinogenesis - reactive oxygen species	7	14.28571	0.024308	MAP2K4, NDUFA5, NDUFS5, NDUFA2, COX7A2, COX5B, COX6A1	2.906609	0.364616
mmu05014:Amyotrophic lateral sclerosis	9	18.36735	0.034208	DCTN2, NDUFA5, NDUFS5, PSMC1, NDUFA2, RAB39B, COX7A2,	2.211735	0.439823

				COX5B, COX6A1		
mmu05100:Bacterial invasion of epithelial cells	4	8.163265	0.039807	ARPC5L, RHOG, CLTB, CLTA	4.982759	0.44783
mmu04714:Thermogenesis	6	12.2449	0.065315	NDUFA5, NDUFS5, NDUFA2, COX7A2, COX5B, COX6A1	2.611446	0.653152
mmu05012:Parkinson disease	8	16.32653	0.072921	NDUFA5, NDUFS5, PSMC1, NDUFA2, COX7A2, COX5B, COX6A1, SNCA	2.049645	0.656292

Wild-Type Basal v. Wild-Type Memory Retrieval- Downregulated

No results.

Wild-Type Basal v. APPtg Basal- Downregulated

Table 37. DAVID annotation tools output of enriched KEGG pathways within proteins downregulated in APPtg mice at the basal level, when compared to WT mice at the basal level.

Term	Count	%	PValue	Genes	Fold Enrichment	FDR
mmu00920:Sulfur metabolism	2	6.060606	0.043509	MPST, BPNT1	42.81481	1
mmu04510:Focal adhesion	3	9.090909	0.091159	ROCK2, TNR, TLN2	5.504762	1

5. Clustering

Wild-Type Basal v. Wild-Type Memory Retrieval- Upregulated

Table 38. DAVID functional annotation clustering tools output within proteins upregulated in WT mice during memory retrieval, when compared to WT mice at the basal level.

Cluster 1-Enrichment Score: 2.6727354428947545						
Term	Count	%	PValue	Genes	Fold Enrichment	FDR
mmu04721:Synaptic vesicle cycle	4	14.2857143	2.54E-04	ATP6V1G2, CLTB, CLTA, ATP6V1E1	29.2564935	0.0149590 6
GO:0030672~synaptic vesicle membrane	4	14.2857143	6.79E-04	ATP6V1G2, CLTB, CLTA, RAB11B	22.1644339	0.0325928 7
mmu04144:Endocytosis	5	17.8571429	8.52E-04	ARPC5L, CLTB, SNX12, CLTA, RAB11B	10.3527114	0.0251340 9
KW-0968~Cytoplasmic vesicle	5	17.8571429	0.013	ATP6V1G2, CLTB, CLTA, ATP6V1E1, RAB11B	5.13821839	0.1944358 4
GO:0031410~cytoplasmic vesicle	5	17.8571429	0.0226989 1	ATP6V1G2, CLTB, CLTA, ATP6V1E1, RAB11B	4.37455933	0.1556496 5
Cluster 2-Enrichment Score: 1.3343973305376122						

Term	Count	%	PValue	Genes	Fold Enrichment	FDR
GO:0015031~protein transport	4	14.2857143	0.04417692	SNX12, LIN7A, NAPG, RAB11B	4.82123173	1
KW-0813~Transport	7	25	0.04519022	ATP6V1G2, SNX12, FXYD6, LIN7A, ATP6V1E1, NAPG, RAB11B	2.34487877	0.28177067
KW-0653~Protein transport	4	14.2857143	0.04972424	SNX12, LIN7A, NAPG, RAB11B	4.40325203	0.28177067
Cluster 3- Enrichment Score: 1.2082765566045408						
Term	Count	%	PValue	Genes	Fold Enrichment	FDR
MOTIF:Effector region	3	10.7142857	0.0047611	RAP1A, RAP2B, RAB11B	27.929347 8	0.1268809 9
GO:0019003~GDP binding	3	10.7142857	0.0055216 6	RAP1A, RAP2B, RAB11B	25.857275 3	0.2772836 9
LIPID:S-geranylgeranyl cysteine	3	10.7142857	0.0060419 5	RAP1A, RAP2B, RAB11B	24.706730 8	0.1268809 9
IPR001806:Small GTPase superfamily	3	10.7142857	0.0114205	RAP1A, RAP2B, RAB11B	17.741880 3	0.2479171 6
IPR005225:Small GTP-binding protein domain	3	10.7142857	0.0169034 4	RAP1A, RAP2B, RAB11B	14.428637 6	0.2479171 6
KW-0636~Prenylation	3	10.7142857	0.0373947 7	RAP1A, RAP2B, RAB11B	9.3737349 4	0.1529338 2

PROPEP:Removed in mature form	3	10.7142857	0.0393342	RAP1A, RAP2B, RAB11B	9.14412811	0.6195147
GO:0016787~hydrolase activity	6	21.4285714	0.0600069	RAP1A, RAP2B, ATP6V1E1, PRDX6, PAFAH1B2, RAB11B	2.66272189	0.71151038
GO:0005768~endosome	4	14.2857143	0.0610592	RAP1A, RAP2B, ATP6V1E1, RAB11B	4.23466827	0.3448048
GO:0003924~GTPase activity	3	10.7142857	0.0709121 6	RAP1A, RAP2B, RAB11B	6.56316161	0.7357136 5
GO:0005525~GTP binding	3	10.7142857	0.0971794 7	RAP1A, RAP2B, RAB11B	5.46095126	0.8962106 7
KW-0342~GTP-binding	3	10.7142857	0.1081634 8	RAP1A, RAP2B, RAB11B	4.82361516	1
KW-0378~Hydrolase	5	17.8571429	0.1085111 1	RAP1A, RAP2B, PRDX6, PAFAH1B2, RAB11B	2.45092849	1
KW-0488~Methylation	5	17.8571429	0.1095613	RAP1A, TPI1, RAP2B, MBP, RAB11B	2.58822355	0.3286839 1
KW-0967~Endosome	3	10.7142857	0.1977006 7	RAP1A, RAP2B, RAB11B	3.50607843	0.5272017 7
IPR027417:P-loop containing nucleoside triphosphate hydrolase	3	10.7142857	0.3079269 2	RAP1A, RAP2B, RAB11B	2.58376898	1
GO:0000166~nucleotide binding	4	14.2857143	0.4110535 9	RAP1A, RAP2B,	1.66368515	1

				UBE2N, RAB11B		
KW-0449~Lipoprotein	3	10.7142857	0.49153645	RAP1A, RAP2B, RAB11B	1.76822727	0.98307289
KW-0547~Nucleotide-binding	4	14.2857143	0.61260259	RAP1A, RAP2B, UBE2N, RAB11B	1.22283814	1
Cluster 4- Enrichment Score: 0.9278839403716633						
Term	Count	%	PValue	Genes	Fold Enrichment	FDR
KW-0813~Transport	7	25	0.04519022	ATP6V1G2, SNX12, FXYD6, LIN7A, ATP6V1E1, NAPG, RAB11B	2.34487877	0.28177067
GO:0006811~ion transport	3	10.7142857	0.17075903	ATP6V1G2, FXYD6, ATP6V1E1	3.86260079	1
KW-0406~Ion transport	3	10.7142857	0.21326522	ATP6V1G2, FXYD6, ATP6V1E1	3.2496	0.60425145
Cluster 5-Enrichment Score: 0.8840326654392694						
Term	Count	%	PValue	Genes	Fold Enrichment	FDR
mmu01100:Metabolic pathways	7	25	0.03846674	TPI1, ATP6V1G2, AKR1A1, ALDOC, ATP6V1E1, PRDX6, PAFAH1B2	2.43202498	0.43313884
GO:0006629~lipid metabolic process	3	10.7142857	0.22755673	AKR1A1, PRDX6,	3.19755245	1

				PAFAH1B2		
KW-0443~Lipid metabolism	3	10.7142857	0.2545229	AKR1A1, PRDX6, PAFAH1B2	2.8849431	0.6181271
Cluster 6- Enrichment Score: 0.06376776161098885						
Term	Count	%	PValue	Genes	Fold Enrichment	FDR
KW-1017~Isopeptide bond	3	10.7142857	0.7978063	TPI1, CSRP1, UBE2N	1.0077979	1
GO:0005634~nucleus	7	25	0.8565744	TPI1, CSRP1, UBE2N, MBP, TAGLN3, YWHAZ, PRDX6	0.8433421	0.9142857
KW-0832~Ubl conjugation	3	10.7142857	0.9419636	TPI1, CSRP1, UBE2N	0.6800874	1
Cluster 7- Enrichment Score: 0.0229646082740319						
Term	Count	%	PValue	Genes	Fold Enrichment	FDR
KW-1133~Transmembrane helix	3	10.7142857	0.9117983	PCMT1, CLPTM1, FXYD6	0.7895995	1
KW-0812~Transmembrane	3	10.7142857	0.9373833	PCMT1, CLPTM1, FXYD6	0.7312930	1
TRANSMEM:Helical	3	10.7142857	0.9983668	PCMT1, CLPTM1, FXYD6	0.3863909	1

Wild-Type Basal v. APPtg Basal- Upregulated

Table 39. DAVID functional annotation clustering tools output within proteins upregulated in APPtg mice at the basal level, when compared to WT mice at the basal level.

Cluster 1- Enrichment Score: 3.6288747828858954						
Term	Count	%	PValue	Genes	Fold Enrichment	FDR
GO:0005743~mitochondrial inner membrane	12	26.086965	5.95E-09	HADHB, CHCHD3, NDUFA5, TIMM9, NDUFS5, NDUFA2, COX7A2, DHRS1, COX5B, COX6A1, HSD17B10, SNCA	10.9168535	8.39E-07
mmu05022:Pathways of neurodegeneration - multiple diseases	12	26.086965	2.31E-07	DCTN2, NDUFA5, NDUFS5, PSMC1, NDUFA2, RAB39B, COX7A2, COX5B, COX6A1, HSD17B10, PPID, SNCA	7.17436306	9.20E-06
mmu00190:Oxidative phosphorylation	8	17.391304	2.82E-07	ATP6V1G2, NDUFA5, NDUFS5, NDUFA2, COX7A2, ATP6V1E1, COX5B, COX6A1	16.687037	9.20E-06
mmu05010:Alzheimer disease	11	23.913043	3.41E-07	NDUFA5, NDUFS5, PSMC1, NDUFA2, COX7A2, APOE, COX5B, COX6A1, HSD17B10, PPID, SNCA	8.08754896	9.20E-06
mmu05016:Huntington disease	10	21.739304	4.98E-07	DCTN2, NDUFA5, NDUFS5, PSMC1, NDUFA2, CLTB, CLTA, COX7A2, COX5B, COX6A1	9.32429636	1.01E-05
KW-0999~Mitochondrion inner membrane	9	19.565217	7.19E-07	HADHB, CHCHD3, NDUFA5, TIMM9, NDUFS5, NDUFA2, COX7A2, COX5B, COX6A1	11.5867953	2.01E-05
GO:00057GT39~mitochondrion	16	34.782608	2.74E-06	NDUFA5, TIMM9, NDUFA2, COX7A2, DBI, DHRS1, COX5B, COX6A1, HSD17B10, HADHB, HINT2, CHCHD3, NDUFS5, ATP6V1E1, PPID, SNCA	4.02250083	1.93E-04

mmu05012:Parkinson disease	8	17.391304	2.46E-05	NDUFA5, NDUFS5, PSMC1, NDUFA2, COX7A2, COX5B, COX6A1, SNCA	8.53314394	3.41E-04
mmu05014:Amyotrophic lateral sclerosis	9	19.565217	2.52E-05	DCTN2, NDUFA5, NDUFS5, PSMC1, NDUFA2, RAB39B, COX7A2, COX5B, COX6A1	6.86814024	3.41E-04
mmu05208:Chemical carcinogenesis - reactive oxygen species	7	15.217391	9.18E-05	MAP2K4, NDUFA5, NDUFS5, NDUFA2, COX7A2, COX5B, COX6A1	8.87908221	0.00106283
mmu04932:Non-alcoholic fatty liver disease	6	13.043478	1.72E-04	NDUFA5, NDUFS5, NDUFA2, COX7A2, COX5B, COX6A1	10.8305288	0.00174384
mmu05020:Prion disease	7	15.217391	2.58E-04	NDUFA5, NDUFS5, PSMC1, NDUFA2, COX7A2, COX5B, COX6A1	7.35506063	0.00231756
KW-0496~Mitochondrion	11	23.913043	5.06E-04	HADHB, HINT2, CHCHD3, NDUFA5, TIMM9, NDUFS5, NDUFA2, COX7A2, COX5B, COX6A1, HSD17B10	3.65644229	0.00707882
mmu05415:Diabetic cardiomyopathy	6	13.043478	6.94E-04	NDUFA5, NDUFS5, NDUFA2, COX7A2, COX5B, COX6A1	8.00740521	0.00562354
GO:0006123~mitochondrial electron transport, cytochrome c to oxygen	3	6.5217391	8.66E-04	COX7A2, COX5B, COX6A1	67.063333	0.38718243
mmu04714:Thermogenesis	6	13.043478	0.001044	NDUFA5, NDUFS5, NDUFA2, COX7A2, COX5B, COX6A1	7.31412338	0.00769231
GO:0005751~mitochondrial respiratory chain complex IV	3	6.5217391	0.001088	COX7A2, COX5B, COX6A1	59.928 9773	0.05116978

KW-0809~Transit peptide	5	10.869565 2	0.003734 61	HADHB, HINT2, COX7A2, COX5B, COX6A1	7.12060205	0.02987685
GO:0005747~mitochondrial respiratory chain complex I	3	6.521739 13	0.005044 91	NDUFA5, NDUFS5, NDUFA2	27.659528	0.08891 66
mmu01100:Metabolic pathways	13	28.26086 96	0.005311 44	ATP6V1G2, NDUFA5, NDUFA2, AK1, COX7A2, COX5B, COX6A1, HSD17B10, HADHB, NDUFS5, CMPK1, ATP6V1E1, CDS2	2.25830891	0.03073 05
GO:0070469~respiratory chain	3	6.521739 13	0.007102 48	NDUFA5, NDUFS5, NDUFA2	23.1983138	0.10170868
GO:0032981~mitochondrial respiratory chain complex I assembly	3	6.521739 13	0.008133 47	NDUFA5, NDUFS5, NDUFA2	21.6333333	0.91842305
GO:0042776~mitochondrial ATP synthesis coupled proton transport	3	6.521739 13	0.008388 55	NDUFA5, NDUFS5, NDUFA2	21.2899471	0.91842305
KW-0679~Respiratory chain	3	6.521739 13	0.008723 21	NDUFA5, NDUFS5, NDUFA2	20.31	0.13084812
GO:0009060~aerobic respiration	3	6.521739 13	0.010273 19	NDUFA5, NDUFS5, NDUFA2	19.1609524	0.91842305
TRANSIT:Mitochondrion	5	10.869565 2	0.014919 94	HADHB, HINT2, COX7A2, COX5B, COX6A1	5.10475885	0.24617901
KW-0249~Electron transport	3	6.521739 13	0.023974 71	NDUFA5, NDUFS5, NDUFA2	11.9251376	0.23974709
mmu04260:Cardiac muscle contraction	3	6.521739 13	0.035752 49	COX7A2, COX5B, COX6A1	9.71012931	0.19306343

mmu04723:Retrograde endocannabinoid signaling	3	6.521739 13	0.091464 08	NDUFA5, NDUFS5, NDUFA2	5.70798142	0.38992579
Cluster 2-Enrichment Score: 1.8056004803969787						
Term	Count	%	PValue	Genes	Fold Enrichment	FDR
MOTIF:Effector region	4	8.695652 17	6.04E-04	RAP1A, RAP2B, RHOG, RAB39B	23.6150583	0.04267962
LIPID:S-geranylgeranylcysteine	4	8.695652 17	8.62E-04	RAP1A, RAP2B, RHOG, RAB39B	20.8902439	0.04267962
IPR001806:Small GTPase superfamily	4	8.695652 17	0.002932 02	RAP1A, RAP2B, RHOG, RAB39B	13.6678189	0.10853191
IPR027417:P-loop containing nucleoside triphosphate hydrolase	8	17.39130 43	0.003127	GNA13, RAP1A, RAP2B, PSMC1, AK1, RHOG, CMPK1, RAB39B	3.98091813	0.10853191
GO:0000166~nucleotide binding	11	23.91304 35	0.004991 2	GNA13, MAP2K4, RAP1A, HINT2, RAP2B, PSMC1, AK1, UBE2N, RHOG, CMPK1, RAB39B	2.70348837	0.40264951
IPR005225:Small GTP-binding protein domain	4	8.695652 17	0.005230 45	RAP1A, RAP2B, RHOG, RAB39B	11.1153949	0.10853191
GO:0003924~GTPase activity	5	10.86956 52	0.006748 32	GNA13, RAP1A, RAP2B, RHOG, RAB39B	6.46371977	0.40264951
GO:0005525~GTP binding	5	10.86956 52	0.012657 34	GNA13, RAP1A, RAP2B, RHOG, RAB39B	5.37820958	0.56641 59
KW-0636~Prenylation	4	8.695652 17	0.013437 58	RAP1A, RAP2B, RHOG, RAB39B	7.81144578	0.06880 65

KW-0449~Lipoprotein	8	17.391304	0.014744	GNA13, RAP1A, CHCHD3, RAP2B, PSMC1, RHOG, RAB39B, APOE	2.94704545	0.06880
KW-0488~Methylation	8	17.391304	0.028017	MAP2K4, RAP1A, RAP2B, PITPNM2, RHOG, RAB39B, DHRS1, GFAP	2.58822355	0.09806
KW-0342~GTP-binding	5	10.869565	0.033110	GNA13, RAP1A, RAP2B, RHOG, RAB39B	3.85889213	0.33212
PROPEP:Removed in mature form	3	6.521739	0.090536	RAP1A, RAP2B, RHOG	5.79871539	0.74692
KW-0547~Nucleotide-binding	11	23.913043	0.090580	GNA13, MAP2K4, RAP1A, HINT2, RAP2B, PSMC1, AK1, UBE2N, RHOG, CMPK1, RAB39B	1.61414634	0.33212
GO:0007165~signal transduction	3	6.521739	0.819134	GNA13, RAP1A, RAP2B	0.96148148	1
KW-1003~Cell membrane	5	10.869565	0.981677	RAP1A, RHOG, RAB39B, LIN7A, ATP6V1E1	0.57167612	1
Cluster 3- Enrichment Score: 1.7268722322639372						
Term	Count	%	PValue	Genes	Fold Enrichment	FDR
mmu04721:Synaptic vesicle cycle	4	8.695652	0.002270	ATP6V1G2, CLTB, CLTA, ATP6V1E1	14.6282468	0.01414
GO:0030672~synaptic vesicle membrane	4	8.695652	0.002966	ATP6V1G2, CLTB, CLTA, SNCA	13.6009026	0.08366
GO:0031410~cytoplasmic vesicle	6	13.043478	0.034263	ATP6V1G2, RHOG, CLTB, CLTA, RAB39B, ATP6V1E1	3.22126642	0.20130
KW-0968~Cytoplasmic vesicle	5	10.869565	0.079567	ATP6V1G2, CLTB, CLTA, RAB39B, ATP6V1E1	2.98733627	0.55696

GO:0016192~vesicle-mediated transport	3	6.521739 13	0.126382 99	CLTB, CLTA, RAB39B	4.756264 78	1
Cluster 4- Enrichment Score: 1.280973968300595						
Term	Count	%	PValue	Genes	Fold Enrichment	FDR
GO:0008289~lipid binding	6	13.04347 83	0.00118107	GLTP, FABP3, PITPNM2, DBI, APOE, SNCA	7.309405 29	0.21141103
REPEAT:1	3	6.521739 13	0.03502465	GLTP, APOE, SNCA	9.935603 81	0.35448 59
REPEAT:2	3	6.521739 13	0.03580666	GLTP, APOE, SNCA	9.815897 74	0.35448 59
GO:0042802~identical protein binding	7	15.21739 13	0.31589723	GLTP, DCTN2, DBI, APOE, HSD17B10, GFAP, SNCA	1.476592 27	1
KW-0677~Repeat	5	10.86956 52	0.84134121	GLTP, ABLIM2, APOE, PPID, SNCA	0.869679 76	1
Cluster 5- Enrichment Score: 1.14970951287547						
Term	Count	%	PValue	Genes	Fold Enrichment	FDR
GO:0008289~lipid binding	6	13.04347 83	0.00118107	GLTP, FABP3, PITPNM2, DBI, APOE, SNCA	7.309405 29	0.21141103
KW-0446~Lipid-binding	4	8.695652 17	0.06243111	FABP3, PITPNM2, DBI, APOE	4.168818 9	0.33212 739
GO:0005794~Golgi apparatus	4	8.695652 17	0.57908491	RAB39B, DBI, APOE, SNCA	1.314412 11	0.89808 917

GO:0005615~extracellular space	5	10.869565	0.5898534	PCMT1, FABP3, DBI, APOE, SNCA	1.2015835	0.89808917
Cluster 6- Enrichment Score: 0.8102218884501934						
Term	Count	%	PValue	Genes	Fold Enrichment	FDR
GO:0006629~lipid metabolic process	5	10.869565	0.0733549	HADHB, HINT2, APOE, HSD17B10, CDS2	3.07912458	1
KW-0443~Lipid metabolism	4	8.695652	0.2021957	HADHB, HINT2, HSD17B10, CDS2	2.46181818	0.94852985
GO:0005783~endoplasmic reticulum	6	13.04348	0.2501074	HADHB, DBI, APOE, DHRS1, HSD17B10, CDS2	1.7266452	0.89808917
Cluster 7- Enrichment Score: 0.4356841414680946						
Term	Count	%	PValue	Genes	Fold Enrichment	FDR
KW-0808~Transferase	7	15.21739	0.1537361	HADHB, PCMT1, MAP2K4, AK1, UBE2N, CMPK1, CDS2	1.80875408	1
GO:0016740~transferase activity	7	15.21739	0.2231541	HADHB, PCMT1, MAP2K4, AK1, UBE2N, CMPK1, CDS2	1.66803321	1
KW-0418~Kinase	3	6.521739	0.3851583	MAP2K4, AK1, CMPK1	2.17117605	1
GO:0016310~phosphorylation	3	6.521739	0.3995913	MAP2K4, AK1, CMPK1	2.14259851	1
GO:0016301~kinase activity	3	6.521739	0.4548983	MAP2K4, AK1, CMPK1	1.91858066	1
GO:0005524~ATP binding	5	10.869565	0.4763982	MAP2K4, PSMC1, AK1, UBE2N, CMPK1	1.38146168	1

KW-0067~ATP-binding	5	10.869565 2	0.7792738 6	MAP2K4, PSMC1, AK1, UBE2N, CMPK1	0.94542857	1
Cluster 8- Enrichment Score: 0.08332821304949985						
Term	Count	%	PValue	Genes	Fold Enrichment	FDR
GO:0005524~ATP binding	5	10.869565 2	0.4763982	MAP2K4, PSMC1, AK1, UBE2N, CMPK1	1.38146168	1
KW-0067~ATP-binding	5	10.869565 2	0.7792738 6	MAP2K4, PSMC1, AK1, UBE2N, CMPK1	0.94542857	1
KW-0539~Nucleus	9	19.56521 74	0.9288090 6	GNA13, PURA, MAP2K4, CHCHD3, PSMC1, UBE2N, CMPK1, PPID, SNCA	0.75454332	1
KW-1017~Isopeptide bond	3	6.521739 13	0.9555460 5	PSMC1, UBE2N, CMPK1	0.6298737	1
KW-0832~Ubl conjugation	4	8.695652 17	0.9777993 4	PSMC1, UBE2N, CMPK1, SNCA	0.56673951	1
GO:0005654~nucleoplasm	4	8.695652 17	0.9816184 1	PSMC1, UBE2N, CMPK1, PPID	0.54760916	0.98161841
Cluster 9- Enrichment Score: 0.020102842657520582						
Term	Count	%	PValue	Genes	Fold Enrichment	FDR
GO:0046872~metal ion binding	7	15.21739 13	0.8708072	GNA13, ABLIM2, TIMM9, PITPNM2, HDHD2, COX5B, SNCA	0.81450342	1
KW-0862~Zinc	3	6.521739 13	0.9997051 3	ABLIM2, TIMM9, COX5B	0.33131414	1
KW-0479~Metal-binding	7	15.21739 13	0.9997641 1	GNA13, ABLIM2, TIMM9, PITPNM2, HDHD2, COX5B, SNCA	0.48344378	1
Cluster 10- Enrichment Score: 0.008274601304265694						

Term	Count	%	PValue	Genes	Fold Enrichment	FDR
KW-1133~Transmembrane helix	5	10.869565	0.952888	PCMT1, COX7A2, FXYD6, COX6A1, CDS2	0.69263121	1
KW-0812~Transmembrane	5	10.869565	0.973081	PCMT1, COX7A2, FXYD6, COX6A1, CDS2	0.64148515	1
TRANSMEM:Helical	5	10.869565	0.999370	PCMT1, COX7A2, FXYD6, COX6A1, CDS2	0.40838071	0.99937
GO:0016021~integral component of membrane	4	8.695652	0.999970	PCMT1, COX7A2, COX6A1, CDS2	0.29722989	0.99997

Wild-Type Basal v. Wild-Type Memory Retrieval- Downregulated

Table 40. DAVID functional annotation clustering tools output within proteins downregulated in WT mice during memory retrieval, when compared to WT mice at the basal level.

Cluster 1-Enrichment Score: 2.0535043689081363						
Term	Count	%	PValue	Genes	Fold Enrichment	FDR
GO:0045202~synapse	5	50	5.65E-04	CYFIP2, MPST, MADD, DMXL2, SRCIN1	10.3305583	0.02430271
KW-0770~Synapse	4	40	0.00171378	CYFIP2, MPST, DMXL2, SRCIN1	13.9968689	0.01885156
GO:0043005~neuron projection	3	30	0.02538632	CYFIP2, MPST, SRCIN1	10.5651085	0.36387059

KW-0963~Cytoplasm	5	50	0.24845167	CYFIP2, MPST, AGL, MADD, SRCIN1	1.72230784	0.54659366
Cluster 2-Enrichment Score: 1.6409272143117863						
Term	Count	%	PValue	Genes	Fold Enrichment	FDR
TRANSIT:Mitochondrion	3	30	0.01834819	OPA1, IMMT, ACO2	12.5577068	1
KW-0809~Transit peptide	3	30	0.0185246	OPA1, IMMT, ACO2	11.5964091	0.0648361
GO:0005743~mitochondrial inner membrane	3	30	0.01996245	MPST, OPA1, IMMT	12.0085389	0.36387059
KW-0496~Mitochondrion	4	40	0.02085027	MPST, OPA1, IMMT, ACO2	5.71734612	0.11107807
KW-0007~Acetylation	6	60	0.02465781	CYFIP2, MPST, OPA1, IMMT, EPS15L1, ACO2	2.73046957	0.09863125
GO:0005739~mitochondrion	4	40	0.0409086	MPST, OPA1, IMMT, ACO2	4.42475092	0.37421852
Cluster 3-Enrichment Score: 0.6174083404230949						
Term	Count	%	PValue	Genes	Fold Enrichment	FDR
KW-0175~Coiled coil	5	50	0.01208345	OPA1, DMXL2, IMMT, EPS15L1, SRCIN1	3.91828445	0.0648361
GO:0016020~membrane	5	50	0.44828129	OPA1, MADD,	1.34175041	1

				DMXL2, IMMT, EPS15L1		
KW-0472~Membrane	5	50	0.76887877	OPA1, MADD, DMXL2, IMMT, EPS15L1	0.9768903	1
GO:0016021~integral component of membrane	3	30	0.81426758	OPA1, MADD, IMMT	0.98085865	1
Cluster 4-Enrichment Score: 0.6153177973596772						
Term	Count	%	PValue	Genes	Fold Enrichment	FDR
COMPBIAS:Polar residues	6	60	0.10071838	MADD, DMXL2, IMMT, EPS15L1, ACO2, SRCIN1	1.98948779	1
KW-0597~Phosphoprotein	7	70	0.31128052	MPST, MADD, DMXL2, IMMT, EPS15L1, ACO2, SRCIN1	1.30050863	0.62256105
REGION:Disordered	7	70	0.45476384	CYFIP2, MADD, DMXL2, IMMT, EPS15L1, ACO2, SRCIN1	1.18876687	1

Wild-Type Basal v. APPtg Basal- Downregulated

Table 41. DAVID functional annotation clustering tools output within proteins downregulated in APPtg mice at the basal level, when compared to WT mice at the basal level.

Cluster 1- Enrichment Score: 2.9130033402577626						
Term	Count	%	PValue	Genes	Fold Enrichment	FDR
GO:0014069~postsynaptic density	6	17.6470588	2.46E-04	CAPZB, CASK, ADD3, DLGAP2, DCLK1, ADD2	10.1199328	0.0092952
KW-0112~Calmodulin-binding	4	11.7647059	0.0016794	CASK, ATP2B2, ADD3, ADD2	15.8121511	0.0386228
GO:0005516~calmodulin binding	4	11.7647059	0.0044103	CASK, ATP2B2, ADD3, ADD2	11.625	0.1897176
Cluster 2-Enrichment Score: 2.510948644137548						
Term	Count	%	PValue	Genes	Fold Enrichment	FDR
REPEAT:HEAT 8	3	8.8235294	5.52E-04	AP3D1, CLASP2, IPO5	83.50875	0.0485167
REPEAT:HEAT 7	3	8.8235294	6.93E-04	AP3D1, CLASP2, IPO5	74.5613839	0.0485167
REPEAT:HEAT 6	3	8.8235294	9.64E-04	AP3D1, CLASP2, IPO5	63.2642045	0.0506072
REPEAT:HEAT 5	3	8.8235294	0.0012116	AP3D1, CLASP2, IPO5	56.4248311	0.0508906
REPEAT:HEAT 4	3	8.8235294	0.0017887	AP3D1, CLASP2, IPO5	46.39375	0.0626049

REPEAT:HEAT 3	3	8.82352941	0.00211743	AP3D1, CLASP2, IPO5	42.6065051	0.06352287
REPEAT:HEAT 1	3	8.82352941	0.0029532	AP3D1, CLASP2, IPO5	35.9951509	0.06890792
REPEAT:HEAT 2	3	8.82352941	0.0029532	AP3D1, CLASP2, IPO5	35.9951509	0.06890792
IPR011989:Armadillo-like helical	3	8.82352941	0.0506822	AP3D1, CLASP2, IPO5	8.03017408	0.70338597
IPR016024:Armadillo-type fold	3	8.82352941	0.10397641	AP3D1, CLASP2, IPO5	5.30081716	1
Cluster 3- Enrichment Score: 2.3105108203304665						
Term	Count	%	PValue	Genes	Fold Enrichment	FDR
GO:0014069~postsynaptic density	6	17.6470588	2.46E-04	CAPZB, CASK, ADD3, DLGAP2, DCLK1, ADD2	10.1199328	0.00929522
GO:0051016~barbed-end actin filament capping	3	8.82352941	5.55E-04	CAPZB, ADD3, ADD2	83.1363636	0.2425389
GO:0051015~actin filament binding	5	14.7058824	5.70E-04	CAPZB, TLN2, ADD3, CLASP2, ADD2	12.5269397	0.0649336
GO:0005200~structural constituent of cytoskeleton	3	8.82352941	0.0063903	TLN2, ADD3, ADD2	24.21875	0.18977176
GO:0005856~cytoskeleton	7	20.5882353	0.0173227	CAPZB, ROCK2, TLN2, ADD3, GLG1,	3.19393074	0.2648407

				CLASP2, ADD2		
KW-0206~Cytoskeleton	7	20.5882353	0.01954887	CAPZB, ROCK2, TLN2, ADD3, GLG1, CLASP2, ADD2	3.09161192	0.08601504
GO:0003779~actin binding	4	11.7647059	0.02699377	CAPZB, TLN2, ADD3, ADD2	5.93112245	0.61545795
KW-0009~Actin-binding	3	8.82352941	0.07214115	CAPZB, ADD3, ADD2	6.4163113	0.82962323
Cluster 4-Enrichment Score: 1.7045369396938246						
Term	Count	%	PValue	Genes	Fold Enrichment	FDR
GO:0016020~membrane	21	61.7647059	0.00327591	SH3GLB1, ATP8A1, ROCK2, NRXN1, AP3D1, ADAM22, CASK, ATP2B2, ADD3, GLG1, MTDH, ADD2, ABHD16A, AIFM1, CAPZB, MADD, CSPG5, TLN2, OSBPL1A, DLGAP2, CLASP2	1.70768234	0.08244373

KW-1003~Cell membrane	14	41.1764706	0.00360476	ATP8A1, ROCK2, NRXN1, ADAM22, CASK, ATP2B2, ADD3, GLG1, ADD2, MADD, CSPG5, TLN2, DLGAP2, CLASP2	2.22031628	0.01982617
GO:0005886~plasma membrane	15	44.1176471	0.05934162	ATP8A1, ROCK2, NRXN1, ADAM22, CASK, ATP2B2, ADD3, GLG1, ADD2, CACNB4, MADD, CSPG5, TLN2, DLGAP2, CLASP2	1.54680374	0.47160975
KW-0472~Membrane	19	55.8823529	0.21691256	SH3GLB1, ATP8A1, ROCK2, NRXN1, AP3D1, ADAM22, CASK, ATP2B2, ADD3, GLG1, MTDH, ADD2, ABHD16A, AIFM1, MADD,	1.19747843	0.6817252

				CSPG5, TLN2, DLGAP2, CLASP2		
Cluster 5- Enrichment Score: 1.697495763657739						
Term	Count	%	PValue	Genes	Fold Enrichment	FDR
KW-0333~Golgi apparatus	7	20.5882353	0.00337764	SH3GLB1, ATP8A1, PACS1, AP3D1, CSPG5, GLG1, CLASP2	4.48129319	0.01982617
GO:0005794~Golgi apparatus	7	20.5882353	0.02076513	SH3GLB1, ATP8A1, PACS1, AP3D1, CSPG5, GLG1, CLASP2	3.0669616	0.28504855
GO:0005802~trans-Golgi network	3	8.82352941	0.04483469	ATP8A1, AP3D1, CLASP2	8.59967387	0.40674991
GO:0000139~Golgi membrane	4	11.7647059	0.05157692	SH3GLB1, AP3D1, CSPG5, GLG1	4.59060987	0.43267302
Cluster 6- Enrichment Score: 1.380168497405341						
Term	Count	%	PValue	Genes	Fold Enrichment	FDR
DOMAIN:SH3	3	8.82352941	0.03500332	SH3GLB1, CACNB4, CASK	9.84772995	0.43239394
KW-0728~SH3 domain	3	8.82352941	0.04515805	SH3GLB1,	8.44834123	0.27094828

				CACNB4, CASK		
IPR001452:Src homology-3 domain	3	8.82352941	0.0457773	SH3GLB1, CACNB4, CASK	8.5004095	0.70338597
Cluster 7- Enrichment Score: 1.0752605000676703						
Term	Count	%	PValue	Genes	Fold Enrichment	FDR
GO:0030424~axon	4	11.764705	0.04129484	MADD, AP3D1, ADAM22, DCLK1	5.0235161	0.40674991
GO:0042995~cell projection	5	14.705882	0.11227982	NRXN1, MADD, ADAM22, DCLK1, CLASP2	2.6091527	0.6307357
KW-0966~Cell projection	5	14.705882	0.12823925	NRXN1, MADD, ADAM22, DCLK1, CLASP2	2.4755641	0.4702105
Cluster 8- Enrichment Score: 0.6661971154272402						
Term	Count	%	PValue	Genes	Fold Enrichment	FDR
KW-0245~EGF-like domain	4	11.764705	0.00678865	NRXN1, ADAM22, CSPG5, TNR	9.7810699	0.0814637
DOMAIN:EGF-like	3	8.82352941	0.03321534	NRXN1, ADAM22, CSPG5	10.134557	0.43239394
IPR000742:Epidermal growth factor-like domain	3	8.82352941	0.05457952	NRXN1, ADAM22, TNR	7.7024118	0.7033859
TOPO_DOM:Cytoplasmic	8	23.529411	0.1609141	ATP8A1, ABHD16A,	1.6994047	0.9722222

				NRXN1, ADAM22, CSPG5, ATP2B2, GLG1, MTDH		
GO:0009986~cell surface	3	8.82352941	0.34042165	NRXN1, CSPG5, TNR	2.41527364	0.9869281
TOPO_DOM:Extracellular	5	14.7058824	0.43746937	NRXN1, ADAM22, CSPG5, ATP2B2, GLG1	1.44139654	0.9722222
CARBOHYD:N-linked (GlcNAc...) asparagine	5	14.7058824	0.78270849	NRXN1, ADAM22, CSPG5, TNR, GLG1	0.93838491	0.9722222
KW-0732~Signal	5	14.7058824	0.97251943	NRXN1, ADAM22, CSPG5, TNR, GLG1	0.62626476	1
KW-1015~Disulfide bond	5	14.7058824	0.97379016	MPST, NRXN1, ADAM22, CSPG5, TNR	0.61118967	1
KW-0325~Glycoprotein	5	14.7058824	0.99621844	NRXN1, ADAM22, CSPG5, TNR, GLG1	0.48880428	1
Cluster 9- Enrichment Score: 0.6658390986531371						
Term	Count	%	PValue	Genes	Fold Enrichment	FDR
GO:0005524~ATP binding	6	17.6470588	0.10667338	MTHFD1L, ATP8A1, ROCK2,	2.27941176	1

				CASK, ATP2B2, DCLK1		
SM00220:S_TKc	3	8.82352941	0.13486827	ROCK2, CASK, DCLK1	4.39991712	1
KW-0723~Serine/threonine-protein kinase	3	8.82352941	0.1432112	ROCK2, CASK, DCLK1	4.26692662	0.90055039
GO:0000166~nucleotide binding	6	17.6470588	0.15356553	MTHFD1L, ATP8A1, ROCK2, CASK, ATP2B2, DCLK1	2.02761628	1
KW-0067~ATP-binding	6	17.6470588	0.15566287	MTHFD1L, ATP8A1, ROCK2, CASK, ATP2B2, DCLK1	1.89085714	0.67453911
GO:0004674~protein serine/threonine kinase activity	3	8.82352941	0.16269097	ROCK2, CASK, DCLK1	4.01785714	1
DOMAIN:Protein kinase	3	8.82352941	0.16289734	ROCK2, CASK, DCLK1	4.01484375	0.97222222
GO:0004712~protein serine/threonine/tyrosine kinase activity	3	8.82352941	0.17037833	ROCK2, CASK, DCLK1	3.90100671	1
IPR000719:Protein kinase, catalytic domain	3	8.82352941	0.1879971	ROCK2, CASK, DCLK1	3.66425419	1
IPR011009:Protein kinase-like domain	3	8.82352941	0.21221903	ROCK2, CASK, DCLK1	3.38188335	1
GO:0004672~protein kinase activity	3	8.82352941	0.2139597	ROCK2, CASK, DCLK1	3.35982659	1

GO:0016310~phosphorylation	3	8.82352941	0.26258359	ROCK2, CASK, DCLK1	2.92172524	1
GO:0006468~protein phosphorylation	3	8.82352941	0.27746065	ROCK2, CASK, DCLK1	2.80952381	1
GO:0016301~kinase activity	3	8.82352941	0.30224455	ROCK2, CASK, DCLK1	2.63804841	1
KW-0418~Kinase	3	8.82352941	0.32135345	ROCK2, CASK, DCLK1	2.48134405	1
KW-0547~Nucleotide-binding	6	17.6470588	0.32730259	MTHFD1L, ATP8A1, ROCK2, CASK, ATP2B2, DCLK1	1.46740576	0.8509867
KW-0808~Transferase	5	14.7058824	0.40712599	MPST, ROCK2, AGL, CASK, DCLK1	1.47653394	1
GO:0016740~transferase activity	4	11.7647059	0.57813155	MPST, ROCK2, CASK, DCLK1	1.31059752	1
Cluster 10- Enrichment Score: 0.4804720355052125						
Term	Count	%	PValue	Genes	Fold Enrichment	FDR
KW-0460~Magnesium	5	14.7058824	0.03852383	FAHD2, ATP8A1, ROCK2, BPNT1, ATP2B2	3.47401575	0.2566486
KW-0106~Calcium	4	11.7647059	0.27410021	FAHD2, CACNB4, NRXN1, ATP2B2	2.03787529	0.8509867

KW-0378~Hydrolase	5	14.7058824	0.33149171	FAHD2, ATP8A1, ABHD16A, AGL, BPNT1	1.63395233	1
GO:0016787~hydrolase activity	4	11.7647059	0.51088875	FAHD2, ATP8A1, ABHD16A, BPNT1	1.44230769	1
GO:0046872~metal ion binding	6	17.6470588	0.75171057	FAHD2, ATP8A1, ROCK2, NRXN1, BPNT1, ATP2B2	0.95995045	1
KW-0479~Metal-binding	6	17.6470588	0.97426999	FAHD2, ATP8A1, ROCK2, NRXN1, BPNT1, ATP2B2	0.69063397	1
Cluster 11- Enrichment Score: 0.36761776802788915						
Term	Count	%	PValue	Genes	Fold Enrichment	FDR
TOPO_DOM:Cytoplasmic	8	23.5294118	0.1609141	ATP8A1, ABHD16A, NRXN1, ADAM22, CSPG5, ATP2B2, GLG1, MTDH	1.69940476	0.97222222
KW-0472~Membrane	19	55.8823529	0.21691256	SH3GLB1, ATP8A1, ROCK2, NRXN1, AP3D1, ADAM22, CASK, ATP2B2,	1.19747843	0.6817252

				ADD3, GLG1, MTDH, ADD2, ABHD16A, AIFM1, MADD, CSPG5, TLN2, DLGAP2, CLASP2		
TOPO_DOM:Extracellular	5	14.7058824	0.43746937	NRXN1, ADAM22, CSPG5, ATP2B2, GLG1	1.44139654	0.97222222
KW-1133~Transmembrane helix	10	29.411764	0.59614453	ATP8A1, ABHD16A, AIFM1, NRXN1, ADAM22, CSPG5, CASK, ATP2B2, GLG1, MTDH	1.05279943	1
TRANSMEM:Helical	10	29.411764	0.60718802	ATP8A1, ABHD16A, AIFM1, NRXN1, ADAM22, CSPG5, CASK, ATP2B2, GLG1, MTDH	1.04647556	0.97222222
GO:0016021~integral component of membrane	10	29.411764	0.68221723	ATP8A1, ABHD16A, AIFM1, NRXN1, MADD,	0.99076631	0.9869281

				ADAM22, CASK, ATP2B2, GLG1, MTDH		
KW-0812~Transmembrane	10	29.4117647	0.70835624	ATP8A1, ABHD16A, AIFM1, NRXN1, ADAM22, CSPG5, CASK, ATP2B2, GLG1, MTDH	0.97505743	1

SECTION 2- 20% DIFFERENTIAL REGULATION THRESHOLD RESULTS

1. **<u>Gene Ontology-Biological Process</u>**

Wild-Type Basal v. Wild-Type Memory Retrieval- 20% Upregulated

Table 42. DAVID Gene Ontology output table for enriched biological processes within proteins upregulated in WT mice during memory retrieval, when compared to WT mice at the basal level.

Term	Count	%	PValue	Genes	Fold Enrichment	FDR
GO:0042776~ mitochondrial ATP synthesis coupled	14	9.79021	6.56E-06	NDUFA7, NDUFA6, NDUFA5, NDUFB6, NDUFB4, NDUFA2, NDUFB2, ATP5K,	4.353199	6.53E-03

proton transport				NDUFB1, ATP5H, ATP5O, NDUFS5, NDUFS4, NDUFV2		
GO:0009060~aerobic respiration	12	8.391608	5.89E-05	NDUFA7, NDUFA6, NDUFB6, NDUFA5, UQCRB, NDUFB4, NDUFS5, NDUFA2, NDUFS4, NDUFB2, NDUFB1, NDUFV2	4.197727	2.60E-02
GO:0042744~hydrogen peroxide catabolic process	6	4.195804	7.85E-05	PRDX3, PRDX2, PRDX5, PRDX1, HBB-BS, PRDX6	10.49432	0.026023
GO:0034599~cellular response to oxidative stress	7	4.895105	5.04E-04	PRDX3, PRDX2, PRDX5, GSR, PARK7, PPIA, SNCA	6.121686	0.125269
GO:0045454~cell redox homeostasis	6	4.195804	8.79E-04	PRDX3, PRDX2, PRDX5, PRDX1, GSR, PRDX6	6.996212	0.174867
GO:0032981~mitochondrial respiratory chain complex I assembly	9	6.293706	0.001944	NDUFA6, NDUFB6, NDUFA5, NDUFB4, NDUFS5, NDUFA2, NDUFS4, NDUFB2, NDUFB1	3.703877	0.322424
GO:0006979~response to oxidative stress	9	6.293706	0.002372	PRDX3, PRDX2, PRDX5, NDUFA6, NDUFB4, PRDX1, PEBP1, PARK7, PRDX6	3.598052	0.337193
GO:0010499~proteasomal ubiquitin-independent protein catabolic process	5	3.496503	0.013839	PSMA6, PSMA3, PSMB2, PSMA7, PSMA8	4.997294	0.997994
GO:0006301~postreplication repair	3	2.097902	0.014286	UBE2N, UBE2V2, UBE2V1	13.99242	0.997994

GO:0006123~mitochondrial electron transport, cytochrome c to oxygen	4	2.797203	0.014996	CYCS, COX7A2, COX6A1, COX5A	6.996212	0.997994
GO:0051014~actin filament severing	3	2.097902	0.027248	CFL2, CFL1, DSTN	10.49432	0.997994
GO:0042743~hydrogen peroxide metabolic process	3	2.097902	0.027248	PRDX2, CYCS, PARK7	10.49432	0.997994
GO:0030043~actin filament fragmentation	3	2.097902	0.027248	CFL2, CFL1, DSTN	10.49432	0.997994
GO:0051092~positive regulation of NF-kappaB transcription factor activity	5	3.496503	0.027872	PRDX3, PSMA6, UBE2N, UBE2V1, PPIA	4.115419	0.997994
GO:0051603~proteolysis involved in cellular protein catabolic process	5	3.496503	0.033917	PSMA6, PSMA3, PSMB2, PSMA7, PSMA8	3.886785	0.997994
GO:0010498~proteasomal protein catabolic process	5	3.496503	0.040666	PSMA6, PSMA3, PSMB2, PSMA7, PSMA8	3.682217	0.997994
GO:0030836~positive regulation of actin filament depolymerization	3	2.097902	0.04332	CFL2, CFL1, DSTN	8.395455	0.997994

GO:0070534~ protein K63-linked ubiquitination	3	2.097902	0.04332	UBE2N, UBE2V2, UBE2V1	8.395455	0.997994
GO:0021766~ hippocampus development	5	3.496503	0.056289	YWHAE, UQCRQ, NEFL, PEBP1, NME1	3.33153	0.997994
GO:0043161~ proteasome-mediated ubiquitin-dependent protein catabolic process	8	5.594406	0.064647	PSMA6, NSFL1C, PSMA3, PSMD4, PSMB2, PCBP2, PSMA7, PSMA8	2.19489	0.997994
GO:0001933~ negative regulation of protein phosphorylation	5	3.496503	0.084917	MYADM, PEBP1, PARK7, PPIA, SNCA	2.915088	0.997994

APPtg Basal v. APPtg Memory Retrieval- 20% Upregulated

Table 43. DAVID Gene Ontology output table for enriched biological processes within proteins upregulated in APPtg mice during memory retrieval, when compared to APPtg mice during basal levels.

Term	Count	%	PValue	Genes	Fold Enrichment	FDR
GO:0042776~ mitochondrial ATP synthesis coupled proton transport	15	14.70588	2.07E-08	NDUFA8, NDUFB7, NDUFA5, NDUFB10, NDUFA2, NDUFB3, ATP5K, NDUFB1, ATP5H, ATP5O, SDHB, ATP5L, NDUFS5, NDUFS4, NDUFV2	6.282313	1.40E-05

GO:0009060~aerobic respiration	13	12.7451	3.68E-07	NDUFA8, NDUFB7, NDUFA5, UQCRB, NDUFB10, NDUFA2, NDUFB3, NDUFB1, UQCR10, SDHB, NDUFS5, NDUFS4, NDUFV2	6.125255	1.24E-04
GO:0032981~mitochondrial respiratory chain complex I assembly	9	8.823529	2.53E-04	NDUFA8, NDUFB7, NDUFB10, NDUFA5, NDUFS5, NDUFA2, NDUFS4, NDUFB3, NDUFB1	4.988896	0.0569
GO:0000302~response to reactive oxygen species	4	3.921569	0.006486	PRDX1, SOD2, PRDX6, SOD1	9.423469	0.845091
GO:0008206~bile acid metabolic process	3	2.941176	0.007912	SCP2, ACAA1B, ACAA1A	18.84694	0.845091
GO:0006122~mitochondrial electron transport, ubiquinol to cytochrome c	4	3.921569	0.009362	UQCRB, UQCRQ, CYCS, UQCR10	8.376417	0.845091
GO:0046034~ATP metabolic process	6	5.882353	0.009822	AK1, ATP5K, AK4, ATP5H, ATP5O, ATP5L	4.349294	0.845091
GO:0051092~positive regulation of NF-kappaB transcription factor activity	5	4.901961	0.010031	MTPN, PSMA6, UBE2N, PPIA, CLU	5.543217	0.845091
GO:0022904~respiratory electron transport chain	4	3.921569	0.01287	NDUFA5, NDUFS4, SOD2, SDHB	7.538776	0.937734
GO:0019430~removal of	3	2.941176	0.015283	PRDX1, SOD2, SOD1	14.1352	0.937734

superoxide radicals						
GO:0043161~ proteasome-mediated ubiquitin-dependent protein catabolic process	8	7.843137	0.015304	PSMA5, PSMA6, NSFL1C, PSMD6, PSMC6, PSMD7, PSMA1, PSMA2	2.956383	0.937734
GO:0015986~ ATP synthesis coupled proton transport	4	3.921569	0.01703	ATP5K, ATP5H, ATP5O, ATP5L	6.853432	0.956528
GO:0045333~cellular respiration	4	3.921569	0.021855	UQCRB, UQCRQ, NDUFS4, UQCR10	6.282313	1
GO:0010499~ proteasomal ubiquitin-independent protein catabolic process	4	3.921569	0.033507	PSMA5, PSMA6, PSMA1, PSMA2	5.38484	1
GO:0022900~ electron transport chain	3	2.941176	0.035656	NDUFA4, NDUFS4, NDUFB3	9.423469	1
GO:1902600~ hydrogen ion transmembrane transport	5	4.901961	0.049521	ATP6V1G1, ATP6V1G2, UQCRQ, NDUFA4, ATP6V1E1	3.490174	1
GO:0090141~ positive regulation of mitochondrial fission	3	2.941176	0.062149	FIS1, PGAM5, MCU	7.067602	1
GO:0042744~ hydrogen peroxide	3	2.941176	0.062149	PRDX5, PRDX1, PRDX6	7.067602	1

catabolic process						
GO:0006123~ mitochondrial electron transport, cytochrome c to oxygen	3	2.941176	0.062149	CYCS, COX6C, COX6A1	7.067602	1
GO:0051603~ proteolysis involved in cellular protein catabolic process	4	3.921569	0.064575	PSMA5, PSMA6, PSMA1, PSMA2	4.188209	1
GO:0010498~ proteasomal protein catabolic process	4	3.921569	0.073858	PSMA5, PSMA6, PSMA1, PSMA2	3.967777	1
GO:0051881~regulation of mitochondrial membrane potential	3	2.941176	0.093321	NDUFS4, SOD2, SOD1	5.654082	1

Wild-Type Basal v. APPtg Basal- 20% Upregulated

Table 44. DAVID Gene Ontology output table for enriched biological processes within proteins upregulated in APPtg mice at the basal level, when compared to WT mice at the basal level.

Term	Count	%	PValue	Genes	Fold Enrichment	FDR
GO:0006897~endocytosis	11	7.971014	7.25E-03	APP, EHD3, DBNL, MYO6, ITSN1, HIP1R, EPS15L1, TLN2,	2.604744	1.00E+00

				PIP5K1C, SYNJ2BP, EPN1		
GO:0009156~ribonucleoside monophosphate biosynthetic process	3	2.173913	1.39E-02	PRPS2, PRPS1, PRPS1L3	14.20769	1.00E+00
GO:0048477~oogenesis	3	2.173913	1.39E-02	SRC, HEXB, FMN2	14.20769	1
GO:0035249~synaptic transmission, glutamatergic	5	3.623188	0.016941	GRM2, UNC13A, CACNB4, TNR, GRIN1	4.735897	1
GO:0007268~chemical synaptic transmission	10	7.246377	0.018832	GRM2, UNC13A, CACNB4, NRXN1, MYO6, KCNMA1, SYNJ2BP, CACNA1E, PAFAH1B1, GRIN1	2.408083	1
GO:0007628~adult walking behavior	5	3.623188	0.021391	ABHD12, EPHA4, CACNB4, KCNMA1, SCN1A	4.439904	1
GO:0050885~neuromuscular process controlling balance	6	4.347826	0.026277	APP, HEXB, NRXN1, KCNMA1, TNR, PAFAH1B1	3.409846	1
GO:0036035~osteoclast development	3	2.173913	0.026459	ATP6AP1, SRC, PAFAH1B1	10.65577	1
GO:1900454~positive regulation of long term synaptic depression	3	2.173913	0.026459	APP, IQSEC2, PPP1R9A	10.65577	1
GO:0006015~5-phosphoribose 1-diphosphate biosynthetic process	3	2.173913	0.026459	PRPS2, PRPS1, PRPS1L3	10.65577	1
GO:0014047~glutamate secretion	3	2.173913	0.026459	GRM2, GJA1, MYO6	10.65577	1

GO:1902961~positive regulation of aspartic-type endopeptidase activity involved in amyloid precursor protein catabolic process	3	2.173913	0.026459	APP, EPHA4, ROCK2	10.65577	1
GO:0051968~positive regulation of synaptic transmission, glutamatergic	5	3.623188	0.026495	CACNG8, IQSEC2, NRXN1, TNR, GRIN1	4.178733	1
GO:2000300~regulation of synaptic vesicle exocytosis	6	4.347826	0.030762	RIMS1, CACNB4, MYO6, CSPG5, CASK, PPFIA2	3.278698	1
GO:1900272~negative regulation of long-term synaptic potentiation	3	2.173913	0.042097	APP, EPHA4, PPP1R9A	8.524615	1
GO:0008344~adult locomotory behavior	5	3.623188	0.045863	GRM2, APP, ADAM22, PAFAH1B1, GRIN1	3.551923	1
GO:0019722~calcium-mediated signaling	4	2.898551	0.045971	APP, RYR2, PPP1R9A, PPP1R9B	4.735897	1
GO:0070059~intrinsic apoptotic signaling pathway in response to endoplasmic reticulum stress	3	2.173913	0.060297	BRSK2, AIFM1, ITPR1	7.103846	1
GO:0009116~nucleoside metabolic process	3	2.173913	0.060297	PRPS2, PRPS1, PRPS1L3	7.103846	1
GO:0007155~cell adhesion	11	7.971014	0.072063	BCAN, APP, EPHA4, SRC, PCDHGC5, NRXN1, TNR, TLN2, PIP5K1C, PCDH1, HAPLN1	1.817263	1
GO:0016081~synaptic vesicle docking	3	2.173913	0.08063	RIMS1, UNC13A, PPFIA3	6.089011	1

GO:0007269~neurotransmitter secretion	5	3.623188	0.081195	RIMS1, GRM2, UNC13A, NRXN1, PPFIA3	2.959936	1
GO:0051897~positive regulation of protein kinase B signaling	4	2.898551	0.081644	SRC, NRXN1, ITSN1, MTDH	3.788718	1
GO:0061003~positive regulation of dendritic spine morphogenesis	4	2.898551	0.095548	ACTR2, DBNL, CASK, PAFAH1B1	3.551923	1

Wild-Type Memory Retrieval v. APPtg Memory Retrieval- 20% Upregulated

No results.

Wild-Type Basal v. Wild-Type Memory Retrieval- 20% Downregulated

Table 45. DAVID Gene Ontology output table for enriched biological processes within proteins downregulated in WT mice during memory retrieval, when compared to WT mice at the basal level.

Term	Count	%	PValue	Genes	Fold Enrichment	FDR
GO:0046488~phosphatidylinositol metabolic process	3	6	1.13E-02	SYNJ1, PIP5K1C, PLCB1	17.20807	1.00E+00
GO:0016081~synaptic vesicle docking	3	6	1.13E-02	RIMS1, UNC13A, PPFIA3	17.20807	1.00E+00
GO:0007269~neurotransmitter secretion	4	8	1.91E-02	RIMS1, UNC13A, PPFIA3, SNAP91	6.692029	1
GO:0098974~postsynaptic actin cytoskeleton organization	3	6	4.39E-02	ROCK2, PPP1R9A, DBN1	8.604037	1
GO:0016082~synaptic vesicle priming	3	6	4.98E-02	RIMS1, UNC13A, SYNJ1	8.030435	1

GO:0030833~regulation of actin filament polymerization	3	6	0.062611	CYFIP2, PPP1R9A, DBN1	7.085678	1
GO:1903140~regulation of establishment of endothelial barrier	2	4	0.071363	ROCK2, PLCB1	26.76812	1
GO:0031915~positive regulation of synaptic plasticity	2	4	0.071363	UNC13A, DBN1	26.76812	1
GO:0035556~intracellular signal transduction	5	10	0.084205	UNC13A, ROCK2, WNK2, PLCB1, ADCY5	2.909578	1
GO:0006099~tricarboxylic acid cycle	3	6	0.098555	OGDHL, ACO2, SDHA	5.475296	1

APPtg Basal v. APPtg Memory Retrieval- 20% Downregulated

Table 46. DAVID Gene Ontology output table for enriched biological processes within proteins downregulated in APPtg mice during memory retrieval, when compared to APPtg mice at the basal level.

Term	Count	%	PValue	Genes	Fold Enrichment	FDR
GO:0035654~cargo loading into clathrin-coated vesicle, AP-3-mediated	3	20	3.18E-04	AP3D1, AP3S1, AP3B2	92.35	2.40E-02
GO:0016183~synaptic vesicle coating	3	20	3.18E-04	AP3D1, AP3S1, AP3B2	92.35	2.40E-02
GO:0048490~anterograde synaptic vesicle transport	3	20	5.27E-04	AP3D1, AP3S1, AP3B2	73.88	0.02652
GO:0046907~intracellular transport	3	20	0.001456	AP3D1, AP3S1, AP3B2	46.175	0.043976
GO:0036465~synaptic vesicle recycling	3	20	0.001456	AP3D1, AP3S1, AP3B2	46.175	0.043976

GO:0008089~anterograde axonal transport	3	20	0.00232	AP3D1, AP3S1, AP3B2	36.94	0.058388
GO:0006886~intracellular protein transport	4	26.66667	0.031742	AP3D1, VPS26A, AP3S1, AP3B2	5.184561	0.613408
GO:0060155~platelet dense granule organization	2	13.33333	0.037369	AP3D1, AP3S1	49.25333	0.613408
GO:1903232~melanosome assembly	2	13.33333	0.037369	AP3D1, AP3S1	49.25333	0.613408
GO:0005975~carbohydrate metabolic process	3	20	0.043865	GSK3A, HEXB, PDK1	8.208889	0.613408
GO:0006896~Golgi to vacuole transport	2	13.33333	0.044685	AP3D1, AP3S1	41.04444	0.613408
GO:0045944~positive regulation of transcription from RNA polymerase II promoter	3	20	0.067152	GSK3A, HEXB, AP3D1	6.480702	0.844994
GO:0090090~negative regulation of canonical Wnt signaling pathway	2	13.33333	0.094472	GSK3A, SCYL2	18.94359	1

Wild-Type Basal v. APPtg Basal- 20% Downregulated

Table 47. DAVID Gene Ontology output table for enriched biological processes within proteins downregulated in APPtg mice at the basal level, when compared to WT mice at the basal level.

Term	Count	%	PValue	Genes	Fold Enrichment	FDR
GO:0006123~mitochondrial electron transport, cytochrome c to oxygen	4	2.352941	0.022208824	COX7A2, COX5B, COX6A1, COX5A	6.139068	1.00E+00

GO:0031584 ~activation of phospholipase D activity	3	1.764706	0.028009446	GNA13, MARCKS, HPCA	10.35968	1.00E+00
GO:0006979 ~response to oxidative stress	7	4.117647	0.050863059	ALAD, PRDX3, PSMB5, PRDX1, APOE, PARK7, PPID	2.544482	1
GO:0090314 ~positive regulation of protein targeting to membrane	4	2.352941	0.061184405	FIS1, HPCA, MFF, HRAS	4.250124	1
GO:0030168 ~platelet activation	3	1.764706	0.063639986	GNA13, RAP2B, PDIA6	6.906452	1
GO:0006165 ~nucleoside diphosphate phosphorylation	3	1.764706	0.063639986	AK1, CMPK1, AK4	6.906452	1
GO:0009142 ~nucleoside triphosphate biosynthetic process	3	1.764706	0.063639986	AK1, CMPK1, AK4	6.906452	1
GO:0007266 ~Rho protein signal transduction	4	2.352941	0.073894507	GNA13, RHOG, CDH13, BAIAP2	3.946544	1
GO:0000266 ~mitochondrial fission	3	1.764706	0.084975852	FIS1, MTFP1, MFF	5.919816	1
GO:0090141 ~positive regulation of mitochondrial fission	3	1.764706	0.084975852	FIS1, PGAM5, MFF	5.919816	1
GO:0032482 ~Rab protein	3	1.764706	0.084975852	RAB21, RAB35, RAB39B	5.919816	1

signal transduction						
GO:0006139 ~nucleobase-containing compound metabolic process	3	1.764706	0.084975852	AK1, CMPK1, AK4	5.919816	1
GO:0007005 ~mitochondrion organization	6	3.529412	0.092411508	PRDX3, MARCKS, MTFP1, MTX2, PARK7, HSD17B10	2.437571	1
GO:0006631 ~fatty acid metabolic process	8	4.705882	0.095550598	HADHB, ACADVL, NDUFS6, DBI, ACAA1A, HSD17B10, DECR1, SNCA	2.00915	1

Wild-type Memory Retrieval v. APPtg Memory Retrieval- 20% Downregulated

Table 48. DAVID Gene Ontology output table for enriched biological processes within proteins downregulated in APPtg mice during memory retrieval, when compared to WT mice during memory retrieval.

Term	Count	%	PValue	Genes	Fold Enrichment	FDR
GO:0071456~cellular response to hypoxia	2	40	2.54E-02	NDRG1, SIRT2	62.43721	1.00E+00
GO:0008285~negative regulation of cell proliferation	2	40	8.29E-02	NDRG1, SIRT2	18.6877	1.00E+00

2. Gene Ontology- Cellular Component

Wild-Type Basal v. Wild-Type Memory Retrieval- 20% Upregulated

Table 49. DAVID Gene Ontology output table for enriched cellular components within proteins upregulated in WT mice during memory retrieval, when compared to WT mice at the basal level.

Term	Count	%	PValue	Genes	Fold Enrichment	FDR
GO:0070469~respiratory chain	14	9.79021	2.86E-06	NDUFA7, NDUFA6, NDUFA5, UQCRB, NDUFB6, NDUFA4, NDUFA2, NDUFB2, NDUFB1, UQCRQ, NDUFS5, NDUFS4, CYCS, NDUFV2	4.654321	7.83E-04
GO:0005747~mitochondrial respiratory chain complex I	12	8.391608	7.82E-06	NDUFA7, NDUFA6, NDUFB6, NDUFA5, NDUFA4, NDUFB4, NDUFS5, NDUFA2, NDUFS4, NDUFB2, NDUFB1, NDUFV2	5.077441	1.07E-03
GO:0031966~mitochondrial membrane	12	8.391608	8.92E-04	SLC25A27, NDUFA6, NDUFB6, NDUFA4, FAM162A, NDUFA2, CFL1, COX7A2, ABCB8, COX6A1,	3.161426	8.14E-02

				COX5A, COX6B1		
GO:0043209~myelin sheath	23	16.08392	1.51E-03	NAPB, CNRIP1, PEBP1, ATP5H, ATP5O, COX6A1, NDRG1, COX5A, NAPG, GFAP, NME1, PRDX3, PRDX2, RAP1A, PRDX1, CYCS, NEFL, MBP, TAGLN3, TPPP, NDUFV2, INA, PPIA	1.994709	0.103405
GO:0005743~mitochondrial inner membrane	25	17.48252	0.00297	SLC27A1, UQCRB, NDUFB6, NDUFB4, NDUFB2, ATP5K, NDUFB1, COX7A2, ABCB8, ATP5H, ATP5O, COX6A1, COX5A, NDUFV2, SNCA, NDUFA7, NDUFA6, APOOL, NDUFA5, NDUFA4, NDUFA2, COX6B1, UQCRQ,	1.827613	0.162782

				NDUFS5, NDUFS4		
GO:0005739~mitochondrion	52	36.36364	0.005253	YWHAE, SLC27A1, PEBP1, PARK7, COX6A1, HINT2, SCP2, FAM162A, ATP6V1E1, DYNLL1, YWHAZ, NME1, COX6B1, NDUFS5, NDUFS4, ALDOC, NDUFB6, UQCRB, RAB1B, NDUFB4, ATP5K, NDUFB2, NDUFB1, COX7A2, ABCB8, ATP5H, ATP5O, COX5A, NAPG, SLC25A27, PRDX3, PRDX2, PRDX5, PRDX1, TPPP, NDUFV2, SNCA, NIPSNAP3B, FIS1, NDUFA7, NDUFA6, APOOL, NDUFA5, NDUFA4, MTX2, GSR,	1.380369	0.212959

				NDUFA2, PRDX6, RAB11A, RAB11B, UQCRQ, CYCS		
GO:0005751~mitochondrial respiratory chain complex IV	5	3.496503	0.005441	NDUFA4, COX7A2, COX6A1, COX5A, COX6B1	6.346801	0.212959
GO:0005839~proteasome core complex	5	3.496503	0.013956	PSMA6, PSMA3, PSMB2, PSMA7, PSMA8	4.986772	0.459564
GO:0019773~proteasome core complex, alpha-subunit complex	4	2.797203	0.015095	PSMA6, PSMA3, PSMA7, PSMA8	6.981481	0.459564
GO:0000502~proteasome complex	7	4.895105	0.025892	PSMA6, PSMA3, PSMD4, PSMB2, TXNL1, PSMA7, PSMA8	2.961841	0.709428
GO:0005634~nucleus	44	30.76923	0.064353	YWHAE, PARK7, NDRG1, PSMA7, NUDT3, PSMA8, PURB, PURA, PRDX5, PSMB2, CSRP1, PSMD4, SCP2, ARHGDIA, CFL2, PRDX1, PCBP1, CFL1,	1.24872	0.992754

				PCBP2, MBP, TPPP, SNCA, CBR1, DUSP3, TPI1, TXNL1, SGTA, ARPC5, DYNLL1, YWHAZ, PRDX6, NME1, PSMA6, NSFL1C, PSMA3, TMX4, FABP5, UBE2N, UBE2V2, CYCS, UBE2V1, MAPT, TAGLN3, PPIA		
GO:0005882~intermediate filament	4	2.797203	0.099582	NEFL, INA, GFAP, NME1	3.490741	0.992754

APPtg Basal v. APPtg Memory Retrieval- 20% Upregulated

Table 50. DAVID Gene Ontology output table for enriched cellular components within proteins upregulated in APPtg mice during memory retrieval, when compared to APPtg mice at the basal level.

Term	Count	%	PValue	Genes	Fold Enrichment	FDR
GO:0070469~respiratory chain	15	14.70588	7.60E-09	NDUFA8, NDUFB7, NDUFA5, UQCRB, NDUFB10, NDUFA4, NDUFA2, NDUFB3, NDUFB1, UQCR10, UQCRQ,	6.732143	1.81E-06

				NDUFS5, NDUFS4, CYCS, NDUFV2		
GO:0005747~mitochondrial respiratory chain complex I	11	10.78431	3.43E-06	NDUFA8, NDUFB7, NDUFB10, NDUFA5, NDUFA4, NDUFS5, NDUFA2, NDUFS4, NDUFB3, NDUFB1, NDUFV2	6.283333	4.08E-04
GO:0005743~mitochondrial inner membrane	26	25.4902	6.87E-06	NDUFB7, UQCRB, NDUFB10, NDUFB3, ATP5K, NDUFB1, UQCR10, ATP5H, ATP5O, COX6A1, CLU, ATP5L, NDUFV2, NDUFA8, NDUFA5, NDUFA4, NDUFA2, TIMM44, COX6C, SOD2, SDHB, COX6B1, UQCRQ, NDUFS5, NDUFS4, MCU	2.565969	5.45E-04
GO:0005739~mitochondrion	47	46.07843	4.02E-05	NDUFB7, UQCRB, NDUFB10, NDUFB3, CISD1, ATP5K, NDUFB1, ACAA1B, AK4, ACAA1A, UQCR10, ATP5H, ATP5O, COX6A1, CLU, ATP5L, PGRMC1, PRDX5, COMTD1, HINT2, SCP2, PRDX1, CKB, ATP6V1E1, NDUFV2, FIS1, NDUFA8, NDUFA5, NDUFA4, MTX2, NDUFA2, TIMM44, COX6C, DYNLL1, SOD2, SDHB, PRDX6, SOD1, COX6B1, UQCRQ, NDUFS5, NDUFS4, RAB35, CYCS, GARS, PGAM5, MCU	1.684316	0.00239
GO:0000502~proteasome complex	8	7.843137	0.001232	PSMA5, PSMA6, PSMD6, PSMC6, PSMD7, PSMA1, PSMA2, TXNL1	4.569697	0.05866
GO:0019773~proteasome core complex, alpha-subunit complex	4	3.921569	0.00649	PSMA5, PSMA6, PSMA1, PSMA2	9.425	0.193086
GO:0005782~peroxisomal matrix	4	3.921569	0.00649	PRDX5, SCP2, PRDX1, ACAA1A	9.425	0.193086

GO:0000276~mitochondrial proton-transporting ATP synthase complex, coupling factor F(o)	4	3.921569	0.006499	ATP5K, ATP5H, ATP5O, ATP5L	9.425	0.193086
GO:0005753~mitochondrial proton-transporting ATP synthase complex	4	3.921569	0.012877	ATP5K, ATP5H, ATP5O, ATP5L	7.54	0.340522
GO:0005751~mitochondrial respiratory chain complex IV	4	3.921569	0.017039	NDUFA4, COX6C, COX6A1, COX6B1	6.854545	0.371616
GO:0005777~peroxisome	6	5.882353	0.018039	FIS1, PRDX5, SCP2, ACAA1B, ACAA1A, SOD1	3.77	0.371616
GO:0031966~mitochondrial membrane	8	7.843137	0.018737	NDUFA4, NDUFA2, CFL1, COX6C, COX6A1, SDHB, CLU, COX6B1	2.845283	0.371616
GO:0097418~neurofibrillary tangle	3	2.941176	0.024611	NEFM, MAPT, CLU	11.31	0.450568
GO:0005839~proteasome core complex	4	3.921569	0.033523	PSMA5, PSMA6, PSMA1, PSMA2	5.385714	0.569889
GO:0043209~myelin sheath	15	14.70588	0.037765	SNAP25, ATP5H, SOD2, ATP5O, COX6A1, SOD1, STIP1, PRDX1, CYCS, MBP, NEFM, CKB, TAGLN3, NDUFV2, PPIA	1.756211	0.599207
GO:0045263~proton-transporting ATP synthase complex, coupling factor F(o)	3	2.941176	0.048243	ATP5K, ATP5H, ATP5L	8.078571	0.717618
GO:0005758~mitochondrial intermembrane space	5	4.901961	0.061943	NDUFA8, NDUFB7, NDUFS5, CYCS, SOD1	3.25	0.821904

GO:0005750~mitochondrial respiratory chain complex III	3	2.941176	0.062161	UQCRB, UQCRQ, UQCR10	7.06875	0.821904

Wild-Type Basal v. APPtg Basal- 20% Upregulated

Table 51. DAVID Gene Ontology output table for enriched cellular components within proteins upregulated in APPtg mice at the basal level, when compared to WT mice at the basal level.

Term	Count	%	PValue	Genes	Fold Enrichment	FDR
GO:0032587~ruffle membrane	8	5.797101	5.39E-03	SRC, CDC37, MYO6, TPM1, HIP1R, PIP5K1C, CLASP2, PPP1R9B	3.543233	1.00E+00
GO:0048786~presynaptic active zone	7	5.072464	6.15E-03	APP, UNC13A, SLC32A1, GAD1, TPRGL, PPFIA3, PPFIA2	3.968421	1.00E+00
GO:0014069~postsynaptic density	22	15.94203	1.17E-02	EPHA4, ACTR2, DBNL, SRC, ITPR1, HIP1R, CASK, ADD3, PPP1R9A, DCLK1, PPP1R9B, GRIN1, ADD2, RIMS1, CACNG8, CAPZB, LRRC7, MYO6, ADGRL1, PIP5K1C, DLGAP2, RAPGEF4	1.722677	1.00E+00
GO:0098685~Schaffer collateral - CA1 synapse	11	7.971014	1.44E-02	EPHA4, CACNG8, IQSEC2, CAPZB, ROCK2, NRXN1, MYO6, ITPR1, TNR, CASK, EPN1	2.362155	1
GO:0098978~glutamatergic synapse	28	20.28986	0.02324	ROCK2, SRC, NRXN1, ITSN1, ADAM22, PPP1R9A, ADD2, RIMS1, CACNG8, MYO6, TNR, PIP5K1C, DLGAP2, PPFIA3, PPFIA2, DLGAP4, EPHA4, UNC13A, IQSEC2, AP3D1, GRIN1, BCAN, CACNB4, LRRC7,	1.497517	1

				KCNMA1, CSPG5, ADGRL1, RAPGEF4		
GO:0002189 ~ribose phosphate diphosphokinase complex	3	2.173913	0.026595	PRPS2, PRPS1, PRPS1L3	10.6297	1
GO:0045202 ~synapse	36	26.08696	0.027325	NRXN1, ITSN1, ITPR1, PPP1R9A, HAPLN1, PPP1R9B, SYNPR, RIMS1, GRM2, CACNG8, GPC1, MYO6, DLGAP2, PPFIA3, PPFIA2, DLGAP4, MPST, EPHA4, UNC13A, DBNL, ATP6AP1, SLC32A1, GAD1, CASK, SLC6A11, GRIN1, BCAN, CACNB4, LRRC7, MADD, CSPG5, ADGRL1, TLN2, PABPC1, TPRGL, PAFAH1B1	1.382725	1
GO:0043025 ~neuronal cell body	23	16.66667	0.027426	SH3GLB1, SRC, NRXN1, ITSN1, ITPR1, HIP1R, CASK, SLC1A4, PPP1R9A, CACNA1E, PPP1R9B, GRIN1, SRR, PDE10A, CAPZB, KIF5C, GPC1, MYO6, KCNMA1, DLGAP4, PAFAH1B1, SCN1A, RAPGEF4	1.567199	1
GO:0031012 ~extracellular matrix	5	3.623188	0.032559	BCAN, GPC1, TNR, GLG1, HAPLN1	3.936926	1
GO:0043197 ~dendritic spine	13	9.42029	0.034515	APP, EPHA4, ITSN1, HIP1R, ASAP1, PPP1R9A, PPP1R9B, GRIN1, CAPZB, LRRC7, DLGAP2, PPFIA2, RAPGEF4	1.899465	1
GO:0005905 ~clathrin-coated pit	6	4.347826	0.036081	APP, MYO6, ITSN1, HIP1R, EPS15L1, EPN1	3.149541	1

GO:0005903 ~brush border	5	3.623188	0.039065	CAPZB, MYO6, MYO18A, ADD3, RAPGEF4	3.729719	1
GO:0099056 ~integral component of presynaptic membrane	7	5.072464	0.040419	EPHA4, NRXN1, ADGRL1, SLC6A11, CACNA1E, SCN1A, GRIN1	2.681366	1
GO:0031410 ~cytoplasmic vesicle	21	15.21739	0.048917	SH3GLB1, APP, DBNL, ATP6AP1, SLC32A1, ATP8A1, HEXB, ITSN1, AP1B1, ITPR1, HIP1R, FMN2, ADD2, SYNPR, EHD3, RAB12, MYO6, TPRGL, TECPR1, SCYL2, PPFIA3	1.518528	1
GO:0098831 ~presynaptic active zone cytoplasmic component	4	2.898551	0.057178	RIMS1, UNC13A, IQSEC2, PPFIA3	4.360902	1
GO:0030665 ~clathrin-coated vesicle membrane	3	2.173913	0.060591	DBNL, AP1B1, HIP1R	7.086466	1
GO:0031594 ~neuromuscular junction	7	5.072464	0.062238	APP, EPHA4, UNC13A, NRXN1, SYNJ2BP, PPP1R9A, DLGAP4	2.419769	1
GO:0009986 ~cell surface	13	9.420289	0.065644	APP, EPHA4, SLC32A1, NRXN1, SYNJ2BP, CKAP4, GRIN1, BCAN, GPC1, TNR, CSPG5, LRRC8A, PPFIA2	1.721945	1
GO:0098982 ~GABA-ergic synapse	8	5.797101	0.072557	BCAN, RIMS1, SLC32A1, NRXN1, ITPR1, CSPG5, SLC6A11, CACNA1E	2.139311	1
GO:0000139 ~Golgi membrane	9	6.521739	0.074116	SH3GLB1, DBNL, VAPA, RAB12, AP3D1, GNAI3, MYO18A, CSPG5, GLG1	1.993069	1

GO:0097060~synaptic membrane	6	4.347826	0.075955	UNC13A, SRC, ITPR1, HIP1R, CASK, GRIN1	2.576897	1
GO:0005938~cell cortex	8	5.797101	0.078698	ACTR2, DBNL, GAD1, HIP1R, FMN2, ADD3, CLASP2, PAFAH1B1	2.099694	1
GO:0098839~postsynaptic density membrane	5	3.623188	0.092376	EPHA4, CACNG8, IQSEC2, SYNJ2BP, GRIN1	2.834586	1

Wild-Type Memory Retrieval v. APPtg Memory Retrieval- 20% Upregulated

No results.

Wild-Type Basal v. Wild-Type Memory Retrieval- 20% Downregulated

Table 52. DAVID Gene Ontology output table for enriched cellular components within proteins downregulated in WT mice during memory retrieval, when compared to WT mice at the basal level.

Term	Count	%	PValue	Genes	Fold Enrichment	FDR
GO:0005759~mitochondrial matrix	8	16	4.28E-03	HSPA9, OAT, PCX, ABAT, OGDHL, ACADSB, DLD, GLS	3.696078	8.00E-01
GO:0098871~postsynaptic actin cytoskeleton	3	6	2.41E-02	MYO6, PPP1R9A, DBN1	11.78125	1.00E+00
GO:0098978~glutamatergic synapse	13	26	2.49E-02	UNC13A, ROCK2, AP3D1, AKAP5, PPP1R9A, GRM3, RIMS1, SYNJ1, MYO6,	1.926494	1.00E+00

				PIP5K1C, PLCB1, DBN1, PPFIA3		
GO:0098831~presynaptic active zone cytoplasmic component	3	6	3.99E-02	RIMS1, UNC13A, PPFIA3	9.0625	1
GO:0098830~presynaptic endosome	2	4	0.049259	AP3D1, SNAP91	39.27083	1
GO:0043005~neuron projection	10	20	0.073395	GRM3, CYFIP2, MPST, SYNPR, UNC13A, SYNJ1, DCTN1, ABAT, PPP1R9A, SNAP91	1.852398	1
GO:0045252~oxoglutarate dehydrogenase complex	2	4	0.09614	OGDHL, DLD	19.63542	1

APPtg Basal v. APPtg Memory Retrieval- 20% Downregulated

Table 53. DAVID Gene Ontology output table for enriched cellular components within proteins downregulated in APPtg mice during memory retrieval, when compared to APPtg mice at the basal level.

Term	Count	%	PValue	Genes	Fold Enrichment	FDR
GO:0030123~AP-3 adaptor complex	3	20	3.05E-04	AP3D1, AP3S1, AP3B2	94.25	1.86E-02
GO:0030117~membrane coat	3	20	3.24E-03	AP3D1, AP3S1, AP3B2	31.41667	9.89E-02
GO:1904115~axon cytoplasm	3	20	1.62E-02	AP3D1, AP3S1, AP3B2	13.96296	2.63E-01
GO:0005769~early endosome	4	26.66667	1.72E-02	AP3D1, VPS26A, AP3S1, AP3B2	6.528139	0.262844

GO:0010008~endosome membrane	3	20	0.026505	AP3D1, VPS26A, SCYL2	10.77143	0.284109
GO:0005802~trans-Golgi network	3	20	0.027945	AP3D1, AP3S1, AP3B2	10.47222	0.284109
GO:0005794~Golgi apparatus	5	33.33333	0.041683	PACS1, AP3D1, AP3S1, AP3B2, SCYL2	3.378136	0.363235

Wild-Type Basal v. APPtg Basal- 20% Downregulated

Table 54. DAVID Gene Ontology output table for enriched cellular components within proteins downregulated in WT mice at the basal level, when compared to APPtg mice at the basal level.

Term	Count	%	PValue	Genes	Fold Enrichment	FDR
GO:0005743~mitochondrial inner membrane	26	15.29412	3.75E-03	ACADVL, UQCRB, NDUFB6, MTFP1, TIMM9, COX7A2, UQCR10, COX5B, COX6A1, HSD17B10, COX5A, CHCHD3, CHCHD6, SLC25A22, SNCA, NDUFA7, NDUFA5, NDUFA2, IDH2, DHRS1, COQ6, HADHB, UQCRQ, NDUFS6, NDUFS5, PGAM5	1.779523	1.00E+00
GO:0070469~respiratory chain	9	5.294118	9.85E-03	NDUFA7, NDUFB6, NDUFA5, UQCRB, UQCRQ, NDUFS6, NDUFS5, NDUFA2, UQCR10	2.897947	1.00E+00
GO:0032432~actin filament bundle	3	1.764706	1.40E-02	MARCKS, PLS3, CRYAB	14.16774	1.00E+00

GO:0005739 ~mitochondrion	51	30	4.02E-02	ALDH1L1, ACADVL, SLC44A2, DBI, ETFA, PARK7, COX6A1, COMTD1, CHCHD3, HINT2, CHCHD6, C1QBP, ATP6V1E1, ACOT9, HADHB, NDUFS6, NDUFS5, RAB35, PGAM5, CRYAB, PPID, NDUFB6, MTFP1, UQCRB, TIMM9, COX7A2, AK4, ACAA1A, UQCR10, COX5B, MFF, HSD17B10, COX5A, SLC25A27, PRDX3, PRDX1, SLC25A22, DECR1, SNCA, FIS1, NDUFA7, NDUFA5, MTX2, NDUFA2, IDH2, HSPE1, DHRS1, COQ6, QDPR, UQCRQ, OCIAD1	1.261003	1
GO:0005751 ~mitochondrial respiratory chain complex IV	4	2.352941	0.046538	COX7A2, COX5B, COX6A1, COX5A	4.722581	1
GO:0005839 ~proteasome core complex	4	2.352941	0.057473	PSMA3, PSMB5, PSMA1, PSMA7	4.359305	1
GO:0005615 ~extracellular space	12	7.058824	0.060684	ALAD, PCMT1, FABP3, C1QBP, CDH13, CPE, DBI, APOE, NPTXR, PAM, PDIA6, SNCA	1.808648	1
GO:0000502 ~proteasome complex	6	3.529412	0.076583	PSMA3, PSMB5, PSMD7, PSMA1, PSMC1, PSMA7	2.575953	1
GO:0019773 ~proteasome core complex, alpha-subunit complex	3	1.764706	0.081264	PSMA3, PSMA1, PSMA7	6.071889	1

GO:0030125~clathrin vesicle coat	3	1.764706	0.081264	NECAP1, CLTB, CLTA	6.071889	1
GO:0005747~mitochondrial respiratory chain complex I	6	3.529412	0.084938	NDUFA7, NDUFB6, NDUFA5, NDUFS6, NDUFS5, NDUFA2	2.50019	1

Wild-Type Memory Retrieval v. APPtg Memory Retrieval - 20% Downregulated

Table 55. DAVID Gene Ontology output table for enriched cellular components within proteins downregulated in APPtg mice during memory retrieval, when compared to WT mice during memory retrieval.

Term	Count	%	PValue	Genes	Fold Enrichment	FDR
GO:0048471~perinuclear region of cytoplasm	3	60	4.31E-03	PAM, NDRG1, SIRT2	19.51195	2.07E-01
GO:0043209~myelin sheath	2	40	2.69E-02	NDRG1, SIRT2	55.28385	4.90E-01
GO:0043204~perikaryon	2	40	3.06E-02	PAM, SIRT2	48.46804	4.90E-01
GO:0005874~microtubule	2	40	5.04E-02	NDRG1, SIRT2	29.24105	0.604776
GO:0098978~glutamatergic synapse	2	40	0.071971	NDRG1, SIRT2	20.33429	0.604776
GO:0005813~centrosome	2	40	0.075597	NDRG1, SIRT2	19.33424	0.604776

3. <u>Gene Ontology- Molecular Function</u>

Wild-Type Basal v. WT Memory Retrieval - 20% Upregulated

Table 56. DAVID Gene Ontology output table for enriched molecular function within proteins upregulated in WT mice during memory retrieval, when compared to WT mice at the basal level.

Term	Count	%	PValue	Genes	Fold Enrichment	FDR
GO:0051920~peroxiredoxin activity	6	4.195804	7.94E-06	PRDX3, PRDX2, PRDX5, PRDX1, PARK7, PRDX6	14.47154	0.002683
GO:0004601~peroxidase activity	5	3.496503	6.26E-04	PRDX3, PRDX2, PRDX5, PRDX1, PRDX6	10.33682	0.101003
GO:0016209~antioxidant activity	5	3.496503	0.001186	PRDX3, PRDX2, PRDX5, PRDX1, PRDX6	9.044715	0.101003
GO:0008379~thioredoxin peroxidase activity	4	2.797203	0.001195	PRDX3, PRDX2, PRDX5, PRDX1	14.47154	0.101003
GO:0003697~single-stranded DNA binding	5	3.496503	0.002023	PURB, PURA, PCBP1, PCBP2, NME1	8.039747	0.136722
GO:0044877~macromolecular complex binding	22	15.38462	0.015404	YWHAE, FIS1, UQCRB, NDUFA4, ATP5K, CLTA, HBB-BS, PARK7,	1.675653	0.867782

				ATP5H, DYNLL1, ATP5O, DYNLL2, YWHAZ, SLC9A3R1, RAP1A, SCP2, GNA11, NEFL, ALDOC, MAPT, INA, PAFAH1B2		
GO:0008137~NADH dehydrogenase (ubiquinone) activity	5	3.496503	0.02487	NDUFA7, NDUFA5, NDUFA2, NDUFS4, NDUFV2	4.256337	0.958294
GO:0043027~cysteine-type endopeptidase inhibitor activity involved in apoptotic process	3	2.097902	0.025517	PRDX3, PRDX5, SNCA	10.85366	0.958294
GO:0000981~RNA polymerase II transcription factor activity, sequence-specific DNA binding	3	2.097902	0.025517	PURB, PURA, PCBP1	10.85366	0.958294
GO:0004175~endopeptidase activity	5	3.496503	0.058692	PSMA6, PSMA3, PSMB2, PSMA7, PSMA8	3.288987	1
GO:0042626~ATPase activity, coupled to transmembrane movement of substances	3	2.097902	0.077971	ATP6V1G2, ABCB8, ATP6V1D	6.202091	1
GO:0000977~RNA polymerase II regulatory region sequence-specific DNA binding	3	2.097902	0.077971	PURB, PURA, NME1	6.202091	1
GO:0005507~copper ion binding	3	2.097902	0.077971	PARK7, PAM, SNCA	6.202091	1

GO:0046332~SMAD binding	3	2.097902	0.077971	FKBP1A, PURB, PURA	6.202091	1
GO:0004129~cytochrome-c oxidase activity	3	2.097902	0.077971	COX7A2, COX6A1, COX5A	6.202091	1

APPtg Basal v. APPtg Memory Retrieval - 20% Upregulated

Table 57. DAVID Gene Ontology output table for enriched molecular function within proteins upregulated in APPtg mice during memory retrieval, when compared to APPtg mice at the basal level.

Term	Count	%	PValue	Genes	Fold Enrichment	FDR
GO:0008137~NADH dehydrogenase (ubiquinone) activity	6	5.882353	0.001378	NDUFB7, NDUFB10, NDUFA5, NDUFA2, NDUFS4, NDUFV2	6.613003	0.315491
GO:0016209~antioxidant activity	4	3.921569	0.006583	PRDX5, PRDX1, PRDX6, SOD1	9.368421	0.753719
GO:0046933~proton-transporting ATP synthase activity, rotational mechanism	4	3.921569	0.013056	ATP5K, ATP5H, ATP5O, ATP5L	7.494737	0.884123
GO:0050633~acetyl-CoA C-myristoyltransferase activity	3	2.941176	0.015443	SCP2, ACAA1B, ACAA1A	14.05263	0.884123
GO:0051537~2 iron, 2 sulfur cluster binding	3	2.941176	0.036017	CISD1, NDUFV2, SDHB	9.368421	1
GO:0051920~peroxiredoxin activity	3	2.941176	0.036017	PRDX5, PRDX1, PRDX6	9.368421	1

GO:0003988~acetyl-CoA C-acyltransferase activity	3	2.941176	0.036017	SCP2, ACAA1B, ACAA1A	9.368421	1
GO:0004601~peroxidase activity	3	2.941176	0.048712	PRDX5, PRDX1, PRDX6	8.030075	1
GO:0016747~transferase activity, transferring acyl groups other than amino-acyl groups	3	2.941176	0.048712	SCP2, ACAA1B, ACAA1A	8.030075	1
GO:0051087~chaperone binding	5	4.901961	0.092461	STIP1, DNAJA2, TIMM44, MAPT, SOD1	2.838915	1

Wild-Type Basal v. APPtg Basal - 20% Upregulated

Table 58. DAVID Gene Ontology output table for enriched molecular function within proteins upregulated in APPtg mice at the basal level, when compared to WT mice at the basal level.

Term	Count	%	PValue	Genes	Fold Enrichment	FDR
GO:0030246~carbohydrate binding	8	5.797101	0.004063	PRPS2, BCAN, PRPS1, AGL, HEXB, ADGRL1, PYGM, GLG1	3.708333	1
GO:0051015~actin filament binding	13	9.42029	0.009386	ACTR2, DBNL, TPM1, HIP1R, ADD3, PPP1R9A, ACTR3B, PPP1R9B, ADD2, MYO6, MYO18A, TLN2, CLASP2	2.259766	1

GO:0008022~protein C-terminus binding	11	7.971014	0.016221	DBNL, PABPC6, LRRC7, SRC, CDC37, ITPR1, CASK, PABPC1, SYNJ2BP, PPP1R9A, PPP1R9B	2.317708	1
GO:0005262~calcium channel activity	6	4.347826	0.024145	RYR2, CACNG8, CACNB4, ITPR1, CACNA1E, GRIN1	3.476563	1
GO:0005524~ATP binding	28	20.28986	0.027279	PRPS2, PRPS1, BRSK2, ATP8A1, ROCK2, SRC, ACTR3B, SRR, HSPH1, MTHFD1L, KIF5C, MYO6, MYO18A, PIP5K1C, STK32C, SCYL2, PRPS1L3, CCT4, CCT3, EPHA4, ACTR2, ATP6AP1, GK, CASK, BCS1L, DCLK1, EHD3, UBE2O	1.474905	1
GO:0004749~ribose phosphate diphosphokinase activity	3	2.173913	0.027552	PRPS2, PRPS1, PRPS1L3	10.42969	1
GO:0005102~receptor binding	9	6.521739	0.041686	APP, GJA1, MECR, SRC, NRXN1, TNR, CASK, SCYL2, GRIN1	2.234933	1
GO:0005216~ion channel activity	6	4.347826	0.050721	RYR2, KCNMA1, ITPR1, CACNA1E, SCN1A, GRIN1	2.877155	1

GO:0003779~actin binding	13	9.42029	0.069157	ACTR2, DBNL, TPM1, HIP1R, FMN2, ADD3, ACTR3B, PPP1R9B, ADD2, CAPZB, MYO6, KCNMA1, TLN2	1.705483	1
GO:0030170~pyridoxal phosphate binding	4	2.898551	0.072333	SRR, OAT, GAD1, PYGM	3.973214	1
GO:0030276~clathrin binding	5	3.623188	0.075976	TOM1L2, AP1B1, HIP1R, TLN2, EPN1	3.023098	1
GO:0016208~AMP binding	3	2.173913	0.083714	PRPS2, PRPS1, PYGM	5.959821	1
GO:0005244~voltage-gated ion channel activity	5	3.623188	0.09736	CACNG8, CACNB4, KCNMA1, CACNA1E, SCN1A	2.78125	1

Wild-Type Memory Retrieval v. APPtg Memory Retrieval - 20% Upregulated

Table 59. DAVID Gene Ontology output table for enriched molecular function within proteins upregulated in APPtg mice during memory retrieval, when compared to WT mice during memory retrieval.

Term	Count	%	PValue	Genes	Fold Enrichment	FDR
GO:0042802~identical protein binding	3	75	9.56E-02	APP, PSMC6, PIP4K2C	3.921533	1

Wild-Type Basal v. Wild-Type Memory Retrieval - 20% Downregulated

Table 60. DAVID Gene Ontology output table for enriched molecular function within proteins downregulated in WT mice during memory retrieval, when compared to WT mice at the basal level.

Term	Count	%	PValue	Genes	Fold Enrichment	FDR
GO:0030170~pyridoxal phosphate binding	3	6	4.50E-02	OAT, ABAT, PYGM	8.47619	1
GO:0005516~calmodulin binding	5	10	5.23E-02	UNC13A, RASGRF2, MYO6, AKAP5, PLCB1	3.409962	1

APPtg Basal v. APPtg Memory Retrieval - 20% Downregulated

Table 61. DAVID Gene Ontology output table for enriched molecular function within proteins downregulated in APPtg mice during memory retrieval, when compared to APPtg mice at the basal level.

Term	Count	%	PValue	Genes	Fold Enrichment	FDR
GO:0004177~aminopeptidase activity	2	13.33333	0.038733	TPP2, BLMH	46.23377	1
GO:0004672~protein kinase activity	3	20	0.058855	GSK3A, SCYL2, PDK1	6.742424	1

Wild-Type Basal v. APPtg Basal- 20% Downregulated

Table 62. DAVID Gene Ontology output table for enriched molecular function within proteins downregulated in APPtg mice at the basal level, when compared to WT mice at the basal level.

Term	Count	%	PValue	Genes	Fold Enrichment	FDR
GO:0016491~oxidoreductase activity	20	11.76471	0.008529	CBR1, ALDH1L1, ACADVL, CTBP1, IDH2, AKR1A1, COX7A2, ETFA, DHRS1, COX6A1, HSD17B10, COQ6,	1.84955	1

				PRDX3, QDPR, PRDX1, PHGDH, PAM, PCYOX1, DECR1, SNCA		
GO:0019205 ~nucleobase-containing compound kinase activity	3	1.764706	0.045236	AK1, CMPK1, AK4	8.212	1
GO:0019003 ~GDP binding	7	4.117647	0.052689	RAB21, RAP1A, MRAS, RAP2B, RAB35, HRAS, RHOB	2.521228	1
GO:0016616 ~oxidoreductase activity, acting on the CH-OH group of donors, NAD or NADP as acceptor	5	2.941176	0.069925	CBR1, CTBP1, IDH2, PHGDH, DHRS1	3.110606	1
GO:0051920 ~peroxiredoxin activity	3	1.764706	0.086315	PRDX3, PRDX1, PARK7	5.865714	1
GO:0004550 ~nucleoside diphosphate kinase activity	3	1.764706	0.086315	AK1, CMPK1, AK4	5.865714	1

Wild-Type Memory Retrieval v. APPtg Memory Retrieval- 20% Downregulated

No results.

4. <u>KEGG Pathways</u>

Wild-Type Basal v. Wild-Type Memory Retrieval- 20% Upregulated

Table 63. DAVID annotation tools output table of enriched KEGG pathways within proteins upregulated in WT mice during memory retrieval, when compared to WT mice at the basal level.

Term	Count	%	PValue	Genes	Fold Enrichment	FDR
mmu00190:Oxidative phosphorylation	25	17.48252	3.25E-10	UQCRB, NDUFB6, NDUFB4, NDUFB2, ATP5K, COX7A2, ATP5H, ATP5O, COX6A1, COX5A, ATP6V1E1, NDUFV2, ATP6V1D, NDUFA7, NDUFA6, ATP6V1G2, NDUFA5, NDUFA4, NDUFA2, COX6B1, UQCRQ, PPA1, NDUFS5, NDUFS4, CYCS	4.089311	4.78E-08
mmu04932:Non-alcoholic fatty liver disease	18	12.58741	2.73E-07	NDUFA7, NDUFA6, NDUFA5, UQCRB, NDUFB6, NDUFA4, NDUFB4, NDUFA2, NDUFB2, COX7A2, COX6A1, COX5A, COX6B1, UQCRQ, NDUFS5, NDUFS4, CYCS, NDUFV2	4.080702	1.93E-05
mmu05012:Parkinson disease	29	20.27972	3.94E-07	UQCRB, NDUFB6, NDUFB4, NDUFB2, COX7A2, PARK7, ATP5H, ATP5O, COX6A1, COX5A, PSMA7, PSMA8, PSMB2, PSMD4, NDUFV2, SNCA, NDUFA7, NDUFA6, NDUFA5, NDUFA4, NDUFA2, COX6B1, PSMA6, PSMA3, UQCRQ, NDUFS5, NDUFS4, CYCS, MAPT	2.639045	1.93E-05
mmu05014:Amyotrophic lateral sclerosis	29	20.27972	8.60E-07	UQCRB, DCTN2, NDUFB6, NDUFB4, NDUFB2, COX7A2, ATP5H, ATP5O, COX6A1, COX5A, PSMA7, PSMA8, PSMB2, PSMD4, NEFL, NDUFV2, RAB8A, NDUFA7, NDUFA6, NDUFA5, NDUFA4, NDUFA2, COX6B1, PSMA6, PSMA3, UQCRQ, NDUFS5, NDUFS4, CYCS	2.549282	3.16E-05

mmu05016:Huntington disease	29	20.27972	1.16E-06	UQCRB, DCTN2, NDUFB6, NDUFB4, CLTB, NDUFB2, CLTA, COX7A2, ATP5H, ATP5O, COX6A1, COX5A, PSMA7, PSMA8, PSMB2, PSMD4, NDUFV2, NDUFA7, NDUFA6, NDUFA5, NDUFA4, NDUFA2, COX6B1, PSMA6, PSMA3, UQCRQ, NDUFS5, NDUFS4, CYCS	2.515063	3.42E-05
mmu05208:Chemical carcinogenesis - reactive oxygen species	21	14.68531	2.27E-06	CBR1, NDUFA7, NDUFA6, NDUFA5, UQCRB, NDUFB6, NDUFA4, NDUFB4, NDUFA2, NDUFB2, AKR1A1, COX7A2, ATP5H, ATP5O, COX6A1, COX5A, COX6B1, UQCRQ, NDUFS5, NDUFS4, NDUFV2	3.119157	5.57E-05
mmu04714:Thermogenesis	20	13.98601	4.62E-06	NDUFA7, NDUFA6, NDUFA5, UQCRB, NDUFB6, NDUFA4, NDUFB4, NDUFA2, NDUFB2, ATP5K, COX7A2, ATP5H, ATP5O, COX6A1, COX5A, COX6B1, UQCRQ, NDUFS5, NDUFS4, NDUFV2	3.113788	9.70E-05
mmu05010:Alzheimer disease	28	19.58042	5.52E-06	UQCRB, NDUFB6, NDUFB4, NDUFB2, COX7A2, ATP5H, ATP5O, COX6A1, COX5A, PSMA7, PSMA8, PSMB2, PSMD4, NDUFV2, SNCA, NDUFA7, NDUFA6, NDUFA5, NDUFA4, NDUFA2, COX6B1, PSMA6, PSMA3, UQCRQ, NDUFS5, NDUFS4, CYCS, MAPT	2.396174	1.01E-04
mmu05022:Pathways of neurodegeneration - multiple diseases	32	22.37762	1.70E-05	UQCRB, DCTN2, NDUFB6, NDUFB4, NDUFB2, COX7A2, PARK7, ATP5H, ATP5O, COX6A1, COX5A, PSMA7, PSMA8, PSMB2, PSMD4, NEFL, NDUFV2, RAB8A, SNCA, NDUFA7, NDUFA6, NDUFA5, NDUFA4, NDUFA2, COX6B1, PSMA6, PSMA3, UQCRQ, NDUFS5, NDUFS4, CYCS, MAPT	2.08844	2.77E-04

mmu05020:Prion disease	26	18.18182	2.14E-05	UQCRB, NDUFB6, NDUFB4, NDUFB2, COX7A2, ATP5H, ATP5O, COX6A1, COX5A, PSMA7, PSMA8, PSMB2, PSMD4, NDUFV2, NDUFA7, NDUFA6, NDUFA5, NDUFA4, NDUFA2, COX6B1, PSMA6, PSMA3, UQCRQ, NDUFS5, NDUFS4, CYCS	2.349495	3.14E-04
mmu05415:Diabetic cardiomyopathy	20	13.98601	3.27E-05	NDUFA7, NDUFA6, NDUFA5, UQCRB, NDUFB6, NDUFA4, NDUFB4, NDUFA2, GSR, NDUFB2, COX7A2, ATP5H, ATP5O, COX6A1, COX5A, COX6B1, UQCRQ, NDUFS5, NDUFS4, NDUFV2	2.749409	4.37E-04
mmu01100:Metabolic pathways	39	27.27273	0.006946	UQCRB, NDUFB6, NDUFB4, AK1, NDUFB2, ATP5K, COX7A2, HSD17B12, ATP5H, ATP5O, COX6A1, COX5A, SCP2, ATP6V1E1, NDUFV2, ATP6V1D, CBR1, NDUFA7, TPI1, NDUFA6, ATP6V1G2, NDUFA5, NDUFA4, NDUFA2, GSR, AKR1A1, PRDX6, DDOST, ASRGL1, COX6B1, NME1, UQCRQ, PSAT1, NDUFS5, NDUFS4, CYCS, ALDOC, PAFAH1B2, CDS2	1.427668	0.085086
mmu04962:Vasopressin-regulated water reabsorption	6	4.195804	0.026189	DCTN2, ARHGDIA, DYNLL1, DYNLL2, RAB11A, RAB11B	3.371014	0.296143
mmu04723:Retrograde endocannabinoid signaling	12	8.391608	0.029988	NDUFA7, NDUFA6, NDUFB6, NDUFA5, NDUFA4, NDUFB4, GNG7, NDUFS5, NDUFA2, NDUFS4, NDUFB2, NDUFV2	1.988034	0.314879
mmu03050:Proteasome	6	4.195804	0.0643	PSMA6, PSMA3, PSMD4, PSMB2, PSMA7, PSMA8	2.673563	0.630145

APPtg Basal v. APPtg Memory Retrieval- 20% Upregulated

Table 64. DAVID annotation tools output table of enriched KEGG pathways within proteins upregulated in APPtg mice during memory retrieval, when compared to APPtg mice at the basal level.

Term	Count	%	PValue	Genes	Fold Enrichment	FDR
mmu00190: Oxidative phosphorylation	25	24.5098	1.38E-11	NDUFB7, UQCRB, NDUFB10, NDUFB3, ATP5K, UQCR10, ATP5H, ATP5O, COX6A1, ATP5L, ATP6V1E1, NDUFV2, NDUFA8, ATP6V1G1, ATP6V1G2, NDUFA5, NDUFA4, NDUFA2, COX6C, SDHB, COX6B1, UQCRQ, NDUFS5, NDUFS4, CYCS	4.658709	1.42E-09
mmu05016: Huntington disease	31	30.39216	1.96E-09	NDUFB7, UQCRB, NDUFB10, NDUFB3, CLTB, CLTA, UQCR10, ATP5H, ATP5O, COX6A1, PSMD6, PSMD7, NDUFV2, NDUFA8, NDUFA5, NDUFA4, NDUFA2, COX6C, SOD2, SDHB, SOD1, COX6B1, PSMA5, PSMA6, PSMC6, PSMA1, UQCRQ, PSMA2, NDUFS5, NDUFS4, CYCS	3.062866	8.91E-08
mmu05012: Parkinson disease	30	29.41176	2.89E-09	NDUFB7, UQCRB, NDUFB10, NDUFB3, UQCR10, ATP5H, ATP5O, COX6A1, PSMD6, PSMD7, NDUFV2, NDUFA8, NDUFA5, NDUFA4, NDUFA2, COX6C, SDHB, SOD1, COX6B1, PSMA5, PSMA6, PSMC6, PSMA1, UQCRQ, PSMA2, NDUFS5, NDUFS4, CYCS, MAPT, MCU	3.11018	8.91E-08
mmu05020: Prion disease	30	29.41176	3.46E-09	NDUFB7, UQCRB, NDUFB10, NDUFB3, UQCR10, ATP5H, ATP5O, COX6A1, STIP1, PSMD6, PSMD7, NDUFV2, NDUFA8, NDUFA5, NDUFA4, NDUFA2, COX6C, SDHB, SOD1, COX6B1, PSMA5, PSMA6,	3.088431	8.91E-08

				PSMC6, PSMA1, UQCRQ, PSMA2, NDUFS5, NDUFS4, CYCS, MCU		
mmu05208: Chemical carcinogenesis - reactive oxygen species	23	22.54902	6.48E-09	NDUFA8, CBR1, NDUFB7, NDUFA5, UQCRB, NDUFB10, NDUFA4, NDUFA2, NDUFB3, AKR1A1, UQCR10, ATP5H, COX6C, SOD2, ATP5O, COX6A1, SDHB, SOD1, COX6B1, UQCRQ, NDUFS5, NDUFS4, NDUFV2	3.891896	1.20E-07
mmu05014: Amyotrophic lateral sclerosis	30	29.41176	6.98E-09	NDUFB7, UQCRB, NDUFB10, NDUFB3, UQCR10, ATP5H, ATP5O, COX6A1, PSMD6, PSMD7, NEFM, NDUFV2, NDUFA8, NDUFA5, NDUFA4, NDUFA2, COX6C, SDHB, SOD1, COX6B1, PSMA5, PSMA6, PSMC6, PSMA1, UQCRQ, PSMA2, NDUFS5, NDUFS4, CYCS, MCU	3.004392	1.20E-07
mmu04932: Non-alcoholic fatty liver disease	18	17.64706	3.33E-08	NDUFA8, NDUFB7, NDUFA5, UQCRB, NDUFB10, NDUFA4, NDUFA2, NDUFB3, UQCR10, COX6C, COX6A1, SDHB, COX6B1, UQCRQ, NDUFS5, NDUFS4, CYCS, NDUFV2	4.648901	4.89E-07
mmu05010: Alzheimer disease	29	28.43137	6.32E-08	NDUFB7, UQCRB, NDUFB10, NDUFB3, UQCR10, ATP5H, ATP5O, COX6A1, PSMD6, PSMD7, NDUFV2, NDUFA8, NDUFA5, NDUFA4, NDUFA2, COX6C, SDHB, COX6B1, PSMA5, PSMA6, PSMC6, PSMA1, UQCRQ, PSMA2, NDUFS5, NDUFS4, CYCS, MAPT, MCU	2.827312	8.14E-07
mmu04714:Thermogenesis	21	20.58824	9.31E-08	NDUFA8, NDUFB7, NDUFA5, UQCRB, NDUFB10, NDUFA4, NDUFA2, NDUFB3, ATP5K, UQCR10, ATP5H, COX6C, ATP5O, COX6A1, SDHB, ATP5L, COX6B1, UQCRQ, NDUFS5, NDUFS4, NDUFV2	3.724722	1.07E-06

mmu05022: Pathways of neurodegeneration - multiple diseases	31	30.39216	2.21E-06	NDUFB7, UQCRB, NDUFB10, NDUFB3, UQCR10, ATP5H, ATP5O, COX6A1, PSMD6, PSMD7, NEFM, NDUFV2, NDUFA8, NDUFA5, NDUFA4, NDUFA2, COX6C, SDHB, SOD1, COX6B1, PSMA5, PSMA6, PSMC6, PSMA1, UQCRQ, PSMA2, NDUFS5, NDUFS4, CYCS, MAPT, MCU	2.304884	2.28E-05
mmu05415: Diabetic cardiomyopathy	19	18.62745	1.74E-05	NDUFA8, NDUFB7, NDUFA5, UQCRB, NDUFB10, NDUFA4, NDUFA2, NDUFB3, UQCR10, ATP5H, COX6C, ATP5O, COX6A1, SDHB, COX6B1, UQCRQ, NDUFS5, NDUFS4, NDUFV2	2.975626	1.63E-04
mmu01100: Metabolic pathways	37	36.27451	0.001702	NDUFB7, UQCRB, NDUFB10, AK1, NDUFB3, ATP5K, ACAA1B, AK4, ACAA1A, UQCR10, ATP5H, ATP5O, COX6A1, ATP5L, SCP2, CKB, ATP6V1E1, NDUFV2, CBR3, NDUFA8, CBR1, ATP6V1G1, TPI1, ATP6V1G2, NDUFA5, NDUFA4, NDUFA2, AKR1A1, COX6C, SDHB, PRDX6, COX6B1, UQCRQ, PSAT1, NDUFS5, NDUFS4, CYCS	1.543049	0.014346
mmu04146: Peroxisome	7	6.862745	0.001811	PRDX5, SCP2, PRDX1, ACAA1B, ACAA1A, SOD2, SOD1	4.907173	0.014346
mmu03050: Proteasome	7	6.862745	0.010273	PSMA5, PSMA6, PSMD6, PSMC6, PSMD7, PSMA1, PSMA2	3.55347	0.075578
mmu05017:Spinocerebellar ataxia	9	8.823529	0.035031	PSMA5, PSMA6, PSMD6, PSMC6, PSMD7, PSMA1, PSMA2, CYCS, MCU	2.284374	0.240544

Wild-Type Basal v. APPtg Basal- 20% Upregulated

Table 65. DAVID annotation tools output table of enriched KEGG pathways within proteins upregulated in APPtg mice at the basal level, when compared to WT mice at the basal level.

Term	Count	%	PValue	Genes	Fold Enrichment	FDR
mmu05010:Alzheimer disease	27	15.88235	2.12E-05	UQCRB, NDUFB6, COX7A2, UQCR10, KLC1, COX5B, COX6A1, HSD17B10, COX5A, PSMA7, PSMB5, PSMD7, APOE, HRAS, SNCA, NDUFA7, NDUFA5, NDUFA2, CSNK2A2, PSMA3, PSMA1, UQCRQ, NDUFS6, NDUFS5, PSMC1, CALM1, PPID	2.318146	4.22E-03
mmu05208:Chemical carcinogenesis - reactive oxygen species	18	10.58824	9.23E-05	CBR1, MAP2K4, NDUFA7, NDUFA5, UQCRB, NDUFB6, NDUFA2, AKR1A1, COX7A2, UQCR10, COX5B, COX6A1, COX5A, UQCRQ, NDUFS6, NDUFS5, HRAS, GSTM5	2.788881	7.78E-03
mmu00190:Oxidative phosphorylation	16	9.411765	1.17E-04	NDUFA7, ATP6V1G2, NDUFA5, UQCRB, NDUFB6, NDUFA2, COX7A2, UQCR10, COX5B, COX6A1, COX5A, UQCRQ, NDUFS6, NDUFS5, ATP6V1E1, ATP6V1D	2.995465	7.78E-03
mmu05012:Parkinson disease	23	13.52941	2.75E-04	NDUFA7, NDUFA5, UQCRB, NDUFB6, NDUFA2, COX7A2, PARK7, UQCR10, KLC1, COX5B, COX6A1, COX5A, PSMA7, PSMA3, PSMB5, PSMD7, PSMA1, UQCRQ, NDUFS6, NDUFS5, PSMC1, CALM1, SNCA	2.198799	1.35E-02
mmu05022:Pathways of neurodegeneration - multiple diseases	29	17.05882	3.39E-04	UQCRB, DCTN2, NDUFB6, COX7A2, PARK7, UQCR10, KLC1, COX5B, COX6A1, HSD17B10, COX5A, PSMA7, PSMB5, PSMD7, HRAS, SNCA, NDUFA7, NDUFA5, NDUFA2, CSNK2A2, RAB39B, PSMA3, PSMA1, UQCRQ, NDUFS6, NDUFS5, PSMC1, CALM1, PPID	1.916216	1.35E-02

mmu05016:Huntington disease	23	13.52941	5.68E-04	NDUFA7, NDUFA5, UQCRB, DCTN2, NDUFB6, NDUFA2, CLTB, CLTA, COX7A2, UQCR10, KLC1, COX5B, COX6A1, COX5A, PSMA7, PSMA3, PSMB5, PSMD7, PSMA1, UQCRQ, NDUFS6, NDUFS5, PSMC1	2.094801	1.88E-02
mmu04932:Non-alcoholic fatty liver disease	13	7.647059	1.42E-03	NDUFA7, NDUFA5, UQCRB, NDUFB6, NDUFA2, COX7A2, UQCR10, COX5B, COX6A1, COX5A, UQCRQ, NDUFS6, NDUFS5	2.781503	3.57E-02
mmu05020:Prion disease	21	12.35294	1.49E-03	NDUFA7, NDUFA5, UQCRB, NDUFB6, NDUFA2, CSNK2A2, COX7A2, UQCR10, KLC1, COX5B, COX6A1, COX5A, PSMA7, PSMA3, PSMB5, PSMD7, PSMA1, UQCRQ, NDUFS6, NDUFS5, PSMC1	2.051242	3.57E-02
mmu05014:Amyotrophic lateral sclerosis	22	12.94118	1.62E-03	NDUFA7, NDUFA5, UQCRB, DCTN2, NDUFB6, NDUFA2, RAB39B, COX7A2, UQCR10, KLC1, COX5B, COX6A1, COX5A, PSMA7, PSMA3, PSMB5, PSMD7, PSMA1, UQCRQ, NDUFS6, NDUFS5, PSMC1	1.990275	3.57E-02
mmu01100:Metabolic pathways	41	24.11765	4.47E-03	PDXK, DGKE, ALDH1L1, ACADVL, UQCRB, NDUFB6, PDE1A, AK1, COX7A2, AK4, ACAA1A, UQCR10, COX5B, COX6A1, HSD17B10, COX5A, ALAD, PDE4B, PHGDH, ATP6V1E1, ATP6V1D, CBR1, NDUFA7, ATP6V1G2, NDUFA5, NDUFA2, IDH2, AKR1A1, TALDO1, ASRGL1, COQ6, HADHB, QDPR, UQCRQ, NDUFS6, NDUFS5, CMPK1, PFKP, PAFAH1B2, GSTM5, CDS2	1.45056	8.20E-02
mmu04714:Thermogenesis	14	8.235294	4.53E-03	NDUFA7, NDUFA5, UQCRB, NDUFB6, NDUFA2, COX7A2, UQCR10, COX5B, COX6A1,	2.329806	8.20E-02

				COX5A, UQCRQ, NDUFS6, NDUFS5, HRAS		
mmu05415:Diabetic cardiomyopathy	13	7.647059	0.022915	NDUFA7, NDUFA5, UQCRB, NDUFB6, NDUFA2, COX7A2, UQCR10, COX5B, COX6A1, COX5A, UQCRQ, NDUFS6, NDUFS5	1.991303	0.380003
mmu04137:Mitophagy - animal	5	2.941176	0.053198	FIS1, MRAS, CSNK2A2, PGAM5, HRAS	3.369898	0.814345
mmu03050:Proteasome	6	3.529412	0.063114	PSMA3, PSMB5, PSMD7, PSMA1, PSMC1, PSMA7	2.695918	0.897122
mmu04260:Cardiac muscle contraction	7	4.117647	0.081463	UQCRB, UQCRQ, COX7A2, UQCR10, COX5B, COX6A1, COX5A	2.246599	0.97549
mmu01240:Biosynthesis of cofactors	7	4.117647	0.089269	ALAD, PDXK, AK1, AKR1A1, CMPK1, AK4, COQ6	2.194352	0.97549

Wild-Type Memory Retrieval v. APPtg Memory Retrieval- 20% Upregulated

No results.

Wild-Type Basal v. Wild-Type Memory Retrieval-20% downregulated

Table 66. DAVID annotation tools output table of enriched KEGG pathways within proteins downregulated in WT mice during memory retrieval, when compared to WT mice at the basal level.

Term	Count	%	PValue	Genes	Fold Enrichment	FDR
mmu00020:Citrate cycle (TCA cycle)	5	10	3.98E-03	PCX, OGDHL, ACO2, SDHA, DLD	7.048485	3.78E-01

mmu01100:Metabolic pathways	18	36	5.37E-03	MPST, OAT, PCX, AGL, OGDHL, PYGM, ABAT, SDHA, ACADSB, ADCY5, GLS, ALDH6A1, SYNJ1, ACO2, PIP5K1C, PLCB1, DLD, ATP6V0A1	1.797064	3.78E-01
mmu00562:Inositol phosphate metabolism	4	8	9.91E-03	ALDH6A1, SYNJ1, PIP5K1C, PLCB1	8.292335	4.66E-01
mmu01200:Carbon metabolism	6	12	2.91E-02	ALDH6A1, PCX, OGDHL, ACO2, SDHA, DLD	3.253147	1.00E+00
mmu00280:Valine, leucine and isoleucine degradation	4	8	5.90E-02	ALDH6A1, ABAT, ACADSB, DLD	4.271809	1.00E+00
mmu00640:Propanoate metabolism	3	6	6.16E-02	ALDH6A1, ABAT, DLD	7.048485	1.00E+00
mmu04072:Phospholipase D signaling pathway	4	8	6.82E-02	GRM3, PIP5K1C, PLCB1, ADCY5	4.027706	1.00E+00

APPtg Basal v. APPtg Memory Retrival-20% downregulated

Table 67. DAVID annotation tools output table of enriched KEGG pathways within proteins downregulated in APPtg mice during memory retrieval, when compared to APPtg mice at the basal level.

Term	Count	%	PValue	Genes	Fold Enrichment	FDR
mmu04142:Lysosome	4	26.66667	6.47E-04	HEXB, AP3D1, AP3S1, AP3B2	18.46032	1.62E-02

Wild-Type Basal v. APPtg Basal-20% downregulated

Table 68. DAVID annotation tools output table of enriched KEGG pathways within proteins downregulated in APPtg mice at the basal level, when compared to WT mice at the basal level.

Term	Count	%	PValue	Genes	Fold Enrichment	FDR
mmu04144:Endocytosis	12	8.695652	4.59E-02	SH3GLB1, ACTR2, EHD3, IQSEC2, CAPZB, SRC, KIF5C, ASAP1, EPS15L1, PIP5K1C, ACTR3B, EPN1	1.85956	1.00E+00

Wild-Type Memory Retrieval v. APPtg Memory Retreival-20% downregulated

No results

5. Clustering

Wild-Type Basal v. Wild-Type Memory Retrieval-20% upregulated

Table 69. DAVID functional annotation clustering output table for annotation clusters enriched within proteins upregulated in WT mice during memory retrieval, when compared to WT mice at the basal level.

Cluster 1- Enrichment Score: 4.645429266363802						
Term	**Count**	**%**	**PValue**	**Genes**	**Fold Enrichment**	**FDR**
mmu00190: Oxidative phosphorylation	25	17.48252	3.25E-10	UQCRB, NDUFB6, NDUFB4, NDUFB2, ATP5K, COX7A2, ATP5H, ATP5O, COX6A1, COX5A, ATP6V1E1, NDUFV2, ATP6V1D, NDUFA7, NDUFA6, ATP6V1G2, NDUFA5, NDUFA4, NDUFA2, COX6B1, UQCRQ, PPA1, NDUFS5, NDUFS4, CYCS	4.089311	4.78E-08
KW-0249~Electron transport	17	11.88811	2.06E-07	NDUFA7, NDUFA6, NDUFA5, UQCRB, NDUFB6, NDUFA4, NDUFB4, TXNL1, NDUFA2, NDUFB2, NDUFB1, TMX4, UQCRQ, NDUFS5, NDUFS4, CYCS, NDUFV2	4.386696	9.08E-06
mmu04932: Non-alcoholic fatty liver disease	18	12.58741	2.73E-07	NDUFA7, NDUFA6, NDUFA5, UQCRB, NDUFB6, NDUFA4, NDUFB4, NDUFA2, NDUFB2, COX7A2, COX6A1, COX5A, COX6B1, UQCRQ, NDUFS5, NDUFS4, CYCS, NDUFV2	4.080702	1.93E-05
KW-0679~Respiratory chain	15	10.48951	3.63E-07	NDUFA7, NDUFA6, NDUFA5, UQCRB, NDUFB6, NDUFA4, NDUFB4, NDUFA2, NDUFB2, NDUFB1, UQCRQ, NDUFS5, NDUFS4, CYCS, NDUFV2	4.860771	9.08E-06
mmu05012: Parkinson disease	29	20.27972	3.94E-07	UQCRB, NDUFB6, NDUFB4, NDUFB2, COX7A2, PARK7, ATP5H, ATP5O, COX6A1, COX5A, PSMA7, PSMA8, PSMB2, PSMD4, NDUFV2, SNCA, NDUFA7, NDUFA6, NDUFA5, NDUFA4, NDUFA2, COX6B1,	2.639045	1.93E-05

				PSMA6, PSMA3, UQCRQ, NDUFS5, NDUFS4, CYCS, MAPT		
mmu05014: Amyotrophic lateral sclerosis	29	20.27972	8.60E-07	UQCRB, DCTN2, NDUFB6, NDUFB4, NDUFB2, COX7A2, ATP5H, ATP5O, COX6A1, COX5A, PSMA7, PSMA8, PSMB2, PSMD4, NEFL, NDUFV2, RAB8A, NDUFA7, NDUFA6, NDUFA5, NDUFA4, NDUFA2, COX6B1, PSMA6, PSMA3, UQCRQ, NDUFS5, NDUFS4, CYCS	2.549282	3.16E-05
mmu05016: Huntington disease	29	20.27972	1.16E-06	UQCRB, DCTN2, NDUFB6, NDUFB4, CLTB, NDUFB2, CLTA, COX7A2, ATP5H, ATP5O, COX6A1, COX5A, PSMA7, PSMA8, PSMB2, PSMD4, NDUFV2, NDUFA7, NDUFA6, NDUFA5, NDUFA4, NDUFA2, COX6B1, PSMA6, PSMA3, UQCRQ, NDUFS5, NDUFS4, CYCS	2.515063	3.42E-05
mmu05208: Chemical carcinogenesis - reactive oxygen species	21	14.68531	2.27E-06	CBR1, NDUFA7, NDUFA6, NDUFA5, UQCRB, NDUFB6, NDUFA4, NDUFB4, NDUFA2, NDUFB2, AKR1A1, COX7A2, ATP5H, ATP5O, COX6A1, COX5A, COX6B1, UQCRQ, NDUFS5, NDUFS4, NDUFV2	3.119157	5.57E-05
GO:0070469~respiratory chain	14	9.79021	2.86E-06	NDUFA7, NDUFA6, NDUFA5, UQCRB, NDUFB6, NDUFA4, NDUFA2, NDUFB2, NDUFB1, UQCRQ, NDUFS5, NDUFS4, CYCS, NDUFV2	4.654321	7.83E-04
mmu04714:Thermogenesis	20	13.98601	4.62E-06	NDUFA7, NDUFA6, NDUFA5, UQCRB, NDUFB6, NDUFA4, NDUFB4, NDUFA2, NDUFB2, ATP5K, COX7A2, ATP5H, ATP5O, COX6A1, COX5A, COX6B1, UQCRQ, NDUFS5, NDUFS4, NDUFV2	3.113788	9.70E-05
mmu05010: Alzheimer disease	28	19.58042	5.52E-06	UQCRB, NDUFB6, NDUFB4, NDUFB2, COX7A2, ATP5H, ATP5O, COX6A1, COX5A, PSMA7, PSMA8, PSMB2, PSMD4, NDUFV2, SNCA, NDUFA7, NDUFA6, NDUFA5, NDUFA4, NDUFA2, COX6B1, PSMA6, PSMA3, UQCRQ, NDUFS5, NDUFS4, CYCS, MAPT	2.396174	1.01E-04

GO:0042776~mitochondrial ATP synthesis coupled proton transport	14	9.79021	6.56E-06	NDUFA7, NDUFA6, NDUFA5, NDUFB6, NDUFB4, NDUFA2, NDUFB2, ATP5K, NDUFB1, ATP5H, ATP5O, NDUFS5, NDUFS4, NDUFV2	4.353199	6.53E-03
GO:0005747~mitochondrial respiratory chain complex I	12	8.391608	7.82E-06	NDUFA7, NDUFA6, NDUFB6, NDUFA5, NDUFA4, NDUFB4, NDUFS5, NDUFA2, NDUFS4, NDUFB2, NDUFB1, NDUFV2	5.077441	1.07E-03
mmu05022: Pathways of neurodegeneration - multiple diseases	32	22.37762	1.70E-05	UQCRB, DCTN2, NDUFB6, NDUFB4, NDUFB2, COX7A2, PARK7, ATP5H, ATP5O, COX6A1, COX5A, PSMA7, PSMA8, PSMB2, PSMD4, NEFL, NDUFV2, RAB8A, SNCA, NDUFA7, NDUFA6, NDUFA5, NDUFA4, NDUFA2, COX6B1, PSMA6, PSMA3, UQCRQ, NDUFS5, NDUFS4, CYCS, MAPT	2.08844	2.77E-04
mmu05020: Prion disease	26	18.18182	2.14E-05	UQCRB, NDUFB6, NDUFB4, NDUFB2, COX7A2, ATP5H, ATP5O, COX6A1, COX5A, PSMA7, PSMA8, PSMB2, PSMD4, NDUFV2, NDUFA7, NDUFA6, NDUFA5, NDUFA4, NDUFA2, COX6B1, PSMA6, PSMA3, UQCRQ, NDUFS5, NDUFS4, CYCS	2.349495	3.14E-04
mmu05415: Diabetic cardiomyopathy	20	13.98601	3.27E-05	NDUFA7, NDUFA6, NDUFA5, UQCRB, NDUFB6, NDUFA4, NDUFB4, NDUFA2, GSR, NDUFB2, COX7A2, ATP5H, ATP5O, COX6A1, COX5A, COX6B1, UQCRQ, NDUFS5, NDUFS4, NDUFV2	2.749409	4.37E-04
GO:0009060~aerobic respiration	12	8.391608	5.89E-05	NDUFA7, NDUFA6, NDUFB6, NDUFA5, UQCRB, NDUFB4, NDUFS5, NDUFA2, NDUFS4, NDUFB2, NDUFB1, NDUFV2	4.197727	2.60E-02
KW-0999~Mitochondrion inner membrane	23	16.08392	8.31E-05	NDUFA7, NDUFA6, NDUFA5, UQCRB, APOOL, NDUFB6, NDUFA4, NDUFB4, NDUFA2, NDUFB2, ATP5K, NDUFB1, COX7A2, ABCB8, ATP5H, ATP5O, COX6A1, COX5A,	2.41968	2.41E-03

				COX6B1, UQCRQ, NDUFS5, NDUFS4, NDUFV2		
GO:0032981 ~mitochondrial respiratory chain complex I assembly	9	6.293706	1.94E-03	NDUFA6, NDUFB6, NDUFA5, NDUFB4, NDUFS5, NDUFA2, NDUFS4, NDUFB2, NDUFB1	3.703877	3.22E-01
GO:0005743 ~mitochondrial inner membrane	25	17.48252	2.97E-03	SLC27A1, UQCRB, NDUFB6, NDUFB4, NDUFB2, ATP5K, NDUFB1, COX7A2, ABCB8, ATP5H, ATP5O, COX6A1, COX5A, NDUFV2, SNCA, NDUFA7, NDUFA6, APOOL, NDUFA5, NDUFA4, NDUFA2, COX6B1, UQCRQ, NDUFS5, NDUFS4	1.827613	1.63E-01
GO:0005739 ~mitochondrion	52	36.36364	5.25E-03	YWHAE, SLC27A1, PEBP1, PARK7, COX6A1, HINT2, SCP2, FAM162A, ATP6V1E1, DYNLL1, YWHAZ, NME1, COX6B1, NDUFS5, NDUFS4, ALDOC, NDUFB6, UQCRB, RAB1B, NDUFB4, ATP5K, NDUFB2, NDUFB1, COX7A2, ABCB8, ATP5H, ATP5O, COX5A, NAPG, SLC25A27, PRDX3, PRDX2, PRDX5, PRDX1, TPPP, NDUFV2, SNCA, NIPSNAP3B, FIS1, NDUFA7, NDUFA6, APOOL, NDUFA5, NDUFA4, MTX2, GSR, NDUFA2, PRDX6, RAB11A, RAB11B, UQCRQ, CYCS	1.380369	0.212959
mmu01100: Metabolic pathways	39	27.27273	6.95E-03	UQCRB, NDUFB6, NDUFB4, AK1, NDUFB2, ATP5K, COX7A2, HSD17B12, ATP5H, ATP5O, COX6A1, COX5A, SCP2, ATP6V1E1, NDUFV2, ATP6V1D, CBR1, NDUFA7, TPI1, NDUFA6, ATP6V1G2, NDUFA5, NDUFA4, NDUFA2, GSR, AKR1A1, PRDX6, DDOST, ASRGL1, COX6B1, NME1, UQCRQ, PSAT1, NDUFS5, NDUFS4, CYCS, ALDOC, PAFAH1B2, CDS2	1.427668	8.51E-02
GO:0008137 ~NADH dehydrogenase	5	3.496503	2.49E-02	NDUFA7, NDUFA5, NDUFA2, NDUFS4, NDUFV2	4.256337	0.958294

(ubiquinone) activity						
mmu04723: Retrograde endocannabinoid signaling	12	8.391608	0.029988	NDUFA7, NDUFA6, NDUFB6, NDUFA5, NDUFA4, NDUFB4, GNG7, NDUFS5, NDUFA2, NDUFS4, NDUFB2, NDUFV2	1.988034	0.314879
KW-0496~Mitochondrion	35	24.47552	0.036196	SLC27A1, UQCRB, NDUFB6, NDUFB4, NDUFB2, ATP5K, NDUFB1, COX7A2, ABCB8, PARK7, ATP5H, ATP5O, COX6A1, COX5A, PRDX3, PRDX5, HINT2, SCP2, FAM162A, NDUFV2, FIS1, NDUFA7, NDUFA6, APOOL, NDUFA5, NDUFA4, MTX2, NDUFA2, GSR, DYNLL1, COX6B1, UQCRQ, NDUFS5, NDUFS4, CYCS	1.36034	0.349899
Cluster 2- Enrichment Score: 2.916384813651269						
Term	Count	%	PValue	Genes	Fold Enrichment	FDR
GO:0051920~peroxiredoxin activity	6	4.195804	7.94E-06	PRDX3, PRDX2, PRDX5, PRDX1, PARK7, PRDX6	14.47154	0.002683
KW-0676~Redox-active center	8	5.594406	1.39E-05	PRDX3, PRDX2, TMX4, PRDX5, PRDX1, TXNL1, GSR, PRDX6	8.554386	1.53E-04
GO:0042744~hydrogen peroxide catabolic process	6	4.195804	7.85E-05	PRDX3, PRDX2, PRDX5, PRDX1, HBB-BS, PRDX6	10.49432	0.026023
ACT_SITE:Cysteine sulfenic acid (-SOH) intermediate	5	3.496503	9.52E-05	PRDX3, PRDX2, PRDX5, PRDX1, PRDX6	14.65079	0.024941
KW-0049~Antioxidant	5	3.496503	1.63E-04	PRDX3, PRDX2, PRDX5, PRDX1, PRDX6	13.66162	0.006194

KW-0575~Peroxidase	5	3.496503	3.63E-04	PRDX3, PRDX2, PRDX5, PRDX1, PRDX6	11.70996	0.0069
DOMAIN:Thioredoxin	7	4.895105	3.90E-04	PRDX3, PRDX2, TMX4, PRDX5, PRDX1, TXNL1, PRDX6	6.409722	0.051137
IPR013766:Thioredoxin domain	7	4.895105	5.12E-04	PRDX3, PRDX2, TMX4, PRDX5, PRDX1, TXNL1, PRDX6	6.105556	0.100185
GO:0004601~peroxidase activity	5	3.496503	6.26E-04	PRDX3, PRDX2, PRDX5, PRDX1, PRDX6	10.33682	0.101003
GO:0045454~cell redox homeostasis	6	4.195804	8.79E-04	PRDX3, PRDX2, PRDX5, PRDX1, GSR, PRDX6	6.996212	0.174867
GO:0016209~antioxidant activity	5	3.496503	0.001186	PRDX3, PRDX2, PRDX5, PRDX1, PRDX6	9.044715	0.101003
GO:0008379~thioredoxin peroxidase activity	4	2.797203	0.001195	PRDX3, PRDX2, PRDX5, PRDX1	14.47154	0.101003
IPR000866:Alkyl hydroperoxide reductase subunit C/ Thiol specific antioxidant	4	2.797203	0.001336	PRDX3, PRDX2, PRDX1, PRDX6	13.95556	0.100185
IPR019479:Peroxiredoxin, C-terminal	4	2.797203	0.001336	PRDX3, PRDX2, PRDX1, PRDX6	13.95556	0.100185
GO:0006979~response to oxidative stress	9	6.293706	0.002372	PRDX3, PRDX2, PRDX5, NDUFA6, NDUFB4, PRDX1, PEBP1, PARK7, PRDX6	3.598052	0.337193
PIRSF000239:peroxiredoxin, AhpC type	3	2.097902	0.01416	PRDX2, PRDX1, PRDX6	13.2381	0.254887
IPR024706:Peroxiredoxin, AhpC-type	3	2.097902	0.014366	PRDX2, PRDX1, PRDX6	13.95556	0.425167

KW-0560~Oxidoreductase	13	9.090909	0.082289	CBR1, GSR, AKR1A1, COX7A2, HSD17B12, COX6A1, PRDX6, PRDX3, PRDX2, PRDX5, PRDX1, NDUFV2, PAM	1.626879	1
GO:0016491~oxidoreductase activity	14	9.79021	0.137858	CBR1, GSR, AKR1A1, COX7A2, HSD17B12, COX6A1, PRDX6, PRDX3, PRDX2, PRDX5, PRDX1, NDUFV2, PAM, SNCA	1.478844	1
KW-1015~Disulfide bond	15	10.48951	0.63154	TXNL1, NDUFA2, GSR, CLTB, PEBP1, COX6B1, PRDX3, PRDX2, TMX4, PRDX5, FABP5, NDUFS5, PRDX1, MAPT, PAM	1.007427	1
Cluster 3-Enrichment Score: 1.6699615896347273						
Term	Count	%	PValue	Genes	Fold Enrichment	FDR
GO:0051920~peroxiredoxin activity	6	4.195804	7.94E-06	PRDX3, PRDX2, PRDX5, PRDX1, PARK7, PRDX6	14.47154	0.002683
GO:0034599~cellular response to oxidative stress	7	4.895105	5.04E-04	PRDX3, PRDX2, PRDX5, GSR, PARK7, PPIA, SNCA	6.121686	0.125269
GO:0043027~cysteine-type endopeptidase inhibitor activity involved in apoptotic process	3	2.097902	0.025517	PRDX3, PRDX5, SNCA	10.85366	0.958294
GO:0034614~cellular response to reactive oxygen species	3	2.097902	0.207194	PRDX3, PRDX5, PARK7	3.498106	0.997994
GO:0043524~negative regulation of	6	4.195804	0.237056	PRDX3, PRDX2, UBE2V2, NEFL, PARK7, SNCA	1.786267	0.997994

neuron apoptotic process						
GO:0032496 ~response to lipopolysaccharide	3	2.097902	0.493698	PRDX3, PRDX2, SNCA	1.825099	0.997994
GO:0043066 ~negative regulation of apoptotic process	5	3.496503	0.825966	SLC25A27, PRDX3, PRDX5, PARK7, SNCA	0.885596	0.997994
Cluster 4- Enrichment Score: 1.545860359905563						
Term	Count	%	PValue	Genes	Fold Enrichment	FDR
SM00948:SM00948	4	2.797203	0.003765	PSMA6, PSMA3, PSMA7, PSMA8	11.13095	0.08762
DOMAIN:PROTEASOME_ALPHA_1	4	2.797203	0.0132	PSMA6, PSMA3, PSMA7, PSMA8	7.325397	0.886358
GO:0010499 ~proteasomal ubiquitin-independent protein catabolic process	5	3.496503	0.013839	PSMA6, PSMA3, PSMB2, PSMA7, PSMA8	4.997294	0.997994
GO:0005839 ~proteasome core complex	5	3.496503	0.013956	PSMA6, PSMA3, PSMB2, PSMA7, PSMA8	4.986772	0.459564
IPR001353:Proteasome, subunit alpha/beta	5	3.496503	0.013981	PSMA6, PSMA3, PSMB2, PSMA7, PSMA8	4.984127	0.425167
GO:0019773 ~proteasome core complex, alpha-	4	2.797203	0.015095	PSMA6, PSMA3, PSMA7, PSMA8	6.981481	0.459564

subunit complex						
IPR000426:Proteasome, alpha-subunit, N-terminal domain	4	2.797203	0.015117	PSMA6, PSMA3, PSMA7, PSMA8	6.977778	0.425167
IPR023332:Proteasome A-type subunit	4	2.797203	0.015117	PSMA6, PSMA3, PSMA7, PSMA8	6.977778	0.425167
KW-0647~Proteasome	7	4.895105	0.022123	PSMA6, PSMA3, PSMD4, PSMB2, TXNL1, PSMA7, PSMA8	3.060764	0.320779
GO:0000502~proteasome complex	7	4.895105	0.025892	PSMA6, PSMA3, PSMD4, PSMB2, TXNL1, PSMA7, PSMA8	2.961841	0.709428
GO:0051603~proteolysis involved in cellular protein catabolic process	5	3.496503	0.033917	PSMA6, PSMA3, PSMB2, PSMA7, PSMA8	3.886785	0.997994
GO:0010498~proteasomal protein catabolic process	5	3.496503	0.040666	PSMA6, PSMA3, PSMB2, PSMA7, PSMA8	3.682217	0.997994
GO:0004175~endopeptidase activity	5	3.496503	0.058692	PSMA6, PSMA3, PSMB2, PSMA7, PSMA8	3.288987	1
mmu03050: Proteasome	6	4.195804	0.0643	PSMA6, PSMA3, PSMD4, PSMB2, PSMA7, PSMA8	2.673563	0.630145
GO:0043161~proteasome-mediated ubiquitin-dependent protein	8	5.594406	0.064647	PSMA6, NSFL1C, PSMA3, PSMD4, PSMB2, PCBP2, PSMA7, PSMA8	2.19489	0.997994

catabolic process						
GO:0006511 ~ubiquitin-dependent protein catabolic process	6	4.195804	0.210449	PSMA6, PSMA3, TOLLIP, UBE2N, PSMA7, PSMA8	1.865657	0.997994
mmu05017:Spinocerebellar ataxia	7	4.895105	0.279713	PSMA6, PSMA3, PSMD4, PSMB2, CYCS, PSMA7, PSMA8	1.559579	0.948387
Cluster 5- Enrichment Score: 1.2211357672039433						
Term	Count	%	PValue	Genes	Fold Enrichment	FDR
GO:0005751 ~mitochondrial respiratory chain complex IV	5	3.496503	0.005441	NDUFA4, COX7A2, COX6A1, COX5A, COX6B1	6.346801	0.212959
GO:0006123 ~mitochondrial electron transport, cytochrome c to oxygen	4	2.797203	0.014996	CYCS, COX7A2, COX6A1, COX5A	6.996212	0.997994
GO:0004129 ~cytochrome-c oxidase activity	3	2.097902	0.077971	COX7A2, COX6A1, COX5A	6.202091	1
TOPO_DOM: Mitochondrial matrix	5	3.496503	0.180428	APOOL, UQCRQ, NDUFA4, COX7A2, COX6A1	2.219817	1
mmu04260: Cardiac muscle contraction	6	4.195804	0.185342	UQCRB, UQCRQ, COX7A2, COX6A1, COX5A, COX6B1	1.938333	0.948387
TOPO_DOM: Mitochondrial	6	4.195804	0.221488	FIS1, APOOL, UQCRQ, NDUFA4, COX7A2, COX6A1	1.831349	1

intermembrane						
Cluster 6- Enrichment Score: 1.1759359655461907						
Term	Count	%	PValue	Genes	Fold Enrichment	FDR
SM01391:SM01391	3	2.097902	0.02517	NEFL, INA, GFAP	11.13095	0.268484
IPR006821:Intermediate filament head, DNA-binding domain	3	2.097902	0.027397	NEFL, INA, GFAP	10.46667	0.616435
REGION:Coil 1A	3	2.097902	0.056995	NEFL, INA, GFAP	7.325397	0.995513
REGION:Coil 1B	3	2.097902	0.056995	NEFL, INA, GFAP	7.325397	0.995513
REGION:Head	3	2.097902	0.056995	NEFL, INA, GFAP	7.325397	0.995513
REGION:Linker 1	3	2.097902	0.056995	NEFL, INA, GFAP	7.325397	0.995513
REGION:Linker 2	3	2.097902	0.056995	NEFL, INA, GFAP	7.325397	0.995513
REGION:Tail	3	2.097902	0.056995	NEFL, INA, GFAP	7.325397	0.995513
DOMAIN:IF rod	3	2.097902	0.056995	NEFL, INA, GFAP	7.325397	0.995513
IPR018039:Intermediate filament protein, conserved site	3	2.097902	0.062326	NEFL, INA, GFAP	6.977778	1
KW-0403~Intermediate filament	3	2.097902	0.082788	NEFL, INA, GFAP	5.996599	0.586252

GO:0005882 ~intermediate filament	4	2.797203	0.099582	NEFL, INA, GFAP, NME1	3.490741	0.992754
GO:0045109 ~intermediate filament organization	3	2.097902	0.105472	NEFL, INA, GFAP	5.247159	0.997994
GO:0005200 ~structural constituent of cytoskeleton	4	2.797203	0.471506	NEFL, ARPC5, INA, GFAP	1.564491	1
Cluster 7- Enrichment Score: 1.0402843357123028						
Term	Count	%	PValue	Genes	Fold Enrichment	FDR
SM00102:ADF	4	2.797203	0.005476	GMFB, CFL2, CFL1, DSTN	9.89418	0.08762
IPR017904:ADF/Cofilin/Destrin	3	2.097902	0.014366	CFL2, CFL1, DSTN	13.95556	0.425167
DOMAIN:ADF-H	4	2.797203	0.018832	GMFB, CFL2, CFL1, DSTN	6.511464	0.886358
IPR002108:Actin-binding, cofilin/tropomyosin type	4	2.797203	0.021511	GMFB, CFL2, CFL1, DSTN	6.202469	0.537777
GO:0051014 ~actin filament severing	3	2.097902	0.027248	CFL2, CFL1, DSTN	10.49432	0.997994
GO:0030043 ~actin filament fragmentation	3	2.097902	0.027248	CFL2, CFL1, DSTN	10.49432	0.997994
MOTIF:Nuclear localization signal	6	4.195804	0.031747	NSFL1C, FABP5, CSRP1, CFL2, CFL1, DSTN	3.255732	0.995513

GO:0030836~positive regulation of actin filament depolymerization	3	2.097902	0.04332	CFL2, CFL1, DSTN	8.395455	0.997994
GO:0030042~actin filament depolymerization	3	2.097902	0.105472	CFL2, CFL1, DSTN	5.247159	0.997994
GO:0048870~cell motility	3	2.097902	0.207194	CFL2, CFL1, DSTN	3.498106	0.997994
GO:0015629~actin cytoskeleton	7	4.895105	0.326795	CSRP1, CFL2, CFL1, ARPC5L, DSTN, ARPC5, SNCA	1.48092	0.992754
mmu04666:Fc gamma R-mediated phagocytosis	4	2.797203	0.406691	CFL2, CFL1, ARPC5L, ARPC5	1.722963	0.948387
KW-0009~Actin-binding	6	4.195804	0.580407	CFL2, CFL1, TMOD2, ARPC5L, DSTN, ARPC5	1.170996	1
GO:0003779~actin binding	8	5.594406	0.600912	GMFB, CFL2, CFL1, TMOD2, ARPC5L, DSTN, ARPC5, SNCA	1.092192	1
GO:0051015~actin filament binding	5	3.496503	0.812749	CFL2, CFL1, ARPC5L, DSTN, ARPC5	0.904472	1
mmu04810: Regulation of actin cytoskeleton	4	2.797203	0.846163	CFL2, CFL1, ARPC5L, ARPC5	0.876083	0.948387
Cluster 8- Enrichment Score: 0.9359377996355763						
Term	Count	%	PValue	Genes	Fold Enrichment	FDR

GO:0006301~postreplication repair	3	2.097902	0.014286	UBE2N, UBE2V2, UBE2V1	13.99242	0.997994
GO:0070534~protein K63-linked ubiquitination	3	2.097902	0.04332	UBE2N, UBE2V2, UBE2V1	8.395455	0.997994
DOMAIN:UBC core	3	2.097902	0.097364	UBE2N, UBE2V2, UBE2V1	5.494048	1
IPR000608:Ubiquitin-conjugating enzyme, E2	3	2.097902	0.10599	UBE2N, UBE2V2, UBE2V1	5.233333	1
IPR016135:Ubiquitin-conjugating enzyme/RWD-like	3	2.097902	0.155368	UBE2N, UBE2V2, UBE2V1	4.186667	1
GO:0000209~protein polyubiquitination	3	2.097902	0.315496	UBE2N, UBE2V2, UBE2V1	2.62358	0.997994
KW-0833~Ubl conjugation pathway	3	2.097902	0.897058	UBE2N, UBE2V2, UBE2V1	0.803897	1
Cluster 9-Enrichment Score: 0.8845199550684083						
Term	Count	%	PValue	Genes	Fold Enrichment	FDR
KW-1017~Isopeptide bond	17	11.88811	0.099934	YWHAE, TPI1, AHSA1, PARK7, DYNLL1, NME1, CSRP1, PSMD4, PRDX1, PCBP1, ARHGDIA, CFL1, PCBP2, UBE2N, MAPT, RPL18, PPIA	1.46984	0.424718
KW-0832~Ubl conjugation	22	15.38462	0.138147	YWHAE, FIS1, TPI1, AHSA1, DSTN, PARK7, ARPC5, DYNLL1, NME1, CSRP1, PSMD4, PRDX1, PCBP1, ARHGDIA, CFL1, PCBP2, UBE2N, NEFL, MAPT, RPL18, PPIA, SNCA	1.318619	0.469699

CROSSLNK:Glycyl lysine isopeptide (Lys-Gly) (interchain with G-Cter in SUMO2)	9	6.293706	0.160838	PSMD4, CSRP1, PRDX1, PCBP1, CFL1, PCBP2, AHSA1, DYNLL1, RPL18	1.669078	1
Cluster 10- Enrichment Score: 0.8577698811329418						
Term	Count	%	PValue	Genes	Fold Enrichment	FDR
GO:0003697~single-stranded DNA binding	5	3.496503	0.002023	PURB, PURA, PCBP1, PCBP2, NME1	8.039747	0.136722
GO:0000981~RNA polymerase II transcription factor activity, sequence-specific DNA binding	3	2.097902	0.025517	PURB, PURA, PCBP1	10.85366	0.958294
GO:0003677~DNA binding	5	3.496503	0.185924	PURB, PURA, PCBP1, PCBP2, MAPT	2.192658	1
KW-0238~DNA-binding	4	2.797203	0.217658	PURB, PURA, PCBP1, PCBP2	2.428732	1
GO:0003729~mRNA binding	4	2.797203	0.280908	PURB, PCBP1, PCBP2, PARK7	2.143933	1
GO:0003723~RNA binding	7	4.895105	0.358894	PURB, PURA, PSMA6, PCBP1, PCBP2, PARK7, RPL18	1.426772	1
KW-0694~RNA-binding	3	2.097902	0.707233	PCBP1, PCBP2, PARK7	1.229545	1

GO:0045944~positive regulation of transcription from RNA polymerase II promoter	3	2.097902	0.922407	PCBP1, PCBP2, PARK7	0.736443	0.997994
Cluster 11- Enrichment Score: 0.566709575494431						
Term	Count	%	PValue	Genes	Fold Enrichment	FDR
KW-0375~Hydrogen ion transport	6	4.195804	0.027016	ATP6V1G2, ATP5K, ATP5H, ATP5O, ATP6V1E1, ATP6V1D	3.344211	0.3377
GO:0042626~ATPase activity, coupled to transmembrane movement of substances	3	2.097902	0.077971	ATP6V1G2, ABCB8, ATP6V1D	6.202091	1
GO:0000276~mitochondrial proton-transporting ATP synthase complex, coupling factor F(o)	3	2.097902	0.105893	ATP5K, ATP5H, ATP5O	5.236111	0.992754
GO:0046933~proton-transporting ATP synthase activity, rotational mechanism	3	2.097902	0.146223	ATP5K, ATP5H, ATP5O	4.341463	1
GO:0005753~mitochondrial proton-transporting	3	2.097902	0.155234	ATP5K, ATP5H, ATP5O	4.188889	0.992754

ATP synthase complex						
GO:0015986 ~ATP synthesis coupled proton transport	3	2.097902	0.180629	ATP5K, ATP5H, ATP5O	3.816116	0.997994
GO:0046961 ~proton-transporting ATPase activity, rotational mechanism	3	2.097902	0.22237	ATP6V1G2, ATP6V1E1, ATP6V1D	3.339587	1
mmu04721:Synaptic vesicle cycle	6	4.195804	0.257172	ATP6V1G2, SLC6A9, CLTB, CLTA, ATP6V1E1, ATP6V1D	1.722963	0.948387
mmu05323: Rheumatoid arthritis	3	2.097902	0.261891	ATP6V1G2, ATP6V1E1, ATP6V1D	2.982051	0.948387
mmu04966: Collecting duct acid secretion	3	2.097902	0.261891	ATP6V1G2, ATP6V1E1, ATP6V1D	2.982051	0.948387
GO:0046034 ~ATP metabolic process	4	2.797203	0.279051	AK1, ATP5K, ATP5H, ATP5O	2.152681	0.997994
mmu04150: mTOR signaling pathway	3	2.097902	0.683862	ATP6V1G2, ATP6V1E1, ATP6V1D	1.292222	0.948387
mmu05165: Human papillomavirus infection	4	2.797203	0.684769	SLC9A3R1, ATP6V1G2, ATP6V1E1, ATP6V1D	1.148642	0.948387
KW-0406~Ion transport	8	5.594406	0.761362	ATP6V1G2, ATP5K, ABCB8, FXYD6, ATP5H, ATP5O, ATP6V1E1, ATP6V1D	0.936754	1

GO:0006811~ion transport	8	5.594406	0.77133	ATP6V1G2, ATP5K, ABCB8, FXYD6, ATP5H, ATP5O, ATP6V1E1, ATP6V1D	0.925119	0.997994
mmu04145: Phagosome	3	2.097902	0.888962	ATP6V1G2, ATP6V1E1, ATP6V1D	0.824823	0.948387
GO:0016887~ATPase activity	3	2.097902	0.949017	ATP6V1G2, ABCB8, ATP5O	0.657797	1
Cluster 12- Enrichment Score: 0.5145793790856175						
Term	Count	%	PValue	Genes	Fold Enrichment	FDR
GO:0060271~cilium assembly	4	2.797203	0.130364	DYNLL1, DYNLL2, ATP6V1D, RAB8A	3.109428	0.997994
GO:0005813~centrosome	8	5.594406	0.352204	DCTN2, DYNLL1, DYNLL2, NDRG1, ATP6V1D, RAB8A, RAB11A, NME1	1.379058	0.992754
GO:0005929~cilium	3	2.097902	0.622745	DYNLL1, ATP6V1D, RAB8A	1.444444	0.992754
Cluster 13- Enrichment Score: 0.5069982935340182						
Term	Count	%	PValue	Genes	Fold Enrichment	FDR
mmu04962: Vasopressin-regulated water reabsorption	6	4.195804	0.026189	DCTN2, ARHGDIA, DYNLL1, DYNLL2, RAB11A, RAB11B	3.371014	0.296143
KW-0243~Dynein	3	2.097902	0.154551	DCTN2, DYNLL1, DYNLL2	4.197619	0.746997
GO:0030286~dynein complex	3	2.097902	0.155234	DCTN2, DYNLL1, DYNLL2	4.188889	0.992754
GO:0007017~microtubule-based process	3	2.097902	0.342324	DCTN2, DYNLL1, DYNLL2	2.469251	0.997994
GO:0005813~centrosome	8	5.594406	0.352204	DCTN2, DYNLL1, DYNLL2, NDRG1, ATP6V1D, RAB8A, RAB11A, NME1	1.379058	0.992754

KW-0493~Microtubule	6	4.195804	0.466257	DCTN2, MAPT, TPPP, DYNLL1, DYNLL2, NDRG1	1.332577	1
GO:0008017~microtubule binding	5	3.496503	0.571576	MAPT, TPPP, NDRG1, RAB11A, SNCA	1.247547	1
mmu05132:Salmonella infection	7	4.895105	0.648576	DCTN2, ARPC5L, RHOG, CYCS, ARPC5, DYNLL1, DYNLL2	1.064183	0.948387
KW-0206~Cytoskeleton	16	11.18881	0.79222	DCTN2, TMOD2, ARPC5L, CLTA, ARPC5, DYNLL1, DYNLL2, NDRG1, NSFL1C, CFL2, CFL1, NEFL, MAPT, TPPP, ATP6V1D, RAB8A	0.902714	1
GO:0005874~microtubule	6	4.195804	0.820524	DCTN2, MAPT, TPPP, DYNLL1, DYNLL2, NDRG1	0.881871	0.992754
Cluster 14- Enrichment Score: 0.5030037988415091						
Term	Count	%	PValue	Genes	Fold Enrichment	FDR
LIPID:S-geranylgeranyl cysteine	8	5.594406	0.020298	RAP1A, RAP2B, GNG7, RAB1B, RHOG, RAB8A, RAB11A, RAB11B	2.790627	0.886358
MOTIF:Effector region	7	4.895105	0.054325	RAP1A, RAP2B, RAB1B, RHOG, RAB8A, RAB11A, RAB11B	2.501355	0.995513
KW-0636~Prenylation	8	5.594406	0.076295	RAP1A, RAP2B, GNG7, RAB1B, RHOG, RAB8A, RAB11A, RAB11B	2.111473	0.424718
PROPEP:Removed in mature form	8	5.594406	0.106422	RAP1A, RAP2B, GNG7, RHOG, PARK7, RAB8A, RAB11A, RAB11B	1.953439	1
GO:0055038~recycling endosome membrane	5	3.496503	0.120114	RAP2B, NDRG1, RAB8A, RAB11A, RAB11B	2.585734	0.992754
IPR001806:Small GTPase superfamily	7	4.895105	0.120947	RAP1A, RAP2B, RAB1B, RHOG, RAB8A, RAB11A, RAB11B	2.035185	1

IPR005225:Small GTP-binding protein domain	7	4.895105	0.203578	RAP1A, RAP2B, RAB1B, RHOG, RAB8A, RAB11A, RAB11B	1.744444	1
GO:0031489~myosin V binding	3	2.097902	0.248501	RAB8A, RAB11A, RAB11B	3.101045	1
GO:0045335~phagocytic vesicle	4	2.797203	0.26036	RAP1A, RAB8A, RAB11A, RAB11B	2.234074	0.992754
KW-0342~GTP-binding	8	5.594406	0.267482	RAP1A, RAP2B, GNA11, RAB1B, RHOG, RAB8A, RAB11A, RAB11B	1.481607	1
KW-0378~Hydrolase	15	10.48951	0.311321	DUSP3, RAB1B, PARK7, PRDX6, RAB11A, ASRGL1, NUDT3, RAB11B, RAP1A, HINT2, RAP2B, PPA1, TPPP, PAFAH1B2, RAB8A	1.223428	1
KW-0449~Lipoprotein	15	10.48951	0.391975	LRRC57, RAB1B, RHOG, PARK7, RAB11A, RAB11B, PRDX3, GAP43, PRDX5, RAP1A, RAP2B, VSNL1, GNA11, GNG7, RAB8A	1.169242	1
GO:0072659~protein localization to plasma membrane	6	4.195804	0.452196	SLC9A3R1, RAP1A, SCP2, MYADM, RAB8A, RAB11A	1.354106	0.997994
GO:0003924~GTPase activity	9	6.293706	0.496849	RAP1A, RAP2B, GNA11, RAB1B, RHOG, TPPP, RAB8A, RAB11A, RAB11B	1.173368	1
GO:0019003~GDP binding	4	2.797203	0.507358	RAP1A, RAP2B, RAB8A, RAB11B	1.484261	1
GO:0005525~GTP binding	9	6.293706	0.569584	RAP1A, RAP2B, GNA11, RAB1B, RHOG, RAB8A, RAB11A, NME1, RAB11B	1.103762	1
GO:0055037~recycling endosome	4	2.797203	0.632062	RAP2B, RAB8A, RAB11A, RAB11B	1.241152	0.992754

mmu04972: Pancreatic secretion	3	2.097902	0.734384	RAP1A, RAB8A, RAB11A	1.174747	0.948387
KW-0488~Methylation	14	9.79021	0.760647	TPI1, RAB1B, RHOG, RAB11A, GFAP, RAB11B, PURB, RAP1A, RAP2B, GNG7, NEFL, MBP, MAPT, RAB8A	0.92377	1
IPR027417:P-loop containing nucleoside triphosphate hydrolase	10	6.993007	0.867718	RAP1A, RAP2B, GNA11, RAB1B, AK1, RHOG, ABCB8, RAB8A, RAB11A, RAB11B	0.825773	1
KW-0547~Nucleotide-binding	16	11.18881	0.870643	SLC27A1, RAB1B, AK1, GSR, RHOG, PEBP1, ABCB8, RAB11A, NME1, RAB11B, RAP1A, HINT2, RAP2B, GNA11, UBE2N, RAB8A	0.866898	1
GO:0005768~endosome	9	6.293706	0.922535	PRDX3, RAP1A, RAP2B, SLC6A9, ARPC5, ATP6V1E1, RAB8A, RAB11A, RAB11B	0.752495	0.992754
KW-0967~Endosome	6	4.195804	0.950059	PRDX3, RAP1A, RAP2B, RAB8A, RAB11A, RAB11B	0.677035	1
GO:0000166~nucleotide binding	15	10.48951	0.997923	SLC27A1, RAB1B, AK1, RHOG, PEBP1, ABCB8, RAB11A, NME1, RAB11B, RAP1A, HINT2, RAP2B, GNA11, UBE2N, RAB8A	0.59148	1
Cluster 15- Enrichment Score: 0.4130531669447467						
Term	Count	%	PValue	Genes	Fold Enrichment	FDR
KW-0456~Lyase	4	2.797203	0.267189	TPI1, DDT, ALDOC, PAM	2.185859	1
GO:0016829~lyase activity	4	2.797203	0.31955	TPI1, DDT, ALDOC, PAM	1.996075	1
GO:0003824~catalytic activity	6	4.195804	0.675278	HINT2, TPI1, PSAT1, ALDOC, PAM, PRDX6	1.058894	1
Cluster 16- Enrichment Score: 0.2955587956149628						

Term	Count	%	PValue	Genes	Fold Enrichment	FDR
GO:0006869~lipid transport	3	2.097902	0.469922	SLC27A1, FABP5, SCP2	1.908058	0.997994
mmu03320:PPAR signaling pathway	3	2.097902	0.512043	SLC27A1, FABP5, SCP2	1.762121	0.948387
KW-0445~Lipid transport	3	2.097902	0.539499	SLC27A1, FABP5, SCP2	1.672105	1
Cluster 17- Enrichment Score: 0.23447636927361706						
Term	Count	%	PValue	Genes	Fold Enrichment	FDR
mmu04721:Synaptic vesicle cycle	6	4.195804	0.257172	ATP6V1G2, SLC6A9, CLTB, CLTA, ATP6V1E1, ATP6V1D	1.722963	0.948387
GO:0031410~cytoplasmic vesicle	12	8.391608	0.843827	SLC27A1, PRDX5, ATP6V1G2, CLTB, RHOG, CLTA, ATP6V1E1, PAM, ATP6V1D, RAB8A, RAB11A, RAB11B	0.854875	0.992754
KW-0968~Cytoplasmic vesicle	9	6.293706	0.912209	ATP6V1G2, CLTB, CLTA, ATP6V1E1, PAM, ATP6V1D, RAB8A, RAB11A, RAB11B	0.767857	1
Cluster 18- Enrichment Score: 0.16027291243680797						
Term	Count	%	PValue	Genes	Fold Enrichment	FDR
mmu04144:Endocytosis	8	5.594406	0.604546	ARPC5L, CLTB, SNX12, CLTA, ARPC5, RAB8A, RAB11A, RAB11B	1.088187	0.948387
mmu04961:Endocrine and other factor-regulated calcium reabsorption	3	2.097902	0.734384	CLTB, CLTA, RAB11A	1.174747	0.948387

GO:0016192~vesicle-mediated transport	6	4.195804	0.744438	NAPB, CLTB, CLTA, NAPG, RAB11A, RAB11B	0.976216	0.997994
Cluster 19- Enrichment Score: 0.13807052798982092						
Term	Count	%	PValue	Genes	Fold Enrichment	FDR
KW-1133~Transmembrane helix	26	18.18182	0.511938	SLC27A1, LPGAT1, NDUFB6, NDUFB4, NDUFB1, COX7A2, ABCB8, HSD17B12, COX6A1, PURB, PCMT1, FAM162A, CLPTM1, FIS1, TMED9, APOOL, NDUFA4, DDOST, TMX4, SLC6A9, REEP5, UQCRQ, MYADM, FXYD6, PAM, CDS2	1.037787	1
KW-0812~Transmembrane	26	18.18182	0.569163	SLC27A1, LPGAT1, NDUFB6, NDUFB4, NDUFB1, COX7A2, ABCB8, HSD17B12, COX6A1, PURB, PCMT1, FAM162A, CLPTM1, FIS1, TMED9, APOOL, NDUFA4, DDOST, TMX4, SLC6A9, REEP5, UQCRQ, MYADM, FXYD6, PAM, CDS2	1.015833	1
TRANSMEM: Helical	26	18.18182	0.966555	SLC27A1, LPGAT1, NDUFB6, NDUFB4, NDUFB1, COX7A2, ABCB8, HSD17B12, COX6A1, PURB, PCMT1, FAM162A, CLPTM1, FIS1, TMED9, APOOL, NDUFA4, DDOST, TMX4, SLC6A9, REEP5, UQCRQ, MYADM, FXYD6, PAM, CDS2	0.780575	1
GO:0016021~integral component of membrane	26	18.18182	0.99549	SLC27A1, LPGAT1, NDUFB6, NDUFB4, NDUFB1, COX7A2, ABCB8, HSD17B12, COX6A1, SLC25A27, PCMT1, FAM162A, CLPTM1, FIS1, TMED9, APOOL, NDUFA4, DDOST, TMX4, SLC6A9, REEP5, UQCRQ, MYADM, FXYD6, PAM, CDS2	0.695473	0.99549
Cluster 20- Enrichment Score: 0.10722236475766003						
Term	Count	%	PValue	Genes	Fold Enrichment	FDR

GO:0000287~magnesium ion binding	5	3.496503	0.599203	PPA1, TPPP, NUDT3, NME1, SNCA	1.205962	1
KW-0460~Magnesium	5	3.496503	0.83152	PPA1, GNA11, TPPP, NUDT3, NME1	0.878107	1
KW-0479~Metal-binding	13	9.090909	0.956943	COX5A, NUDT3, NME1, VSNL1, CSRP1, PPA1, GNA11, EFHD2, CYCS, TPPP, NDUFV2, PAM, SNCA	0.758846	1
Cluster 21- Enrichment Score: 0.10255971091329887						
Term	Count	%	PValue	Genes	Fold Enrichment	FDR
mmu05170: Human immunodeficiency virus 1 infection	5	3.496503	0.542091	GNA11, GNG7, CFL2, CFL1, CYCS	1.292222	0.948387
mmu05163: Human cytomegalovirus infection	3	2.097902	0.925379	GNA11, GNG7, CYCS	0.731447	0.948387
mmu05200: Pathways in cancer	3	2.097902	0.981588	GNA11, GNG7, CYCS	0.53105	0.981588
Cluster 22-Enrichment Score: 0.0979872041167143						
Term	Count	%	PValue	Genes	Fold Enrichment	FDR
GO:0003824~catalytic activity	6	4.195804	0.675278	HINT2, TPI1, PSAT1, ALDOC, PAM, PRDX6	1.058894	1
mmu01230: Biosynthesis of amino acids	3	2.097902	0.777964	TPI1, PSAT1, ALDOC	1.076852	0.948387
mmu01200: Carbon metabolism	3	2.097902	0.967378	TPI1, PSAT1, ALDOC	0.59641	0.967378

Cluster 23- Enrichment Score: 0.08419959896826314						
Term	Count	%	PValue	Genes	Fold Enrichment	FDR
GO:0030154~cell differentiation	7	4.895105	0.63749	PURB, PURA, GAP43, CLPTM1, INA, NME1, PSMA8	1.07634	0.997994
GO:0007399~nervous system development	6	4.195804	0.771514	PURA, GAP43, RAP1A, NDUFV2, INA, NME1	0.943309	0.997994
KW-0221~Differentiation	5	3.496503	0.80535	GAP43, CLPTM1, INA, NME1, PSMA8	0.916724	1
KW-0524~Neurogenesis	4	2.797203	0.832491	GAP43, RAP1A, INA, NME1	0.898981	1
GO:0007275~multicellular organism development	4	2.797203	0.907785	GAP43, TPI1, CLPTM1, INA	0.756347	0.997994
KW-9996~Developmental protein	3	2.097902	0.927298	GAP43, CLPTM1, INA	0.723262	1
KW-0217~Developmental protein	3	2.097902	0.927298	GAP43, CLPTM1, INA	0.723262	1
Cluster 24- Enrichment Score: 0.07082506632858317						
Term	Count	%	PValue	Genes	Fold Enrichment	FDR
KW-0653~Protein transport	10	6.993007	0.789916	NAPB, TMED9, MTX2, RAB1B, SNX12, LIN7A, NAPG, RAB8A, RAB11A, RAB11B	0.904819	1
GO:0015031~protein transport	10	6.993007	0.836005	NAPB, TMED9, MTX2, RAB1B, SNX12, LIN7A, NAPG, RAB8A, RAB11A, RAB11B	0.858431	0.997994

GO:0005794 ~Golgi apparatus	10	6.99 3007	0.9284	NSFL1C, TMED9, RAB1B, PEBP1, TPPP, NAPG, RAB8A, RAB11A, SNCA, RAB11B	0.75069 7	0.992 754

APPtg Basal v. APPtg Memory Retrieval-20% Upregulated

Table 70. DAVID functional annotation clustering output table for annotation clusters enriched within proteins upregulated in APPtg mice during memory retrieval, when compared to APPtg mice at the basal level.

Cluster 1- Enrichment Score: 6.4083263821861856						
Term	Count	%	PValue	Genes	Fold Enrichment	FDR
mmu00190 :Oxidative phosphorylation	25	24.5 098	1.38E-11	NDUFB7, UQCRB, NDUFB10, NDUFB3, ATP5K, UQCR10, ATP5H, ATP5O, COX6A1, ATP5L, ATP6V1E1, NDUFV2, NDUFA8, ATP6V1G1, ATP6V1G2, NDUFA5, NDUFA4, NDUFA2, COX6C, SDHB, COX6B1, UQCRQ, NDUFS5, NDUFS4, CYCS	4.65 8709	1.42 E-09
KW-0249~Electron transport	17	16.6 6667	5.73E-10	NDUFA8, NDUFB7, NDUFA5, UQCRB, NDUFB10, NDUFA4, TXNL1, NDUFA2, NDUFB3, NDUFB1, UQCR10, SDHB, UQCRQ, NDUFS5, NDUFS4, CYCS, NDUFV2	6.29 0356	2.29 E-08
mmu05016 :Huntington disease	31	30.3 9216	1.96E-09	NDUFB7, UQCRB, NDUFB10, NDUFB3, CLTB, CLTA, UQCR10, ATP5H, ATP5O, COX6A1, PSMD6, PSMD7, NDUFV2, NDUFA8, NDUFA5, NDUFA4, NDUFA2, COX6C, SOD2, SDHB, SOD1, COX6B1, PSMA5, PSMA6, PSMC6, PSMA1, UQCRQ, PSMA2, NDUFS5, NDUFS4, CYCS	3.06 2866	8.91 E-08
KW-0679~Respiratory chain	15	14.7 0588	2.15E-09	NDUFA8, NDUFB7, NDUFA5, UQCRB, NDUFB10, NDUFA4, NDUFA2, NDUFB3, NDUFB1, UQCR10, UQCRQ, NDUFS5, NDUFS4, CYCS, NDUFV2	6.97 0162	4.29 E-08

mmu05012:Parkinson disease	30	29.41176	2.89E-09	NDUFB7, UQCRB, NDUFB10, NDUFB3, UQCR10, ATP5H, ATP5O, COX6A1, PSMD6, PSMD7, NDUFV2, NDUFA8, NDUFA5, NDUFA4, NDUFA2, COX6C, SDHB, SOD1, COX6B1, PSMA5, PSMA6, PSMC6, PSMA1, UQCRQ, PSMA2, NDUFS5, NDUFS4, CYCS, MAPT, MCU	3.11018	8.91E-08
mmu05020:Prion disease	30	29.41176	3.46E-09	NDUFB7, UQCRB, NDUFB10, NDUFB3, UQCR10, ATP5H, ATP5O, COX6A1, STIP1, PSMD6, PSMD7, NDUFV2, NDUFA8, NDUFA5, NDUFA4, NDUFA2, COX6C, SDHB, SOD1, COX6B1, PSMA5, PSMA6, PSMC6, PSMA1, UQCRQ, PSMA2, NDUFS5, NDUFS4, CYCS, MCU	3.08843	8.91E-08
mmu05208:Chemical carcinogenesis - reactive oxygen species	23	22.54902	6.48E-09	NDUFA8, CBR1, NDUFB7, NDUFA5, UQCRB, NDUFB10, NDUFA4, NDUFA2, NDUFB3, AKR1A1, UQCR10, ATP5H, COX6C, SOD2, ATP5O, COX6A1, SDHB, SOD1, COX6B1, UQCRQ, NDUFS5, NDUFS4, NDUFV2	3.891896	1.20E-07
mmu05014:Amyotrophic lateral sclerosis	30	29.41176	6.98E-09	NDUFB7, UQCRB, NDUFB10, NDUFB3, UQCR10, ATP5H, ATP5O, COX6A1, PSMD6, PSMD7, NEFM, NDUFV2, NDUFA8, NDUFA5, NDUFA4, NDUFA2, COX6C, SDHB, SOD1, COX6B1, PSMA5, PSMA6, PSMC6, PSMA1, UQCRQ, PSMA2, NDUFS5, NDUFS4, CYCS, MCU	3.004392	1.20E-07
GO:0070469~respiratory chain	15	14.70588	7.60E-09	NDUFA8, NDUFB7, NDUFA5, UQCRB, NDUFB10, NDUFA4, NDUFA2, NDUFB3, NDUFB1, UQCR10, UQCRQ, NDUFS5, NDUFS4, CYCS, NDUFV2	6.732143	1.81E-06
GO:0042776~mitochondrial ATP synthesis coupled proton transport	15	14.70588	2.07E-08	NDUFA8, NDUFB7, NDUFA5, NDUFB10, NDUFA2, NDUFB3, ATP5K, NDUFB1, ATP5H, ATP5O, SDHB, ATP5L, NDUFS5, NDUFS4, NDUFV2	6.282313	1.40E-05
mmu04932:Non-alcoholic fatty liver disease	18	17.64706	3.33E-08	NDUFA8, NDUFB7, NDUFA5, UQCRB, NDUFB10, NDUFA4, NDUFA2, NDUFB3, UQCR10, COX6C, COX6A1, SDHB, COX6B1, UQCRQ, NDUFS5, NDUFS4, CYCS, NDUFV2	4.648901	4.89E-07

mmu05010:Alzheimer disease	29	28.43137	6.32E-08	NDUFB7, UQCRB, NDUFB10, NDUFB3, UQCR10, ATP5H, ATP5O, COX6A1, PSMD6, PSMD7, NDUFV2, NDUFA8, NDUFA5, NDUFA4, NDUFA2, COX6C, SDHB, COX6B1, PSMA5, PSMA6, PSMC6, PSMA1, UQCRQ, PSMA2, NDUFS5, NDUFS4, CYCS, MAPT, MCU	2.827312	8.14E-07
mmu04714:Thermogenesis	21	20.58824	9.31E-08	NDUFA8, NDUFB7, NDUFA5, UQCRB, NDUFB10, NDUFA4, NDUFA2, NDUFB3, ATP5K, UQCR10, ATP5H, COX6C, ATP5O, COX6A1, SDHB, ATP5L, COX6B1, UQCRQ, NDUFS5, NDUFS4, NDUFV2	3.724722	1.07E-06
KW-0999~Mitochondrion inner membrane	24	23.52941	1.95E-07	NDUFA8, NDUFB7, NDUFA5, UQCRB, NDUFB10, NDUFA4, NDUFA2, NDUFB3, ATP5K, NDUFB1, TIMM44, UQCR10, ATP5H, COX6C, ATP5O, COX6A1, SDHB, ATP5L, COX6B1, UQCRQ, NDUFS5, NDUFS4, NDUFV2, MCU	3.279746	5.86E-06
GO:0009060~aerobic respiration	13	12.7451	3.68E-07	NDUFA8, NDUFB7, NDUFA5, UQCRB, NDUFB10, NDUFA2, NDUFB3, NDUFB1, UQCR10, SDHB, NDUFS5, NDUFS4, NDUFV2	6.125255	1.24E-04
mmu05022:Pathways of neurodegeneration - multiple diseases	31	30.39216	2.21E-06	NDUFB7, UQCRB, NDUFB10, NDUFB3, UQCR10, ATP5H, ATP5O, COX6A1, PSMD6, PSMD7, NEFM, NDUFV2, NDUFA8, NDUFA5, NDUFA4, NDUFA2, COX6C, SDHB, SOD1, COX6B1, PSMA5, PSMA6, PSMC6, PSMA1, UQCRQ, PSMA2, NDUFS5, NDUFS4, CYCS, MAPT, MCU	2.304884	2.28E-05
GO:0005747~mitochondrial respiratory chain complex I	11	10.78431	3.43E-06	NDUFA8, NDUFB7, NDUFB10, NDUFA5, NDUFA4, NDUFS5, NDUFA2, NDUFS4, NDUFB3, NDUFB1, NDUFV2	6.283333	4.08E-04
GO:0005743~mitochondrial inner membrane	26	25.4902	6.87E-06	NDUFB7, UQCRB, NDUFB10, NDUFB3, ATP5K, NDUFB1, UQCR10, ATP5H, ATP5O, COX6A1, CLU, ATP5L, NDUFV2, NDUFA8, NDUFA5, NDUFA4, NDUFA2, TIMM44, COX6C, SOD2, SDHB, COX6B1, UQCRQ, NDUFS5, NDUFS4, MCU	2.565969	5.45E-04

KW-0496~Mitochondrion	39	38.23529	7.36E-06	NDUFB7, UQCRB, NDUFB10, NDUFB3, CISD1, ATP5K, NDUFB1, AK4, UQCR10, ATP5H, ATP5O, COX6A1, CLU, ATP5L, PGRMC1, PRDX5, HINT2, SCP2, CKB, NDUFV2, FIS1, NDUFA8, NDUFA5, NDUFA4, MTX2, NDUFA2, TIMM44, COX6C, DYNLL1, SOD2, SDHB, COX6B1, UQCRQ, NDUFS5, NDUFS4, CYCS, GARS, PGAM5, MCU	1.968986	1.10E-04
mmu05415:Diabetic cardiomyopathy	19	18.62745	1.74E-05	NDUFA8, NDUFB7, NDUFA5, UQCRB, NDUFB10, NDUFA4, NDUFA2, NDUFB3, UQCR10, ATP5H, COX6C, ATP5O, COX6A1, SDHB, COX6B1, UQCRQ, NDUFS5, NDUFS4, NDUFV2	2.975626	1.63E-04
GO:0005739~mitochondrion	47	46.07843	4.02E-05	NDUFB7, UQCRB, NDUFB10, NDUFB3, CISD1, ATP5K, NDUFB1, ACAA1B, AK4, ACAA1A, UQCR10, ATP5H, ATP5O, COX6A1, CLU, ATP5L, PGRMC1, PRDX5, COMTD1, HINT2, SCP2, PRDX1, CKB, ATP6V1E1, NDUFV2, FIS1, NDUFA8, NDUFA5, NDUFA4, MTX2, NDUFA2, TIMM44, COX6C, DYNLL1, SOD2, SDHB, PRDX6, SOD1, COX6B1, UQCRQ, NDUFS5, NDUFS4, RAB35, CYCS, GARS, PGAM5, MCU	1.684316	0.00239
KW-0813~Transport	36	35.29412	6.49E-05	VPS29, NDUFB7, UQCRB, NDUFB10, NDUFB3, SNX12, ATP5K, NDUFB1, LIN7A, UQCR10, ATP5H, ATP5O, SLC4A3, ATP5L, SCP2, ATP6V1E1, NDUFV2, NDUFA8, ATP6V1G1, ATP6V1G2, NDUFA5, NDUFA4, MTX2, TXNL1, NDUFA2, TIMM44, DYNLL1, DYNLL2, SDHB, UQCRQ, NDUFS5, NDUFS4, RAB35, CYCS, ARF5, MCU	1.668958	8.65E-04
GO:0032981~mitochondrial respiratory chain complex I assembly	9	8.823529	2.53E-04	NDUFA8, NDUFB7, NDUFB10, NDUFA5, NDUFS5, NDUFA2, NDUFS4, NDUFB3, NDUFB1	4.988896	0.05069
GO:0008137~NADH dehydrogenase	6	5.882353	0.001378	NDUFB7, NDUFB10, NDUFA5, NDUFA2, NDUFS4, NDUFV2	6.613003	0.315491

(ubiquinone) activity						
mmu01100:Metabolic pathways	37	36.27451	0.001702	NDUFB7, UQCRB, NDUFB10, AK1, NDUFB3, ATP5K, ACAA1B, AK4, ACAA1A, UQCR10, ATP5H, ATP5O, COX6A1, ATP5L, SCP2, CKB, ATP6V1E1, NDUFV2, CBR3, NDUFA8, CBR1, ATP6V1G1, TPI1, ATP6V1G2, NDUFA5, NDUFA4, NDUFA2, AKR1A1, COX6C, SDHB, PRDX6, COX6B1, UQCRQ, PSAT1, NDUFS5, NDUFS4, CYCS	1.543049	0.0143446
mmu04723:Retrograde endocannabinoid signaling	10	9.803922	0.070074	NDUFA8, NDUFB7, NDUFB10, NDUFA5, NDUFA4, NDUFS5, NDUFA2, NDUFS4, NDUFB3, NDUFV2	1.887374	0.4511101
Cluster 2- Enrichment Score: 1.8031233955567816						
Term	Count	%	PValue	Genes	Fold Enrichment	FDR
DOMAIN:CHCH	4	3.921569	0.002081	NDUFA8, NDUFB7, NDUFS5, COX6B1	13.37681	0.4786661
MOTIF:Cx9C motif 1	3	2.941176	0.021808	NDUFA8, NDUFB7, NDUFS5	12.03913	0.835957
MOTIF:Cx9C motif 2	3	2.941176	0.021808	NDUFA8, NDUFB7, NDUFS5	12.03913	0.835957
GO:0005758~mitochondrial intermembrane space	5	4.901961	0.061943	NDUFA8, NDUFB7, NDUFS5, CYCS, SOD1	3.25	0.8219044
Cluster 3- Enrichment Score: 1.674569750733893						
Term	Count	%	PValue	Genes	Fold Enrichment	FDR

GO:0000502~proteasome complex	8	7.843137	0.001232	PSMA5, PSMA6, PSMD6, PSMC6, PSMD7, PSMA1, PSMA2, TXNL1	4.569697	0.05866
KW-0647~Proteasome	8	7.843137	0.001249	PSMA5, PSMA6, PSMD6, PSMC6, PSMD7, PSMA1, PSMA2, TXNL1	4.543814	0.012487
SM00948:SM00948	4	3.921569	0.001654	PSMA5, PSMA6, PSMA1, PSMA2	14.60938	0.052937
DOMAIN:PROTEASOME_ALPHA_1	4	3.921569	0.00542	PSMA5, PSMA6, PSMA1, PSMA2	10.03261	0.623326
GO:0019773~proteasome core complex, alpha-subunit complex	4	3.921569	0.00649	PSMA5, PSMA6, PSMA1, PSMA2	9.425	0.193086
IPR000426:Proteasome, alpha-subunit, N-terminal domain	4	3.921569	0.006687	PSMA5, PSMA6, PSMA1, PSMA2	9.326733	0.708848
IPR023332:Proteasome A-type subunit	4	3.921569	0.006687	PSMA5, PSMA6, PSMA1, PSMA2	9.326733	0.708848
mmu03050:Proteasome	7	6.862745	0.010273	PSMA5, PSMA6, PSMD6, PSMC6, PSMD7, PSMA1, PSMA2	3.55347	0.075578
GO:0043161~proteasome-mediated ubiquitin-dependent protein catabolic process	8	7.843137	0.015304	PSMA5, PSMA6, NSFL1C, PSMD6, PSMC6, PSMD7, PSMA1, PSMA2	2.956383	0.937734

GO:0010499~proteasomal ubiquitin-independent protein catabolic process	4	3.921569	0.033507	PSMA5, PSMA6, PSMA1, PSMA2	5.38484	1
GO:0005839~proteasome core complex	4	3.921569	0.033523	PSMA5, PSMA6, PSMA1, PSMA2	5.385714	0.569889
IPR001353: Proteasome, subunit alpha/beta	4	3.921569	0.034454	PSMA5, PSMA6, PSMA1, PSMA2	5.329562	1
mmu05017:Spinocerebellar ataxia	9	8.823529	0.035031	PSMA5, PSMA6, PSMD6, PSMC6, PSMD7, PSMA1, PSMA2, CYCS, MCU	2.284374	0.240544
GO:0051603~proteolysis involved in cellular protein catabolic process	4	3.921569	0.064575	PSMA5, PSMA6, PSMA1, PSMA2	4.188209	1
GO:0010498~proteasomal protein catabolic process	4	3.921569	0.073858	PSMA5, PSMA6, PSMA1, PSMA2	3.967777	1
GO:0004175~endopeptidase activity	4	3.921569	0.10624	PSMA5, PSMA6, PSMA1, PSMA2	3.406699	1
mmu05169:Epstein-Barr virus infection	4	3.921569	0.196296	PSMD6, PSMC6, PSMD7, CYCS	2.560264	0.919643
GO:0006511~ubiquitin-dependent	5	4.901961	0.20817	PSMA5, PSMA6, PSMA1, PSMA2, UBE2N	2.094104	1

protein catabolic process						
GO:0005654~nucleoplasm	12	11.76471	0.862711	PSMA5, PSMA6, NSFL1C, PSMD7, SCP2, PSMA1, PSMA2, UBE2N, NDUFV2, SDHB, CBR3, SOD1	0.837778	0.991667
Cluster 4- Enrichment Score: 1.5973035293716469						
Term	Count	%	PValue	Genes	Fold Enrichment	FDR
KW-0049~Antioxidant	4	3.921569	0.001233	PRDX5, PRDX1, PRDX6, SOD1	15.68116	0.038238
mmu04146:Peroxisome	7	6.862745	0.001811	PRDX5, SCP2, PRDX1, ACAA1B, ACAA1A, SOD2, SOD1	4.907173	0.014346
GO:0000302~response to reactive oxygen species	4	3.921569	0.006486	PRDX1, SOD2, PRDX6, SOD1	9.423469	0.845091
GO:0016209~antioxidant activity	4	3.921569	0.006583	PRDX5, PRDX1, PRDX6, SOD1	9.368421	0.753719
GO:0019430~removal of superoxide radicals	3	2.941176	0.015283	PRDX1, SOD2, SOD1	14.1352	0.937734
ACT_SITE:Cysteine sulfenic acid (-SOH) intermediate	3	2.941176	0.021808	PRDX5, PRDX1, PRDX6	12.03913	0.835957
KW-0575~Peroxidase	3	2.941176	0.031099	PRDX5, PRDX1, PRDX6	10.08075	0.378766

KW-0676~Redox-active center	4	3.921569	0.035635	PRDX5, PRDX1, TXNL1, PRDX6	5.237379	0.288235
GO:0051920~peroxiredoxin activity	3	2.941176	0.036017	PRDX5, PRDX1, PRDX6	9.368421	1
KW-0560~Oxidoreductase	11	10.78431	0.036655	CBR1, PRDX5, PRDX1, AKR1A1, SOD2, NDUFV2, COX6A1, SDHB, PRDX6, CBR3, SOD1	1.975108	0.378766
DOMAIN:Thioredoxin	4	3.921569	0.040707	PRDX5, PRDX1, TXNL1, PRDX6	5.016304	1
GO:0004601~peroxidase activity	3	2.941176	0.048712	PRDX5, PRDX1, PRDX6	8.030075	1
IPR013766:Thioredoxin domain	4	3.921569	0.049094	PRDX5, PRDX1, TXNL1, PRDX6	4.663366	1
GO:0042744~hydrogen peroxide catabolic process	3	2.941176	0.062149	PRDX5, PRDX1, PRDX6	7.067602	1
GO:0006979~response to oxidative stress	5	4.901961	0.107749	PRDX5, PRDX1, SOD2, PRDX6, SOD1	2.69242	1
GO:0045454~cell redox homeostasis	3	2.941176	0.127958	PRDX5, PRDX1, PRDX6	4.711735	1
GO:0016491~oxidoreductase activity	11	10.78431	0.180771	CBR1, PRDX5, PRDX1, AKR1A1, SOD2, NDUFV2, COX6A1, SDHB, PRDX6, CBR3, SOD1	1.504418	1
Cluster 5- Enrichment Score: 1.5039835000209274						
Term	Count	%	PValue	Genes	Fold Enric	FDR

					hme nt	
KW-0375~Hydrogen ion transport	7	6.862745	9.04E-04	ATP6V1G1, ATP6V1G2, ATP5K, ATP5H, ATP5O, ATP6V1E1, ATP5L	5.594717	0.009042
GO:0000276~mitochondrial proton-transporting ATP synthase complex, coupling factor F(o)	4	3.921569	0.00649	ATP5K, ATP5H, ATP5O, ATP5L	9.425	0.193086
GO:0046034~ATP metabolic process	6	5.882353	0.009822	AK1, ATP5K, AK4, ATP5H, ATP5O, ATP5L	4.349294	0.845091
GO:0005753~mitochondrial proton-transporting ATP synthase complex	4	3.921569	0.012877	ATP5K, ATP5H, ATP5O, ATP5L	7.54	0.340522
GO:0046933~proton-transporting ATP synthase activity, rotational mechanism	4	3.921569	0.013056	ATP5K, ATP5H, ATP5O, ATP5L	7.494737	0.884123
GO:0015986~ATP synthesis coupled proton transport	4	3.921569	0.01703	ATP5K, ATP5H, ATP5O, ATP5L	6.853432	0.956528

GO:0045263~proton-transporting ATP synthase complex, coupling factor F(o)	3	2.941176	0.048243	ATP5K, ATP5H, ATP5L	8.078571	0.717618
KW-0138~CF(0)	3	2.941176	0.051517	ATP5K, ATP5H, ATP5L	7.789396	0.309103
KW-0066~ATP synthesis	3	2.941176	0.054774	ATP5K, ATP5O, ATP5L	7.492925	0.438195
GO:0006754~ATP biosynthetic process	3	2.941176	0.127958	ATP5K, ATP5O, ATP5L	4.711735	1
GO:0015078~hydrogen ion transmembrane transporter activity	3	2.941176	0.147557	ATP5K, ATP5H, ATP5L	4.323887	1
KW-0406~Ion transport	9	8.823529	0.220608	ATP6V1G1, ATP6V1G2, ATP5K, ATP5H, ATP5O, ATP6V1E1, SLC4A3, MCU, ATP5L	1.511178	1
GO:0006811~ion transport	9	8.823529	0.299929	ATP6V1G1, ATP6V1G2, ATP5K, ATP5H, ATP5O, ATP6V1E1, SLC4A3, MCU, ATP5L	1.401838	1
Cluster 6- Enrichment Score: 1.4504900303546544						
Term	Count	%	PValue	Genes	Fold Enrichment	FDR
GO:0006122~mitochondrial electron transport, ubiquinol	4	3.921569	0.009362	UQCRB, UQCRQ, CYCS, UQCR10	8.376417	0.845091

to cytochrome c						
GO:0045333~cellular respiration	4	3.921569	0.021855	UQCRB, UQCRQ, NDUFS4, UQCR10	6.282313	1
GO:0005750~mitochondrial respiratory chain complex III	3	2.941176	0.062161	UQCRB, UQCRQ, UQCR10	7.06875	0.821904
mmu04260:Cardiac muscle contraction	6	5.882353	0.124056	UQCRB, UQCRQ, UQCR10, COX6C, COX6A1, COX6B1	2.208228	0.751632
Cluster 7- Enrichment Score: 1.185427793770002						
Term	Count	%	PValue	Genes	Fold Enrichment	FDR
mmu04146:Peroxisome	7	6.862745	0.001811	PRDX5, SCP2, PRDX1, ACAA1B, ACAA1A, SOD2, SOD1	4.907173	0.014346
GO:0005782~peroxisomal matrix	4	3.921569	0.00649	PRDX5, SCP2, PRDX1, ACAA1A	9.425	0.193086
GO:0008206~bile acid metabolic process	3	2.941176	0.007912	SCP2, ACAA1B, ACAA1A	18.84694	0.845091
GO:0050633~acetyl-CoA C-myristoyltransferase activity	3	2.941176	0.015443	SCP2, ACAA1B, ACAA1A	14.05263	0.884123
GO:0005777~peroxisome	6	5.882353	0.018039	FIS1, PRDX5, SCP2, ACAA1B, ACAA1A, SOD1	3.77	0.371616

KW-0576~Peroxisome	5	4.901961	0.028341	FIS1, PRDX5, SCP2, ACAA1B, ACAA1A	4.13074	0.212554
GO:0003988~acetyl-CoA C-acyltransferase activity	3	2.941176	0.036017	SCP2, ACAA1B, ACAA1A	9.368421	1
IPR020615: Thiolase, acyl-enzyme intermediate active site	3	2.941176	0.036375	SCP2, ACAA1B, ACAA1A	9.326733	1
GO:0016747~transferase activity, transferring acyl groups other than amino-acyl groups	3	2.941176	0.048712	SCP2, ACAA1B, ACAA1A	8.030075	1
DOMAIN:Thiolase_N	3	2.941176	0.055439	SCP2, ACAA1B, ACAA1A	7.524457	1
IPR020613: Thiolase, conserved site	3	2.941176	0.063353	SCP2, ACAA1B, ACAA1A	6.99505	1
IPR020616: Thiolase, N-terminal	3	2.941176	0.063353	SCP2, ACAA1B, ACAA1A	6.99505	1
IPR020617: Thiolase, C-terminal	3	2.941176	0.063353	SCP2, ACAA1B, ACAA1A	6.99505	1
IPR016039: Thiolase-like	3	2.941176	0.078698	SCP2, ACAA1B, ACAA1A	6.217822	1

mmu01040:Biosynthesis of unsaturated fatty acids	3	2.941176	0.140886	SCP2, ACAA1B, ACAA1A	4.416456	0.806178
KW-0012~Acyltransferase	3	2.941176	0.20057	SCP2, ACAA1B, ACAA1A	3.528261	1
GO:0016746~transferase activity, transferring acyl groups	3	2.941176	0.285384	SCP2, ACAA1B, ACAA1A	2.810526	1
GO:0006635~fatty acid beta-oxidation	3	2.941176	0.342565	SCP2, ACAA1B, ACAA1A	2.458296	1
KW-0443~Lipid metabolism	7	6.862745	0.403604	CBR1, HINT2, SCP2, AKR1A1, ACAA1B, ACAA1A, PRDX6	1.344884	1
mmu03320:PPAR signaling pathway	3	2.941176	0.440858	SCP2, ACAA1B, ACAA1A	2.00748	0.919643
GO:0006629~lipid metabolic process	7	6.862745	0.534343	CBR1, HINT2, SCP2, AKR1A1, ACAA1B, ACAA1A, PRDX6	1.188546	1
mmu01212:Fatty acid metabolism	3	2.941176	0.610132	SCP2, ACAA1B, ACAA1A	1.472152	0.919643
Cluster 8- Enrichment Score: 1.1808115267293193						
Term	Count	%	PValue	Genes	Fold Enrichment	FDR

KW-0001~2Fe-2S	3	2.941176	0.022206	CISD1, NDUFV2, SDHB	11.83784	0.488538
GO:0051537~2 iron, 2 sulfur cluster binding	3	2.941176	0.036017	CISD1, NDUFV2, SDHB	9.368421	1
KW-0408~Iron	5	4.901961	0.055242	PGRMC1, CISD1, CYCS, NDUFV2, SDHB	3.288288	0.607663
KW-0411~Iron-sulfur	3	2.941176	0.137406	CISD1, NDUFV2, SDHB	4.439189	1
GO:0051536~iron-sulfur cluster binding	3	2.941176	0.205441	CISD1, NDUFV2, SDHB	3.513158	1
Cluster 9- Enrichment Score: 0.8496214981406249						
Term	Count	%	PValue	Genes	Fold Enrichment	FDR
KW-1017~Isopeptide bond	15	14.70588	0.079411	TPI1, CISD1, DYNLL1, STIP1, PSMD7, PSMA1, RPS18, ARPC3, PRDX1, CFL1, DNAJA2, UBE2N, MAPT, RPL18, PPIA	1.575825	0.516173
KW-0832~Ubl conjugation	18	17.64706	0.186967	FIS1, TPI1, CISD1, DYNLL1, SOD2, CLU, STIP1, PSMD7, PSMA1, RPS18, ARPC3, PRDX1, CFL1, DNAJA2, UBE2N, MAPT, RPL18, PPIA	1.310885	0.81019
CROSSLNK: Glycyl lysine isopeptide (Lys-Gly) (interchain with G-Cter in SUMO2)	7	6.862745	0.190322	RPS18, ARPC3, PRDX1, CFL1, DNAJA2, DYNLL1, RPL18	1.777931	1
Cluster 10- Enrichment Score: 0.8490798264872408						

Term	Count	%	PValue	Genes	Fold Enrichment	FDR
KW-0375~Hydrogen ion transport	7	6.862745	9.04E-04	ATP6V1G1, ATP6V1G2, ATP5K, ATP5H, ATP5O, ATP6V1E1, ATP5L	5.594717	0.009042
GO:1902600~hydrogen ion transmembrane transport	5	4.901961	0.049521	ATP6V1G1, ATP6V1G2, UQCRQ, NDUFA4, ATP6V1E1	3.490174	1
GO:0046961~proton-transporting ATPase activity, rotational mechanism	3	2.941176	0.147557	ATP6V1G1, ATP6V1G2, ATP6V1E1	4.323887	1
mmu04721:Synaptic vesicle cycle	6	5.882353	0.178262	SNAP25, ATP6V1G1, ATP6V1G2, CLTB, CLTA, ATP6V1E1	1.962869	0.919643
mmu05323:Rheumatoid arthritis	3	2.941176	0.215011	ATP6V1G1, ATP6V1G2, ATP6V1E1	3.397274	0.919643
mmu04966:Collecting duct acid secretion	3	2.941176	0.215011	ATP6V1G1, ATP6V1G2, ATP6V1E1	3.397274	0.919643
mmu04150:mTOR signaling pathway	3	2.941176	0.610132	ATP6V1G1, ATP6V1G2, ATP6V1E1	1.472152	0.919643
mmu05165:Human papillomavirus infection	3	2.941176	0.819446	ATP6V1G1, ATP6V1G2, ATP6V1E1	0.981435	0.919643

mmu04145:Phagosome	3	2.941176	0.838174	ATP6V1G1, ATP6V1G2, ATP6V1E1	0.939671	0.919643
Cluster 11- Enrichment Score: 0.7479385011099945						
Term	Count	%	PValue	Genes	Fold Enrichment	FDR
GO:0005751~mitochondrial respiratory chain complex IV	4	3.921569	0.017039	NDUFA4, COX6C, COX6A1, COX6B1	6.854545	0.371616
TOPO_DOM:Mitochondrial matrix	6	5.882353	0.020689	UQCRQ, NDUFA4, UQCR10, COX6C, COX6A1, MCU	3.648221	0.835957
TOPO_DOM:Mitochondrial intermembrane	7	6.862745	0.027996	FIS1, UQCRQ, NDUFA4, UQCR10, COX6C, COX6A1, MCU	2.926178	0.919881
mmu04260:Cardiac muscle contraction	6	5.882353	0.124056	UQCRB, UQCRQ, UQCR10, COX6C, COX6A1, COX6B1	2.208228	0.751632
KW-1133~Transmembrane helix	17	16.66667	0.913886	FIS1, NDUFA4, ATL2, NDUFB3, CISD1, NDUFB1, UQCR10, ACAA1A, COX6C, SLC4A3, COX6A1, PCMT1, COMTD1, PGRMC1, UQCRQ, PGAM5, MCU	0.830881	1
KW-0812~Transmembrane	17	16.66667	0.932275	FIS1, NDUFA4, ATL2, NDUFB3, CISD1, NDUFB1, UQCR10, ACAA1A, COX6C, SLC4A3, COX6A1, PCMT1, COMTD1, PGRMC1, UQCRQ, PGAM5, MCU	0.813305	1
TRANSMEM:Helical	15	14.70588	0.996567	FIS1, NDUFA4, ATL2, NDUFB3, NDUFB1, UQCR10, ACAA1A, COX6C, SLC4A3, COX6A1, PCMT1, PGRMC1, UQCRQ, PGAM5, MCU	0.616759	1

GO:0016021~integral component of membrane	16	15.68627	0.999175	FIS1, NDUFA4, ATL2, NDUFB3, CISD1, NDUFB1, UQCR10, COX6C, SLC4A3, COX6A1, PCMT1, COMTD1, PGRMC1, UQCRQ, PGAM5, MCU	0.577778	0.999175
Cluster 12- Enrichment Score: 0.6943031928338689						
Term	Count	%	PValue	Genes	Fold Enrichment	FDR
REPEAT:TPR	3	2.941176	0.18471	STIP1, FIS1, SGTA	3.762228	1
KW-0802~TPR repeat	3	2.941176	0.19889	STIP1, FIS1, SGTA	3.553936	0.795561
IPR011990: Tetratricopeptide-like helical	4	3.921569	0.224898	STIP1, FIS1, PSMD6, SGTA	2.406899	1
Cluster 13- Enrichment Score: 0.331818815851336						
Term	Count	%	PValue	Genes	Fold Enrichment	FDR
KW-0408~Iron	5	4.901961	0.055242	PGRMC1, CISD1, CYCS, NDUFV2, SDHB	3.288288	0.607663
KW-0862~Zinc	4	3.921569	0.896111	VPS29, DNAJA2, CRIP2, SOD1	0.782667	1
KW-0479~Metal-binding	11	10.78431	0.956573	VPS29, PGRMC1, DNAJA2, EFHD2, CISD1, CYCS, CRIP2, SOD2, NDUFV2, SDHB, SOD1	0.746225	1
GO:0046872~metal ion binding	11	10.78431	0.993973	VPS29, PGRMC1, DNAJA2, EFHD2, CISD1, CYCS, CRIP2, SOD2, NDUFV2, SDHB, SOD1	0.593963	1
Cluster 14- Enrichment Score: 0.31461700821456934						
Term	Count	%	PValue	Genes	Fold Enric	FDR

					hme nt	
GO:0005634~nucleus	30	29.41176	0.262585	MTPN, CLU, STIP1, PRDX5, SCP2, RPS18, PRDX1, CFL1, MBP, CKB, CBR1, TPI1, TXNL1, SGTA, DYNLL1, PRDX6, SOD1, PSMA5, PSMA6, NSFL1C, PSMC6, PSMA1, PSMA2, ARPC3, DNAJA2, UBE2N, CYCS, MAPT, TAGLN3, PPIA	1.14939	0.991667
GO:0005829~cytosol	41	40.19608	0.396005	SNAP25, MTPN, VPS29, AK1, CLTB, CLU, STIP1, PCMT1, PRDX5, SCP2, RPS18, PRDX1, CFL1, CKB, ATP6V1E1, NDUFV2, RPL18, CBR3, ATP6V1G1, TPI1, TXNL1, SGTA, AKR1A1, DYNLL1, PRDX6, SOD1, PSMA5, FKBP1A, PSMA6, NSFL1C, IMPACT, MARCKS, PSMA1, PSAT1, PSMA2, DNAJA2, UBE2N, CYCS, GARS, MAPT, PPIA	1.060151	0.991667
KW-0963~Cytoplasm	47	46.07843	0.618341	SNAP25, MTPN, VPS29, WIPF3, AK1, ARPC5L, CLTA, CLU, STIP1, PCMT1, PRDX5, SCP2, DPYSL5, RPS18, PRDX1, CFL1, MBP, NEFM, CKB, RPL18, CBR3, CBR1, TPI1, TXNL1, SGTA, TMOD2, AKR1A1, DYNLL1, DYNLL2, MAPK8IP3, PRDX6, SOD1, PSMA5, FKBP1A, PSMA6, NSFL1C, IMPACT, MARCKS, PSMC6, PSMA1, PSMA2, ARPC3, UBE2N, GARS, MAPT, PPIA, ARF5	0.990994	1
GO:0005737~cytoplasm	54	52.94118	0.857696	SNAP25, VPS29, WIPF3, ARPC5L, CLTA, CLU, PCMT1, HINT2, SCP2, DPYSL5, RPS18, CFL1, NEFM, ATP6V1E1, CBR1, TPI1, TMOD2, AKR1A1, DYNLL1, DYNLL2, MAPK8IP3, PSMA5, PSMA6, IMPACT, PSMA1, PSMA2, GARS, MAPT, PPIA, ARF5, MTPN, AK1, AK4, STIP1, PRDX5, PRDX1, MBP, CKB, RPL18, CBR3, MTX2, TXNL1, SGTA, SOD2, PRDX6, SOD1, FKBP1A, NSFL1C, MARCKS, PSMC6, PSAT1, ARPC3, DNAJA2, UBE2N	0.927894	0.991667
Cluster 15- Enrichment Score: 0.3134074087848435						
Term	Count	%	PValue	Genes	Fold Enrichment	FDR

mmu04144:Endocytosis	9	8.823529	0.300687	VPS29, ARPC3, WIPF3, RAB35, ARPC5L, CLTB, SNX12, CLTA, ARF5	1.39467	0.919643
GO:0006886~intracellular protein transport	6	5.882353	0.566791	VPS29, MARCKS, CLTB, CLTA, TIMM44, ARF5	1.190333	1
GO:0016192~vesicle-mediated transport	5	4.901961	0.673349	RAB35, CLTB, CLTA, MAPK8IP3, ARF5	1.095752	1
Cluster 16- Enrichment Score: 0.2696617649939319						
Term	Count	%	PValue	Genes	Fold Enrichment	FDR
KW-1000~Mitochondrion outer membrane	5	4.901961	0.313173	FIS1, PGRMC1, MTX2, CISD1, PGAM5	1.747621	1
GO:0005741~mitochondrial outer membrane	5	4.901961	0.495725	FIS1, PGRMC1, MTX2, CISD1, PGAM5	1.365942	0.991667
TOPO_DOM:Cytoplasmic	5	4.901961	0.999977	FIS1, PGRMC1, ATL2, CISD1, SLC4A3	0.309648	1
Cluster 17- Enrichment Score: 0.24491615796669305						
Term	Count	%	PValue	Genes	Fold Enrichment	FDR
KW-0009~Actin-binding	7	6.862745	0.128883	IMPACT, MARCKS, ARPC3, CFL1, WIPF3, TMOD2, ARPC5L	1.960145	0.799074
mmu04666:Fc gamma R-mediated	4	3.921569	0.326372	MARCKS, ARPC3, CFL1, ARPC5L	1.962869	0.919643

phagocytosis						
GO:0003779~actin binding	7	6.862745	0.493425	IMPACT, MARCKS, ARPC3, CFL1, WIPF3, TMOD2, ARPC5L	1.237339	1
mmu05135:Yersinia infection	3	2.941176	0.662933	ARPC3, WIPF3, ARPC5L	1.33832	0.919643
GO:0005856~cytoskeleton	14	13.72549	0.681064	SNAP25, TMOD2, ARPC5L, CLTA, DYNLL1, DYNLL2, CLU, NSFL1C, MARCKS, ARPC3, CFL1, NEFM, MAPT, TAGLN3	0.977407	0.991667
GO:0007015~actin filament organization	3	2.941176	0.68326	MARCKS, CFL1, TMOD2	1.285019	1
mmu04810:Regulation of actin cytoskeleton	4	3.921569	0.773109	MRAS, ARPC3, CFL1, ARPC5L	0.998069	0.919643
GO:0051015~actin filament binding	4	3.921569	0.807378	MARCKS, ARPC3, CFL1, ARPC5L	0.936842	1
KW-0206~Cytoskeleton	11	10.78431	0.890269	NSFL1C, MARCKS, ARPC3, CFL1, TMOD2, ARPC5L, CLTA, NEFM, MAPT, DYNLL1, DYNLL2	0.806161	1
GO:0098978~glutamatergic synapse	6	5.882353	0.99914	SNAP25, MARCKS, CFL1, ARPC5L, CLTA, DYNLL2	0.426792	0.99914
Term	Count	%	PValue	Genes	Fold Enrichment	FDR
KW-0009~Actin-binding	7	6.862745	0.128883	IMPACT, MARCKS, ARPC3, CFL1, WIPF3, TMOD2, ARPC5L	1.960145	0.799074

mmu04666:Fc gamma R-mediated phagocytosis	4	3.921569	0.326372	MARCKS, ARPC3, CFL1, ARPC5L	1.962869	0.919643
GO:0003779~actin binding	7	6.862745	0.493425	IMPACT, MARCKS, ARPC3, CFL1, WIPF3, TMOD2, ARPC5L	1.237339	1
mmu05135:Yersinia infection	3	2.941176	0.662933	ARPC3, WIPF3, ARPC5L	1.33832	0.919643
GO:0005856~cytoskeleton	14	13.72549	0.681064	SNAP25, TMOD2, ARPC5L, CLTA, DYNLL1, DYNLL2, CLU, NSFL1C, MARCKS, ARPC3, CFL1, NEFM, MAPT, TAGLN3	0.977407	0.991667
GO:0098978~glutamatergic synapse	6	5.882353	0.99914	SNAP25, MARCKS, CFL1, ARPC5L, CLTA, DYNLL2	0.426792	0.99914
Cluster 18- Enrichment Score: 0.22463220852818871						
Term	Count	%	PValue	Genes	Fold Enrichment	FDR
KW-0168~Coated pit	3	2.941176	0.359192	RAB35, CLTB, CLTA	2.370686	1
GO:0005905~clathrin-coated pit	3	2.941176	0.419167	RAB35, CLTB, CLTA	2.094444	0.991667
GO:0016192~vesicle-mediated transport	5	4.901961	0.673349	RAB35, CLTB, CLTA, MAPK8IP3, ARF5	1.095752	1
GO:0031410~cytoplasmic vesicle	9	8.823529	0.826966	PRDX5, ATP6V1G2, RAB35, CLTB, CLTA, ATP6V1E1, CLU, MAPK8IP3, SOD1	0.865561	0.991667
KW-0968~Cytoplasmic vesicle	7	6.862745	0.898251	ATP6V1G2, RAB35, CLTB, CLTA, ATP6V1E1, CLU, MAPK8IP3	0.775773	1

Cluster 19- Enrichment Score: 0.20816602238532186						
Term	Count	%	PValue	Genes	Fold Enrichment	FDR
GO:0032456~endocytic recycling	3	2.941176	0.342565	VPS29, RAB35, SNX12	2.458296	1
KW-0653~Protein transport	7	6.862745	0.793396	VPS29, MTX2, RAB35, SNX12, TIMM44, LIN7A, ARF5	0.908233	1
GO:0015031~protein transport	7	6.862745	0.873513	VPS29, MTX2, RAB35, SNX12, TIMM44, LIN7A, ARF5	0.809378	1
Cluster 20- Enrichment Score: 0.11805508603252067						
Term	Count	%	PValue	Genes	Fold Enrichment	FDR
LIPID:S-palmitoylcysteine	4	3.921569	0.691527	SNAP25, PRDX5, SLC4A3, SOD1	1.130435	1
KW-0449~Lipoprotein	10	9.803922	0.736993	SNAP25, PRDX5, MARCKS, NDUFB7, MRAS, DNAJA2, RAB35, SLC4A3, ARF5, SOD1	0.947128	1
KW-0564~Palmitate	4	3.921569	0.868085	SNAP25, PRDX5, SLC4A3, SOD1	0.83089	1
Cluster 21- Enrichment Score: 0.04702730058846935						
Term	Count	%	PValue	Genes	Fold Enrichment	FDR
KW-0342~GTP-binding	5	4.901961	0.683484	MRAS, ATL2, RAB35, AK4, ARF5	1.076167	1
IPR005225: Small GTP-binding	3	2.941176	0.809225	MRAS, RAB35, ARF5	0.999293	1

protein domain						
GO:0005525~GTP binding	5	4.901961	0.883606	MRAS, ATL2, RAB35, AK4, ARF5	0.793934	1
IPR027417: P-loop containing nucleoside triphosphate hydrolase	7	6.862745	0.900004	PSMC6, MRAS, AK1, ATL2, RAB35, AK4, ARF5	0.772629	1
GO:0003924~GTPase activity	4	3.921569	0.942241	MRAS, ATL2, RAB35, ARF5	0.675202	1
KW-0547~Nucleotide-binding	12	11.76471	0.957759	PSMC6, HINT2, MRAS, AK1, ATL2, RAB35, UBE2N, TIMM44, GARS, AK4, CKB, ARF5	0.755607	1
KW-0067~ATP-binding	7	6.862745	0.965459	PSMC6, AK1, UBE2N, TIMM44, GARS, AK4, CKB	0.673698	1
GO:0005524~ATP binding	8	7.843137	0.991566	PSMC6, AK1, DNAJA2, UBE2N, TIMM44, GARS, AK4, CKB	0.567783	1
GO:0000166~nucleotide binding	12	11.76471	0.993071	PSMC6, HINT2, MRAS, AK1, ATL2, RAB35, UBE2N, TIMM44, GARS, AK4, CKB, ARF5	0.612649	1
Cluster 22- Enrichment Score: 0.026821790658358116						
Term	Count	%	PValue	Genes	Fold Enrichment	FDR
KW-0418~Kinase	4	3.921569	0.845751	AK1, AK4, CKB, MAPK8IP3	0.871176	1
GO:0016301~kinase activity	4	3.921569	0.931904	AK1, AK4, CKB, MAPK8IP3	0.700443	1

KW-0067~ATP-binding	7	6.862745	0.965459	PSMC6, AK1, UBE2N, TIMM44, GARS, AK4, CKB	0.673698	1
GO:0016310~phosphorylation	3	2.941176	0.973245	AK1, AK4, CKB	0.565408	1
GO:0005524~ATP binding	8	7.843137	0.991566	PSMC6, AK1, DNAJA2, UBE2N, TIMM44, GARS, AK4, CKB	0.567783	1
Cluster 23- Enrichment Score: 0.005204590681130565						
Term	Count	%	PValue	Genes	Fold Enrichment	FDR
GO:0030424~axon	6	5.882353	0.966166	SNAP25, MTPN, GARS, NEFM, MAPT, MAPK8IP3	0.635393	0.9916667
GO:0042995~cell projection	7	6.862745	0.99911	ARPC3, CFL1, GARS, NEFM, MBP, MAPT, MAPK8IP3	0.450341	0.99911
KW-0966~Cell projection	6	5.882353	0.999358	ARPC3, CFL1, GARS, NEFM, MAPT, MAPK8IP3	0.417822	1

Wild-Type Basal v. APPtg Basal- 20% Upregulated

Table 71. DAVID functional annotation clustering output table for annotation clusters enriched within proteins upregulated in APPtg mice at the basal level, when compared to WT mice at the basal level.

Cluster 1- Enrichment Score: 1.7151323831527738						
Term	Count	%	PValue	Genes	Fold Enrichment	FDR
IPR001478:PDZ domain	8	5.797101	1.48E-02	RIMS1, LRRC7, MYO18A, GM20498, CASK, SYNJ2BP, PPP1R9A, PPP1R9B	2.959937	1.00E+00

DOMAIN:PDZ	8	5.797101	1.58E-02	RIMS1, LRRC7, MYO18A, GM20498, CASK, SYNJ2BP, PPP1R9A, PPP1R9B	2.922042	1.00E+00
SM00228:PDZ	8	5.797101	3.05E-02	RIMS1, LRRC7, MYO18A, GM20498, CASK, SYNJ2BP, PPP1R9A, PPP1R9B	2.523617	1.00E+00
Cluster 2- Enrichment Score: 1.6762702598189836						
Term	Count	%	PValue	Genes	Fold Enrichment	FDR
GO:0006897~endocytosis	11	7.971014	7.25E-03	APP, EHD3, DBNL, MYO6, ITSN1, HIP1R, EPS15L1, TLN2, PIP5K1C, SYNJ2BP, EPN1	2.604744	1.00E+00
KW-0254~Endocytosis	9	6.521739	1.06E-02	APP, DBNL, MYO6, ITSN1, HIP1R, EPS15L1, PIP5K1C, SYNJ2BP, EPN1	2.801587	5.94E-01
GO:0005905~clathrin-coated pit	6	4.347826	3.61E-02	APP, MYO6, ITSN1, HIP1R, EPS15L1, EPN1	3.149541	1.00E+00
KW-0168~Coated pit	5	3.623188	7.11E-02	APP, MYO6, ITSN1, EPS15L1, EPN1	3.090813	5.72E-01
Cluster 3- Enrichment Score: 1.1607536263892448						
Term	Count	%	PValue	Genes	Fold Enrichment	FDR
GO:0009156~ribonucleoside monophosphate biosynthetic process	3	2.173913	1.39E-02	PRPS2, PRPS1, PRPS1L3	14.20769	1.00E+00
IPR000842:Phosphoribosyl pyrophosphate synthetase, conserved site	3	2.173913	1.42E-02	PRPS2, PRPS1, PRPS1L3	14.0597	1.00E+00

GO:0006015~5-phosphoribose 1-diphosphate biosynthetic process	3	2.173913	2.65E-02	PRPS2, PRPS1, PRPS1L3	10.65577	1.00E+00
GO:0002189~ribose phosphate diphosphokinase complex	3	2.173913	2.66E-02	PRPS2, PRPS1, PRPS1L3	10.6297	1.00E+00
IPR000836:Phosphoribosyltransferase domain	3	2.173913	2.70E-02	PRPS2, PRPS1, PRPS1L3	10.54478	1.00E+00
IPR005946:Ribose-phosphate diphosphokinase	3	2.173913	2.70E-02	PRPS2, PRPS1, PRPS1L3	10.54478	1.00E+00
GO:0004749~ribose phosphate diphosphokinase activity	3	2.173913	2.76E-02	PRPS2, PRPS1, PRPS1L3	10.42969	1.00E+00
KW-0545~Nucleotide biosynthesis	3	2.173913	3.06E-02	PRPS2, PRPS1, PRPS1L3	9.805556	0.856952
GO:0009116~nucleoside metabolic process	3	2.173913	6.03E-02	PRPS2, PRPS1, PRPS1L3	7.103846	1.00E+00
GO:0006164~purine nucleotide biosynthetic process	3	2.173913	1.51E-01	PRPS2, PRPS1, PRPS1L3	4.262308	1

mmu00230: Purine metabolism	5	3.623188	0.161752	PRPS2, PRPS1, PDE10A, AMPD2, PRPS1L3	2.300237	1
GO:0000287~magnesium ion binding	7	5.072464	0.253254	PRPS2, PRPS1, SRR, BRSK2, ATP8A1, BPNT1, PRPS1L3	1.622396	1
mmu00030: Pentose phosphate pathway	3	2.173913	0.266231	PRPS2, PRPS1, PRPS1L3	2.944304	1
mmu01200: Carbon metabolism	5	3.623188	0.648564	PRPS2, PRPS1, ALDH6A1, SDHC, PRPS1L3	1.132425	1
mmu01230: Biosynthesis of amino acids	3	2.173913	0.709935	PRPS2, PRPS1, PRPS1L3	1.226793	1
Cluster 4- Enrichment Score: 1.1603250694185652						
Term	Count	%	PValue	Genes	Fold Enrichment	FDR
GO:0045202~synapse	36	26.08696	0.027325	NRXN1, ITSN1, ITPR1, PPP1R9A, HAPLN1, PPP1R9B, SYNPR, RIMS1, GRM2, CACNG8, GPC1, MYO6, DLGAP2, PPFIA3, PPFIA2, DLGAP4, MPST, EPHA4, UNC13A, DBNL, ATP6AP1, SLC32A1, GAD1, CASK, SLC6A11, GRIN1, BCAN, CACNB4, LRRC7, MADD, CSPG5, ADGRL1, TLN2, PABPC1, TPRGL, PAFAH1B1	1.382725	1
GO:0030054~cell junction	27	19.56522	0.102666	SRC, NRXN1, ITSN1, MTDH, PPP1R9B, SYNPR, RIMS1, GRM2, GJA1, CACNG8, PIP5K1C, PCDH1, DLGAP2, PPFIA2, MPST, EPHA4, UNC13A, DBNL, ATP6AP1, SYNJ2BP, GRIN1, VAPA, LRRC7, CSPG5, ADGRL1, TLN2, TPRGL	1.315014	1
KW-0770~Synapse	21	15.21739	0.117772	MPST, EPHA4, UNC13A, DBNL, ATP6AP1, SLC32A1, NRXN1, ITSN1, PPP1R9B, GRIN1, SYNPR, RIMS1, GRM2, CACNG8, LRRC7, CSPG5, ADGRL1, TLN2, DLGAP2, TPRGL, PPFIA2	1.363345	0.57179

Cluster 5- Enrichment Score: 1.1422476000488115						
Term	Count	%	PValue	Genes	Fold Enrichment	FDR
GO:0098831~presynaptic active zone cytoplasmic component	4	2.898551	0.057178	RIMS1, UNC13A, IQSEC2, PPFIA3	4.360902	1
GO:0016081~synaptic vesicle docking	3	2.173913	0.08063	RIMS1, UNC13A, PPFIA3	6.089011	1
GO:0007269~neurotransmitter secretion	5	3.623188	0.081195	RIMS1, GRM2, UNC13A, NRXN1, PPFIA3	2.959936	1
Cluster 6- Enrichment Score: 1.1292162684983824						
Term	Count	%	PValue	Genes	Fold Enrichment	FDR
GO:0051015~actin filament binding	13	9.42029	0.009386	ACTR2, DBNL, TPM1, HIP1R, ADD3, PPP1R9A, ACTR3B, PPP1R9B, ADD2, MYO6, MYO18A, TLN2, CLASP2	2.259766	1
KW-0009~Actin-binding	12	8.695652	0.041801	ACTR2, DBNL, CAPZB, MYO6, TPM1, MYO18A, HIP1R, FMN2, ADD3, ACTR3B, PPP1R9B, ADD2	1.885017	0.668817
GO:0003779~actin binding	13	9.42029	0.069157	ACTR2, DBNL, TPM1, HIP1R, FMN2, ADD3, ACTR3B, PPP1R9B, ADD2, CAPZB, MYO6, KCNMA1, TLN2	1.705483	1
KW-0206~Cytoskeleton	23	16.66667	0.130695	ACTR2, BRSK2, DBNL, ROCK2, SRC, TPM1, GNAI3, FMN2, ADD3, ACTR3B, CKAP4, GLG1, PPP1R9B, ADD2, CLIP2, CAPZB, KIF5C, HECW2, MYO18A, TLN2, PAFAH1B1, CCT4, CLASP2	1.318581	0.57179
GO:0005856~cytoskeleton	24	17.3913	0.176148	ACTR2, BRSK2, DBNL, ROCK2, SRC, TPM1, GNAI3, HIP1R, FMN2, ADD3, PPP1R9A, ACTR3B, CKAP4, GLG1, PPP1R9B, ADD2, CLIP2, CAPZB, HECW2,	1.259816	1

				MYO18A, TLN2, PAFAH1B1, CCT4, CLASP2		
GO:0005200 ~structural constituent of cytoskeleton	5	3.623188	0.268583	ACTR2, TPM1, TLN2, ADD3, ADD2	1.879223	1
Cluster 7- Enrichment Score: 1.0711242900625968						
Term	Count	%	PValue	Genes	Fold Enrichment	FDR
IPR013761:Sterile alpha motif/pointed domain	4	2.898551	0.058337	EPHA4, PPP1R9A, PPFIA3, PPFIA2	4.326062	1
IPR001660:Sterile alpha motif domain	4	2.898551	0.058337	EPHA4, PPP1R9A, PPFIA3, PPFIA2	4.326062	1
DOMAIN:SAM	4	2.898551	0.060209	EPHA4, PPP1R9A, PPFIA3, PPFIA2	4.270677	1
SM00454:SAM	4	2.898551	0.084232	EPHA4, PPP1R9A, PPFIA3, PPFIA2	3.688363	1
GO:0061001 ~regulation of dendritic spine morphogenesis	3	2.173913	0.255475	EPHA4, PPP1R9A, PPFIA2	3.044505	1
Cluster 8- Enrichment Score: 1.0404036813316888						
Term	Count	%	PValue	Genes	Fold Enrichment	FDR
KW-0333~Golgi apparatus	14	10.14493	0.045927	SH3GLB1, APP, DBNL, ATP8A1, AP3D1, AP1B1, GLG1, PACS1, RAB12, MYO6, MYO18A, CSPG5, SCYL2, CLASP2	1.76149	0.57179

GO:0000139~Golgi membrane	9	6.521739	0.074116	SH3GLB1, DBNL, VAPA, RAB12, AP3D1, GNAI3, MYO18A, CSPG5, GLG1	1.993069	1
GO:0005794~Golgi apparatus	17	12.31884	0.222234	SH3GLB1, APP, EPHA4, DBNL, ATP8A1, AP3D1, AP1B1, GNAI3, GLG1, GJA1, PACS1, RAB12, MYO6, MYO18A, CSPG5, SCYL2, CLASP2	1.295376	1
Cluster 9- Enrichment Score: 0.9190907758142892						
Term	Count	%	PValue	Genes	Fold Enrichment	FDR
KW-0245~EGF-like domain	5	3.623188	0.054972	BCAN, NRXN1, ADAM22, CSPG5, TNR	3.319717	0.541
IPR000742:Epidermal growth factor-like domain	4	2.898551	0.113094	BCAN, NRXN1, ADAM22, TNR	3.308165	1
DOMAIN:EGF-like	4	2.898551	0.116425	BCAN, NRXN1, ADAM22, CSPG5	3.265812	1
SM00181:EGF	3	2.173913	0.291078	BCAN, NRXN1, TNR	2.766272	1
Cluster 10- Enrichment Score: 0.8460822977190687						
Term	Count	%	PValue	Genes	Fold Enrichment	FDR
GO:0005262~calcium channel activity	6	4.347826	0.024145	RYR2, CACNG8, CACNB4, ITPR1, CACNA1E, GRIN1	3.476563	1
KW-0107~Calcium channel	5	3.623188	0.032742	RYR2, CACNG8, CACNB4, ITPR1, CACNA1E	3.880918	0.668817
GO:0006874~cellular calcium ion homeostasis	5	3.623188	0.126596	RYR2, CACNB4, HEXB, PYGM, GRIN1	2.537088	1

mmu04921: Oxytocin signaling pathway	7	5.072464	0.128938	RYR2, CACNG8, CACNB4, ROCK2, SRC, ITPR1, GNAI3	1.981743	1
mmu05410: Hypertrophic cardiomyopathy	4	2.898551	0.145417	RYR2, CACNG8, CACNB4, TPM1	2.944304	1
KW-0109~Calcium transport	5	3.623188	1.70E-01	RYR2, CACNG8, CACNB4, ITPR1, CACNA1E	2.254151	1
GO:0006816~calcium ion transport	6	4.347826	0.176876	RYR2, CACNG8, CACNB4, ITPR1, CACNA1E, GRIN1	1.982469	1
mmu05412: Arrhythmogenic right ventricular cardiomyopathy	4	2.898551	0.196296	RYR2, CACNG8, GJA1, CACNB4	2.560264	1
mmu05414: Dilated cardiomyopathy	4	2.898551	0.250827	RYR2, CACNG8, CACNB4, TPM1	2.264849	1
Cluster 11- Enrichment Score: 0.8060151352635841						
Term	Count	%	PValue	Genes	Fold Enrichment	FDR
DOMAIN:Ion_trans	5	3.623188	0.002374	RYR2, KCNMA1, ITPR1, CACNA1E, SCN1A	7.710944	0.407211
IPR005821:Ion transport domain	5	3.623188	0.013624	RYR2, KCNMA1, ITPR1, CACNA1E, SCN1A	5.021322	1
GO:0007628~adult walking behavior	5	3.623188	0.021391	ABHD12, EPHA4, CACNB4, KCNMA1, SCN1A	4.439904	1
GO:0005262~calcium	6	4.347826	0.024145	RYR2, CACNG8, CACNB4, ITPR1, CACNA1E, GRIN1	3.476563	1

channel activity						
KW-0107~Calcium channel	5	3.623188	0.032742	RYR2, CACNG8, CACNB4, ITPR1, CACNA1E	3.880918	0.668817
KW-0407~Ion channel	9	6.521739	0.03839	RYR2, CACNG8, CACNB4, KCNMA1, ITPR1, LRRC8A, CACNA1E, SCN1A, GRIN1	2.240681	0.668817
GO:0005216~ion channel activity	6	4.347826	0.050721	RYR2, KCNMA1, ITPR1, CACNA1E, SCN1A, GRIN1	2.877155	1
GO:0005244~voltage-gated ion channel activity	5	3.623188	0.09736	CACNG8, CACNB4, KCNMA1, CACNA1E, SCN1A	2.78125	1
GO:0034765~regulation of ion transmembrane transport	5	3.623188	0.102727	CACNG8, CACNB4, KCNMA1, CACNA1E, SCN1A	2.732249	1
KW-0851~Voltage-gated channel	5	3.623188	0.110535	CACNG8, CACNB4, KCNMA1, CACNA1E, SCN1A	2.639024	1
GO:0006874~cellular calcium ion homeostasis	5	3.623188	0.126596	RYR2, CACNB4, HEXB, PYGM, GRIN1	2.537088	1
GO:0042391~regulation of membrane potential	5	3.623188	0.152566	RIMS1, CACNB4, KCNMA1, SCN1A, GRIN1	2.367949	1
KW-0109~Calcium transport	5	3.623188	0.169901	RYR2, CACNG8, CACNB4, ITPR1, CACNA1E	2.254151	1
GO:0006816~calcium ion transport	6	4.347826	0.176876	RYR2, CACNG8, CACNB4, ITPR1, CACNA1E, GRIN1	1.982469	1

GO:0051649 ~establishment of localization in cell	5	3.623188	0.256018	RYR2, CASK, CACNA1E, PAFAH1B1, SCN1A	1.919958	1
GO:0005245 ~voltage-gated calcium channel activity	3	2.173913	0.263533	CACNG8, CACNB4, CACNA1E	2.979911	1
GO:0070588 ~calcium ion transmembrane transport	4	2.898551	0.271191	RYR2, CACNB4, ITPR1, CACNA1E	2.185799	1
KW-0675~Receptor	7	5.072464	0.289097	GRM2, EPHA4, RYR2, ITPR1, ADAM22, ADGRL1, GRIN1	1.539431	1
GO:0006811 ~ion transport	11	7.971014	0.335096	RYR2, CACNG8, CACNB4, ATP6AP1, KCNMA1, ITPR1, LRRC8A, CACNA1E, SCN1A, GRIN1, ADD2	1.291608	1
KW-1071~Ligand-gated ion channel	3	2.173913	0.367741	RYR2, ITPR1, GRIN1	2.328551	1
KW-0106~Calcium	13	9.42029	0.41098	RYR2, UNC13A, NRXN1, ITSN1, ITPR1, EPS15L1, CACNA1E, GRIN1, EHD3, CACNG8, CACNB4, KCNMA1, FKBP8	1.171123	1
GO:0001666 ~response to hypoxia	4	2.898551	0.446985	RYR2, KCNMA1, ITPR1, PYGM	1.623736	1
mmu04713: Circadian entrainment	4	2.898551	0.544688	RYR2, ITPR1, GNAI3, GRIN1	1.402049	1
GO:0055085 ~transmembrane transport	6	4.347826	0.548555	RYR2, GJA1, KCNMA1, ITPR1, CACNA1E, SCN1A	1.217802	1

KW-0406~Ion transport	10	7.246377	0.555677	RYR2, CACNG8, CACNB4, ATP6AP1, KCNMA1, ITPR1, LRRC8A, CACNA1E, SCN1A, GRIN1	1.098662	1
mmu04972: Pancreatic secretion	3	2.173913	0.662933	RYR2, KCNMA1, ITPR1	1.33832	1
mmu04020: Calcium signaling pathway	4	2.898551	0.692642	RYR2, ITPR1, CACNA1E, GRIN1	1.132425	1
mmu04724: Glutamatergic synapse	4	2.898551	0.740918	GRM2, ITPR1, GNAI3, GRIN1	1.051537	1
mmu04010: MAPK signaling pathway	3	2.173913	0.913342	CACNG8, CACNB4, CACNA1E	0.761458	1
Cluster 12- Enrichment Score: 0.7627320185852414						
Term	Count	%	PValue	Genes	Fold Enrichment	FDR
GO:0030170~pyridoxal phosphate binding	4	2.898551	0.072333	SRR, OAT, GAD1, PYGM	3.973214	1
KW-0663~Pyridoxal phosphate	4	2.898551	0.10026	SRR, OAT, GAD1, PYGM	3.435294	1
GO:0003824~catalytic activity	6	4.347826	0.710137	SRR, PDE10A, OAT, ECI1, GAD1, PYGM	1.01753	1
Cluster 13- Enrichment Score: 0.7497953782446511						
Term	Count	%	PValue	Genes	Fold Enrichment	FDR
IPR000261:EPS15 homology (EH)	3	2.173913	0.027008	EHD3, ITSN1, EPS15L1	10.54478	1

DOMAIN:EH	3	2.173913	0.027674	EHD3, ITSN1, EPS15L1	10.40977	1
SM00027:EH	3	2.173913	0.036025	EHD3, ITSN1, EPS15L1	8.990385	1
GO:0005509~calcium ion binding	13	9.42029	0.10123	RYR2, UNC13A, PCDHGC5, NRXN1, ITSN1, ITPR1, EPS15L1, CACNA1E, GRIN1, BCAN, EHD3, SRR, PCDH1	1.599834	1
GO:0016197~endosomal transport	3	2.173913	0.308885	EHD3, ITSN1, EPS15L1	2.663942	1
DOMAIN:EF-hand	5	3.623188	0.403578	RYR2, EHD3, ITSN1, EPS15L1, CACNA1E	1.542189	1
KW-0106~Calcium	13	9.42029	0.41098	RYR2, UNC13A, NRXN1, ITSN1, ITPR1, EPS15L1, CACNA1E, GRIN1, EHD3, CACNG8, CACNB4, KCNMA1, FKBP8	1.171123	1
IPR002048:EF-hand domain	5	3.623188	0.426855	RYR2, EHD3, ITSN1, EPS15L1, CACNA1E	1.495713	1
IPR011992:EF-hand-like domain	4	2.898551	0.711475	RYR2, EHD3, ITSN1, EPS15L1	1.102722	1
IPR018247:EF-Hand 1, calcium-binding site	3	2.173913	0.749149	EHD3, ITSN1, EPS15L1	1.139976	1
Cluster 14- Enrichment Score: 0.728040228641575						
Term	Count	%	PValue	Genes	Fold Enrichment	FDR
KW-0654~Proteoglycan	4	2.898551	0.010196	BCAN, GPC1, CSPG5, TNR	7.897793	0.121878
GO:0031012~extracellular matrix	5	3.623188	0.032559	BCAN, GPC1, TNR, GLG1, HAPLN1	3.936926	1

KW-0272~Extracellular matrix	3	2.173913	1.51E-01	BCAN, TNR, HAPLN1	4.265323	0.58542
KW-0964~Secreted	6	4.347826	0.323118	BCAN, APP, GPC1, TNR, HAPLN1, ITFG1	1.579749	0.846623
GO:0007417~central nervous system development	3	2.173913	0.387322	BCAN, APP, HAPLN1	2.24332	1
GO:0005576~extracellular region	7	5.072464	0.43037	BCAN, APP, HSPH1, GPC1, TNR, HAPLN1, ITFG1	1.322807	1
IPR013783:Immunoglobulin-like fold	5	3.623188	0.709646	BCAN, EPHA4, VAPA, TNR, HAPLN1	1.049231	1
GO:0005615~extracellular space	5	3.623188	0.78454	BCAN, APP, HEXB, GPC1, TNR	0.944862	1
Cluster 15-Enrichment Score: 0.7272420296787512						
Term	Count	%	PValue	Genes	Fold Enrichment	FDR
REPEAT:4	4	2.898551	0.116425	SYNPR, RYR2, FMN2, EPN1	3.265812	1
REPEAT:3	4	2.898551	0.149812	SYNPR, RYR2, FMN2, EPN1	2.922042	1
REPEAT:1	4	2.898551	0.223863	SYNPR, RYR2, FMN2, EPN1	2.413861	1
REPEAT:2	4	2.898551	0.223863	SYNPR, RYR2, FMN2, EPN1	2.413861	1
REPEAT:5	3	2.173913	0.264382	SYNPR, FMN2, EPN1	2.974221	1

Cluster 16- Enrichment Score: 0.6555755563868145						
Term	Count	%	PValue	Genes	Fold Enrichment	FDR
KW-1003~Cell membrane	40	28.98551	0.090471	APP, ATP8A1, ROCK2, SRC, NRXN1, ITSN1, GNAI3, ADAM22, FMN2, ADD3, GLG1, PPP1R9B, ADD2, RIMS1, GRM2, GJA1, CACNG8, GPC1, MYO6, LRRC8A, PIP5K1C, DLGAP2, CLASP2, SCN1A, EPHA4, UNC13A, DBNL, CASK, SLC6A11, EPS15L1, CKAP4, EPN1, GRIN1, EHD3, VAPA, MADD, KCNMA1, CSPG5, ADGRL1, TLN2	1.233644	0.57179
KW-0472~Membrane	78	56.52174	0.175769	APP, RYR2, ATP8A1, ITSN1, FMN2, PPP1R9B, ABHD12, LACTB, GRM2, SYNPR, RIMS1, GJA1, AIFM1, ABHD16A, PSMD1, DLGAP2, SCYL2, SCN1A, DLGAP4, SH3GLB1, EPHA4, UNC13A, DBNL, ATP6AP1, SLC32A1, VPS13C, AP1B1, CASK, SDHC, SLC6A11, EPS15L1, BCS1L, CKAP4, EPN1, ITFG1, MADD, KCNMA1, FKBP8, GM20498, TLN2, PAFAH1B1, RAPGEF4, BRSK2, ROCK2, SRC, NRXN1, ITPR1, GNAI3, ADAM22, ASAP1, SLC1A4, ADD3, CACNA1E, GLG1, MTDH, ADD2, CACNG8, GPC1, MYO6, LRRC8A, PIP5K1C, SRGAP3, PCDH1, CLASP2, GK, PCDHGC5, AP3D1, HIP1R, SYNJ2BP, ACADSB, GRIN1, EHD3, VAPA, RAB12, CSPG5, ADGRL1, TPRGL, TECPR1	1.080881	0.611692
GO:0005886~plasma membrane	52	37.68116	0.378567	APP, RYR2, ATP8A1, ITSN1, FMN2, PPP1R9B, GRM2, RIMS1, GJA1, DLGAP2, SCN1A, TBC1D10B, DLGAP4, EPHA4, UNC13A, DBNL, SLC32A1, CASK, EPS15L1, CKAP4, EPN1, ITFG1, CACNB4, LRRC7, MADD, KCNMA1, TLN2, RAPGEF4, ROCK2, SRC, NRXN1, ITPR1, GNAI3, ADAM22, SLC1A4, ADD3, GLG1, ADD2, SRR, CACNG8, GPC1, MYO6, LRRC8A, PIP5K1C, CLASP2, HIP1R, GRIN1, EHD3, VAPA, RAB12, CSPG5, ADGRL1	1.055863	1

GO:0016020~membrane	76	55.07246	0.39637	APP, RYR2, ATP8A1, HEXB, ITSN1, FMN2, PPP1R9B, ABHD12, GRM2, SYNPR, RIMS1, GJA1, AIFM1, CAPZB, ABHD16A, SBF1, DLGAP2, SCYL2, SCN1A, DLGAP4, SH3GLB1, EPHA4, UNC13A, DBNL, ATP6AP1, SLC32A1, VPS13C, AP1B1, CASK, SDHC, SLC6A11, EPS15L1, BCS1L, CKAP4, EPN1, ITFG1, TOM1L2, MADD, KCNMA1, FKBP8, TLN2, PAFAH1B1, RAPGEF4, ROCK2, SRC, NRXN1, ITPR1, GNAI3, ADAM22, ASAP1, SLC1A4, ADD3, CACNA1E, GLG1, MTDH, ADD2, CACNG8, GPC1, MYO6, LRRC8A, PIP5K1C, CLASP2, GK, PCDHGC5, AP3D1, HIP1R, GRIN1, EHD3, PDE10A, VAPA, RAB12, CSPG5, ADGRL1, OSBPL1A, TPRGL, TECPR1	1.032735	1
Cluster 17- Enrichment Score: 0.6427160416532073						
Term	Count	%	PValue	Genes	Fold Enrichment	FDR
KW-0268~Exocytosis	6	4.347826	0.053705	RIMS1, BRSK2, UNC13A, ITSN1, PIP5K1C, RAPGEF4	2.801587	1
GO:0042734~presynaptic membrane	7	5.072464	0.114394	RIMS1, GRM2, UNC13A, NRXN1, ITSN1, CASK, ADGRL1	2.066886	1
GO:0006887~exocytosis	6	4.347826	0.142209	RIMS1, BRSK2, UNC13A, ITSN1, PIP5K1C, RAPGEF4	2.131154	1
IPR000008:C2 calcium-dependent membrane targeting	4	2.898551	0.527774	RIMS1, UNC13A, HECW2, ITSN1	1.442021	1
DOMAIN:C2	4	2.898551	0.53677	RIMS1, UNC13A, HECW2, ITSN1	1.423559	1
SM00239:C2	4	2.898551	0.562501	RIMS1, UNC13A, HECW2, ITSN1	1.369963	1
Cluster 18- Enrichment Score: 0.6250763033721854						

Term	Count	%	PValue	Genes	Fold Enrichment	FDR
GO:0005524~ATP binding	28	20.28986	0.027279	PRPS2, PRPS1, BRSK2, ATP8A1, ROCK2, SRC, ACTR3B, SRR, HSPH1, MTHFD1L, KIF5C, MYO6, MYO18A, PIP5K1C, STK32C, SCYL2, PRPS1L3, CCT4, CCT3, EPHA4, ACTR2, ATP6AP1, GK, CASK, BCS1L, DCLK1, EHD3, UBE2O	1.474905	1
KW-0067~ATP-binding	26	18.84058	0.056449	PRPS2, PRPS1, BRSK2, ATP8A1, ROCK2, SRC, ACTR3B, SRR, HSPH1, MTHFD1L, KIF5C, MYO6, MYO18A, PIP5K1C, STK32C, PRPS1L3, CCT4, CCT3, EPHA4, ACTR2, GK, CASK, BCS1L, DCLK1, EHD3, UBE2O	1.361549	1
GO:0016301~kinase activity	12	8.695652	0.134789	PRPS2, PRPS1, EPHA4, BRSK2, GK, ROCK2, SRC, CASK, PIP5K1C, PRPS1L3, DCLK1, STK32C	1.559579	1
GO:0004672~protein kinase activity	9	6.521739	0.135949	EPHA4, BRSK2, ROCK2, SRC, CASK, DCLK1, STK32C, SCYL2, PPP1R9B	1.738281	1
GO:0016310~phosphorylation	11	7.971014	0.154486	PRPS2, PRPS1, EPHA4, BRSK2, GK, ROCK2, SRC, CASK, PIP5K1C, DCLK1, STK32C	1.562846	1
KW-0418~Kinase	12	8.695652	0.173979	PRPS2, PRPS1, EPHA4, BRSK2, GK, ROCK2, SRC, CASK, PIP5K1C, PRPS1L3, DCLK1, STK32C	1.466125	1
IPR000719:Protein kinase, catalytic domain	8	5.797101	0.179648	EPHA4, BRSK2, ROCK2, SRC, CASK, DCLK1, STK32C, SCYL2	1.704206	1
DOMAIN:Protein kinase	8	5.797101	0.18792	EPHA4, BRSK2, ROCK2, SRC, CASK, DCLK1, STK32C, SCYL2	1.682388	1
IPR011009:Protein kinase-like domain	8	5.797101	0.199596	EPHA4, BRSK2, ROCK2, SRC, CASK, DCLK1, STK32C, SCYL2	1.654083	1

GO:0035556 ~intracellular signal transduction	8	5.797101	0.202275	BRSK2, UNC13A, ROCK2, SRC, ITSN1, DCLK1, STK32C, RAPGEF4	1.647269	1
GO:0006468 ~protein phosphorylation	9	6.521739	0.238173	APP, EPHA4, BRSK2, ROCK2, SRC, CASK, DCLK1, STK32C, SCYL2	1.504344	1
KW-0808~Transferase	19	13.76812	0.250564	PRPS2, MPST, PRPS1, EPHA4, BRSK2, OAT, GK, ROCK2, SRC, AGL, CASK, PYGM, DCLK1, HECW2, DBT, UBE2O, PIP5K1C, PRPS1L3, STK32C	1.228957	1
GO:0018105 ~peptidyl-serine phosphorylation	5	3.623188	0.256018	BRSK2, ROCK2, SRC, DCLK1, STK32C	1.919958	1
GO:0016740 ~transferase activity	17	12.31884	0.280978	PRPS2, MPST, PRPS1, EPHA4, BRSK2, OAT, GK, ROCK2, SRC, CASK, PYGM, DCLK1, HECW2, DBT, UBE2O, PIP5K1C, STK32C	1.237729	1
SM00220:S_TKc	7	5.072464	0.310516	EPHA4, BRSK2, ROCK2, CASK, DCLK1, STK32C, SCYL2	1.498397	1
IPR017441:Protein kinase, ATP binding site	6	4.347826	0.332281	EPHA4, BRSK2, ROCK2, SRC, DCLK1, STK32C	1.562189	1
GO:0000166 ~nucleotide binding	29	21.01449	0.37578	PRPS2, PRPS1, BRSK2, ATP8A1, ROCK2, SRC, GNAI3, PYGM, ACTR3B, SRR, HSPH1, MTHFD1L, MYO6, MYO18A, PIP5K1C, STK32C, CCT4, CCT3, EPHA4, ACTR2, GK, CASK, BCS1L, DCLK1, EHD3, PDE10A, RAB12, UBE2O, RAPGEF4	1.098859	1
KW-0547~Nucleotide-binding	31	22.46377	0.422557	PRPS2, PRPS1, BRSK2, ATP8A1, ROCK2, SRC, GNAI3, PYGM, ACTR3B, SRR, HSPH1, MTHFD1L, KIF5C, MYO6, MYO18A, PIP5K1C, STK32C, PRPS1L3, CCT4, CCT3, EPHA4, ACTR2, GK, CASK, BCS1L, DCLK1, EHD3, PDE10A, RAB12, UBE2O, RAPGEF4	1.062109	1

KW-0723~Serine/threonine-protein kinase	5	3.623188	0.631966	BRSK2, ROCK2, CASK, DCLK1, STK32C	1.157467	1
GO:0004674~protein serine/threonine kinase activity	5	3.623188	0.65807	BRSK2, ROCK2, CASK, DCLK1, STK32C	1.121472	1
IPR008271:Serine/threonine-protein kinase, active site	4	2.898551	0.724009	BRSK2, ROCK2, DCLK1, STK32C	1.081515	1
ACT_SITE:Proton acceptor	10	7.246377	0.809221	EPHA4, SRR, BRSK2, ALDH2, ROCK2, SRC, AMPD2, ACADSB, DCLK1, STK32C	0.884057	1
Cluster 18- Enrichment Score: 0.605543791475061						
Term	Count	%	PValue	Genes	Fold Enrichment	FDR
IPR001452:Src homology-3 domain	8	5.797101	0.151466	SH3GLB1, DBNL, CACNB4, SRC, ITSN1, CASK, ASAP1, SRGAP3	1.785359	1
DOMAIN:SH3	8	5.797101	0.158762	SH3GLB1, DBNL, CACNB4, SRC, ITSN1, CASK, ASAP1, SRGAP3	1.762501	1
KW-0728~SH3 domain	8	5.797101	0.248407	SH3GLB1, DBNL, CACNB4, SRC, ITSN1, CASK, ASAP1, SRGAP3	1.542062	1
GO:0002102~podosome	3	2.173913	0.25646	DBNL, SRC, ASAP1	3.037057	1
SM00326:SH3	7	5.072464	0.295375	SH3GLB1, DBNL, SRC, ITSN1, CASK, ASAP1, SRGAP3	1.525641	1
IPR027267:Arfaptin homology (AH)	3	2.173913	0.514183	SH3GLB1, ASAP1, SRGAP3	1.757463	1

domain/BAR domain						
Cluster 19- Enrichment Score: 0.590718535893234						
Term	Count	%	PValue	Genes	Fold Enrichment	FDR
REPEAT:HEAT 8	3	2.173913	0.156716	AP3D1, CLASP2, IPO5	4.163991	1
REPEAT:HEAT 7	3	2.173913	0.182971	AP3D1, CLASP2, IPO5	3.785373	1
REPEAT:HEAT 6	3	2.173913	0.209806	AP3D1, CLASP2, IPO5	3.469925	1
GO:0005802~trans-Golgi network	5	3.623188	0.241823	ATP8A1, AP3D1, AP1B1, MYO18A, CLASP2	1.968463	1
REPEAT:HEAT 1	3	2.173913	0.264382	AP3D1, CLASP2, IPO5	2.974221	1
REPEAT:HEAT 2	3	2.173913	0.264382	AP3D1, CLASP2, IPO5	2.974221	1
REPEAT:HEAT 3	3	2.173913	0.264382	AP3D1, CLASP2, IPO5	2.974221	1
REPEAT:HEAT 4	3	2.173913	0.264382	AP3D1, CLASP2, IPO5	2.974221	1
REPEAT:HEAT 5	3	2.173913	0.264382	AP3D1, CLASP2, IPO5	2.974221	1
IPR011989:Armadillo-like helical	6	4.347826	0.289386	AP3D1, AP1B1, PSMD1, SCYL2, CLASP2, IPO5	1.654083	1
IPR016024:Armadillo-type fold	6	4.347826	0.584313	AP3D1, AP1B1, PSMD1, SCYL2, CLASP2, IPO5	1.171642	1

Cluster 20- Enrichment Score: 0.5864480699218039						
Term	Count	%	PValue	Genes	Fold Enrichment	FDR
DOMAIN:PH	7	5.072464	0.195488	IQSEC2, ROCK2, ITSN1, ASAP1, OSBPL1A, SBF1, TECPR1	1.766507	1
IPR011993:Pleckstrin homology-like domain	9	6.521739	0.198513	APP, IQSEC2, ROCK2, ITSN1, ASAP1, TLN2, OSBPL1A, SBF1, TECPR1	1.581716	1
GO:0005085~guanyl-nucleotide exchange factor activity	5	3.623188	0.252378	IQSEC2, MADD, ITSN1, SBF1, RAPGEF4	1.931424	1
IPR001849:Pleckstrin homology domain	6	4.347826	0.289386	IQSEC2, ROCK2, ITSN1, ASAP1, OSBPL1A, SBF1	1.654083	1
SM00233:PH	6	4.347826	0.412403	IQSEC2, ROCK2, ITSN1, ASAP1, OSBPL1A, SBF1	1.410256	1
Cluster 21- Enrichment Score: 0.5761192610698398						
Term	Count	%	PValue	Genes	Fold Enrichment	FDR
GO:0098982~GABA-ergic synapse	8	5.797101	0.072557	BCAN, RIMS1, SLC32A1, NRXN1, ITPR1, CSPG5, SLC6A11, CACNA1E	2.139311	1
GO:0006836~neurotransmitter transport	3	2.173913	0.335357	RIMS1, SLC32A1, SLC6A11	2.50724	1
KW-0532~Neurotransmitter transport	3	2.173913	0.343748	RIMS1, SLC32A1, SLC6A11	2.451389	1

mmu04721:Synaptic vesicle cycle	4	2.898551	0.593059	RIMS1, UNC13A, SLC32A1, SLC6A11	1.308579	1
Cluster 22- Enrichment Score: 0.5430841630153816						
Term	Count	%	PValue	Genes	Fold Enrichment	FDR
TRANSMEM:Helical	41	29.71014	0.172338	RYR2, APP, BRSK2, ATP8A1, NRXN1, ADAM22, ITPR1, SLC1A4, CACNA1E, GLG1, MTDH, ABHD12, SYNPR, LACTB, GRM2, GJA1, CACNG8, ABHD16A, AIFM1, PSMD1, LRRC8A, SRGAP3, PCDH1, SCN1A, EPHA4, ATP6AP1, SLC32A1, PCDHGC5, CASK, SDHC, SLC6A11, BCS1L, ACADSB, CKAP4, ITFG1, GRIN1, VAPA, KCNMA1, FKBP8, CSPG5, ADGRL1	1.166122	1
KW-0472~Membrane	78	56.52174	0.175769	APP, RYR2, ATP8A1, ITSN1, FMN2, PPP1R9B, ABHD12, LACTB, GRM2, SYNPR, RIMS1, GJA1, AIFM1, ABHD16A, PSMD1, DLGAP2, SCYL2, SCN1A, DLGAP4, SH3GLB1, EPHA4, UNC13A, DBNL, ATP6AP1, SLC32A1, VPS13C, AP1B1, CASK, SDHC, SLC6A11, EPS15L1, BCS1L, CKAP4, EPN1, ITFG1, MADD, KCNMA1, FKBP8, GM20498, TLN2, PAFAH1B1, RAPGEF4, BRSK2, ROCK2, SRC, NRXN1, ITPR1, GNAI3, ADAM22, ASAP1, SLC1A4, ADD3, CACNA1E, GLG1, MTDH, ADD2, CACNG8, GPC1, MYO6, LRRC8A, PIP5K1C, SRGAP3, PCDH1, CLASP2, GK, PCDHGC5, AP3D1, HIP1R, SYNJ2BP, ACADSB, GRIN1, EHD3, VAPA, RAB12, CSPG5, ADGRL1, TPRGL, TECPR1	1.080881	0.615192
GO:0016021~integral component of membrane	42	30.43478	0.211678	RYR2, APP, BRSK2, ATP8A1, NRXN1, ADAM22, ITPR1, SLC1A4, CACNA1E, GLG1, MTDH, ABHD12, SYNPR, LACTB, GRM2, GJA1, CACNG8, ABHD16A, AIFM1, PSMD1, LRRC8A, SRGAP3, SCN1A, EPHA4, ATP6AP1, SLC32A1, CASK, SDHC, SLC6A11, BCS1L, ACADSB, CKAP4, ITFG1, GRIN1, VAPA, MADD, KCNMA1, FKBP8, GM20498, CSPG5, ADGRL1, TECPR1	1.140351	1

TOPO_DOM: Cytoplasmic	28	20.28986	0.211987	RYR2, APP, ATP8A1, NRXN1, ADAM22, ITPR1, SLC1A4, CACNA1E, GLG1, MTDH, ABHD12, SYNPR, GRM2, GJA1, ABHD16A, LRRC8A, SCN1A, EPHA4, ATP6AP1, SLC32A1, SLC6A11, SYNJ2BP, CKAP4, GRIN1, VAPA, KCNMA1, CSPG5, ADGRL1	1.19948	1
TOPO_DOM: Extracellular	18	13.04348	0.290428	APP, EPHA4, NRXN1, ADAM22, SLC6A11, SLC1A4, CACNA1E, CKAP4, GLG1, GRIN1, ABHD12, GRM2, GJA1, KCNMA1, CSPG5, ADGRL1, LRRC8A, SCN1A	1.218705	1
KW-0812~Transmembrane	43	31.15942	0.628853	RYR2, APP, BRSK2, ATP8A1, NRXN1, ADAM22, ITPR1, SLC1A4, CACNA1E, GLG1, MTDH, ABHD12, SYNPR, LACTB, GRM2, GJA1, CACNG8, ABHD16A, AIFM1, PSMD1, LRRC8A, SRGAP3, PCDH1, SCN1A, EPHA4, ATP6AP1, SLC32A1, PCDHGC5, CASK, SDHC, SLC6A11, BCS1L, SYNJ2BP, ACADSB, CKAP4, ITFG1, GRIN1, VAPA, KCNMA1, FKBP8, GM20498, CSPG5, ADGRL1	0.988254	1
KW-1133~Transmembrane helix	42	30.43478	0.636086	RYR2, APP, BRSK2, ATP8A1, NRXN1, ADAM22, ITPR1, SLC1A4, CACNA1E, GLG1, MTDH, ABHD12, SYNPR, LACTB, GRM2, GJA1, CACNG8, ABHD16A, AIFM1, PSMD1, LRRC8A, SRGAP3, PCDH1, SCN1A, EPHA4, ATP6AP1, SLC32A1, CASK, SDHC, SLC6A11, BCS1L, SYNJ2BP, ACADSB, CKAP4, ITFG1, GRIN1, VAPA, KCNMA1, FKBP8, GM20498, CSPG5, ADGRL1	0.986132	1
Cluster 23- Enrichment Score: 0.516427100104354						
Term	Count	%	PValue	Genes	Fold Enrichment	FDR
GO:0005783~endoplasmic reticulum	20	14.49275	0.189973	SH3GLB1, APP, EPHA4, RYR2, BRSK2, ATP6AP1, ATP8A1, NRXN1, ITPR1, AHSA1, FMN2, CKAP4, MTDH, GRIN1, ABHD12, GJA1, VAPA, KCNMA1, FKBP8, CSPG5	1.288448	1

GO:0005789~endoplasmic reticulum membrane	11	7.971014	0.300001	ABHD12, RYR2, VAPA, ATP6AP1, ITPR1, GNAI3, CSPG5, FMN2, CKAP4, MTDH, GRIN1	1.332498	1
KW-0256~Endoplasmic reticulum	13	9.42029	0.495342	APP, BRSK2, ATP6AP1, ATP8A1, VPS13C, ITPR1, AHSA1, CKAP4, MTDH, ABHD12, GJA1, VAPA, CSPG5	1.113438	1
Cluster 24-Enrichment Score: 0.49205374415864234						
Term	Count	%	PValue	Genes	Fold Enrichment	FDR
GO:0006915~apoptotic process	9	6.521739	0.172786	SH3GLB1, APP, GJA1, BRSK2, AIFM1, MADD, ITPR1, HIP1R, FKBP8	1.639349	1
KW-0053~Apoptosis	7	5.072464	0.338263	SH3GLB1, APP, BRSK2, AIFM1, MADD, ITPR1, FKBP8	1.452675	1
CROSSLNK:Glycyl lysine isopeptide (Lys-Gly) (interchain with G-Cter in ubiquitin)	4	2.898551	0.57158	APP, AIFM1, ITPR1, FKBP8	1.354117	1
Cluster 25- Enrichment Score: 0.44442737704350754						
Term	Count	%	PValue	Genes	Fold Enrichment	FDR
GO:0098839~postsynaptic density membrane	5	3.623188	0.092376	EPHA4, CACNG8, IQSEC2, SYNJ2BP, GRIN1	2.834586	1
GO:0045211~postsynaptic membrane	6	4.347826	0.602004	GRM2, EPHA4, CACNG8, DBNL, KCNMA1, GRIN1	1.149157	1
KW-0628~Postsynaptic cell membrane	3	2.173913	0.834758	EPHA4, CACNG8, GRIN1	0.947849	1

Cluster 26- Enrichment Score: 0.43142361258397044						
Term	Count	%	PValue	Genes	Fold Enrichment	FDR
TOPO_DOM: Cytoplasmic	28	20.28986	0.211987	RYR2, APP, ATP8A1, NRXN1, ADAM22, ITPR1, SLC1A4, CACNA1E, GLG1, MTDH, ABHD12, SYNPR, GRM2, GJA1, ABHD16A, LRRC8A, SCN1A, EPHA4, ATP6AP1, SLC32A1, SLC6A11, SYNJ2BP, CKAP4, GRIN1, VAPA, KCNMA1, CSPG5, ADGRL1	1.19948	1
CARBOHYD: N-linked (GlcNAc...) asparagine	24	17.3913	0.226526	APP, EPHA4, ATP6AP1, PCDHGC5, HEXB, NRXN1, ADAM22, SLC6A11, SLC1A4, CACNA1E, GLG1, HAPLN1, ITFG1, GRIN1, ABHD12, BCAN, SYNPR, GRM2, GPC1, TNR, CSPG5, ADGRL1, LRRC8A, SCN1A	1.21574	1
TOPO_DOM: Extracellular	18	13.04348	0.290428	APP, EPHA4, NRXN1, ADAM22, SLC6A11, SLC1A4, CACNA1E, CKAP4, GLG1, GRIN1, ABHD12, GRM2, GJA1, KCNMA1, CSPG5, ADGRL1, LRRC8A, SCN1A	1.218705	1
KW-1015~Disulfide bond	19	13.76812	0.337166	CCT3, MPST, APP, ATP6AP1, HEXB, NRXN1, ADAM22, CACNA1E, HAPLN1, GRIN1, BCAN, GRM2, GJA1, GPC1, TNR, CSPG5, ADGRL1, LRRC8A, SCN1A	1.172329	1
KW-0325~Glycoprotein	23	16.66667	0.610777	APP, EPHA4, ATP6AP1, HEXB, NRXN1, ADAM22, SLC6A11, SLC1A4, CACNA1E, GLG1, HAPLN1, ITFG1, GRIN1, ABHD12, BCAN, SYNPR, GRM2, GPC1, TNR, CSPG5, ADGRL1, LRRC8A, SCN1A	1.002796	1
KW-0732~Signal	19	13.76812	0.89798	APP, EPHA4, ATP6AP1, PCDHGC5, HEXB, NRXN1, ADAM22, SLC1A4, GLG1, ITFG1, GRIN1, BCAN, SYNPR, GRM2, GPC1, TNR, CSPG5, ADGRL1, PCDH1	0.834811	1
Cluster 27- Enrichment Score: 0.42843596578515575						
Term	Count	%	PValue	Genes	Fold Enrichment	FDR
mmu04921: Oxytocin	7	5.072464	0.128938	RYR2, CACNG8, CACNB4, ROCK2, SRC, ITPR1, GNAI3	1.981743	1

signaling pathway						
mmu04713: Circadian entrainment	4	2.898551	0.544688	RYR2, ITPR1, GNAI3, GRIN1	1.402049	1
mmu04371: Apelin signaling pathway	3	2.173913	0.738183	RYR2, ITPR1, GNAI3	1.162225	1
Cluster 28- Enrichment Score: 0.41677775713331566						
Term	Count	%	PValue	Genes	Fold Enrichment	FDR
GO:0030175~filopodium	5	3.623188	0.305882	EPHA4, LRRC7, MYO6, PPP1R9A, PPP1R9B	1.771617	1
GO:0007015~actin filament organization	5	3.623188	0.369646	MYO6, TPM1, HIP1R, PPP1R9A, PPP1R9B	1.61451	1
GO:0015629~actin cytoskeleton	6	4.347826	0.496965	LRRC7, MYO6, TPM1, FMN2, PPP1R9A, PPP1R9B	1.288448	1
Cluster 29- Enrichment Score: 0.40666102707893154						
Term	Count	%	PValue	Genes	Fold Enrichment	FDR
GO:0007399~nervous system development	9	6.521739	0.278943	PRPS1, APP, EPHA4, BRSK2, CSPG5, PRPS1L3, DCLK1, PPP1R9B, PAFAH1B1	1.436733	1
KW-0524~Neurogenesis	7	5.072464	0.32422	EPHA4, BRSK2, CSPG5, PPP1R9A, DCLK1, PPP1R9B, PAFAH1B1	1.476105	1
KW-9996~Developmental protein	7	5.072464	0.400512	EPHA4, RYR2, CSPG5, FMN2, DCLK1, PPP1R9B, PAFAH1B1	1.358321	1

KW-0217~Developmental protein	7	5.072464	0.400512	EPHA4, RYR2, CSPG5, FMN2, DCLK1, PPP1R9B, PAFAH1B1	1.358321	1
GO:0007275~multicellular organism development	7	5.072464	0.414918	EPHA4, RYR2, CSPG5, FMN2, DCLK1, PPP1R9B, PAFAH1B1	1.343971	1
GO:0030154~cell differentiation	8	5.797101	0.453835	RIMS1, UNC13A, SRC, CSPG5, LRRC8A, DCLK1, PPP1R9B, PAFAH1B1	1.249028	1
KW-0221~Differentiation	7	5.072464	0.521107	RIMS1, UNC13A, CSPG5, LRRC8A, DCLK1, PPP1R9B, PAFAH1B1	1.204191	1
Cluster 30- Enrichment Score: 0.38742507577246776						
Term	Count	%	PValue	Genes	Fold Enrichment	FDR
GO:0051010~microtubule plus-end binding	3	2.173913	0.156142	CLIP2, CLASP2, PAFAH1B1	4.171875	1
GO:0005881~cytoplasmic microtubule	3	2.173913	0.283273	CLIP2, CLASP2, PAFAH1B1	2.834586	1
GO:0008017~microtubule binding	6	4.347826	0.399282	CLIP2, VAPA, KIF5C, FMN2, CLASP2, PAFAH1B1	1.438578	1
GO:0015630~microtubule cytoskeleton	5	3.623188	0.484626	CLIP2, VAPA, DBT, CLASP2, PAFAH1B1	1.389503	1
GO:0005874~microtubule	7	5.072464	0.667101	CCT3, CLIP2, HSPH1, KIF5C, CCT4, CLASP2, PAFAH1B1	1.044321	1
KW-0493~Microtubule	4	2.898551	0.829559	CLIP2, KIF5C, CLASP2, PAFAH1B1	0.902714	1
Cluster 31- Enrichment Score: 0.37748973227547744						

Term	Count	%	PValue	Genes	Fold Enrichment	FDR
mmu04611: Platelet activation	5	3.623188	0.11237	ROCK2, SRC, ITPR1, GNAI3, TLN2	2.628843	1
mmu04921: Oxytocin signaling pathway	7	5.072464	0.128938	RYR2, CACNG8, CACNB4, ROCK2, SRC, ITPR1, GNAI3	1.981743	1
mmu04360: Axon guidance	5	3.623188	0.38832	EPHA4, ROCK2, SRC, GNAI3, SRGAP3	1.566119	1
mmu04540: Gap junction	4	2.898551	0.475519	GJA1, SRC, ITPR1, GNAI3	1.549634	1
mmu05205: Proteoglycans in cancer	4	2.898551	0.527866	ROCK2, SRC, GPC1, ITPR1	1.436246	1
mmu04915:Estrogen signaling pathway	3	2.173913	0.679233	SRC, ITPR1, GNAI3	1.298958	1
mmu05163: Human cytomegalovirus infection	4	2.898551	0.705296	ROCK2, SRC, ITPR1, GNAI3	1.111058	1
mmu04062: Chemokine signaling pathway	3	2.173913	0.751422	ROCK2, SRC, GNAI3	1.132425	1
mmu05417:Lipid and atherosclerosis	3	2.173913	0.787781	ROCK2, SRC, ITPR1	1.051537	1
Cluster 32- Enrichment Score: 0.34248816289494405						
Term	Count	%	PValue	Genes	Fold Enrichment	FDR

KW-0021~Allosteric enzyme	3	2.173913	0.339594	SRR, PDE10A, PYGM	2.474085	1
GO:0008152~metabolic process	4	2.898551	0.389254	SRR, PDE10A, HEXB, PYGM	1.775962	1
GO:0003824~catalytic activity	6	4.347826	0.710137	SRR, PDE10A, OAT, ECI1, GAD1, PYGM	1.01753	1
Cluster 33- Enrichment Score: 0.33783160389972017						
Term	Count	%	PValue	Genes	Fold Enrichment	FDR
GO:0006457~protein folding	6	4.347826	0.142209	CCT3, HSPH1, CDC37, FKBP8, AHSA1, CCT4	2.131154	1
GO:0050821~protein stabilization	5	3.623188	0.498123	CCT3, EPHA4, CDC37, HIP1R, CCT4	1.366124	1
KW-0143~Chaperone	5	3.623188	0.587645	CCT3, CDC37, AHSA1, BCS1L, CCT4	1.221771	1
GO:0051082~unfolded protein binding	3	2.173913	0.695447	CCT3, CDC37, CCT4	1.264205	1
GO:0016887~ATPase activity	5	3.623188	0.70664	CCT3, HSPH1, KIF5C, BCS1L, CCT4	1.053504	1
Cluster 34- Enrichment Score: 0.31022443064517663						
Term	Count	%	PValue	Genes	Fold Enrichment	FDR
mmu05135:Yersinia infection	5	3.623188	0.17519	ACTR2, ROCK2, SRC, PIP5K1C, ACTR3B	2.230533	1
mmu04666:Fc gamma R-	4	2.898551	0.326372	ACTR2, ASAP1, PIP5K1C, ACTR3B	1.962869	1

mediated phagocytosis						
mmu04810: Regulation of actin cytoskeleton	5	3.623188	0.569413	ACTR2, ROCK2, SRC, PIP5K1C, ACTR3B	1.247586	1
mmu05100: Bacterial invasion of epithelial cells	3	2.173913	0.679233	ACTR2, SRC, ACTR3B	1.298958	1
mmu04530:Tight junction	4	2.898551	0.740918	ACTR2, ROCK2, SRC, ACTR3B	1.051537	1
mmu05132:Salmonella infection	5	3.623188	0.839874	ACTR2, ROCK2, KIF5C, MYO6, ACTR3B	0.865972	1
Cluster 35- Enrichment Score: 0.19788208376236902						
Term	Count	%	PValue	Genes	Fold Enrichment	FDR
GO:0016477~cell migration	6	4.347826	0.295704	SRC, GPC1, MYO18A, CLASP2, PPP1R9B, PAFAH1B1	1.639349	1
GO:0005813~centrosome	7	5.072464	0.506756	BRSK2, LRRC7, ROCK2, GNAI3, SLC1A4, CCT4, PAFAH1B1	1.224821	1
KW-0498~Mitosis	3	2.173913	0.711827	BRSK2, CLASP2, PAFAH1B1	1.225694	1
GO:0051301~cell division	4	2.898551	0.752553	BRSK2, GNAI3, CLASP2, PAFAH1B1	1.033287	1
GO:0007049~cell cycle	5	3.623188	0.773768	BRSK2, SRC, GNAI3, CLASP2, PAFAH1B1	0.959979	1
KW-0132~Cell division	4	2.898551	0.792165	BRSK2, GNAI3, CLASP2, PAFAH1B1	0.96845	1

KW-0131~Cell cycle	5	3.623188	0.837205	BRSK2, SRC, GNAI3, CLASP2, PAFAH1B1	0.871605	1
Cluster 36- Enrichment Score: 0.18219104899292218						
Term	Count	%	PValue	Genes	Fold Enrichment	FDR
KW-0460~Magnesium	11	7.971014	0.392742	PRPS2, PRPS1, SRR, BRSK2, ATP8A1, ROCK2, KCNMA1, GNAI3, BPNT1, STK32C, GRIN1	1.221602	1
GO:0046872~metal ion binding	22	15.94203	0.838858	PRPS2, PRPS1, APP, BRSK2, UNC13A, ATP8A1, ROCK2, NRXN1, ITSN1, GNAI3, SDHC, AMPD2, ASAP1, EPS15L1, CACNA1E, RIMS1, EHD3, SRR, PDE10A, KCNMA1, BPNT1, STK32C	0.881664	1
KW-0479~Metal-binding	24	17.3913	0.862246	PRPS2, PRPS1, APP, BRSK2, UNC13A, ATP8A1, ROCK2, PCDHGC5, NRXN1, ITSN1, GNAI3, SDHC, AMPD2, ASAP1, EPS15L1, CACNA1E, RIMS1, EHD3, SRR, PDE10A, KCNMA1, BPNT1, PRPS1L3, STK32C	0.885892	1
Cluster 37- Enrichment Score: 0.13798793171570653						
Term	Count	%	PValue	Genes	Fold Enrichment	FDR
mmu04924:Renin secretion	3	2.173913	0.392736	KCNMA1, ITPR1, GNAI3	2.208228	1
mmu04022:cGMP-PKG signaling pathway	4	2.898551	0.608448	ROCK2, KCNMA1, ITPR1, GNAI3	1.280132	1
KW-0564~Palmitate	5	3.623188	0.890376	CACNG8, KCNMA1, ITPR1, GNAI3, CKAP4	0.785292	1
LIPID:S-palmitoyl cysteine	3	2.173913	0.968941	KCNMA1, ITPR1, GNAI3	0.586466	1

KW-0449~Lipoprotein	8	5.797101	0.990524	CACNG8, SRC, RAB12, GPC1, KCNMA1, ITPR1, GNAI3, CKAP4	0.572897	1
Cluster 38- Enrichment Score: 0.09281867333534953						
Term	Count	%	PValue	Genes	Fold Enrichment	FDR
TRANSMEM: Helical; Name=7	3	2.173913	0.606627	GRM2, ADGRL1, SLC6A11	1.487111	1
TRANSMEM: Helical; Name=3	3	2.173913	0.825896	GRM2, ADGRL1, SLC6A11	0.968351	1
TRANSMEM: Helical; Name=6	3	2.173913	0.825896	GRM2, ADGRL1, SLC6A11	0.968351	1
TRANSMEM: Helical; Name=5	3	2.173913	0.844945	GRM2, ADGRL1, SLC6A11	0.925313	1
TRANSMEM: Helical; Name=1	3	2.173913	0.862097	GRM2, ADGRL1, SLC6A11	0.885938	1
TRANSMEM: Helical; Name=2	3	2.173913	0.862097	GRM2, ADGRL1, SLC6A11	0.885938	1
TRANSMEM: Helical; Name=4	3	2.173913	0.862097	GRM2, ADGRL1, SLC6A11	0.885938	1
Cluster 39- Enrichment Score: 0.08519842492929318						
Term	Count	%	PValue	Genes	Fold Enrichment	FDR
mmu00280: Valine, leucine and isoleucine degradation	4	2.898551	0.383327	ALDH6A1, ALDH2, DBT, ACADSB	1.784427	1

TRANSIT:Mitochondrion	12	8.695652	0.746111	LACTB, PDHX, ALDH6A1, OAT, MECR, ALDH2, MTHFD1L, AIFM1, ECI1, DBT, SDHC, ACADSB	0.93571	1
KW-0496~Mitochondrion	22	15.94203	0.858657	MPST, SH3GLB1, PDHX, OAT, MECR, GK, SRC, VPS13C, ECI1, SDHC, BCS1L, SYNJ2BP, ACADSB, ABHD12, LACTB, ALDH6A1, AIFM1, ALDH2, MTHFD1L, DBT, FKBP8, GM20498	0.868862	1
KW-0809~Transit peptide	12	8.695652	0.923843	LACTB, PDHX, ALDH6A1, OAT, MECR, ALDH2, MTHFD1L, AIFM1, ECI1, DBT, SDHC, ACADSB	0.775199	1
KW-0520~NAD	3	2.173913	0.940413	ALDH6A1, ALDH2, AIFM1	0.690126	1
GO:0005739~mitochondrion	27	19.56522	0.99052	APP, OAT, SRC, ECI1, ABHD12, LACTB, GJA1, ALDH2, MTHFD1L, AIFM1, DBT, MPST, SH3GLB1, PDHX, MECR, GK, GAD1, VPS13C, HIP1R, SDHC, BCS1L, SYNJ2BP, ACADSB, SND1, ALDH6A1, KCNMA1, FKBP8	0.727508	1
GO:0016491~oxidoreductase activity	5	3.623188	0.991828	ALDH6A1, MECR, ALDH2, AIFM1, ACADSB	0.507527	1
KW-0560~Oxidoreductase	5	3.623188	0.993123	ALDH6A1, MECR, ALDH2, AIFM1, ACADSB	0.503631	1
Cluster 40- Enrichment Score: 0.05833628612767439						
Term	Count	%	PValue	Genes	Fold Enrichment	FDR
GO:0006886~intracellular protein transport	6	4.347826	0.808335	RIMS1, TOM1L2, AP3D1, AP1B1, TBC1D10B, IPO5	0.897328	1
GO:0015031~protein transport	9	6.521739	0.899426	TOM1L2, EHD3, RAB12, MYO6, ITSN1, AP3D1, AP1B1, FMN2, IPO5	0.784474	1
KW-0653~Protein transport	9	6.521739	0.919251	TOM1L2, EHD3, RAB12, MYO6, ITSN1, AP3D1, AP1B1, FMN2, IPO5	0.764069	1

Cluster 41- Enrichment Score: 0.009614575327307622						
Term	Count	%	PValue	Genes	Fold Enrichment	FDR
mmu05017:Spinocerebellar ataxia	3	2.173913	0.913342	ITPR1, PSMD1, GRIN1	0.761458	1
mmu05020: Prion disease	6	4.347826	0.973982	RYR2, KIF5C, ITPR1, PSMD1, SDHC, GRIN1	0.617686	1
mmu05010: Alzheimer disease	6	4.347826	0.982735	APP, KIF5C, ITPR1, PSMD1, SDHC, GRIN1	0.584961	1
mmu05012: Parkinson disease	5	3.623188	0.991145	KIF5C, ITPR1, GNAI3, PSMD1, SDHC	0.518363	1
mmu05016: Huntington disease	5	3.623188	0.994098	KIF5C, ITPR1, PSMD1, SDHC, GRIN1	0.494011	1
mmu05022: Pathways of neurodegeneration - multiple diseases	7	5.072464	0.995819	APP, RYR2, KIF5C, ITPR1, PSMD1, SDHC, GRIN1	0.520458	1
mmu05014: Amyotrophic lateral sclerosis	4	2.898551	0.998459	KIF5C, PSMD1, SDHC, GRIN1	0.400586	1

Wild-Type Memory Retrieval v. APPtg Memory Retrieval-20% Upregulated

Table 72. DAVID functional annotation clustering output table for annotation clusters enriched within proteins upregulated in APPtg mice during memory retrieval, when compared to WT mice during memory retrieval.

Cluster 1- Enrichment Score: 0.47186001504263037

Term	Count	%	PValue	Genes	Fold Enrichment	FDR
GO:0042802~identical protein binding	3	75	9.56E-02	APP, PSMC6, PIP4K2C	3.921533	1.00E+00
KW-0597~Phosphoprotein	4	100	4.50E-01	APP, PSMC6, PIP4K2C, SLC4A3	1.304768	1.00E+00
KW-0963~Cytoplasm	3	75	4.85E-01	APP, PSMC6, PIP4K2C	1.530057	1.00E+00
GO:0005737~cytoplasm	3	75	6.21E-01	APP, PSMC6, PIP4K2C	1.290541	1.00E+00

Wild-Type Basal v. Wild-Type Memory Retrieval- 20% Downregulated

Table 73. DAVID functional annotation clustering output table for annotation clusters enriched within proteins downregulated in WT mice during memory retrieval, when compared to WT mice at the basal level.

Cluster 1- Enrichment Score: 1.6885023696804387						
Term	Count	%	PValue	Genes	Fold Enrichment	FDR
GO:0016081~synaptic vesicle docking	3	6	1.13E-02	RIMS1, UNC13A, PPFIA3	17.20807	1.00E+00
GO:0007269~neurotransmitter secretion	4	8	1.91E-02	RIMS1, UNC13A, PPFIA3, SNAP91	6.692029	1.00E+00
GO:0098831~presynaptic active zone cytoplasmic component	3	6	3.99E-02	RIMS1, UNC13A, PPFIA3	9.0625	1.00E+00
Cluster 2- Enrichment Score: 1.6815504597577644						
Term	Count	%	PValue	Genes	Fold Enrichment	FDR

KW-0809~Transit peptide	14	28	1.39E-03	HSPA9, OAT, PCX, IMMT, OGDHL, ABAT, SDHA, ACADSB, LRPPRC, GLS, ALDH6A1, OPA1, ACO2, DLD	2.493207	1.67E-02
TRANSIT:Mitochondrion	13	26	1.39E-03	HSPA9, OAT, PCX, IMMT, ABAT, SDHA, ACADSB, LRPPRC, GLS, ALDH6A1, OPA1, ACO2, DLD	2.751433	1.96E-01
GO:0005759~mitochondrial matrix	8	16	4.28E-03	HSPA9, OAT, PCX, ABAT, OGDHL, ACADSB, DLD, GLS	3.696078	8.00E-01
KW-0496~Mitochondrion	15	30	4.87E-02	HSPA9, MPST, OAT, PCX, IMMT, ABAT, SDHA, BCS1L, ACADSB, LRPPRC, GLS, ALDH6A1, OPA1, ACO2, DLD	1.632407	9.63E-01
GO:0005739~mitochondrion	16	32	3.18E-01	HSPA9, MPST, OAT, PCX,	1.19455	1.00E+00

				IMMT, OGDHL, ABAT, SDHA, BCS1L, ACADSB, LRPPRC, GLS, ALDH6A1, OPA1, ACO2, DLD		
KW-0007~Acetylation	22	44	6.36E-01	HSPA9, MPST, CYFIP2, OAT, PCX, AP3D1, IMMT, PYGM, ABAT, EPS15L1, SDHA, ACADSB, LRPPRC, GLS, ALDH6A1, OPA1, DNAJC5, KIF21A, ACO2, PIP5K1C, DLD, DBN1	0.993941	1.00E+00
Cluster 3- Enrichment Score: 1.3431177983554679						
Term	Count	%	PValue	Genes	Fold Enrichment	FDR
mmu00562:Inositol phosphate metabolism	4	8	9.91E-03	ALDH6A1, SYNJ1, PIP5K1C, PLCB1	8.292335	4.66E-01
GO:0046488~phosphatidylinositol metabolic process	3	6	1.13E-02	SYNJ1, PIP5K1C, PLCB1	17.20807	1.00E+00
mmu04070:Phosphatidylinositol signaling system	3	6	1.30E-01	SYNJ1, PIP5K1C, PLCB1	4.596838	1.00E+00

KW-0443~Lipid metabolism	5	10	2.93E-01	PCX, SYNJ1, PIP5K1C, PLCB1, ACADSB	1.755637	1.00E+00
Cluster 4- Enrichment Score: 1.304834281238411						
Term	Count	%	PValue	Genes	Fold Enrichment	FDR
mmu00020:Citrate cycle (TCA cycle)	5	10	3.98E-03	PCX, OGDHL, ACO2, SDHA, DLD	7.048485	0.378293
mmu01200:Carbon metabolism	6	12	0.029055	ALDH6A1, PCX, OGDHL, ACO2, SDHA, DLD	3.253147	1
GO:0006099~tricarboxylic acid cycle	3	6	0.098555	OGDHL, ACO2, SDHA	5.475296	1
KW-0560~Oxidoreductase	5	10	0.529004	ALDH6A1, OGDHL, SDHA, ACADSB, DLD	1.290553	1
Cluster 5- Enrichment Score: 0.6061209927480975						
Term	Count	%	PValue	Genes	Fold Enrichment	FDR
mmu00280:Valine, leucine and isoleucine degradation	4	8	5.90E-02	ALDH6A1, ABAT, ACADSB, DLD	4.271809	1.00E+00
GO:0050660~flavin adenine dinucleotide binding	3	6	1.01E-01	SDHA, ACADSB, DLD	5.393939	1
KW-0274~FAD	3	6	2.04E-01	SDHA, ACADSB, DLD	3.421875	1

KW-0285~Flavoprotein	3	6	2.23E-01	SDHA, ACADSB, DLD	3.220588	1
KW-0560~Oxidoreductase	5	10	5.29E-01	ALDH6A1, OGDHL, SDHA, ACADSB, DLD	1.290553	1
ACT_SITE:Proton acceptor	5	10	5.94E-01	ROCK2, WNK2, SDHA, ACADSB, DLD	1.199792	1
GO:0016491~oxidoreductase activity	4	8	6.72E-01	ALDH6A1, SDHA, ACADSB, DLD	1.154907	1
Cluster 6- Enrichment Score: 0.5575145686405505						
Term	Count	%	PValue	Genes	Fold Enrichment	FDR
IPR000008:C2 calcium-dependent membrane targeting	3	6	0.25392	RIMS1, UNC13A, PLCB1	3.019231	1
DOMAIN:C2	3	6	0.269409	RIMS1, UNC13A, PLCB1	2.897959	1
SM00239:C2	3	6	0.310704	RIMS1, UNC13A, PLCB1	2.585253	1
Cluster 7- Enrichment Score: 0.5573508417842515						
Term	Count	%	PValue	Genes	Fold Enrichment	FDR
KW-0268~Exocytosis	3	6	0.16727	RIMS1, UNC13A, PIP5K1C	3.912562	1
GO:0006887~exocytosis	3	6	0.254527	RIMS1, UNC13A, PIP5K1C	3.011413	1
KW-0965~Cell junction	4	8	0.499799	RIMS1, UNC13A,	1.478407	1

				PIP5K1C, DBN1		
Cluster 8- Enrichment Score: 0.5461070715501117						
Term	Count	%	PValue	Genes	Fold Enrichment	FDR
GO:0035556~intracellular signal transduction	5	10	8.42E-02	UNC13A, ROCK2, WNK2, PLCB1, ADCY5	2.909578	1
mmu04611:Platelet activation	3	6	1.78E-01	ROCK2, PLCB1, ADCY5	3.775974	1
mmu04270:Vascular smooth muscle contraction	3	6	0.239637	ROCK2, PLCB1, ADCY5	3.109626	1
mmu04062:Chemokine signaling pathway	3	6	0.29172	ROCK2, PLCB1, ADCY5	2.710956	1
mmu04022:cGMP-PKG signaling pathway	3	6	0.36401	ROCK2, PLCB1, ADCY5	2.298419	1
mmu04921:Oxytocin signaling pathway	3	6	0.423995	ROCK2, PLCB1, ADCY5	2.033217	1
mmu05163:Human cytomegalovirus infection	3	6	0.433741	ROCK2, PLCB1, ADCY5	1.994854	1
mmu05200:Pathways in cancer	3	6	0.608799	ROCK2, PLCB1, ADCY5	1.448319	1
Cluster 9- Enrichment Score: 0.5429970838995531						
Term	Count	%	PValue	Genes	Fold Enrichment	FDR
GO:0030170~pyridoxal phosphate binding	3	6	0.045018	OAT, ABAT, PYGM	8.47619	1

KW-0663~Pyridoxal phosphate	3	6	0.056278	OAT, ABAT, PYGM	7.3	1
GO:0003824~catalytic activity	4	8	0.330667	OAT, PCX, ABAT, PYGM	1.929539	1
GO:0016740~transferase activity	7	14	0.331345	MPST, OAT, ROCK2, WNK2, ABAT, PYGM, PIP5K1C	1.44968	1
KW-0808~Transferase	8	16	0.364533	MPST, OAT, ROCK2, WNK2, AGL, ABAT, PYGM, PIP5K1C	1.32598	1
GO:0016310~phosphorylation	3	6	0.711591	ROCK2, WNK2, PIP5K1C	1.204565	1
GO:0016301~kinase activity	3	6	0.754478	ROCK2, WNK2, PIP5K1C	1.109034	1
KW-0418~Kinase	3	6	0.833714	ROCK2, WNK2, PIP5K1C	0.939236	1
Cluster 10- Enrichment Score: 0.5134083673497215						
Term	Count	%	PValue	Genes	Fold Enrichment	FDR
GO:0098871~postsynaptic actin cytoskeleton	3	6	0.02411	MYO6, PPP1R9A, DBN1	11.78125	1
GO:0014069~postsynaptic density	8	16	0.158065	GRM3, RIMS1, MYO6, AKAP5, PIP5K1C, PPP1R9A,	1.735727	1

				DBN1, SNAP91		
GO:0030175~filopodium	3	6	0.263109	MYO6, PPP1R9A, DBN1	2.945313	1
GO:0007015~actin filament organization	3	6	0.291219	MYO6, PPP1R9A, DBN1	2.737648	1
GO:0019901~protein kinase binding	5	10	0.425714	RIMS1, DCTN1, AKAP5, PPP1R9A, SNAP91	1.475954	1
GO:0043197~dendritic spine	4	8	4.39E-01	GRM3, AKAP5, PPP1R9A, DBN1	1.619416	1
GO:0015629~actin cytoskeleton	3	6	0.495829	MYO6, PPP1R9A, DBN1	1.785038	1
GO:0051015~actin filament binding	3	6	0.5973	MYO6, PPP1R9A, DBN1	1.483333	1
GO:0043025~neuronal cell body	6	12	0.605744	DCTN1, MYO6, AKAP5, PPP1R9A, DBN1, SNAP91	1.132813	1
GO:0003779~actin binding	3	6	0.749714	MYO6, AKAP5, DBN1	1.119497	1
Cluster 11- Enrichment Score: 0.5124874513268287						
Term	Count	%	PValue	Genes	Fold Enrichment	FDR
KW-0966~Cell projection	10	20	0.19261	RIMS1, UNC13A, MADD, MYO6, KIF21A, DIP2B,	1.501064	0.963051

				PIP5K1C, DLD, DBN1, ADCY5		
GO:0042995~cell projection	10	20	0.301344	RIMS1, UNC13A, MADD, MYO6, KIF21A, DIP2B, PIP5K1C, DLD, DBN1, ADCY5	1.340301	1
KW-0965~Cell junction	4	8	0.499799	RIMS1, UNC13A, PIP5K1C, DBN1	1.478407	1
Cluster 12- Enrichment Score: 0.4581309414439043						
Term	Count	%	PValue	Genes	Fold Enrichment	FDR
GO:0030054~cell junction	10	20	0.294067	CYFIP2, MPST, SYNPR, RIMS1, UNC13A, AKAP5, PIP5K1C, PCDH1, DBN1, ATP6V0A1	1.349513	1
GO:0045202~synapse	12	24	0.304738	CYFIP2, MPST, SYNPR, RIMS1, UNC13A, MADD, MYO6, AKAP5, PPP1R9A, PPFIA3, GLS, ATP6V0A1	1.2771	1

KW-0770~Synapse	7	14	0.471231	CYFIP2, MPST, SYNPR, RIMS1, UNC13A, AKAP5, ATP6V0A1	1.252258	1
Cluster 13- Enrichment Score: 0.4472887691783924						
Term	Count	%	PValue	Genes	Fold Enrichment	FDR
KW-0067~ATP-binding	9	18	0.303843	HSPA9, PCX, ROCK2, WNK2, MYO6, KIF21A, PIP5K1C, BCS1L, ADCY5	1.335366	1
GO:0005524~ATP binding	9	18	0.323644	HSPA9, PCX, ROCK2, WNK2, MYO6, KIF21A, PIP5K1C, BCS1L, ADCY5	1.348485	1
KW-0547~Nucleotide-binding	12	24	0.391215	HSPA9, PCX, OPA1, ROCK2, WNK2, MYO6, KIF21A, PYGM, PIP5K1C, BCS1L, DLD, ADCY5	1.164894	1
GO:0000166~nucleotide binding	11	22	0.422389	HSPA9, PCX, OPA1, ROCK2,	1.185589	1

				WNK2, MYO6, KIF21A, PYGM, PIP5K1C, BCS1L, ADCY5		
Cluster 14- Enrichment Score: 0.3960294616922943						
Term	Count	%	PValue	Genes	Fold Enrichment	FDR
TOPO_DOM:Mitochondrial matrix	3	6	0.210937	OPA1, IMMT, BCS1L	3.424861	1
TOPO_DOM:Mitochondrial intermembrane	3	6	0.356901	OPA1, IMMT, BCS1L	2.354592	1
GO:0005743~mitochondrial inner membrane	6	12	0.52596	MPST, PCX, OPA1, IMMT, SDHA, BCS1L	1.233639	1
KW-0999~Mitochondrion inner membrane	4	8	0.658005	OPA1, IMMT, SDHA, BCS1L	1.178279	1
Cluster 15- Enrichment Score: 0.24486774799172586						
Term	Count	%	PValue	Genes	Fold Enrichment	FDR
KW-0968~Cytoplasmic vesicle	6	12	0.390078	SYNPR, DNAJC5, MYO6, DLD, PPFIA3, ATP6V0A1	1.433333	1
GO:0031410~cytoplasmic vesicle	6	12	0.55011	SYNPR, DNAJC5, MYO6, DLD, PPFIA3, ATP6V0A1	1.202168	1

GO:0005794~Golgi apparatus	4	8	0.858609	DNAJC5, MYO6, AP3D1, ATP6V0A1	0.844534	1
Cluster 16- Enrichment Score: 0.23194655220642907						
Term	Count	%	PValue	Genes	Fold Enrichment	FDR
KW-0965~Cell junction	4	8	0.499799	RIMS1, UNC13A, PIP5K1C, DBN1	1.478407	1
KW-0221~Differentiation	3	6	0.610181	RIMS1, UNC13A, DBN1	1.44147	1
GO:0030154~cell differentiation	3	6	0.660551	RIMS1, UNC13A, DBN1	1.323698	1
Cluster 17- Enrichment Score: 0.15281022367099661						
Term	Count	%	PValue	Genes	Fold Enrichment	FDR
KW-0863~Zinc-finger	3	6	0.419072	RIMS1, UNC13A, ROCK2	2.059122	1
GO:0046872~metal ion binding	8	16	0.78422	RIMS1, UNC13A, PCX, ROCK2, ABAT, EPS15L1, ACO2, ADCY5	0.911944	1
KW-0862~Zinc	3	6	0.850153	RIMS1, UNC13A, ROCK2	0.904959	1
KW-0479~Metal-binding	8	16	0.876064	RIMS1, UNC13A, PCX, ROCK2, ABAT, EPS15L1,	0.836676	1

				ACO2, ADCY5		
Cluster 18- Enrichment Score: 0.0787361314319916						
Term	Count	%	PValue	Genes	Fold Enrichment	FDR
GO:0015031~protein transport	4	8	0.77462	MYO6, AP3D1, STAM, SNAP91	0.985329	1
KW-0653~Protein transport	4	8	0.798617	MYO6, AP3D1, STAM, SNAP91	0.9485	1
KW-0813~Transport	9	18	0.938349	RIMS1, DCTN1, MYO6, AP3D1, STAM, SDHA, LRPPRC, SNAP91, ATP6V0A1	0.762541	1
Cluster 19- Enrichment Score: 0.012330157984083462						
Term	Count	%	PValue	Genes	Fold Enrichment	FDR
TRANSMEM:Helical	10	20	0.921986	GRM3, SYNPR, OPA1, IMMT, ELFN2, BCS1L, PCDH1, ACADSB, ADCY5, ATP6V0A1	0.771997	1
GO:0016021~integral component of membrane	10	20	0.936647	GRM3, SYNPR, OPA1, MADD, IMMT, ELFN2, BCS1L,	0.752315	1

				ACADSB, ADCY5, ATP6V0A1		
TOPO_DOM:Extracellular	3	6	0.976664	GRM3, ELFN2, ADCY5	0.551319	1
TOPO_DOM:Cytoplasmic	5	10	9.79E-01	GRM3, SYNPR, ELFN2, ADCY5, ATP6V0A1	0.581381	1
KW-0325~Glycoprotein	5	10	0.979544	GRM3, SYNPR, ELFN2, SNAP91, ADCY5	0.58291	1
CARBOHYD:N-linked (GlcNAc...) asparagine	4	8	0.981588	GRM3, SYNPR, ELFN2, ADCY5	0.549978	1
KW-1133~Transmembrane helix	10	20	0.989351	GRM3, SYNPR, OPA1, IMMT, ELFN2, BCS1L, PCDH1, ACADSB, ADCY5, ATP6V0A1	0.647268	1
KW-0812~Transmembrane	10	20	0.992043	GRM3, SYNPR, OPA1, IMMT, ELFN2, BCS1L, PCDH1, ACADSB, ADCY5, ATP6V0A1	0.633576	1
KW-0732~Signal	4	8	0.993455	GRM3, SYNPR,	0.484499	1

				ELFN2, PCDH1		

APPtg Basal v. APPtg Memory Retrieval- 20% Downregulated

Table 74. DAVID functional annotation clustering output table for annotation clusters enriched within proteins downregulated in APPtg mice during memory retrieval, when compared to APPtg mice at the basal level.

Cluster 1- Enrichment Score: 2.0391349263929923						
Term	Count	%	PValue	Genes	Fold Enrichment	FDR
GO:0030123~AP-3 adaptor complex	3	20	3.05E-04	AP3D1, AP3S1, AP3B2	94.25	1.86E-02
GO:0016183~synaptic vesicle coating	3	20	3.18E-04	AP3D1, AP3S1, AP3B2	92.35	2.40E-02
GO:0035654~cargo loading into clathrin-coated vesicle, AP-3-mediated	3	20	3.18E-04	AP3D1, AP3S1, AP3B2	92.35	2.40E-02
GO:0048490~anterograde synaptic vesicle transport	3	20	5.27E-04	AP3D1, AP3S1, AP3B2	73.88	2.65E-02
mmu04142:Lysosome	4	26.66667	6.47E-04	HEXB, AP3D1, AP3S1, AP3B2	18.46032	1.62E-02
GO:0036465~synaptic	3	20	1.46E-03	AP3D1, AP3S1, AP3B2	46.175	4.40E-02

vesicle recycling						
GO:0046907~intracellular transport	3	20	1.46E-03	AP3D1, AP3S1, AP3B2	46.175	4.40E-02
GO:0008089~anterograde axonal transport	3	20	2.32E-03	AP3D1, AP3S1, AP3B2	36.94	5.84E-02
GO:0030117~membrane coat	3	20	3.24E-03	AP3D1, AP3S1, AP3B2	31.41667	9.89E-02
IPR011989:Armadillo-like helical	4	26.66667	5.51E-03	AP3D1, PSMD1, AP3B2, SCYL2	9.85098	2.37E-01
KW-0333~Golgi apparatus	5	33.33333	7.29E-03	PACS1, AP3D1, AP3S1, AP3B2, SCYL2	5.572061	8.74E-02
IPR016024:Armadillo-type fold	4	26.66667	1.44E-02	AP3D1, PSMD1, AP3B2, SCYL2	6.977778	3.09E-01
GO:1904115~axon cytoplasm	3	20	1.62E-02	AP3D1, AP3S1, AP3B2	13.96296	2.63E-01
GO:0005769~early endosome	4	26.66667	1.72E-02	AP3D1, VPS26A, AP3S1, AP3B2	6.528139	2.63E-01
GO:0005802~trans-Golgi network	3	20	2.79E-02	AP3D1, AP3S1, AP3B2	10.47222	2.84E-01
GO:0006886~intracellular protein transport	4	26.66667	3.17E-02	AP3D1, VPS26A, AP3S1, AP3B2	5.184561	6.13E-01
GO:0005794~Golgi apparatus	5	33.33333	4.17E-02	PACS1, AP3D1, AP3S1, AP3B2, SCYL2	3.378136	3.63E-01
KW-0653~Protein transport	4	26.66667	6.76E-02	AP3D1, VPS26A, AP3S1, AP3B2	3.438312	5.64E-01

KW-0968~Cytoplasmic vesicle	4	26.66667	1.13E-01	HEXB, AP3S1, AP3B2, SCYL2	3.071429	6.78E-01
GO:0015031~protein transport	4	26.66667	1.19E-01	AP3D1, VPS26A, AP3S1, AP3B2	3.021677	1.00E+00
GO:0016192~vesicle-mediated transport	3	20	1.36E-01	AP3D1, AP3S1, AP3B2	4.295349	1
GO:0031410~cytoplasmic vesicle	4	26.66667	1.72E-01	HEXB, AP3S1, AP3B2, SCYL2	2.564626	1.00E+00
KW-0813~Transport	4	26.66667	5.96E-01	AP3D1, VPS26A, AP3S1, AP3B2	1.228538	1
Cluster 2- Enrichment Score: 0.8175527336699847						
Term	Count	%	PValue	Genes	Fold Enrichment	FDR
GO:0004672~protein kinase activity	3	20	0.058855	GSK3A, SCYL2, PDK1	6.742424	1
GO:0006468~protein phosphorylation	3	20	0.133201	GSK3A, SCYL2, PDK1	4.345882	1
GO:0005524~ATP binding	3	20	0.449834	GSK3A, SCYL2, PDK1	1.838843	1
Cluster 3- Enrichment Score: 0.5972928979715888						
Term	Count	%	PValue	Genes	Fold Enrichment	FDR
KW-0378~Hydrolase	3	20	0.15904	HEXB, TPP2, BLMH	3.229851	0.7952

GO:0016787 ~hydrolase activity	3	20	0.31 1998	HEXB, TPP2, BLMH	2.427273	1
GO:0042802 ~identical protein binding	4	26. 666 67	0.32 5434	HEXB, TPP2, BLMH, PDK1	1.808024	1

Wild-Type Basal v. APPtg Basal- 20% Downregulated

Table 75. DAVID functional annotation clustering output table for annotation clusters enriched within proteins downregulated in APPtg mice at the basal level, when compared to WT mice at the basal level.

Cluster 1- Enrichment score: 2.3155376205714786						
Term	**Count**	**%**	**PValue**	**Genes**	**Fold Enrichment**	**FDR**
mmu05010: Alzheimer disease	27	15.8 8235	2.12E-05	UQCRB, NDUFB6, COX7A2, UQCR10, KLC1, COX5B, COX6A1, HSD17B10, COX5A, PSMA7, PSMB5, PSMD7, APOE, HRAS, SNCA, NDUFA7, NDUFA5, NDUFA2, CSNK2A2, PSMA3, PSMA1, UQCRQ, NDUFS6, NDUFS5, PSMC1, CALM1, PPID	2.318146	4.22E-03
mmu05208: Chemical carcinogenesis - reactive oxygen species	18	10.5 8824	9.23E-05	CBR1, MAP2K4, NDUFA7, NDUFA5, UQCRB, NDUFB6, NDUFA2, AKR1A1, COX7A2, UQCR10, COX5B, COX6A1, COX5A, UQCRQ, NDUFS6, NDUFS5, HRAS, GSTM5	2.788881	7.78E-03
mmu00190: Oxidative phosphorylation	16	9.41 1765	1.17E-04	NDUFA7, ATP6V1G2, NDUFA5, UQCRB, NDUFB6, NDUFA2, COX7A2, UQCR10, COX5B, COX6A1, COX5A, UQCRQ, NDUFS6,	2.995465	7.78E-03

				NDUFS5, ATP6V1E1, ATP6V1D		
mmu05012: Parkinson disease	23	13.52941	2.75E-04	NDUFA7, NDUFA5, UQCRB, NDUFB6, NDUFA2, COX7A2, PARK7, UQCR10, KLC1, COX5B, COX6A1, COX5A, PSMA7, PSMA3, PSMB5, PSMD7, PSMA1, UQCRQ, NDUFS6, NDUFS5, PSMC1, CALM1, SNCA	2.198799	1.35E-02
mmu05022: Pathways of neurodegeneration - multiple diseases	29	17.05882	3.39E-04	UQCRB, DCTN2, NDUFB6, COX7A2, PARK7, UQCR10, KLC1, COX5B, COX6A1, HSD17B10, COX5A, PSMA7, PSMB5, PSMD7, HRAS, SNCA, NDUFA7, NDUFA5, NDUFA2, CSNK2A2, RAB39B, PSMA3, PSMA1, UQCRQ, NDUFS6, NDUFS5, PSMC1, CALM1, PPID	1.916216	1.35E-02
mmu05016: Huntington disease	23	13.52941	5.68E-04	NDUFA7, NDUFA5, UQCRB, DCTN2, NDUFB6, NDUFA2, CLTB, CLTA, COX7A2, UQCR10, KLC1, COX5B, COX6A1, COX5A, PSMA7, PSMA3, PSMB5, PSMD7, PSMA1, UQCRQ, NDUFS6, NDUFS5, PSMC1	2.094801	1.88E-02
KW-0999~Mitochondrion inner membrane	21	12.35294	1.18E-03	ACADVL, NDUFA7, NDUFA5, UQCRB, NDUFB6, MTFP1, TIMM9, NDUFA2, COX7A2, UQCR10, COX5B, COX6A1, COX5A, COQ6, HADHB, CHCHD3, UQCRQ, NDUFS6, NDUFS5, CHCHD6, SLC25A22	2.136207	3.77E-02
mmu04932: Non-alcoholic fatty liver disease	13	7.647059	1.42E-03	NDUFA7, NDUFA5, UQCRB, NDUFB6, NDUFA2, COX7A2, UQCR10, COX5B, COX6A1, COX5A, UQCRQ, NDUFS6, NDUFS5	2.781503	3.57E-02
mmu05020: Prion disease	21	12.35294	1.49E-03	NDUFA7, NDUFA5, UQCRB, NDUFB6, NDUFA2, CSNK2A2, COX7A2,	2.051242	3.57E-02

				UQCR10, KLC1, COX5B, COX6A1, COX5A, PSMA7, PSMA3, PSMB5, PSMD7, PSMA1, UQCRQ, NDUFS6, NDUFS5, PSMC1		
mmu05014: Amyotrophic lateral sclerosis	22	12.94118	1.62E-03	NDUFA7, NDUFA5, UQCRB, DCTN2, NDUFB6, NDUFA2, RAB39B, COX7A2, UQCR10, KLC1, COX5B, COX6A1, COX5A, PSMA7, PSMA3, PSMB5, PSMD7, PSMA1, UQCRQ, NDUFS6, NDUFS5, PSMC1	1.990275	3.57E-02
GO:0005743~mitochondrial inner membrane	26	15.29412	3.75E-03	ACADVL, UQCRB, NDUFB6, MTFP1, TIMM9, COX7A2, UQCR10, COX5B, COX6A1, HSD17B10, COX5A, CHCHD3, CHCHD6, SLC25A22, SNCA, NDUFA7, NDUFA5, NDUFA2, IDH2, DHRS1, COQ6, HADHB, UQCRQ, NDUFS6, NDUFS5, PGAM5	1.779523	1.00E+00
mmu04714:Thermogenesis	14	8.235294	4.53E-03	NDUFA7, NDUFA5, UQCRB, NDUFB6, NDUFA2, COX7A2, UQCR10, COX5B, COX6A1, COX5A, UQCRQ, NDUFS6, NDUFS5, HRAS	2.329806	8.20E-02
KW-0679~Respiratory chain	9	5.294118	7.17E-03	NDUFA7, NDUFB6, NDUFA5, UQCRB, UQCRQ, NDUFS6, NDUFS5, NDUFA2, UQCR10	3.007317	3.60E-01
GO:0070469~respiratory chain	9	5.294118	9.85E-03	NDUFA7, NDUFB6, NDUFA5, UQCRB, UQCRQ, NDUFS6, NDUFS5, NDUFA2, UQCR10	2.897947	1.00E+00
KW-0249~Electron transport	10	5.882353	1.09E-02	NDUFA7, NDUFB6, NDUFA5, UQCRB, UQCRQ, NDUFS6, NDUFS5, NDUFA2, ETFA, UQCR10	2.592515	3.60E-01
mmu05415: Diabetic	13	7.647059	2.29E-02	NDUFA7, NDUFA5, UQCRB, NDUFB6, NDUFA2, COX7A2, UQCR10, COX5B,	1.991303	3.80E-01

cardiomyopathy				COX6A1, COX5A, UQCRQ, NDUFS6, NDUFS5		
GO:0005747~mitochondrial respiratory chain complex I	6	3.529412	8.49E-02	NDUFA7, NDUFB6, NDUFA5, NDUFS6, NDUFS5, NDUFA2	2.50019	1.00E+00
GO:0042776~mitochondrial ATP synthesis coupled proton transport	6	3.529412	1.22E-01	NDUFA7, NDUFB6, NDUFA5, NDUFS6, NDUFS5, NDUFA2	2.23993	1.00E+00
GO:0009060~aerobic respiration	6	3.529412	1.33E-01	NDUFA7, NDUFB6, NDUFA5, NDUFS6, NDUFS5, NDUFA2	2.180985	1.00E+00
GO:0032981~mitochondrial respiratory chain complex I assembly	5	2.941176	2.25E-01	NDUFB6, NDUFA5, NDUFS6, NDUFS5, NDUFA2	2.031309	1.00E+00
GO:0006120~mitochondrial electron transport, NADH to ubiquinone	3	1.764706	3.49E-01	NDUFA7, NDUFB6, NDUFS6	2.437571	1
mmu04723: Retrograde endocannabinoid signaling	6	3.529412	7.16E-01	NDUFA7, NDUFB6, NDUFA5, NDUFS6, NDUFS5, NDUFA2	1.010969	9.75E-01
Cluster 2- Enrichment Score: 1.6761186901128533						
GO:0005743~mitochondrial inner membrane	26	15.29412	0.003754	ACADVL, UQCRB, NDUFB6, MTFP1, TIMM9, COX7A2, UQCR10, COX5B, COX6A1, HSD17B10, COX5A, CHCHD3, CHCHD6, SLC25A22, SNCA, NDUFA7,	1.779523	1

				NDUFA5, NDUFA2, IDH2, DHRS1, COQ6, HADHB, UQCRQ, NDUFS6, NDUFS5, PGAM5		
GO:0005739~mitochondrion	51	30	0.04018	ALDH1L1, ACADVL, SLC44A2, DBI, ETFA, PARK7, COX6A1, COMTD1, CHCHD3, HINT2, CHCHD6, C1QBP, ATP6V1E1, ACOT9, HADHB, NDUFS6, NDUFS5, RAB35, PGAM5, CRYAB, PPID, NDUFB6, MTFP1, UQCRB, TIMM9, COX7A2, AK4, ACAA1A, UQCR10, COX5B, MFF, HSD17B10, COX5A, SLC25A27, PRDX3, PRDX1, SLC25A22, DECR1, SNCA, FIS1, NDUFA7, NDUFA5, MTX2, NDUFA2, IDH2, HSPE1, DHRS1, COQ6, QDPR, UQCRQ, OCIAD1	1.261003	1
KW-0496~Mitochondrion	36	21.17647	0.06211	ACADVL, UQCRB, NDUFB6, MTFP1, TIMM9, COX7A2, AK4, ETFA, PARK7, UQCR10, MFF, COX5B, COX6A1, HSD17B10, COX5A, PRDX3, CHCHD3, HINT2, C1QBP, CHCHD6, SLC25A22, DECR1, FIS1, ACOT9, NDUFA7, NDUFA5, MTX2, NDUFA2, IDH2, HSPE1, COQ6, HADHB, UQCRQ, NDUFS6, NDUFS5, PGAM5	1.304554	0.717584
Cluster 3- Enrichment score: 1.35823518151106						
GO:0006123~mitochondrial electron transport, cytochrome c to oxygen	4	2.352941	0.022209	COX7A2, COX5B, COX6A1, COX5A	6.139068	1
GO:0005751~mitochondrial	4	2.352941	0.046538	COX7A2, COX5B, COX6A1, COX5A	4.722581	1

respiratory chain complex IV						
mmu04260: Cardiac muscle contraction	7	4.117647	0.081463	UQCRB, UQCRQ, COX7A2, UQCR10, COX5B, COX6A1, COX5A	2.246599	0.97549
Cluster 4- Enrichment score: 1.3300330059604775						
MOTIF:Cx9C motif 1	3	1.764706	0.041487	CHCHD3, CHCHD6, NDUFS5	8.604	1
MOTIF:Cx9C motif 2	3	1.764706	0.041487	CHCHD3, CHCHD6, NDUFS5	8.604	1
DOMAIN:CHCH	3	1.764706	0.059441	CHCHD3, CHCHD6, NDUFS5	7.17	1
Cluster 5- Enrichment score: 1.055156481280672						
PROPEP:Removed in mature form	12	7.058824	0.002478	RAB21, RAP1A, PSMB5, MRAS, RAP2B, PALM, DNAJA2, RHOG, CDH13, PARK7, HRAS, RHOB	2.820984	0.859857
KW-0636~Prenylation	11	6.470588	0.005153	RAB21, RAP1A, MRAS, RAP2B, PALM, DNAJA2, RAB35, RHOG, RAB39B, HRAS, RHOB	2.73252	0.054104
MOTIF:Effector region	9	5.294118	0.00589	RAB21, RAP1A, MRAS, RAP2B, RAB35, RHOG, RAB39B, HRAS, RHOB	3.147805	1
IPR020849:Small GTPase superfamily, Ras type	5	2.941176	0.007765	RAB21, RAP1A, MRAS, RAP2B, HRAS	5.819979	1
IPR001806:Small GTPase superfamily	9	5.294118	0.015826	RAB21, RAP1A, MRAS, RAP2B, RAB35, RHOG, RAB39B, HRAS, RHOB	2.674714	1
KW-0449~Lipoprotein	23	13.52941	0.026701	LRRC57, HPCA, RHOG, RAB39B, PARK7, RHOB, PRDX3, GNA13, RAB21, MARCKS, RAP1A, CHCHD3, MRAS, RAP2B, PSMC1, CHCHD6, PALM, DNAJA2,	1.573269	0.186907

				RAB35, S1PR1, CDH13, APOE, HRAS		
IPR005225:Small GTP-binding protein domain	9	5.294118	0.041537	RAB21, RAP1A, MRAS, RAP2B, RAB35, RHOG, RAB39B, HRAS, RHOB	2.244849	1
GO:0019003~GDP binding	7	4.117647	0.052689	RAB21, RAP1A, MRAS, RAP2B, RAB35, HRAS, RHOB	2.521228	1
LIPID:S-geranylgeranyl cysteine	7	4.117647	0.054059	RAB21, RAP1A, MRAS, RAP2B, RAB35, RHOG, RAB39B	2.5095	1
KW-0342~GTP-binding	11	6.470588	0.265861	GNA13, RAB21, RAP1A, MRAS, RAP2B, RAB35, RHOG, RAB39B, AK4, HRAS, RHOB	1.361359	1
GO:0005525~GTP binding	11	6.470588	0.371265	GNA13, RAB21, RAP1A, MRAS, RAP2B, RAB35, RHOG, RAB39B, AK4, HRAS, RHOB	1.254611	1
GO:0003924~GTPase activity	10	5.882353	0.404594	GNA13, RAB21, RAP1A, MRAS, RAP2B, RAB35, RHOG, RAB39B, HRAS, RHOB	1.244242	1
GO:0007264~small GTPase mediated signal transduction	4	2.352941	0.407826	RAP1A, RHOG, HRAS, RHOB	1.726613	1
IPR027417:P-loop containing nucleoside triphosphate hydrolase	14	8.235294	0.556134	AK1, RHOG, RAB39B, AK4, RHOB, GNA13, RAB21, RAP1A, MRAS, RAP2B, PSMC1, RAB35, CMPK1, HRAS	1.062779	1
KW-0488~Methylation	18	10.58824	0.604252	MAP2K4, RHOG, RAB39B, DHRS1, RHOB, GFAP, RAB21, RAP1A, MRAS, RAP2B, DPYSL5, PALM,	1.015417	1

				DNAJA2, PITPNM2, CALM1, HRAS, CRYAB, VTI1B		
GO:0007165 ~signal transduction	12	7.058824	0.654356	GNA13, DGKE, RAP1A, MRAS, RAP2B, PDE1A, PDE4B, S1PR1, GPR37L1, NDRG1, HRAS, RHOB	1.004575	1
GO:0000166 ~nucleotide binding	22	12.94118	0.980409	DARS, MAP2K4, PDXK, DGKE, CSNK2A2, AK1, RHOG, RAB39B, AK4, RHOB, GNA13, RAB21, RAP1A, HINT2, MRAS, RAP2B, PSMC1, RAB35, UBE2N, CMPK1, HRAS, PFKP	0.730841	1
KW-0547~Nucleotide-binding	22	12.94118	0.991696	DARS, MAP2K4, PDXK, DGKE, CSNK2A2, AK1, RHOG, RAB39B, AK4, RHOB, GNA13, RAB21, RAP1A, HINT2, MRAS, RAP2B, PSMC1, RAB35, UBE2N, CMPK1, HRAS, PFKP	0.724334	1
Cluster 6- Enrichment score: 0.9885424355458768						
SM00102:ADF	3	1.764706	0.066756	GMFB, CFL2, TWF1	6.746914	1
DOMAIN:ADF-H	3	1.764706	0.12453	GMFB, CFL2, TWF1	4.78	1
IPR002108:Actin-binding, cofilin/tropomyosin type	3	1.764706	0.130199	GMFB, CFL2, TWF1	4.655983	1
Cluster 7- Enrichment score: 0.9362489505165028						
REGION:LID	3	1.764706	0.026067	AK1, CMPK1, AK4	10.755	1
REGION:NMP	3	1.764706	0.026067	AK1, CMPK1, AK4	10.755	1
IPR000850:Adenylate kinase	3	1.764706	0.04359	AK1, CMPK1, AK4	8.380769	1

GO:0019205 ~nucleobase-containing compound kinase activity	3	1.764706	0.045236	AK1, CMPK1, AK4	8.212	1
GO:0006165 ~nucleoside diphosphate phosphorylation	3	1.764706	0.06364	AK1, CMPK1, AK4	6.906452	1
GO:0009142 ~nucleoside triphosphate biosynthetic process	3	1.764706	0.06364	AK1, CMPK1, AK4	6.906452	1
GO:0006139 ~nucleobase-containing compound metabolic process	3	1.764706	0.084976	AK1, CMPK1, AK4	5.919816	1
GO:0004550 ~nucleoside diphosphate kinase activity	3	1.764706	0.086315	AK1, CMPK1, AK4	5.865714	1
mmu01240: Biosynthesis of cofactors	7	4.117647	8.93E-02	ALAD, PDXK, AK1, AKR1A1, CMPK1, AK4, COQ6	2.194352	0.97549
mmu01232: Nucleotide metabolism	3	1.764706	0.412504	AK1, CMPK1, AK4	2.128357	0.97549
KW-0418~Kinase	8	4.705882	0.733924	MAP2K4, PDXK, DGKE, AK1, CSNK2A2, CMPK1, AK4, PFKP	0.962338	1
GO:0016310 ~phosphorylation	8	4.705882	0.759901	MAP2K4, PDXK, DGKE, AK1, CSNK2A2, CMPK1, AK4, PFKP	0.936468	1
GO:0016301 ~kinase activity	8	4.705882	0.824753	MAP2K4, PDXK, DGKE, AK1, CSNK2A2, CMPK1, AK4, PFKP	0.868995	1

Cluster 8- Enrichment score: 0.8749102997698915						
SM00948:SM00948	3	1.764706	0.041436	PSMA3, PSMA1, PSMA7	8.674603	1
GO:0005839~proteasome core complex	4	2.352941	0.057473	PSMA3, PSMB5, PSMA1, PSMA7	4.359305	1
IPR001353:Proteasome, subunit alpha/beta	4	2.352941	0.059535	PSMA3, PSMB5, PSMA1, PSMA7	4.29783	1
mmu03050: Proteasome	6	3.529412	0.063114	PSMA3, PSMB5, PSMD7, PSMA1, PSMC1, PSMA7	2.695918	0.897122
KW-0647~Proteasome	6	3.529412	0.067274	PSMA3, PSMB5, PSMD7, PSMA1, PSMC1, PSMA7	2.670259	0.717584
GO:0000502~proteasome complex	6	3.529412	0.076583	PSMA3, PSMB5, PSMD7, PSMA1, PSMC1, PSMA7	2.575953	1
DOMAIN:Proteasome alpha-type subunits	3	1.764706	0.079509	PSMA3, PSMA1, PSMA7	6.145714	1
GO:0019773~proteasome core complex, alpha-subunit complex	3	1.764706	0.081264	PSMA3, PSMA1, PSMA7	6.071889	1
IPR023332:Proteasome A-type subunit	3	1.764706	0.083331	PSMA3, PSMA1, PSMA7	5.986264	1
IPR000426:Proteasome, alpha-subunit, N-terminal domain	3	1.764706	0.083331	PSMA3, PSMA1, PSMA7	5.986264	1

GO:0051603 ~proteolysis involved in cellular protein catabolic process	4	2.352941	0.151862	PSMA3, PSMB5, PSMA1, PSMA7	2.90798	1
GO:0010498 ~proteasomal protein catabolic process	4	2.352941	0.151862	PSMA3, PSMB5, PSMA1, PSMA7	2.90798	1
mmu05017:Spinocerebellar ataxia	6	3.529412	0.484074	PSMA3, PSMB5, PSMD7, PSMA1, PSMC1, PSMA7	1.304477	0.97549
CROSSLNK:Glycyl lysine isopeptide (Lys-Gly) (interchain with G-Cter in ubiquitin)	4	2.352941	0.671865	PSMD7, PSMA1, PSMC1, HRAS	1.170612	1
GO:0006511 ~ubiquitin-dependent protein catabolic process	4	2.352941	0.735565	PSMA3, PSMA1, UBE2N, PSMA7	1.062531	1
GO:0043161 ~proteasome-mediated ubiquitin-dependent protein catabolic process	3	1.764706	0.879176	PSMB5, PSMD7, PSMC1	0.845688	1
Cluster 9- Enrichment score: 0.8516868568025209						
mmu04260: Cardiac muscle contraction	7	4.117647	0.081463	UQCRB, UQCRQ, COX7A2, UQCR10, COX5B, COX6A1, COX5A	2.246599	0.97549

GO:0005750~mitochondrial respiratory chain complex III	3	1.764706	0.127134	UQCRB, UQCRQ, UQCR10	4.722581	1
GO:0006122~mitochondrial electron transport, ubiquinol to cytochrome c	3	1.764706	0.158272	UQCRB, UQCRQ, UQCR10	4.143871	1
GO:0045333~cellular respiration	3	1.764706	0.239126	UQCRB, UQCRQ, UQCR10	3.187593	1
Cluster 10- Enrichment score: 0.8011875047990299						
KW-0496~Mitochondrion	36	21.17647	0.06211	ACADVL, UQCRB, NDUFB6, MTFP1, TIMM9, COX7A2, AK4, ETFA, PARK7, UQCR10, MFF, COX5B, COX6A1, HSD17B10, COX5A, PRDX3, CHCHD3, HINT2, C1QBP, CHCHD6, SLC25A22, DECR1, FIS1, ACOT9, NDUFA7, NDUFA5, MTX2, NDUFA2, IDH2, HSPE1, COQ6, HADHB, UQCRQ, NDUFS6, NDUFS5, PGAM5	1.304554	0.717584
KW-0809~Transit peptide	16	9.411765	0.137538	ACOT9, ACADVL, IDH2, COX7A2, ETFA, ACAA1A, COX5B, COX6A1, COX5A, COQ6, HADHB, PRDX3, HINT2, NDUFS6, C1QBP, DECR1	1.411938	1
TRANSIT:Mitochondrion	15	8.823529	0.462223	ACOT9, ACADVL, IDH2, COX7A2, ETFA, COX5B, COX6A1, COX5A, COQ6, HADHB, PRDX3, HINT2, NDUFS6, C1QBP, DECR1	1.120313	1
Cluster 11- Enrichement score: 0.6014299531903391						

mmu04260: Cardiac muscle contraction	7	4.117647	0.081463	UQCRB, UQCRQ, COX7A2, UQCR10, COX5B, COX6A1, COX5A	2.246599	0.97549
TOPO_DOM: Mitochondrial intermembrane	6	3.529412	0.374502	FIS1, UQCRQ, COX7A2, UQCR10, MFF, COX6A1	1.483448	1
TOPO_DOM: Mitochondrial matrix	4	2.352941	0.514394	UQCRQ, COX7A2, UQCR10, COX6A1	1.470769	1
Cluster 12: Enrichment score: 0.5796867098295971						
GO:0006631~fatty acid metabolic process	8	4.705882	0.095551	HADHB, ACADVL, NDUFS6, DBI, ACAA1A, HSD17B10, DECR1, SNCA	2.00915	1
GO:0006635~fatty acid beta-oxidation	5	2.941176	0.111742	HADHB, ACADVL, ACAA1A, HSD17B10, DECR1	2.656328	1
KW-0443~Lipid metabolism	13	7.647059	0.113604	CBR1, ACADVL, DGKE, LPGAT1, AKR1A1, ACAA1A, HSD17B10, HADHB, HINT2, PAM, PAFAH1B2, DECR1, CDS2	1.551394	1
GO:0006629~lipid metabolic process	14	8.235294	0.148136	CBR1, ACADVL, DGKE, LPGAT1, AKR1A1, ACAA1A, HSD17B10, HADHB, HINT2, APOE, PAM, PAFAH1B2, DECR1, CDS2	1.465005	1
GO:0042645~mitochondrial nucleoid	3	1.764706	0.337156	HADHB, ACADVL, HSD17B10	2.50019	1
KW-0276~Fatty acid metabolism	5	2.941176	0.342032	HADHB, ACADVL, ACAA1A, HSD17B10, DECR1	1.670732	1
mmu00071:Fatty acid degradation	3	1.764706	0.622407	HADHB, ACADVL, ACAA1A	1.444242	0.97549

mmu01212:Fatty acid metabolism	3	1.764706	0.660538	HADHB, ACADVL, ACAA1A	1.347959	0.97549
mmu00280: Valine, leucine and isoleucine degradation	3	1.764706	0.71194	HADHB, ACAA1A, HSD17B10	1.225417	0.97549
Cluster 13: Enrichment score: 0.5670517176501461						
GO:0090141~positive regulation of mitochondrial fission	3	1.764706	0.084976	FIS1, PGAM5, MFF	5.919816	1
GO:0005741~mitochondrial outer membrane	7	4.117647	0.457372	HADHB, FIS1, SLC44A2, MTX2, PGAM5, MFF, SNCA	1.287977	1
KW-1000~Mitochondrion outer membrane	5	2.941176	0.512012	HADHB, FIS1, MTX2, PGAM5, MFF	1.343526	1
Cluster 14: Enrichment score: 0.5603187619854242						
GO:0016616~oxidoreductase activity, acting on the CH-OH group of donors, NAD or NADP as acceptor	5	2.941176	0.069925	CBR1, CTBP1, IDH2, PHGDH, DHRS1	3.110606	1
GO:0051287~NAD binding	4	2.352941	0.373117	CTBP1, IDH2, PHGDH, HSD17B10	1.824889	1
KW-0520~NAD	4	2.352941	0.79904	CTBP1, PHGDH, DHRS1, HSD17B10	0.955939	1
Cluster 15- Enrichment score: 0.5224654391300952						

KW-0143~Chaperone	8	4.705882	0.086512	ST13, TIMM9, DNAJA2, PARK7, HSPE1, CRYAB, PDIA6, PPID	2.036948	1
GO:0006457~protein folding	5	2.941176	0.374315	DNAJA2, HSPE1, PPIB, CRYAB, PPID	1.606152	1
GO:0051082~unfolded protein binding	4	2.352941	0.491789	ST13, DNAJA2, HSPE1, CRYAB	1.520741	1
GO:0051087~chaperone binding	4	2.352941	0.510556	ST13, TIMM9, DNAJA2, HSPE1	1.47964	1
Cluster 16- Enrichment score: 0.5180979126620917						
GO:0030125~clathrin vesicle coat	3	1.764706	0.081264	NECAP1, CLTB, CLTA	6.071889	1
GO:0005905~clathrin-coated pit	4	2.352941	0.430483	NECAP1, RAB35, CLTB, CLTA	1.666793	1
GO:0016192~vesicle-mediated transport	6	3.529412	0.797724	NECAP1, RABEP1, CLTB, CLTA, RAB39B, VTI1B	0.910741	1
Cluster 17- Enrichment score: 0.4648374090140741						
m_fcer1Pathway:Fc Epsilon Receptor I Signaling in Mast Cells	3	1.764706	0.167273	MAP2K4, CALM1, HRAS	3.75	1
m_tcrPathway:T Cell Receptor Signaling Pathway	3	1.764706	0.167273	MAP2K4, CALM1, HRAS	3.75	1
m_pyk2Pathway:Links between Pyk2 and Map Kinases	3	1.764706	0.238705	MAP2K4, CALM1, HRAS	3	1

m_at1rPathway:Angiotensin II mediated activation of JNK Pathway via Pyk2 dependent signaling	3	1.764706	0.26315	MAP2K4, CALM1, HRAS	2.8125	1
mmu05417:Lipid and atherosclerosis	4	2.352941	0.640389	MAP2K4, RAP1A, CALM1, HRAS	1.225417	0.97549
mmu05167: Kaposi sarcoma-associated herpesvirus infection	3	1.764706	0.695561	MAP2K4, CALM1, HRAS	1.263712	0.97549
mmu04912: GnRH signaling pathway	3	1.764706	0.71194	MAP2K4, CALM1, HRAS	1.225417	0.97549
Cluster 18- Enrichment score: 0.4382309567673749						
REPEAT:TPR	4	2.352941	0.1399	FIS1, ST13, KLC1, PPID	3.018947	1
KW-0802~TPR repeat	4	2.352941	0.190896	FIS1, ST13, KLC1, PPID	2.601626	1
SM00028:TPR	3	1.764706	0.289399	ST13, KLC1, PPID	2.760101	1
IPR019734:Tetratricopeptide repeat	3	1.764706	0.471337	ST13, KLC1, PPID	1.90472	1
REPEAT:TPR 3	3	1.764706	0.503605	ST13, KLC1, PPID	1.7925	1
REPEAT:TPR 1	3	1.764706	0.5474	ST13, KLC1, PPID	1.654615	1
REPEAT:TPR 2	3	1.764706	0.5474	ST13, KLC1, PPID	1.654615	1

IPR011990:Tetratricopeptide-like helical	4	2.352941	0.567559	FIS1, ST13, KLC1, PPID	1.362727	1
Cluster 19- Enrichment score: 0.4324686054574155						
IPR020849:Small GTPase superfamily, Ras type	5	2.941176	0.007765	RAB21, RAP1A, MRAS, RAP2B, HRAS	5.819979	1
mmu05417:Lipid and atherosclerosis	4	2.352941	0.640389	MAP2K4, RAP1A, CALM1, HRAS	1.225417	0.97549
mmu04722:Neurotrophin signaling pathway	3	1.764706	0.660538	RAP1A, CALM1, HRAS	1.347959	0.97549
mmu04010:MAPK signaling pathway	5	2.941176	0.682412	MAP2K4, RAP1A, MRAS, DUSP3, HRAS	1.087064	0.97549
mmu04015:Rap1 signaling pathway	4	2.352941	0.726024	RAP1A, MRAS, CALM1, HRAS	1.078367	0.97549
mmu04720:Long-term potentiation	3	1.764706	0.756746	RAP1A, CALM1, HRAS	1.123299	0.97549
mmu04014:Ras signaling pathway	4	2.352941	0.762554	RAP1A, MRAS, CALM1, HRAS	1.017328	0.97549
Cluster 20- Enrichment score: 0.423258239239409						
KW-0676~Redox-active center	3	1.764706	0.353816	PRDX3, PRDX1, PDIA6	2.394678	1
DOMAIN:Thioredoxin	3	1.764706	0.383236	PRDX3, PRDX1, PDIA6	2.264211	1
IPR013766:Thioredoxin domain	3	1.764706	0.396262	PRDX3, PRDX1, PDIA6	2.205466	1

Cluster 21- Enrichment score: 0.41674600283241503						
REPEAT:1	4	2.352941	0.325567	GLTP, APOE, NDRG1, SNCA	1.977931	1
REPEAT:2	4	2.352941	0.325567	GLTP, APOE, NDRG1, SNCA	1.977931	1
GO:0008289~lipid binding	7	4.117647	0.530251	GLTP, FIS1, FABP3, PITPNM2, DBI, APOE, SNCA	1.197583	1
Cluster 22- Enrichment score: 0.40948001669903844						
GO:0000221~vacuolar proton-transporting V-type ATPase, V1 domain	3	1.764706	0.127134	ATP6V1G2, ATP6V1E1, ATP6V1D	4.722581	1
GO:0046961~proton-transporting ATPase activity, rotational mechanism	3	1.764706	0.214666	ATP6V1G2, ATP6V1E1, ATP6V1D	3.421667	1
mmu04966: Collecting duct acid secretion	3	1.764706	0.218405	ATP6V1G2, ATP6V1E1, ATP6V1D	3.369898	0.97549
KW-0375~Hydrogen ion transport	3	1.764706	0.233245	ATP6V1G2, ATP6V1E1, ATP6V1D	3.222125	1
mmu05323: Rheumatoid arthritis	3	1.764706	0.246475	ATP6V1G2, ATP6V1E1, ATP6V1D	3.110675	0.97549
GO:0097401~synaptic vesicle lumen acidification	3	1.764706	0.266664	ATP6V1G2, ATP6V1E1, ATP6V1D	2.959908	1
GO:0098850~extrinsic	3	1.764706	0.337156	ATP6V1G2, ATP6V1E1, ATP6V1D	2.50019	1

component of synaptic vesicle membrane						
mmu04721:Synaptic vesicle cycle	5	2.941176	0.474819	ATP6V1G2, CLTB, CLTA, ATP6V1E1, ATP6V1D	1.404124	0.97549
mmu04150: mTOR signaling pathway	4	2.352941	0.500558	ATP6V1G2, ATP6V1E1, HRAS, ATP6V1D	1.497732	0.97549
GO:1902600~hydrogen ion transmembrane transport	3	1.764706	0.501215	ATP6V1G2, ATP6V1E1, ATP6V1D	1.801683	1
mmu05165: Human papillomavirus infection	5	2.941176	0.570792	ATP6V1G2, PSMC1, ATP6V1E1, HRAS, ATP6V1D	1.24811	0.97549
mmu04145: Phagosome	3	1.764706	0.895027	ATP6V1G2, ATP6V1E1, ATP6V1D	0.808776	0.97549
KW-0406~Ion transport	4	2.352941	0.991128	ATP6V1G2, FXYD6, ATP6V1E1, ATP6V1D	0.493003	1
GO:0006811~ion transport	4	2.352941	0.995771	ATP6V1G2, FXYD6, ATP6V1E1, ATP6V1D	0.442013	1
Cluster 23- Enrichment score: 0.37605817559074595						
GO:0043524~negative regulation of neuron apoptotic process	6	3.529412	0.347096	SLC25A27, PRDX3, APOE, PARK7, HRAS, SNCA	1.534767	1
GO:0043066~negative regulation of apoptotic process	8	4.705882	0.449318	SLC25A27, PRDX3, PDXK, AKR1A1, PARK7, CRYAB, PPID, SNCA	1.255718	1

GO:0034599 ~cellular response to oxidative stress	3	1.764706	0.477334	PRDX3, PARK7, SNCA	1.883578	1
Cluster 24- Enrichment score: 0.3667035900306337						
SM00033:CH	3	1.764706	0.252494	SPTBN4, PLS3, TAGLN3	3.036111	1
DOMAIN:Calponin-homology (CH)	3	1.764706	0.480715	SPTBN4, PLS3, TAGLN3	1.870435	1
IPR001715:Calponin homology domain	3	1.764706	0.518208	SPTBN4, PLS3, TAGLN3	1.745994	1
GO:0051015 ~actin filament binding	8	4.705882	0.542679	SPTBN4, MARCKS, ABLIM2, CFL2, ARPC5L, PLS3, TWF1, TAGLN3	1.152561	1
Cluster 25- Enrichment score: 0.32358477443081507						
KW-0274~FAD	4	2.352941	0.440826	ACADVL, ETFA, COQ6, PCYOX1	1.630719	1
KW-0285~Flavoprotein	4	2.352941	0.479371	ACADVL, ETFA, COQ6, PCYOX1	1.540123	1
GO:0050660 ~flavin adenine dinucleotide binding	3	1.764706	0.506182	ACADVL, ETFA, COQ6	1.785217	1
Cluster 26- Enrichment score: 0.32025544790384614						
GO:0005791 ~rough endoplasmic reticulum	4	2.352941	0.19683	BAIAP2, RPL18, RPL6, SNCA	2.575953	1
GO:0005840 ~ribosome	4	2.352941	0.590676	RPLP1, RPL18, RPL6, SNCA	1.317929	1

GO:0098794~postsynapse	7	4.117647	0.941442	PURA, RPLP1, HPCA, BAIAP2, RPL6, PSMA7, SNCA	0.703363	1
Cluster 27- Enrichment score: 0.31688808123193835						
GO:0000122~negative regulation of transcription from RNA polymerase II promoter	5	2.941176	0.457721	PURA, CTBP1, C1QBP, TAGLN3, PPID	1.438844	1
KW-0804~Transcription	5	2.941176	0.494729	PURA, CHCHD3, CTBP1, C1QBP, CSNK2A2	1.366962	1
KW-0805~Transcription regulation	5	2.941176	0.494729	PURA, CHCHD3, CTBP1, C1QBP, CSNK2A2	1.366962	1
Cluster 28- Enrichment score: 0.3070828474198248						
SM00054:EFh	4	2.352941	0.251696	HPCA, EFHD2, PLS3, CALM1	2.248971	1
DOMAIN:EF-hand 4	3	1.764706	0.357621	CAPNS1, HPCA, CALM1	2.39	1
DOMAIN:EF-hand 2	5	2.941176	0.363734	CAPNS1, HPCA, EFHD2, PLS3, CALM1	1.629545	1
DOMAIN:EF-hand	5	2.941176	0.491241	CAPNS1, HPCA, EFHD2, PLS3, CALM1	1.378846	1
IPR002048:EF-hand domain	5	2.941176	0.512661	CAPNS1, HPCA, EFHD2, PLS3, CALM1	1.343072	1
DOMAIN:EF-hand 3	3	1.764706	0.52584	CAPNS1, HPCA, CALM1	1.7208	1
DOMAIN:EF-hand 1	4	2.352941	0.565725	HPCA, EFHD2, PLS3, CALM1	1.365714	1
IPR018247:EF-Hand 1, calcium-binding site	4	2.352941	0.600679	CAPNS1, HPCA, PLS3, CALM1	1.299344	1

IPR011992:EF-hand-like domain	5	2.941176	0.60137	CAPNS1, HPCA, EFHD2, PLS3, CALM1	1.204134	1
KW-0106~Calcium	12	7.058824	0.666211	CAPNS1, HPCA, PITPNM2, EFHD2, CLTB, PLS3, CLTA, CDH13, KLC1, CALM1, NPTXR, PAM	0.996008	1
GO:0005509~calcium ion binding	9	5.294118	0.70962	CAPNS1, HPCA, PITPNM2, EFHD2, PLS3, CDH13, CALM1, PAM, SNCA	0.977619	1
Cluster 29- Enrichment score: 0.300079764872977						
GO:0015629~actin cytoskeleton	8	4.705882	0.259024	ABLIM2, CSRP1, CFL2, ARPC5L, TWF1, TAGLN3, BAIAP2, SNCA	1.531648	1
GO:0003779~actin binding	11	6.470588	0.351018	SPTBN4, MARCKS, GMFB, ABLIM2, CFL2, HPCA, TMOD2, ARPC5L, PLS3, TWF1, SNCA	1.275876	1
GO:0051015~actin filament binding	8	4.705882352941177+A271:C273	0.542679	SPTBN4, MARCKS, ABLIM2, CFL2, ARPC5L, PLS3, TWF1, TAGLN3	1.152561	1
KW-0009~Actin-binding	7	4.117647	0.579073	SPTBN4, MARCKS, CFL2, TMOD2, ARPC5L, PLS3, TWF1	1.137657	1
mmu04666:Fc gamma R-mediated phagocytosis	3	1.764706	0.678432	MARCKS, CFL2, ARPC5L	1.304477	0.97549
GO:0005884~actin filament	3	1.764706	0.816712	SPTBN4, PLS3, TWF1	0.988447	1
Cluster 30- Enrichment score: 0.28131427577325174						
KW-0865~Zymogen	3	1.764706	0.177372	PSMB5, CPE, PARK7	3.86166	0.931205

GO:0006508~proteolysis	6	3.529412	0.562069	PSMB5, CAPNS1, SCRN3, CPE, PARK7, ASRGL1	1.201122	1
GO:0008233~peptidase activity	5	2.941176	0.631665	PSMB5, PSMD7, CPE, PARK7, ASRGL1	1.159887	1
KW-0645~Protease	4	2.352941	0.680325	PSMB5, CPE, PARK7, ASRGL1	1.152989	1
ACT_SITE:Nucleophile	3	1.764706	0.91527	PSMB5, PARK7, ASRGL1	0.754737	1
Cluster 31- Enrichment score: 0.27349858416720274						
LIPID:S-palmitoyl cysteine	7	4.117647	0.355823	GNA13, RAP2B, PALM, S1PR1, PARK7, HRAS, RHOB	1.434	1
KW-0564~Palmitate	8	4.705882	0.457912	GNA13, PRDX3, RAP2B, PALM, S1PR1, PARK7, HRAS, RHOB	1.244784	1
GO:0001525~angiogenesis	3	1.764706	0.665711	GNA13, S1PR1, RHOB	1.336733	1
mmu04071:Sphingolipid signaling pathway	3	1.764706	0.742513	GNA13, S1PR1, HRAS	1.155394	0.97549
Cluster 32- 0.2557899536726249						
mmu04218:Cellular senescence	4	2.352941	0.359713	MRAS, CALM1, HRAS, PPID	1.859254	0.97549
mmu04625:C-type lectin receptor signaling pathway	3	1.764706	0.412504	MRAS, CALM1, HRAS	2.128357	0.97549
mmu04371:Apelin signaling pathway	4	2.352941	0.640389	GNA13, MRAS, CALM1, HRAS	1.225417	0.97549
mmu04015:Rap1	4	2.352941	0.726024	RAP1A, MRAS, CALM1, HRAS	1.078367	0.97549

signaling pathway						
mmu04014: Ras signaling pathway	4	2.352941	0.762554	RAP1A, MRAS, CALM1, HRAS	1.017328	0.97549
Cluster 33- Enrichment score- 0.21966773969124903						
KW-0862~Zinc	13	7.647059	0.356789	PDXK, DGKE, TIMM9, PDE1A, ADAP1, COX5B, ALAD, ABLIM2, CSRP1, DNAJA2, CPE, PAM, CRYAB	1.21753	1
KW-0479~Metal-binding	29	17.05882	0.762176	PDXK, DGKE, PDE1A, TIMM9, HPCA, COX5B, COX5A, NUDT3, ALAD, GNA13, ABLIM2, CSRP1, CAPNS1, EFHD2, PDE4B, PLS3, SNCA, IDH2, ADAP1, HDHD2, PITPNM2, DNAJA2, CDH13, CPE, CALM1, NPTXR, CRYAB, PAM, PFKP	0.941387	1
GO:0046872~metal ion binding	28	16.47059	0.806361	PDXK, DGKE, PDE1A, TIMM9, HPCA, ENDOD1, COX5B, COX5A, ALAD, GNA13, ABLIM2, CSRP1, CAPNS1, EFHD2, PDE4B, PLS3, SNCA, IDH2, HSPE1, HDHD2, PITPNM2, DNAJA2, CDH13, CPE, NPTXR, CRYAB, PAM, PFKP	0.90812	1
Cluster 34- Enrichment score: 0.2180493204604778						
mmu04810: Regulation of actin cytoskeleton	6	3.529412	0.569442	GNA13, MRAS, CFL2, ARPC5L, BAIAP2, HRAS	1.189376	0.97549
mmu04072: Phospholipase D signaling pathway	4	2.352941	0.608077	GNA13, DGKE, MRAS, HRAS	1.283771	0.97549
mmu04371: Apelin signaling pathway	4	2.352941	0.640389	GNA13, MRAS, CALM1, HRAS	1.225417	0.97549

Cluster 35- Enrichment score: 0.2164945144060664						
GO:0005905~clathrin-coated pit	4	2.352941	0.430483	NECAP1, RAB35, CLTB, CLTA	1.666793	1
KW-0168~Coated pit	3	1.764706	0.572084	RAB35, CLTB, CLTA	1.582375	1
mmu04144:Endocytosis	6	3.529412	0.910124	RABEP1, RAB35, ARPC5L, CLTB, CLTA, HRAS	0.755865	0.97549
Cluster 36- Enrichment score: 0.2004230482210217						
KW-0967~Endosome	12	7.058824	0.533363	RAB21, PRDX3, RAP1A, RAP2B, RABEP1, RAB35, S1PR1, FLOT1, OCIAD1, APOE, RHOB, VTI1B	1.095491	1
GO:0005769~early endosome	7	4.117647	0.667642	RAB21, PRDX3, RAP1A, RABEP1, FLOT1, APOE, RHOB	1.043939	1
GO:0005768~endosome	14	8.235294	0.703339	RHOB, PRDX3, RAB21, RABEP1, RAP1A, RAP2B, RAB35, S1PR1, FLOT1, EXOC4, OCIAD1, APOE, ATP6V1E1, VTI1B	0.962856	1
Cluster 37-Enrichment score: 0.1668294690842498						
KW-0964~Secreted	6	3.529412	0.546793	C1QBP, ENDOD1, CPE, APOE, CRYAB, SNCA	1.22069	1
GO:0005576~extracellular region	7	4.117647	0.580183	C1QBP, ENDOD1, CPE, APOE, PAM, CRYAB, SNCA	1.139933	1
GO:0009986~cell surface	4	2.352941	0.995689	C1QBP, APOE, PAM, CRYAB	0.442742	1
Cluster 38- Enrichment score: 0.15665707396650488						
GO:0022625~cytosolic large ribosomal subunit	3	1.764706	0.463714	RPLP1, RPL18, RPL6	1.931965	1
GO:0003735~structural	4	2.352941	0.528959	NDUFA7, RPLP1, RPL18, RPL6	1.440702	1

constituent of ribosome						
GO:0005840~ribosome	4	2.352941	0.590676	RPLP1, RPL18, RPL6, SNCA	1.317929	1
mmu03010: Ribosome	3	1.764706	0.71194	RPLP1, RPL18, RPL6	1.225417	0.97549
GO:0022626~cytosolic ribosome	3	1.764706	0.716732	RPLP1, RPL18, RPL6	1.214378	1
GO:0002181~cytoplasmic translation	3	1.764706	0.730193	RPLP1, RPL18, RPL6	1.183963	1
KW-0689~Ribosomal protein	3	1.764706	0.745149	RPLP1, RPL18, RPL6	1.145783	1
KW-0687~Ribonucleoprotein	3	1.764706	0.831022	RPLP1, RPL18, RPL6	0.954819	1
mmu05171: Coronavirus disease - COVID-19	3	1.764706	0.857063	RPLP1, RPL18, RPL6	0.898639	0.97549
GO:1990904~ribonucleoprotein complex	3	1.764706	0.946895	RPLP1, RPL18, RPL6	0.664113	1
Cluster 39- Enrichment score: 0.11036781972394576						
TRANSMEM: Helical; Name=7	3	1.764706	0.724936	SLC2A13, S1PR1, GPR37L1	1.195	1
TRANSMEM: Helical; Name=3	4	2.352941	0.757865	SLC2A13, S1PR1, GPR37L1, SLC25A22	1.024286	1
TRANSMEM: Helical; Name=6	4	2.352941	0.757865	SLC2A13, S1PR1, GPR37L1, SLC25A22	1.024286	1
TRANSMEM: Helical; Name=5	4	2.352941	0.778849	SLC2A13, S1PR1, GPR37L1, SLC25A22	0.988966	1

TRANSMEM: Helical; Name=4	4	2.352941	0.798327	SLC2A13, S1PR1, GPR37L1, SLC25A22	0.956	1
TRANSMEM: Helical; Name=1	4	2.352941	0.807521	SLC2A13, S1PR1, GPR37L1, SLC25A22	0.940328	1
TRANSMEM: Helical; Name=2	4	2.352941	0.807521	SLC2A13, S1PR1, GPR37L1, SLC25A22	0.940328	1
Cluster 40- Enrichment score: 0.09743139654225756						
KW-0808~Transferase	17	10	0.506859	MAP2K4, PDXK, DGKE, LPGAT1, CSNK2A2, AK1, TALDO1, AK4, ACAA1A, HADHB, PCMT1, COMTD1, UBE2N, CMPK1, PFKP, GSTM5, CDS2	1.073185	1
GO:0016740~transferase activity	17	10	0.593208	MAP2K4, PDXK, DGKE, LPGAT1, CSNK2A2, AK1, TALDO1, AK4, ACAA1A, HADHB, PCMT1, COMTD1, UBE2N, CMPK1, PFKP, GSTM5, CDS2	1.024993	1
KW-0418~Kinase	8	4.705882	0.733924	MAP2K4, PDXK, DGKE, AK1, CSNK2A2, CMPK1, AK4, PFKP	0.962338	1
GO:0016310~phosphorylation	8	4.705882	0.759901	MAP2K4, PDXK, DGKE, AK1, CSNK2A2, CMPK1, AK4, PFKP	0.936468	1
GO:0016301~kinase activity	8	4.705882	0.824753	MAP2K4, PDXK, DGKE, AK1, CSNK2A2, CMPK1, AK4, PFKP	0.868995	1
GO:0000166~nucleotide binding	22	12.94118	0.980409	DARS, MAP2K4, PDXK, DGKE, CSNK2A2, AK1, RHOG, RAB39B, AK4, RHOB, GNA13, RAB21, RAP1A, HINT2, MRAS, RAP2B, PSMC1, RAB35, UBE2N, CMPK1, HRAS, PFKP	0.730841	1
GO:0005524~ATP binding	15	8.823529	0.988116	DARS, MAP2K4, PDXK, DGKE, CSNK2A2, AK1, TWF1, AK4, HSPE1,	0.660129	1

				PRPSAP1, PSMC1, DNAJA2, UBE2N, CMPK1, PFKP		
KW-0547~Nucleotide-binding	22	12.94118	0.991696	DARS, MAP2K4, PDXK, DGKE, CSNK2A2, AK1, RHOG, RAB39B, AK4, RHOB, GNA13, RAB21, RAP1A, HINT2, MRAS, RAP2B, PSMC1, RAB35, UBE2N, CMPK1, HRAS, PFKP	0.724334	1
KW-0067~ATP-binding	11	6.470588	0.999302	DARS, MAP2K4, PDXK, DGKE, PSMC1, AK1, CSNK2A2, UBE2N, CMPK1, AK4, PFKP	0.527586	1
Cluster 41- Enrichment score: 0.09707518932629637						
mmu04371: Apelin signaling pathway	4	2.352941	0.640389	GNA13, MRAS, CALM1, HRAS	1.225417	0.97549
mmu05200: Pathways in cancer	5	2.941176	0.848729	GNA13, CTBP1, CALM1, HRAS, GSTM5	0.853139	0.97549
mmu05163: Human cytomegalovirus infection	3	1.764706	0.940939	GNA13, CALM1, HRAS	0.685403	0.97549
Cluster 42- Enrichment score: 0.052663319924344844						
KW-0732~Signal	19	11.17647	0.551888	CADM4, HEPACAM, ENDOD1, AK4, GPR37L1, PDIA6, COQ6, HINT2, PSMD7, EMC1, CMPK1, CDH13, CPE, FXYD6, APOE, PPIB, NPTXR, PAM, PCYOX1	1.039435	1
KW-0325~Glycoprotein	17	10	0.992214	CADM4, SLC44A2, HEPACAM, SLC2A13, GPR37L1, PSMA7, PSMA1, EMC1, S1PR1, CDH13, CPE, MAL2, APOE, NPTXR, PAM, PFKP, PCYOX1	0.657678	1
CARBOHYD: N-linked	13	7.647059	0.996742	CADM4, SLC44A2, HEPACAM, SLC2A13, GPR37L1, EMC1, S1PR1,	0.582563	1

(GlcNAc...) asparagine				CDH13, CPE, MAL2, NPTXR, PAM, PCYOX1		
TOPO_DOM: Extracellular	8	4.705882	0.99937	CADM4, SLC44A2, HEPACAM, SLC2A13, S1PR1, FXYD6, GPR37L1, NPTXR	0.453439	1
TOPO_DOM: Cytoplasmic	14	8.235294	0.999811	FIS1, CADM4, SLC44A2, HEPACAM, SLC2A13, GPR37L1, MFF, EMC1, S1PR1, MAL2, FXYD6, NPTXR, PAM, VTI1B	0.505693	1
Cluster 43- Enrichment score: 0.012813607896924083						
KW-1133~Transmembrane helix	30	17.64706	0.925236	DGKE, LPGAT1, NDUFB6, MTFP1, SLC44A2, HEPACAM, ENDOD1, COX7A2, ACAA1A, UQCR10, MFF, COX6A1, PCMT1, COMTD1, EMC1, S1PR1, MAL2, SLC25A22, VTI1B, FIS1, CADM4, SLC2A13, GPR37L1, UQCRQ, FXYD6, PGAM5, NPTXR, PAM, PCYOX1, CDS2	0.853856	1
KW-0812~Transmembrane	30	17.64706	0.94029	DGKE, LPGAT1, NDUFB6, MTFP1, SLC44A2, HEPACAM, ENDOD1, COX7A2, ACAA1A, UQCR10, MFF, COX6A1, PCMT1, COMTD1, EMC1, S1PR1, MAL2, SLC25A22, VTI1B, FIS1, CADM4, SLC2A13, GPR37L1, UQCRQ, FXYD6, PGAM5, NPTXR, PAM, PCYOX1, CDS2	0.84158	1
TRANSMEM: Helical	29	17.05882	0.995025	DGKE, LPGAT1, NDUFB6, MTFP1, SLC44A2, HEPACAM, ENDOD1, COX7A2, ACAA1A, UQCR10, MFF, COX6A1, PCMT1, EMC1, S1PR1, MAL2, SLC25A22, VTI1B, FIS1, CADM4, SLC2A13,	0.709659	1

				GPR37L1, UQCRQ, FXYD6, PGAM5, NPTXR, PAM, PCYOX1, CDS2		
GO:0016021 ~integral component of membrane	27	15.88235	0.996933	DGKE, LPGAT1, MTFP1, SLC44A2, HEPACAM, ENDOD1, COX7A2, ACAA1A, MFF, COX6A1, SLC25A27, PCMT1, COMTD1, EMC1, S1PR1, MAL2, SLC25A22, VTI1B, FIS1, CADM4, SLC2A13, GPR37L1, PGAM5, NPTXR, PAM, PCYOX1, CDS2	0.683088	1
TOPO_DOM: Cytoplasmic	14	8.235294	0.999811	FIS1, CADM4, SLC44A2, HEPACAM, SLC2A13, GPR37L1, MFF, EMC1, S1PR1, MAL2, FXYD6, NPTXR, PAM, VTI1B	0.505693	1

Wild-Type Memory Retrieval v. APPtg Memory Retrieval- 20% Downregulated

Table 76. DAVID functional annotation clustering output table for annotation clusters enriched within proteins downregulated in APPtg mice during memory retrieval, when compared to WT mice during memory retrieval.

Cluster 1- Enrichment Score: 0.842334358003652						
Term	Count	%	PValue	Genes	Fold Enrichment	FDR
GO:0048471 ~perinuclear region of cytoplasm	3	60	0.004314	PAM, NDRG1, SIRT2	19.51195	0.207074
GO:0005829 ~cytosol	3	60	0.102552	PAM, NDRG1, SIRT2	3.778299	0.703217
GO:0005886 ~plasma membrane	3	60	0.195509	PAM, NDRG1, SIRT2	2.645688	1
GO:0016020 ~membrane	3	60	0.239425	PAM, NDRG1, SIRT2	2.356334	1

KW-0472~Membrane	3	60	0.269133	PAM, NDRG1, SIRT2	1.927549	0.733556
KW-0597~Phosphoprotein	3	60	0.364694	PAM, NDRG1, SIRT2	1.655863	1
REGION:Disordered	3	60	0.624594	PAM, NDRG1, SIRT2	1.284587	1

6. Functional Classification

Wild-Type Basal v. Wild-Type Memory Retrieval-20% Upregulated

Table 77. DAVID functional classification output table for proteins upregulated in WT mice during memory retrieval, when compared to WT mice at the basal level.

Gene Group 1 Enrichment Score: 4.56061471590555
Ndufb4 NADH:ubiquinone oxidoreductase subunit B4(Ndufb4)
Uqcrq ubiquinol-cytochrome c reductase, complex III subunit VII(Uqcrq)
Ndufs4 NADH:ubiquinone oxidoreductase core subunit S4(Ndufs4)
Uqcrb ubiquinol-cytochrome c reductase binding protein(Uqcrb)
Ndufa4 Ndufa4, mitochondrial complex associated(Ndufa4)
Ndufa2 NADH:ubiquinone oxidoreductase subunit A2(Ndufa2)
Cox7a2 cytochrome c oxidase subunit 7A2(Cox7a2)
Ndufb1 NADH:ubiquinone oxidoreductase subunit B1(Ndufb1)
Cox6a1 cytochrome c oxidase subunit 6A1(Cox6a1)
Cox5a cytochrome c oxidase subunit 5A(Cox5a)
Ndufs5 NADH:ubiquinone oxidoreductase core subunit S5(Ndufs5)
Atp5o ATP synthase, H+ transporting, mitochondrial F1 complex, O subunit(Atp5o)

Atp5k ATP synthase, H+ transporting, mitochondrial F1F0 complex, subunit E(Atp5k)
Cox6b1 cytochrome c oxidase, subunit 6B1(Cox6b1)
Ndufa6 NADH:ubiquinone oxidoreductase subunit A6(Ndufa6)
Apool apolipoprotein O-like(Apool)
Ndufb6 NADH:ubiquinone oxidoreductase subunit B6(Ndufb6)
Ndufa7 NADH:ubiquinone oxidoreductase subunit A7(Ndufa7)
Ndufa5 NADH:ubiquinone oxidoreductase subunit A5(Ndufa5)
Atp5h ATP synthase, H+ transporting, mitochondrial F0 complex, subunit D(Atp5h)
Ndufv2 NADH:ubiquinone oxidoreductase core subunit V2(Ndufv2)
Gene Group 2 Enrichment Score: 2.5369240722120243
Prdx6 peroxiredoxin 6(Prdx6)
Prdx3 peroxiredoxin 3(Prdx3)
Prdx1 peroxiredoxin 1(Prdx1)
Prdx5 peroxiredoxin 5(Prdx5)
Prdx2 peroxiredoxin 2(Prdx2)
Gene Group 3 Enrichment Score: 2.2542664079951886
Psma8 proteasome subunit alpha 8(Psma8)
Psma6 proteasome subunit alpha 6(Psma6)
Psma3 proteasome subunit alpha 3(Psma3)
Psmd4 proteasome (prosome, macropain) 26S subunit, non-ATPase, 4(Psmd4)
Psmb2 proteasome (prosome, macropain) subunit, beta type 2(Psmb2)
Psma7 proteasome subunit alpha 7(Psma7)
Gene Group 4 Enrichment Score: 0.6346788572182275
Rab11b RAB11B, member RAS oncogene family(Rab11b)
Rab8a RAB8A, member RAS oncogene family(Rab8a)

Rap2b RAP2B, member of RAS oncogene family(Rap2b)
Rhog ras homolog family member G(Rhog)
Rab11a RAB11A, member RAS oncogene family(Rab11a)
Rab1b RAB1B, member RAS oncogene family(Rab1b)
Gene Group 5 Enrichment Score: 0.2751755184711442
Apool apolipoprotein O-like(Apool)
Clptm1 cleft lip and palate associated transmembrane protein 1(Clptm1)
Tmx4 thioredoxin-related transmembrane protein 4(Tmx4)
Fxyd6 FXYD domain-containing ion transport regulator 6(Fxyd6)

APPtg Basal v. APPtg Memory Retrieval- 20% Upregulated

Table 78. DAVID functional classification output table for proteins upregulated in APPtg mice during memory retrieval, when compared to APPtg mice at the basal level.

Gene Group 1 Enrichment Score: 6.386830970422354
Uqcrq ubiquinol-cytochrome c reductase, complex III subunit VII(Uqcrq)
Ndufs4 NADH:ubiquinone oxidoreductase core subunit S4(Ndufs4)
Ndufa4 Ndufa4, mitochondrial complex associated(Ndufa4)
Uqcrb ubiquinol-cytochrome c reductase binding protein(Uqcrb)
Ndufa2 NADH:ubiquinone oxidoreductase subunit A2(Ndufa2)
Ndufb3 NADH:ubiquinone oxidoreductase subunit B3(Ndufb3)
Ndufa8 NADH:ubiquinone oxidoreductase subunit A8(Ndufa8)
Ndufb7 NADH:ubiquinone oxidoreductase subunit B7(Ndufb7)
Mcu mitochondrial calcium uniporter(Mcu)
Ndufb1 NADH:ubiquinone oxidoreductase subunit B1(Ndufb1)

Cox6c	cytochrome c oxidase subunit 6C(Cox6c)
Cox6a1	cytochrome c oxidase subunit 6A1(Cox6a1)
Atp5l	ATP synthase, H+ transporting, mitochondrial F0 complex, subunit G(Atp5l)
Uqcr10	ubiquinol-cytochrome c reductase, complex III subunit X(Uqcr10)
Ndufs5	NADH:ubiquinone oxidoreductase core subunit S5(Ndufs5)
Atp5o	ATP synthase, H+ transporting, mitochondrial F1 complex, O subunit(Atp5o)
Atp5k	ATP synthase, H+ transporting, mitochondrial F1F0 complex, subunit E(Atp5k)
Cox6b1	cytochrome c oxidase, subunit 6B1(Cox6b1)
Ndufa5	NADH:ubiquinone oxidoreductase subunit A5(Ndufa5)
Ndufb10	NADH:ubiquinone oxidoreductase subunit B10(Ndufb10)
Atp5h	ATP synthase, H+ transporting, mitochondrial F0 complex, subunit D(Atp5h)
Ndufv2	NADH:ubiquinone oxidoreductase core subunit V2(Ndufv2)
Sdhb	succinate dehydrogenase complex, subunit B, iron sulfur (Ip)(Sdhb)
Gene Group 2	**Enrichment Score: 2.7421860596388368**
Psma6	proteasome subunit alpha 6(Psma6)
Psma5	proteasome subunit alpha 5(Psma5)
Psma1	proteasome subunit alpha 1(Psma1)
Psmd7	proteasome (prosome, macropain) 26S subunit, non-ATPase, 7(Psmd7)
Psmd6	proteasome (prosome, macropain) 26S subunit, non-ATPase, 6(Psmd6)
Psma2	proteasome subunit alpha 2(Psma2)
Psmc6	proteasome (prosome, macropain) 26S subunit, ATPase, 6(Psmc6)

Wild-Type Basal v. APPtg Basal- 20% Upregulated

Table 79. DAVID functional classification output table for proteins upregulated in APPtg mice at the basal level, when compared to WT mice at the basal level.

Gene Group 1	**Enrichment Score: 3.090680163702553**
Pacs1	phosphofurin acidic cluster sorting protein 1(Pacs1)
Ccdc177	coiled-coil domain containing 177(Ccdc177)

Kbtbd11	kelch repeat and BTB (POZ) domain containing 11(Kbtbd11)
6430548M08Rik	RIKEN cDNA 6430548M08 gene(6430548M08Rik)

Wild-Type Memory Retrieval v. APPtg Memory Retrieval-20% Upregulated

No results.

Wild-Type Basal v. Wild-Type Memory Retrieval- 20% Downregulated

No results.

APPtg Basal v. APPtg Memory Retrieval- 20% Downregulated

No results.

Wild-Type Basal v. APPtg Basal- 20% Downregulated

Table 80. DAVID functional classification output table for proteins downregulated in APPtg mice at the basal level, when compared to WT mice at the basal level.

Gene Group 1	**Enrichment Score: 3.090680163702553**
Pacs1	phosphofurin acidic cluster sorting protein 1(Pacs1)
Ccdc177	coiled-coil domain containing 177(Ccdc177)
Kbtbd11	kelch repeat and BTB (POZ) domain containing 11(Kbtbd11)
6430548M08Rik	RIKEN cDNA 6430548M08 gene(6430548M08Rik)

Wild-Type Memory Retrieval v. APPtg Memory Retrieval- 20% Downregulated

No results.

DAVID Analysis on Proteins that fail to become appropriately regulated during memory retrieval and proteins that are inappropriately regulated during memory retrieval in APPtg mice, when compared to WT mice during memory retrieval

Proteins that fail to become upregulated during memory retrieval

Biological Process

Table 81. DAVID Gene Ontology output table for enriched biological processes within proteins that fail to become upregulated during memory retrieval in APPtg mice, when compared to WT mice during memory retrieval.

Term	Count	%	PValue	Genes	Fold Enrichment	FDR
GO:0034599~cellular response to oxidative stress	5	5.05050505	0.01138131	PRDX3, PRDX2, GSR, PARK7, SNCA	5.42171717	1
GO:0042776~mitochondrial ATP synthesis coupled proton transport	5	5.05050505	0.06424051	NDUFA7, NDUFA6, NDUFB6, NDUFB4, NDUFB2	3.22372372	1
GO:0009060~aerobic respiration	5	5.05050505	0.06960885	NDUFA7, NDUFA6, NDUFB6, NDUFB4, NDUFB2	3.13888889	1
GO:0006979~response to oxidative stress	5	5.05050505	0.06960885	PRDX3, PRDX2, NDUFA6, NDUFB4, PARK7	3.13888889	1

GO:0043524~negative regulation of neuron apoptotic process	6	6.06060606	0.0700410 9	SLC25A27, PRDX3, PRDX2, NEFL, PARK7, SNCA	2.6506172 8	1
GO:0006268~DNA unwinding involved in DNA replication	2	2.02020202	0.0812065 3	PURB, PURA	23.855555 6	1
GO:0051252~regulation of RNA metabolic process	2	2.02020202	0.0812065 3	PCBP1, PCBP2	23.855555 6	1
GO:0045109~intermediate filament organization	3	3.03030303	0.0856327 7	NEFL, INA, GFAP	5.9638888 9	1
GO:0001933~negative regulation of protein phosphorylation	4	4.04040404	0.0900683 1	MYADM, PEBP1, PARK7, SNCA	3.6700854 7	1

Molecular Function

Table 82. DAVID Gene Ontology output table for enriched molecular functions within proteins that fail to become upregulated during memory retrieval in APPtg mice, when compared to WT mice during memory retrieval.

Term	**Count**	**%**	**PValue**	**Genes**	**Fold Enrichment**	**FDR**
GO:0003697~single-stranded DNA binding	5	5.05050505	6.44E-04	PURB, PURA, PCBP1, PCBP2, NME1	11.185064 9	0.16924539
GO:0000981~RNA polymerase II transcription factor activity, sequence-specific DNA binding	3	3.03030303	0.0147232	PURB, PURA, PCBP1	14.764285 7	1
GO:0000977~RNA polymerase II regulatory region sequence-specific DNA binding	3	3.03030303	0.0293395	PURB, PURA, NME1	10.545918 4	1

GO:0051920~peroxiredoxin activity	3	3.03030303	0.0293395	PRDX3, PRDX2, PARK7	10.5459184	1
GO:0005507~copper ion binding	3	3.03030303	0.04774316	PARK7, PAM, SNCA	8.20238095	1
GO:0019900~kinase binding	5	5.05050505	0.0684069 2	PRDX3, TOLLIP, PEBP1, PARK7, GFAP	3.1547619	1
GO:0003924~GTPase activity	9	9.09090909	0.0702566 7	RAP1A, RAP2B, GNA11, RAB1B, RHOG, TPPP, RAB6B, RAB8A, RAB11B	2.0133116 9	1
GO:0032422~purine-rich negative regulatory element binding	2	2.02020202	0.0787158 7	PURB, PURA	24.607142 9	1
GO:0003691~double-stranded telomeric DNA binding	2	2.02020202	0.0787158 7	PURB, PURA	24.607142 9	1
GO:0004332~fructose-bisphosphate aldolase activity	2	2.02020202	0.0787158 7	ALDOC, ALDOA	24.607142 9	1

Cellular Component

Table 83. DAVID Gene Ontology output table for enriched cellular components within proteins that fail to become upregulated during memory retrieval in APPtg mice, when compared to WT mice during memory retrieval.

Term	Count	%	PValue	Genes	Fold Enrichment	FDR

GO:0043209~myelin sheath	14	14.1414141	0.00957118	CNRIP1, PEBP1, NDRG1, COX5A, NAPG, GFAP, NME1, PRDX3, PRDX2, RAP1A, NEFL, TPPP, ALDOA, INA	2.16462518	1
GO:0005793~endoplasmic reticulum-Golgi intermediate compartment	4	4.04040404	0.02492203	TMED9, RAB1B, RAB6B, PDIA6	6.06868132	1
GO:0005882~intermediate filament	4	4.04040404	0.03424857	NEFL, INA, GFAP, NME1	5.39438339	1
GO:0005615~extracellular space	9	9.09090909	0.03484422	FABP5, DDT, ARHGDIA, SPARCL1, PEBP1, ALDOA, PAM, PDIA6, SNCA	2.32417582	1
GO:0000502~proteasome complex	5	5.05050505	0.04273988	PSMA3, PSMD4, PSMB2, PSMC1, PSMA7	3.67798868	1
GO:0005747~mitochondrial respiratory chain complex I	5	5.05050505	0.04697697	NDUFA7, NDUFA6, NDUFB6, NDUFB4, NDUFB2	3.56981254	1
GO:0005839~proteasome core complex	3	3.03030303	0.09569237	PSMA3, PSMB2, PSMA7	5.60185968	1

Proteins that are inappropriately upregulated in APPtg mice during memory retrieval (upregulated when they are not upregulated in WT mice)

Biological Process

Table 84. DAVID Gene Ontology output table for enriched biological processes within proteins that are inappropriately upregulated during memory retrieval in APPtg mice, when compared to WT mice during memory retrieval.

Term	Count	%	PValue	Genes	Fold Enrichment	FDR
GO:0042776~mitochondrial ATP synthesis coupled proton transport	6	10.5263158	0.0019713	NDUFA8, NDUFB9, NDUFB7, NDUFB10, NDUFB3, SDHB	6.33022113	0.46544945
GO:0009060~aerobic respiration	6	10.5263158	0.0022270	NDUFA8, NDUFB9, NDUFB7, NDUFB10, NDUFB3, SDHB	6.16363636	0.46544945
GO:0032981~mitochondrial respiratory chain complex I assembly	5	8.7719298	0.0094743	NDUFA8, NDUFB9, NDUFB7, NDUFB10, NDUFB3	5.74064171	1
GO:0042554~superoxide anion generation	2	3.5087719	0.0496815	SOD2, SOD1	39.036363	1
GO:0000303~response to superoxide	2	3.5087719	0.0496815	SOD2, SOD1	39.036363	1
GO:0006801~superoxide metabolic process	2	3.5087719	0.0496815	SOD2, SOD1	39.036363	1

GO:0050665~hydrogen peroxide biosynthetic process	2	3.50877193	0.07360568	SOD2, SOD1	26.0242424	1
GO:0051603~proteolysis involved in cellular protein catabolic process	3	5.26315789	0.08083706	PSMA5, PSMA1, PSMA2	6.16363636	1
GO:0010498~proteasomal protein catabolic process	3	5.26315789	0.08083706	PSMA5, PSMA1, PSMA2	6.16363636	1
GO:0019430~removal of superoxide radicals	2	3.50877193	0.09693837	SOD2, SOD1	19.5181818	1

Cellular Component

Table 85. DAVID Gene Ontology output table for enriched cellular components within proteins that are inappropriately upregulated during memory retrieval in APPtg mice, when compared to WT mice during memory retrieval.

Term	Count	%	PValue	Genes	Fold Enrichment	FDR
GO:0000502~proteasome complex	6	10.5263158	0.00102026	PSMA5, PSMD6, PSMC6, PSMD7, PSMA1, PSMA2	7.30247934	0.11181579
GO:0005743~mitochondrial inner membrane	14	24.5614035	0.00121539	NDUFB9, NDUFA8, NDUFB7, NDUFB10, NDUFB3, TIMM44, UQCR10, COX6C, SOD2, SDHB,	2.66488583	0.11181579

				CLU, CHCHD3, PGAM5, MCU		
GO:0070469~respiratory chain	6	10.5263158	0.0038057 2	NDUFA8, NDUFB9, NDUFB7, NDUFB10, NDUFB3, UQCR10	5.4768595	0.2334174 5
GO:0005747~mitochondrial respiratory chain complex I	5	8.7719298 2	0.0085887 3	NDUFA8, NDUFB9, NDUFB7, NDUFB10, NDUFB3	5.9064171 1	0.3532780 4
GO:0019773~proteasome core complex, alpha-subunit complex	3	5.2631578 9	0.0113875 5	PSMA5, PSMA1, PSMA2	17.212987	0.3532780 4
GO:0005739~mitochondrion	23	40.350877 2	0.0115199 4	NDUFB9, NDUFA8, NDUFB7, NDUFB10, NDUFB3, CISD1, TIMM44, AK4, UQCR10, ACAA1A, COX6C, SOD2, SDHB, CLU, SOD1, COMTD1, PGRMC1, CHCHD3, RAB35, GARS, PGAM5,	1.6121529 4	0.3532780 4

				CKB, MCU		
GO:0005839~proteasome core complex	3	5.26315789	0.03851033	PSMA5, PSMA1, PSMA2	9.26853147	1
GO:0099026~anchored component of presynaptic membrane	2	3.50877193	0.09431611	SNAP25, MARCKS	20.0818182	1

Molecular Function

Table 86. DAVID Gene Ontology output table for enriched biological processes within proteins that are inappropriately upregulated during memory retrieval in APPtg mice, when compared to WT mice during memory retrieval.

Term	Count	%	PValue	Genes	Fold Enrichment	FDR
GO:0004784~superoxide dismutase activity	2	3.50877193	0.04497026	SOD2, SOD1	43.0625	1
GO:0051087~chaperone binding	4	7.01754386	0.04990131	STIP1, DNAJA2, TIMM44, SOD1	4.65540541	1

<u>Proteins that fail to become downregulated during memory retrieval in APPtg mice</u>

Biological Process

Table 87. DAVID Gene Ontology output table for enriched biological processes within proteins that fail to become downregulated during memory retrieval in APPtg mice, when compared to WT mice during memory retrieval.

Term	Count	%	PValue	Genes	Fold Enrichment	FDR
GO:0007612~learning	12	11.0091743	7.37E-07	NTRK2, SLC12A5, SYNJ1, PRKAR2B, CTNND2, NRXN1, NRXN3, AMPH, PLCB1, SHANK3, SHANK2, PPP1R9B	6.50770397	8.88E-04
GO:0016079~synaptic vesicle exocytosis	7	6.42201835	9.98E-05	RPH3A, UNC13A, SV2B, SYT1, CADPS, PPFIA3, SPTBN2	8.262232	0.06014038
GO:0061001~regulation of dendritic spine morphogenesis	6	5.50458716	3.74E-04	DNM3, EPHA4, ABI2, PPP1R9A, SHANK3, SRCIN1	8.59946595	0.11223141
GO:0050808~synapse organization	9	8.25688073	4.64E-04	PCDHGC5, CTNND2, CTNNB1, ATP2B2, BSN, SHANK3,	4.63048167	0.11223141

				SHANK2, PPFIA3, SYN1		
GO:0007416~synapse assembly	8	7.33944954	4.66E-04	DNM3, NRXN1, MYO6, NRXN3, BSN, SHANK3, SHANK2, SPTBN2	5.35077882	0.11223141
GO:2000300~regulation of synaptic vesicle exocytosis	8	7.33944954	0.00104455	RIMS1, SV2B, SYT1, PRKCB, MYO6, NRXN3, SYN1, STXBP5L	4.72127543	0.20978024
GO:0007269~neurotransmitter secretion	7	6.42201835	0.00128936	RIMS1, UNC13A, SYT1, NRXN1, NRXN3, PPFIA3, SYN1	5.40222861	0.22195416
GO:0050804~modulation of synaptic transmission	10	9.17431193	0.00478912	GRM3, SYNPR, SYNGAP1, CAMKV, PRKAR2B, DLGAP1, PPP1R9A, DLGAP2, SHANK3, PPP1R9B	2.99483889	0.72136061
GO:0048167~regulation of synaptic plasticity	6	5.50458716	0.00764702	RIMS1, SYNGAP1, CTNND2, MYO6,	4.63048167	0.86472559

				ATP2B2, SHANK3		
GO:0051963~regulation of synapse assembly	4	3.66972477	0.00790356	CTNNB1, PPP1R9A, OGT, SRCIN1	8.91796469	0.8647255
GO:0016082~synaptic vesicle priming	5	4.58715596	0.00811763	RPH3A, RIMS1, UNC13A, SYNJ1, CADPS	5.90159428	0.8647255
GO:0007155~cell adhesion	12	11.0091743	0.0087917	CYFIP2, EPHA4, PCDHGC5, CTNND2, NRXN1, NRXN3, CTNNB1, PKP4, NRCAM, TLN2, PLCB1, PCDH1	2.40785047	0.8647255
GO:0030534~adult behavior	5	4.58715596	0.0100466	NRXN1, NRXN3, SHANK3, SHANK2, SPTBN2	5.57372793	0.8647255
GO:0098974~postsynaptic actin cytoskeleton organization	5	4.58715596	0.0100466	ABI2, ROCK2, PPP1R9A, SRCIN1, DBN1	5.57372793	0.8647255
GO:0097091~synaptic vesicle clustering	4	3.66972477	0.01088931	NRXN1, CTNNB1, BSN, SYN1	8.02616822	0.8747749
GO:0007268~chemical synaptic transmission	9	8.25688073	0.0119277	SLC12A5, UNC13A	2.82169977	0.8983051

				, SV2B, NRXN1, MYO6, NRXN3, CTNNB1, DLGAP1, GLS		
GO:0060291~long-term synaptic potentiation	6	5.50458716	0.01623407	NTRK2, RIMS1, UNC13A, RASGRF2, SHANK3, SHANK2	3.88362979	1
GO:0006874~cellular calcium ion homeostasis	6	5.50458716	0.01623407	PRKCB, ANXA7, ATP2B3, ATP2B2, PYGM, ATP2B1	3.88362979	1
GO:0071625~vocalization behavior	4	3.66972477	0.01857397	NRXN1, NRXN3, SHANK3, SHANK2	6.68847352	1
GO:0099525~presynaptic dense core vesicle exocytosis	3	2.75229358	0.02189735	RIMS1, UNC13A, CADPS	12.0392523	1
GO:0061669~spontaneous neurotransmitter secretion	3	2.75229358	0.02189735	RPH3A, RIMS1, SYT1	12.0392523	1
GO:0046777~protein autophosphorylation	6	5.50458716	0.02653329	HSPA9, NTRK2, EPHA4, WNK2, CAMK2G, HK1	3.43978638	1
GO:0007249~I-kappaB kinase/NF-kappaB signaling	3	2.75229358	0.03179664	ROCK2, MYO18A, CTNNB1	10.0327103	1

GO:0016081~synaptic vesicle docking	3	2.75229358	0.03179664	RIMS1, UNC13A, PPFIA3	10.0327103	1
GO:0032024~positive regulation of insulin secretion	5	4.58715596	0.03626215	GLUD1, PRKCB, ANXA7, ABAT, PLCB1	3.85873472	1
GO:0018105~peptidyl-serine phosphorylation	6	5.50458716	0.04028649	NTRK2, BRSK2, CAMKV, ROCK2, PRKCB, HK1	3.08698778	1
GO:0001843~neural tube closure	4	3.66972477	0.04096861	NCKAP1, MTHFD1L, OPA1, ROCK2	5.01635514	1
GO:0040011~locomotion	3	2.75229358	0.04309876	WDR1, ATP2B2, SHANK3	8.59946595	1
GO:0046847~filopodium assembly	3	2.75229358	0.04309876	DNM3, NRXN1, PPP1R9B	8.59946595	1
GO:2000310~regulation of NMDA receptor activity	3	2.75229358	0.04309876	RPH3A, RASGRF2, NRXN1	8.59946595	1
GO:0007207~phospholipase C-activating G-protein coupled acetylcholine receptor signaling pathway	3	2.75229358	0.04309876	PRKCB, ANXA7, PLCB1	8.59946595	1
GO:0051968~positive regulation of synaptic transmission, glutamatergic	4	3.66972477	0.0480081	NTRK2, NRXN1, SHANK3, SHANK2	4.72127543	1
GO:0007399~nervous system development	10	9.17431193	0.04917735	NTRK2, EPHA4, BRSK2, ABI2, CTNNB1	2.04749189	1

				, DIP2B, SDHA, CAMK2G, DBN1, PPP1R9B		
GO:0030036~actin cytoskeleton organization	8	7.33944954	0.05409056	CAP1, WDR1, ROCK2, ACTN1, SPTAN1, SPTBN1, SPTBN2, PPP1R9B	2.29319092	1
GO:0061098~positive regulation of protein tyrosine kinase activity	3	2.75229358	0.06928382	EPHA4, ABI2, SRCIN1	6.68847352	1
GO:0098884~postsynaptic neurotransmitter receptor internalization	3	2.75229358	0.06928382	DNM3, SYNJ1, MYO6	6.68847352	1
GO:0016358~dendrite development	4	3.66972477	0.07237317	SYNGAP1, ABI2, MYO6, PPP1R9B	4.01308411	1
GO:0006887~exocytosis	6	5.50458716	0.07321935	RPH3A, RIMS1, BRSK2, UNC13A, SRCIN1, STXBP5L	2.61722877	1
GO:0098609~cell-cell adhesion	6	5.50458716	0.07885241	CYFIP2, CTNND2, CTNNB1, PKP4, NRCAM, TLN2	2.56154305	1

GO:0035640~exploration behavior	3	2.752293 58	0.083882 45	ABAT, SHANK3, SHANK2	6.019626 17	1
GO:0048015~phosphatidylinositol-mediated signaling	3	2.752293 58	0.083882 45	SYNJ1, PLCB1, OGT	6.019626 17	1
GO:2000463~positive regulation of excitatory postsynaptic potential	4	3.669724 77	0.091125 94	RIMS1, NRXN1, SHANK3, DBN1	3.648258 28	1
GO:0000902~cell morphogenesis	4	3.669724 77	0.091125 94	CYFIP2, CAP1, NCKAP1, ATP2B2	3.648258 28	1
GO:0048617~embryonic foregut morphogenesis	2	1.834862 39	0.096326 78	NCKAP1, CTNNB1	20.06542 06	1
GO:0097338~response to clozapine	2	1.834862 39	0.096326 78	PRKAR2B, PPP1R9B	20.06542 06	1
GO:0097117~guanylate kinase-associated protein clustering	2	1.834862 39	0.096326 78	NRXN1, SHANK3	20.06542 06	1
GO:0051571~positive regulation of histone H3-K4 methylation	2	1.834862 39	0.096326 78	CTNNB1, OGT	20.06542 06	1
GO:0007015~actin filament organization	6	5.504587 16	0.097107 48	CAP1, ACTN1, MYO6, PPP1R9A, DBN1, PPP1R9B	2.407850 47	1
GO:0009410~response to xenobiotic stimulus	7	6.422018 35	0.098004 86	POR, SLC12A5, PRKCB, MYO6, CTNNB1, ABAT, SHANK2	2.160891 45	1

GO:0018108~peptidyl-tyrosine phosphorylation	3	2.75229358	0.09931374	EPHA4, ABI2, HK1	5.47238743	1
GO:0006103~2-oxoglutarate metabolic process	3	2.75229358	0.09931374	OGDH, OGDHL, DLD	5.47238743	1

Cellular Component

Table 88. DAVID Gene Ontology output table for enriched cellular components within proteins that fail to become downregulated during memory retrieval in APPtg mice, when compared to WT mice during memory retrieval.

Term	Count	%	PValue	Genes	Fold Enrichment	FDR
GO:0098978~glutamatergic synapse	41	37.6146789	1.99E-08	ROCK2, NRXN1, CTNND2, NRXN3, ADAM22, PPP1R9A, GRM3, RIMS1, SYNGAP1, CAMKV, SV2B, PRKAR2B, MYO6, NRCAM, DLGAP1, BSN, SPTAN1, DLGAP2, SPTBN1, PPFIA3, SPTBN2, EPHA4, NTRK2, UNC13A,	2.40287064	5.79E-06

				SYT1, ACTN1, CADPS, ATP2B3, ATP2B2, ATP2B1, SRCIN1, DNM3, ABI2, SYNJ1, CTNNB1, AMPH, PLCB1, SHANK3, OGT, DBN1, SHANK2		
GO:0030864~cortical actin cytoskeleton	10	9.17431193	1.53E-05	CAP1, WDR1, ACTN1, LANCL2, PPP1R9A, SPTAN1, DBN1, SPTBN1, SPTBN2, PPP1R9B	6.19809203	0.00157205
GO:0042995~cell projection	34	31.1926606	1.62E-05	NCKAP1, WDR1, NRXN1, CTNND2, ADAM22, ADCY5, PPP1R9B, RPH3A, RIMS1, MYO6, MAP6, NRCAM, KIF21A, DIP2B, BSN, SPTAN1, SPTBN1, SPTBN2, CLASP2,	2.0946564	0.00157205

				EPHA4, NTRK2, UNC13A, SLC12A5, ACTN1, ATP2B1, SRCIN1, ABI2, MADD, CTNNB1, DLD, SHANK3, OGT, DBN1, SHANK2		
GO:0045202~synapse	38	34.8623853	2.60E-04	CYFIP2, NRXN1, PPP1R9A, GLS, PPP1R9B, RPH3A, SYNPR, RIMS1, SYNGAP1, SV2B, MYO6, NRCAM, DLGAP1, BSN, DLGAP2, PPFIA3, ATP6V0A1, MPST, EPHA4, NTRK2, UNC13A, SLC12A5, ATP6AP1, SYT1, CADPS, ATP2B2, ATP2B1, SRCIN1, SYN1, DNM3, ABI2, MADD,	1.74269224	0.01888904

				CTNNB1, AMPH, TLN2, SHANK3, OGT, SHANK2		
GO:0043005~neuron projection	23	21.1009174	0.0016600 2	MPST, CYFIP2, EPHA4, UNC13A, SLC12A5, SYT1, DCTN1, ATP2B2, ABAT, PPP1R9A, SRCIN1, PPP1R9B, GRM3, RPH3A, SYNPR, SYNJ1, SV2B, MAP6, NRCAM, CAMK2G, SHANK3, OGT, SHANK2	1.9766184 3	0.0833815 5
GO:0014069~postsynaptic density	21	19.266055	0.0017192 1	NTRK2, EPHA4, CTNND2, PPP1R9A, SRCIN1, SYN1, PPP1R9B, GRM3, DNM3, RIMS1, SYNGAP1, MYO6, PKP4, DLGAP1, BSN, CAMK2G, DLGAP2,	2.0650373 9	0.0833815 5

				SHANK3, DBN1, SHANK2, SPTBN1		
GO:0048786~presynaptic active zone	7	6.42201835	0.00214144	GRM3, NTRK2, UNC13A, BSN, SHANK2, PPFIA3, SYN1	4.93710089	0.08827681
GO:0005886~plasma membrane	56	51.3761468	0.00260465	NCKAP1, WDR1, RASGRF2, CTNND2, PPP1R9B, GRM3, RPH3A, SMPD3, RIMS1, SYNGAP1, CAMKV, ANXA7, NRCAM, KIF21A, DLGAP1, SPTAN1, DLGAP2, CAP1, EPHA4, UNC13A, PRKCB, ACTN1, EPS15L1, DNM3, DNAJC5, MADD, LANCL2, AMPH, PKP4, TLN2, PLCB1, SHANK3, DBN1, SHANK2, ROCK2,	1.36520549	0.08827681

				NRXN1, ADAM22, ADCY5, PRKAR2B, MYO6, PCDH1, SPTBN1, SPTBN2, ATP6V0A1, CLASP2, NTRK2, SLC12A5, SYT1, ATP2B3, ATP2B2, ATP2B1, STXBP5L, WNK2, CTNNB1, SMAP1, OGT		
GO:0043197~dendritic spine	14	12.8440367	0.00273021	NTRK2, EPHA4, ACTN1, PPP1R9A, PPP1R9B, GRM3, RPH3A, DNM3, ABI2, PRKAR2B, DLGAP2, SHANK3, DBN1, SHANK2	2.51185835	0.08827681
GO:0060076~excitatory synapse	7	6.42201835	0.0036282	NTRK2, UNC13A, SYT1, NRXN1, BSN, SHANK3, DBN1	4.47424769	0.10558067
GO:0005759~mitochondrial matrix	12	11.009174	0.00439611	HSPA9, GLUD1, OAT, PCX,	2.63918757	0.1138694

				OGDH, LONP1, ABAT, OGDHL, ACO2, ACADSB, DLD, GLS		
GO:0098831~presynaptic active zone cytoplasmic component	5	4.58715596	0.0046956	RIMS1, UNC13A, CTNNB1, BSN, PPFIA3	6.81790123	0.1138694
GO:0030175~filopodium	7	6.42201835	0.0066601	EPHA4, ABI2, MYO6, PPP1R9A, SRCIN1, DBN1, PPP1R9B	3.97710905	0.1490857
GO:0005916~fascia adherens	4	3.66972477	0.0074965	ACTN1, CTNNB1, TLN2, SPTAN1	9.09053498	0.1558217
GO:0030672~synaptic vesicle membrane	11	10.091743	0.0094429	RPH3A, SYNPR, UNC13A, SV2B, SYT1, ATP6AP1, DNAJC5, ATP2B1, BSN, SYN1, ATP6V0A1	2.52798585	0.1745872
GO:0030054~cell junction	9	8.25688073	0.0097585	WDR1, ABI2, ACTN1, CTNNB1, PKP4, PCDH1, SPTAN1, SPTBN1, SPTBN2	2.92195767	0.1745872

GO:0042734~presynaptic membrane	11	10.0917431	0.0101992	GRM3, RIMS1, EPHA4, UNC13A, SYT1, NRXN1, NRXN3, CTNNB1, ATP2B3, ATP2B2, ATP2B1	2.49989712	0.1745872
GO:0045252~oxoglutarate dehydrogenase complex	3	2.75229358	0.0130829	OGDH, OGDHL, DLD	15.3402778	0.2115068
GO:0043229~intracellular organelle	5	4.58715596	0.0138237	SYT1, AMPH, SYN1, SPTBN1, ATP6V0A1	5.11342593	0.2117220
GO:0098982~GABA-ergic synapse	9	8.25688073	0.0152347	RIMS1, NRXN1, NRXN3, ATP2B3, ATP2B2, ATP2B1, BSN, PLCB1, OGT	2.70710784	0.2216652
GO:0031594~neuromuscular junction	7	6.42201835	0.0176303	RPH3A, EPHA4, UNC13A, DNAJC5, NRXN1, PPP1R9A, STXBP5L	3.25399832	0.2443055
GO:0008021~synaptic vesicle	12	11.009174	0.0185045	RPH3A, SYNPR, SV2B, SYT1, DNAJC5, MADD, WDR7, AMPH, BSN,	2.17207473	0.2447643

				SYN1, SPTBN2, ATP6V0A1		
GO:0005856~cytoskeleton	24	22.0183486	0.0195946	BRSK2, WDR1, ROCK2, DCTN1, ACTN1, PPP1R9A, SRCIN1, LRPPRC, SYN1, PPP1R9B, DNM3, ABI2, MYO18A, MAP6, CTNNB1, PKP4, KIF21A, AMPH, TLN2, BSN, SPTAN1, DBN1, SPTBN1, CLASP2	1.5886371	0.2479154
GO:0098871~postsynaptic actin cytoskeleton	4	3.66972477	0.0221537	ABI2, MYO6, PPP1R9A, DBN1	6.2934472	0.2686145
GO:0042584~chromaffin granule membrane	3	2.75229358	0.0306844	SYT1, DNAJC5, ANXA7	10.226851	0.3434292
GO:0008091~spectrin	3	2.75229358	0.0306844	PRKCB, SPTBN1, SPTBN2	10.226851	0.3434292
GO:0070161~anchoring junction	10	9.17431193	0.0332333	EPHA4, WDR1, ABI2, CTNND2, ACTN1, CTNNB1, PKP4,	2.1993229	0.3581819

				TLN2, DBN1, PPP1R9B		
GO:0030424~axon	17	15.5963303	0.0345812 4	NTRK2, EPHA4, UNC13A, SYT1, DCTN1, ADAM22, SRCIN1, SYN1, GRM3, DNM3, MYO6, MADD, MAP6, NRCAM, KIF21A, DIP2B, BSN	1.6961607 9	0.3593979
GO:0031209~SCAR complex	3	2.7522935 8	0.0416164	CYFIP2, NCKAP1, ABI2	8.7658730 2	0.4036790 4
GO:0005798~Golgi-associated vesicle	3	2.7522935 8	0.0416164	UNC13A, MAP6, BSN	8.7658730 2	0.4036790 4
GO:0000922~spindle pole	4	3.6697247 7	0.0530543	DCTN1, CTNNB1, PKP4, CLASP2	4.5452674 9	0.4929497
GO:0030425~dendrite	17	15.5963303	0.0542075 3	NTRK2, EPHA4, CTNND2, ATP2B2, PPP1R9A, SRCIN1, SYN1, PPP1R9B, ABI2, OPA1, PRKAR2B, MAP6, KIF21A, DIP2B, BSN,	1.6023638 8	0.4929497

				DLGAP2, DBN1		
GO:0098688~parallel fiber to Purkinje cell synapse	4	3.66972477	0.06084962	SYNJ1, ATP2B3, ATP2B2, SPTBN2	4.30604288	0.52810759
GO:0098793~presynapse	12	11.0091743	0.06343404	RPH3A, DNM3, UNC13A, SYNJ1, DNAJC5, CADPS, NRXN3, AMPH, BSN, SRCIN1, SYN1, SPTBN2	1.79156529	0.52810759
GO:0005912~adherens junction	6	5.50458716	0.06351809	EPHA4, ABI2, CTNND2, CTNNB1, PKP4, PPP1R9B	2.72716049	0.52810759
GO:0099092~postsynaptic density, intracellular component	5	4.58715596	0.07229607	SYNGAP1, CTNNB1, DLGAP1, DLGAP2, SHANK3	3.09904602	0.5843932
GO:0044295~axonal growth cone	4	3.66972477	0.07793097	EPHA4, NRXN1, DBN1, CLASP2	3.89594356	0.61291652
GO:0098684~photoreceptor ribbon synapse	3	2.75229358	0.08114234	ATP2B2, AMPH, ATP2B1	6.13611111	0.62137948
GO:0030285~integral component of synaptic vesicle membrane	5	4.58715596	0.08601527	SYNPR, SV2B, SYT1, ATP2B1, ATP6V0A1	2.92195767	0.63142956

GO:0045211~postsynaptic membrane	11	10.0917431	0.0867944	GRM3, RPH3A, NTRK2, EPHA4, CTNNB1, NRCAM, ATP2B2, DLGAP1, SHANK3, DBN1, SHANK2	1.75774016	0.6314295
GO:0098683~cochlear hair cell ribbon synapse	2	1.83486239	0.0945510	MYO6, BSN	20.453703	0.6660147
GO:0032591~dendritic spine membrane	3	2.75229358	0.0961258	ATP2B2, ATP2B1, PPP1R9B	5.57828283	0.6660147

Molecular Function

Table 89. DAVID Gene Ontology output table for enriched molecular functions within proteins that fail to become downregulated during memory retrieval in APPtg mice, when compared to WT mice during memory retrieval.

Term	Count	%	PValue	Genes	Fold Enrichment	FDR
GO:0005516~calmodulin binding	12	11.009174	3.70E-04	UNC13A, SYT1, CAMKV, RASGRF2, MYO6, MAP6, ATP2B2, ATP2B1, PLCB1, SPTAN1, CAMK2G, SPTBN1	3.52579957	0.1173487
GO:0051015~actin filament binding	13	11.926605	0.0022661	WDR1, ACTN1,	2.69383459	0.3591886

				PPP1R9A, PPP1R9B, RPH3A, MYO6, MYO18A, TLN2, SPTAN1, DBN1, SPTBN1, SPTBN2, CLASP2		
GO:1905056~calcium-transporting ATPase activity involved in regulation of presynaptic cytosolic calcium ion concentration	3	2.75229358	0.00727745	ATP2B3, ATP2B2, ATP2B1	19.6857143	0.76898354
GO:0098919~structural constituent of postsynaptic density	4	3.66972477	0.01519418	CTNND2, DLGAP1, SHANK3, SHANK2	7.15844156	0.99459105
GO:0005509~calcium ion binding	13	11.9266055	0.02158521	UNC13A, SYT1, PCDHGC5, NRXN1, ACTN1, CADPS, ATP2B2, EPS15L1, RPH3A, ANXA7, PLCB1, PCDH1, SPTAN1	2.03106576	0.99459105
GO:0019829~cation-transporting ATPase activity	3	2.75229358	0.02269589	ATP2B3, ATP2B2, ATP2B1	11.8114286	0.99459105
GO:0009055~electron carrier activity	4	3.66972477	0.02447461	POR, NDUFS1, SDHA, ACADSB	6.05714286	0.99459105
GO:0008022~protein C-terminus binding	9	8.25688073	0.02974635	SYT1, SYNJ1,	2.39420849	0.99459105

				CTNNB1, ATP2B2, AMPH, PPP1R9A, SHANK3, SHANK2, PPP1R9B		
GO:0005246~calcium channel regulator activity	4	3.66972477	0.0300323	GRM3, PRKCB, NRXN1, NRXN3	5.6244898	0.99459105
GO:0004672~protein kinase activity	10	9.17431193	0.0318894 5	NTRK2, EPHA4, BRSK2, CAMKV, ROCK2, PRKCB, WNK2, CAMK2G, PPP1R9B, HK1	2.2118780 1	0.99459105
GO:0005524~ATP binding	24	22.018348 6	0.0345126 2	HSPA9, NTRK2, EPHA4, BRSK2, PCX, ATP6AP1, ROCK2, PRKCB, ATP2B3, ATP2B2, ATP2B1, BCS1L, SYN1, ADCY5, HK1, GLUD1, CAMKV, MTHFD1L, WNK2, MYO6, MYO18A, LONP1, KIF21A, CAMK2G	1.5046405 8	0.99459105

GO:0005515~protein binding	61	55.9633028	0.0428536	CYFIP2, NCKAP1, GDA, PPP1R9A, PPP1R9B, HK1, GLS, RPH3A, SMPD3, RIMS1, SYNGAP1, OPA1, ANXA7, NRCAM, DLGAP1, BSN, SPTAN1, CAP1, EPHA4, UNC13A, PRKCB, ACTN1, EPS15L1, SRCIN1, DNM3, DNAJC5, AMPH, NDUFS1, TLN2, PLCB1, DLD, SHANK3, DBN1, BRSK2, DCTN1, ROCK2, NRXN1, NRXN3, ADAM22, ADCY5, SAMM50, PRKAR2B, MYO6, PCDH1, SPTBN1, ATP6V0A1, CLASP2, HSPA9,	1.18541814	1

				NTRK2, SYT1, AGL, CADPS, IMMT, ATP2B1, STAM, LRPPRC, GLUD1, SYNJ1, CTNNB1, SMAP1, OGT		
GO:0005388~calcium-transporting ATPase activity	3	2.75229358	0.04461601	ATP2B3, ATP2B2, ATP2B1	8.43673469	1
GO:0017124~SH3 domain binding	6	5.50458716	0.05662882	RIMS1, SYNGAP1, ABI2, SYNJ1, SHANK3, SHANK2	2.8122449	1
GO:0003779~actin binding	11	10.0917431	0.06850855	CAP1, WDR1, ACTN1, MYO6, TLN2, SPTAN1, SHANK3, DBN1, SYN1, SPTBN1, PPP1R9B	1.83510896	1
GO:0042731~PH domain binding	2	1.83486239	0.09812051	EPHA4, LONP1	19.685714 3	1

Proteins inappropriately downregulated in APPtg mice during memory retrieval (proteins downregulated in APPtg mice during memory retrieval but not in WT mice during memory retrieval)

Biological Process

Table 90. DAVID Gene Ontology output table for enriched biological processes within proteins that are inappropriately downregulated during memory retrieval in APPtg mice, when compared to WT mice during memory retrieval.

Term	Count	%	PValue	Genes	Fold Enrichment	FDR
GO:0006468~protein phosphorylation	8	20	0.00196859	GSK3A, PTK2B, TNIK, CDC42BPB, STK32C, SCYL2, MTOR, PDK1	4.19438339	1
GO:0016310~phosphorylation	8	20	0.00385143	GSK3A, PTK2B, TNIK, CDC42BPB, PFKP, STK32C, MTOR, PDK1	3.73229031	1
GO:0007268~chemical synaptic transmission	5	12.5	0.02479324	USP14, GRM2, GABBR1, NRXN2, PAFAH1B1	4.30088141	1
GO:0018105~peptidyl-serine phosphorylation	4	10	0.03015603	GSK3A, STK32C, MTOR, PDK1	5.64628534	1
GO:0042220~response to cocaine	3	7.5	0.03131687	GRM2, PTK2B, MTOR	10.3221154	1
GO:0051012~microtubule sliding	2	5	0.03509307	MAP4, PAFAH1B1	55.0512821	1

GO:1904000~positive regulation of eating behavior	2	5	0.03509307	SGIP1, MTOR	55.0512821	1
GO:0007166~cell surface receptor signaling pathway	3	7.5	0.03905462	ADGRB2, PTK2B, PDK1	9.17521368	1
GO:0018107~peptidyl-threonine phosphorylation	3	7.5	0.04316954	GSK3A, CDC42BPB, MTOR	8.69230769	1
GO:0005975~carbohydrate metabolic process	4	10	0.04603269	GSK3A, HEXB, MPI, PDK1	4.787068	1
GO:0014048~regulation of glutamate secretion	2	5	0.052187	GRM2, GABBR1	36.7008547	1
GO:0007165~signal transduction	7	17.5	0.0663871	GRM2, GSK3A, GABBR1, ADGRB2, PTK2B, NRXN2, ANK1	2.33550894	1
GO:0051896~regulation of protein kinase B signaling	2	5	0.06898592	GRM2, MTOR	27.525641	1
GO:0016183~synaptic vesicle coating	2	5	0.06898592	AP3S1, AP3B2	27.525641	1
GO:0007281~germ cell development	2	5	0.06898592	MTOR, PAFAH1B1	27.525641	1
GO:0035654~cargo loading into clathrin-coated vesicle, AP-3-mediated	2	5	0.06898592	AP3S1, AP3B2	27.525641	1
GO:0070885~negative regulation of calcineurin-NFAT signaling cascade	2	5	0.0854948	ATP2B4, MTOR	22.0205128	1
GO:0033173~calcineurin-NFAT signaling cascade	2	5	0.0854948	ADGRB2, MTOR	22.0205128	1
GO:0048490~anterograde synaptic vesicle transport	2	5	0.0854948	AP3S1, AP3B2	22.0205128	1

Cellular Component

Table 91. DAVID Gene Ontology output table for enriched cellular components within proteins that are inappropriately downregulated during memory retrieval in APPtg mice, when compared to WT mice during memory retrieval.

Term	Count	%	PValue	Genes	Fold Enrichment	FDR
GO:0030117~membrane coat	3	7.5	0.02189119	CLTC, AP3S1, AP3B2	12.4567669	1
GO:0016020~membrane	27	67.5	0.03763336	USP14, ATP8A1, HEXB, CLTC, NRXN2, VPS26A, GRM2, APMAP, PTK2B, AP3S1, SLC25A22, SCYL2, GABBR1, SGIP1, SACM1L, SLC2A13, ATP2B4, CDC42BPB, ANK1, AP3B2, MTOR, AFG3L2, PPP5C, ADGRB2, RIMBP2, PFKP, PAFAH1B1	1.30037501	1
GO:0030136~clathrin-coated vesicle	3	7.5	0.073732	SGIP1, CLTC, SCYL2	6.45906433	1
GO:0031410~cytoplasmic vesicle	8	20	0.07375388	USP14, ATP8A1, HEXB, CLTC, AP3S1, AP3B2,	2.07612782	1

				SCYL2, MTOR		
GO:1904115~axon cytoplasm	3	7.5	0.07858633	AP3S1, AP3B2, PAFAH1B1	6.22838346	1
GO:0030123~AP-3 adaptor complex	2	5	0.0964872	AP3S1, AP3B2	19.377193	1

Molecular Function

Table 92. DAVID Gene Ontology output table for enriched molecular functions within proteins that are inappropriately downregulated during memory retrieval in APPtg mice, when compared to WT mice during memory retrieval.

Term	Count	%	PValue	Genes	Fold Enrichment	FDR
GO:0004672~protein kinase activity	8	20	6.52E-04	GSK3A, PTK2B, TNIK, CDC42BPB, STK32C, SCYL2, MTOR, PDK1	5.02156089	0.09512927
GO:0005524~ATP binding	13	32.5	0.00490739	GSK3A, ATP8A1, ATP2B4, CDC42BPB, MTOR, AFG3L2, PPP5C, PTK2B, TNIK, PFKP, STK32C, SCYL2, PDK1	2.31287657	0.24336857

GO:0016301~kinase activity	8	20	0.0050007 2	GSK3A, PTK2B, TNIK, CDC42BPB , PFKP, STK32C, MTOR, PDK1	3.5469755 5	0.2433685 7
GO:0004674~protein serine/threonine kinase activity	6	15	0.0085983 6	GSK3A, TNIK, CDC42BPB , STK32C, MTOR, PDK1	4.4691891 9	0.2653862 7
GO:0004712~protein serine/threonine/tyrosine kinase activity	6	15	0.0090885 7	GSK3A, PTK2B, TNIK, CDC42BPB , STK32C, MTOR	4.4103840 7	0.2653862 7
GO:0044877~macromolecular complex binding	9	22.5	0.0226179 8	PDP1, PPP5C, HEXB, PTK2B, CDC42BPB , PFKP, MTOR, PAFAH1B1 , PDK1	2.4289071 7	0.5503707 7
GO:0004888~transmembrane signaling receptor activity	3	7.5	0.0303691 1	GABBR1, ADGRB2, NRXN2	10.474662 2	0.6334128 2
GO:0004930~G-protein coupled receptor activity	3	7.5	0.0418887 1	GRM2, GABBR1, ADGRB2	8.8207681 4	0.7644689 7
GO:0016787~hydrolase activity	9	22.5	0.0641634 3	PDP1, USP14, AFG3L2, PPP5C, ATP8A1, SACM1L, HEXB, TPP2, BLMH	1.9872876 8	1

GO:0008233~peptidase activity	4	10	0.0810994 3	USP14, AFG3L2, TPP2, BLMH	3.7874484 7	1
GO:0000166~nucleotide binding	12	30	0.0853324 3	AFG3L2, GSK3A, ATP8A1, ATP2B4, PTK2B, TNIK, CDC42BPB , ADSS, PFKP, STK32C, MTOR, PDK1	1.6271319 9	1
GO:0016740~transferase activity	8	20	0.0917338 8	GSK3A, PTK2B, TNIK, CDC42BPB , PFKP, STK32C, MTOR, PDK1	1.9688058 1	1
GO:0005515~protein binding	23	57. 5	0.0970673 4	USP14, GSK3A, GABBR1, ATP8A1, SGIP1, SACM1L, CLTC, ATP2B4, NRXN2, VPS26A, CDC42BPB , ANK1, MTOR, AFG3L2, PPP5C, ADGRB2, PSMD3, PSMD1, PTK2B, TNIK, MAP4,	1.2684026 6	1

				SCYL2, PAFAH1B1		